1949

THE
REVIEW

THE PHYSICAL REVIEW

A journal of experimental and theoretical physics established by E. L. Nichols in 1893

Published by the American Institute of Physics
for the
AMERICAN PHYSICAL SOCIETY

Officers

President

F. W. Loomis
University of Illinois
Urbana, Illinois

Vice-President

I. I. Rabi
Columbia University
New York, New York

Secretary

K. K. Darrow
Bell Telephone Laboratories
Office:
Columbia University
New York 27, New York

Treasurer

G. B. Pegram
Columbia University
New York 27, New York

Local Secretary
for the Pacific Coast

J. Kaplan
University of California at Los Angeles
Los Angeles, California

Managing Editor

John T. Tate
University of Minnesota
Minneapolis, Minnesota

BOARD OF EDITORS

Editor

John T. Tate

Assistant Editor

J. W. Beams

Associate Editors

S. A. Goudsmit — W. E. Lamb, Jr.
E. M. Purcell — R. G. Sachs
V. F. Weisskopf — J. Rainwater

Manuscripts for publication should be submitted to John T. Tate, University of Minnesota, Minneapolis, Minnesota. The authors' institutions are requested to pay a publication charge of $4 per page which, if honored, entitles them to 100 free reprints. Instructions will be sent with galley proof.

Proofs and all correspondence concerning papers in the process of publication should be addressed to the Publication Manager, American Institute of Physics, 57 East 55 Street, New York 22, New York.

Subscription Price

United States and Canada ..... $[illegible]
Elsewhere ..... $[illegible]

Back Numbers[1]

Quarterly back number rate when complete year is available:
Prior to 1949: $20.00
Thereafter: $27.00
Single copies: $2.00 each, prior to July, 1929;
$[illegible] each, July, 1929–December, 1941;
$2.00 each, January, 1942–December, 1946;
$3.00 each, January, 1947–December, 1948.
Current issues: $0.75 each.
General index, 1893–1920: $4.00.

Subscriptions and orders for back numbers should be addressed to the Business Office, [illegible] Streets, Lancaster, Pennsylvania, or to the American Institute of Physics, 57 East 55 Street, New York 22, New York.

Changes of address in the case of members of the American Physical Society should be addressed to the Treasurer; in the case of other subscribers, to the Circulation Manager, American Institute of Physics.

[1] Inquire of Physics Department, Cornell University, Ithaca, New York.

The Physical Review is published monthly at Prince and Lemon Streets, Lancaster, Pennsylvania.

Entered as second-class matter March [illegible], 1913, at the Post Office at Lancaster, Pennsylvania, under the Act of March 3, 1879.

Acceptance for mailing at special rate of postage provided for in paragraph 4, section 538, P. L. & R., authorized January 27, [illegible].

THE
PHYSICAL REVIEW

A journal of experimental and theoretical physics established by E. L. Nichols in 1893

SECOND SERIES, VOL. 76, No. 9 NOVEMBER 1, 1949

Notes on the *j–j* Coupling Shell Model*

EUGENE FEENBERG
*Washington University, St. Louis, Missouri, and Oak Ridge National Laboratory,** Oak Ridge, Tennessee*
(Received July 29, 1949)

A study of the nuclear shell model based on the hypothesis of strong spin-orbit coupling yields a number of interesting results for even–even and odd–odd nuclei. To secure simple relations all calculations are based on the extreme limiting situation of complete *j–j* coupling. Maximum symmetry in the space wave function and *j–j* coupling are generally in sharp conflict. On occasion there is no conflict and then the consequences of the *j–j* coupling model are found to agree with experiment (notably the spin and magnetic moment of B^{10} and the sign of the magnetic moment of K^{40}). The *j–j* coupling model yields good results for the magnetic moments of N^{14} and Ne^{22}, but in both cases the agreement may be illusory because the computed moments are nearly independent of the amount of singlet wave function in the representation of the ground state. Also the model favors $I=5$ for the ground state of Na^{22}.

INTRODUCTION

THREE aspects of nuclear structure are particularly relevant for the present discussion:

(a) *Spin-orbit coupling.* Experimental results on nuclear spins and magnetic moments of light nuclei suggest that parallel orientation of the orbital and spin angular momentum vectors of the individual particles is favored energetically over the antiparallel orientation.[1] The rule may be stated in the form that nuclear multiplets are inverted or regular according as the last orbital shell is less or more than half-filled.[2] Actually the theoretical basis for the rule is somewhat confused and equivocal because of uncertainty in the form, exchange properties and spin dependence of nuclear forces and the associated relativistic corrections[3–5] as well as in the best choice of nuclear model and the magnitude of configuration interaction.[6,7]

(b) *Odd–even structure of the energy surface.* In the successive addition of neutrons (or protons), the odd neutron (or proton) is less tightly bound than the preceding and following even neutron (or proton).[8–10] The simplest interpretation is that two nucleons interact most strongly when both are in essentially equivalent space orbits. With two particles in an orbit, energy is gained from the direct interaction of the particles and from a second-order polarization effect which simulates a direct interaction.[11] In the space orbital approximation, two like particles outside of a closed shell or missing from a closed shell are described by singlet wave functions completely symmetrical in the space coordinates of the two particles.

From a more general standpoint, the odd–even structure of the energy surface can be correlated with a pronounced tendency for the ground state space wave function to possess the maximum possible symmetry consistent with the exclusion principle. The actual maximum is associated with Wigner's first approximation[12] in which the space wave functions belong to irreducible representations of the symmetric group. The ground states have then the following spin properties:

Type of nucleus	*Spin character*
even–even	singlet ($S=0$)
odd–odd	singlet ($S=0$) or triplet ($S=1$)
even–odd	doublet ($S=\frac{1}{2}$).

* Assisted by the Joint Program of the ONR and the AEC.
** Temporary, summer, 1949.
[1] D. R. Inglis, Phys. Rev. **50**, 783 (1936); also G. Breit, lectures at Ann Arbor, summer, 1936.
[2] L. Rosenfeld, *Nuclear Forces* (Interscience Publishers, Inc., New York, 1948), p. 317. Denoted by NF in later references.
[3] S. Dancoff and D. R. Inglis, Phys. Rev. **50**, 784 (1936).
[4] W. Furry, Phys. Rev. **50**, 784 (1936).
[5] G. Breit, Phys. Rev. **51**, 248, 778 (1937).
[6] M. Phillips, Phys. Rev. **57**, 160 (1940); NF, p. 410.
[7] R. Sacks, Phys. Rev. **55**, 825 (1939); NF, p. 411.
[8] N. Bohr and J. A. Wheeler, Phys. Rev. **56**, 426 (1939); particularly Eq. (6).
[9] See reference 2, Fig. 3.221–1.
[10] K. Way, Phys. Rev. **75**, 1448 (1949).
[11] C. F. V. Weizacker, Zeits. f. Physik **96**, 432 (1935).
[12] E. P. Wigner, Phys. Rev. **51**, 106, 947 (1937).

TABLE I. Single particle Landé g factors.

State	g factor Neutron g_1	Proton g_2
$^2S_{1/2}$	−3.82	5.58
$^2P_{3/2}$	−1.27	2.53
$^2P_{1/2}$	1.27	−0.53
$^2D_{5/2}$	−0.76	1.92
$^2D_{3/2}$	0.76	0.08
$^2F_{7/2}$	−0.55	1.65
$^2F_{5/2}$	0.55	0.35
$^2G_{9/2}$	−0.42	1.51
$^2G_{7/2}$	0.42	0.49
$^2H_{11/2}$	−0.35	1.42
$^2H_{9/2}$	0.35	0.58

There is good evidence from the analysis of binding energies supporting the approximate validity of Wigner's first approximation up to $A\sim 50$.[12,13] The absence of a noticeable trend with Z or A in the values of allowed (favored)[14] and allowed (unfavored)[15,16] beta-decay matrix elements suggests a much wider range of validity.

(c) *$I=0$ for even–even nuclei.* As yet no exception is known to the rule that even–even nuclei have $I=0$ in the ground state. However, the existence of two even–even nuclei with isomeric states ($_{82}Pb^{204}$ and $_{32}Ge^{72}$) and the probable existence of others suggests the advisability of caution in stating and applying the rule. In terms of the explanation offered for *b*, the rule implies that the state of lowest energy has neither orbital nor spin angular momentum. Studies of exchange force models by variational and perturbation methods yield results conforming to the rule.[17–19]

Among recently discussed nuclear shell models, one is based on the hypothesis that (i) strong spin-orbit coupling exists in accordance with the Breit-Inglis rule[1] and (ii) the effective magnitude of the coupling grows with increasing angular momentum in an unspecified, but decisive manner.[20,21]

The present note develops certain consequences of the strong spin-orbit coupling model for two particles with respect to the symmetry properties of the space wave function. To secure simple relations, all calculations are based on the extreme limiting situation of complete j–j coupling. It will be shown that j–j coupling on the one hand and maximum symmetry in the space wave function on the other are generally in sharp conflict. On occasion there is no conflict and then the consequences of the j–j coupling model are found to agree with experiment (notably the spin and magnetic moment of B^{10} and the sign of the magnetic moment of $_{19}K^{40}$). The j–j coupling model yields good results for the magnetic moments of $_7N^{14}$ and $_{11}Ne^{22}$, but in both cases the agreement may be illusory because the computed moments are nearly independent of the amount of singlet wave function in the representation of the ground state. Also, the model favors $I=5$ for the ground state of $_{11}Na^{22}$ rather than the actual $I=3$.

NOTATION

$\Theta_{lm}(\theta, \varphi)$—normalized single particle angular wave function.

$$(2l+1)^{\frac{1}{2}}\psi_{l+\frac{1}{2},\,p+\frac{1}{2}}=(l+1+p)^{\frac{1}{2}}\Theta_{l,p}\delta(m_s,\tfrac{1}{2})+(l-p)^{\frac{1}{2}}\Theta_{l,p+1}\delta(m_s,-\tfrac{1}{2}),$$

$$(2l+1)^{\frac{1}{2}}\psi_{l-\frac{1}{2},\,p+\frac{1}{2}}=(l-p)^{\frac{1}{2}}\Theta_{l,p}\delta(m_s,\tfrac{1}{2})-(l+1+p)^{\frac{1}{2}}\Theta_{l,p+1}\delta(m_s,-\tfrac{1}{2}),$$

$$^3S_1(1,2)=\delta(m_{s1},\tfrac{1}{2})\delta(m_{s2},\tfrac{1}{2}),$$

$$^3S_0(1,2)=2^{-\frac{1}{2}}[\delta(m_{s1},\tfrac{1}{2})\delta(m_{s2},-\tfrac{1}{2})+\delta(m_{s2},\tfrac{1}{2})\delta(m_{s1},-\tfrac{1}{2})],$$

$$^3S_{-1}(1,2)=\delta(m_{s1},-\tfrac{1}{2})\delta(m_{s2},-\tfrac{1}{2}),$$

$$^1S_0(1,2)=2^{-\frac{1}{2}}[\delta(m_{s1},\tfrac{1}{2})\delta(m_{s2},-\tfrac{1}{2})-\delta(m_{s2},\tfrac{1}{2})\delta(m_{s1},-\tfrac{1}{2})],$$

$$(p+\tfrac{1}{2},q+\tfrac{1}{2})_\pm{}^j=2^{-\frac{1}{2}}[\psi_{j,\,p+\frac{1}{2}}(1)\psi_{j,\,q+\frac{1}{2}}(2)\pm\psi_{j,\,p+\frac{1}{2}}(2)\psi_{j,\,q+\frac{1}{2}}(1)],$$

$$(p,q)_\pm=2^{-\frac{1}{2}}[\Theta_{l,p}(1)\Theta_{l,q}(2)\pm\Theta_{l,p}(2)\Theta_{l,q}(1)].$$

The last two definitions fail for $p=q$. Obvious modifications are then required to maintain the normalization of the symmetrical combination.

TWO LIKE PARTICLES IN EQUIVALENT ORBITS

The wave function

$$(l+1)^{\frac{1}{2}}\Psi_0(1,2)=\sum_0^l(-1)^p(p+\tfrac{1}{2},-p-\tfrac{1}{2})_-^{l+\frac{1}{2}} \quad (1)$$

describes two like particles in $j=l+\frac{1}{2}$ orbits combined to produce an antisymmetrical state with zero angular momentum. The problem set here is the determination of the statistical weight of the singlet component in Ψ_0. A straightforward calculation yields

$$\begin{aligned}(2l+1)(l+1)^{\frac{1}{2}}\Psi_0(1,2)&=\,^3S_1\sum_0^l(-1)^p\{(l+1+p)(l-p)\}^{\frac{1}{2}}(p,-p-1)\\&+\,^3S_{-1}\sum_0^l(-1)^p\{(l+1+p)(l-p)\}^{\frac{1}{2}}(p+1,-p)_-\\&+\,^3S_0 2^{\frac{1}{2}}\sum_1^l(-1)^p p(p,-p)_-\\&+(l+1)\,^1S_0\left[(0,0)_+ +2^{\frac{1}{2}}\sum_1^l(-1)^p(p,-p)_+\right]. \quad (2)\end{aligned}$$

[12] W. Barkas, Phys. Rev. **55**, 691 (1939).
[14] E. P. Wigner, Phys. Rev. **56**, 519 (1939); A. M. Feingold and E. P. Wigner, unpublished notes (1949).
[15] N. Feather and H. O. W. Richardson, Proc. Phys. Soc. **61**, 452 (1948).
[16] E. Feenberg and K. C. Hammack, Phys. Rev. **75**, 1877 (1949).
[17] W. Heisenberg, Zeits. f. Physik **96**, 473 (1935).
[18] E. Feenberg and M. Phillips, Phys. Rev. **51**, 597 (1937).
[19] Tyrrell, Carroll, and Margenau, Phys. Rev. **55**, 790 (1939).
[20] M. G. Mayer, Phys. Rev. **75**, 1969 (1949).
[21] Haxel, Jensen, and Suess, Phys. Rev. **75**, 1766 (1949).

The singlet term is found to occur with the statistical weight

$$(l+1)/(2l+1).$$

Similarly, one finds

$$l^1\Phi_0(1,2)=\sum_0^{l-1}(-1)^p(p+\tfrac{1}{2},-p-\tfrac{1}{2})_-{}^{l-1}, \qquad (3)$$

the antisymmetric wave function with zero angular momentum constructed from pairs of orbits with $j=l-\frac{1}{2}$. Proceeding as before, the singlet term is found to occur with the statistical weight $l/(2l+1)$. The single formula $(2j+1)/2(2l+1)$ includes both cases.

As illustrations, consider the application to $_{38}Sr^{88}$ and $_{40}Zr^{92}$ assuming $I=0$ for the ground states of both nuclei as required by c. In Wigner's first approximation, the space part of the wave functions belong to irreducible representations of the symmetric group denoted by the partition symbol $4\cdot\cdots42\cdot\cdot2$. In the language of the shell model, assuming L–S coupling, two holes in the proton $3p$ shell or two particles in the neutron $4d$ shell generate $^1S_0$ ground states, completely symmetrical in the space coordinates of the two particles. With complete j–j coupling on the other hand, the statistical weight of the $^1S_0$ component is 0.33 ($l=1$, $j=\frac{1}{2}$) and 0.60 ($l=2$, $j=5/2$).

The only certain conclusion warranted by the preceding argument is that the hypothesis of strong spin-orbit coupling as postulated by Mayer requires an extreme degree of departure from the maximum possible symmetry, consistent with the exclusion principle, in the space wave function. However, continuing on less certain ground, several plausible lines of argument may be cited against the possibility of such large admixture of triplet components as occur in the preceding examples. The simple and qualitatively satisfying explanation discussed under b of the greater binding energy of the even particle now fails. The ground states of even-even nuclei are now linear combinations of $^1S_0$ and $^3P_0$ components with approximately equal statistical weights. Also the theoretical basis for the separation of allowed beta-transitions into distinct favored and unfavored groups is lost.

One can, however, find in property c an argument for a tendency toward j–j coupling. The two particle wave functions with maximum spin are

$$\Psi_{2l}=(l+\tfrac{1}{2},l-\tfrac{1}{2})_-{}^{l+1},$$
$$\Psi_{2l-2}=(l-\tfrac{1}{2},l-\tfrac{3}{2})_-{}^{l-1},\quad l>0. \qquad (4)$$

The statistical weight of the singlet component is $(2l+1)^{-1}$ for the first and $(4l-1)(2l+1)^{-2}$ for the second. In view of these results it is a reasonable supposition that the statistical weight of the singlet component for states in the antisymmetric j^2 function space attains a maximum at $I=0$. If now strong forces tending to favor energetically states of maximum symmetry in the space wave function (i.e., Majorana forces) coexist with strong spin-orbit forces, the opposing tendencies should favor zero spin for the ground state.

These remarks leave the issue unsettled, but may help to direct attention to an important problem.

TABLE II. Spins and magnetic moments of odd–odd nuclei.

Nucleus	Spin	Experimental* Magnetic moment	Computed magnetic moment j–j coupling	Computed magnetic moment Singlet component removed	Statistical weight of the triplet component in j–j coupling	Predicted spin in j–j coupling
$_3Li^6$	1	0.82	0.63	0.785	0.444	3
$_5B^{10}$	3	1.80	1.88	1.88	1.000	3
$_7N^{14}$	1	0.40	0.37	0.34	0.778	1
$_{11}Na^{22}$	3	1.75	1.73	1.86	0.640	5
$_{19}K^{40}$	4	−1.29	−1.70	1.16	0.74	—

*S. Millman and B. Kusch, Phys. Rev. **60**, 91 (1941); J. Zacharias, Phys. Rev. **61**, 270 (1942); Gordy, Ring, and Burg, Phys. Rev. **74**, 1191 (1948); and L. David, Phys. Rev. **74**, 1193 (1948).

TWO UNLIKE PARTICLES

The spins and magnetic moments of odd–odd nuclei offer further opportunities for testing the hypothesis of strong spin-orbit coupling. A table of Landé g factors facilitates the calculations (see Table I).

The formula

$$\mu/\mu_0=\tfrac{1}{2}I\left[g_1+g_2+(g_1-g_2)\frac{(j_1-j_2)(j_1+j_2+1)}{I(I+1)}\right], \qquad (5)$$

valid for pure j–j coupling, yields the magnetic moments listed in column 4 of Table II.

The excellent agreement of j–j coupling moments with the experimental values may be illusory. First of all, the values listed in the last column of Table II represent the ground state spins expected if strong forces tending to produce j–j coupling are associated with strong forces tending to favor energetically states of maximum symmetry in the space wave function. The discrepancies at Li^6 and Na^{22} suggest that spin-orbit coupling plays a secondary role in determining the ground state angular momenta of these nuclei. Secondly, the complete omission of the singlet components in the j–j coupling wave functions (excluding K^{40}) does not change the moments appreciably (except in Li^6 where the omission of the singlet component results in a notable improvement).

In the shell model description of K^{40}, the $(3d)^{-1}(4f)^1$ configuration generates four L–S coupling type states with $I=4$; $^3H_4$, $^3G_4$, $^3F_4$, and $^1G_4$ all with positive magnetic moments.[22] The alternative simple possibility of j–j coupling yields one state with $I=4$ from each of the configurations $^2D_{3/2}\,{}^2F_{5/2}$, $^2D_{5/2}\,{}^2F_{5/2}$, $^2D_{5/2}\,{}^2F_{7/2}$, and $^2D_{3/2}\,{}^2F_{7/2}$. Only the last named possesses a negative

[22] D. R. Inglis, Phys. Rev. **60**, 837 (1941); NF, p. 416.

magnetic moment. Thus the negative magnetic moment of K^{40} may be cited as supporting the j–j coupling shell model. Considering, however, the absence of symmetry effects (because of the non-equivalence of the $3d$ and $4f$ orbits), it is not unlikely that the appearance of extreme j–j coupling may be produced by a relatively weak coupling of the spin and orbital motion. Within the limits of the ground state configuration, the most general wave function is a linear combination of the four above-mentioned L–S coupling states. The expectation value of the magnetic moment operator then contains cross terms connecting the several pure L–S type components. These cross terms create the possibility of a negative magnetic moment.

Recent studies of energy distribution in the $_{38}Sr^{90}$ and $_{39}Y^{90}$ beta-transitions[23,24] provide unambiguous evidence for the assignment $I=2$ to the ground state of $_{39}Y^{90}$. A direct measurement of the spin and magnetic moment of this nucleus would yield information on the coupling scheme in a $(3p)^{-1}(4d)^{1}$ configuration. The various simple ways of constructing states with $I=2$ and the associated magnetic moments are tabulated below:

State	$^1D_2$	$^3P_2$	$^3D_2$	$^3F_2$	$P_{3/2}D_{5/2}$	$P_{3/2}D_{3/2}$	$P_{1/2}D_{3/2}$	$P_{1/2}D_{5/2}$
μ/μ_0	0.33	0.38	0.57	0.30	−0.97	3.29	0.88	−1.60

The wave functions listed in the Appendix may be used to compute quadrupole moments. It is uncertain whether such calculations can yield significant results because of the sensitivity of quadrupole matrix elements to the admixture of small components in the wave function from excited configurations. Whereas magnetic moments depend quadratically on the amplitudes of the admixture, quadrupole moments are linear functions when these amplitudes are small. Consequently, a simple wave function may produce a significant result for the magnetic moment while failing completely on the quadrupole moment (i.e., the $^2P_{3/2}$ wave function derived from $(2p)^3$ for Li^7).[25]

[23] Braden, Slack, and Shull, Phys. Rev. **75**, 1964 (1949).
[24] E. N. Jensen and L. J. Laslett, Phys. Rev. **75**, 1949 (1949).
[25] P. Kusch, Phys. Rev. **76**, 138 (1949).

APPENDIX

Li^6: $^2P_{3/2}$(neutron)$^2P_{3/2}$(proton), $j_1=j_2=3/2$, $I=1$.

$$(45)^{1/2}\psi_{1,1}=3[3^{1/2}(3/2,-1/2)_+^{3/2}-2^{1/2}(1/2,1/2)_+^{3/2}]$$
$$={}^3S_1\{3(1,-1)_+-2^{3/2}(0,0)_+\}+{}^3S_0(0,1)_+$$
$$-2^{1/2}\,{}^3S_{-1}(1,1)_+ +5\,{}^1S_0(1,0)_-.$$

B^{10}: $^2P_{3/2}\binom{\text{neutron}}{\text{hole}}$ $^2P_{3/2}\binom{\text{proton}}{\text{hole}}$,

$j_1=j_2=3/2$, $I=3$.

$$\psi_{3,3}(3/2,3/2)_+={}^3S_1(1,1)_+.$$

N^{14}: $^2P_{1/2}\binom{\text{neutron}}{\text{hole}}$ $^2P_{1/2}\binom{\text{proton}}{\text{hole}}$,

$j_1=j_2=1/2$, $I=1$.

$$3\psi_{1,1}=3(1/2,1/2)_+$$
$$={}^3S_1(0,0)_+-2^{1/2}\,{}^3S_0(0,1)_++2\,{}^3S_{-1}(1,1)_+$$
$$-2^{1/2}\,{}^1S_0(0,1)_-.$$

Na^{22}: $^2D_{5/2}$(neutron) $^2D_{5/2}$(proton),

$j_1=j_2=5/2$, $I=3$.

$$15\psi_{3,3}=5[5^{1/2}(5/2,1/2)_+-2(3/2,3/2)_+]$$
$$={}^3S_1[(75)^{1/2}(2,0)_+-8(1,1)_+]+{}^3S_0(2,1)_+$$
$$-2\,{}^3S_{-1}(2,2)_+ +9\,{}^1S_0(2,1)_-.$$

K^{40}: $^2D_{3/2}\binom{\text{proton}}{\text{hole}}$ $^2F_{7/2}$(neutron),

$j_1=3/2$, $j_2=7/2$, $I=4$.

$$(350)^{1/2}\psi_{4,4}=(35)^{1/2}[3^{1/2}\psi_{3/2\ 3/2}(1)\psi_{7/2\ 5/2}(2)$$
$$-7^{1/2}\psi_{3/2\ 1/2}(1)\psi_{7/2\ 7/2}(2)]$$
$$={}^3S_1[(18)^{1/2}\Theta_{21}(1)\Theta_{32}(2)$$
$$-(98)^{1/2}\Theta_{20}(1)\Theta_{33}(2)]$$
$$+{}^3S_0[(96)^{1/2}\Theta_{21}(1)\Theta_{33}(2)$$
$$-6\Theta_{22}(1)\Theta_{32}(2)]$$
$$-(12)^{1/2}\,{}^3S_{-1}\Theta_{22}(1)\Theta_{33}(2)$$
$$-{}^1S_0[(54)^{1/2}\Theta_{21}(1)\Theta_{33}(2)$$
$$-6\Theta_{22}(1)\Theta_{32}(2)]$$

A Photographic Study of Neutrons from Al+H²*

R. A. Peck, Jr.
Brown University, Providence, Rhode Island
(Received May 19, 1949)

The (dn) reaction on aluminum has been studied using Eastman NTB emulsions. Twenty-two hundred head-on recoil tracks are plotted, and ten groups identified (with widths and intensities), extending up to 9 Mev excitation of the product Si^{28} nucleus. The first two excited levels, at 1.8 and 4.5 Mev, agree with gamma-ray energies and inelastic scattering. The reaction Q value (9.08±0.20 Mev) determines the mass difference $Si^{28}-Al^{27}=+0.996\,05\pm0.20\times10^{-3}$ mass unit.

EXPERIMENTAL

THE reaction studied is

$$Al^{27}+H^2=Si^{28}+n+Q_1. \quad (1)$$

Deuterons were accelerated in the Yale cyclotron, to energy 3.68±0.05 Mev (mean).[1] The target was an aluminum foil of thickness 1.5 mg cm^{-2} placed perpendicular to the direction of the incident beam. After passing through the target, the deuterons were stopped in a thick backing of pure tin. (Tin was used to minimize neutrons from the backing. No exposures were made with backing only, but the Coulomb barrier height is about 2.8 Mev for aluminum, 6.8 Mev for tin.) Bombardment took place in a thick-walled brass chamber,[1] and the photographic plates were exposed immediately outside.

The plates were held (up to six at a time) in brass containers with $\frac{1}{16}$-in. walls. The emulsions lay approximately in the target plane, so that neutrons emitted at 90° to the incident beam were recorded. The nearest end of each plate was about 6 cm from the target area (intersection of beam with target foil, about 1 cm² in extent), so that the detector half-angle ranged between 0.08 radian and 0.19 radian over the whole area of each plate. An exposure of about 20 microampere minutes was found to give a suitable balance of neutron recoil yield and gamma-ray fog. This figure refers to the beam current as read via the tin backing on which the thin aluminum target was mounted.

Two Eastman NTB emulsions were used, Nos. 361281 and 361399, of thickness 21 and 113 microns respectively. Development was for 10 minutes in D-19 after soaking for 10 minutes in water at 30°C, and followed by fixation in F-5. Even with agitation and replenishing of the F-5, fixation times of several hours were required. After washing for 30 minutes or more the plates were dried by evaporation, lying emulsion up on absorbent paper, under an inverted dish. When completely dry the emulsions were covered with No. 0 cover glasses, using as adhesive a resin suspension (damar) in xylene.

A two-point calibration of emulsion 361281 was carried out by plotting tracks of long-range protons from $B^{10}(dp)B^{11}$ with two different values of basic absorption in the protons' path.[2] These emulsion ranges were compared with the air range of the same protons as determined with proportional counters.[3] In this way, two values of emulsion stopping power (range in air/range in emulsion) were determined: 1975±70 at 6.0 Mev and 1960±180 at 3.6 Mev. Most of the assigned uncertainty is associated with the air range, and in view of the close agreement of the two stopping powers an assessment of about 1 percent error (1975±20 above 3.6 Mev) seems more realistic. It is interesting that this agrees precisely with the corresponding value of Lattes, Fowler, and Cuer[4] for the Ilford C2 plates.

Emulsion 361399 was calibrated by comparison with 361281. Six corresponding ranges in the Al(dn) spectrum were identified from each emulsion, giving a stopping power for 361399 lower by 4 percent ±1 percent than for 361281.

Tracks of recoil protons were observed with a binocular microscope (Bausch and Lomb, Model CT). To locate measurable tracks, the plates were scanned with 10X eyepieces and a 10X objective, using an oblique system of illumination. The concave mirror is adjusted to direct light obliquely through the substage condenser, with iris diaphragm wide open. Observation is at the periphery of the conic section of light which appears on the object slide. Such illumination provides the comfort of quasi-dark field, and illuminates only tracks moving in roughly the forward direction. Both features are highly desirable for the scanning operation. For measurements, a 97X oil immersion objective was used, with the same eyepieces and the plane substage mirror (light field illumination). To be suitable for measurement, recoil tracks were required to lie within ±10° of the direction of neutron incidence, both in the horizontal and vertical planes. These angles were checked, respectively, by reference to the eyepiece scale and by the observed length of track which was in focus at a single setting. (A smaller angular spread was allowed in the vertical direction, because of the emulsion shrinkage on processing.) A criterion for the maximum acceptable elastic scattering along a track was based on

* The major part of this work was done at Sloane Physics Laboratory, Yale University, New Haven, Connecticut, and assisted by the ONR under Contract No. N6ori-44.

[1] A. B. Martin, Phys. Rev. 72, 378 (1947).

[2] R. A. Peck, Jr., Phys. Rev. 72, 1121 (1947).

[3] A. B. Martin, unpublished.

[4] Lattes, Fowler, and Cuer, Proc. Phys. Soc. 59, 883 (1947).

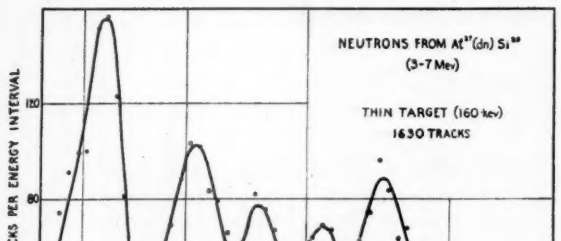

FIG. 1. Distribution of recoil energies (first part). Histogram interval = 1.7 cm air equivalent in range. Each point set is a complete histogram, the two being displaced one-half interval from one another. Six groups are identified—in order of decreasing energy, III *A*, III *B*, III *C*, III *D*, III *E* and IV (see Tables I and II). 230 tracks (lying above 3.7 Mev) from the 113-micron thick emulsions, others from 21-micron emulsions.

the requirement that (assuming the scattering atom to be one of the lightest emulsion constituents—C, N, O) the energy lost to the recoiling atom should correspond to less than the least count of observable proton range in emulsion.

For each acceptable track, the projection on the focal plane was measured with a calibrated eyepiece scale, and the depth coordinate by the vertical travel in focussing on one end at a time (at 970X, the focal depth was about one micron). Since measured tracks lay within small angles of the horizontal plane, a sufficient correction term for the depth coordinate was the first term in the binomial expansion of $(l^2+z^2)^{\frac{1}{2}}$ (l = length of projection on focal plane, z = depth difference between track ends). In view of a strong observer bias in estimating fractions of eyepiece scale divisions, all track lengths were rounded to the nearest whole scale division before further consideration. The recoil proton ranges, in the calibrated emulsions, lead to values for proton energies which, for the 0° recoils measured, are presumed to give the neutron energies directly.

The track measurements have been plotted in histogram form in Figs. 1 and 2. Against neutron energy is plotted the number of recoils observed within a fixed interval about this energy. The scale of abscissas is actually linear in range, not energy, and the collection interval is constant in range—5 scale divisions, or 1.7 cm air equivalent. In Fig. 2 this interval has been doubled because of the reduced yield at high energy. Two histograms are plotted in each of the figures, for better definition of the curve shape. The histograms are displaced from one another by a half-interval.

The distribution of observed tracks must be corrected for the energy dependence of the emulsion efficiency for neutron recording. Part of this effect is simply geometrical, due to a greater tendency for long tracks to pass out of the emulsion, and part derives from the energy dependence of the neutron-proton scattering cross section. Both effects are calculable,[5] and were combined in a single range-dependent correction factor applied to each ordinate in the histograms (this correction factor varied over the energy spectrum by a factor 50 for the 21-micron emulsions, a factor 6 for the 113-micron emulsions). Finally the ordinate scales were "normalized"—multiplied by the factor necessary to restore the area of each histogram (total number of tracks) to the number actually observed. Consequently the ordinates of Figs. 1 and 2 are corrected for efficiency change, but still represent correctly the over-all number of tracks observed.

EVALUATION OF GROUPS

In Figs. 1 and 2 ten groups have been identified, though the resolution in Fig. 1 does not allow much confidence in the precise location of the components of this part of the spectrum. For locating groups, the curves of Figs. 1 and 2 were used as shown. However in the determination of group parameters (range, width, intensity) each histogram was plotted and resolved separately. Thus two values were obtained for each parameter, and in Tables I and II the average of these values is used, with an assigned error equal to ± the difference between the two values. Sole departure from this procedure was in connection with the end group, for which the yield was too low for an accurate curve shape. Here the mean range was determined arithmetically, and the width identified from the calculated standard deviation of the tracks comprising the group (root-mean-square deviation from the mean range). The intensity of the group was then taken as the height of a Gaussian curve of area equal to the number of tracks in the group, and the same width as that just determined. This procedure assumes symmetry of the end group about its mean. A partial justification of that assumption is the agreement of extrapolated—mean range, for this group, with the calculation of that quantity from expected straggling (see below).

Group symmetry was again assumed in the process of resolving Fig. 1 into separate group curves. Starting at the high energy end, the first half-group was reflected about the peak ordinate line and subtracted from the rest of the curve. The next high energy side thus "revealed" was treated in a similar fashion, and so to the low energy end of the curve. Since the group of lowest energy is quite well defined, it is possible to check the accuracy of this resolution into groups. The accumulated discrepancy (i.e., the area in Fig. 1 not accounted for) corresponds to 60 tracks, a few percent of the total number represented in Fig. 1.

Table I shows the result of reducing group energies to Q values for the reaction. The range corresponding

[5] Geometrical correction: H. T. Richards, Phys. Rev. **59**, 796 (1941). Cross section *vs.* energy: see R. A. Peck, Jr., Phys. Rev. **73**, 947 (1948), footnote 9.

to the group peak was taken as mean range, converted to energy (via calibration and air range-energy curve[6]), and increased[6] by $X_0^2E/2=1.52\times10^{-2}E$ for critical angle $\pm10°$. The Q value was then calculated, using the known beam energy[1] and the formula for 90° observation.

It is possible to predict the over-all spread of these groups, to compare with the observed spreads.[7] The contributing effects are range and angle straggling of protons in the emulsion, target thickness, $\pm10°$ spread allowed in collecting data, intrinsic inhomogeneity of deuteron beam and the finite size of histogram interval. The first three effects may be estimated following the procedures of Bethe.[6] Independent information is available[1] respecting the beam inhomogeneity, and may be combined with the other straggling parameters by root-sum-squares addition.[6] The effect of finite histogram interval may be measured empirically by applying histogram collection to a curve of known initial shape. The combination of these effects yields a prediction for the difference between extrapolated and mean range, for each group. Using the observed extrapolated range in each case, predicted mean ranges have been calculated and, in Table II, compared with the observed mean ranges. For each group, there is agreement within the cited experimental error.

The above calculations also provide predictions for half-width at half-value, which may be compared with those observed (Table II). Agreement is adequate (within cited errors) except for groups I, III E and IV, which may indicate that these three are multiple groups. Respecting the others it may be concluded that no intrinsic level width is observable in these experiments, and that the number of groups extracted from Fig. 1 is about correct.

DISCUSSION OF RESULTS

The excited levels of Si^{28} indicated by this work are listed in Table I. The end group, $Q=9.08\pm0.20$ Mev, leads to the mass difference $Si^{28}-Al^{27}=+0.99605\pm0.20\times10^{-3}$ mass unit.

A comparison value for the reaction Q is available from the chain

$$Al^{27}+H^2=Al^{28}+H^1+Q_2, \quad (2)$$

$$Al^{28}=Si^{28}+Q_3 \text{ (beta-decay)} \quad (3)$$

with (1). Eliminating the three nuclear masses, one has

$$Q_1=p-n+Q_2+Q_3=Q_2+Q_3-0.80 \text{ Mev}.$$

Experimental values are $Q_2=5.45\pm0.05$ Mev[8] and $Q_3=4.55\pm0.2$ Mev[9] giving $Q_1=9.20\pm0.25$ Mev, in adequate agreement with the present observation. The agreement is impaired, however, by the choice of a higher Q_3.[10]

The energy level scheme may be compared with gamma-ray energies from Si^{28}. When that nucleus is formed by reaction (3) the disintegration energy (maximum excitation of Si^{28}) is about 4.5 Mev and a single gamma-ray is observed, energy 1.8 Mev.[9] This agrees well with the location of the first excited level here obtained. The absence of radiation from the second and third levels of the present scheme might indicate a Q_3 too small to excite the Si^{28} level at 4.5 Mev, or a selection rule concerning that state.

The gamma-rays from Al+H² were observed by

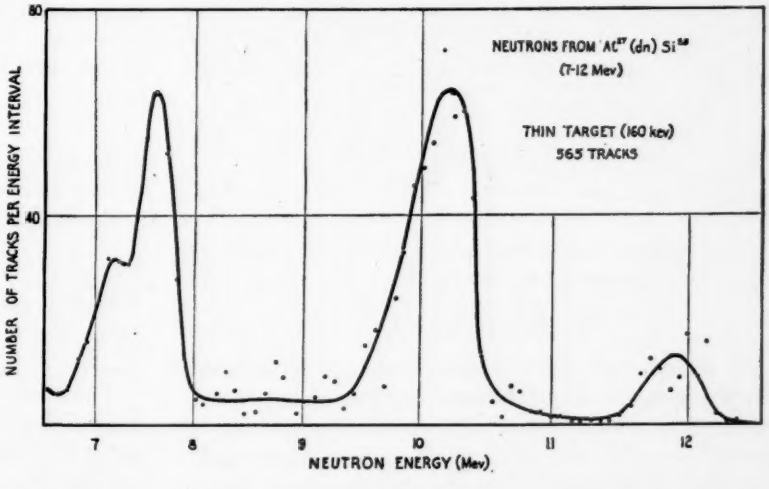

FIG. 2. Distribution of recoil energies (second part). Histogram interval=3.4 cm air equivalent in range. Each point set is a complete histogram, the two being displaced one-half interval from one another. Four groups are identified—in order of decreasing energy 0, I, II A and II B (see Tables I and II). 365 of the tracks from 113-micron emulsions, others from 21-micron emulsions.

[6] M. S. Livingston and H. A. Bethe, Rev. Mod. Phys. **9**, 245 (1937).

[7] These calculations follow a procedure worked out by H. T. Motz, to whom the author is indebted for helpful discussions of straggling problems. See R. F. Humphreys and H. T. Motz, Phys. Rev. **74**, 1232 (1948). The arbitrary choice of a histogram interval in photographic work is tantamount to arbitrary "peaking" of proportional counters.

[8] Pollard, Sailor, and Wyly, Phys. Rev. **75**, 725 (1949).

[9] W. H. Barkas, Phys. Rev. **72**, 346 (1947).

[10] Footnote 8 of reference 9. Also Benes, Hedgran and Hole, Arkiv. **35A**, 12 (1948); Dunworth, Nature **159**, 436 (1947). These papers suggest that Q_3 is 0.25 Mev higher than the value compared in the text.

TABLE I. Groups in the neutron spectrum. All energies in Mev. Reliability refers to certainty or uncertainty of existence of some group, not to group location. Errors listed are exclusive of that in stopping power, which introduces an additional ±0.07 Mev in the end group Q value.

Group	Reliability	Relative intensity	Mean energy	Q	Si^{28} excitation
0	+	1.0±0.1	12.09±0.08	9.08±0.13	0.00
I	+	4.4±0.9	10.37±0.05	7.30±0.10	1.78±0.13
II *A*	+	4.0±0.2	7.75±0.02	4.61±0.07	4.47±0.10
II *B*	−	2.1±0.1	7.32±0.13	4.17±0.18	4.91±0.21
III *A*	+	5.4±0.8	6.16±0.02	2.97±0.07	6.11±0.10
III *B*	+	12.0±1.6	5.65±0.06	2.43±0.11	6.65±0.14
III *C*	−	9.4±0.1	5.21±0.04	1.98±0.09	7.10±0.12
III *D*	−	10.6±1.0	4.77±0.04	1.53±0.09	7.55±0.12
III *E*	+	13.8±0.2	4.17±0.02	0.90±0.04	8.18±0.10
IV	+	20.6±0.6	3.23±0.09	−0.08±0.14	9.16±0.17

TABLE II. Group widths. First column is predicted from observed extrapolated ranges and straggling calculations. Unit is eyepiece scale division=0.34 cm air equivalent. Last column lists half-widths calculated due to straggling only (histogram interval approaching zero). Comparison with column 5 shows the effect of finite histogram interval.

Group	Mean range in scale div. Predicted	Mean range in scale div. Observed	Half-width at half maximum value (in cm air equivalent) Observed	Calculated	Differential
0	464	465±6	5.0	4.8	2.8
I	355±9	354±3	5.7±2.0	4.1	2.4
II *A*	213±4	211±1	3.7±0.8	3.2	1.8
II *B*	187±4	191±6	3.5±1.3	3.0	1.7
III *A*	144±7	142±1	2.7±0.1	2.6	1.5
III *B*	121±1	121±2	2.6±0.7	2.4	1.4
III *C*	104±1	105±2	2.4±0.2	2.3	1.3
III *D*	88±1	90±2	2.0±0.5	2.1	1.2
III *E*	75±2	72±1	2.6±0.2	1.9	1.1
IV	49±1	46±2	2.4±0.3	1.6	0.9

Alburger,[11] who found the same low energy gamma (1.72±0.08 Mev), and others at 8.5±0.5 Mev and possibly 3.0±0.2 Mev. The 8.5 Mev radiation is consistent with a transition from level III *E*, or even IV, to ground. The 3 Mev would fit a transition to the first excited level from either of the pair II *A*, *B* (or a combination), in which connection it may be recalled that the beta-transition from Al^{28} is also to the first excited state (1.8 Mev), not directly to ground.[9] It is possible, of course, that Alburger's gammas do not derive from the (dn) reaction.

Si^{28} gamma-radiation has also been studied by Plain *et al.*,[12] as a result or proton bombardment of aluminum. At proton energies corresponding to excitation in Si^{28} of 11.1, 11.2, 11.6 and 12.0 Mev they found average gamma-energy (respectively) 6.1, 6.5, 7.7 and 8.2 Mev. If the excitation levels found in the present work are weighted by the observed group intensities and averaged, the value 7.0 Mev is obtained; if the highest group (9 Mev) is omitted, the average falls to 6.3 Mev.

A direct check on the second excited level here reported is provided by the inelastic scattering studies of Fulbright and Bush,[13] who assign to Si^{28} a level at 4.6±0.3 Mev.

According to the statistical theory of Weisskopf[14] the spectrum is expected to have a Maxwellian form

$$W_n(E) \propto E \exp(-E/T)$$

(on which the group structure already discussed is superimposed). The left-hand member represents the number of neutrons emitted (per unit energy interval) with energy E. T is the nuclear temperature (in energy units) corresponding to the maximum excitation energy of the product nucleus Si^{28} (E_A-E_0, in the notation of Weisskopf). The latter is

$$\begin{aligned} E_A-E_0 &= Al^{27}+H^2+\text{beam energy}-Si^{28}-n^1 \\ &= \text{maximum } Q \text{ value}+\text{beam energy} \\ &= 9.08+3.68=12.76 \text{ Mev.} \end{aligned}$$

Hence, if the data are plotted in the form $\ln(W/E)$ *vs.* E, a straight line is expected whose slope is negative and equal to the reciprocal of the nuclear temperature at excitation 12.8 Mev.

When the present data are so plotted there remains considerable scattering of points. The best visually fitted straight line has a slope

$$\frac{d[\ln(W/E)]}{dE} = -0.69\pm0.16 \text{ Mev}^{-1}$$

from which $T=1.5\pm0.4$ Mev at 12.8 Mev excitation. We may also estimate the proportionality constant a[14] (representative of the low lying level spacing),

$$a=T^2/E=0.19\pm0.09 \text{ Mev.}$$

This is in line with the estimates of Weisskopf (0.1–0.2 Mev) but is an order of magnitude smaller than the spacing of the low lying levels in Si^{28} here observed.

The Maxwell distribution corresponding to the above temperature has mean energy 3.0 Mev, its peak at $E=T=1.5$ Mev, and falls to $1/e$ of maximum at $E=0.2$ and 4.8 Mev. The data do not extend to sufficiently low neutron energies to permit observation of the peak of this Maxwell curve.

[11] D. E. Alburger, Phys. Rev. **75**, 51 (1949).
[12] Plain, Herb, Hudson, and Warren, Phys. Rev. **57**, 187 (1940).
[13] H. W. Fulbright and R. R. Bush, Phys. Rev. **74**, 1323 (1948).
[14] V. F. Weisskopf, Phys. Rev. **52**, 295 (1937).

Range Distribution of the Charged Particles from the D–D Reactions for 10-Mev Deuterons: Differential Elastic Scattering Cross Section at 40 Degrees, 60 Degrees, and 80 Degrees in the Center-of-Mass System*

LOUIS ROSEN, FRANCIS K. TALLMADGE, AND JOHN H. WILLIAMS**
Los Alamos Scientific Laboratory, Los Alamos, New Mexico
(Received June 6, 1949)

Microphotographic techniques have been used to obtain the range distribution of the charged particles resulting from the D−D reactions at center of mass angles of 40 degrees, 60 degrees, and 80 degrees for 10-Mev deuterons. At 80 degrees all of the groups of charged particles from the above reactions are clearly resolved. The differential D−D elastic scattering cross sections have been obtained for the same angles and for these angles the cross sections per unit solid angle in the center-of-mass system are in the ratios of 1.00:0.51:0.42, respectively. Only one group of protons is observed from the $D(d,H)H^3$ reaction, thus indicating that the H^3 nucleus is not formed in an excited state for the energy region investigated when He^4 is the compound nucleus.

ALTHOUGH a large number of investigators[1] have studied the D−D reactions, practically all this work has been done with relatively low incident deuteron energies. The only investigations in an energy region comparable to the energy region available to us in the present experiments were carried out by Guggenheimer, Heitler, and Powell.[2] These experiments were concerned with D−D elastic scattering and no attempt was made to resolve the various groups of charged particles arising from the D−D reactions. In fact, the differential scattering cross sections themselves are given in relative units.

In the present experiments photographic plate detectors were utilized to obtain the range distribution of the charged particles resulting from the D−D reactions and also to make absolute determinations of the D−D elastic scattering cross section at angles of 20 degrees, 30 degrees, and 40 degrees with respect to the incident beam in the laboratory system for 10-Mev deuterons from the Los Alamos cyclotron. The general instrumentation for this paper is the same as that described in a forthcoming paper by Curtis, Fowler, and Rosen.[3] The experimental arrangement is given in Figs. 1 and 2. The experiment consisted of bombarding thin gas targets with 10-Mev deuterons and simultaneously recording on photographic plates the numbers and ranges of the disintegration particles and scattered deuterons emitted into a known solid angle in a given direction.

Deuterium gas of 99.4 percent purity at an accurately determined pressure in the region of 20 cm Hg was contained in the gas targets by thin mica windows: beam entrance and exit windows, and one window on each side of the target for the emergence of the reaction products at the desired angle (in the case of the 40 degree target only one such window was used for the emergence of the scattered particles). The beam, focused at approximately the center of the gas target, was diaphragmed to a diameter of $\frac{1}{4}$ inch immediately in front of the target. Additional slits defined the beam to an angular divergence of 1.2 degrees in the horizontal direction and 0.85 degree in the vertical direction. Coulomb scattering by the entrance target windows never caused more than 2.5 percent of the incident deuterons to be scattered through an angle greater than 1.0 degree. The deuteron current which passed through the target was collected in a nine-inch long Faraday cage and integrated with an electronic current integrator.

Three different gas targets were used, one for each of the angles investigated, the reaction products being simultaneously recorded by two cameras, one on each side of the target, with the exception of the 40 degree target for which only one camera was used. Each camera contained a 100-micron Ilford C-2 plate behind a thin aluminum window at the front of the camera. The plates made angles of approximately seven degrees with the axes of the slit systems.

The cameras were set at accurately determined angles with respect to a 0–180 degree line, which line corre-

* This document is based on work performed at the Los Alamos Scientific Laboratory of the University of California, under Government Contract W-7405-eng-36.

** Now at the University of Minnesota, Minneapolis, Minnesota.

[1] T. W. Bonner and W. M. Brubaker, Phys. Rev. **49**, 19 (1936); Kempton, Browne, and Massdorp, Proc. Roy. Soc. **A157**, 386 (1936); H. Neuert, Physik Zeits. **38**, 122, 618 (1937); T. W. Bonner, Phys. Rev. **52**, 685 (1937); R. Ladenburg and M. H. Kanner, Phys. Rev. **52**, 911 (1937); R. B. Roberts, Phys. Rev. **51**, 810 (1937); R. Dopel, Ann. d. Physik **28**, 1, 87 (1937); T. W. Bonner, Phys. Rev. **53**, 711 (1938); H. Neuert, Zeits. f. tech. Physik **19**, 12, 576 (1938); A. Ellett and R. D. Huntoon, Phys. Rev. **54**, 87 (1938); Hoxby, Allen, and Williams, Phys. Rev. **55**, 140 (1939); N. P. Heydenburg and R. B. Roberts, Phys. Rev. **56**, 1092 (1939); E. Hudspeth and H. Dunlap, Phys. Rev. **57**, 971 (1940); Huntoon, Ellett, Bayley, and Van Allen, Phys. Rev. **58**, 97 (1941); T. W. Bonner, Phys. Rev. **59**, 237 (1941); Manning, Huntoon, Myers, and Young, Phys. Rev. **61**, 371 (1942); Bennett, Mandeville, and Richards, Phys. Rev. **69**, 418 (1946); Bretscher, French, and Seidl, Phys. Rev. **73**, 815 (1948); H. V. Argo, Phys. Rev. **74**, 1293 (1948); Blair, Freier, Lampi, Sleator, and Williams, Phys. Rev. **74**, 1594, 1599 (1948).

[2] Guggenheimer, Heitler, and Powell, Proc. Roy. Soc. **190**, 196 (1947).

[3] Curtis, Fowler, and Rosen, Rev. Sci. Inst. **20**, 388 (1949).

sponded to the axis of the beam direction to within 0.3 degree. The angular resolution of the camera-target slit system geometry (Fig. 2) was ±1.4 degrees for the 20 degree target, ±1.2 degrees for the 30 degree target, and ±1.0 degree for the 40 degree target. When the scattered deuterons were recorded simultaneously on each side of the target, as was the case for the 20 degree and 30 degree targets, both the energy and the direction of the beam were determined from the mean ranges of the deuteron groups. By using the range-energy relations given by Lattes, Fowler, and Cuer[4] and making allowance for the loss in range which the particles suffer in traversing the target window, target gas, and camera window, the average energy of the beam prevailing during all the exposures was calculated to be 10.0 Mev ±0.3 Mev at the center of the gas targets.

The direction of the beam which prevailed during the exposures was accurately determined from the mean scattered deuteron ranges at two angles with respect to the incident beam (see Fig. 6). The measurements of the ranges of the scattered deuterons were made by the same observer using the same equipment, the two sets of tracks having been recorded on plates which came from the same batch. Under such conditions the ratio of the mean ranges could be determined to an accuracy of ±1.5 percent. It is noteworthy that it is necessary to know neither the absolute ranges nor the absolute value of the energy in order to accurately determine the beam direction from this method, for from Fig. 2:

$$R_1(\theta)=K_1E_0\cos^2\theta,$$
$$R_2(\theta'-\theta)=K_2E_0\cos^2(\theta'-\theta),$$

and

$$R_1/R_2=K_1/K_2\times\frac{\cos^2(\theta)}{\cos^2(\theta'-\theta)}, \quad (1)$$

where E_0 = incident deuteron energy at center of target, R_1 and R_2 are the ranges of the deuterons at their respective angles, corrected for the absorbers between the center of the target and the photographic plate, and K_1/K_2 is determined from the range-energy relations (1). The direction of the beam determined in this manner for the 30 degree point was calculated to be accurate to ±0.25 degree. The beam maintained this direction during the 20 degree exposures and was

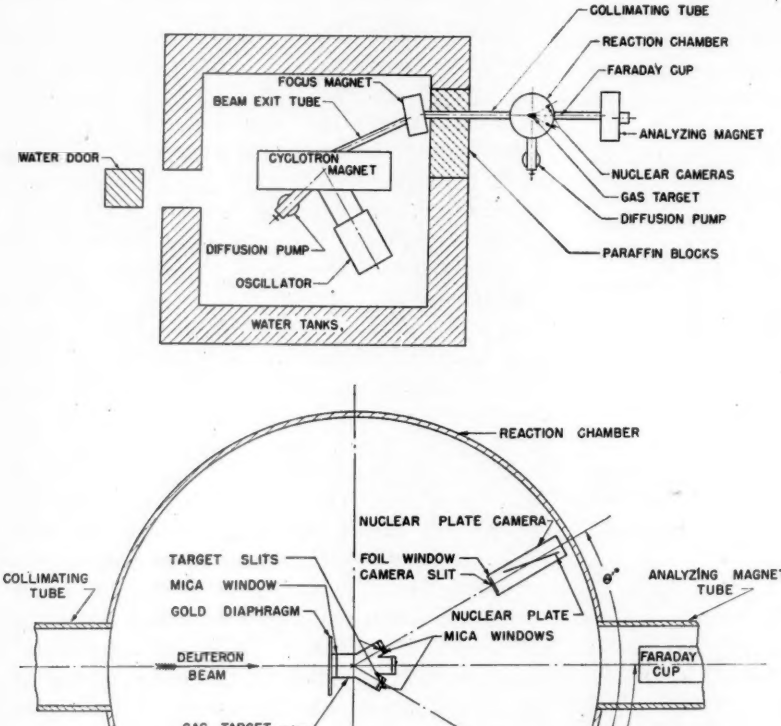

FIG. 1. Plan view of experimental arrangement.

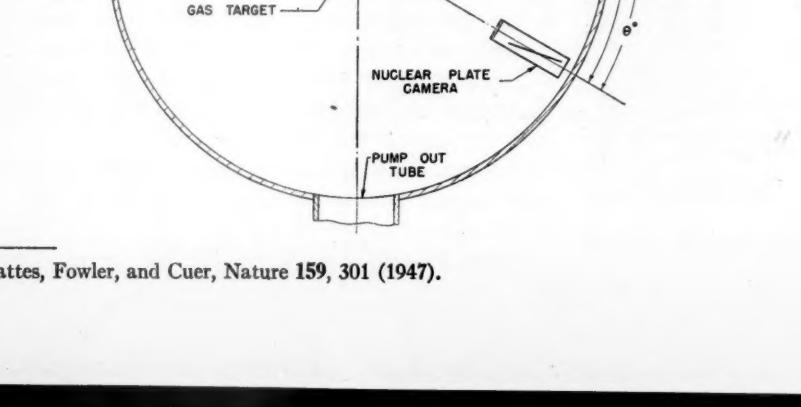

FIG. 2. Plan view of reaction chamber.

[4] Lattes, Fowler, and Cuer, Nature 159, 301 (1947).

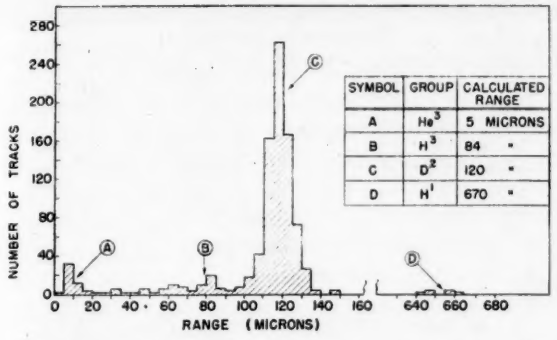

FIG. 3. Range distribution of charged particles from D−D reaction. Ten-Mev deuterons. Forty degrees (laboratory system).

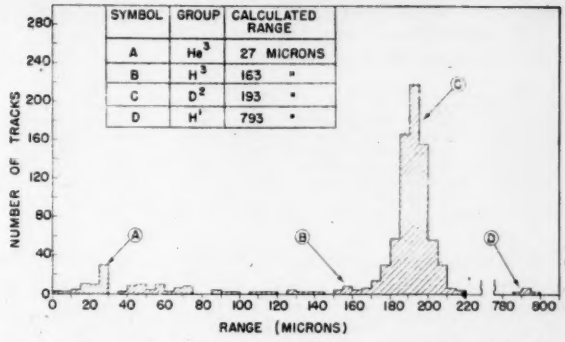

FIG. 4. Range distribution of charged particles from D−D reaction. Ten-Mev deuterons. Thirty degrees (laboratory system).

therefore assumed to have this same direction during the 40 degree exposures.

The experimental procedure for making the range and cross-section measurements was quite simple and straightforward. It consisted of lining up the cameras with respect to the center of the target and axis of the beam, pumping down the vacuum chamber, Fig. 2, and then turning on the cyclotron with the focus magnet off, thus preventing the beam from reaching the scattering chamber during the "warm-up" period. When a steady external beam of the proper magnitude was obtained, the focus magnet was turned on and a beam of approximately 0.2 microampere was permitted to pass through the target. With such a beam an exposure of one to three minutes gave an ample track density in our geometry.

The gas temperature in the target was taken to be the same as the temperature of the water cooling the target. Since the cyclotron was on for a very short time this temperature never changed measurably during an exposure.

Since many particles besides elastically scattered deuterons are produced when high energy deuterons impinge upon a deuterium target, protons and tritons from the reaction $D+D\rightarrow H^3+H^1$, He^3 particles from the $D+D\rightarrow He^3+n$ reaction and possibly protons from the disintegration of the deuteron ($Q=-2.2$ Mev), it was felt desirable, in order to accurately determine the D−D scattering cross section, to make range analyses of the charged particles which come off at each of the angles investigated. Only tracks starting on the surface of the emulsion and traveling in the proper direction were included in this range analysis, thus effectively eliminating all background due to proton recoils from neutrons as well as all charged particle background which did not originate from the gas target. It was necessary to eliminate about two percent of the tracks which started on the surface of the emulsion because they did not travel in the proper direction. These tracks were caused by particles which either did not originate inside the gas target or else suffered scattering by the slit systems. In either case the tracks due to such particles were justifiably eliminated. The probability of the change of direction of scattered deuterons by Coulomb scattering in the target and camera windows and in the target gas to such an extent that they would not be counted was calculated to be completely negligible. Figures 3–5 give the results of range analyses at laboratory angles of 40.3 degrees, 30.0 degrees, and 20.1 degrees with respect to the incident beam direction. All of the charged particle groups from the D−D reactions are seen to be clearly resolved at 40 degrees. At 20 degrees the triton peak cannot be resolved from the deuteron peak, for at this angle the mean ranges of the two groups of particles differ by only 2.5 percent. It should be pointed out that some of the short range tracks (tracks whose length is less than that to be expected for elastically scattered deuterons) were undoubtedly caused either by the scattering of deuterons from the walls of the target or by slit penetration. Others of these short range tracks, however, may have been caused by protons arising from deuteron disintegration. The various groups are labeled with the particles producing them and with their calculated residual*** ranges in the emulsion. The energy widths at half-maximum of

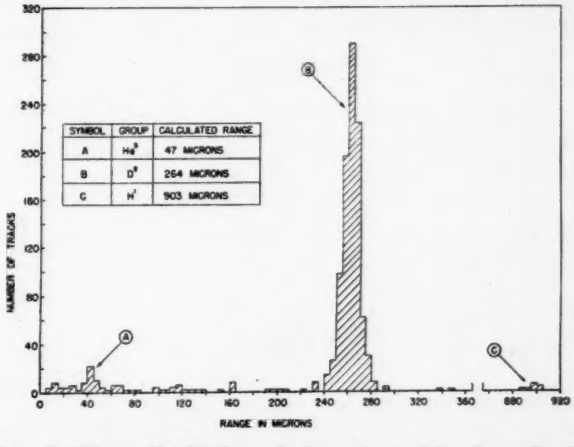

FIG. 5. Range distribution of charged particles from D−D reaction. Ten-Mev deuterons. Twenty degrees (laboratory system).

*** Range which particle has left after passing through the absorbing materials in its path on the way to the detector—D^2 gas, mica window in target, and aluminum window in camera.

TABLE I. D−D scattering cross sections per unit solid angle in the laboratory and center-of-mass coordinate systems.

θ (lab)	$\sigma(\theta)$ (cm²)	ϕ (cm)	$\sigma(\phi)$ (cm²)
40.3°±0.25°	0.324±0.020×10⁻²⁴	80.6°±0.5°	0.106±0.006×10⁻²⁴
30.0°±0.25°	0.456±0.027×10⁻²⁴	60.0°±0.5°	0.132±0.008×10⁻²⁴
29.7°±0.25°	0.467±0.029×10⁻²⁴	59.4°±0.5°	0.134±0.008×10⁻²⁴
20.1°±0.25°	0.955±0.057×10⁻²⁴	40.2°±0.5°	0.254±0.015×10⁻²⁴
19.7°±0.25°	0.980±0.059×10⁻²⁴	39.4°±0.5°	0.260±0.016×10⁻²⁴

the deuteron peaks are approximately three percent of the scattered deuteron energy which is quite close to what one expects from the geometry in these experiments. From such a range analysis it is a simple matter to determine with rather high precision the total number of tracks which are due to the properly collimated elastically scattered deuterons. (At 20 degrees a two percent correction was applied for the tritons which were counted in the deuteron peak.) Having made such a determination, the procedure was adopted of counting all tracks originating in a swath of accurately known width, again only tracks being counted which originated on the surface of the emulsion and which proceeded in the proper direction. The charged particles coming from the target were collimated by two slits of accurately known dimensions, which slits were sufficiently narrow such that all the tracks in a swath were clustered approximately at the center of the plate. In order to make an absolute cross-section determination it was necessary to accurately determine the following: the number of tracks per swath, width of swath, diameter of slits and their relative geometry with respect to the center of the plate and the center of the target, the number of target gas atoms per unit volume, the angle of the axis of the slit system with respect to the incident deuteron beam and the integrated beam current. The equation giving the absolute cross sections in terms of the above was developed by Dr. C. L. Critchfield. The geometrical factors which enter into this equation for the 30 degree points are illustrated in Fig. 6. The equation is as follows:

$$Y = NI\sigma(\theta)n_0, \tag{2}$$

$$I = \frac{4abw}{Ll\sin\theta}\left\{1 - \frac{a^2+b^2}{2l^2} - \frac{Pa^2+b^2\cot\alpha}{3l^2} + \frac{P^2a^2+Q^2b^2}{3l^2}\right\}, \tag{3}$$

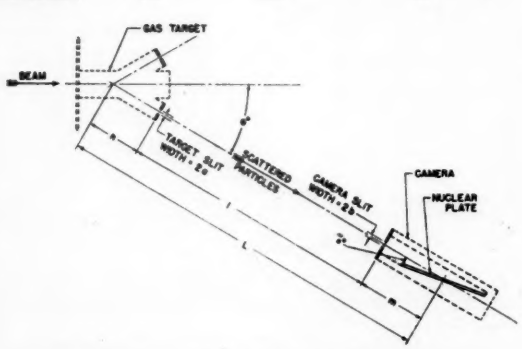

FIG. 6. Geometrical factors which enter into cross-section determinations.

TABLE II. Comparison of the present data with those of other observers.

	E_d	$\frac{\sigma(40\text{ degrees})}{\sigma(80\text{ degrees})}$
Present data	10 Mev	2.40
Guggenheimer *et al*	6.6 Mev	3.58
Blair *et al*	3.5 Mev	2.02
Blair *et al*	2.5 Mev	2.05

where

$$P = \frac{m[\cot\alpha - \cot\theta]}{L}, \quad Q = \frac{(m+l)[\cot\alpha - \cot\theta]}{L},$$

Y = number of tracks appearing on a swath of width w, N = number of incident beam particles that passed through the target, n_0 = number of scattering centers per unit volume, and $\sigma(\theta)$ = differential cross section in laboratory system.

By diaphragming the scattered particles so that they are concentrated about the center of the plate, the necessity for making accurate measurements of the angle that the surface of the emulsion makes with the direction of the scattered deuterons was eliminated. This technique also essentially eliminated errors due to surface irregularities in the emulsion.

The errors in the measurements which enter into the cross-section determination (Eq. (2)) were determined to be as follows:

Quantity	Y	ab	w	Ll	$\sin\theta$	n_0	N
Error (± percent)	3.5	1.5	1.0	2.0	1.0	0.5	3.5

Since the first term in the expansion for I (Eq. (3)) determined approximately 99.5 percent of I for our geometries, the remaining terms need not be considered as far as errors are concerned. It is therefore seen that the r.m.s. of all the above errors, which enter linearly into our cross-section determination is approximately ±5.5 percent.

The D^2 gas used was specified as 99.4 percent pure by the manufacturer. As a check on the purity with respect to heavy atoms (i.e., O_2 and N_2), it is noticed that, in Fig. 5, deuterons scattered by such atoms would have formed a peak at 328±7 microns and deuterons scattered by protons would have formed a peak at 193±4 microns. It is therefore seen that the number of tracks due to scattering from heavy nuclei for which the Coulomb scattering cross sections would be many times the D−D cross section indicates that the total amount of impurities in the D^2 gas from heavy elements is completely negligible. For D−P scattering, on the other hand, the cross section at 20 degrees is probably about one-half the D−D cross section. If this be so it would indicate a maximum hydrogen impurity of less than one percent, in good agreement with the manufacturer's specifications.

In order to check the contribution made to the elastically scattered deuteron peak by deuterons scattered from the walls of the target, the deuterium gas

was replaced by hydrogen and a run made at a scattering angle of 20 degrees. An analysis of the plate showed that less than one percent of the particles recorded had a range between 240 and 280 microns which would correspond to the range of deuterons scattered elastically through 20 degrees by deuterons.

Several of the plates were analyzed by two observers using different microscopes and calibration equipment. It was a gratifying verification of the method to find that the number of tracks recorded per unit swath width always agreed to within the statistical accuracy of the determinations.

The results for the D−D scattering cross sections are given in Table I. Figure 7 gives the differential cross-section values as a function of angle in the center-of-mass system and also the differential cross sections for Coulomb scattering as a function of angle in the same coordinate system.

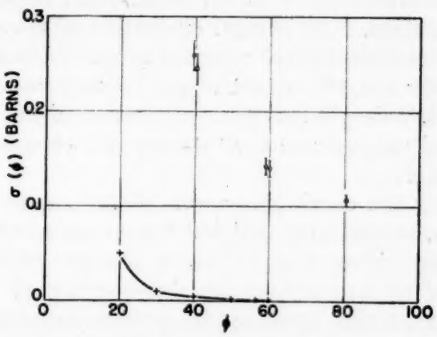

FIG. 7. Upper curve: Differential D−D scattering cross section in the center-of-mass coordinate system. Lower curve: Calculated differential cross section for Coulomb scattering in the center-of-mass coordinate system.

The present data may be compared to the results of Guggenheimer, Heitler, and Powell[2] for 6.6-Mev deuterons and Blair *et al*[1] for 3.5- and 2.5-Mev deuterons. The results of Guggenheimer *et al.* are given in arbitrary units for the cross section and a comparison can only be made by considering the ratios of the cross sections at two scattering angles, $\phi=40$ degrees and 80 degrees. The results of such a comparison are shown in Table II. The marked disagreement with the 6.6-Mev data is disturbing.

Although both theoretical and experimental evidence[5,6] suggest the non-existence of excited levels in the H^3 nucleus, it was felt worth while to investigate this possibility in the energy region available to us, since this region is considerably higher than that heretofore utilized for this investigation.

The method employed to look for energy levels in the H^3 nucleus consisted of determining the energy distribution of the protons from the $H^2+H^2\rightarrow H^3+H^1$ reaction, since a group of protons of energy below that of the primary group would constitute strong proof of the existence of an excited state of the H^3 nucleus.

[5] S. S. Share, Phys. Rev. **53**, 875 (1938).
[6] F. E. Myers and L. M. Langer, Phys. Rev. **54**, 90 (1938).

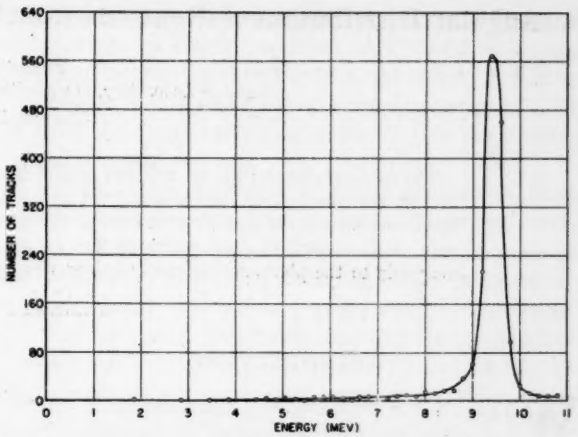

FIG. 8. "Residual" energy distribution of protons from $D(d,p)H^3$ reaction at 20 degrees.

The experimental arrangement was identical with that illustrated in Fig. 2. Since, however, the cross section for elastic scattering of deuterons is much higher than for the production of protons by the reaction $D(d,H)H^3$, it is necessary, in order to record a suitable number of proton tracks without simultaneously obscuring them with deuteron tracks, to prevent the elastically scattered deuterons from being recorded by the photographic detector. This was accomplished by utilizing an aluminum absorber of appropriate thickness between the camera windows and the photographic plate. The proton tracks were recorded at 20 degrees to the incident beam direction.

The plates having been exposed and developed, a range analysis of the tracks on the plate yielded a number *vs.* range curve for the protons from the above reaction which was then converted to a number *vs.* energy curve, the energy representing the residual energy of the protons after penetrating the target gas, target, camera window, and absorber. Figure 8 shows such a curve, an analysis of which brings one to the conclusion that, to within one percent of the primary group intensity, no second group of protons exists which would correspond to an energy level of the H^3 nucleus between one and 5.2 Mev.

In view of the apparent success of the above experiments, a camera is now being constructed for recording the ranges and intensities of the products of nuclear disintegrations and scatterings at 2.5 degree intervals from 10 degrees to 170 degrees with respect to the incident beam. When this is completed, we hope to repeat the D−D elastic scattering experiment over a much larger range of angles and with higher absolute precision.

We wish to thank Mrs. Virginia Stovall and Mrs. Lois Tallmadge for analyzing most of the plates from which were taken the data for this paper. We wish to express our indebtedness to the Los Alamos cyclotron group, and in particular to Dr. J. L. Fowler for the use of the cyclotron.

Angular Distribution of Neutrons from the Photo-Disintegration of the Deuteron*

FRANK GENEVESE**
Randall Laboratory, University of Michigan, Ann Arbor, Michigan
(Received June 30, 1949)

The angular distribution of neutrons arising from the photo-disintegration of deuterons by gamma-rays of 2.76 Mev energy has been investigated under conditions requiring no corrections for neutron scattering by the walls or by the heavy water. Inverse square law tests using balloon suspension indicated the clearance required for which the apparatus was free of the effects of scattering. The weighted ratio of the photo-magnetic to the photoelectric cross sections was found to be 0.295 ± 0.036.

INTRODUCTION

WITHIN the past decade, a considerable amount of effort has been expended by numerous investigators[1–5] toward the experimental determination of the angular distribution with which neutrons or protons are ejected when deuterons are photo-disintegrated. These earlier attempts have in general been handicapped by low intensity; the rather weak effects attending photo-disintegration have made angular distribution measurements very difficult. In consequence, it has not been possible to attain the accuracy required for verification of the theoretical analysis from the experimental data.

The method to be reported here is an attempt toward a more satisfactory investigation of the angular distribution of the photo-neutrons using the 2.76 Mev gamma-rays from Na^{24}. An experimental arrangement was selected in which the geometrical conditions were such as to give improved definition of angle while at the same time providing a higher intensity photo-neutron yield.

In the photo-disintegration of the deuteron, theoretical considerations[6] have indicated not only the existence of a photoelectric effect, i.e., the influence of the electric field of the gamma-ray upon the deuteron, but also of a photo-magnetic effect due to the magnetic field of the gamma-ray. In the former, the disintegrations are the result of electric dipole transitions of the deuteron; in the latter, a magnetic dipole transition is involved. It has been shown that the above two effects result in a superposition of a ^3P, i.e., $\sin^2$, distribution and a spherically symmetrical ^1S distribution, for the ejected nucleons in the center of gravity system. For photons whose energy is not too high, and therefore of small momentum, the center of gravity system may be identified here with the laboratory system.

Since the photo-disintegration differential cross section consists of two terms of different origin, it is possible to distinguish one from the other by the difference in their dependence on the angle of ejection of the nucleons with respect to the direction of the incident photon. Thus, experimental evaluation of the ratio of intensities of the ejected neutrons at two different directions with respect to that of the incident radiation is required. This will lead to an evaluation of the ratio of the total magnetic to the total electric cross sections, $\tau = \sigma_m/\sigma_{el}$.

During the concluding weeks of the current investigation, several brief articles[7–9] have appeared in the literature giving the results of recent experiments designed to measure the angular distribution of neutrons or protons produced by photo-disintegration of the deuteron. In general, only preliminary results are reported. Nevertheless, comparisons may be drawn between the numerical results of these investigations and that to be reported here.

EXPERIMENTAL APPARATUS

The gamma-ray sources were prepared by cyclotron bombardment of sodium with deuterons. Sodium metaborate targets were prepared by fusing 40 mg of the compound onto the grooved face of a copper target head of 1.7 cm diameter. By internal bombardment with beam currents of 350 microamperes at 7 Mev for six to eight hours, it was possible to prepare sources having strengths up to 500 millicuries.

The neutron detector consisted of a proportional counter containing BF_3 at one-third of an atmosphere of pressure. The gas was extracted from a boron trifluoride-calcium fluoride complex. As furnished by the Atomic Energy Commission, Isotopes Branch, the boron in the complex is 96 percent B^{10}. By the addition of 10 percent of argon of 99.6 percent purity, it was possible to hold the operating potential of the counter down to a value of 2100 volts. The over-all length of the cylindrical counter was 8 inches; its diameter was $1\frac{1}{2}$ inches. A three mil tungsten wire served as the anode.

* Condensation of a dissertation submitted in partial fulfillment of the requirements for the degree of Doctor of Philosophy at the University of Michigan.
** Now with The Kellex Corporation, New York, New York.
[1] Chadwick, Feather and Bretscher, Proc. Roy. Soc. **A163**, 366 (1937).
[2] J. R. Richardson and L. Emo, Phys. Rev. **53**, 234 (1938).
[3] H. v. Halban, Nature **141**, 644 (1938).
[4] F. E. Myers and L. C. Van Atta, Phys. Rev. **61**, 19 (1942).
[5] G. A. R. Graham and H. v. Halban, Rev. Mod. Phys. **17**, 297 (1945).
[6] H. A. Bethe and R. F. Bacher, Rev. Mod. Phys. **8**, 83 (1936); H. A. Bethe and R. E. Peierls, Proc. Roy. Soc. **A148**, 146 (1935).
[7] N. O. Lassen, Phys. Rev. **74**, 1533 (1948).
[8] B. Hamermesh and A. Wattenberg, Phys. Rev. **76**, 1290 (1949).
[9] Meiners, Smith and Slack, Phys. Rev. **75**, 1632 (1949).

The pulses produced by the disintegration products from the capture of slow neutrons by B^{10} in the reaction $B^{10}(n,\alpha)Li^7$ were amplified by a general purpose linear amplifier constructed on the design developed by Jordan and Bell.[10] After the signals were differentiated and amplified, they were allowed to pass through a discriminator or pulse height selector so that only pulses larger than a selected value were recorded by a scaling circuit. With proper selector setting, it was readily possible to exclude all but those pulses arising from the above reaction. Extreme care was exercised in the construction and operation of the apparatus to exclude all background of mechanical and electrical origin. External sources of interference which could give rise to spurious counts were minimized by operating only at night.

The counter was surrounded by a paraffin form which acted as a moderator for slowing down the fast neutrons produced in the photo-disintegration process. A cadmium covering of 10 mil thickness completely surrounded the detector. Preliminary tests showed that an increase by a factor of approximately four or five in the number of counts recorded could be gained by orienting the cylindrical counter so as to present a side view instead of an end view to the incident photo-neutron beam. Experimentally, the optimum paraffin thickness necessary for maximum counting efficiency was found by irradiating 25 cc of D_2O with gamma-rays from radio-sodium. By interposing 1-cm slabs of paraffin between the neutron source and counter, a maximum counting efficiency was found for a thickness of approximately 5.5 cm of paraffin. Guided by these results, a paraffin form was constructed such that the front portion facing the neutron source was cylindrical in shape with axis parallel to the counter axis and of 5.5 cm paraffin thickness while the rear portion was a hemisphere of 15.5 cm diameter. For purposes of symmetry, the front cylindrical portion was then machined so as to present a circular area of 15.5 cm diameter through which the photo-neutrons had to pass in order to be detected. Only those neutrons emitted by the heavy water and contained in an angular opening of 5° could be slowed down and detected in the paraffin. As shown in Fig. 1, the detector was maintained at a fixed distance of 177.6 cm from the heavy water in order to give the desired angular opening.

To gain a high intensity of photo-neutrons a large volume of heavy water is desirable. However, three factors militate against such a choice: the increase in photo-neutron internal scattering with increase in volume, the departure from a point source of neutrons, and the increase in the angular opening for the gamma-rays effective in producing photo-disintegration. To avoid these objections and still permit effective use of as much as 30 cc of D_2O at one time, a toroid or anchor ring of small diameter copper tubing (0.08-cm wall thickness) was filled with heavy water and placed concentric with the axis of the apparatus. The toroid had a radius of 10 cm; the internal diameter of the copper tubing, and hence, of the heavy water was slightly less than 8 mm. With this choice of geometry, it was possible to meet the requirements satisfactorily. Scattering by the heavy water was thereby reduced to a value not detectable outside the probable error of the data (see below); the point source requirement considering the distances involved was essentially satisfied; and the angular opening of the gamma-rays was maintained within a value of 8.4° or less.

The sodium source was located on the axis of the heavy water toroid. By positioning the source at specified distances from the plane of the toroid and concentric thereto, it was possible to vary the angle, γ, between the primary gamma-rays and the observed photo-neutrons. Figure 2 serves to illustrate the arrangement of the principal components of the apparatus. It is apparent that this geometry is such as to select for detection only those neutrons having the same direction (within the angular openings allowed the neutrons and the gamma-rays) with respect to the primary gamma-rays. As this direction is changed by

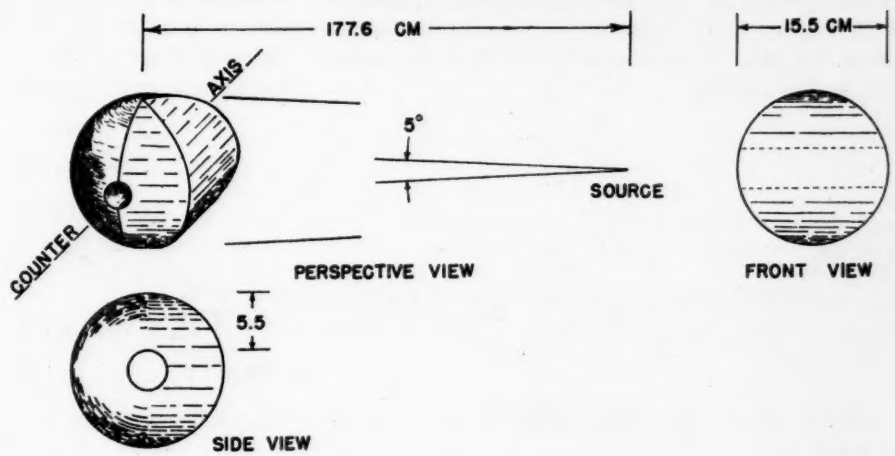

FIG. 1. Paraffin moderator.

[10] W. H. Jordan and P. R. Bell, Rev. Sci. Inst. 18, 703 (1947).

FIG. 2. Experimental set-up (not to scale).

movement of the sodium source, the gamma-ray flux traversing the toroid is likewise changed, thereby necessitating a solid angle correction for the intensity. To keep this correction factor within a reasonably small range of values, the angle, γ, was varied only from 90° to 45° in 15° steps. This required motion of the source throughout a total distance of 11 cm as measured out along the axis of the toroid. For angles less than 45°, this distance increases rapidly with consequent decrease in neutron production. Hence, measurements at the smaller angles were avoided. The gamma-rays effective in producing photo-disintegration had a variable opening due to the finite size of the source and to the fact that the source distance varied with the angle, γ. These angular openings corresponding to γ-angles of 90°, 75°, 60° and 45° were 5.1°, 7.2°, 8.4°, and 7.8°, respectively. Figure 3 shows a dimensional view of the apparatus to scale.

SCATTERING BY THE HEAVY WATER

The extent to which the photo-neutrons scattered by the heavy water affect the angular measurements may be determined by a separate investigation. So far as the isotropic component of the photo-effect is concerned, the scattering would have no influence upon the measured angular distribution. This is not the case, however, for the $\sin^2$ component. The net result of scattering would be to enhance the isotropic component at the expense of the anisotropic component. For this reason, the effect of the scattering by the heavy water must be kept small.

To investigate the optimum toroid dimensions which would allow substantial intensity without excessive scattering, the following test was conducted. Into each of four 10-cm radius toroids having inside sectional diameters of 0.439, 0.630, 0.795, and 1.092 cm a constant volume (9.53 cc) of D_2O was added. This volume completely filled the 0.439 cm toroid. The remaining toroids were then filled to full capacity with H_2O such that the ratio of H_2O to D_2O was 0, 0.98, 2.16 and 5.23, respectively.

Using toroids filled in this manner, it was possible to investigate the effect of the increased volume of water upon the scattering while at the same time to hold constant the number of photo-neutrons produced in the photo-disintegration process. Any change in the number of neutrons detected with change of toroid could quite correctly be attributed to the effect of the additional water upon the scattering. This method has the obvious disadvantage of using the scattering in H_2O to tell us something about the scattering in D_2O.

A radio-sodium source was prepared by a six and one-half hour cyclotron bombardment at an average deuteron beam current of 350 microamperes. Observations of one hour duration using the arrangement shown in Fig. 2 were made for each toroid. Two background observations, each of one hour duration, were made near the start and at the end of the run—an empty copper toroid replacing the water-filled toroids during these periods. This background amounted to an average value of 1.29 counts per minute with the sodium source still positioned on the apparatus. Because of the decay of the sodium source with half-life of 14.8 hours during the course of an experimental run, it was necessary to apply a decay correction factor to the data so as to normalize the counting rates to a constant source intensity. The data from this test for $\gamma = 90°$ are shown plotted in Fig. 4.

The interpretation given to this result rests in general upon the fact that, within the probable error of the data, no increase in intensity is apparent for toroid volumes up to 30 cc for which the radius of the toroid section is 0.398 cm. As the volume becomes greater, however, those neutrons which travel in the plane of the toroid have greater probability for scattering since their

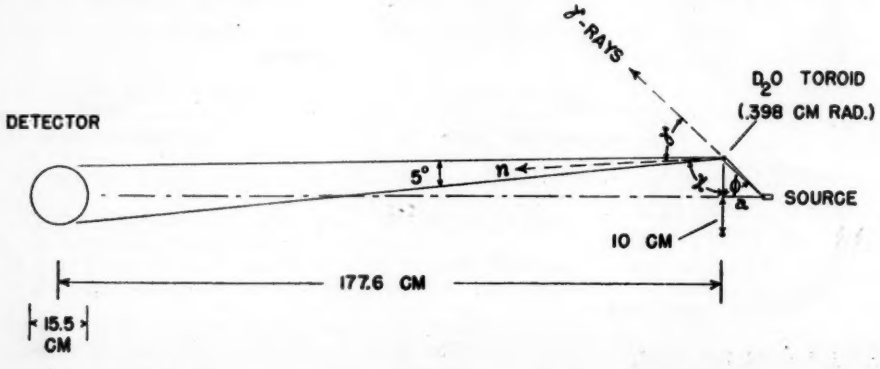

FIG. 3. Dimensional view of apparatus (scale: 1 cm = 10 cm).

path lengths in water have become greater. Hence, some neutrons which were not initially directed toward the detector may now suffer single or multiple scattering and be recorded. These scattered neutrons augment the unscattered intensity recorded for the smaller volumes. Thus, a rise in the curve sets in at volumes for which the amount of scattering is detectable outside the probable error of the counting rate. In consequence, the 0.398-cm radius toroid was used throughout all subsequent angular distribution tests. This choice permitted as large a neutron intensity as possible consistent with a minimum detectable scattering effect.

SCATTERING BY THE WALLS

A potential source of error in experiments in which fast neutrons are formed at one position and detected as slow neutrons at another position removed from the source is that due to scattering of neutrons by parts of the apparatus and by the walls of the room. The material forming the framework of the apparatus and the supports for holding the components of the apparatus at fixed positions were kept as small as possible to make their contribution to this effect negligible. However, the contribution from the walls of the room may be considerable. For this reason, it was necessary to measure the scattered neutron intensity to determine the extent to which this effect influenced the experiment.

The scattering by the walls of the room was studied by measuring the deviations from the $1/r^2$ law for the neutrons observed with the detector at various distances from a small photo-neutron source. For this purpose, a freshly bombarded Na^{24} source was surrounded by a metal cup containing 190 cc of heavy water. This, and the detector heretofore described, were mounted six feet above the floor of a medium sized laboratory room whose dimensions in meters was $7\times14\times4$. Readings of the neutron intensity were made with the photo-neutron source placed at various distances from the detector. The latter was maintained at a fixed position in the center of the room.

The results of this test, corrected for decay of the source and with background (approximately one count/min.) subtracted, are shown in the upper curve of Fig. 5. Here the photo-neutron intensity per minute and distance in meters are plotted on logarithmic scales. It is apparent that the deviation from the inverse square law is extremely large; the exponent evaluated for these data was found to be -1.15.

In consequence of this result, the apparatus was next mounted on the parapet fringing the roof of a four-story laboratory building. The detector, still supported on a thin stand six feet high, was placed at one corner of the parapet. Its over-all height above the roof was $8\frac{1}{2}$ feet. The neutron source, consisting of 150 cc of heavy water surrounding a Na^{24} target of approximately 400 mc strength, was similarly mounted on top of the parapet. By moving the source at various intervals along one side of the building, the variation of intensity at the detector could be recorded.

The data resulting from this test, when corrected for decay and with background (approximately 3 counts/min.) subtracted, are shown marked "roof-top" in Fig. 5. These data have been normalized at the one meter position with the previous data taken indoors. A considerable improvement toward an inverse square fall-off is apparent with the exponent now decreasing to -1.66.

To reduce still further the effect of neutron scattering by the surrounding objects, the equipment was adapted so as to permit measurements aloft. Ten Neoprene captive balloons, each inflated with hydrogen to a diameter of six feet, provided sufficient lifting force to raise the twenty-five pounds of equipment consisting of cadmium-covered paraffin moderator, counter and counter basket, preamplifier, filter box, heavy water cup and source, five-conductor shielded cable, and unshielded high voltage cable. The ten balloons were

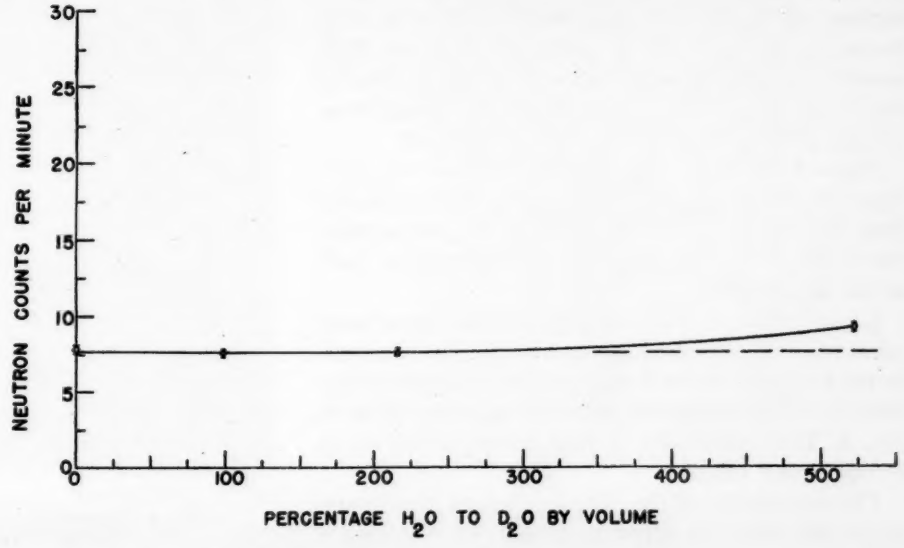

FIG. 4. D_2O scattering test.

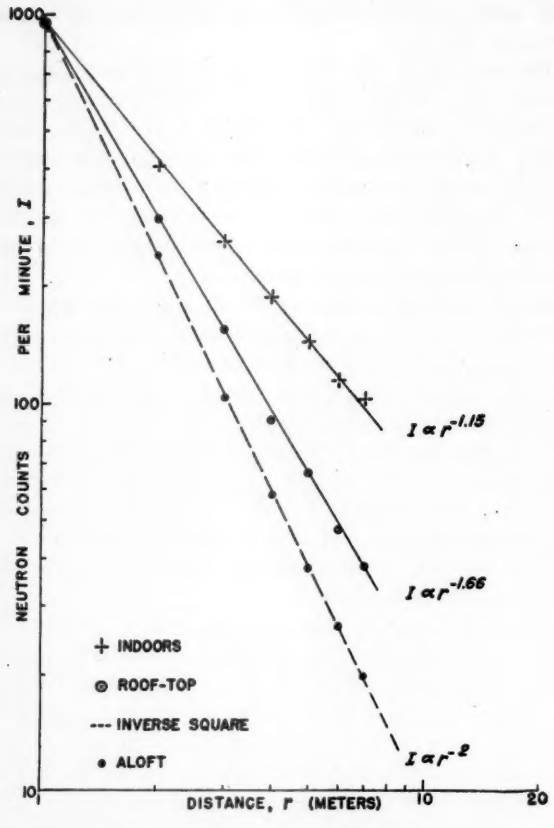

FIG. 5. Photo-neutron background.

linked together into a compact group so as to minimize excessive jarring of the apparatus which otherwise would occur if the ballons were allowed to separate and then be blown against each other. The balloons were positioned approximately one hundred and twenty-five feet above the apparatus so as to minimize the effect of scattering by the hydrogen gas. The distance between source and detector was made variable in intervals of one meter by linking together a number of one-meter sections of $\frac{1}{16}$-inch stranded steel cable with snap hooks. By lowering the apparatus, sections of cable would be quickly added or removed as desired. During the course of a run, the apparatus was maintained at an average distance of sixty feet from the building.

Figure 6 shows an approximately vertical view indicating the manner in which the apparatus was suspended from the mooring line. The weight of the power cables was removed from the detector by looping these back to the line as shown.

Using 190 cc of D_2O, intensity measurements were taken at six positions in random order. The data corrected for decay of the source and for background (approximately three counts/min.) are shown plotted in Fig. 5. The dashed line is that corresponding to an inverse square fall-off.

The consistency of the data in obeying the inverse square law when the apparatus is kept clear of walls is apparent. To make unambiguous tests on the angular distribution, these results show that it will be sufficient to suspend the apparatus outdoors and at least sixty feet away from surrounding objects. Such a procedure will effectively eliminate the need for a wall scattering correction to the data.

MEASUREMENTS USING OUT-OF-DOOR SUSPENSION

The conduct of the experiments on the angular distribution measurements was next altered to permit an out-of-doors test without the use of ballons. For this purpose, a three-hundred foot suspension cable ($\frac{1}{8}$-inch stranded steel) was fastened so as to extend between structures atop the roofs of two four-story buildings. The apparatus previously described and shown suspended in Fig. 7 was equipped with Nylon lines to permit its being drawn out with the aid of pulleys to a point midway between and slightly above the two buildings. In this fashion the equipment remained suspended one hundred feet from the buildings and approximately ninety feet above the ground. Checks on the inverse square law in the manner described above showed that with this arrangement the wall scattering effect was absent when the apparatus occupied the operating position at the center of the cable.

In the conduct of the angular distribution measurements, the activated source of sodium, mounted on its support rod, was placed in the aluminum holder located

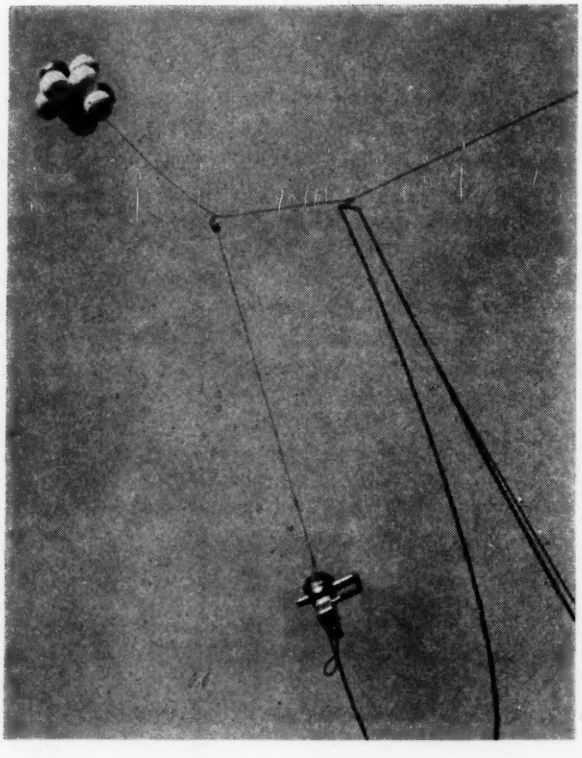

FIG. 6. Apparatus for inverse square law test in flight—vertical close-up.

above the toroid in the upper frame of Fig. 7. An empty or heavy water filled toroid shown clamped to the wire basket allowed either a background or an angular distribution measurement. The detector, with accompanying preamplifier and filter box, was supported by the four $\frac{1}{16}$-inch stranded cables which extended down from the toroid as shown in the lower frame of Fig. 7. These cables in turn fastened to an empty copper toroid which encircled the top portion of the cadmium-covered paraffin form. This toroid served to prevent the cables from cutting into the paraffin. Only the sensitive volume of the counter was enclosed in the paraffin. The horizontal portions seen extending beyond the form on either side consisted of the shielding caps and sleeves and were not regions sensitive to neutron detection. However, these portions were covered with sheet cadmium to permit absorption of slow neutrons which approached the sensitive volume from either end of the counter.

Between measurements, the apparatus was drawn in, the source reoriented to a new position by means of stop grooves in the source support rod, and then drawn out to its operating position at the center of the suspension cable.

A total of six complete and independent measurements were made of the intensity at each of the 45°, 60°, 75°, and 90° positions. Each measurement at a single position lasted for one hour.

The total number of neutron counts (less background) recorded at each position during the six one-hour observation periods is shown in Table I, column 2. The average background in these tests was 1.77 counts per minute.

The neutron intensity recorded at each angular position requires the application of several correction factors before useful information may be obtained from the data. One such correction relates to the decay of the radio-sodium source during the period of observation; a second correction must be applied to the recorded intensity by virtue of the fact that the gamma-ray flux streaming through the heavy water toroid varies with the axial distance "a". The values of this correction factor ranged from 1.00 at the 90° position to 2.23 at the 45° position. Application of these corrections yields the average number of counts per minute, $\bar{I}$, shown in column 3 of Table I. The probable error associated with each counting rate is likewise presented in this same column.

RESULTS AND CONCLUSIONS

From the results of theoretical analysis of the nuclear photo-effect, we consider that the total cross section consists of an isotropic component due to magnetic interaction and an anisotropic component due to electric interaction. The differential cross section of the latter is expected to conform to a $\sin^2$ distribution. In consequence, we assume that, at the angle, γ, the average intensity of the photo-neutrons can be described by a relation of the form

$$\bar{I}(\gamma)=\frac{\int_{\gamma_1}^{\gamma_2}(a+b\sin^2\gamma)\sin\gamma d\gamma}{\int_{\gamma_1}^{\gamma_2}\sin\gamma d\gamma}, \quad (1)$$

where the limits of integration are chosen to include the total angular opening allowed the photo-neutrons and primary gamma-rays by the finite size of the detector and toroid. The constants, a and b, represent the number of photo-neutrons projected into unit solid angle, at the angle $\gamma=90°$, by the magnetic and electric photo-effects, respectively.

Upon integration, we obtain for the average intensity at the angle, γ, and for the angular opening from γ_1 to γ_2, the value

$$\bar{I}(\gamma)=a+b-\tfrac{1}{3}b(\cos^2\gamma_1+\cos\gamma_1\cos\gamma_2+\cos^2\gamma_2). \quad (2)$$

The ratio of the intensities corresponding to measurements taken at two different γ-angles will yield information on the value of the quotient, a/b. Designating the ratio of intensities measured at the γ-angles, γ_A and

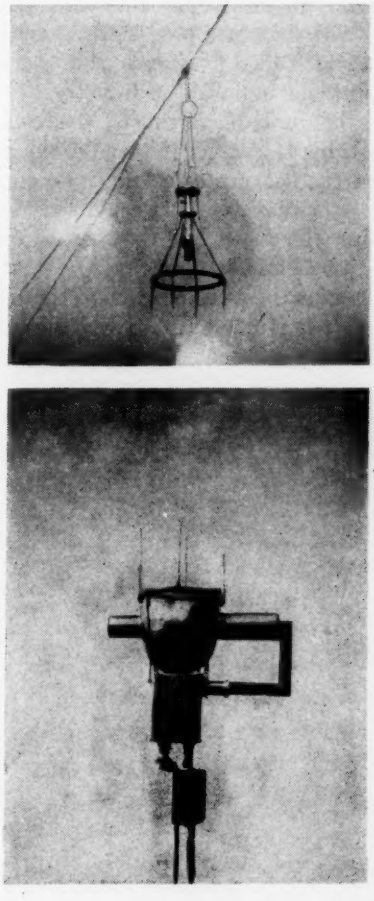

FIG. 7. Apparatus for angular distribution test in suspension—composite close-up.

TABLE I. Composite angular distribution data.

1 γ-angle	2 Total no. counts	3 $\bar{I}$, average no. of counts/min. (corrected)
45°	1415	9.34±0.23
60°	2929	12.66±0.19
75°	4307	15.03±0.18
90°	5133	15.94±0.17

γ_B, by the symbol $B_{A,B}$, we have, therefore, a set of equations as:

$$(a/b)_{A,B}=\frac{B_{A,B}\{1-\frac{1}{3}(\cos^2\gamma_3+\cos\gamma_3\cos\gamma_4+\cos^2\gamma_4)\}-\{1-\frac{1}{3}(\cos^2\gamma_1+\cos\gamma_1\cos\gamma_2+\cos^2\gamma_2)\}}{1-B_{A,B}}, \quad (3)$$

where γ_1 and γ_2 represent the integration limits associated with the angle γ_A, while γ_3 and γ_4 represent the corresponding limits for the angle γ_B.

Upon applying the average counting rates per minute, $\bar{I}$, of Table I to the above set of equations, we obtain values for the quotient, a/b, corresponding to all possible combinations of pairs of angles at which observations have been made. A probable error to be assigned each of these quotients was evaluated in accordance with standard practice by propagating the errors listed in Table I through the various mathematical operations indicated in Eqs. (3).

Because the probable error of the counting rate (column 3, Table I) is larger the smaller the γ-angle, the resulting percentage errors of the quotients, each of which involves intensity measurements at two γ-angles, will vary over wide limits. For this reason, it is desirable to evaluate a weighted average, $\langle a/b\rangle_{Av}$, in such fashion that greater emphasis is placed on those quotients having the smaller error. To this end, a weighting factor was assigned to each quotient which is inversely proportional to the square of the probable error of that quotient.[11] This procedure permits evaluation of a grand mean and its probable error in accordance with Eqs. (27) and (28), Chapter VIII, of the reference cited. The value so obtained is:

$$\langle a/b\rangle_{Av}=0.196\pm0.024.$$

From this experimental result, we obtain the ratio, τ, of probabilities of the magnetic to the electric effect, since $a/b=\frac{2}{3}\tau$. Hence, for the Na^{24} gamma-ray energy of 2.76 Mev we have

$$\tau=0.295\pm0.036.$$

The ratio of the photo-magnetic to the total cross section becomes, therefore

$$\tau/(\tau+1)=0.228\pm0.028.$$

The value of a/b from this investigation is found to lie below that of Lassen[7] who gives a value of 0.22±0.04. On the other hand, it exceeds the Hamermesh and Wattenberg value of 0.15±0.04 which was revised downward from 0.24 after publication of the Bulletin.[8]

In consequence of the difficulties attending the measurement of the weak effects associated with photodisintegration by current techniques, verification of the existence of the additional $^3D-{}^3P$ and $^3D-{}^1D$ transitions predicted by non-central force theory, lies well beyond present experimental capabilities.

ACKNOWLEDGMENTS

The author wishes to express his appreciation to Professors H. R. Crane and M. L. Wiedenbeck and to Dr. E. S. Lennox for their interest and helpful discussions throughout the course of this investigation. It is a pleasure to record here my indebtedness to the University of Michigan cyclotron staff for their valuable and untiring efforts in assisting in the preparation of the radio-sodium sources and aiding in the conduct of the night operations.

Finally, the stimulation and encouragement afforded me through the Horace H. Rackham Special Fellowship appointments for the school years 1947–1948 and 1948–1949 are gratefully acknowledged.

[11] A. G. Worthing and J. Geffner, *Treatment of Experimental Data* (John Wiley and Sons, Inc., New York, 1943).

PHYSICAL REVIEW VOLUME 76, NUMBER 9 NOVEMBER 1, 1949

Molecular Dipole Moments and Stark Effects

I. Stark Effects on Symmetric Top Molecules with Nuclear Quadrupole Coupling

W. Low and C. H. Townes
Columbia Radiation Laboratory, Columbia University, New York, New York
(Received July 12, 1949)

The hyperfine structure of rotational levels of a symmetric top molecule in which one nucleus has an electric quadrupole moment is derived for weak, strong, and intermediate fields. Intensities of the hyperfine components are discussed. Solution of a second-order secular equation is shown to suffice for the evaluation of dipole moments from microwave spectra. A sample calculation is given for nuclear spin of $\frac{3}{2}$ and $J=1\rightarrow 2$ transition.

INTRODUCTION

STARK effects on molecular spectra are easily observed with the techniques of microwave spectroscopy and have proved useful in detecting molecular absorption lines, in identifying transitions, and in measuring molecular dipole moments. A number of papers[1] have discussed the effects of quadrupole interaction between nuclei and the molecular electrons. Fano[2] has studied the case of Stark effects on linear molecules with hyperfine structure. The present work is an extension to symmetric top molecules, i.e., molecules with two equal principal moments of inertia.[3] Expressions for the first- and second-order terms of the Stark effects are given for the case of nuclear quadrupole coupling for a single nucleus with the molecular field and for Stark interactions which are either small or large compared with the quadrupole coupling. The secular equation is derived for the intermediate case and it is shown that for dipole moment determination no more than a second-order equation need be solved. Other miscellaneous cases as well as relative intensities of the Stark components of a molecular transition are discussed.

The Hamiltonian in an external field with quadrupole interaction is given by

$$H=H_O+H_E+H_Q, \tag{1}$$

where H_O is the unperturbed Hamiltonian, H_E is due to the electric field and given by $\boldsymbol{\mu}\cdot\boldsymbol{E}$ where $\boldsymbol{\mu}$ is the molecular dipole moment and $\boldsymbol{E}$ is the electric field. H_Q is due to the quadrupole coupling and is given by

$$H_Q=\frac{eqQ}{2I(2I-1)(2J-1)}\{3(\boldsymbol{I}\cdot\boldsymbol{J})^2+\tfrac{3}{2}(\boldsymbol{I}\cdot\boldsymbol{J}) -I(I+1)J(J+1)\}\left\{\frac{3K^2}{J(J+1)}-1\right\} \tag{2}$$

where e is the charge of the proton, Q=nuclear quadrupole moment, $q=\partial^2V/\partial z^2$ or the second derivative of the electrostatic potential along the molecular axis, I=nuclear angular momentum, J=molecular angular momentum, K=component of J along the molecular symmetry axis.

The energy of a rigid rotating symmetric top is characterized by the two quantum numbers J and K and is given by

$$W(J,K)=BJ(J+1)+(A-B)K^2, \tag{3}$$

where A and B are rotational constants related to the molecular moments of inertia. In an external electric field (Hamiltonian $H=H_O+H_E$) expression (3) is modified[4] to

$$W(J,K,m_J)=W(J,K)-\frac{\mu E m_J K}{J(J+1)} +4\frac{\mu^2E^2}{B}[\Phi(J,m_J,K)-\Phi(J+1,m_J,K)] \tag{4}$$

where

$$\Phi(J,m_J,K)=\frac{(J^2-m_J^2)(J^2-K^2)}{(2J-1)(2J)^3(2J+1)}$$

and m_J is the projection of J on E, or the magnetic quantum number.

In the case of nuclear quadrupole coupling ($H=H_O+H_Q$) the eigenvalues have been obtained[1] as

$$W(F,J,K)=W(J,K)+eqQ \times\left\{\frac{\frac{3}{4}C(C+1)-I(I+1)J(J+1)}{2I(2I-1)(2J-1)(2J+3)}\right\}\left\{\frac{3K^2}{J(J+1)}-1\right\} \tag{5}$$

where $C=2(\boldsymbol{I}\cdot\boldsymbol{J})=F(F+1)-J(J+1)-I(I+1)$ and F is the total quantum number, i.e.,

$$F=J+I,\ J+I-1,\ \cdots J-I.$$

[1] W. B. G. Casimir, *On the Interaction between Atomic Nuclei and Electrons* (Teylor's Tweede Genootshop, Harlem, Netherlands, 1936); A. Nordsieck, Phys. Rev. **58**, 310 (1940); J. H. Van Vleck, Phys. Rev. **71**, 468 (1947); J. Bardeen and C. H. Townes, Phys. Rev. **73**, 97–107 (1948); D. K. Coles and W. E. Good, Phys. Rev. **70**, 979 (1946).

[2] U. Fano, J. Research Nat. Bur. Stand. **40** (1948).

[3] R. Karplus and A. H. Sharbaugh, Phys. Rev. **75**, 889 (1949) have solved the special case of methyl chloride for $K=0$. Their solution is similar to that of Fano, and shows none of the effects peculiar to symmetric top molecules.

[4] Mannebeck, Physik Zeits. **28**, 72 (1927); R. Kronig and I. Rabi, Phys. Rev. **29**, 262 (1927); and D. M. Dennison, Rev. Mod. Phys. **3**, 34 (1931).

In the case to be considered here, when both an external field and quadrupole interaction are present, two extreme cases can relatively easily be solved.

A. The electric field is weak so that the Stark splittings are small compared with the quadrupole splittings, i.e.,

$$\mu E \ll eqQ \quad \text{when} \quad m_J, K \neq 0$$
$$(\mu E/B)^2 \ll eqQ \quad \text{when} \quad m_J, K = 0.$$

B. The electric field is strong compared to the quadrupole interaction, but not strong enough to distort appreciably the rotational wave functions, i.e.,

$$B \gg \mu E \gg eqQ \quad \text{if} \quad m_J, K \neq 0$$
$$B \gg \mu^2 E^2/B \gg eqQ \quad \text{if} \quad m_J, K = 0.$$

C. In the intermediate case, which is often encountered in microwave spectroscopy, secular equations must be solved to obtain the energy levels.

(A) The Weak Field Case. $\mu E \ll eqQ$

Let only one nucleus have a quadrupole moment. In the zero field case (pure quadrupole interaction) the total angular momentum F is a constant of motion and all states with the same F but different M the total magnetic quantum number $M=m_j+m_I$) have the same energy. In the case of near-zero field (i.e., weak field) F will still remain constant and the effect of the field can be treated as a small perturbation. It is therefore appropriate to use the F, M, J, I, representation which diagonalizes H_Q and treat H_E as a small perturbation.

Expanding the wave function $\Psi(F, M, J, I)$ in terms of the molecular rotational wave function $U(J, m_j, K)$ and the nuclear spin function $\Phi(I, m_I)$ one gets

$$\Psi(F, M, J, I) = \sum_{m_J} C(F, M, J, I, m_J) U(J, m_J, K) \Phi(I, m_I) \quad (6)$$

where the coefficients $C(FMJIm_J)$ can be evaluated.[5] Using the perturbation H_E, the first-order correction is

$$W^{(1)} = \langle FMJI|H_E|FMJI\rangle = -\frac{\mu EK}{J(J+1)} \sum_{m_J} |C(FMJIm_J)|^2 m_J.$$

Noting that $\sum_{m_J} |C(FMJIm_J)|^2 m_J$ is the average of the quantum number m_J one can easily show this to be

$$M\frac{\boldsymbol{F}\cdot\boldsymbol{J}}{F(F+1)} = M\frac{[F(F+1)+J(J+1)-I(I+1)]}{2F(F+1)}.$$

The first-order correction therefore becomes

$$W^{(1)} = -\frac{\mu EK}{2J(J+1)} \frac{[F(F+1)+J(J+1)-I(I+1)]}{F(F+1)}. \quad (7)$$

It is to be noticed that

(a) When $K=0$, the expression vanishes as in the case of the diatomic or linear molecule.

(b) When $F=I+J=M$, the expression is independent of the presence of the quadrupole effects, for then

$$W^{(1)} = -\mu EK/(J+1).$$

The second-order correction due to the perturbation H_E is given by

$$W^{(2)} = \sum_{F'} \sum_{J'} 1 \frac{\langle F'J'MI|H_E|FJMI\rangle\langle FJMI|H_E|F'J'MI\rangle}{E_{FJMI} - E_{F'J'MI}}$$

where the term $F=F'$, $J=J'$ is omitted from this sum. The sum $\sum_{F'} \sum_{J'}$ can be broken up into the two sums

$$\sum_{F'} \sum_{J' \neq J} + \sum_{F' \neq F} \sum_{J'}.$$

Considering the first summation, expanding by means of (6) and remembering that

$$\Phi(Im_I)\Phi(Im_I') = \delta m_I m_I',$$

where δ is the Kronecker symbol, one obtains

$$\sum_{F'} \sum_{J' \neq J} \sum_{m_J} C^*(F'J'm_Jm_I) C(FJm_Jm_I) \frac{\langle J'm_JK|H_E|Jm_JK\rangle}{E_{FJMI} - E_{F'J'MI}} \times C^*(FJm_Jm_I) C(F'J'm_Jm_I) \langle Jm_JK|H_E|J'm_JK\rangle.$$

But since

$$\sum_{F'} C^*(F'J'm_Jm_I) C(F'J'm_Jm_I) = 1$$

this reduces to

$$\sum_{J' \neq J} \sum_{m_J} |C(FJm_Jm_I)|^2 \frac{|\langle J'm_JK|H_E|Jm_JK\rangle|^2}{E_{FJMI} - E_{F'J'MI}}.$$

Since

$$E_{F'J'MI} - E_{FJMI} \approx E_{J'} - E_J,$$

$$W_{(a)}^{(2)} = \sum_{J' \neq J} \sum_{m_J} |C(FJm_Jm_I)|^2 \frac{|\langle J'm_JK|H_E|Jm_JK\rangle|^2}{E_J - E_{J'}}, \quad (8)$$

or

$$W_{(a)}^{(2)} = \frac{\mu^2 E^2}{B} \sum_{m_J} |C(FJm_Jm_I)|^2 \left\{ \frac{3m_J^2 - J(J+1)}{(J+1)(2J)(2J+3)(2J-1)} \right\} + \frac{(\mu E)^2}{B} \sum_{m_J} |C(FJm_Jm_I)|^2 K^2 \left[m_J^2 \frac{\{(2J+3)(J+1)^3 - J^3(2J-1)\} - 3J^2(J+1)^2(2J+1)}{2(2J-1)(2J+1)J^3(J+1)^3(2J+3)} \right].$$

[5] E. U. Condon and G. H. Shortley, *The Theory of Atomic Spectra* (The Macmillan Company, New York, 1935), pp. 76–77.

By similar reasoning the second sum becomes

$$W_{(b)}{}^{(2)}=\sum_{F'\neq F}\sum_{m_J}|C(F'Jm_Jm_I)|^2\frac{|\langle Jm_JK|H_E|Jm_JK\rangle|^2}{E_F-E_{F'}},$$

where $E_F-E_{F'}=W(Q)-W(Q')$ or the difference in the quadrupole energies. Hence we obtain

$$W_b{}^{(2)}=\mu^2E^2\sum_{F'\neq F}\sum_{m_J}\frac{|C(FJm_Jm_I)|^2}{E_F-E_{F'}}\left(\frac{m_JK}{J(J+1)}\right)^2 \quad (9)$$

One notices that

(a) When $K=0$ the only term remaining is

$$W_{(a)}{}^{(2)}=\frac{\mu^2E^2}{B}\sum_{m_J}|C(FJm_Jm_I)|^2 \times\left\{\frac{3m_J{}^2-J(J+1)}{(J+1)(2J)(2J+3)(2J-1)}\right\},$$

which is the term obtained by Fano[2] (formula 13) for a linear molecule and is given as

$$W_{(a)}{}^{(2)}=-\frac{\mu^2E^2}{B}\frac{[3M^2-F(F+1)][3D(D-1)-4F(F+1)J(J+1)]}{2J(J+1)(2J-1)(2J+3)(2F)(2F+1)(2F-1)(2F+3)}, \quad (10)$$

and $D=2(\mathbf{J}\cdot\mathbf{F})=F(F+1)+J(J+1)-I(I+1)$.

(b) The contribution due to $W_b{}^2$ is greater than $W_a{}^2$ because

$$E_J-E_{J'}\gg E_F-E_{F'}.$$

(c) The coefficients* $C(FJm_Jm_I)$ can be found in Condon and Shortley.[5]

The total energy for the weak field case is hence given as

$$W(FJMIK)=W(FJK)+W^{(1)}+W_{(a)}{}^{(2)}+W_{(b)}{}^{(2)}. \quad (11)$$

(B) The Strong Field Case. $\mu E\gg eqQ$

In a strong electric field the interaction with the field is stronger than with the nuclear quadrupole moment ($\mu E\gg eqQ$) but not strong enough to distort the original rotational wave function ($\mu E\ll B$) to a considerable extent. Hence the perturbing term results from the electrical quadrupole interaction between the nucleus and the rest of the molecule, i.e.,

$$H_Q=\frac{eqQ}{(2J+3)2I(2I-1)(2J-1)}\left\{\frac{3K^2}{J(J+1)}-1\right\} \times[3(\mathbf{I}\cdot\mathbf{J})^2+\tfrac{3}{2}(\mathbf{I}\cdot\mathbf{J})-I(I+1)J(J+1)]. \quad (12)$$

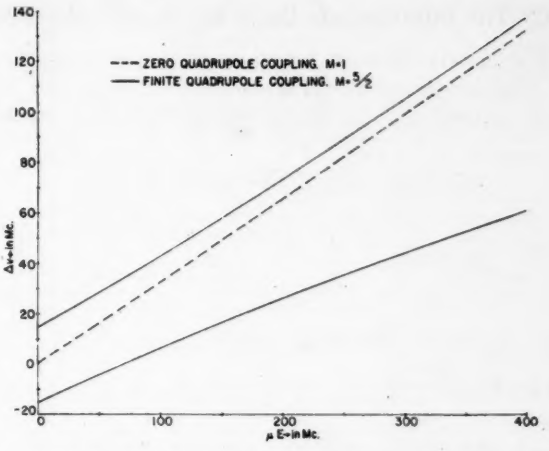

FIG. 1. Stark effect in symmetric top with quadrupole coupling. $J=1\rightarrow2$, $I=\frac{3}{2}$, $eqQ=-235$ Mc.

Case I. $|m_J|\neq1$. The first-order correction is given by

$$W(Jm_Jm_IK)=W(Jm_JK)+\langle Jm_Jm_IK|H_Q|Jm_Jm_IK\rangle.$$

Referring to the operator of H_Q (Eq. (12)) in square brackets as A we get

$$\langle Jm_Jm_IK|A|Jm_Jm_IK\rangle=\tfrac{1}{2}[3m_I{}^2-I(I+1)][3m_J{}^2-J(J+1)],$$

and hence

$$W(Jm_Jm_IK)=W(Jm_JK)+W(Q), \quad (13)$$

where

$$W(Q)=\frac{eqQ}{4I(2I-1)(2J-1)(2J+3)}\left\{\frac{3K^2}{J(J+1)}-1\right\} \times[3m_I{}^2-I(I+1)][3m_J{}^2-J(J+1)]. \quad (13a)$$

A similar expression is obtained for two quadrupole moments, i.e.,

$$W(Jm_Jm_IK)=W(Jm_JK)+W(Q_1)+W(Q_2).$$

Case II. $\mu E\gg eqQ$, $|m_J|=1$. For $M=I$, $I+1$, and $m_J=1$ the term energy is still given by the above Eq. (13). However, for $M=1$, $m_J=1$ is not a good quantum number but $|m_J|=1$ is. The term energy then is given as a solution of the secular equation

$$\begin{vmatrix} W(J,I,K)+\langle J,1,K|H_Q|J,1,K\rangle-W & \langle J,1,K|H_Q|J,-1,K\rangle \\ \langle J,-1,K|H_Q|J,1,K\rangle & W(J,I,K)+\langle J,-1,K|H_Q|J,-1,K\rangle-W \end{vmatrix}=0. \quad (14)$$

* From Fano one can obtain for

$$\sum_{m_J}(C_{m_J})^2m_J{}^2=[3M^2-F(F+1)]\frac{[3D(D-1)-4F(F+1)J(J+1)]}{2F(F+1)(2F-1)(2F+3)3}+\frac{J(J+1)}{3}.$$

(C) The Intermediate Case. $K>0$, $\mu E \simeq eqQ \ll B$

The matrix elements for states with the same value of JIM are given by $\langle JIMm_{J'}|H_E|JIMm_J\rangle$, and the term energy can be found by solving the secular determinant.

$$|\langle JIMm_{J'}|H_E|JIMm_J\rangle - W\delta m_J m_{J'}|=0. \quad (15)$$

The matrix is of the form

	$M=J+I$	$M=J+I-1$	$M=J+I-2$
$M=J+I$	$W(J+I)$	0	0
$M=J+I-1$	0	$W(J+1)$ $\langle J+I\|H_E\|J+I-1\rangle$ $\langle J+I-1\|H_E\|J+I\rangle$ $W(J+I-1)$	0
$M=J+I-2$	0	0	$W(J+I)$ $\langle J+I\|H_E\|J+I-1\rangle$ 0 $\langle J+I-1\|H_E\|J+I\rangle$ $W(J+I-1)$ $\langle J+I-1\|H_E\|J+I-2\rangle$ 0 $\langle J+I-2\|H_E\|J+I-1\rangle$ $W(J+I-2)$

The matrix can be divided into submatrices of the first, second or higher order. The highest degree of the equation is $2J+1$ or $2I+1$, depending which is smaller. $W(J+I)$ represent the diagonal elements of the matrix and they are of the form

$$W(J+I)=W\{Q(I+J)\}+\langle J+I|H_E|J+I\rangle$$

where $W\{Q(I+J)\}$ refers to the quadrupole energy for the level $F=J+I$. The various matrix elements can be found from the tables in Condon and Shortley.[5]

The strongest hyperfine line in a transition $J\rightarrow J+1$, for a given K is the transition $F=J+I\rightarrow F=J+I+1$. The most widely split Stark component of this line for such a transition has $M=J+I$. It can be seen therefore that for convenient dipole moment determination it is sufficient to evaluate the first and second degree secular determinants. A sample calculation as well as an illustrative graph is given in the Appendix.

INTENSITIES

Knowledge of the relative intensities of the various components help very often in identifying their quantum numbers. The intensities of the various lines involve the elements of the dipole moment matrix $\langle\Psi^*|H_E|\Psi\rangle$. The same three cases can therefore be distinguished:

(A) Using the zero field approximation and hence F, M, J, I, K, representation one easily finds for

$\Delta F=0$ (center line)

$$I_M=PM^2,$$

$\Delta F=+1$ (satellite)

$$I_M=Q(F^2-M^2), \quad (16)$$

where P, Q are parameters independent of M, and F is the larger of the two levels.

(B) Using the very strong field approximation (the (Jm_JK) representation, the intensity of the components is given by

$\Delta J=0$ (center line)

$$Im=Rm_J^2,$$

$\Delta J=+1$ (satellite)

$$Im=S(J^2-m_J^2), \quad (17)$$

where R and S are parameters independent of m_J, and J is the larger of the two levels.

(C) In intermediate fields approximate intensities may be determined by interpolating between the two extreme cases (A) and (B). Exact intensities may be obtained by solving equations of the type encountered in Part C (in the intermediate case).

ACKNOWLEDGMENT

The authors appreciate several very helpful discussions with Professor H. M. Foley.

APPENDIX

A sample calculation of energy levels for intermediate field strengths, is given for the transition

$$J\rightarrow J+1,$$
$$F\rightarrow F+1,$$
$$\Delta M=0, \quad K=1,$$
$I=3/2, \quad J=1, \quad M=5/2=F$ is the lower state,
$I=3/2, \quad J=2, \quad M=5/2=F-1$ the upper state.

(a) $F=M=I+J$.

The ground state wave function is given by

$$\Psi(JIMm_J)=f(Jm_J=J)\Phi(Im_I),$$

and therefore

$$\langle\Psi(JIMm_J|H_E|\Psi(JIMm_J\rangle,$$

which reduces to

$$\langle f(J, m_J=J|H_E|f(J, m_J=J\rangle=-(\mu EK/J+1)=-(\mu E/2).$$

Hence the term value is given as

$$W_1=W(Q)-\mu E/2.$$

(b) $M=F-1=J+I-1$.

In this case there are two eigenfunctions corresponding to the two ways M can be formed, i.e.,

$$M=m_J=J+m_I=I-1,$$
$$=m_J=J-1+m_I=I,$$

$$\Psi_1=a_1f_1(J, m_J=J)\Phi(I, m_I=I-1)+a_2f_2(J, m_J=J-1)\Phi(I, m_I),$$
$$\Psi_2=-a_2f_1(J, m_J=J)\Phi(I, m_I=I-1)+a_1f_2(J, m_J=J-1)\Phi(I, m_I).$$

The coefficients a_1 and a_2 are obtained from Condon and Shortley and are

$$a_1=(2J/2J+3)^{\frac{1}{2}}, \quad a_2=(3/2J+3)^{\frac{1}{2}}.$$

The determinant to be solved is

$$\begin{vmatrix} W(Q_1)+\langle\Psi_1|H_E|\Psi_1\rangle-W & \langle\Psi_1|H_E|\Psi_2\rangle \\ \langle\Psi_2|H_E|\Psi_1\rangle & W(Q_2)+\langle\Psi_2|H_E|\Psi_2\rangle-W \end{vmatrix}=0,$$

where

$$\langle\Psi_1|H_E|\Psi_1\rangle=\frac{3}{2J+3}|\langle J, m_J=J|H_E|J, m_J=J\rangle|^2$$
$$+\frac{2J}{(2J+3)}\langle J, m_J=J-1|H_E|J, m_J=J-1\rangle|^2$$
$$=-\mu EK\left[\frac{2J+1}{(2J+3)(J+1)}\right]=a;$$

similarly

$$\langle\Psi_2|H_E|\Psi_2\rangle=-\mu EK\left[\frac{3(J-1)+2J^2}{J(J+1)(2J+3)}\right]=b,$$

$$\langle\Psi_1|H_E|\Psi_2\rangle=-\mu EK\left[\frac{(6J)^{\frac{1}{2}}}{J(J+1)(2J+3)}\right]=c.$$

The solution of the determinant is given by

$$W_2=-\frac{(W(Q_1)+W(Q_2)+a+b)}{2}\pm\tfrac{1}{2}[(W(Q_1)+W(Q_2)+a+b)^2$$
$$-4(W(Q_1)W(Q_2)+ab+aW(Q_2)+bW(Q_1))-c^2]^{\frac{1}{2}}.$$

In the specific case of AsF_3($-eqQ=-235$ Mc) introducing numbers we obtain

$$\Delta\nu=W_2-W_1=[-0.4+(\mu E/4)]\pm[((25.3+\mu E)/4)^2$$
$$-2.8\mu E-(\mu E/18)^2+176.0]^{\frac{1}{2}}.$$

Figure 1 shows $\Delta\nu$ as a function of μE in megacycles/sec.

For $M=F-2$ the equation is a cubic and can be solved in a similar fashion.

PHYSICAL REVIEW VOLUME 76, NUMBER 9 NOVEMBER 1, 1949

The Effect of Nuclear Motion on the Hyperfine Structure of Hydrogen*

G. Breit, G. E. Brown, and G. B. Arfken
Yale University, New Haven, Connecticut

(Received July 18, 1949)

The problem is considered from the point of view of a Hamiltonian which is relativistic to order v^2/c^2. The discussion results in a clearer separation of the non-relativistic correction factor $1-3m/M$ from relativistic effects than in previous treatments. The Hamiltonian applies through the interior as well as the exterior of the proton. By means of it the potential energy can be rounded off at small distances without contradiction to relativity, within the order v^2/c^2. A transformation involving a new effective charge allows the calculation of part of the effect without approximation and it becomes clear that higher order effects are not separable from the so far arbitrary assumptions concerning the proton's radius. Relativistic corrections to the fine structure are reconsidered by means of this transformation and the effect of the acceleration of the proton on the hyperfine structure is discussed.

I. INTRODUCTION

THE effect under discussion has been treated by Breit and Meyerott[1] with the conclusion that the important correction factor is $1-3m/M$ where the mathematical notation is explained at the end of the present section. Some of the reservations which have to be made in connection with higher order terms have been brought out by the same authors.[2] The present note has two main objects: (a) To simplify the considerations so as to make the conclusion less dependent on the manipulative details of the previous work, (b) to improve the logical consistency of the reasoning by employing a Hamiltonian which is relativistically invariant to order v^2/c^2 not only outside the proton radius but through the whole range of values of the relative distance r between the particles.

The main step in the simplification consists in a transformation which appears under Eqs. (7.6), (7.6′) below. The equations which are being transformed are those listed in Eq. (7.3) with neglect of the terms in $(\hbar/2Mc)$ which are present in Eq. (7.5). The latter can be taken account of by a perturbation calculation. The transformation brings the equations back to the form of radial equations for a Dirac electron in a Coulomb field. It involves changes in the linear scale, the charge and the ratio of the radial functions. The effect of the transformation is to change the hyperfine structure in the ratio given by Eq. (9.6) and contains all the terms of interest for comparison with experiment.

Improvement in logical consistency is obtained by employing one of the relativistically invariant forms of the Hamiltonian outside the proton radius. This form

* Assisted by the Joint Program of the ONR and AEC.

[1] G. Breit and R. E. Meyerott, Phys. Rev. **72**, 1023 (1947).

[2] G. Breit and R. E. Meyerott, Phys. Rev. **75**, 1447 (1948).

agrees with the equation which follows from quantum electrodynamics for two charged particles.[3] Inside the proton radius the Coulomb potential is replaced by the function J. In order to avoid a logical failure of this scheme care must be taken to have J reasonably small inside the proton radius so as to keep the electron from moving too fast. This feature of the present note is admittedly arbitrary in its quantitative aspects for the numerical value of the proton radius and regarding the way in which the function J is rounded off. Qualitatively, however, there would appear to be little doubt concerning the inapplicability of the Coulomb potential e^2/r inside the proton radius. The Hamiltonian used here is believed therefore to approximate reality better than a Coulomb potential and the logical consistency is improved by the inclusion of correction terms for the relative velocity which appear in terms of the function J and its derivatives.

The conclusion reached is in agreement with previous work:[1] the correction to the hyperfine structure caused by the finiteness of the proton's mass is represented by the factor $1-3m/M$ within terms which do not involve the products $\alpha^2 m/M$. The effect of the part of the proton's magnetic moment which is not a consequence of Dirac's equation is not explicitly treated in this note. The considerations mentioned toward the end of reference 1 apply to this contribution and the changes in the radial functions which are discussed here bring about uncertainties of relative order $\alpha^2 m/M$.

The transformation with changed charge is also made use of to present the effects of order $\alpha^2 m/M$ on the fine structure in a way different from that of Breit and Brown.[4] Effects on the hyperfine structure which arise from the effect of the acceleration of the proton are discussed by means of Eqs. (6.2)–(6.4). These are analogous to the Thomas terms for ordinary spectroscopic fine structure. They disappear for s terms. For p terms they are so small as to make their experimental detection very improbable.

The following notation is used except where stated:

α = fine structure constant.
v = relative velocity.
r = distance between proton and electron.
m = electronic mass.
M = mass of proton.
e = charge of proton.
c = velocity of light.
$\hbar$ = Planck's h divided by 2π.
$\mathbf{p}_e = (\hbar/i)(\partial/\partial x_e, \partial/\partial y_e, \partial/\partial z_e)$.
$\mathbf{p}_M = (\hbar/i)(\partial/\partial x_M, \partial/\partial y_M, \partial/\partial z_M)$.
$p_0 = -\hbar\partial/ic\partial t + e^2/cr$.
$\boldsymbol{\alpha}_e, \beta$ = the four matrices, $\alpha_1, \alpha_2, \alpha_3, \alpha_4$, of Dirac. These matrices operate on the spin coordinates of the electron; $\beta = \rho_3$.
$\boldsymbol{\alpha}_M, \beta_M$ = the four matrices of Dirac which operate on the proton spin coordinates; conventions followed for $\boldsymbol{\alpha}_M$ are similar to those for $\boldsymbol{\alpha}_e$.
$a_H = \hbar^2/me^2$ = Bohr radius.
Ry = absolute value of energy of ground state of hydrogen for $M = \infty$; $Ry = e^2/2a_H$.
$<A>$ = expectation value of operator A.

II. GENERAL REDUCTIONS

The Hamiltonian will be taken to be[5]

$$H = -c(\boldsymbol{\alpha}_e\mathbf{p}_e) - c(\boldsymbol{\alpha}_M\mathbf{p}_M) - \beta mc^2 - \beta_M Mc^2 - J + Q \quad (1)$$

where Q is given by

$$Q = \tfrac{1}{2}(\boldsymbol{\alpha}_e\boldsymbol{\alpha}_M)J - \tfrac{1}{2}(\boldsymbol{\alpha}_e\mathbf{r})(\boldsymbol{\alpha}_M\mathbf{r})dJ/rdr. \quad (2)$$

Subscripts e, M refer to the electron and proton respectively. Elimination of "small" components for the proton leads to

$$\{\mathcal{E} - [(\boldsymbol{\sigma}_M\mathbf{p}) + Q'/c](\mathcal{E} + 2Mc)^{-1} \times [(\boldsymbol{\sigma}_M\mathbf{p}) + Q'/c]\}\Psi = 0 \quad (3)$$

where

$$Q' = \tfrac{1}{2}(\boldsymbol{\alpha}_e\boldsymbol{\sigma}_M)J - \tfrac{1}{2}(\boldsymbol{\alpha}_e\mathbf{r})(\boldsymbol{\sigma}_M\mathbf{r})dJ/rdr, \quad (3.1)$$

$$\mathbf{p} = \mathbf{p}_e = -\mathbf{p}_M, \quad (3.2)$$

$$\mathcal{E} = p_0 + (\boldsymbol{\alpha}_e\mathbf{p}_e) + \beta mc; \quad (3.3)$$

$$p_0 = (E + J)/c. \quad (3.4)$$

The spin operator $\boldsymbol{\sigma}_M$ for the proton is a two-row square matrix. Introduction of $\Psi^{(1)}$ by[6]

$$\Psi^{(1)} = \{1 + (P^2 + i[\mathbf{P}\times\mathbf{P}]\cdot\boldsymbol{\sigma}_M)/8M^2c^2\}\Psi \quad (3.5)$$

with

$$\mathbf{P} = \mathbf{p} + [\boldsymbol{\alpha}J - \mathbf{r}(\boldsymbol{\alpha}\mathbf{r})dJ/rdr]/2c \quad (3.6)$$

yields

$$\{\mathcal{E} + \mathcal{E}_1 + \mathcal{E}_2 + \mathcal{E}_3 + \mathcal{E}_4\}\Psi^{(1)} = 0 \quad (4)$$

where

$$\mathcal{E}_1 = -P^2/2Mc, \quad \mathcal{E}_2 = [\mathbf{P}, [\mathcal{E}, \mathbf{P}]]/8M^2c^2, \quad (4.1)$$

$$\mathcal{E}_3 = -i\boldsymbol{\sigma}_M[\mathbf{P}\times\mathbf{P}]/2Mc, \quad (4.2)$$

$$\mathcal{E}_4 = i\boldsymbol{\sigma}_M([\mathbf{P}\times[\mathcal{E}, \mathbf{P}]] - [[\mathcal{E}, \mathbf{P}]\times\mathbf{P}])/8M^2c^2. \quad (4.3)$$

In order to obtain answers for the hyperfine structure accurate within the order of the small quantity $m\alpha^2/M$ it is necessary to take into account the terms in J^2 which are contained in $P^2/2M$. These terms produce effects of relative order $m\alpha^2/M$ on the wave function and consequently also on the hyperfine structure energy. Since these terms arise from Q and since only the expectation value $<Q>$ can be considered as certain for any choice of Q one cannot expect[7] Eq. (4) to be more than an ap-

[3] G. Breit, Phys. Rev. **51**, 248 (1937).
[4] G. Breit and G. E. Brown, Phys. Rev. **74**, 1278 (1948).

[5] Here J is a generalization of the Coulomb potential, arranged to be finite everywhere; Q corrects the non-relativistic features of J to order v^2/c^2 and is arranged to give the effects of retardation and of magnetic interaction in the limit of J approaching the Coulomb interaction. Both J and Q are discussed in Sections 1 and 2 of reference 3 for the case of two nucleons.
[6] This reduction is analogous to Eqs. (9), (9′) of the reference in footnote 3.
[7] G. Breit, Phys. Rev. **39**, 616 (1932).

proximation. The result of the reductions is given here because it makes it possible to exhibit the hyperfine structure effects contained in $\mathfrak{L}_3+\mathfrak{L}_4$ and to show by comparison with an alternative calculation that the effects on hyperfine structure splitting of relative order $m\alpha^2/M$ cannot be definitely predicted and that it is probably incorrect to calculate them by means of Eq. (4).

If Q is first omitted from the Hamiltonian and if its expectation value is calculated afterward then one first obtains

$$\{\mathfrak{L}-p^2/2Mc+[\mathbf{p},[\mathfrak{L},\mathbf{p}]]/8M^2c^2 +\hbar\sigma_M(dJ/rdr)[\mathbf{r}\times\mathbf{p}]/4M^2c^3\}\Psi^{(1)}=0. \quad (5)$$

Here the perturbation energy Q' is given by

$$Q'=(\mathbf{u}\sigma_M); \quad (5.1)$$

where

$$\mathbf{u}=\alpha J-(\alpha\nabla)(\nabla K)/2=\alpha J/2-(\alpha\mathbf{r})\mathbf{r}dJ/2rdr \quad (5.2)$$

with

$$K=\int^r rJdr, \quad \alpha=\alpha_e. \quad (5.3)$$

In Eq. (5.2) the operations ∇ do not extend beyond K. The nuclear spin enters through Q'. The calculation of the expectation value of the terms containing Q' in Eq. (3) brings in the nuclear spin operator σ_M once more resulting in a quadratic entrance of the nuclear spin operators.

The addition to the hyperfine structure splitting is obtained by linearizing

$$(\sigma_M\mathbf{p})(\mathfrak{L}+2Mc)^{-1}(\mathbf{u}\sigma_M)+(\mathbf{u}\sigma_M)(\mathfrak{L}+2Mc)^{-1}(\sigma_M\mathbf{p})$$

in σ_M. The difference between Ψ and $\Psi^{(1)}$ may be neglected in taking the expectation value of this operator for it introduces effects of relative order $\alpha^2(m/M)^2$ which are consistently neglected here. The spin dependent part of Q is then found to be the expectation value of Q'' where Q'' is

$$Q''=\frac{\hbar}{2Mc}\left(1-\frac{J}{2Mc^2}\right)\frac{dJ}{rdr}[\mathbf{r}\times\alpha]\sigma_M. \quad (5.4)$$

Here there is the factor differing from unity by the quantity $J/2Mc^2$ which contains correction effects of order $(m/M)\alpha^2$. Aside from this factor Eq. (5.4) is the ordinary operator for the hyperfine structure interaction. The literal application of the two-particle wave equation which is followed in the reductions leading to Eq. (4) is somewhat analogous to a similar reduction which has been tried out for two electrons.[8] Comparison with experiment as well as theoretical considerations have indicated for two electrons that it is unjustifiable and incorrect to make literal use of the terms corresponding to Q in the two-electron case.[7] For this reason the discussion below is carried out along lines which have proved to be more adequate in the two-electron case. These correspond to attaching significance only to first-order effects of Q. It should be noted that this limitation makes all effects of order α^2m/M somewhat uncertain. The consideration of effects of this order which follow from Eq. (1) is not pointless, however, because if the numerical coefficients with which the questionable effects appear were to be large one would have serious doubts concerning the applicability of the non-relativistic correction factor $1-3m/M$.

III. THE THOMAS-TYPE TERMS

The first, second and fourth terms in Eq. (5) contain effects easily describable in terms of current nomenclature. The operator $\mathfrak{L}$ corresponds to the Dirac equation in the approximation of neglecting nuclear mass motion. The second term brings in the kinetic energy of the proton. The last term corresponds to effects of the proton's acceleration on the hyperfine structure. These effects were absent in the treatment of Breit and Meyerott[1] because the latter was concerned exclusively with s terms. The effect of these terms can be found by the consideration of the matrix vector

$$\mathbf{B}^{\mathrm{IV}}=-(\hbar/2M^2c^2)(dJ/rdr)[\mathbf{r}\times\mathbf{p}] \quad (6)$$

which combines with[9] $\mathbf{B}'$ to give the hyperfine structure energy as Eq. (2) of the above reference which corresponds to representing the interval factor as

$$((\mathbf{B}'+\mathbf{B}^{\mathrm{IV}})\cdot\mathbf{J})_j/j(j+1) \quad (6.1)$$

where $\mathbf{J}$ is the inner quantum number operator, j the inner quantum number, and the symbol $(\ )_j$ stands for the common value of the diagonal element of the submatrix of the operator enclosed in ( ), with both rows and columns of the submatrix labeled by the same j.

Straightforward calculation yields

$$((\mathbf{B}'+\mathbf{B}^{\mathrm{IV}})\cdot\mathbf{J})_j\cong 8\pi\mu_0\mu_N(1-3m/M)\Psi s^2(0) +\mu_0\mu_N\langle r^{-3}\rangle\delta_{L,0}'\{4k(1+k)(1-3m/M) +(k+1)(2k-1)(m/M)\} \quad (6.2)$$

where k is the Dirac quantum number which takes on values $-1, +1, -2, +2$ for $s_{1/2}$, $p_{1/2}$, $p_{3/2}$, $d_{3/2}$ terms, and L is the azimuthal quantum number. The symbol δ' is 1 minus the Kronecker δ. In Eq. (6.2) there is included the ordinary mass correction effect in the first term which contains the square of the Schrödinger function Ψs at $r=0$ and in the first part of the second term. The last part of the second term in Eq. (6.2) represents the effect of the Thomas-type terms. This effect vanishes for s terms to the present order of approximation as has been found by Breit and Meyerott.[1] Comparison of the regular mass effect which is contained in the first term

[8] G. Breit, Phys. Rev. **34**, 553 (1929).

[9] G. Breit, Phys. Rev. **74**, 656 (1948).

with the special mass effect gives

$$\text{special mass effect/regular mass effect} = -\delta_{L,0}'(2k-1)/12k. \quad (6.3)$$

For $L\neq 0$ this effect is seen to be of the same order of magnitude as the regular mass effect. It is nevertheless of no practical interest at this time because the experimental accuracy does not suffice for its detection in view of the much larger effect of the natural breadth of the levels from which this effect would have to be separated. In the present approximation the effect is

$$(\Delta E)_{Thom} = -\frac{\hbar^2\delta'}{4M^2c^2}\cdot\frac{2L(L+1)}{L+\frac{1}{2}}\left\langle\frac{dJ}{rdr}\right\rangle \cong\left(\frac{m}{M}\right)^2\frac{Ry\alpha^2\delta'}{(L+\frac{1}{2})^2n^3} \quad (6.4)$$

which corresponds to

$$\Delta E_T(2p_{3/2}) = 0.0029Mc/s = \Delta E_T(2p_{1/2}). \quad (6.5)$$

IV. RELATION TO FINE STRUCTURE

In the present section a transformation will be considered which enables one to understand the result of Breit and Brown[4] for the fine structure from a different viewpoint and will also be found useful for the understanding of mass effects on hyperfine structure. The first two terms of Eq. (5) give

$$[p_0+mc-(p_0^2-m^2c^2)/2Mc]f-\hbar O_+g -(\hbar/2Mc^2)(dJ/dr)g=0, \quad (7)$$

$$[p_0-mc-(p_0^2-m^2c^2)/2Mc]g+\hbar O_-f +(\hbar/2Mc^2)(dJ/dr)f=0,$$

where

$$O_+=d/dr+(1+k)/r; \quad O_-=d/dr+(1-k)/r. \quad (7.1)$$

Introduction of Ω_+, Ω_-, F, G by means of

$$\Omega_+=O_+-1/r, \quad \Omega_-=O_--1/r, \quad F=rf, \quad G=rg \quad (7.2)$$

and division by $1-J/2Mc^2$ gives

$$\begin{aligned}(W+J+mc^2)BF-c\hbar\Omega_+[1+J/2Mc^2]G=0,\\ (W+J-mc^2)AG+c\hbar\Omega_-[1+J/2Mc^2]F=0\end{aligned} \quad (7.3)$$

where

$$A=1-(W+mc^2)/2Mc^2, \quad B=1-(W-mc^2)/2Mc^2 \quad (7.4)$$

and W stands for the energy $-Mc^2$. It will be remembered, however, that in Eq. (4) the operator p^2 is replaced by P^2. The operator $\mathfrak{L}_2$ contains only effects of relative order $(m/M)^2$ and will, therefore, be neglected. The addition of $-(P^2-p^2)/2M$ to the left side of Eqs. (7.3) gives

$$\begin{aligned}(W+J+mc^2)BF-c\hbar\Omega_+G-(\hbar/2Mc)UG=0,\\ (W+J-mc^2)AG+c\hbar\Omega_-F+(\hbar/2Mc)UF=0,\\ U=r\Delta J/2+(rdJ/dr)(d/dr)\end{aligned} \quad (7.5)$$

which is seen to contain correction terms in $\hbar/Mc$ which do not depend on the quantum number k. It would be surprising if the correction for P^2-p^2 which has just been made did not have some good quantitative meaning because, as may be seen from Eq. (3.6), it contains in it the usual effects of the vector potential caused by the electron on the momentum operator of the proton with an additional correction for retardation. There is thus a reason for believing Eq. (7.5) in preference to Eq. (7.3).

It will now be shown how Eq. (7.5) gives results for the fine structure of hydrogen. The terms in $\hbar/Mc$ will be treated as a perturbation and will be used only to the first order. Omitting these terms one has two simultaneous equations which agree exactly with corresponding Dirac's equations for a Coulomb field without nuclear motion provided one approximates A and B by unity. Since A, B do not contain r it is possible to transform the equations by means of

$$r'=(AB)^{\frac{1}{2}}r, \quad F'=(B/A)^{\frac{1}{2}}F, \quad G'=G, \quad e'^2=(AB)^{\frac{1}{2}}e^2 \quad (7.6)$$

which gives

$$\begin{aligned}[W+mc^2+e'^2/r']F'-c\hbar\Omega_+'G'=0,\\ [W-mc^2+e'^2/r']G'+c\hbar\Omega_-'F'=0\end{aligned} \quad (7.6')$$

a set of two equations identical in form with the radial equations for an electron in a central field. The energy which corresponds to Eqs. (7.6′) differs from that for the problem with infinite nuclear mass. For the latter

$$(1+W/mc^2)^{\frac{1}{2}}/(1-W/mc^2)^{\frac{1}{2}}-(1-W/mc^2)^{\frac{1}{2}}/(1+W/mc^2)^{\frac{1}{2}}=2(p+s)/\alpha \quad (7.7)$$

where

$$p=(k^2-\alpha^2)^{\frac{1}{2}}-1 \quad (7.8)$$

and

$$-1+|k|+s=\text{principal quantum number.}$$

By means of the above relation between W and α one finds the first-order effect of m/M on W to be

$$\delta W=-\left(\frac{W^2-m^2c^4}{2Mc^2}\right)\cdot\frac{W^2}{m^2c^4}\left[1+\frac{\alpha^2}{(p+1)(p+s)}\right]. \quad (7.9)$$

On the other hand the terms which have been omitted in Eq. (7.5) contribute a first-order effect to the energy which also contains the first power of m/M and amounts to

$$\Delta W=(he^2/2Mc)\int(1/r)[GdF/dr-FdG/dr]dr. \quad (7.9')$$

Evaluating the integral on the right side of this expression and adding the two energy changes one obtains

$$\delta W+\Delta W=-(W^2-m^2c^4)/2Mc^2. \quad (8)$$

This is identical with the quantity called E_1 by Breit and Brown[4] as is seen by comparing with their Eq. (6) and agrees with a previous result of Bechert and Meixner.[10] The meaning of the result in the present

[10] K. Bechert and J. Meixner, Ann. d. Physik **22**, 525 (1935).

paper and in that of Breit and Brown is slightly different from that of Bechert and Meixner. In both of the later papers the energy correction is worked out as an addition to the exact energy of Dirac's equation while Bechert and Meixner's calculation does not consider the higher powers of α.

It has thus been verified that Eqs. (7.5) give the correction to the fine structure within terms of degree m/M in an expansion in powers of m/M within the limitations of the Hamiltonian. No approximation regarding the entrance of α has been made. For the ground term of hydrogen the integrand in Eq. (7.9′) vanishes and the distortion of the wave function caused by the perturbing terms involving $1/M$ in the Eqs. (7.5) is accordingly small. It is therefore convenient to make use of Eq. (7.6′) as a starting point for the calculation of the hyperfine structure effect.

V. THE MASS CORRECTION TO HYPERFINE STRUCTURE OF GROUND TERM NEGLECTING NUCLEAR VOLUME

In the present discussion quantities obtained by setting $M=\infty$ will be denoted by the subscript 0; the radial functions corresponding to F', G' by f', g' in the same sense as in Eq. (7.2) for f, g. One is concerned with the value of

$$-I=\int_0^\infty fgdr \Big/ \int_0^\infty (f^2+g^2)r^2dr \tag{9}$$

which is the most important factor in the usual formula for hyperfine splitting which depends on m/M. In terms of the primed quantities one has

$$I=-qp^{-2}\int_0^\infty f'g'dr' \Big/ \int_0^\infty (g'^2+q^2f'^2)r'^2dr' \tag{9.1}$$

where

$$q=(A/B)^{\frac{1}{2}}, \quad p=1/(AB)^{\frac{1}{2}} \tag{9.2}$$

are the factors brought in by the transformations of f and r respectively. Taking into account that for the ground term

$$f_0^2/g_0^2\cong\alpha^2/4 \tag{9.3}$$

and that $q^2f'^2$ is the same as f'^2 within terms of order m/M one has to a sufficient approximation

$$I=-qp^{-2}[1-(1-q^2)(\alpha^2/4)]^{-1} \times\int_0^\infty f'g'dr' \Big/ \int_0^\infty (f'^2+g'^2)r'^2dr'. \tag{9.4}$$

In the last formula there are three correction factors which multiply the ratio of two integrals. The latter ratio is identical in form with that for the value of I without nuclear mass motion. It differs from it, however, on account of the replacement of the unprimed quantities by primed ones. Without nuclear mass motion the value of I is[11]

$$I_0=\alpha(2\rho^2-\rho)^{-1}a_H^{-2}; \quad \rho=(1-\alpha^2)^{\frac{1}{2}} \tag{9.5}$$

where a_H is the Bohr radius. Within relative order α^2 it follows that

$$I_0=\alpha(1+3\alpha^2/2)a_H^{-2}. \tag{9.5′}$$

Taking into account the occurrence of e in α and a_H there results from Eqs. (9.4), (9.5′) together with the transformation formulas (7.6), (9.2) that

$$I/I_0=1-3m/M+0\cdot\alpha^2m/M+\cdots. \tag{9.6}$$

At this stage of the calculation the corrections of order α^2m/M have disappeared and the mass correction to the hyperfine structure for the Dirac part of the proton's moment is expressed by the factor $1-3m/M$.

The contribution to hyperfine structure arising from the difference between $1-(J/2Mc^2)$ and unity in Eq. (5.4) has been neglected so far. The term in $-J/2Mc^2$ gives rise to an integral in the first-order perturbation energy which diverges as $\int\exp[(-1-\alpha^2)\ln r]dr$ and this term cannot be treated in the usual manner. The function J should be considered, however, as being finite everywhere for otherwise the justification for Eq. (1) breaks down. It is probable, furthermore, that at distances smaller than $\sim e^2/mc^2$ the field of the proton deviates from the inverse square law and that the whole method of treatment loses meaning on account of the presence of mesons. It would be unreasonable to attach much meaning to the divergence just mentioned since it disappears if one makes J finite by rounding off the $1/r$-type potential. The exact way in which it should be rounded off is subject to question. Speculatively it will be supposed that J has the constant value e^2/b from $r=0$ to $r=b$ and that for $r>b$ the value e^2/r applies. The ratio of the extra effect to the regular effect is

$$\text{extra effect/regular effect}\cong-(e^2/2Mc^2a_H) \times\int_b^\infty r^{-1}\exp(-2r)dr \Big/ \int_0^\infty \exp(-2r)dr \tag{10}$$

where r is expressed in units a_H and the relativistic radial functions are replaced by their non-relativistic values with sufficient accuracy. The above ratio is expressible in terms of the Ei integral and can be approximated by

$$-(m/M)\alpha^2[\ln(1/2b''\alpha^2)-0.577\cdots] \tag{10.1}$$

where b'' is the value of b in units e^2/mc^2 and where terms containing additional factors α have been neglected.

Since dJ/dr vanishes in the cut off region the hyperfine structure splitting is smaller than it would be without cutting off J even if m/M is not considered. The correction factor introduced by this effect is approximately

$$\int_b^\infty e^{-2r}dr \Big/ \int_0^\infty e^{-2r}dr\cong 1-2b=1-2b''\alpha^2$$

[11] G. Breit, Phys. Rev. **35**, 1447 (1930).

where b is in Bohr radii. Since the mass correction corresponds approximately to multiplication by $1-3m/M$ one can expect an additional effect of approximate value $6b''\alpha^2 m/M$ which has its origin in the combined action of changes of relative order α^2 produced by a finite nuclear radius and of the mass effect. Such changes cannot be treated with certainty because the nuclear radius is not understood in a precise sense. Effects of order $(m/M)\alpha^2$ as well as that described by Eqs. (10), (10.1) are much too small to be detected with the accuracy reported in the experiments.

The Hamiltonian employed here is only approximately relativistic. The function J cannot be made too large and the introduction of a proton radius is, therefore, unavoidable in the present approach. The uncertainties in the answer which are a consequence of the arbitrariness in the value of the radius b and the shape of $J(r)$ are thus an inherent limitation of the method. Similar uncertainties arise from the fact that for a finite nuclear radius the transformation to Eqs. (7.6′) can be made only in the region $r>b$. These effects can be discussed properly only if one takes into account the change in the wave function brought about by the finite rather than zero value of b. The expectation value of the hyperfine structure energy Q'' when calculated with such an improved wave function contains additional corrections of relative order $m\alpha^2/M$. These corrections are worked out in the adjoining paper[12] by G. E. Brown and G. B. Arfken.

There is an additional effect of the terms in $(\hbar/2Mc)\times(rdJ/dr)(d/dr)$ in Eq. (7.5) which also brings in b explicitly. This effect is similar to that in Eq. (10.1). It also depends on b logarithmically and becomes infinite for zero nuclear radius. The terms in ΔJ contained in Eq. (7.5) produce in general effects of relative order $m\alpha^2/M$. For the special case of J being constant in the interval $0<r<b$ their effect is of a higher order in α as is shown in the adjoining paper.[12] Their evaluation does not depend on the effect of the cut-off of the Coulomb potential on the wave function but it proved easier to present the matter in this order. The evaluation of the effect of terms involving dJ/dr in Eq. (7.5) will now be described. The functions F, G are represented as $(1+u)F_0$, $(1+v)G_0$ where F_0, G_0 are solutions of Eq. (7.5) in the absence of the terms under consideration. Substitution into Eq. (7.5) then shows that regularity of F and G at $r=\infty$ requires

$$u=v=K+(\alpha^2\beta/2)(-\rho/r-\ln r) \tag{11}$$

where $\beta=m/M$, $\rho=(1-\alpha^2)^{\frac{1}{2}}$ and where the unit of length is $\hbar^2/me^2$. The constant of integration remains undetermined at this stage. Since the effect of $u-K=v-K$ on F and G can be represented by the correction factor $\exp(u-K)$ to within the relative order $\alpha^2\beta$, the effect of K amounts to employing $(1+K)F_0$, $(1+K)G_0$ in place of F_0, G_0. This effect cannot be distinguished, therefore, from the determination of the normalization factor. The correction factor to the hyperfine structure is thus found to be

$$1+\delta \tag{11.1}$$

where

$$\delta=\delta_1+\delta_2 \tag{11.2}$$

and

$$\delta_1=-\alpha^2\beta[\ln b-3Ei(-2b)], \tag{11.3}$$

$$\delta_2=\alpha^2\beta[\ln b+(5/2)-Ei(-2b)]. \tag{11.4}$$

The contributions δ_1, δ_2 arise from the inclusion of the factors $\exp(u-K)$ in the integrals of FG/r^2 and F^2+G^2 respectively. The first of these integrals arises from Q'', the second on account of normalization. Combining the two contributions

$$\delta=\alpha^2\beta[(5/2)+2Ei(-2b)]\cong\alpha^2\beta[(5/2)-2\ln(1/2b\gamma)] \tag{11.5}$$

where $\ln\gamma=0.577\cdots$. Combining with Eq. (10.1) the correction factor for both effects is

$$1+\epsilon \tag{12}$$

where

$$\epsilon=\alpha^2\beta[(5/2)-3\ln(1/2b''\alpha^2\gamma)]. \tag{12.1}$$

The correctness of the argument for the elimination of K has been verified by the extension of the phase amplitude perturbation method to Dirac's equation.[13] For $b''=1$ the value of ϵ is 7×10^{-7} which is negligible in comparison with experimental errors and is of the same order as the effects in $\beta^2=(m/M)^2$ which have been neglected here.

It appears from the considerations presented that the "approximately relativistic" equation considered here gives a result which for practical purposes is the same as that of Breit and Meyerott.[1] It is desirable to emphasize again that neither treatment is free from ambiguities. There is a difference between the method of Eqs. (4), (4.1), (4.2), (4.3) and the method of Eqs. (5), (5.4) which has been adopted here. A complete treatment of the problem requires a more consistent application of electrodynamics than that attempted here.

It should also be mentioned that the transformation of Eqs. (7.6), (7.6′) is not closely related to the stretching of the wave function which corresponds to the introduction of the reduced mass in the non-relativistic problem. The charge is not transformed in the latter. It is possible to employ the ordinary reduced mass transformation but the classification of effects does not appear as clearly as by means of Eq. (7.6′).

[12] G. E. Brown and G. B. Arfken, Phys. Rev. **76**, 1305 (1949).

[13] G. Breit and G. E. Brown, Phys. Rev. **76**, 1307 (1949).

Effects of the Proton Radius on Nuclear Motion Correction for the Hyperfine Structure of Hydrogen*

G. E. Brown and G. B. Arfken
Yale University, New Haven, Connecticut
(Received July 18, 1949)

Contributions to the hyperfine structure of the ground state of hydrogen resulting from the assumption of a non-vanishing proton radius are evaluated in this paper. These effects occur because of the assumed modification of the Coulomb potential inside the proton and the consequent change in the wave function the above assumption implies. Since the proton radius and the shape of the potential function in the interior are not known, there occur uncertainties of relative order $\alpha^2 m/M$ in the hyperfine structure arising from nuclear mass motion.

I. INTRODUCTION

THE transformation[1] (I, 7.6) brings the Eqs. (I, 7.5), with neglect of the terms in $\hbar/Mc$, to the form of radial equations for a Dirac electron in a Coulomb field, and allows calculation of the effects of the mass motion terms if the assumption is made that the potential in Eq. (I, 7.5) is Coulombian. This potential is modified inside the proton if one assumes a non-vanishing proton radius,[1] however, and there result effects the evaluation of which is the object of this note. The potential function in the interior of the proton is assumed to have the constant value $J=e^2/b$, corresponding to the potential of a charged shell of radius b. This modification of the Coulomb potential is an admittedly arbitrary one. It has advantages of simplicity, however. Since it is the change in the wave functions and the approximate values of the quantities dJ/dr, ΔJ that are of primary importance, it is believed that the results of the calculations give the correct order of magnitude of the effects under consideration. The details of the way in which the potential energy curve is rounded off are believed to be immaterial provided the curve is nearly smooth and reproduces approximately the values used below. The change in the wave function produced by the change of the potential from the Coulombian is considered below. It will be seen that this effect combines with the effects of nuclear mass motion to change the hyperfine structure splitting to relative order $\alpha^2 m/M$.

II. CALCULATIONS AND CONCLUSIONS

Effects of the modification of the Coulomb potential inside the proton will now be considered. The potential function J is assumed to have the constant value e^2/b inside this region as discussed in the preceding section. Consequently the quantity dJ/dr vanishes in the nuclear interior and the integral which arises in the calculation of the hyperfine structure splitting through the evaluation of $<Q''>$ of the preceding paper[1] has the limits $r=b$ and ∞. This effect of the exclusion of the region $0<r<b$ from the hyperfine structure integral, just referred to, has been discussed in Section V of I.

There is now a second effect to be considered. From the modification of the potential in the interior there results a change of order α^2 in the wave function in the exterior region $r>b$ and the hyperfine structure integral is changed also.

Effects of relative order α^2 and $\alpha^2 m/M$ result from both of the above causes. Only the latter type is concerned with nuclear mass motion and its evaluation will now be made.

In order to obtain the change in the wave function for $r>b$, one first considers the wave function inside the nucleus. For $r<b$, the modified potential $J=e^2/b$ is transformed by Eq. (I, 7.6) into $J'=e'^2/(AB)^{\frac{1}{2}}b$, to replace e'^2/r' in Eq. (I, 7.6′). Equations (I, 7.6′) take the form

$$\begin{aligned}(W+1+J')F'-(1/\alpha')\Omega_+'G'=0,\\ (W-1+J')G'+(1/\alpha')\Omega_-'F'=0\end{aligned} \tag{1}$$

with

$$\alpha'=e'^2/\hbar c \tag{1.1}$$

and with the other quantities defined by Eqs. (I, 7.2), (I, 7.6). Here energies are expressed in units mc^2 and lengths in e'^2/mc^2. For the ground state of hydrogen the Dirac quantum number k appearing in the Ω's, which are defined by Eq. (I, 7.2), has the value -1. On elimination of F' from Eqs. (1), one obtains

$$d^2G'/dr'^2+\kappa^2G'=0 \tag{1.2}$$

where

$$\kappa=\alpha'[(W+J')^2-1]^{\frac{1}{2}} \tag{1.3}$$

giving $G'=\sin\kappa r'$. The function F' may be obtained from the first of the two Eqs. (1). The ratio of the functions is

$$F'/G'\cong-(1/3)\alpha'(W+J'-1)r'\cong-(1/3)\alpha'J'r' \tag{2}$$

where the second approximate equality holds because $W\cong 1$ in mc^2 units. The ratio F/G has to vary continuously at the nuclear radius $r=b$ as a general property of Dirac's equation. The value of F'/G' for $r=b-0$ is the same as for $r=b+0$ and will be used below to determine the solution for $r>b$. For the special case of the spherical shell distribution the right side of Eq. (2) simplifies to

$$F'/G'\cong-(1/3)\alpha'. \tag{2.1}$$

* Assisted by the Joint Program of the ONR and the AEC.
[1] Breit, Brown, and Arfken, Phys. Rev. **76**, 1299 (1949). This paper will be referred to as I in the text. Formulas occurring in this paper will be referred to by prefixing the Roman numeral I ahead of the number of the formula.

By a method discussed in III,[2] the difference between this ratio and the ratio of solutions F_0'/G_0' obtained using $J'=e'^2/r$, which follows from a Coulomb potential in Eq. (I, 7.5), can be used to calculate changes in the wave function for $r>b$ produced by the cut-off of the Coulomb potential. Employing a notation similar to that of III one obtains

$$y'=F'/G', \quad y_0'=F_0'/G_0', \quad \delta y'=y'-y_0'. \tag{2.2}$$

The quantity y_0' is easily found since equations for F_0' and G_0' take the form of Dirac equations for an electron in a Coulomb field. The known solutions of these yield $y_0'=-\alpha'/2$. The cut-off, therefore, produces a change in y which when evaluated at the proton radius is

$$\delta y'=y'-y_0'\cong\alpha'/6. \tag{2.3}$$

For $r>b$ the same equations hold for F', G' as for F_0', G_0' and one can find $\delta y'$ in this region by employing Eq. (III, 3.1). Equation (III, 3.1) becomes

$$(d/dr')(G_0'^2\delta y')+(F_0'^2+G_0'^2)\delta W/\alpha'=0 \tag{2.4}$$

with energy in units mc^2 and lengths in $a_H'=\hbar^2/me'^2$. The primes in this formula as in Eqs. (1) and following denote quantities transformed by Eqs. (I, 7.6). On integration from the proton radius b to infinity one finds δW, the change in energy produced by the cut-off, to be of order $\alpha^4 Ry$ and hence negligible. Employing Eq. (2.4) and the known value of δy at $r=b$, one finds

$$\delta y'\cong(\alpha'/6)b'^2\alpha'^4(1/r'^2+2/r'+2). \tag{3}$$

Here b' is the value of r' at the proton radius[3] in units e'^2/mc^2. The integral of interest for the hyperfine structure is

$$-I'=\int f'g'dr'\cong\int y_0'g_0'^2(1+\delta y'/y_0')dr' + \int 2g_0'y_0'\delta g'dr' \tag{3.1}$$

where f' and g' are given by $r'f'=F'$, $r'g'=G'$. The first integral on the right of the approximate equality sign is

$$[1-(8/3)b'\alpha'^2]I_0=[1-(8/3)b'\alpha^2(1-m/M)]I_0$$

where

$$-I_0=\int_0^\infty f_0'g_0'dr',$$

the hyperfine structure integral without cut-off. The second integral is of order $\alpha^4 I_0$ and will be neglected.

The term in α^2 in the above factor multiplying I_0 includes the effect of the exclusion of the region $0<r<b$ from the integral and the effect of the cut-off on the wave functions exterior to the proton. The term in $\alpha^2 m/M$ arises from the combination of both of these effects with mass motion effects. Because the proton radius and the shape of the interior potential are not known, uncertainties in the mass correction to the hyperfine structure of this latter order $\alpha^2 m/M$ occur.

The terms in ΔJ in Eqs. (I, 7.5) must also be considered, although it will be shown that their effect is negligible for the particular J assumed here. Equations (I, 7.5) relating unprimed quantities are employed to describe the behavior of the wave functions through the charged shell of radius b, which is taken to be the limit of a shell of finite thickness. Only terms in ΔJ, dG/dr and dF/dr are large in this transition region. Consequently, the first of Eqs. (I, 7.5) becomes

$$[1+r(dJ/dr)/2Mc^2]dG/dr+(rG\Delta J)/4Mc^2=0 \tag{4}$$

with the same equation holding for F. This yields with neglect of terms in $(m/M)^2$,

$$G_{(b-0)}\cong G_{(b+0)}\exp\left\{(1/4Mc^2)\int_{(b-0)}^{(b+0)} r\Delta J dr\right\} \cong G_{(b+0)}(1-m/4Mb'') \tag{4.1}$$

where b'' is the value of b in units e^2/mc^2 as in I. The functions for $r>b$ can be taken to be the same as before the introduction of the charged shell, since the change in normalization caused by the decrease in the functions in the interior is found to be negligible. Consequently, the only effect of the transition region is to diminish F and G inside the proton. This region is excluded from the hyperfine structure integral I for that special case of a constant J as discussed above and therefore the transition region does not have an appreciable effect on the hyperfine structure.

If one assumes a potential which is not constant in the region $0<r<b$, however, the quantity dJ/dr is not zero there and the hyperfine structure integral will include this region. In this case, the transition region contributes effects of order $\alpha^2 m/M$ since the wave functions are decreased in order m/M over a region of order α^2 of the important range of integration.

ACKNOWLEDGMENTS

The authors would like to acknowledge their indebtedness to Professor Breit for his preliminary work, which provided the methods used in this note, and their appreciation for helpful discussions throughout the work.

[2] G. Breit and G. E. Brown, Phys. Rev. **76**, 1307 (1949). This paper will be referred to as III in the text. Formulas occurring in this paper will be referred to by prefixing the Roman numeral III ahead of the number of the formula.

[3] The quantity b' does not correspond to b of the preceding paper in a manner strictly adhering to the relations of the other primed quantities in this note to the unprimed ones in I. In I, b is expressed in units a_H whereas b'' is its value in e^2/mc^2 and corresponds to the b' of the present paper.

Perturbation Methods for Dirac Radial Equations*

G. Breit and G. E. Brown
Yale University, New Haven, Connecticut
(Received July 18, 1949)

Two methods of calculating perturbation effects for the Dirac electron equation are discussed. The two radial functions enter symmetrically in the main contributions to the effects calculated. The first method is related to the method of the Riccati equation for ordinary second-order differential equations but differs from it through the use of the ratio of the two radial functions rather than that of the logarithmic derivative of one of them. The second method has some similarity to Milne's phase amplitude method. The methods described have been helpful in the two preceding papers.

I. INTRODUCTION[1,2]

THE Schrödinger single particle wave equation can often be conveniently treated by introducing the logarithmic derivative of the radial wave function. Perturbation calculations can at times be made very conveniently by this method. Useful results for nuclear scattering theory[3,4] and for the JWKB method have been obtained in this manner. The general plan is as follows. The linear second-order equation is transformed into a non-linear first-order equation of the Riccati type, the dependent variable being the logarithmic derivative. Perturbation calculations can then be made conveniently. A special advantage of this method is that an estimate of the effect of an inaccuracy can be made by a simple quadrature. For the Dirac equation in a central field one deals with two simultaneous radial equations which connect the two radial functions. One of these functions can be eliminated and there results an ordinary second-order differential equation which can be dealt with in the same general way as in the Schrödinger case. Such a procedure has been used[5] and is feasible. It has certain disadvantages, however. In the first place the second-order differential equation for a Dirac radial function has to be reduced to a standard form by a transformation. Secondly the physically important radial functions are lost track of in the manipulations. It is clear on the other hand that the Rayleigh-Schrödinger perturbation calculus can be applied to this problem, that in general the perturbation Hamiltonian can then be represented by two-row square matrices with operators for elements and that the two radial functions enter explicitly in the calculations. It is a disadvantage of the method of elimination of one of the radial functions that expressions obtainable from it are not simply related to those of the Rayleigh-Schrödinger perturbation calculus. It will be shown below that equations of a simpler and more practical form can be obtained by a different choice of the dependent variable. Two methods will be described. In the first the variable $y=f/g$ will be used. Here f, g are the two radial functions in a rather usual choice of the Dirac matrices which will become directly obvious through the formulas below. The employment of the variable y yields convenient results whenever the change in y caused by the perturbation, which is here called δy, does not become too large in the region of distances r for which the calculation is made. Experience with a similar equation for the Schrödinger case[4] has shown that analytic approximations can be improved by employing step by step numerical constructions for taking into account non-linear terms in δy. The method requires special consideration close to a node of g, a case which arises often and leads to an infinite δy. In order to have available a treatment in which infinities do not occur a second perturbation method has been worked out and is reported on also. This is suggested by Milne's phase amplitude method for the Schrödinger equation.[6] The amplitude A is here $r(f^2+g^2)^{\frac{1}{2}}$ and the phase φ is introduced by $\tan\varphi=f/g$. The direct application of Milne's method would bring in variables different from those used here. The equations reported on have been found useful in the two preceding papers.[1,2]

The feature which is especially convenient in both phase amplitude methods is the replacement of oscillatory functions by the monotonic φ and the smoothly varying A.

II. THE LOGARITHMIC DERIVATIVE METHOD

The radial equations can be written in the form

$$\{\|\epsilon_{ij}\|(d/idr)+\|P_{ij}\|\}\chi=0, \quad (i=1,2;j=1,2) \quad (1)$$

where χ is a column matrix with two rows. The two matrix elements of χ are denoted by

$$\chi_1=F=rf, \quad \chi_2=G=rg \quad (1.1)$$

and the normalization integral is

$$\int_0^\infty (\chi_1^2+\chi_2^2)dr=1. \quad (1.2)$$

* Assisted by the Joint Program of the ONR and the AEC.
[1] The methods described in this paper have been helpful in Breit, Brown, and Arfken, Phys. Rev. 76, 1299 (1949).
[2] The methods described in this paper have been helpful in G. E. Brown and G. B. Arfken, Phys. Rev. 76, 1305 (1949).
[3] Breit, Thaxton, and Eisenbud, Phys. Rev. 55, 1018 (1939).
[4] The possibilities of step by step numerical constructions of perturbation effects by means of the Riccati equation have been successfully tried out by M. H. Hull at the suggestion of one of the writers in connection with the calculation of Coulomb functions.
[5] G. Breit and R. E. Meyerott, Phys. Rev. 72, 1023 (1947).
[6] W. E. Milne, Phys. Rev. 35, 863 (1930).

The relation of the other symbols in Eq. (1) to the scalar potential A_0, the electronic charge and mass $-e$, m is

$$\|P_{ij}\|=(E+eA_0+mc^2\rho_3)/\hbar c+ik\epsilon\rho_3/r, \quad (1.3)$$

in the notation of Dirac.[7] The quantum number k is the characteristic value of

$$\rho_3[(\mathbf{L}\sigma)+1],$$

while

$$\epsilon=\|\epsilon_{ij}\|=\rho_1(\sigma\mathbf{r})/r. \quad (1.4)$$

The matrices ρ_3 and ϵ/i are taken in the representation

$$\rho_3=\begin{pmatrix}1, & 0\\ 0, & -1\end{pmatrix}, \quad \epsilon/i=\begin{pmatrix}0, & -1\\ 1, & 0\end{pmatrix}. \quad (1.5)$$

Employing the abbreviation $p_0=(E+eA_0)/c$ the matrix elements of $\|P_{ij}\|$ are

$$P_{11}=(p_0+mc)/\hbar, \quad P_{12}=P_{21}=-k/r, \quad P_{22}=(p_0-mc)/\hbar. \quad (1.6)$$

The definitions made above describe the connection with standard theory. Changes in A_0 are seen to affect only the diagonal elements P_{11}, P_{22}. For the treatment of problems in which perturbation effects of the central potential are needed it suffices to consider the special case of a diagonal perturbation matrix

$$\|\delta P_{ij}\|=\|P_{ij}\|-\|P_{ij}{}^0\| \quad (1.7)$$

with c numbers as the perturbing elements.

In the problem of nuclear mass motion[1,2,5] and in other questions[8] there occur more general changes of the δP_{ij}. The calculations below will be made in part without any restriction on the δP_{ij} and in part with the specialization of all the δP_{ij} being c numbers. In the latter case the restrictions $\delta P_{12}=\delta P_{21}$, $P_{ij}=P_{ij}{}^*$ will be used. The functions F, G will be supposed real throughout.

Extensions of the general formulas to complex P_{ij} are obvious. The simplicity of reductions in the special case, just mentioned, seems to be lost, however, when extensions to complex χ_i are made. It may be noted that if the equations are not reducible to real χ_i, $y=F/G$ contains two functions rather than one and the application of the methods under discussion is necessarily more involved. It will be recalled that if the P_{ij} are c numbers then the Hermitian requirement for $\|P_{ij}\|$ is

$$\int_0^\infty \Sigma P_{ij}{}^*\chi_j{}^*\chi_i dr=\int_0^\infty \Sigma P_{ij}\chi_i{}^*\chi_j dr$$

and this can be satisfied for arbitrary χ_i, χ_j only if $P_{ij}{}^*=P_{ji}$. This condition reduces to $P_{ij}=P_{ji}$ if all the quantities are real. Only symmetric matrices $\|P_{ij}\|$ are, therefore, considered below. For differential operators P_{12} the requirement of symmetry cannot be used. An example is the Hermitian operator $(\epsilon/i)(d/dr)$.

It will now be supposed that there is available a solution of Eq. (1) for some set of values of the P_{ij} given by Eqs. (1.3), (1.6) with a suitable choice of the scalar potential. The quantities corresponding to this solution will be referred to as unperturbed quantities. The unperturbed matrix will be denoted by

$$\|P_{ij}{}^0\|\equiv\|p_{ij}\|. \quad (2)$$

The perturbed function satisfies Eq. (1) with a different set of matrix elements. The relation between the two sets of elements will be taken as in Eq. (1.7). Introducing

$$y=F/G, \quad y_0=F_0/G_0, \quad \delta y=y-y_0 \quad (2.1)$$

with the convention of denoting unperturbed quantities by subscripts or superscripts 0, one obtains

$$d(\delta y)/dr\equiv -G^{-2}\Sigma\chi_i(\delta P_{ij})\chi_j +\Sigma p_{ij}(G_0{}^{-2}\chi_i{}^0\chi_j{}^0-G^{-2}\chi_i\chi_j). \quad (2.2)$$

Here and below it will be understood that the summations are performed over both i and j. By straightforward calculation one can remove first-order effects from the right side of the above formula with the result

$$d(G_0{}^2\delta y)/dr=-(G_0{}^2/G^2)\Sigma\chi_i(\delta P_{ij})\chi_j-G_0{}^2p_{11}(\delta y)^2. \quad (3)$$

The last term on the right side is of the second order in the small quantity δy. The main effects are contained in the first term. To the first order of small quantities one has the approximation

$$d(G_0{}^2\delta y)/dr\cong-\Sigma\chi_i{}^0(\delta P_{ij})\chi_j{}^0. \quad (3.1)$$

If the boundary conditions are such that $G_0{}^2\delta y$ vanishes at $r=0$ and $r=\infty$ this formula implies with neglect of higher order effects,

$$\int_0^\infty \Sigma\chi_i{}^0(\delta P_{ij})\chi_j{}^0 dr=0 \quad (3.2)$$

which gives the Rayleigh-Schrödinger first-order perturbation formula for the energy. Account has to be taken of the fact that, in general, Eq. (3.2) cannot be satisfied unless E is changed from its unperturbed value.

By integration of Eq. (3.1) one obtains δy to the first order within an interval $r_1<r<r_2$ provided δy is known either at r_1 or r_2 and provided the nodes of G and G_0 do not interfere with the calculation. Having δy to the first order one also has first-order corrections to F and G because Eq. (1) gives

$$d(\delta G)/dr=[\delta(P_{11}y+P_{12})]G+(p_{11}y_0+p_{12})\delta G \quad (3.3)$$

so that $\delta G=G-G_0$ is determined for known $\delta(P_{11}y+P_{12})$ and G as the solution of an ordinary linear inhomogeneous differential equation. Similarly δF is determined by Eq. (1). An iteration procedure for the solution of Eq.

[7] P. A. M. Dirac, Proc. Roy. Soc. A117, 611 (1928).

[8] The method outlined proved useful in unpublished calculations made by one of the authors (G.B.) on the distortion of the electronic wave functions produced by the nuclear magnetic moment.

(1) is thus possible, in the general case. It has practical value only if the convergence is rapid.

In the special case of $P_{12}=P_{21}$ and of c numbers for the P_{ij} the consideration of δF and δG can be avoided. One finds in this case

$$-d(G_0^2\delta y)/dr=G_0^2(y^2\delta P_{11}+2y\delta P_{12}+\delta P_{22}) +G_0^2p_{11}(\delta y)^2=\Sigma\chi_i^0(\delta P_{ij})\chi_j^0+2G_0(F_0\delta P_{11} +G_0\delta P_{12})\delta y+G_0^2P_{11}(\delta y)^2. \quad (3.4)$$

In the latter form there are only known functions multiplying the unknown δy. The second and third terms are of second order of small quantities. The term $P_{11}(\delta y)^2$ contains the third-order effect $(\delta P_{11})(\delta y)^2$, since $P_{11}=p_{11}+\delta P_{11}$. The error committed by neglecting them can be readily estimated and either an iteration procedure or a numerical step by step construction is relatively simple. In this case the knowledge of y gives G and F directly from Eq. (1) because

$$dG/Gdr=P_{11}y+P_{12} \quad (3.5)$$

so that G is obtainable by a quadrature.

If the δP_{ij} are differential operators it is also possible to perform reductions similar to that of Eq. (3.4). The differentiations on the χ_i which occur in Eq. (3) bring in either dG/dr which is expressible as $P_{11}yG+P_{12}G$, which in turn contains dG/dr, dy/dr, y, G. The relation thus obtained can be solved for dG/dr resulting in an expression for dG/Gdr in y and dy/dr. Since $dF/Fdr=dy/ydr+dG/Gdr$ one is also able to deal with dF/Fdr. The iteration via F and G discussed in connection with Eq. (3.3) is thus not a necessary step and is only one of several possibilities.[9]

III. THE PHASE-AMPLITUDE METHOD

In order to avoid special considerations at the poles of y equations somewhat similar to those of the phase amplitude method of Milne have been worked out. The defining relations are

$$F=A\mathbf{s}, \quad G=A\mathbf{c}, \quad \mathbf{s}=\sin\varphi, \quad \mathbf{c}=\cos\varphi. \quad (4)$$

The quantities φ and A will be referred to as phase and amplitude respectively. The equations on A and φ can be put in various forms having their respective advantages. The forms listed below have been decided on with the view of classifying effects according to different orders of smallness. The relations between A and φ can be put in the form

$$\begin{aligned} -Ad\varphi/dr&=\Sigma u_iP_{ij}u_jA, \\ dA/dr&\equiv\Sigma u_iR_{ij}u_jA, \end{aligned} \quad (4.1)$$

with

$$u_1\equiv\mathbf{s}, \quad u_2=\mathbf{c} \quad (4.2)$$

and

$$\|R_{ij}\|=\begin{pmatrix} -P_{21}, & -P_{22} \\ P_{11}, & P_{12} \end{pmatrix}. \quad (4.3)$$

Adhering to the previously introduced meaning of superscript and subscript 0 as well as the symbol δ for difference between perturbed and unperturbed quantities one finds

$$-d(\delta\varphi)/dr=A^{-2}\Sigma\chi_i(\delta P_{ij})\chi_j +2Q_2'^0\delta_1-Q_1'^0\delta_2-Q_2'^0\delta_3, \quad (4.4)$$

where

$$\delta_1=\delta\varphi, \quad \delta_2=1-\cos2\delta_1, \quad \delta_3=2\delta_1-\sin2\delta_1, \quad (4.5)$$

$$Q_1'=Q_1\mathbf{C}_0+Q_2\mathbf{S}_0, \quad Q_2'=-Q_1\mathbf{S}_0+Q_2\mathbf{C}_0, \quad (4.6)$$

$$\mathbf{C}=\cos2\varphi, \quad \mathbf{S}=\sin2\varphi \quad (4.7)$$

and the superscript ^{0} on the Q' indicates that the quantities Q in Eq. (4.6) take the values Q^0. The Q are as follows

$$Q_1=(P_{22}-P_{11})/2, \quad Q_2=(P_{12}+P_{21})/2. \quad (4.8)$$

The notation

$$P=(P_{11}+P_{22})/2 \quad (4.9)$$

will also be used.

The quantities Q_i' are connected with the Q_i by an orthogonal transformation. The latter has coefficients which are determined by the known value φ_0 of φ in the zeroth approximation. The value of φ_0 does not change during the improvement of values of $\delta\varphi$. The orthogonal transformation can be conveniently remembered as corresponding to a rotation through an angle $2\varphi_0$. Removal of first-order terms on the right side of Eq. (4.4) gives

$$-A_0^{-2}d(A_0^2\delta\varphi)/dr =A^{-2}\Sigma\chi_i(\delta P_{ij})\chi_j-Q_1'^0\delta_2-Q_2'^0\delta_3 \quad (5)$$

which is analogous to Eq. (3). The quantities δ_2, δ_3 are of second and third order respectively. The first term on the right side of Eq. (5) is seen to be the main one for small perturbations. It does not become infinite at a node of G and is more convenient in this respect than the first term on the right side of Eq. (3). Iteration procedures for Eq. (5) are similar to those for Eq. (3). The special case which was considered for Eq. (3.4) leads to the following form

$$-A_0^{-2}d(A_0^2\delta\varphi)/dr=\delta P+\delta Q_1' +2(\delta Q_2')\delta_1-Q_1'\delta_2-Q_2'\delta_3. \quad (5.1)$$

On the right side of this equation the quantities Q' are completely known and the δ_j are definitely determined by $\delta\varphi$. For a sufficiently small $\delta\varphi$ the δ_j can be approximated by one or two terms of the power series in δ_1, which represent them. Iteration or step by step constructions are again practical.

It is clear from Eq. (4.1) that in a calculation of δA the matrix $\|R_{ij}\|$ plays a part similar to that of P in the calculation of $\delta\varphi$. Replacement of the P_{ij} by the R_{ij}

[9] Another possibility for treating higher order effects is the expansion of δy in a power series similar to that discussed by Breit, Thaxton, and Eisenbud (see reference 3) for the Schrödinger equation. Coefficients of the terms in this series are given by relations similar to Eqs. (9.1) of reference 3.

changes P into $(P_{12}-P_{21})/2$, Q_1 into Q_2, Q_2 into $-Q_1$, Q_1' into Q_2', Q_2' into $-Q_1'$. These relations will be helpful to those who wish to verify the calculations. It is found that

$$d(\delta \ln A)/dr = A^{-2}\Sigma\chi_i(\delta R_{ij})\chi_j - 2Q_1'^0\delta_1 - Q_2'^0\delta_2 + Q_1'^0\delta_3 \quad (6)$$

and for the special case of c numbers for the P_{ij} the corresponding formula is

$$d(\delta \ln A)/dr = \delta Q_2' - 2Q_1'\delta_1 - Q_2'\delta_2 + Q_1'\delta_3. \quad (6.1)$$

The calculation of changes in the amplitude A is thus reducible to the evaluation of simple expressions.

PHYSICAL REVIEW VOLUME 76, NUMBER 9 NOVEMBER 1, 1949

Electron-Nuclear Potential Fields from Hyperfine Structure

M. F. CRAWFORD AND A. L. SCHAWLOW
McLennan Laboratory, University of Toronto, Toronto, Canada

(Received July 26, 1949)

Theoretical predictions for the effects of nuclear size on hyperfine structure are compared with experimental data. New data show that isotope shifts of *ns* levels in Tl III are proportional to $\psi^2(0)$ as predicted. The fractional change in nuclear radius for the addition of two neutrons, determined from *s* electron shifts in Hg II, Tl III, Pb IV, is the same for the three elements. Köhler's results for Tl II are consistent with those for Tl III when allowance is made for the mutual screening of the valence electrons.

Corrections for the approximation of the perturbation method and for screening of inner electrons by the valence electron are considered and found to be appreciable. Even after applying the corrections, the fractional change in nuclear radius is smaller than expected if the charge is uniformly distributed throughout the nucleus and the volume is proportional to the mass.

Values of nuclear magnetic moments of thallium deduced from hyperfine structure measurements are compared with those measured by radiofrequency induction and found to be 15 percent lower. This discrepancy is removed by the correction for finite nuclear size assuming either a uniform charge distribution or a concentration of charge toward the surface of the nucleus. Thus both the isotope shift and the magnetic effect indicate that the electron-nuclear potential is consistent with a charge distribution of this form and that the non-electrical forces between electrons and nuclei are relatively small.

1. INTRODUCTION

A RELATIVISTIC theory of the effects of finite nuclear size, with a consequent departure from a Coulomb field, on the atomic energy levels has been formulated by Rosenthal and Breit[1,2] and Racah.[3] The first two authors have also considered the effect of a finite nucleus on the interaction between electrons and the nuclear magnetic moment. The first effect leads to an isotope shift, and the second to a correction for the nuclear magnetic moment deduced from hyperfine structure splittings. Previous comparisons[2,4,5] of the theory with experimental data on isotope shifts agreed only as to order of magnitude; in general, the theoretical and observed values differed by a factor of the order of three. In many of these cases the comparison was complicated by the mutual screening of several electrons outside closed shells and by inter-configuration perturbations. It is therefore desirable to consider unperturbed levels arising from one-electron configurations, preferably those of penetrating *s* electrons. Such configurations occur in the Hg II, Tl III, Pb IV sequence and their isotope shifts are analyzed here.

The analysis shows that significant information about electron-nuclear potential fields can be obtained from the absolute magnitude of the shifts. The corrections for the approximations in the perturbation method and for the screening of electrons in completed shells are found to be important.

Hitherto the effect of nuclear radius on the magnetic interaction between electrons and the nuclear spin has not been confirmed experimentally. Evidence confirming this effect is presented. Both the isotope shifts and the magnetic effect are more consistent with a uniform charge distribution in the nucleus than with a well-type potential for the electron-nuclear interaction.

2. ISOTOPE SHIFT

The isotope shift for a single *s* electron as derived by Rosenthal and Breit[1] using the perturbation method is

$$\Delta\delta W = \frac{4\pi R a_H^3 \psi^2(0)}{Z} \frac{1+\rho}{[\Gamma(2\rho+1)]^2} y_0^{2\rho} \frac{\Delta y_0}{y_0} \cdot B, \quad (1)$$

where R is the Rydberg constant,

$a_H = h^2/4\pi^2 me^2$ is the radius of the first Bohr orbit for hydrogen,
Z is the nuclear charge,
$\psi^2(0)$ is the square of the non-relativistic atomic wave function at the center of the nucleus,
$\rho = (1-Z^2\alpha^2)^{\frac{1}{2}}$,
$\alpha = 2\pi e^2/hc$ is the fine structure constant
$y_0 = 2Zr_0/a_H$ where r_0 is the radius of the nucleus,

[1] J. E. Rosenthal and G. Breit, Phys. Rev. **41**, 459 (1932).
[2] G. Breit, Phys. Rev. **42**, 348 (1932).
[3] G. Racah, Nature **129**, 723 (1932).
[4] P. Köhler, Zeits. f. Physik **113**, 306 (1939).
[5] S. Mrozowski, Phys. Rev. **61**, 605 (1942).

$\Delta y_0/y_0$ is the fractional change in y_0 for two isotopes,
B is a factor depending on the potential within the nucleus.

The datum for the shifts given by Eq. (1) is zero shift when the s electron is completely removed. Following Goudsmit,[6] Breit,[2] and Fermi and Segrè,[7]

$$\psi^2(0)=\frac{Z_i Z_0^2}{\pi a_H^3 n_0^3}\left(1-\frac{d\sigma}{dn}\right), \tag{2}$$

where Z_i is the effective nuclear charge in the inner region and can be put equal to Z for an s electron,
Z_0 is the effective nuclear charge in the outer region,
n_0 is the effective principal quantum number,
σ is the quantum defect.

Since the term value

$$T=RZ_0^2/n_0^2, \tag{3}$$

$$n_0^3=(R/T)^{\frac{3}{2}}Z_0^3. \tag{4}$$

Substituting Eq. (2) and Eq. (4) in Eq. (1),

$$\Delta\delta W=\frac{4T^{\frac{3}{2}}}{Z_0R^{\frac{1}{2}}}\left(1-\frac{d\sigma}{dn}\right)\frac{1+\rho}{[\Gamma(2\rho+1)]^2}y_0^{2\rho}\frac{\Delta y_0}{y_0}\cdot B. \tag{5}$$

Case 1. For a constant potential within the nucleus[1]

$$B=[1+vy_0/2a^2], \tag{6}$$

where $a=Z_i\alpha$, $v=V/mc^2$ and V is the potential energy of the electron inside the nucleus.

Equation (6) is based on the assumption that v is the same for both nuclei.

Case 2. If v is a constant for a given nucleus, but a function of y_0, then by the perturbation method

$$B=\left[1+\frac{vy_0}{2a^2}+\frac{1}{2a^2}\frac{y_0^2}{2\rho+1}\frac{dv}{dy_0}\right]. \tag{7}$$

Case 3. If the non-electrical forces between the electron and the nucleus are negligible and all the charge is concentrated at the surface of the nucleus, then $V=-Ze^2/r_0$, and $v=-2a^2/y_0$ and is different for each isotope. For this case,[3] from Eq. (7),

$$B=\left[1-\frac{2a^2y_0}{2a^2y_0}+\frac{1}{2\rho+1}\right]=\frac{1}{2\rho+1}. \tag{8}$$

If the forces are purely electrical, any other charge distribution will give $V<-Ze^2/r_0$ inside the nucleus. $V>-Ze^2/r_0$ implies the existence of non-electrical forces.

Case 4. If V is the same for each isotope and equal to $-Ze^2/r_0$ for one of the isotopes, then $dv/dr_0=0$ and from either Eq. (6) or Eq. (7),

$$B=0. \tag{9}$$

This corresponds to the case where the addition of neutrons does not change the proton distribution.

Case 5. If the non-electrical forces are negligible but, in contrast to *Case 3*, the charge is uniformly distributed throughout the nucleus,[1]

$$V=\left[-\frac{3}{2}+\frac{1}{2}\left(\frac{r}{r_0}\right)^2\right]\frac{Ze^2}{r_0}=\left[-\frac{3}{2}+\frac{1}{2}\left(\frac{y}{y_0}\right)^2\right]\frac{2a^2}{y_0},$$

and

$$B=3/(2\rho+1)(2\rho+3). \tag{10}$$

Figure 1 shows the potential energy distributions discussed above. In each case the curve for the heavier isotope is represented by a broken line where it differs from that of the lighter isotope.

A. Experimental Data

To test Rosenthal and Breit's theory it is best to study the ns term sequences of one-electron spectra of elements with relatively heavy, and therefore relatively large nuclei. Since the contributions of non-s electrons to the shifts are small, these data can be supplemented by those for terms of more complex configurations with one or two s electrons. Mrozowski[5] has given shifts for

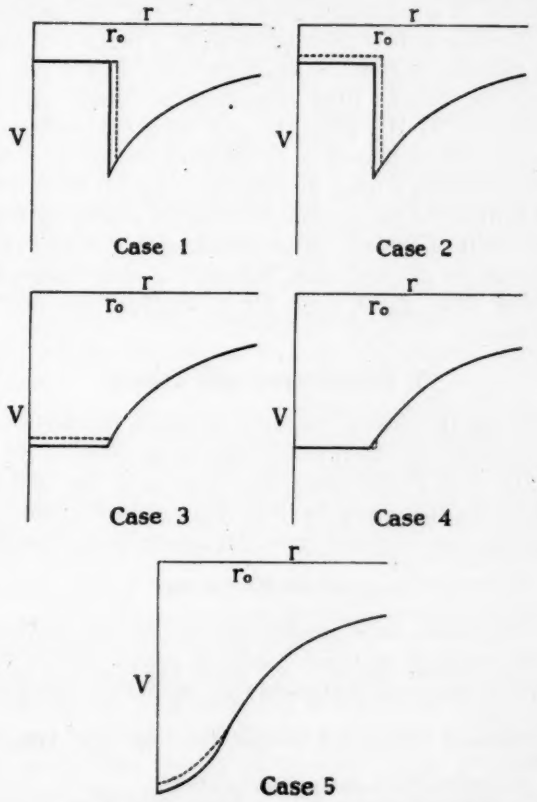

FIG. 1. Potential energy of the valence electron for five nuclear models.

[6] L. Pauling and S. Goudsmit, *The Structure of Line Spectra* (McGraw-Hill Book Company, Inc., New York, 1930); S. Goudsmit, Phys. Rev. 43, 636 (1933).
[7] E. Fermi and E. Segrè, Zeits. f. Physik 82, 729 (1933).

TABLE I. Isotope shifts in Tl III.

Term	Term value cm^{-1}	Isotope shift cm^{-1}
$5d^9 6s^2 2_{1\frac{1}{2}}$	156,001.0	0.710
$5d^9 6s6p3_{2\frac{1}{2}}{}^0$	113,220.0	0.385
$5d^9 6s6p4_{1\frac{1}{2}}{}^0$	111,436.2	0.343
$7s\ ^2S_{\frac{1}{2}}$	101,377.5	0.090
$5d^9 6s6p10_{\frac{1}{2}}{}^0$	97,224.5	0.407
$5d^9 6s6p13_{\frac{1}{2}}{}^0$	89,746.2	0.397
$5d^9 6s6p14_{1\frac{1}{2}}{}^0$	84,739.4	0.378
$5d^9 6s6p18_{1\frac{1}{2}}{}^0$	80,585.4	0.410
$6d^9 6s6p22_{\frac{1}{2}}{}^0$	65,858.7	0.422
$8s\ ^2S_{\frac{1}{2}}$	56,402.0	0.046

Hg II; Crawford, McLay, and Crooker[8] have given shifts for eight terms of Pb IV involving a 6*s* electron. Shifts have been measured by Crawford and Convey[9] as part of an extensive analysis of the hyperfine structures of Tl III. This spectrum was excited in an electrodeless discharge and the hyperfine structures were resolved by a 21-foot concave grating of 80,000 lines in the third to eight orders. Table I gives the isotope shifts observed by Crawford and Convey for terms involving one unpaired *s* electron and for one level of $5d^9 6s^2$. The shifts are relative to a datum of zero shift for the $7d\ ^2D_{5/2}$ level which shows no magnetic splitting. For all levels listed the lighter isotope has the greater binding energy.

Since the shift of the $6s\ ^2S_{\frac{1}{2}}$ level was not observed directly, it is evaluated here as 0.38 cm^{-1} by reducing the average shift of the 6*s*6*p* levels by 2 percent to allow for the contribution of the *p* electron. This 2 percent correction follows from Rosenthal and Breit's theory which, for Tl III, gives the shift of a $6p_{\frac{1}{2}}$ electron as about 1/20 of that of a 6*s* electron and gives a negligible shift for a $6p_{3/2}$. In this way we get 0.38 cm^{-1} for the shift of the $6s\ ^2S_{\frac{1}{2}}$ level. As a further check, the 0.710 cm^{-1} shift of $5d^9 6s^2 2_{1\frac{1}{2}}$ gives a shift of 0.355 cm^{-1} per *s* electron in $6s^2$ and thus indicates a shift somewhat greater than 0.355 cm^{-1} for a single unscreened 6*s* electron.

B. Comparison with Theory

To test the theory, the value of $\Delta y_0/y_0$ has been computed from the experimental data for *ns* levels of Hg II, Tl III, and Pb IV using the value of *B* for uniform charge density given by Eq. (10). y_0 used in the calculation was obtained from the approximate formula[10]

$$r_0 = 1.5\times 10^{-13} A \text{ cm}, \tag{11}$$

where *A* is the mass number. $(1-d\sigma/dn)$ was evaluated from a plot of quantum defect, σ, against term value. If the terms are unperturbed they should fit a Rydberg-Ritz equation[11]

$$T = RZ_0^2/(n-\alpha-\beta T)^2, \tag{12}$$

so that

$$\sigma = \alpha+\beta T, \tag{13}$$

and

$$d\sigma/dn = \beta dT/dn.$$

But from Eq. (12),

$$(n-\alpha-\beta T) = R^{\frac{1}{2}}Z_0/T^{\frac{1}{2}}.$$

Differentiating,

$$1-\beta\frac{dT}{dn} = -\frac{R^{\frac{1}{2}}Z_0}{2T^{\frac{3}{2}}}\frac{dT}{dn}$$

so that

$$dT/dn = 1/(\beta - R^{\frac{1}{2}}Z_0/2T^{\frac{3}{2}}).$$

Finally

$$d\sigma/dn = \beta/(\beta - R^{\frac{1}{2}}Z_0/2T^{\frac{3}{2}}) = \beta/(\beta - n_0/2T). \tag{14}$$

To evaluate β and check for perturbations, σ was plotted against *T*. By Eq. (13), this graph for an unperturbed series is a straight line of slope β.

The values obtained for the apparent fractional change in nuclear radius, $\Delta y_0/y_0$, for the addition of two neutrons, are tabulated in Table II. These values are termed apparent because, as will be shown, they must be corrected for the approximations in the perturbation method and for the effect of the decrease in screening of the inner electrons by removal of the outer *s* electron.

Within the precision of the measured intervals, the shifts of the 6*s*, 7*s*, and 8*s* levels in Tl III give the same value of $\Delta r_0/r_0$. This confirms the predicted variation of the isotope shift with $T^{\frac{1}{2}}(1-d\sigma/dn)$ and hence with $\psi^2(0)$, and shows that the isotope shift in the heavy elements is primarily due to the finite size of the nucleus.

In the case of Hg II, the 6*s* and 7*s* levels give equal values of $\Delta y_0/y_0$. The other three levels give much larger values of the ratio, but these are not free from perturbations since the plot of quantum defect against term value starts to depart from a straight line at 8*s* and is curving strongly at 9*s* and 10*s*. This shows that they are perturbed by at least one level above the 10*s*. Although levels of the configuration $5d^9 6s6d$ have not been identified, they are expected in this position and some of them are capable of producing the perturbation. Furthermore, these levels would have large isotope shifts and on sharing their properties with the 8*s*, 9*s*, and 10*s* would increase the shifts of the latter and account for the large values of $\Delta y_0/y_0$. Therefore the 8*s*, 9*s*, and 10*s* levels are not suitable for testing the theory.

Table II shows another confirmation of the field effect theory. The addition of two neutrons to a nucleus of each of the three elements causes the same fractional

[8] Crawford, McLay, and Crooker, Proc. Roy. Soc. **A158**, 455 (1937).
[9] J. Convey, Ph.D. thesis, Toronto (1940).
[10] H. Bethe, *Elementary Nuclear Theory* (John Wiley and Sons, Inc., New York, 1947). See also E. Amaldi and B. N. Cacciapuoti, Phys. Rev. **71**, 739 (1947).
[11] A. G. Shenstone and H. N. Russell, Phys. Rev. **39**, 415 (1932).

change in nuclear radius, as would be expected since the binding energies for the addition of two neutrons are equal within a few percent[12] for thallium and lead. Binding energies for mercury are not available.

Köhler[4] has analyzed the shifts observed by him for the $6sns$ sequence of Tl II and concluded that for a reasonable choice of datum they could be fitted to a $(1-d\sigma/dn)/n_0^3$ law as predicted by Eq. (1) and Eq. (2). Mrozowski[5] has pointed out that the higher members of the $^1S_0$ sequence are known to be perturbed by a term that is capable of lowering their isotope shifts. Furthermore, Köhler made no estimate of the effect on the shifts of the change in screening of the $6s$ electron by the removal of the outer ns electron. Until such an estimate is made this confirmation of theory is not as conclusive as the results of Table II.

In the following, the shifts for the $6sns$ sequence of Tl II are calculated making allowance for screening and using the value of $\Delta y_0/y_0=1.1\times10^{-3}$ established in Tl III. This is done primarily to show that the shifts in Tl II are not inconsistent with the value of $\Delta y_0/y_0$ obtained from Tl III when calculated on the same basis [Eqs. (5), (10), and (11)]. The results of the calculations are summarized in Table III. The shifts of the $6sns$ levels, tabulated in the third column, were calculated treating the outer ns electron as a one-electron system and using the term values from Tl II. The datum for the calculated shifts is zero shift for $6s$ of Tl III. The shift listed in the third column for the $5d^96s^26p$ is that given in Table II as the measured shift of the $6s$ level of Tl III. This value is in accord with $\Delta y_0/y_0=1.1\times10^{-3}$.

The shifts in the last column of Table III are obtained from those in column 3 by correcting for screening. The change in the screening of the $6s$ by the ns can be estimated from the change in the magnetic hyperfine structure of the $6sns\ ^3S_1$ sequence because both the magnetic hyperfine structure and the isotope shift depend on $\psi^2(0)$ of each electron. The interaction constant of the $6s$ electron in the $6sns$ configuration was evaluated from the observed interval factors[13] by treating the outer s electron as a one-electron system and calculating its contribution to the interval factor. The interaction constant, a_{ns}, of the outer electron was evaluated by the Goudsmit expression

$$a_{ns}=8\pi R\alpha^2 a_H{}^3\kappa g(I)\psi^2(0)/3\times1837$$

using $g(I)$ deduced from $a_{6s}(\text{Tl III})=5.85\ \text{cm}^{-1}$. This interval factor is a reliable limiting value obtained from the hyperfine structures of $6sng$ levels and $6sns\ ^3S_1$ levels of Tl II, and also by calculation from the structures of higher members of the ns sequence of Tl III (see Section 3). It is found that for the $6s7s$ level a_{6s} is reduced 3 percent at most by the presence of the $7s$ electron. Thus the corrected shifts of the $6s7s$ levels are smaller than the calculated by not more than 0.011 cm^{-1}, 3 percent of 0.38. For the $6s8s$ and $6s9s$ the screening correction is negligible.

TABLE II. Apparent change in nuclear radius (uniform charge distribution).

	Hg II		Tl III		Pb IV	
Level	Isotope shift cm^{-1}	$\frac{\Delta y_0}{y_0}=\frac{\Delta r_0}{r_0}$ apparent	Isotope shift cm^{-1}	$\frac{\Delta y_0}{y_0}=\frac{\Delta r_0}{r_0}$ apparent	Isotope shift cm^{-1}	$\frac{\Delta y_0}{y_0}=\frac{\Delta r_0}{r_0}$ apparent
$6s$	0.276	1.05×10^{-3}	0.38	1.13×10^{-3}	0.5	$1.(2)\times10^{-3}$
$7s$	0.050	1.02×10^{-3}	0.090	1.01×10^{-3}		
$8s$	0.080*	4.2×10^{-3}	0.046	1.2×10^{-3}		
$9s$	0.10 ± 0.025*	11×10^{-3}				
$10s$	0.05 ± 0.03*	10×10^{-3}				

* Perturbed—see text.

For the $5d^96s^26p$ levels the important screening correction will be the mutual screening of the $6s$ electrons. The isotope shift due to a $6s$ electron is $5d^{10}6s^2$ can be evaluated from the isotope shift of a single $6s$ electron (Tl III) by approximating to the Z_0 and n_0 of a $6s^2$ as follows. Consider the two s electrons of $6s^2$ as a single electron of charge 2. For them Z_0 is 2.5 since the probability of either $6s$ being nearer the nucleus than the other is one-half and their charge distribution is spherically symmetrical. From this value of Z_0 and the sum of the ionization potentials of Tl II and Tl III, which is the energy required to remove the pair to infinity, one obtains $n_0=1.840$ for either electron of the pair. For the $6s$ electron of Tl III, $Z_0=3$, $n_0=2.026$ and its isotope shift is 0.38 cm^{-1} relative to ionization. A shift of 0.352 cm^{-1} for each $6s$ electron of $6s^2$ of Tl II is obtained from these data by the relation $\Delta\delta W\propto Z_0{}^2/n_0{}^3$, which follows from Eqs. (1) and (2) assuming a constant Fermi-Segrè correction. That is, the mutual screening of the two $6s$ electrons decreases the shift per 6s electron by 7 percent. The shift for $6s^2$ of Tl II then is 0.704 cm^{-1} relative to ionization of Tl III (double ionization of Tl II). This shift agrees well with the 0.710 cm^{-1} shift observed for the $5d^96s^2$ of Tl III, which differs from $5d^{10}6s^2$ only by the absence of a d electron.

But the datum for the calculated shifts is $6s$ of Tl III. To get the shift relative to this datum it is necessary to subtract the shift produced by taking a $6s$ electron in Tl III to infinity. Thus the shift of the $6s^2$ configuration of Tl II relative to the $6s$ level of Tl III is $0.704-0.38=0.32$ cm^{-1}. For a $5d^96s^26p$ configuration the shift will be from 0 to 5 percent greater because of the presence of the $6p$ electron; the absence of a d electron should have a negligible effect.

The agreement between the observed values and the values corrected for screening is very good except for $6s8s$ and $6s9s$, for which the observed shifts are smaller. But, as pointed out by Mrozowski,[4] these levels are perturbed, presumably by $6p^2\ ^1S_0$,[14] which would reduce

[12] J. Mattauch, *Nuclear Physics Tables* (Interscience Publishers Inc., New York, 1946).

[13] S. Smith and J. Convey, Can. J. Research **A14**, 139 (1936). The intervals given by Smith and Convey for $6s8s$ and $6s10s$ are incorrect; they are 4.68 and 4.47 cm^{-1}, respectively, from our unpublished data.

[14] C. B. Ellis and R. A. Sawyer, Phys. Rev. **49**, 145 (1936).

TABLE III. Isotope shifts in Tl II.

Level	Observed (datum 6s9s of Tl II) cm^{-1}	Isotope shift Calculated (datum 6s of Tl III) cm^{-1}	Calculated with screening correction cm^{-1}
$5d^96s^26p4_2{}^0$	0.348*	0.38	0.32–0.34
$5d^96s^26p8_1{}^0$	0.338*		
$5d^96s^26p5_1{}^0$	0.302*		
$6s7s\ {}^3S_1$	0.059	0.066	0.055
$6s7s\ {}^1S_0$	0.060	0.063	0.052
$6s8s\ {}^1S_0$	0.015	0.023	0.023
$6s9s\ {}^1S_0$	0.000	0.011	0.011

* There is some perturbation between these levels and those of $6s7p$ and it would reduce the observed shifts. This spread in the shifts is probably caused by this perturbation.

their shifts and, in particular, make the shift of $6s9s$ less than the calculated 0.011 cm^{-1}. As a result of this perturbation, Köhler's original datum of zero shift for $6s9s$ is probably equivalent to zero shift for $6s$ of Tl III, the datum for the calculated values. Thus the shifts in Tl II as well as those listed in Table II are consistent with the field effect theory.

C. Validity of the Perturbation Method

Because the fields responsible for the energy perturbation are so large, even though they act only in a small region, it is necessary to examine the accuracy of the perturbation method. Rosenthal and Breit[1] have considered the case where v is constant and the same for both nuclei, but their method is not suitable for cases where the v's are different. An alternative treatment by E. K. Broch[15] avoids the use of the perturbation method and permits the derivation of an expression for the isotope shift which is not dependent on the assumption that the perturbed wave functions differ only slightly from the unperturbed in the region of the perturbation. By Broch's method the change in energy due to the finite nuclear radius is

$$\delta W=-2\left(\frac{C-}{C}\right)C^2Ze^2\frac{\rho}{\Gamma(1+2\rho)\Gamma(1-2\rho)}, \quad (15)$$

where $C-$ and C are the coefficients used by Rosenthal and Breit in the solution of the wave equations for $y>y_0$. Equation (15) differs from Broch's Eq. (4–3) only by a factor $a_H/2Z$ which converts Broch's normalization to that of Rosenthal and Breit.

The wave functions are

$$\phi_1/a=CJ_{2\rho}(2y^{\frac{1}{2}})+C_-J_{-2\rho}(2y^{\frac{1}{2}}), \quad (16)$$

$$\phi_2=CA_{2\rho}(2y^{\frac{1}{2}})+C_-A_{-2\rho}(2y^{\frac{1}{2}}), \quad (17)$$

where

$$A_{2\rho}(2y^{\frac{1}{2}})=(j-\rho)J_{2\rho}(2y^{\frac{1}{2}})+y^{\frac{1}{2}}J_{2\rho+1}(2y^{\frac{1}{2}}), \quad (18)$$

$$A_{-2\rho}(2y^{\frac{1}{2}})=(j-\rho)J_{-2\rho}(2y^{\frac{1}{2}})-y^{\frac{1}{2}}J_{-2\rho-1}(2y^{\frac{1}{2}}), \quad (19)$$

the J's are Bessel functions,

j is the quantum number taking the values -1, 1, -2, 2, -3, $\cdots$ for $s_{\frac{1}{2}}$, $p_{\frac{1}{2}}$, $p_{3/2}$, $d_{3/2}$, $d_{5/2}$, $\cdots$ electrons, respectively,

C is a constant and equals $(-a_H\psi(0)/2Z)$,

C_- depends on y_0 and on the potential inside the nucleus.

From Eq. (15), by differentiating, the isotope shift is

$$\Delta\delta W=-2Ze^2C^2\frac{2\rho}{\Gamma(1+2\rho)\Gamma(1-2\rho)}\times\left[\frac{d}{dy_0}\left(\frac{C-}{C}\right)\right]_{y_0}\frac{\delta y_0}{y_0}, \quad (20)$$

where[1,15]

$$\frac{C_-}{C}=\frac{(\phi_1/a\phi_2)_{y_0}A_{2\rho}(2y_0^{\frac{1}{2}})-J_{2\rho}(2y_0^{\frac{1}{2}})}{J_{-2\rho}(2y_0^{\frac{1}{2}})-(\phi_1/a\phi_2)_{y_0}A_{-2\rho}(2y_0^{\frac{1}{2}})}. \quad (21)$$

$(\phi_1/a\phi_2)_{y_0}$ is obtained by putting $y=y_0$ in the solutions of the wave equation for $y\leqslant y_0$. These solutions for v constant are given by Rosenthal and Breit; those for the uniform charge distribution were obtained as power series in y. It can be shown that $(\phi_1/a\phi_2)_{y_0}$ is very nearly independent of y_0 so that its derivative can be set equal to zero in the differentiation.

The isotope shift for an s electron of thallium has been evaluated by Eq. (20) for *Case 3* ($V=-Ze^2/r_0$) and *Case 5* (uniform charge density), and compared with the shift calculated by the perturbation method, Eq. (5). The error in the perturbation method was found to be 36 percent for *Case 3* and 34 percent for *Case 5*. Thus for this reason alone the values of $\Delta y_0/y_0$ (apparent) in Table II must be multiplied by 1.35.

D. Screening of Inner Electrons by the Valence Electron

Since a penetrating s-type valence electron has a finite probability of being near the nucleus, it has an appreciable probability of being inside the orbit of any of the inner electrons. For that fraction of the time when the valence electron is inside the orbit of the inner electron, the effective nuclear charge for the inner electron is reduced by one unit. Thus the binding of the inner electron to the nucleus is reduced by the presence of the valence electron and thus the contribution of the inner electron to the isotope shift of the entire atom is reduced.

The change caused by this screening of an inner electron by the valence electron is a small fraction of the isotope shift in the binding energy of the inner

[15] E. K. Broch, Archiv. f. Mat. o. Nat. 48, 25 (1945). J. Smorodinsky, J. Phys. U.S.S.R. 10, 419 (1946), has used essentially the same method, but his result is inaccurate because of the approximations used.

electron. But the inner electron is closely bound to the nucleus, and a small fractional change in its isotope shift is an appreciable fraction of the isotope shift of the valence electron.

A direct evaluation of this screening would require a very accurate value of $\psi^2(0)$ for the inner electrons when the valence electron is present and when it is removed to ionization. The wave function of the 1*s* electron would need to be accurate to one part in 10^5 or 10^6 so that the uncertainty in its value of $\psi^2(0)$ would be a small fraction of $\psi^2(0)$ for the valence electron. This accuracy is far beyond the limit of the Hartree self-consistent field method.

However, an estimate of the screening effect can be obtained in the following way. From the Hartree wave functions for mercury[16] the probability, p, of a 6*s* valence electron being closer to the nucleus than each of the 1*s*, 2*s*, 3*s*, 4*s*, and 5*s* electrons is evaluated. From Eq. (1) the ratio of the isotope shift for the *ns* electron to the isotope shift for the 6*s* electron is

$$(\Delta\delta W)_n/(\Delta\delta W)_6=\psi_{ns}^2(0)/\psi_{6s}^2(0), \tag{22}$$

but $\psi_{ns}^2(0)=Z_i Z_0^2/\pi a_H^3 n_0^3$ from Eq. (2). During a fraction p of the total time, the valence electron is closer to the nucleus than the inner electron and reduces Z_0 by one unit. For this fraction of the time $\psi_{ns}^2(0)$ is reduced by the fraction $[Z_0^2-(Z_0-1)^2]/Z_0^2\simeq 2/Z_0$. Thus the change in the isotope shift of the *ns* electron due to the presence of the 6*s* electron, expressed as a fraction of the isotope shift of the 6*s* is

$$\frac{\psi_{ns}^2(0)}{\psi_{6s}^2(0)}\cdot\frac{2}{Z_0}\cdot p. \tag{23}$$

p is obtained by evaluating numerically the integral

$$p=\int_0^\infty\left[P_{ns}^2\int_0^{r_1}P_{6s}^2 dr\right]dr_1 \tag{24}$$

using the Hartree wave functions to get P^2, the probability of the electron being between r and $r+dr$. $\psi_{ns}^2(0)$ and $\psi_{6s}^2(0)$ are taken from the Hartree wave functions. Z_0, from a shell model of the atom, is approximately 80 for 1*s* electrons, 78 for 2*s* electrons, 70 for 3*s* electrons, 52 for 4*s* electrons, and 20 for 5*s* electrons. These values of Z_0 are not inconsistent with the Hartree and Fermi-Thomas fields.

The values of p and of the change in the isotope shift of the atomic energy levels caused by the change in screening of each inner pair of *s* electrons, expressed as a fraction of the shift for the 6*s* electron, are given in Table IV.

Thus this calculation shows that the observed shifts should be 16 percent smaller than those calculated neglecting screening. It is difficult to assess the accuracy of this calculation, but it is believed that the correction should be of the right order of magnitude. It is realized that the Hartree wave function for ψ_{6s} does not give a good value of $\psi_{6s}^2(0)$ because the amplitude in the inner region is very sensitive to the normalization integral, which is determined mainly in the region of large r. However in the expression for the screening, Eq. (23), p appears in the numerator and $\psi_{6s}^2(0)$ in the denominator. Since they are both dependent on the amplitude of the 6*s* wave function, the error is reduced. This compensation is best for the 1*s* electron. For the 5*s* electron this compensation is worst since p is not as dependent on the amplitude of ψ_{6s} near the nucleus, but the error in $\psi_{6s}^2(0)$ probably is partially compensated by an error of the same sense in $\psi_{5s}^2(0)$.

In the calculation it has been assumed that n_0 is independent of the screening by the valence electron. This approximation is very good for the inner electrons, for which the effective field is nearly Coulombian, but is not as accurate for the outer electrons. As a result of these two effects the calculated screening corrections should be regarded as upper limits.

The 6*s* electron also screens inner p and d electrons, but since the latter have very small isotope shifts, the change in the screening of these electrons by the valence electron has a negligible effect on the shifts.

E. Conclusions

When the corrections for both the approximation of the perturbation method and the screening of the inner electrons are applied to the apparent $\Delta y_0/y_0$ for uniform charge density (*Case 5*), its value is raised from 1.1×10^{-3} (Table II) to $1.1\times10^{-3}\times1.35\times1.16=1.7\times10^{-3}$. This fractional change in nuclear radius is only half of 3.3×10^{-3}, the value expected on the assumption that the protons remain uniformly distributed throughout the volume of the nucleus, and that the volume is proportional to the mass. Therefore the isotope shifts indicate that the addition of two neutrons to a lead, mercury, or thallium nucleus does not cause a complete redistribution of the charge in the nucleus. This result favors the existence of some type of reasonably stable structure in the nucleus, such as the shell structures discussed by Feenberg and Hammack, Mayer, and Nordheim.[17]

If any of the other potentials (*Cases 1* to *3*) are assumed, $\Delta y_0/y_0$ calculated from the observed shifts is still smaller. For *Case 3*, charge on surface, $\Delta y_0/y_0$ is $\frac{2}{3}$ of that calculated assuming uniform charge density. For the deep potential well ($v\simeq 0$), $\Delta y_0/y_0$ is one-fourth that calculated on the basis of uniform charge distribution. Thus the deep potential well does not seem probable and the charge on surface is somewhat less satisfactory than the uniform charge density.

[16] D. R. Hartree and W. Hartree, Proc. Roy. Soc. **A149**, 210 (1934).

[17] M. G. Mayer, Phys. Rev. **74**, 235 (1948); E. Feenberg and K. C. Hammack, Phys. Rev. **75**, 1877 (1949); L. Nordheim, Phys. Rev. **75**, 1894 (1949).

TABLE IV. Isotope shift screening correction.

Electron	$\psi^2(0)\cdot\pi a_H^3$ (Hartree)	p	Screening correction per ns^2 as a fraction of $(\Delta\delta W)_{6s}$
$1s$	5.06×10^{5}	2.034×10^{-5}	0.016
$2s$	5.56×10^{4}	1.912×10^{-4}	0.017
$3s$	1.23×10^{4}	9.010×10^{-4}	0.020
$4s$	3.06×10^{3}	3.846×10^{-3}	0.028
$5s$	6.10×10^{2}	2.090×10^{-2}	0.079
$6s$	3.2×10^{1}		
		Total	0.16

The specific mass effect has generally been neglected for heavy elements and has not been considered here. The best justification for this is experimental: in elements of intermediate mass only very small isotope shifts are observed, and in heavy elements different levels of an unperturbed configuration have practically the same isotope shifts (see Table I). If the specific mass effect were invoked to account for the smallness of $\Delta y_0/y_0$ obtained from the observed shift of the $6s$ level of Tl III in particular, it would have to be in the opposite sense to the field effect and have a magnitude of 0.2 cm^{-1}. Then differences of this order between shifts of the levels of the same configuration would be expected. Since such large differences do not occur, the specific mass effect must be relatively small.

3. EFFECT OF NUCLEAR SIZE OF MAGNETIC INTERACTION

Rosenthal and Breit have considered the effect of the finite size of the nucleus on the interaction of an electron with the nuclear magnetic moment and have shown that for heavy nuclei the effect may be appreciable. Thallium is the only heavy element whose nuclear magnetic moment has been measured by an induction method,[18] and the value so obtained is higher than any of the spectroscopic values. The correction factors to be applied to the spectroscopic values have been computed for a deep potential well with $v=0$ (*Case 1*), but not for *Case 3* and *Case 5*. Since the latter are more consistent with the observed isotope shifts than *Case 1*, their correction factors are evaluated here.

The coupling of the electron and the nuclear magnetic moment is proportional to the integral

$$I=\int_0^\infty \phi_1\phi_2 y^{-2}dy, \tag{25}$$

where ϕ_1 and ϕ_2 are the Darwin-Gordon radial functions. It is evident from the form of this integral that the values of the product $\phi_1\phi_2$ are weighted most heavily for small values of y where, for a nucleus of finite size, ϕ_1 and ϕ_2 depart most from their values in a purely Coulomb field.

For all the charge on the surface of the nucleus, *Case 3*, analytical expressions for ϕ_1 and ϕ_2 are given by Rosenthal and Breit. For uniform charge distribution, *Case 5*, ϕ_1 and ϕ_2 inside the nucleus were obtained as power series in y. The Rosenthal-Breit solutions with the value of C_-/C given by Eq. (21) apply outside.

The integrand $\phi_1\phi_2 y^{-2}$ was evaluated and plotted against y for the range $0\leq y\leq 0.2$, taking $y_0=0.0271$, the radius used for isotope shifts. This plot was compared with a similar plot of the unperturbed $\phi_1^{(0)}\phi_2^{(0)}y^{-2}$, corresponding to a point nucleus. From this comparison a particular value $y=y_1$ is found such that the total area under the perturbed $\phi_1\phi_2 y^{-2}$ curve is the same as the area under the unperturbed curve from y_1 to infinity. Thus,

$$\begin{aligned} I&=\int_0^\infty \phi_1\phi_2 y^{-2}dy=\int_{y1}^\infty \phi_1^{(0)}\phi_2^{(0)}y^{-2}dy \\ &=I^{(0)}-\int_0^{y1}\phi_1^{(0)}\phi_2^{(0)}y^{-2}dy \\ &=\left\{1-\frac{2(j-\rho)\rho(2\rho+1)y_1^{2\rho-1}}{(2j-1)[\Gamma(2\rho+1)]^2}\right\}I^{(0)}. \end{aligned} \tag{26}$$

The values of y_1 and the correction factor, $I^{(0)}/I$, as obtained from Eq. (26), are given in Table V.

Spectroscopic values of μ, the magnetic moment of Tl^{205}, derived from splittings of unperturbed levels of the first three spectra, are given in Table VI. These have been calculated from the observed splittings by the method of Goudsmit[19] and Fermi and Segrè.[6] The interaction constants for the s electrons of Tl III are from Convey's thesis.[9] The origins of the others are indicated. The values of μ in column 4 of Table VI, multiplied by the appropriate value of $I^{(0)}/I$ from Table V, give the corrected values of μ listed in columns 5 and 6.

All the uncorrected values in column 4 of Table VI are appreciably lower than the induction measurement; 16 percent for s electrons and 9 percent for the $p_{\frac{1}{2}}$ electron. The discrepancy is almost completely removed by the corrections for both cases, with *Case 3* slightly closer. Since the difference between the correction factors for the two cases is smaller than the spread in the spectroscopic values, the comparison does not significantly discriminate between the two models. However, the deep potential well of *Case 1* gives a 30 percent correction and is thus untenable on the basis of this comparison.

TABLE V. Correction factors for thallium ($y_0=0.0271$).

	Case 3		*Case 5*	
	y_1	$I^{(0)}/I$	y_1	$I^{(0)}/I$
$^2S_{\frac{1}{2}}$	0.032	1.17	0.024	1.14
$^2P_{\frac{1}{2}}$	0.030	1.05	0.024	1.04

[18] H. L. Poss, Phys. Rev. **72**, 637 (1947).

[19] S. Goudsmit, Phys. Rev. **43**, 636 (1933).

Although the correction decreases with decreasing atomic number, it appears to be significant for intermediate elements. For caesium, Millman and Kusch[20] obtained $\Delta(6^2S_{\frac{1}{2}})=0.30665$ cm^{-1}. This gives, by the Goudsmit-Fermi-Segrè formula, $g(I)=0.7025$. The directly measured value,[21,22] $g(I)=0.7315$, is 3.9 percent higher. If we assume that $y_1=y_0$, as indicated by the values of y_1 in Table V, the corrected hyperfine structure value is $g(I)=0.728$, which differs from the directly measured value by only 0.4 percent. For lanthanum[23] $\Delta(6s\,^2S_{\frac{1}{2}}$ of La III$)=1.076$ cm^{-1} from which, by the Goudsmit-Fermi-Segrè formula, $g(I)=2.65$. The induction method[22] gives $g(I)=2.761$, which is 4.2 percent higher. The correction for nuclear radius, calculated as above, is 4.1 percent.

Thus when the values of the nuclear moments obtained from the interaction constants of s electrons by the Goudsmit-Fermi-Segrè formula are corrected for the finite size of the nucleus, they are in excellent agreement with those from direct induction measurements. The Goudsmit-Fermi-Segrè formula appears to be sufficiently accurate to warrant the use of $d\sigma/dn$, as obtained from Eq. (14), in the Fermi-Segrè factor rather than the rougher approximation $\Delta\sigma/\Delta n$.

Bitter[24] has pointed out that the ratio of the magnetic moments of the rubidium isotopes indicates that the spectroscopic values of the magnetic moments should be further corrected if the nuclear magnetic moment is distributed over the volume of the nucleus. It is indicated that this correction is of the same order as the Rosenthal-Breit correction. This is true only for Z small. For thallium, an upper limit for the correction arising from the distribution of magnetic moment within the nucleus can be determined as follows. As an extreme, the distribution of the magnetic moment could reduce the integrand of Eq. (25) to zero for $y<y_0$. A numerical calculation shows that this would increase the values of $I^{(0)}/I$ for an s electron, as given in Table V, by 3 percent. This additional correction is small because for a finite charge distribution the product $\phi_1\phi_2 y^{-2}$ is much smaller in the region $y<y_0$ than it is for a point nucleus.

It is interesting to note that the formula for the magnetic distribution correction, $(2Zr_0/a_H)$, which is a justifiable approximation for light elements happens to be of the right order for heavy elements when the charge distribution is taken into account. On the other hand $(2Zr_0/a_H)$ is a fair approximation to the Rosenthal-Breit correction to the magnetic interaction only for light elements. For the heavy elements the Rosenthal-Breit correction increases much more rapidly with Z. Although the difference in the magnetic distribution correction for different isotopes may well account for the difference in the ratios of the magnetic moments determined spectroscopically and inductively, this correction is too small relative to the Rosenthal-Breit correction for heavy elements to modify our conclusions about the electron-nuclear potentials.

TABLE VI. Nuclear moment of thallium.

Spectrum	Term	Interaction constant a_{ns} cm^{-1}	Uncorrected	μ, nuclear magnetons: Charge on surface	μ, nuclear magnetons: Uniform charge distribution
Tl III	$7s\,^2S_{\frac{1}{2}}$	1.348	1.37	1.60	1.56
	$8s\,^2S_{\frac{1}{2}}$	0.565	1.38	1.61	1.58
	$9s\,^2S_{\frac{1}{2}}$	0.295	1.39	1.63	1.59
Tl II	$6s5g$, $6sns$	5.88	1.44[b]	1.68	1.64
Tl I	$6p\,^2P_{\frac{1}{2}}$	0.710	1.49[c]	1.57	1.55
	$7s\,^2S_{\frac{1}{2}}$	0.400	1.35[d]	1.58	1.54
Average				1.61	1.58
Radio frequency induction[a]			1.628		

[a] See reference 18.
[b] Unpublished data by M. F. Crawford. In the $6s5g$ configuration, the multiplet structure is of the same order of size as the h.f.s. When the perturbations are taken into account, the separations of the hyperfine structure states of the configuration are consistent to within 0.010 cm^{-1} with $a_{6s}=5.88$. This value of a_{6s} is in agreement with that obtained from other high $6snx$ terms. μ was calculated taking 5.88 as the value of a_{6s} for Tl III.
[c] The value quoted in the table is that calculated by G. Breit (Phys. Rev. **38**, 463 (1931) increased by a 3 percent perturbation correction estimated by L. A. Wills (Phys. Rev. **45**, 883 (1934)). The Goudsmit-Fermi-Segrè method cannot be applied because the doublet splitting is required and the $^2P_{1/2}$ term is perturbed.
[d] Measurement by D. A. Jackson (Zeits. f. Physik **75**, 223 (1932)). calculation by H. Schüler and Th. Schmidt (Zeits. f. Physik **104**, 468 (1936)).

The effect of nuclear size on magnetic interaction is not consistent with a deep potential well, but is in agreement with either a uniform charge density or a concentration of the charge on the surface of the nucleus. The magnitude of the isotope shift is in best agreement with the uniform charge distribution. Even for this distribution it is necessary to conclude that the fractional change in the radius of the positive charge distribution for the addition of two neutrons is less than that given by radius $\propto$ (mass)$^{\frac{1}{3}}$. This suggests that the added neutrons do not cause a complete redistribution of the protons, and so may be considered as evidence for some form of stable shell structure in the nucleus. Both effects, particularly the magnetic interaction, lead to the conclusion that non-electrical forces between electrons and nuclei are small in comparison with the electrical forces. This conclusion is consistent with results on slow neutron scattering[25] which show that forces between neutrons and electrons are small.

The authors wish to thank Mr. F. M. Kelly and Dr. W. M. Gray for many helpful discussions. They are indebted to the Computing Centre of the University of Toronto for the numerical evaluation of the integrals in Section 2D.

[20] S. Millman and P. Kusch, Phys. Rev. **58**, 438 (1940).
[21] Kusch, Millman, and Rabi, Phys. Rev. **55**, 1176 (1939).
[22] W. H. Chambers and D. Williams, Phys. Rev. **76**, 461 (1949).
[23] M. F. Crawford and N. S. Grace, Phys. Rev. **47**, 536 (1935); H. Wittke, Zeits. f. Physik **116**, 547 (1940).
[24] F. Bitter, Phys. Rev. **76**, 150 (1949); H. Kopfermann, *Kernmomente* (Akademische Verlagesellschaft, M.B.H., Leipzig, 1940), p. 17.
[25] Rainwater, Rabi, and Havens, Phys. Rev. **75**, 1295 (1949).

Theory of the Lithium Two-Alpha-Reactions. II. Angular Distribution of $Li^6(d,\alpha)\alpha$

ROBERT RESNICK* AND D. R. INGLIS
The Johns Hopkins University, Baltimore, Maryland
(Received June 2, 1949)

An analysis is presented of the variation of the intensity of alphas from $Li^6(d,\alpha)\alpha$ with angle and energy. This variation has been observed to have the form $1+A(E)\cos^2\theta+B(E)\cos^4\theta$, just as in the case of $Li^7(p,\alpha)\alpha$ for which an analysis has already been given. For $Li^6(d,\alpha)\alpha$ it is again the Bose statistics and consequent even parity of the alphas that makes analysis possible. It is assumed that Li^6 has even parity so that only $s,d,\cdots$ deuterons are relevant here, in contrast to $Li^7(p,\alpha)\alpha$ in which $p,f,\cdots$ protons are involved. The two analyses differ also in the spin combinations, but are similar in the assumption of only two contributing states of the compound nucleus, with angular momentum quantum numbers 0 and 2. An expression for the energy variation of the angular distribution in $Li^6(d,\alpha)\alpha$ is derived from the dispersion formula and the treatment with two sharp levels is compared with that for one sharp and one broad level. The latter is found simpler and adequate for obtaining agreement with the experimental $A(E)$ and $B(E)$. After recognizing limitations on the parameters consistent with order-of-magnitude estimates of the matrix elements involved, it is found that the theoretical formulas rather naturally give the general form of the experimental results, including the feature that both $A(E)$ and $B(E)$ rise more slowly in the $Li^6(d,\alpha)\alpha$ reaction than in the $Li^7(p,\alpha)\alpha$ reaction as the bombarding energy is increased from zero, a consequence of the spherical symmetry of the entering s waves which participate in the Li^6 reaction only.

I. INTRODUCTION

THE angular distribution of the $Li^6(d,\alpha)\alpha$ reaction has been investigated by Heydenburg, Hudson, Inglis, and Whitehead.[1] The intensity of the reaction was observed to vary with angle as $1+A(E)\cos^2\theta+B(E)\cos^4\theta$, as expected from the Bose statistics of the product alphas. $A(E)$ rises gradually beginning just below 1 Mev to a broad maximum a little below unity at a bombarding energy E in the neighborhood of 2 Mev, and falls rapidly to zero at 3.5 Mev. The coefficient $B(E)$ remains zero up to almost 1.5 Mev and rises to a positive value of about 0.35 at higher energies. The yield curve observed at right angles to the beam displays a sharp maximum at 0.75 Mev and there is evidence to the approach to another peak just beyond the highest bombarding energy employed, 3.75 Mev.

The reaction $Li^6(d,\alpha)\alpha$ involves the formation of the same compound nucleus Be^8 as is formed in $Li^7(p,\alpha)\alpha$ but the binding energy of a deuteron to Li^6 is 4.96 Mev higher than the binding energy of a proton to Li^7, so the compound nucleus is in a more highly excited state in the Li^6 reaction than in the Li^7 reaction, for comparable bombarding energies. The Li^6 reaction thus makes it possible to explore a different part of the Be^8 spectrum than that explored as yet by the Li^7 reaction.

It is assumed throughout this work that the parity of the ground state of Li^6 is even, since it may be described as an alpha plus two p-nucleons. The results show that the data are compatible with this assumption. This theoretical interpretation of the Li^6 reaction includes the effects of entering s and d deuterons. The s deuterons by themselves give spherical symmetry, and the penetration of d deuterons is necessary for the appearance of the asymmetry. The product of an s wave and a d wave introduces a term $\cos^2\theta$ into the angular distribution, whereas the square of the d wave is responsible for the $\cos^4\theta$ term.

II. CALCULATION OF ANGULAR DISTRIBUTION OF THE Li^6+DEUTERON REACTION

The calculation is based on the Briet-Wigner dispersion formula[2] extended to several compound states, which for a system prepared in a well-defined initial state P may be written

$$\sigma(E,\theta)\sim\lambda\!\!\!^{-2}\left|\sum_r (P/H/r)(r/H/Q)/(E-E_R+(i/2)\Gamma_r)\right|^2. \quad (1)$$

In the paper[3] on $Li^7(p,\alpha)\alpha$ (hereafter referred to as I) it is shown that the cross section for finding an alpha in a small element of solid angle at θ is

$$\sigma(E,\theta)=\sum_P \sigma_P(E,\theta) \quad (2)$$

for an incident unpolarized beam and unpolarized target, where

$$\sigma_P(E,\theta)=4\pi\lambda\!\!\!^{-2}\left|\sum_{lr}\frac{\{(lSom/lSj_rm)[lSj_r/X_{lr}]\phi_l(E)\alpha_{lr}P_{j_r}{}^m(\cos\theta)\}}{(E-E_r+(i/2)\Gamma_r)}\right|^2. \quad (3)$$

Here, $(lSom/lSj_rm)$ is a transformation coefficient transforming from a representation in which l and S are diagonal to that in which the total angular momentum is diagonal; $[lSj_r/X_{lr}]$ transforms from lSj_r to the in-

* Now at the University of Pittsburgh, Pittsburgh, Pennsylvania.

[1] Heydenburg, Hudson, Inglis, and Whitehead, Phys. Rev. 74, 405 (1948).

[2] G. Breit and E. Wigner, Phys. Rev. 49, 519 (1936).

[3] D. R. Inglis, Phys. Rev. 74, 21 (1948). (See also C. L. Critchfield and E. Teller, Phys. Rev. 60, 10 (1941).)

coming wave function X_{lr}, having angular properties most nearly matching those of the resonant state r of the compound nucleus, having $j=j_r$. The product $(X_{lr}/H/r)(r/H/Q)$ is factored thus: $\varphi_l(E)\alpha_{lr}P_{j_r}^m(\cos\theta)$. Here, Q is the final state. α_{lr} is a complex number; $\varphi_l(E)$ is real and arises from penetration of the nuclear barrier; and $P_{j_r}^m$ is the associated Legendre polynomial introducing the angle factor.

In the reaction $Li^6(d,\alpha)\alpha$ the deuteron spin is $s=1$, the target nucleus has angular momentum $I=1$, and these combine to give spin states $S=0$, 1, 2. The ground state of Li^6 is assumed to be even, so s, d, $g\cdots$ waves may give the even states of the compound nucleus required for the reaction. The successively higher values of l find penetration more and more difficult, so it will suffice to consider only $l=0$ and $l=2$. The Bose statistics of the product alphas also demands that the compound state have even angular momentum j_r. With $l=0$, the spin state $S=0$ gives $j_r=0$, and $S=2$ gives $j_r=2$. With $l=2$, $S=2$ leads to $j_r=0$, 2, 4, $S=1$ to $j_r=2$ and $S=0$ to $j_r=2$.

We are free to assume such disposition of virtual levels of the compound nucleus having $j_r=0$, 2, or 4 as may be necessary to account for the observations. It may be assumed in the interests of simplicity, that the d wave reacts only with states having $j_r=0$ or $j_r=2$ without invoking $j_r=4$. It is found unnecessary to introduce more than two such states to explain the details of the reaction so far as they have been observed.

Our first set of assumptions about the compound nucleus is that it has just two states which contribute appreciably to the reaction in the energy range investigated, a state numbered $r=0$ having $j_0=0$ and a half-width Γ_0 much greater than the range of energies covered by the experiments, so that the energy variation of its resonance denominator may be neglected, and a state numbered $r=2$ having $j_2=2$, and Γ_2 small enough to account for the rapid energy variation of the angular distribution of the product alphas.

With these states, the cross section given by (1), (2), and (3) is

$$\sigma(E,\theta)=\frac{16\pi\lambda^2}{\Gamma_2^2(\epsilon^2+1)}\sum_{S,m}\Big|(\Gamma_2/i\Gamma_0)(\epsilon+i)\sum_{l=0,2}(lSom/lSom)[lSo/lo]\alpha_{lo}\phi_l+\sum_{l=0,2}(lSom/lS2m)\times[lS2/l2]\alpha_{l2}\phi_lP_2^m\Big|^2. \quad (4)$$

TABLE I. Transformation coefficients $(lSom/lSj_rm)$.

m	(2000/2020)	(210m/212m)	(220m/220m)	(220m/222m)	(020m/022m)	(0000/0000)
2		0	0	$(2/7)^{\frac{1}{2}}$	1	
1		$-(1/2)^{\frac{1}{2}}$	0	$-(1/14)^{\frac{1}{2}}$	1	
0	1	0	$(1/5)^{\frac{1}{2}}$	$-(2/7)^{\frac{1}{2}}$	1	1
−1		$(1/2)^{\frac{1}{2}}$	0	$-(1/14)^{\frac{1}{2}}$	1	
−2		0	0	$(2/7)^{\frac{1}{2}}$	1	

Here we have put

$$(E-E_2)/(\Gamma_2/2)=\epsilon, \quad (5)$$

which then measures the energy deviation from resonance with the state $r=2$ in units of its half-width. The summation indices S and m are implicit in the initial state P. More explicitly we have,

$$\sigma=[16\pi\lambda^2/\Gamma_2^2(\epsilon^2+1)]\Big\{\sum_{m\neq0}\Big|\sum_{l=0,2}(l20m/l22m)\times[l22/l2]\alpha_{l2}\phi_l\Big|^2(P_2^m)^2+\Big|(\Gamma_2/i\Gamma_0)(\epsilon+i)(2200/2200)[220/20]\alpha_{20}\phi_2+\sum_{l=0,2}(l200/l220)[l22/l2]\alpha_{l2}\phi_lP_2^0\Big|^2+\sum_m\Big|(210m/212m)[212/22]\alpha_{22}\phi_2\Big|^2(P_2^m)^2+\Big|(\Gamma_2/i\Gamma_0)(\epsilon+i)(0000/0000)\alpha_{00}\phi_0+(2000/2020)[202/22]\alpha_{22}\phi_2(P_2^0)\Big|^2\Big\}. \quad (6)$$

The factor $(\Gamma_2/i\Gamma_0)$ appears here twice since $j_r=0$ arises from both $l=0$, $S=0$ and $l=2$, $S=2$. The sums over m appearing here are easily evaluated by use of the values[4] for $(lSom/lSj_rm)$ given in Table I. In order to simplify the terms in the brackets, we divide through by $a=[202/22]\alpha_{22}$ and we put

$$\begin{aligned}&\Gamma_2[000/00]\alpha_{00}/i\Gamma_0a=R_0+iI_0\\&\Gamma_2[220/20]\alpha_{20}/i\Gamma_0a=R_1+iI_1\\&[022/02]\alpha_{02}/a=R_2+iI_2\\&[222/22]/[202/22]=R_3+iI_3\\&[212/22]/[202/22]=R_4+iI_4.\end{aligned} \quad (7)$$

Here R is the real part and I the imaginary part. In Table II are listed sums used in the Li^6 reaction with $j_r=0$ and $j_r=2$. Using Tables I and II with definitions (7), we find

$$\sigma=[16\pi\lambda^2\phi_0^2/\Gamma_2^2(\epsilon^2+1)][202/22]\alpha_{22}^2R^2\times\{[(\epsilon^2+1)+b]+\phi[c+d\epsilon+\cos^2\theta(e\epsilon+f)]+\phi^2[(\epsilon^2+1)g+h\epsilon+i+(j+k'\epsilon)\cos^2\theta+l\cos^4\theta]\}. \quad (8)$$

TABLE II. Sums used in Li^6 reaction with $j_r=0$ and 2.

l_1	l_2	$\sum_{m=-2}^{2}(l_120m/l_122m)\times(l_220m/l_222m)(P_2^m)^2$	$\sum_{m=-2}^{2}(l_110m/l_112m)\times(l_210m/l_212m)(P_2^m)^2$
0	0	5	
0	2	$(5/14)^{\frac{1}{2}}(1-3\cos^2\theta)$	
2	2	$5/14(4-9\cos^2\theta+9\cos^4\theta)$	$15/2(\cos^2\theta-\cos^4\theta)$

[4] See E. U. Condon and G. H. Shortley, *Theory of Atomic Spectra* (Oxford University Press, New York, 1935), pp. 76–77.

TABLE III. Barrier penetrabilities of the s and d waves.

$R/(e^2/mc^2)$	E/mc^2	1	1.5	2	3	4	6	8
1.50	φ_0	0.500	0.820	1.207	1.127	0.887	0.725	0.648
	φ_2	0.021	0.046	0.076	0.146	0.225	0.399	0.591
	φ	0.042	0.056	0.063	0.130	0.254	0.550	0.912
2.25	φ_0	0.936		1.190	0.904	0.795	0.687	0.626
	φ_2	0.076		0.258	0.479	0.734		0.800
	φ	0.081		0.217	0.530	0.923		1.278
3.00	φ_0		1.253	1.025	0.851	0.766	0.672	
	φ_2	0.187	0.381	0.604		1.126	0.786	
	φ		0.304	0.589		1.470	1.170	

In Eq. (8) we have put

$$
\begin{aligned}
R^2&=(R_0^2+I_0^2)\\
b&=5(R_2^2+I_2^2)/R^2\\
c&=\{(50/7)^{\frac{1}{2}}(R_2R_3+I_2I_3)-(R_1I_2-I_1R_2)+(5)^{\frac{1}{2}}I_0\}/R^2\\
d&=\{-(R_1R_2+I_1I_2)-(5)^{\frac{1}{2}}R_0\}/R^2\\
e&=\{3(R_1R_2+I_1I_2)+(9/5)^{\frac{1}{2}}R_0\}/R^2\\
f&=\{[-30/(14)^{\frac{1}{2}}](R_2R_3+I_2I_3)\\
&\qquad+3(R_1I_2-I_1R_2)-3(5)^{\frac{1}{2}}I_0\}/R^2\\
g&=(1/5)(R_1^2+I_1^2)/R^2\\
h&=(10/35)^{\frac{1}{2}}(R_3R_1+I_3I_1)/R^2\\
i&=\{(10/7)(R_3^2+I_3^2)+5/4\\
&\qquad+(10/35)^{\frac{1}{2}}(I_3R_1-I_1R_3)\}/R^2\\
j&=\{-(45/14)(R_3^2+I_3^2)+(15/2)(R_4^2+I_4^2)\\
&\qquad-(30/4)-(18/7)^{\frac{1}{2}}(I_3R_1-I_1R_3)\}/R^2\\
k'&=-(18/7)^{\frac{1}{2}}(R_3R_1+I_3I_1)/R^2\\
l&=\{(45/14)(R_3^2+I_3^2)\\
&\qquad-(15/2)(R_4^2+I_4^2)+45/4\}/R^2. \qquad (9)
\end{aligned}
$$

Also, $\phi=\phi_2/\varphi_0$ is the ratio of the penetration amplitudes of the incoming d and s waves.

With these definitions we can write finally,

$$\sigma=C(\epsilon)[1+A(\epsilon)\cos^2\theta+B(\epsilon)\cos^4\theta] \qquad (10)$$

where

$$
\begin{aligned}
C(\epsilon)&=\pi\{4\lambda\phi_0[202/22]\alpha_{22}\}^2D(\epsilon)/\Gamma_2^2(\epsilon^2+1)\\
D(\epsilon)&=a+(\epsilon^2+1)+\varphi(c+d\epsilon)+\varphi^2\{(\epsilon^2+1)g+h\epsilon+i\}\\
A(\epsilon)&=\phi[e\epsilon+f+\phi(j+k'\epsilon)]/D(\epsilon)\\
B(\epsilon)&=l\phi^2/D(\epsilon).
\end{aligned} \qquad (11)
$$

Here $C(\epsilon)$ represents the yield at $\theta=90°$. It need not be considered however in a study of the angular distribution. Its form illustrates our assumption of a broad state with $j_r=0$ and a sharp state with $j_r=2$, since ϵ is related to the resonant energy E_2 and the bombarding energy E in center-of-mass coordinates by Eq. (5).

If there were no entering d wave, φ would become zero and $A(\epsilon)$ and $B(\epsilon)$ would vanish, the d wave being necessary for the appearance of the asymmetry. Also since φ is more important than φ^2 at low energies, $B(\epsilon)$ should rise from zero at a higher energy than $A(\epsilon)$.

The explicit form of the parameters is given here so that a comparison of their values in terms of the integrals appearing in the theory with the values required to fit the data can be made.

III. PENETRABILITY OF THE NUCLEAR POTENTIAL BARRIER

In both of the lithium two-alpha-reactions the "outgoing" matrix element $(r/H/Q)$ can be assumed to be independent of the energy in the ranges considered, since these reactions are highly exoergic. The energy dependence of $\phi_l(E)$ arises almost entirely from the penetration of the incoming wave.

Tabulated values of the amplitudes of the regular and irregular solutions of the wave equation with Coulomb field at the edge of the nucleus are not available as yet for the required values of the parameters and the WKB approximation method is used for the calculation of penetrability. In the case Li^6+deuteron we deal with $l=0$ and $l=2$. For a given l the barrier for the Li^6 case is lower than that for Li^7 due to the greater reduced mass of the system Li^6+H^2 and the larger radius, R, of the top of the barrier one must assume to allow for the extension of the deuteron. This brings the barrier height into the region of experimental energies for $l=0$, and also for $l=2$ if we take $R<1.8\ e^2/mc^2$. φ_l is put equal to $|B_l-E|^{-\frac{1}{4}}e^{-C_l}$ with B_l the barrier height and C_l defined as $[(2M)^{\frac{1}{2}}/\hbar]\int_R^{r_l}(U_l-E)^{\frac{1}{2}}dr$, the usual integral across the barrier.[5] The use of $(l+\frac{1}{2})^2\hbar^2/2Mr^2$ as the l-barrier in $U_l(r)$ keeps the WKB approximation a good one for energies closer to the barrier height than the use of $l(l+1)\hbar^2/2Mr^2$ would permit.[6]

Calculations were made for three values of R, the effective nuclear radius. For $R=1.50e^2/mc^2$, $B_0=2.38\ mc^2$ and $B_2=11.51mc^2$. For $R=2.25e^2/mc^2$, $B_0=1.50mc^2$ and $B_2=5.56mc^2$. For $R=3.00e^2/mc^2$, $B_0=1.10mc^2$ and $B_2=3.38mc^2$. Values of φ_l and φ are tabulated in Table III for the three radii assumed and for some of the values of E used.

Values for $\varphi_l(E)$ are calculated on both sides of the barrier height and a smooth curve is drawn through this region.[7] The arbitrariness of the curve near the peak does not greatly affect our final results because the nuclear radius chosen avoids the use of this region.

In Fig. 1, $\varphi=\varphi_2/\varphi_0$ is plotted against the energy for

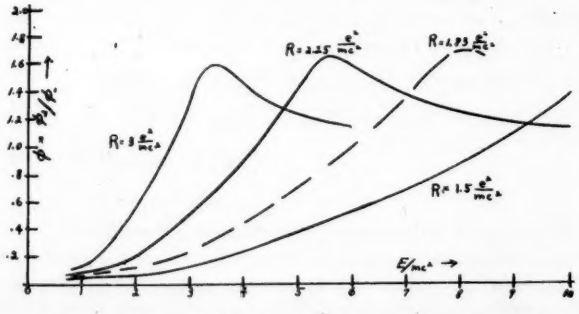

FIG. 1. Ratio of penetrabilities of $l=2$ wave to $l=0$ wave as function of incoming energy for several assumed radii in d+Li^6.

[5] H. A. Bethe, Rev. Mod. Phys. 9, 178 (1937).
[6] Breit, Wheeler, and Yost, Phys. Rev. 49, 174 (1936).
[7] N. H. Frank and L. A. Young, Phys. Rev. 38, 80 (1931).

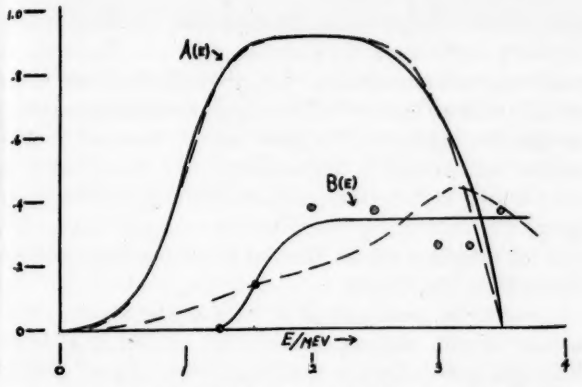

FIG. 2. Theoretical (dashes) and experimental (straight line) curves for $A(E)$ and $B(E)$ in $Li^6(d,\alpha)\alpha$ with $\Phi=kE$.

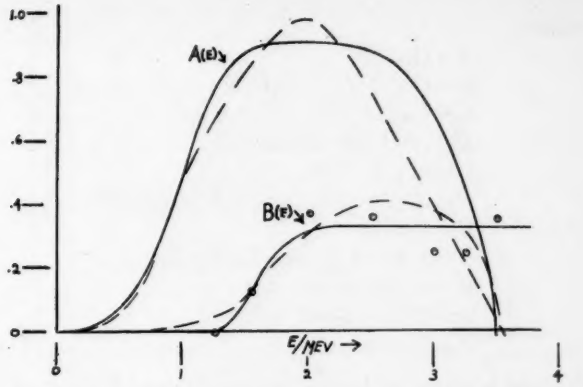

FIG. 3. Theoretical (dashes) and experimental (straight line) curves for $A(E)$ and $B(E)$ in $Li^6(d,\alpha)\alpha$ with $\Phi=kE^2$, rough choice of coefficients.

each assumed radius. The ratio for $R=1.83e^2/mc^2$ interpolated from the calculated values is shown also in Fig. 1. The choice of this radius will be discussed below. It is worth noting here that for $R=1.83e^2/mc^2$, $B_4=22.36mc^2$ and φ_4 is negligible compared to φ_0 and φ_2 in the energy range considered, so that $l=4$ can be omitted in the analysis.

IV. COMPARISON WITH EXPERIMENTAL RESULTS

We test the assumption that a broad state with $j_r=0$ and a sharp state with $j_r=2$ will account for the experimental results, the first peak in the observed excitation curve at 0.75 Mev being the $j_r=2$ resonance where $\epsilon=0$, and the subsequent approach to a second peak being due to increasing penetrability of the $l=2$ wave.

Under this assumption we first choose R for Li^6+H^2 such that $l=2$ has its maximum penetrability "at the second peak," or more specifically, at $E=4$ Mev. This corresponds to $R=1.83e^2/mc^2$. This radius would put the maximum penetrability for $l=0$ between the peak at 0.75 Mev and 1 Mev and would account for the broadness of the peak on the high energy side and the more gradual descent to a higher minimum there. This value of R is larger than the corresponding value for Li^7+H^1 ($R=1.5e^2/mc^2$) as taken in I, and by Christy and Latter,[8] and is easily accounted for as the distance out to the center-of-mass of the deuteron when the two nuclei begin to interact strongly.

Under these assumptions we obtained (10) and (11). Since the maximum for φ occurs in the observed energy range, we cannot neglect φ^2 in our determination of $A(\epsilon)$ and $B(\epsilon)$. This, of course, introduces a large number of undetermined constants. In order to cut these parameters to a minimum we set $\varphi=kE$ for the range considered and we choose k so that this will be a fair approximation in the region from 1.5 to 3.5 Mev (e.g., $k=0.3$ (Mev)$^{-1}$).

Putting in $E=(\Gamma_2/2)\epsilon+E_2$ [9] and $\varphi=kE$ we obtain

$$A(E)=(HE^3+JE^2+KE)/(E^4+BE^3+CE^2+DE+F) \quad (12)$$

and

$$B(E)=LE^2/(E^4+BE^3+CE^2+DE+F)$$

where the coefficients are expressible in terms of the constants in (9) and E_2, Γ_2 and k.

The quickest and best fit of these expressions to the experimental curves is obtained by solving simultaneously for the seven coefficients in $A(E)$. A choice of L in $B(E)$ then normalizes this curve. This has been done and with the following values for the coefficients the curves have been plotted in Fig. 2 with the experimental curves.

$H=-0.4577$ (Mev)	$C=26.584$ (Mev)^2
$J=1.6020$ (Mev)^2	$D=-33.483$ (Mev)^3
$K=0$ (Mev)^3	$F=16.879$ (Mev)^4
$B=-8.6540$ (Mev)	$L=0.1375$ (Mev)^2.

From Fig. 2 it is evident that $A(E)$ is an excellent fit to experiment, lying everywhere within the experimental uncertainty. $B(E)$, however, is a very poor fit indeed, and attempts to improve the fit to $B(E)$ with Eqs. (12) resulted in a much poorer fit for $A(E)$. A more exact expression for φ appears to be necessary in order to provide an $A(E)$ and $B(E)$ with sufficient parameters to obtain a good fit with experiment everywhere. This indicates that the results are sensitive to the exact assumptions made, thus making our assumptions more significant.

It is clear from Fig. 1 that $\varphi=kE^2$ will represent the curve for $R=1.83e^2/mc^2$ better than $\varphi=kE$. In fact, if we take $k=0.114$ (Mev)$^{-2}$, $\varphi=kE^2$ is almost an exact fit over the whole range $0<E<3.75$ Mev. Putting in kE^2 for φ and $E=(\Gamma_2/2)\epsilon+E_2$ in (11) we obtain

$$A(E)=(AE^5+BE^4+CE^3+DE^2)/(E^6+FE^5+GE^4+HE^3+JE^2+KE+M) \quad (13)$$

and

$$B(E)=LE^4/(E^6+FE^5+GE^4+HE^3+JE^2+KE+M)$$

[8] R. F. Christy and R. Latter, Rev. Mod. Phys. **20**, 185 (1948).

[9] Defined in laboratory system, which introduces factor $(\frac{3}{4})^2$ in $C(\epsilon)$. See footnote 12 of I.

where

$$\begin{aligned}
A&=(\Gamma_2/2)k'\\
B&=(\Gamma_2^2/4)j-E_2\Gamma_2k'/2\\
C&=\Gamma_2e/2k\\
D&=(\Gamma_2^2f/4k-E_2\Gamma_2e/2k)\\
F&=h\Gamma_2/2-2gE_2\\
G&=i\Gamma_2^2/4-hE_2\Gamma_2/2+g(\Gamma_2^2/4+E_2^2)\\
H&=\Gamma_2d/2k\\
J&=1/k^2+\Gamma_2^2c/4k-\Gamma_2dE_2/2k\\
K&=-2E_2/k^2\\
M&=\Gamma_2^2(a+1)/4k^2+E_2^2/k^2\\
L&=\Gamma_2^2l/4
\end{aligned}\qquad(14)$$

defined in terms of the constants in (9), and E_2, Γ_2, and k.

Before fixing our coefficients to give the best fit to experiment, we inquire whether or not the values of the coefficients determined from their definition in terms of the matrix elements, etc., in the theoretical treatment can give us the general form of the experimental curves. The exact values of the matrix elements cannot be calculated but one may conclude that the coefficients $a, b, c, \cdots$ are probably of the order of magnitude 1, varying perhaps from $\frac{1}{5}$ to 5, and that some (a, g) are required to be positive. It is possible that some of these coefficients may be zero since they involve differences of matrix elements, but the probability of such an occurrence seems small. Furthermore $k\cong\frac{1}{9}$, $\Gamma_2\cong(\frac{1}{4})$ Mev, and $E_2\cong(\frac{3}{4})$ Mev. The "expected" range of the coefficients in (14) is not sufficiently narrow to yield a curve of any definite shape, but with a small amount of trial adjustment of the coefficients within this range a rough fit was easily obtained (Fig. 3). Here

$$\begin{aligned}
A&=-0.008\text{ Mev} & M&=48.0\text{ (Mev)}^6\\
B&=0.80\text{ (Mev)}^2 & K&=-91.0\text{ (Mev)}^5\\
C&=-2.92\text{ (Mev)}^3 & J&=55.0\text{ (Mev)}^4\\
D&=4.64\text{ (Mev)}^4 & H&=-5.98\text{ (Mev)}^3\\
L&=0.11\text{ (Mev)}^2 & G&=2.00\text{ (Mev)}^2\\
& & F&=-4.02\text{ Mev.}
\end{aligned}\qquad(15)$$

The appearance of the late and sharp rise of the $B(E)$ curve is a feature of these equations obtained even with only rough values of the coefficients which the previous Eqs. (12) could not yield while still retaining a good fit to $A(E)$. Hence the improved fit of equations (13) with coefficients (14), obtained by use of the more nearly correct expression for the penetration ratio $\varphi=kE^2$, rather than $\varphi=kE$, seems quite significant even though the improvement involved an increase in the number of arbitrary parameters. By more careful curve-fitting still better coefficients could be obtained, but as Fig. 3 implies, these would compare favorably with the ranges of values allowed by order-of-magnitude estimates in the theory.

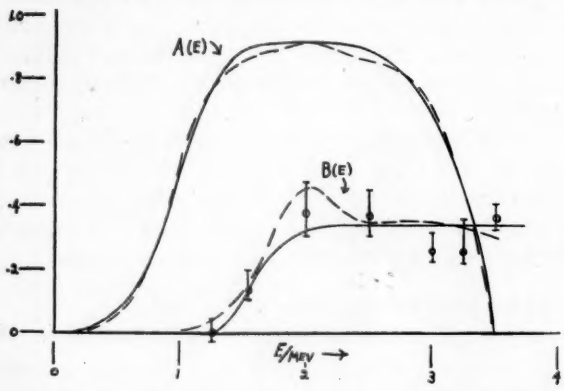

FIG. 4. Theoretical (dashes) and experimental (straight line) curves for $A(E)$ and $B(E)$ in $Li^6(d,\alpha)\alpha$ with $\Phi=kE^2$.

It would be gratifying if it were evident from comparison of the theoretical expressions for $A(E)$ and $B(E)$ in the $Li^7(p,\alpha)\alpha$ reaction with those of the $Li^6(d,\alpha)\alpha$ reaction, that the $A(E)$ and $B(E)$ curves rise from zero at a higher energy in the Li^6 case. This would correspond to the physical situation that the easy entrance of s-waves makes the $Li^6(d,\alpha)\alpha$ reaction symmetric at very low energies and that the p-waves responsible for the Li^7 reaction at low energies may introduce asymmetry in that reaction. For $Li^7(p,\alpha)\alpha$ the result[3] comparable to (13) is

$$\begin{aligned}
A(E)&=(C_0E^2+C_1E+C_2)/(E^2+C_3E+C_4)\\
B(E)&=(C_5E^2+C_6E)/(E^2+C_3E+C_4).
\end{aligned}\qquad(16)$$

For both $A(E)$ and $B(E)$ the form of the numerator in $Li^6(d,\alpha)\alpha$ requires a later rise with energy than the numerators in $Li^7(p,\alpha)\alpha$. In (13) the lowest power of E is 2 in $A(E)$ and 4 in $B(E)$, whereas in (16) the lowest power of E is 0 in $A(E)$ and 1 in $B(E)$. The qualitative differences being considered in these reactions appear in the energy region $0<E<1$ Mev, and in this region one can claim that in effect, the denominators in (13) and (16) have the same form. Not only are high powers of E less important here, but (14) and (15) show also that the coefficients of the high powers of E in the denominators of (13) are relatively very small. Hence, the nature of the numerator predominates and the results give rise somewhat naturally to the later rise in the angular distribution curves of $Li^6(d,\alpha)\alpha$ observed experimentally. The observed vanishing of $A(E)$ near $E=0$ for $Li^7(p,\alpha)\alpha$ is caused[3] by a pure coincidence in the placing of the resonant state of the compound nucleus, and there is no consideration of barrier penetration to oppose a rapid rise.

In order to demonstrate that an improved fit can be obtained with (14) by more exact curve-fitting, we choose values for our parameters by solving simultaneously fixing four coefficients by the $B(E)$ experimental curve and the remaining seven by the $A(E)$ experimental curve. The resulting curves are plotted in Fig. 4 with the experimental curves for comparison. The coefficients are assigned the following values

$$\begin{aligned}
A&=-0.2648\text{ (Mev)} & G&=63.248\text{ (Mev)}^2\\
B&=1.8966\text{ (Mev)}^2 & H&=-164.215\text{ (Mev)}^3\\
C&=-4.3292\text{ (Mev)}^3 & J&=232.222\text{ (Mev)}^4\\
D&=3.2706\text{ (Mev)}^4 & K&=-171.094\text{ (Mev)}^5\\
F&=-12.531\text{ (Mev)} & L&=0.0110\text{ (Mev)}^2\\
& & M&=52.379\text{ (Mev)}^6.
\end{aligned}\qquad(17)$$

The localized hump in the $B(E)$ curve and the dips in the $A(E)$ curve both derive from the curve fitting condition $[dB(E)/dE]_{E=2.5}=0$. Had another condition been imposed in its place the fit could be better than shown. However, the already good fit obtained and the uncertainty in the experimental values make further fitting seem superfluous.

In this case, with $\varphi=kE^2$, both $A(E)$ and $B(E)$ can be considered good fits. The $B(E)$ curve shows the late and rapid rise characteristic of this reaction. The experimental uncertainty in the points is also shown in Fig. 4, and $B(E)$ is seen to be a good fit, in spite of the localized hump which is not considered significant. $A(E)$ again lies everywhere within the experimental uncertainty in the curve. The values of this set of coefficients are also fairly reasonable from the point of view discussed in connection with (14) and (15). For example, C in (17) makes $|e|=0.9$ after Γ_2 from the observed resonance and k from penetration calculations have been used, and similarly D makes $f\approx 1$. The value of $|H|$ in (17) is unreasonably large, requiring $|d|\approx 30$, but seems to be associated with the unexpected localized hump in $B(E)$, and this somewhat unlikely value would probably disappear with more refined curve fitting.

V. ALTERNATIVE SET OF COMPOUND STATES

The assumption investigated above that the angular distribution is to be attributed to a broad state of the compound nucleus with $j_r=0$ and a sharp state with $j_r=2$, seems to be the simplest basis for interpretation of the experimental results. The sharp state $j_r=2$ gives rise to the observed resonance, and the great breadth of the state with $j_r=0$ is naturally associated with the ease with which such a state is expected to break up into two alphas.

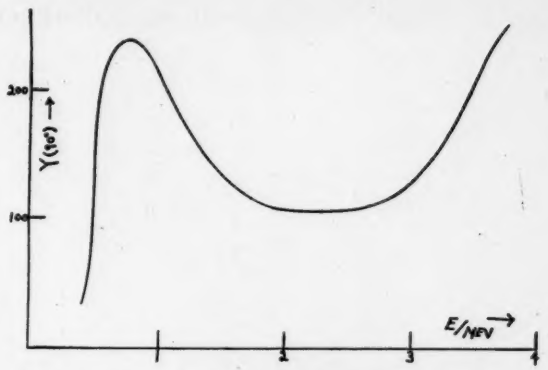

FIG. 5. Relative cross section for $Li^6(d,\alpha)\alpha$ at 90°.

The fitting of the data with the above assumptions does not guarantee their validity, however, and, in fact, a simple modification of them suggests itself when one investigates the $\sigma(E, 90°)$ curve, Fig. 5. The rise to a second peak near 3.5 Mev can also be attributed to a sharp s-state, rather than due only to increasing penetrability of d-wave deuterons. Under the assumption of two sharp states, with $j_r=0$ and $j_r=2$, one can carry out the calculations, closely paralleling those already carried out, and one finds

$$A(\epsilon_0,\epsilon_2)=\frac{\phi(p+q\epsilon_0+r\epsilon_2+s\epsilon_0\epsilon_2+t\epsilon_0^2)+\phi^2(u+v\epsilon_0^2+w\epsilon_0+y\epsilon_2+z\epsilon_0\epsilon_2)}{(a\epsilon_0^2+b\epsilon_2^2+c)+\phi(d+e\epsilon_0+f\epsilon_2+g\epsilon_0\epsilon_2+h\epsilon_0^2)+\phi^2(i+j\epsilon_0^2+k\epsilon_2^2+l\epsilon_0+m\epsilon_2+h\epsilon_0\epsilon_2)}. \quad (18)$$

$B(\epsilon_0,\epsilon_2)$ has the same denominator as $A(\epsilon_0,\epsilon_2)$ but its numerator is $l'\varphi^2(1+\epsilon_0^2)$.

Here,

$$\epsilon_0=(E-E_0)/(\Gamma_0/2) \quad \text{and} \quad \epsilon_2=(E-E_2)/(\Gamma_2/2) \quad (19)$$

and the coefficients a, b, $\cdots z$ are defined in terms of matrix elements as in (9) but they are more involved and more numerous, and interpretation of their roles becomes quite complex.

Substitution of (19) in (18) and taking $\varphi=kE^2$ gives

$$A(E)=(C_1E^6+C_2E^5+C_3E^4+C_4E^3+C^5E^2)/(E^6+C_7E^5+C_8E^4+C_9E^3+C_{10}E^2+C_{11}E+C_{12}).$$

$B(E)$ has the same denominator as $A(E)$, but its numerator is $C_6E^6+C_{13}E^5+C_{14}E^4$.

Hence, we arrive at expressions giving one additional curve-fitting parameter in $A(E)$ and two additional parameters in $B(E)$. Of course, the number of implicit parameters has increased and the relation of the explicit ones to the matrix elements has become more complex. Also, both numerator and denominator are now the same order in E.

Since the simpler assumptions fit the experimental results, it is clear that these assumptions give more parameters than are necessary. A fit in this case would be less significant than with fewer parameters and its interpretation would be more involved. These assumptions may have to be invoked only if experiments obtaining $A(E)$ and $B(E)$ and $\sigma(E, 90°)$ are performed for $E>3.75$ Mev and the added complexity requires the greater freedom allowed by (18). If extension of the experiments demonstrates that a resonance does in fact exist near 4 Mev, then these assumptions will be the simplest valid ones. However, we may than have to consider the small effect of the $l=4$ wave, and the effect of the fact that φ may not behave as E^2 beyond the peak.

Some Properties of Superconductors below 1°K. II. Aluminum and Zinc

J. G. DAUNT AND C. V. HEER
The Mendenhall Laboratory, The Ohio State University, Columbus, Ohio
(Received July 25, 1949)

Magnetic measurements of the threshold curves of superconducting aluminum and zinc of very high purity have been carried out down to 0.3°K. Calculations have been made therefrom of the entropy differences between the normal and superconducting states and of the specific heats of the electron assemblies in both the normal and superconducting states. The value of the linear term for the normal electronic specific heat for Al was found to be $2.59\times10^{-4}T$ cal./mole/degree and for Zn $1.36\times10^{-4}T$ cal./mole/degree.

INTRODUCTION

IN continuation of investigations[1] on techniques required for the observation of nuclear paramagnetism the properties of superconducting aluminum and zinc have been studied below 1°K, details of which are reported herewith. A detailed examination has been made of the magnetic properties of these elements in the temperature range 0.3°K to 1°K, since it is considered that these metals will be of value for the establishment of thermal contact switches at very low temperatures.*

Previous work by Daunt and Mendelssohn,[2] on the magnetic properties of superconductors in the liquid helium temperature range, has shown that it is possible therefrom to calculate reliable values for the specific heats of the electron assemblies both in the normal and in the superconducting states. Furthermore such evaluations are free of any obscuring effects of the vibrations of the crystal lattice, as would be present in direct calorimetric observations. The accuracy of our measurements of the magnetic threshold curves of superconducting aluminum and zinc was sufficiently good to enable such evaluations of their specific heats to be carried out by this method for the first time. A comparison of our results with those obtained by other methods disclosed satisfactory agreement and emphasizes the confidence previously established in the reliability of our method.

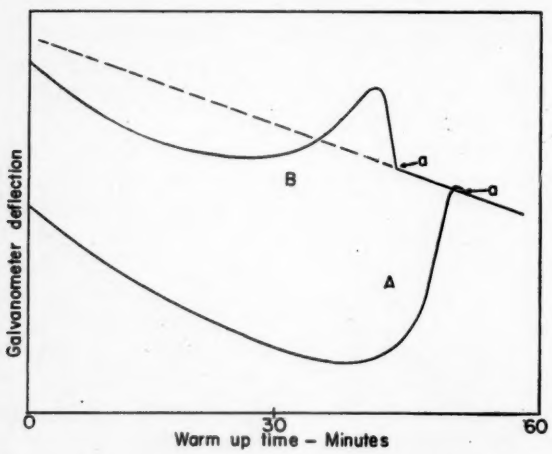

FIG. 1. Change of susceptibility with warm-up time; curve A for zero exterior magnetic field, curve B for a finite applied magnetic field.

EXPERIMENTAL ARRANGEMENTS

Temperatures below 1°K were produced by the magnetic method starting from the temperatures obtained with liquid helium.[3] The paramagnetic salt used was chromium potassium alum, the magnetic field being provided by a large permanent magnet.

To achieve thermal contact between the salt and the superconducting metal under investigation, the metal in the form of small pieces was compressed together with the powdered salt into an ellipsoidal pill under a pressure of 200–300 atmospheres. It was found that good temperature equilibrium was maintained between the salt and the metal by this method down to about 0.2°K, as previously observed by Kurti and Simon[4] and by us,[1] and as is indicated by the agreement between the two sets of measurements reported here for zinc of different average particle size.

The susceptibility of the specimen was measured by the ballistic mutual inductance method,[5] from which measurements both the Curie temperatures and the superconducting transitions could be obtained. The specimen was mounted on a thin-walled glass rod, the lower end of which was fixed to the bottom of a brass vacuum vessel immersed in liquid helium. The mutual inductance used to measure the variation of susceptibility of the specimen was wound around this vacuum vessel and consisted of two secondary coils of 3800 turns each wound in series opposition, and a single layer primary coil of 100 turns per cm. The specimen was mounted coaxially inside one of the secondary coils, the other serving as a compensator. The primary coil produced a measuring field of between 1 and 5 gauss. A solenoidal coil, which could be demounted during the adiabatic demagnetizations, was mounted coaxially

[1] J. G. Daunt and C. V. Heer, Phys. Rev. **76**, 715 (1949).
* Detail of experiments carried out on these problems will be published separately.
[2] J. G. Daunt and K. Mendelssohn, Proc. Roy. Soc. **A160**, 127 (1937); Daunt, Horseman, and Mendelssohn, Phil. Mag. **27**, 754 (1939).
[3] Daunt, Heer, and Silvidi, Phys. Rev. **75**, 1113 (1949).
[4] N. Kurti and F. Simon, Proc. Roy. Soc. **A151**, 610 (1935).
[5] N. Kurti and F. Simon, Proc. Roy. Soc. **A149**, 152 (1935); de Haas and Wiersma, Physica **2**, 335 (1935).

TABLE I. Data on the Al and Zn specimens.

No.	Specimen composition	Linear dimensions of metal particles mm	Major axis mm	Minor axis mm	f	Δ
2	Cr alum and Al	1	29	13	0.55	0.008
4	Cr alum and Zn	1–2	38	13	0.63	0.011
5	Cr alum and Zn	0.1–0.5	32	13	0.80	0.013

with the mutual inductance and provided the small fields necessary for the observation of the magnetic transitions of the superconducting metals. All metal joints at liquid helium temperatures were silver soldered to avoid the presence of undesired superconducting material.

It was found that with this arrangement the rate of warming of the specimen at the lowest temperatures was moderately small, thus ensuring good conditions for temperature equilibrium between the salt and the metal. Approximately one hour was required to warm up from 0.3 to 1°K, corresponding to an average heat influx of 8 ergs per second.

In Table I, details of the aluminum and the two zinc specimens are given. The aluminum used in specimen #2 was 30 mesh chips from Coleman and Bell having a purity >99.9 percent. Spectroscopic analysis showed that the amount of other superconducting material present, namely Pb, was probably less than 0.001 percent. The zinc used in specimens #4 and #5 was H-S spectroscopic zinc, Lab. No. 1790B supplied by Johnson, Matthey and Company having a stated purity of 99.999 percent and containing less than 0.0001 percent Pb.

TABLE II. Observed magnetic thresholds for Al and Zn for difference Curie temperatures.

Al (#2)		Zn (#4)		Zn (#5)	
T_s^*(deg)	H_c(gauss)	T_s^*(deg)	H_c(gauss)	T_s^*(deg)	H_c(gauss)
0.734	60.0	0.959	0.0	0.910	0.0
0.688	65.4	0.865	8.8	0.845	13.2
0.636	71.0	0.787	16.4	0.725	22.2
0.600	76.2	0.623	31.6	0.573	37.6
0.526	82.0	0.519	42.0	0.501	42.8
0.454	87.4	0.511	42.2	0.377	53.0
		0.507	42.0		
		0.495	44.2		
		0.447	48.4		
		0.383	52.0		
		0.321	55.0		
		0.283	55.4		

In Table I, f denotes the filling factor, namely the ratio of the distributed density of the powdered salt to the crystalline density and Δ is given by

$$\Delta = cf(4\pi/3 - N),$$

where c is the Curie constant per cc and N the demagnetization factor of the specimen. The listed values of Δ were used in the calculation T_s^*, the extrapolated temperature based on Curie's law for a spherical specimen.[6]

In order to observe the superconducting transitions the specimen was allowed to warm up either in zero magnetic field or in a small d.c. field provided by the external magnetizing coil, susceptibility measurements being made at regular time intervals, a method previously used successfully by Kurti and Simon[4] and by us.[1] Typical curves showing the change of the susceptibility with time are given in Fig. 1, the curve A showing the typical behavior in zero exterior magnetic

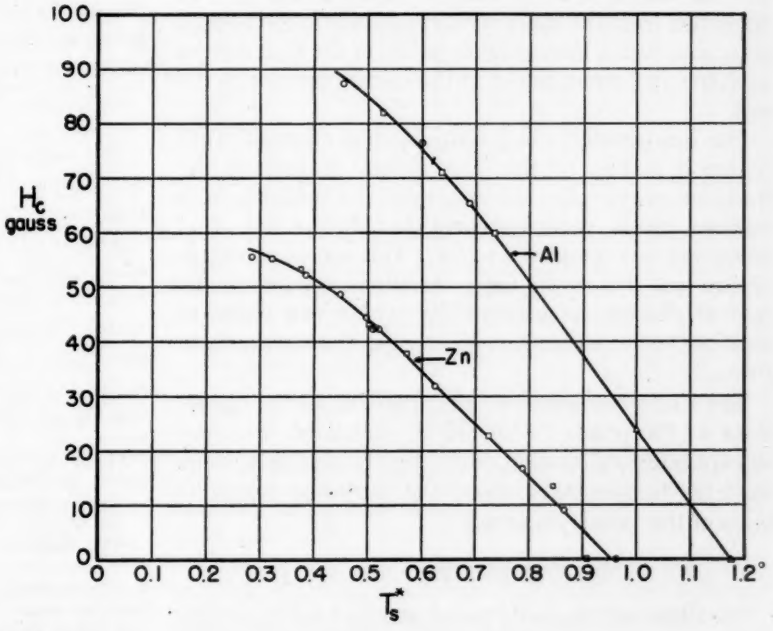

FIG. 2. Observed magnetic threshold for Al and Zn as a function of the Curie temperature T_s^*.

[6] N. Kurti and F. Simon, Phil. Mag. 26, 849 (1938).

TABLE III. Comparison of the values of gamma for Al and Zn obtained by various methods, and the value of the constant A in the equation for the specific heat of superconducting electrons.

	Al	Zn
γ from our experimental ΔS values	2.59×10^{-4} cal./mole/deg.^{2}	1.36×10^{-4} cal./mole/deg.^{2}
γ from Sommerfeld's formula	2.18×10^{-4} cal./mole/deg.^{2} (for $n=3$)	1.80×10^{-4} cal./mole/deg.^{2} (for $n=2$)
γ from calorimetric measurements		
Kok and Keesom*	3.48×10^{-4} cal./mole/deg.^{2}	
Keesom and van den Ende**		1.25×10^{-4} cal./mole/deg.^{2}†
Daunt and Silvidi***		1.50×10^{-4} cal./mole/deg.^{2}
A	5.6×10^{-4} cal./mole/deg.^{4}	4.8×10^{-4} cal./mole/deg.^{4}

* See reference 14.
** See reference 15.
*** See reference 15a.
† This value is obtained from Keesom and van den Ende's measurements by plotting C_s/T against T^2 which yields a straight line the intercept of which on the C/T axis enables the γ-value to be calculated. We are indebted to Mr. A. A. Silvidi for pointing this out to us. This value is somewhat lower than the value given by the interpretation of Burton, Grayson-Smith, and Wilhelm, *Phenomena at the Temperature of Liquid Helium* (Reinhold Publishing Company, New York, 1940), p. 348, of the same measurements of Keesom and van den Ende.

field and the curve B in a finite applied magnetic field. For both curves a marked kink at the points marked "a" was observed which indicated the disappearance of the last remnants of superconductivity in each specimen at the value of field given by the strength of the applied exterior d.c. field.

For measurements in zero applied magnetic field (curve A in Fig. 1) the specimens showed a susceptibility less than that due to the paramagnetism of the salt on account of the diamagnetism of the superconducting metal, as is shown by the difference between the full curve and the extrapolated dashed curve in Fig. 1. From this diamagnetic component of the total susceptibility it was possible to calculate that for all specimens the full volume of metal became superconducting. The transition from the superconducting state to the normal state was over a broad region owing to the distribution in shape and arrangement of the metal particles in the salt.

For measurements in a finite applied magnetic field (curve B in Fig. 1), the same general features of the warm-up curve were evident with the addition of a marked excess paramagnetism just before the final transition was completed at "a". This excess paramagnetism was due to the large variations possible in the rate of change of susceptibility which can occur in multiply connected superconductors in the intermediate state.

The Curie temperatures corresponding to the transitions at the points "a" could be calculated from the susceptibility calibration curve for the salt specimens made at temperatures above the transition temperatures of the metal concerned.

RESULTS

The observed magnetic thresholds for aluminum and zinc are tabulated in Table II and are shown plotted against the Curie temperatures, T_s^*, in Fig. 2. No significant difference was observed in the results for zinc of two different average particle size. It is estimated that in the temperature range concerned, the differences between the T_s^* values and the absolute temperatures[7] are within the experimental errors which for the magnetic fields are estimated to be ±1 gauss and for T_s^* to be ±0.008 degree for the measurements in finite fields. For the transition in zero field the experimental error in the temperature is greater, being about ±0.025 degree. Other data are given in Table III.

In Fig. 2 the points above 1.0°K for the magnetic threshold curve for aluminum have been taken from Shoenberg's work,[8] the temperatures having been corrected to the 1939 scale proposed by Bleaney and Simon.[9]

The error in the magnetic field depends primarily on estimating the field acting on the small pieces of superconductor imbedded in the salt. The field acting on the interior of a small cavity will be given by

$$H=H_{\text{ext}}+(D-N)\sigma f,$$

where H_{ext} is the exterior applied field, N the demagnetization factor for the entire specimen, D the demagnetization factor for the space occupied by a small superconducting particle, σ the magnetic moment per unit volume and f the filling factor. An accurate evaluation of $(D-N)$ cannot be made since the shapes of the particles were irregular and distributed at random. As long as $(D-N)$ is of the order of unity, errors of the order of 1 percent at 0.5 degree and 2 percent at 0.25 degree may be expected. In the temperature range of our observations therefore, it is assumed that the errors in estimating the magnetic field are within the errors of experimental observation. At lower temperatures the deviations would become large and it would appear that below 0.2 degree, it would be desirable to use particles of regular shape.

DISCUSSION

For aluminum our measurements below 1°K together with those of Shoenberg[8] above 1°K form a satisfactory continuous curve, as shown in Fig. 2.

For zinc the transition temperature of 0.95 degree observed by us lies somewhat higher than the value found by Keesom[10] of 0.81 ± 0.02°K (corrected to 1939 scale).[9] Keesom's measurements, however, were of the electrical resistance of a cold-worked sample and appeared to show a small resistance remaining even at the lowest temperatures.**

[7] See J. H. Van Vleck, J. Chem. Phys. **5**, 320 (1937); M. H. Hebb and E. M. Purcell, J. Chem. Phys. **5**, 388 (1937).
[8] D. Shoenberg, Proc. Camb. Phil. Soc. **36**, 84 (1940).
[9] B. Bleaney and F. Simon, Trans. Faraday Soc. **35**, 1205 (1939).
[10] W. H. Keesom, Physica **1**, 123 (1934).
** Some preliminary experiments using Zn, having a purity spectroscopically found to be 99.99 percent which was therefore less pure than the Johnson Matthey zinc of samples #4 and #5 (see Table I), showed transition points in zero magnetic field as low as 0.82 degree. The magnetic measurements made with this

The transition temperature for zinc found by Shoenberg[8] for which the possible observation error was high (±0.05) lies reasonably close to the value given here. Shoenberg's magnetic threshold curve for zinc, however, differs greatly from that given in Fig. 2 due probably to the uncertainty in his measurements which he reported. A comparison of our results with the work on zinc by Lasarew and Esselson[11] is difficult since they based much of their calculations on the results obtained by Shoenberg.

The slopes of the magnetic transition curves for both Al and Zn, being 136 gauss per degree for Al and 98 gauss per degree for Zn at $H=0$, are small, thus placing these superconductors, as would be expected, into the group of "soft" superconductors.[2]

Following the thermodynamic theory of Gorter and Casimir,[12] the difference in entropy between the normal and the superconducting state is given by

$$\Delta S=S_s-S_n=\frac{V}{4\pi}H_c\left(\frac{dH_c}{dT}\right),$$

where V is the atomic volume. The ΔS values calculated from this formula using the magnetic threshold curves of Al and Zn shown in Fig. 2 are plotted against T_s^* in Fig. 3. It is evident that our measurements have been made to temperatures sufficiently low to allow extrapolation towards absolute zero. As has been pointed out previously by Daunt and Mendelssohn[2] for other superconductors, at sufficiently low temperatures ΔS will be proportional to T and can be identified with the total entropy of the electron gas in the normal state. If, according to Sommerfeld,[13] we put the specific heat of the normal electron gas, $C_n=\gamma T$ then

$$\gamma=\left(\frac{d\Delta S}{dT}\right)_{T=0}.$$

The values of γ obtained in this way for Al and Zn are listed in Table III. For comparison with these results, the γ-values calculated according to the simplified Sommerfeld formula[13] neglecting lattice effects are also listed in Table III, together with the γ-values obtained calorimetrically by Kok and Keesom[14] for Al, and by Keesom and van den Ende,[15] and Daunt and Silvidi[15a] for Zn.

The small differences between our results for γ and the values according to the simplified Sommerfeld formula are not surprising in view of the fact that the latter does not take into account the detailed energy spectrum of the metal.[13,16] The agreement between the values obtained from our ΔS values and those obtained calorimetrically is satisfactory in the case of zinc, although some discrepancy exists for the aluminum. The latter may be explained however in view of the fact that the calorimetric values are strongly dependent on the interpretation of the constants for the lattice specific heat, whereas in the values obtained from the ΔS curves the lattice specific heat does not enter in the calculations. These results, together with those previously obtained in a similar manner for other superconductors,[2] give confidence in the reliability of this method of measurement of the specific heat of the normal electrons, and indicate that our threshold curve measurements represent the reversible equilibrium boundary between the normal and the superconducting states.

As previously shown by Kok[17] and by Daunt and Mendelssohn[2] the specific heat of the system of superconducting electrons can also be calculated from the magnetic threshold curves. Such a determination, however, involves a second differentiation of H_c with respect to T, a process which can result in considerable error. On the other hand the calculation can be greatly simplified if it is assumed, as a first approximation, that the threshold curves are parabolic,[17] which leads to T^3 function for the specific heat of the superconducting electrons, given by

$$C_{s.el}=AT^3=\frac{3VH_0^2}{2\pi T_c^4}\text{ cal./mole/degree},$$

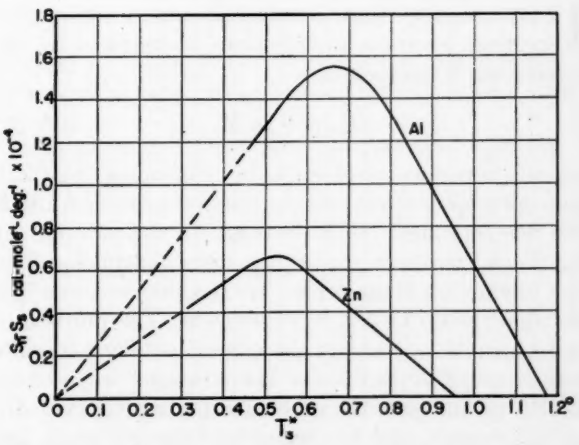

FIG. 3. Calculated values of the difference in entropy ΔS between the normal and the superconducting state plotted as a function of the Curie temperature.

relatively impure zinc have not been used for thermodynamic calculations, as the transitions from the superconducting to the normal state were not reversible.

[11] B. G. Lasarew and B. N. Esselson, J. Phys. U.S.S.R. **15**, 151 (1941).

[12] C. J. Gorter and H. G. B. Casimir, Physica **1**, 305 (1934); Zeits. f. Tech. Physik **15**, 539 (1934).

[13] A. Sommerfeld, Zeits. f. Physik **47**, 1 (1928); Ann. d. Physik **28**, 1 (1937).

[14] J. A. Kok and W. H. Keesom, Physica **4**, 835 (1937).

[15] W. H. Keesom and J. N. van den Ende, Proc. Amst. Akad. Sci. **35**, 143 (1932); Leiden Comm. 219b.

[15a] J. G. Daunt and A. A. Silvidi, to be published shortly.

[16] J. Slater, Phys. Rev. **45**, 794 (1934); N. F. Mott, Proc. Roy. Soc. **A152**, 42 (1936); H. Jones and N. F. Mott, Proc. Roy. Soc. **A162**, 49 (1937); A. Sommerfeld and H. A. Bethe, *Handbuch der Physik* (1933), Vol. 24/2, p. 33.

[17] J. A. Kok, Physica **1**, 1103 (1934).

where V is the atomic volume. The values of A calculated in this way for Zn and Al are given in Table III. The specific heat of the superconducting electrons calculated in this way is 87 times as great as the lattice specific heat for Al (Debye $\theta=419$[14]) and 33 times as great as that for Zn (Debye $\theta=320$[15]). The accuracy of this interpretation of $C_{s.el.}$ is, of course, strongly dependent on the accuracy with which the magnetic threshold curve follows a parabolic law. Our results for Al and Zn as well as those obtained elsewhere[2,18] show that the magnetic threshold curves are not exactly parabolic and consequently it cannot be excluded that for Zn and Al further approximation would lead to some deviation from the T^3 function for $C_{s.el.}$

[18] A. D. Misener, Proc. Roy. Soc. **A166**, 43 (1938).

ACKNOWLEDGMENTS

We wish to thank Professor H. H. Nielsen for his support of this low temperature program in The Mendenhall Laboratory, and The Research Corporation for their grant-in-aid of research on nuclear paramagnetism for which this work is preliminary and for their establishment of a fellowship for one of us (C.V.H.).

Our thanks are also due to the Ohio State University Research Foundation and the Ohio State University Development Fund for their aid. The later stages of the work were assisted by a contract between the Office of Naval Research and The Ohio State University Research Foundation.

We also thank Mr. A. A. Silvidi for his assistance during the experiments.

PHYSICAL REVIEW VOLUME 76, NUMBER 9 NOVEMBER 1, 1949

Magnetic Interaction between Neutrons and Electrons*

H. EKSTEIN
Armour Research Foundation, Chicago, Illinois
(Received July 11, 1949)

The phenomenological interaction operator between neutrons and electrons is usually assumed to be $-\mu\mathbf{s}\cdot\mathbf{B}$. ($\mu\mathbf{s}$ magnetic moment of the neutron, $\mathbf{B}$ magnetic field of the electrons.) Bloch has pointed out that other operators are possible. It is shown that the class of operators considered by Bloch is equivalent with the form $-\mu\mathbf{s}\cdot(\mathbf{H}+4\pi C\mathbf{M})$ where $\mathbf{M}$ is the spin momentum density of the electrons, $\mathbf{H}=\mathbf{B}-4\pi\mathbf{M}$ and C is an indeterminate constant. Diffraction by ferromagnetic crystals and magnetic double refraction are calculated for this interaction. Present experimental evidence excludes the value $C=0$. Experimental methods for measuring C are discussed.

I. THE GENERALIZED INTERACTION OPERATOR

IT is commonly assumed that the magnetic interaction between neutrons and electrons is described by the interaction Hamiltonian

$$H_{\text{int}}=-\mu\mathbf{s}\cdot\mathbf{B}, \tag{1}$$

where μ is the neutron's magnetic moment, $\mathbf{s}$ the Pauli spin operator acting on the neutron wave function and $\mathbf{B}$ the magnetic field of all electrons. It was pointed out by Bloch,[1] however, that other, more general forms of the interaction Hamiltonian are possible and that the decision should be left to experiment. The purpose of this paper is to examine the experimentally verifiable consequences of the class of Hamiltonians proposed by Bloch, to interpret the existing experimental evidence in this respect, and to suggest experiments which can give a definite decision on the interaction operator.

The interaction of neutrons with ferromagnetic crystals is most likely to supply the desired information. For the case of thermal neutrons, inelastic scattering is small, and the neutron can be described by a wave equation

$$(\nabla^2+k_0^2)\psi-(2m/\hbar^2)[V(\mathbf{r})+\langle H_{\text{int}}\rangle_{Av}]\psi=0, \tag{2}$$

where $\langle H_{\text{int}}\rangle_{Av}$ is the interaction operator, averaged over the electron wave functions of the ground state, ψ is the Pauli spinor of the neutron, $k_0^2=2mE/\hbar^2$ in the usual notation and $V(\mathbf{r})$ the nuclear "quasi-potential."

The magnetic field of the electrons $\mathbf{B}(\mathbf{r})$ is

$$\mathbf{B}(\mathbf{r})=e\sum_{i=1}^{z}\int'\varphi_0^*(\mathbf{r}_1\cdots\mathbf{r}_z)\frac{\mathbf{r}-\mathbf{r}_i}{|\mathbf{r}-\mathbf{r}_i|^3}\times\boldsymbol{\alpha}_i\varphi_0(\mathbf{r}_1\cdots\mathbf{r}_z)d\tau_1\cdots d\tau_z. \tag{3}$$

In non-relativistic approximation, and in absence of orbital moments, the expectation value of the current $e\boldsymbol{\alpha}=\mathbf{j}$ is

$$\mathbf{j}=c\nabla\times\mathbf{M},\quad \mathbf{M}=\sum_{i=1}^{z}\left[\int'\Phi_0^*\boldsymbol{\sigma}_i\Phi_0\prod_{n=1}^{z}{}'d\tau_n\right]_{\mathbf{r}_i=\mathbf{r}}, \tag{4}$$

where Φ_0 is the Pauli spinor and $\boldsymbol{\sigma}$ the Pauli moment operator. The symbol $\prod'$ means that the integration is carried out with respect to the space and spin coor-

* This work was sponsored by ONR.
[1] F. Bloch, Phys. Rev. 51, 994 (1937).

dinates of all but the i'th electron.[2] As usual in the classical theory, one can express $\mathbf{B}$ by

$$\mathbf{B}=4\pi\mathbf{M}+\mathbf{H}, \tag{5}$$

where $\mathbf{H}$ is irrotational;

$$\nabla\times\mathbf{H}=0, \tag{6}$$

while

$$\nabla\cdot\mathbf{B}=0. \tag{7}$$

An interaction Hamiltonian more general than (1) is

$$\langle H_{\text{int}}\rangle_{\text{Av}}=-\mu\mathbf{s}\cdot(\mathbf{H}+4\pi C\mathbf{M}), \tag{8}$$

where C is an undetermined constant. If a single magnetic ion interacts with the incident plane wave of neutrons, Born's approximation gives for the scattered amplitude

$$\psi_{sc}\sim\frac{m}{2\pi\hbar^2}\frac{\exp(ik_0r)}{r}\int\exp(i\mathbf{q}\cdot\mathbf{r})\times[V(\mathbf{r})-\mu\mathbf{s}\cdot(\mathbf{H}+4\pi C\mathbf{M})]\chi_0 d\mathbf{r} \tag{9}$$

where χ_0 is the constant spinor of the incident wave

$$\psi_0=\chi_0\exp(i\mathbf{k}_0\cdot\mathbf{r}),\quad \mathbf{q}=\mathbf{k}_0-\mathbf{k} \tag{10}$$

and $\mathbf{k}$ is the propagation vector of the scattered wave.

The Fourier integral

$$\mathbf{h}(\mathbf{q})=\int\mathbf{H}(\mathbf{r})\exp(i\mathbf{q}\cdot\mathbf{r})d\mathbf{r} \tag{11}$$

can be expressed in terms of $\mathbf{M}$ as follows: Let

$$\int\mathbf{M}(\mathbf{r})\exp(i\mathbf{q}\cdot\mathbf{r})d\mathbf{r}=\mathbf{m}(\mathbf{q}), \tag{12}$$

and therefore,

$$\mathbf{M}(\mathbf{r})=\frac{1}{(2\pi)^3}\int\mathbf{m}(\mathbf{q})\exp(-i\mathbf{q}\cdot\mathbf{r})d\mathbf{q}, \tag{13}$$

and

$$\mathbf{H}(\mathbf{r})=\frac{1}{(2\pi)^3}\int\mathbf{h}(\mathbf{q})\exp(-i\mathbf{q}\cdot\mathbf{r})d\mathbf{q}. \tag{14}$$

Substitution of (13) and (14) into (5), (6) and (7) yields

$$\mathbf{q}\times\mathbf{h}=0 \tag{15}$$

and

$$\mathbf{q}\cdot(\mathbf{h}+4\pi\mathbf{m})=0. \tag{16}$$

Equations (15) and (16) can be solved for $\mathbf{h}$:

$$\mathbf{h}=-4\pi\mathbf{q}(\mathbf{q}\cdot\mathbf{m})/\mathbf{q}^2. \tag{17}$$

[2] H. A. Kramers, *Grundlagen der Quantentheorie* (Akademische Verlagsgesellschaft, Leipzig, 1938), p. 408.

The scattered amplitude is now, in terms of $\mathbf{M}$:

$$\psi_{sc}\sim\frac{m\exp(ik_0r)}{2\pi\hbar^2r}\left[\int V(\mathbf{r})\exp(i\mathbf{q}\cdot\mathbf{r})d\mathbf{r}+4\pi\mu\mathbf{s}\cdot\left(\frac{\mathbf{q}(\mathbf{q}\cdot\mathbf{m})}{\mathbf{q}^2}-C\mathbf{m}\right)\right]\chi_0. \tag{18}$$

Equation (18) is identical with Bloch's result.* We have shown that the interaction Hamiltonian (8) is equivalent to Bloch's assumption. If, in particular, $C=1$, we obtain the result derived by Schwinger[3] from the Hamiltonian (1) whereas $C=0$ leads to the earlier formula of Bloch.[4]

II. INTERACTION WITH A FERROMAGNETIC LATTICE

The wave equation of the neutron is

$$(\nabla^2+k_0^2)\psi-\frac{2m}{\hbar^2}[V(\mathbf{r})-\mu\mathbf{s}\cdot(\mathbf{H}+4\pi C\mathbf{M})]\psi=0. \tag{19}$$

In a periodic lattice, V, $\mathbf{H}$ and $\mathbf{M}$ are periodic functions of $\mathbf{r}$ and can be represented by Fourier sums

$$V(\mathbf{r})=\sum v_n\exp(2\pi i\mathbf{A}_n\cdot\mathbf{r}), \tag{20}$$

$$\mathbf{H}(\mathbf{r})=\sum\mathbf{h}_n\exp(2\pi i\mathbf{A}_n\cdot\mathbf{r}), \tag{21}$$

$$\mathbf{M}(\mathbf{r})=\sum\mathbf{m}_n\exp(2\pi i\mathbf{A}_n\cdot\mathbf{r}), \tag{22}$$

where $\mathbf{A}_n$ are the reciprocal lattice vectors, and the summation index n is understood to mean a triplet of integers $(n_1n_2n_3)$. The coefficients $\mathbf{m}_n$ are

$$\mathbf{m}_n=\frac{1}{\tau}\int_{\text{cell}}\mathbf{M}(\mathbf{r})\exp(-2\pi i\mathbf{A}_n\cdot\mathbf{r})d\mathbf{r}, \tag{23}$$

where τ is the volume of the unit cell, which is also the domain of integration. Analogous expressions give v_n and $\mathbf{h}_n$.

Substitution of the Fourier sums into Eqs. (5), (6) and (7) gives

$$\mathbf{A}_n\cdot(\mathbf{h}_n+4\pi\mathbf{m}_n)=0 \tag{24}$$

and

$$\mathbf{A}_n\times\mathbf{h}_n=0. \tag{25}$$

Therefore,

$$\mathbf{h}_n=-\frac{4\pi\mathbf{A}_n(\mathbf{A}_n\cdot\mathbf{m}_n)}{\mathbf{A}_n^2},\quad (n\neq0) \tag{26}$$

whereas $\mathbf{h}_0$ remains indeterminate. This corresponds to

* Bloch defines the constant C as the limit of the integral

$$C=\frac{1}{4\pi}\int_S\frac{z\,ds_z}{r^3}$$

as the surface S is contracted to zero; ds is the surface element. The value of the integral depends on the shape of S.

[3] J. S. Schwinger, Phys. Rev. **51**, 544 (1937).

[4] F. Bloch, Phys. Rev. **50**, 259 (1936).

the physical fact that the macroscopic mean value of $\mathbf{H}$ depends on the shape of the magnet, even if it is infinitely large.

We can now proceed as in the dynamical theory of x-rays.[5] The wave function has the form

$$\psi=\exp(i\mathbf{k}\cdot\mathbf{r})\sum_n c_n \exp(2\pi i\mathbf{A}_n\cdot\mathbf{r}), \tag{27}$$

where the c_n are constant spinors. For convenience we put

$$\begin{aligned} w(\mathbf{r})&=\frac{2m}{\hbar^2}[V(\mathbf{r})-\mu\mathbf{s}\cdot(\mathbf{H}+4\pi C\mathbf{M})] \\ &=\sum w_n \exp(2\pi i\mathbf{A}_n\cdot\mathbf{r}), \end{aligned} \tag{28}$$

where according to Eqs. (20), (21), (22), and (26)

$$w_n=\frac{2m}{\hbar^2}\left[v_n+4\pi\mathbf{s}\cdot\left(\frac{\mathbf{A}_n(\mathbf{A}_n\cdot\mathbf{m}_n)}{\mathbf{A}_n^2}-C\mathbf{m}_n\right)\right]. \tag{29}$$

Substitution of the sums (27) and (28) into Eq. (19) yields:

$$[k_0^2-(\mathbf{k}+2\pi\mathbf{A}_m)^2]c_m-\sum_n w_{m-n}c_n=0. \tag{30}$$

When the direction $\mathbf{k}$ is far from a Laue reflection, only c_0 is large, and we have

$$(k_0^2-k^2)c_0-w_0c_0\approx 0 \tag{31}$$

with

$$w_0=\frac{2m}{\hbar^2}[V_{Av}-\mu\mathbf{s}\cdot(\mathbf{H}_{Av}+4\pi C\mathbf{M}_{Av})], \tag{32}$$

where $\mathbf{V}_{Av}$, $\mathbf{H}_{Av}$ and $\mathbf{M}_{Av}=\mathbf{m}_0$ are the macroscopic mean values of the nuclear potential, the field intensity and the magnetization. If the z direction is chosen parallel to $(\mathbf{H}_{Av}+4\pi C\mathbf{M}_{Av})$, the obvious solutions of Eq. (31) are the two eigen states of the z-component of $\mathbf{s}$, i.e., $\chi_{\frac{1}{2}}$ and $\chi_{-\frac{1}{2}}$, respectively. If we call the corresponding wave numbers $k=2\pi/\lambda$, k_+ and k_-, respectively,[6] we have from Eqs. (31) and (32):

$$k_0^2-k_\pm^2=\frac{2m}{\hbar^2}[V_{Av}\pm\mu|\mathbf{H}_{Av}+4\pi C\mathbf{M}_{Av}|]. \tag{33}$$

This result, with the special value $C=1$, was derived by Achieser and Pomeranchuk[6] for neutron wavelengths large in comparison to the lattice spacing. Equation (33) should be valid for unrestricted wavelengths, except near-Laue interference directions.

We have to justify the approximation made in Eq. (31). If all quantities but w_0 are neglected, we obtain for $c_m(m\neq 0)$

$$c_m=\frac{w_{-m}c_0}{k_0^2-(\mathbf{k}+2\pi\mathbf{A}_{-m})^2}. \tag{34}$$

The approximation in Eq. (31) is justified if

$$\sum_{n\neq 0}\frac{w_nw_{-n}c_0}{k_0^2-(\mathbf{k}+2\pi\mathbf{A}_{-n})^2}\ll w_0c_0. \tag{35}$$

Since we are not interested in the nuclear forces, we consider only the magnetic term in w_n.[7] Furthermore, we consider only lattices with a center of symmetry so that $\mathbf{m}_n=\mathbf{m}_{-n}$.

Because of the anticommutative properties of the Pauli matrices

$$(\mathbf{s}\cdot\mathbf{a})(\mathbf{s}\cdot\mathbf{a})=\mathbf{a}^2 \tag{36}$$

for any vector $\mathbf{a}$.

Equation (35) can be written

$$\left(\frac{8\pi m}{\hbar^2}\right)^2\sum_{n\neq 0}\frac{\mathbf{m}_n^2(C^2+\cos^2\varphi_n-2C\cos^2\varphi_n)}{k_0^2-(\mathbf{k}+2\pi\mathbf{A}_{-n})^2} \ll\frac{2m}{\hbar^2}|\mathbf{H}_{Av}+4\pi C\mathbf{M}_{Av}|, \tag{37}$$

where φ_n is the angle between $\mathbf{m}_n$ and $\mathbf{A}_{-n}$. Usually, $\mathbf{H}_{Av}$ is very small as compared to $4\pi\mathbf{m}_0$. If C is of the order of one, we can neglect the first term of the second member. The validity of Eq. (37) depends then on the numerical value of the dimensionless quantity

$$\frac{8\pi m}{\hbar^2k_0^2}|\mathbf{m}_0|=\alpha, \tag{38}$$

and on the manner in which the function

$$f(n)=\frac{|\mathbf{m}_n|}{|\mathbf{m}_0|} \tag{39}$$

decreases with increasing n.

The Fourier coefficients $\mathbf{m}_n$ of $\mathbf{M}$ have been estimated for Fe by Halpern, Hamermesh, and Johnson[8] and could be used for the estimate. However, it is easier to use an argument due to the analogy with the dynamical theory of x-rays. The quantity α is of the order of $5\cdot 10^{-6}$ for neutrons, the same order as the corresponding quantity in x-rays. The behavior of the function $f(n)$ is determined by the microscopic distribution of $\mathbf{M}(\mathbf{r})$ which is close to the electronic density of the magnetically unsaturated electrons.[8] But in x-ray theory, the corresponding quantity is the total electronic density so that the similarity of the two cases is obvious. We can conclude from the experimental verification of the dynamical theory of x-rays that our approximation is justified.

However, the approximation method breaks down if $C\ll 1$. In this case, the term $\mathbf{m}_n^2\cos^2\varphi_n$ in the first

[5] M. von Laue, *Röntgenstrahlinterferenzen* (Akademische Verlagsgesellschaft, Leipzig, 1941).

[6] A. Achieser and J. Pomeranchuk, J. Exper. and Theor. Phys. U.S.S.R. 18, 475 (1948).

[7] For the nuclear quasi-potential the approximation cannot be justified directly. An indirect justification has been given by M. L. Goldberger and F. Seitz, Phys. Rev. 71, 296 (1947).

[8] Halpern, Hamermesh, and Johnson, Phys. Rev. 59, 981 (1941).

member of Eq. (37) will predominate, and make the justification impossible. But, in this case, the entire effect of "magnetic birefringence" expressed by Eq. (33) will be immeasurably small, unless $\mathbf{H}_{Av}$ is made very large. In this latter case, i.e., when $\mathbf{H}_{Av}$ is of the order of $\mathbf{m}_0$, the above argument holds again.

The case of Laue interference in the dynamical theory will not be investigated here since actual ferromagnetic crystals are so imperfect that they can hardly be expected to approach the infinite ideal crystal.

III. EXPERIMENTAL POSSIBILITIES FOR DETERMINING BLOCH'S CONSTANT C

A. Laue Interference

For a sufficiently small ferromagnetic crystal, Born's approximation can be used to calculate the wave scattered from an incident plane wave of the form (10). It is a well-known result of the kinematic theory of x-rays that the scattered "integrated intensity" of an interference maximum characterized by

$$2\pi\mathbf{A}_n=\mathbf{k}-\mathbf{k}_0 \tag{40}$$

is proportional to the square modulus of $w_n\chi_0$, where w_n is given by (29) and χ_0 is given by the form (10). In general, this scattered intensity will depend on the spin state χ_0 of the incident wave. This results in polarization effects for the beam transmitted through a polycrystalline magnetized plate. These effects have been theoretically investigated by Halpern, Hamermesh, and others[8–10] for the usual assumption $C=1$.

The easiest method for measuring C seems to be an experiment in which the magnetic term in (29) is made to vanish for all existing Laue maxima. In this case, no single transmission effect is observable. If a monoenergetic beam of neutrons has the longest reflecting wave-length for the lattice (e.g., twice the spacing of the 110 planes in Fe), then the incident beam is reflected by 180° by those crystals which are in reflecting position, whereas all other crystals act as a transparent medium. In this case, $\mathbf{k}$, $\mathbf{k}_0$ and $\mathbf{A}_n$ have the same direction. If φ is the angle between the incident beam and the direction of magnetization $\mathbf{M}$ (which is parallel to all $\mathbf{m}_n$'s) then the magnetic term in (29) can be written

$$4\pi\mu\mathbf{m}_n{}^2\mathbf{s}\cdot\mathbf{e}(C^2+\cos^2\varphi-2C\cos^2\varphi), \tag{41}$$

where $\mathbf{e}$ is a unit vector without interest for the following. The magnetic interaction vanishes if

$$C=1,\quad \varphi=0;\quad C=0,\quad \varphi=\pi/2. \tag{42}$$

It should be possible to measure Bloch's constant C by determining that angle φ between magnetization and incident beam which leads to the smallest transmission effect. If the common assumption $C=1$ is correct, then the single transmission effect should vanish when the magnetization is parallel to the incident beam.

The observations of Hughes, Wallace, and Holtzman[11] show a large single transmission effect for the case where the magnetization is normal to the incident beam, i.e., $\varphi=\pi/2$. This seems to rule out the possibility $C=0$. It is true that in these experiments the wave-length band covered a number of reflections, but the contribution of the largest lattice spacing (110) is so large that their results would be difficult to explain if this reflection did not contribute to the magnetic interaction.

B. Total Reflection

If the effective nuclear potential V_{Av} is positive, as in most cases, the birefringence expressed in Eq. (33) can give rise to two angles of total reflection, as pointed out by Achieser and Pomeranchuk.[6] One obtains in the usual way for the two glancing angles of total reflection

$$\theta_\pm=\left(\frac{2m}{\hbar^2k_0{}^2}\right)^{\frac{1}{2}}[V_{Av}\pm\mu|\mathbf{H}_{Av}+4\pi C\mathbf{M}_{Av}|]^{\frac{1}{2}}, \tag{43}$$

corresponding to the total reflection of neutrons with spin either parallel or antiparallel to the vector $\mathbf{H}_{Av}+4\pi C\mathbf{M}_{Av}$. In particular, with the usual assumption $C=1$, we obtain the expression

$$\theta_\pm=\left(\frac{2m}{\hbar^2k_0{}^2}\right)^{\frac{1}{2}}[V_{Av}\pm\mu|\mathbf{B}_{Av}|]^{\frac{1}{2}} \tag{44}$$

in agreement with Achieser and Pomeranchuk, but for unrestricted neutron wave-length. The angles $\theta_\pm$ are independent of the direction of the induction $\mathbf{B}_{Av}$. This conclusion differs from opinions expressed by Halpern[12] and by Hughes and Burgy.[13]

Hughes and Burgy[13] reported observation of two distinct angles of total reflection, in a case where the mean magnetic field $\mathbf{H}_{Av}$ was very small. This is an additional evidence against the assumption $C=0$.

A precise measurement of $\theta_\pm$ with a field $\mathbf{H}_{Av}=0$ provides a method for measuring Bloch's constant by using Eq. (43).

[9] O. Halpern and M. H. Johnson, Phys. Rev. **55**, 898 (1939).
[10] O. Halpern and T. Holstein, Phys. Rev. **59**, 960 (1941).
[11] Hughes, Wallace, and Holtzman, Phys. Rev. **73**, 1277 (1948).
[12] O. Halpern, Phys. Rev. **75**, 343 (1949).
[13] D. J. Hughes, and M. T. Burgy, Phys. Rev. **76**, 463 (1949).

Surface Impedance of Normal and Superconductors at 24,000 Megacycles per Second*

E. MAXWELL,**Δ P. M. MARCUS,*** AND J. C. SLATER
Research Laboratory of Electronics, Massachusetts Institute of Technology, Cambridge, Massachusetts
(Received April 27, 1949)

The surface impedance of tin at 24,000 mc/sec. has been investigated in the range of temperatures from 2°K to 300°K, including both the superconducting and normal states, by means of a resonant cavity technique. The experimental techniques are described and the data for the normal state discussed in terms of the theory of the anomalous skin effect given by Reuter and Sondheimer. Agreement is found between the general features of the theory and the data although numerical estimates for the number of free electrons appear to low. The superconducting data are analyzed in terms of a theory which combines the London and the Reuter and Sondheimer theories. The variation of penetration depth, λ, with temperature is found to be in agreement with other determinations. The best value for λ_0, is estimated at 10^{-5} cm.

INTRODUCTION

THE work reported here represents part of a general program of investigation of the conductivity of metals at low temperatures and microwave frequencies, which was initiated in the Research Laboratory of Electronics at M.I.T. in November 1945. Preliminary reports[1–3] of some phases of this work have already been given elsewhere.

One of the original aims of the investigation was to obtain data on the behavior of superconductors in a microwave range in order to see if the superconducting properties persisted down to wave-lengths of the order of a centimeter. Superconductivity in lead at 3 cm was successfully observed in our laboratory in early 1946. Later that year the bulk of the effort was shifted to 1.25 cm. Also, since lead was not an ideal material to work on because of its inconveniently high transition temperature, attention was shifted from it to tin.

Although the initial interest was largely in the superconducting properties, it became clear by the early part of 1947 that there was a pronounced anomaly in the r-f conductivity at low temperatures. This effect had been noted previously by London[4] at 1500 mc/sec. but was much greater at 24,000 mc/sec. The anomaly has also been reported on in some detail by Pippard.[5]

Following Pippard's observations of the anomalous r-f conductivity Reuter and Sondheimer developed their theory of the effect. A preliminary version of their paper was kindly made available to us in manuscript form in the fall of 1947, and it has since appeared in print.[6] It was soon realized that their theory could be used to derive values for the number of free electrons per atom by comparison with experimental data, and could also be applied to the behavior of the normal electrons in superconductors in the London theory. Some preliminary results of these analyses have already been reported.[2]

SURFACE IMPEDANCE OF A METAL

The surface impedance is the most useful way of characterizing the effect of a metal surface on an electromagnetic field at high frequencies. As pointed out by Pippard,[5] this is particularly important at low temperatures where anomalous effects enter and the conductivity is no longer a precise concept. The current at a point in the metal is no longer proportional to just the field strength at that point, but is given by an integral over the entire field distribution in the metal, although still a linear function in the field amplitude. On the other hand, the surface impedance is always an unambiguous quantity and can be uniquely defined in terms of the field components at the metal surface. It is simply related to the measurable quantities at high frequencies, namely the Q and resonant frequency of a cavity resonator, and therefore offers a convenient phenomenological description of the behavior of the metal.

Consider a general radiation field impinging on a metal surface which is normal to the z direction. If we have strong damping in the z direction, then the derivative of the field with respect to z will be much larger than those with respect to x and y, and it can be shown that the field in the metal consists essentially just of x and y components. Let us take these as E_x and H_y. We define the surface impedance Z as

$$Z=R+iX=\frac{4\pi}{c}\cdot\left[\frac{E_x}{H_y}\right]_{z=0}=\frac{E_x}{\int_0^\infty J_x(z)dz}=4\pi ik\cdot\left[\frac{E_x}{\frac{\partial E_x}{\partial z}}\right]_{z=0} \quad (1)$$

* This work was made possible by support extended to the Research Laboratory of Electronics by the Army Signal Corps, ONR and the Air Force under Signal Corps Contract No. W-36-039-56-SC-32037.
** Now with the Cryogenics Section, National Bureau of Standards.
*** Now with the ONR, London Branch.
Δ This paper is based on a thesis submitted in partial fulfillment of the Degree of Doctor of Philosophy at M.I.T.
[1] Bitter, Garrison, Halpern, Maxwell, Slater, and Squire, Phys. Rev. 70, 97 (1946).
[2] Maxwell, Marcus, and Slater, Phys. Rev. 74, 1234 (1948).
[3] Maxwell, Marcus, and Slater, Tech. Report No. 109, Research Laboratory of Electronics, M.I.T. (May 1, 1949).
[4] H. London, Proc. Roy. Soc. A 176, 522 (1940).
[5] A. B. Pippard, Proc. Roy. Soc. A 191, 370 (1947).
[6] G. E. H. Reuter and E. H. Sondheimer, Proc. Roy. Soc. A 195, 336 (1948).

where J is the current density and $k=\omega/c$. Since the x and y variations are slow compared to the z variation, the former may be ignored in obtaining the field and Z from the intrinsic properties of the metal. We need only consider the normal incidence of a plane wave on an infinite metallic conducting surface. For free space Z becomes

$$Z=\frac{4\pi}{c}\text{ Gaussian units}=120\pi\text{ ohms.} \tag{2}$$

For a classical metal with conductivity, Z is given by

$$Z=\frac{4\pi k}{c\kappa}=\frac{2\pi\omega\delta}{c^2}(1+i)=(1+i)\cdot\left(\frac{2\pi\omega}{c^2\sigma}\right)^{\frac{1}{2}}. \tag{3}$$

κ is the propagation constant in the metal and δ is the ordinary skin depth. These are given by

$$\kappa^2=-\frac{4\pi i\omega\sigma}{c^2}; \tag{4a}$$

$$\delta=\left(\frac{c^2}{2\pi\omega\sigma}\right)^{\frac{1}{2}}. \tag{4b}$$

In the case of a wave guided by metal surfaces, the real and imaginary parts of the surface impedance are related to the attenuation and phase velocity, respectively, or in the specific case of a resonant cavity to the Q and resonant frequency.

For the low temperature case (3) will not be very meaningful because of the impossibility of defining a conductivity. The surface impedance will, however, be useful and may be calculated from the experimentally observed data for attenuation and phase velocity, or Q and resonant frequency. We shall set down the relations which connect the surface impedance and the observable quantities both for the case of a wave guided between parallel plates and for the generalized cavity resonator. Although in practice one always uses a cavity resonator for these measurements, the case of the parallel plate line is instructive because it affords a simple picture of the physical problem. It is also a natural way of introducing the concepts of resistive and inductive skin depth which replace the ordinary skin depth of (4b).

Consider a wave traveling in the z direction between parallel metal surfaces (normal to the y direction), and let the field components be E_y, E_z, and H_z. The field components between the walls are combinations of $\exp(-i\kappa_z z+i\kappa_y y+i\omega t)$ where $\kappa_y^2+\kappa_z^2=k^2$, and are slightly perturbed from the wave which would exist with perfectly conducting walls. We then have the following for E_z, H_z, and Z.

$$E_z=E_{z0}\sin\kappa_y y e^{-i\kappa_z z+i\omega t}, \tag{5a}$$

$$H_z=\frac{ik}{\kappa_y}E_{z0}\cos\kappa_y y e^{-i\kappa_z z+i\omega t}, \tag{5b}$$

$$Z=\frac{4\pi}{c}\left[\frac{E_z}{H_z}\right]_{y=d/2}=\frac{4\pi}{cik}\tan\left(\frac{\kappa_y d}{2}\right). \tag{6}$$

The walls are separated by a distance d and the origin of coordinates is taken at the center.

Now $\kappa_z\sim k$, hence $\kappa_y\ll k$; further $kd\sim 1$ in the microwave region so that $\kappa_y d\ll 1$. It follows then that

$$\kappa_y^2=\frac{icZ}{2\pi}\frac{k}{d} \tag{7}$$

and

$$\kappa_z=k\left[1+\frac{c}{4\pi kd}(X-iR)+\cdots\right]. \tag{8}$$

The wave attenuation is then given by

$$Im(\kappa_z)=Rc/4\pi d \tag{9}$$

and the phase velocity by

$$\frac{\omega}{Re(\kappa_z)}=\frac{\omega}{k(1+Xc/4\pi kd)}\cong c\left(1-\frac{Xc^2}{4\pi\omega d}\right). \tag{10}$$

In the low temperature case as distinguished from the classical case R and X are not in general equal. It is useful to substitute for the simple skin depth concept of (4b) the notions of resistive and inductive skin depths. The resistive skin depth δ defines an equivalent skin depth for power dissipation and is

$$\delta=\frac{c^2R}{2\pi\omega}. \tag{11}$$

This reduces to the ordinary skin depth of (4b) for the

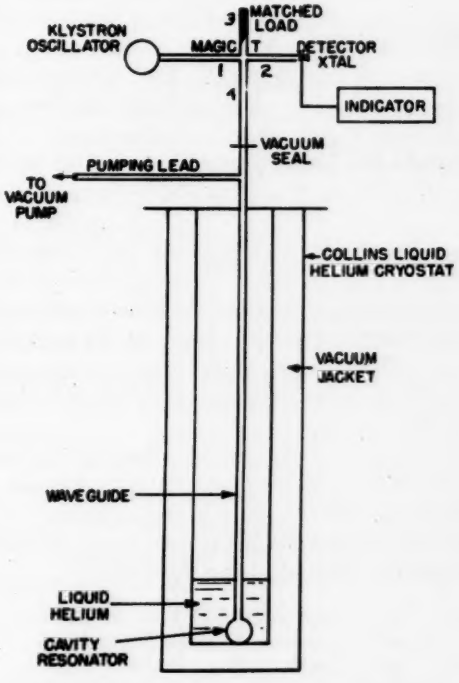

FIG. 1. Schematic diagram of the experiment.

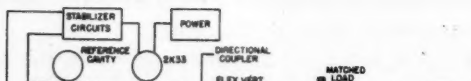

FIG. 2. Details of microwave plumbing for unbalanced bridge.

classical case but is more general since it does not involve the conductivity.

The inductive skin depth δ' has been defined[5] as the distance the walls should be set back (and considered perfectly conducting) in calculating the inductance between them, for the purpose of determining the wave velocity from the inductance and capacitance per unit length. (The capacitance is calculated using the original spacing.)

The treatment of the parallel plate line may be extended to obtain the idea of an inductive skin depth without resorting to the concepts of inductance and capacitance. Thus we may replace a layer of the metal, of thickness δ' by a layer of high dielectric material having zero conductivity. The tangential magnetic field can penetrate this layer but not normal electric field. We set up fields in δ' like those of (5), replacing k by $k\sqrt{\epsilon}$, and match impedances at the surface $y=d/2$. We then find

$$\kappa_y^2=-\frac{2k^2\delta'}{d} \tag{12}$$

analogous to (7) and

$$\kappa_z=\left(1+\frac{\delta'}{d}\right) \tag{13}$$

analagous to (8). Comparing (12) with (10) we obtain

$$\delta'=\frac{Xc^2}{4\pi\omega}. \tag{14}$$

Another approach would be to define δ' such that the magnetic energy stored in a layer of thickness δ' (between the plates) is equal to the magnetic energy stored in the metal. It is easily verified that this definition also leads to (14).

For a resonant cavity, the relation between the surface conductivity and the Q and resonant frequency has been given by Slater,[7] pp. 473–475, especially III-59. Generalizing his formula to the case of an arbitrary surface impedance (and changing units) gives

$$\frac{1}{Q}-2i\frac{\Delta\omega}{\omega_a}=\frac{c^2(R+iX)}{4\pi\omega_a}\cdot\int H_a^2 da \tag{15}$$

where ω_a = the unperturbed resonant frequency, H_a = the magnetic field of the mode with volume integral over the cavity normalized to unity. $\Delta\omega$ is the frequency shift or perturbation due to the finite surface reactance and the integral is over the surface area of the cavity.

The integral $\int H_a^2\cdot da$ is a constant for a given cavity geometry and a given mode. Knowing what this constant is we may evaluate R from the Q and in principle we could evaluate X from the dimensions of the cavity (which would give ω_a) and the measured value of ω (which is the perturbed frequency). In practice this is difficult because it involves knowing the cavity dimensions very accurately including those of the coupling orifice. It is also difficult to evaluate changes in X with temperature (which would be sufficient, since at room temperatures R and X should be equal) and it is only possible below about 20°K, where the frequency shift due to thermal contraction is very small and does not mask the effect due to changing surface reactance. This means that the only information on surface reactance which can be readily obtained is the change which occurs in the superconducting state. The absolute value is not evaluated by direct measurement.

EXPERIMENTAL DETAILS AND MEASUREMENT TECHNIQUES

The low temperatures were obtained with a Collins Liquid Helium Cryostat with the resonant cavities mounted directly in the experimental chamber. This made it possible to take measurements at all temperatures from room temperature down through the liquid helium range, but only those in the liquid helium region could be stabilized and measured with any precision. In the liquid helium region temperature measurements were made with a vapor pressure thermometer using the Leiden 1937 scale, while at other temperatures a constant volume gas thermometer was used.

The cavities were rectangular cavities operating in the TE_{102} mode and were made by cold pressing two identical halves (of tin or lead) with a steel die. The halves were soldered together on the outside seam and to the wave guide. The parting plane was a section of no transverse current flow so contact difficulties were eliminated. The cavities were continuously evacuated during operation to a pressure of about 10^{-5} mm by pumping through the wave guide which was sealed off

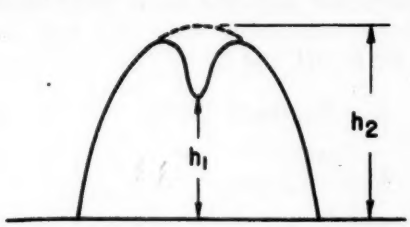

FIG. 3. Oscilloscope deflection pattern for unbalanced bridge. Vertical coordinate is amplitude; horizontal coordinate is frequency.

[7] J. C. Slater, Rev. Mod. Phys. 18, 441 (1946).

with a mica disk. Reflections from the disk were tuned out with an inductive iris clamped to the disk itself.

Surface resistance data were obtained from Q measurements, while the change in surface reactance in the superconducting state was found by measuring the shift in resonant frequency. The Q measurements were made with an unbalanced magic-tee bridge. Most of the measurements were relative measurements made by observing the reflection coefficient at resonance by means of the arrangement of Figs. 1 and 2. A frequency modulated klystron was used as the power source and the power reflected from the cavity was displayed oscillographically as a function of frequency, as in Fig. 3. The solid curve shows the cavity resonance and the dotted line indicates the pattern observed when the klystron center frequency was tuned somewhat off resonance. The ratio h_1/h_2 gives the power reflection coefficient at resonance, which determines the VSWR; the VSWR is equal to the ratio of window Q to unloaded Q and hence gives a number directly proportional to the surface resistance.

To fix the absolute value of the surface resistance, or the unloaded Q, complete resonance curves were taken at 300°K and 4.2°K using a stable c.w. oscillator of variable frequency. The arrangement used is shown schematically in the block diagram of Fig. 4. A 2K-33 klystron was stabilized to a resonant cavity, and a working, or slave oscillator, which was a 2K-50, was tied to the 2K-33 by means of an i.f. link which consisted of a commercial Hallicrafters VHF receiver. The operating frequency of the 2K-50 was varied by tuning the receiver. The over-all stability was about 50 kc. This apparatus was also used to measure the shift in resonant frequency of the cavity while in the superconducting state.

The estimated uncertainties in the measurements are as follows. For the relative measurements in the normal state these range from 10 percent at a VSWR of 10 to about 6 percent at a VSWR of 1.5. For a normalized VSWR in the superconducting state (ratio of the VSWR at the given temperature to the VSWR at the transition temperature) these are of the order of 10 percent at 3.7°K and 20 percent at 2.1°K. A detailed discussion of these and other experimental matters has been given elsewhere.[3]

NORMAL STATE

I. Results

The results of the measurements on tin and lead**** are given in Fig. 5 and the numerical data for tin in Table I. These figures compare the measured value of the surface resistance at 24,000 mc/sec. with the value calculated from the classical formula of Eq. (3) using the measured value of the d.c. resistivity. It is seen that even at room temperatures there is a divergence of 10 or 15 percent between the measured and calculated values.

**** Lead from M.I.T. Ph.D. thesis of J. B. Garrison, 1947.

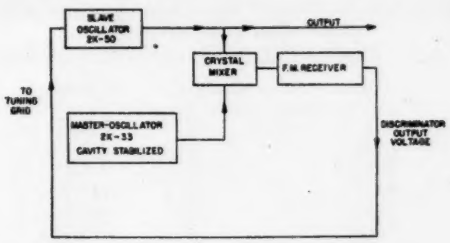

FIG. 4. Block diagram of master and slave oscillator arrangement.

This sort of behavior has been observed before and is presumably due to a condition of surface roughness. Down to about 30°K the two curves continue parallel but below 30°K anomalous behavior sets in rapidly. This phenomenon is of course the mean free path effect.

II. Analysis

London[4] was the first to suggest that the surface resistance at low temperature would depend on the mean free path. Pippard[5] made use of this idea in an approximate way which revealed much of the general physical behavior. Reuter and Sondheimer[6] derived the integro-differential equation for the field which follows precisely for this model and solved two limiting cases rigorously. Their treatment made use of a Boltzmann equation for the distribution function and applied it to calculate the current in terms of the field.

Pippard[5] indicated a kinetic derivation of an integral equation which differed somewhat from Reuter's and Sondheimer's equation, and Harrison[8] independently developed a kinetic approach to the problem. The kinetic method is a useful alternative to the distribution function method because it gives a clearer physical picture of the various contributions to the current at a point in the metal. The kinetic point of view of Harrison or Pippard can be used to derive the integral equations of Reuter and Sondheimer, and such a treatment has been given in Technical Report 109 of the M.I.T. Research Laboratory of Electronics (henceforth referred to as R.L.E. 109).

The calculations are based on the familiar simple model of the electrons in a metal as forming a degenerate Fermi gas. Equilibrium is maintained by collisions with the lattice of positive ions (actually lattice vibrations and irregularities). The energy of an electron is proportional to the velocity squared, but the mass is not necessarily the free electron mass. In the presence of an electric field, electrons acquire small drift velocities in the direction of the field between collisions. The average drift velocity at a point determines the electric current there. Two basic constants determine electron behavior, n the number of free electrons per cm^3, and l the mean free path for electrons at the edge of the Fermi distribution; $l=\tau v_m$ where v_m is the maximum velocity of the

[8] R. J. Harrison, Quarterly Progress Report, Research Laboratory of Electronics, M.I.T., p. 29 (January 15th, 1948).

TABLE I. Smoothed values of the surface resistance of Sn in the normal state at 24,000 mc/sec.

T°K	R (ohms)
300	0.1217
200	0.0995
140	0.0801
100	0.0636
80	0.0532
70	0.0478
60	0.0420
50	0.0358
40	0.0293
35	0.0260
30	0.0227
25	0.0198
20	0.0180
15	0.0175
10	0.0175
5	0.0175
4.2	0.0175

Fermi distribution, τ is the mean time between collisions, and the relaxation time of the electron distribution.

The kinetic treatment derives the expression which follows from the free electron model for the current in a metal in terms of the electric field, and combines it with Maxwell's equations to yield an integro-differential equation for the field. The solution of this equation yields the field in the metal, and the derivative at the surface yields the surface impedance of the metal. In the low temperature region, the surface resistance at high frequencies deviates from the predictions of ordinary skin depth theory in the observed manner.

In the theory of Reuter and Sondheimer, and in the equivalent treatment of R.L.E. 109, the expression for the surface impedance is finally given in the form

$$Z=\frac{4\pi i\omega l}{c^2}\cdot\frac{f(0)}{f'(0)} \tag{16a}$$

where $f(x)$ gives the field distribution in the metal and, $f'(x)$ its derivative. Only the values of these functions at the surface are involved. In addition to n, l, v_m and τ, it is useful to introduce the following parameters.

$$\sigma=\frac{\epsilon}{h}\cdot\frac{2\pi^{\frac{1}{3}}}{3^{\frac{1}{3}}}n^{\frac{1}{3}}l, \tag{17}$$

$$\alpha=\frac{2\pi^{4/3}3^{\frac{1}{3}}}{hc^2}\epsilon^2\omega n^{\frac{1}{3}}l, \tag{18}$$

$$A=\frac{3^{5/18}2^{1/6}\pi^{5/4}h^{\frac{1}{3}}\omega^{\frac{1}{3}}n^{-2/9}}{c^{4/3}\epsilon^{\frac{1}{3}}}$$

$$=\frac{4\pi\omega}{c^2}\left(\frac{3}{8}\right)^{\frac{1}{3}}\frac{l}{\alpha^{\frac{1}{3}}}=\left(\frac{2\pi\omega}{c^2}\right)^{\frac{1}{3}}\frac{\alpha^{1/6}}{\sigma^{\frac{1}{3}}}, \tag{19}$$

$$\delta=\left(\frac{c^2}{2\pi\omega\sigma}\right)^{\frac{1}{3}}=\frac{3^{1/6}}{2\pi^{\frac{1}{3}}}\cdot\frac{h^{\frac{1}{3}}c}{\epsilon\omega^{\frac{1}{3}}}\cdot\frac{1}{h^{\frac{1}{3}}l^{\frac{1}{3}}}, \tag{20}$$

σ and δ are the ordinary d.c. conductivity and classical skin depth, respectively, ϵ is the electronic charge, h and c have their customary meanings.

In terms of these other parameters, Z may be written as

$$Z=i\left(\frac{8}{3}\right)^{\frac{1}{3}}A\alpha^{\frac{1}{3}}\frac{f(0)}{f'(0)}. \tag{16b}$$

Reuter and Sondheimer show the form of this function in Fig. 1 of their paper.[6] In Fig. 6b we have re-plotted the function R/A to logarithmic coordinates. The two cases $p=0$ and $p=1$ correspond respectively to diffuse and specular reflection at the surface of the conductor. For very low temperatures Z takes the limiting forms

$$Z\cong 0.4291A(1+\sqrt{3}i);\quad p=0, \tag{21a}$$

$$Z\cong 0.4827A(1+\sqrt{3}i);\quad p=1. \tag{21b}$$

At room temperatures Z is given by the classical formula

$$Z=\frac{2\pi\omega\delta}{c^2}(1+i)=A\alpha^{1/6}(1+i) \tag{22}$$

good for both $p=0$ and $p=1$.

One expects l to depend on the temperature T, increasing as T decreases until the region of residual resistance is reached, but n should be independent of T. At a given frequency A depends only on n, hence should not depend on T.

The data consists of $\sigma(T)$, $R(T)$ (surface resistance, ReZ) at known frequency. Equation (17) then gives a relation between n and l; (21a) or (21b) give A from the limiting low temperature value of R hence a value of n from (19). Thus n and $l(T)$ may be deduced without using a value for the electron mass m, or equivalently the maximum Fermi velocity v_m. The latter is required to deduce the relaxation time τ.

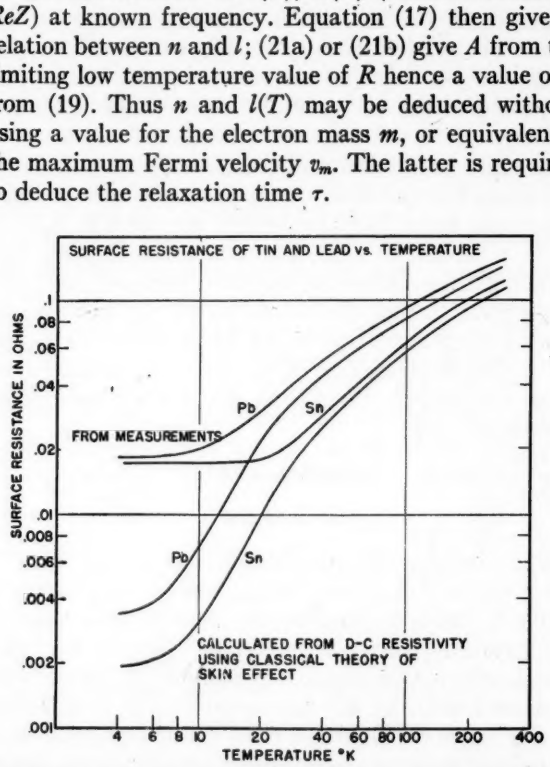

FIG. 5. Surface resistance of Sn and Pb in the normal state at 24,000 mc/sec., Pb measurements by J. B. Garrison.

The theory predicts the dependence of R/A on α. Hence plotting $1/R$ *vs.* $\sigma^{\frac{1}{2}}$ on a log-log scale gives an experimental curve of the same shape but displaced from the universal curve of A/R *vs.* $\alpha^{1/6}$ (which is proportional to $\sigma^{\frac{1}{2}}$). Thus an over-all check of the theory can be obtained. The best position of fit of the two curves gives an average value of n from the displacement of the scales. ($R=(2\pi\omega/c^2\sigma)^{\frac{1}{2}}$, which follows from Eq. (22), must hold between R and $\sigma^{\frac{1}{2}}$ at high temperatures.)

It is possible that the theory is accurate at high temperatures (classical region) and very low temperatures (residual resistance region), in both of which the idea of a mean free path is valid, but is not accurate at intermediate temperatures. Only these regions can be expected to match then, and we can determine n essentially only from the limiting value of R.

In Fig. 6a the data for tin have been plotted in the form of $1/R$, *vs.* $(\sigma/\sigma_{300})^{\frac{1}{2}}$ in logarithmic coordinates. These are to be compared with Fig. 6b, the theoretical curves of Reuter and Sondheimer. The experimental and theoretical curves are of generally similar shape, but of course any theory which predicts that the surface resistance at low temperatures becomes independent of the d.c. resistivity, will give a curve of the same shape.

As mentioned above, by matching the experimental to the theoretical curves we should be able to derive a value for n, the number of free electrons. In practice this amounts to simultaneously superposing the asymptotic and the initial linear portions of the curves, inasmuch as the curves do not match very well in the bends (probably for the reasons quoted). This procedure demands that the measured surface resistivity and d.c. conductivity be consistent at room temperature, or in other words that the curves of Figs. 6a and 6b coincide at room temperature. The procedure adopted here has been to decrease the measured surface resistance data so as to bring it into agreement, at room temperature, with the figure computed from the d.c. conductivity. This seems

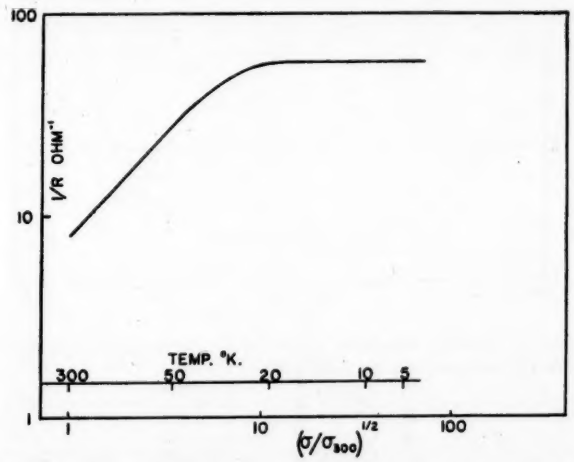

FIG. 6a. Surface resistance data for Sn plotted in form for comparison with theory ($1/R$ *vs.* $(\sigma/\sigma_{300})^{\frac{1}{2}}$). Johnson-Matthey 2135 Sn.

TABLE II. Number of free electrons per atom calculated from surface resistance.

Metal	Authority	Frequency	n (per atom) $p=0$	$p=1$
Sn	Pippard	1200 mc/sec.	1.1	0.67
Sn	Our data	24,000	0.20	0.12
Pb	Garrison	24,000	0.19	0.12
Hg	Pippard	1200	0.57	
Al	Pippard	1200	0.70	0.41
Cu	Pippard	1200	0.11	0.07
Ag	Pippard	1200	0.066	0.038
Au	Pippard	1200	0.021	0.011

reasonable[ΔΔ] since the microscopic parameters of the metal which we seek to determine by this process are related to the true d.c. conductivity and not to geometrical form of the surface.

The results of this analysis of our data and Pippard's[5] data are given in Table II.

Two facts are at once apparent. First, our data for Sn give results that are considerably lower than Pippard's. Second, most of the values given are low. One might expect n to be of the order of one. With the exception of the figures derived from Pippard's data for Sn, Hg, and Al, the numbers are considerably smaller than 1. The numbers for Au, Ag, and Cu are especially low. For these metals Mott and Jones[9] give an estimate of about 0.8 free electrons per atom.

It should also be noted that the number obtained by the fitting process is sensitive to very small changes in the fitting (apart from the uncertainty in p), due to the fact that the constants evaluated in the matching process have to be raised to the 9/2 power in the calculation process. These uncertainties, however, hardly seem adequate to account for the discrepancies noted; even after taking this into account, the numbers seem low.

A possible explanation for the low values of n may be

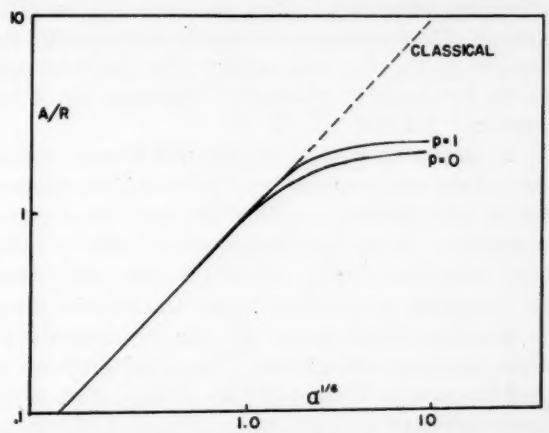

FIG. 6b. A/R as function of parameter $\alpha^{1/6}$ following Reuter and Sondheimer theory; logarithmic plot.

[ΔΔ] If this correction is not made, then the values for n for our tin data are 0.14 for $p=0$ and 0.09 for $p=1$; for Garrison's Pb data the corresponding figures are 0.12 for $p=0$ and 0.08 for $p=1$.

[9] N. F. Mott and H. Jones, *The Theory of the Properties of Metals and Alloys* (Oxford University Press, New York, 1936).

TABLE III. Smoothed values of R/R_t—normalized surface resistance of Sn in superconducting state at 24,000 mc/sec.

T°K	R/R_t
3.751	1.000
3.740	0.932
3.730	0.860
3.720	0.806
3.710	0.749
3.700	0.702
3.680	0.627
3.660	0.569
3.630	0.498
3.600	0.444
3.500	0.319
3.400	0.247
3.300	0.198
3.200	0.171
3.000	0.142
2.800	0.120
2.600	0.109
2.400	0.103
2.100	0.097

that at low temperatures the surface roughness is more important than at high temperatures.[ΔΔΔ] At low temperatures the mean free path (in bulk metal) may be considerably larger than the surface irregularities. Hence the latter may reduce the effective mean free path. This effect would reduce the values of n obtained.

Another aspect of this discrepancy hinges on the value of the d.c. resistivity. The resistivity of our tin as determined by measurements on extruded wires was 13.7×10^{-6} ohm cm as compared with the figure of 11.5×10^{-6} ohm cm given by Onnes and Tuyn for pure tin in the International Critical Tables. The reason for our high resistivity is not known but it was checked on a number of different annealed samples. Pippard apparently did not measure the absolute resistivity of his samples but assumed the values given in the tables. Furthermore he used these values to establish the proportionality between Q and the surface resistance of his resonators. However even making full allowance for this difference in the d.c. resistivities, this could at most account for a factor of about 2 whereas the actual discrepancy is about 5.

It is interesting further, to compare the asymptotic values of the surface resistance reached at low temperatures in our experiments with those found by Pippard. The surface resistance of Sn was 0.0175 ohms at 23,910 mc/sec. as against 0.00147 at 1180 mc/sec. in Pippard's case. According to the Reuter and Sondheimer theory this quantity should go as $\omega^{\frac{1}{3}}$ and consequently the surface resistance should be 7.4 times as great at the higher frequency. The actual ratio is 11.9. Part of this discrepancy may be due to the difference in the d.c. resistivities at room temperature discussed in the previous paragraph. To eliminate this factor we can multiply our figure of 11.9 by $(11.5/13.7)^{\frac{1}{3}}$ which has the effect of making our room temperature surface resistance consistent with those of Pippard and brings the ratio down to 10. The discrepancy is still large.

The corrections for relaxation effects, according to the Reuter and Sondheimer theory are quite small, as previously noted. For the case of tin the theoretical value of the asymptotic surface resistance should be decreased by about 5 percent in our case, which is incidentally, in the wrong direction to rectify the descrepancies noted in the values found for n, and in the frequency dependence of the low temperature surface resistance.

SUPERCONDUCTING STATE

I. Surface Resistance Data

The variation of surface resistance with temperature for the tin-cavities is shown in Fig. 7. This figure includes three separate runs on cavity L as well as points from successful runs on cavities M and H. A set of smoothed values of R/R_t is given in Table III. The transition-temperature, as nearly as can be judged is 3.751°K. This is somewhat higher than that reported by others and may be due to residual strains.

The surface resistance is still appreciable at 2.1°K, the lowest temperature reached, and apparently is not headed for zero at 0°K, but approaches a value of about 0.09. This same sort of behavior was noted by Pippard[5] at 1200 mc/sec. The numerical value of R/R_t at 2.1°K reported by him was 0.009. Later work[10] of Pippard's, at 9200 mc/sec. does, however, seem to indicate that the surface resistance may approach zero at 0°K, so these discrepancies are still to be resolved.

The residual surface resistance may result from two separate mechanisms. First the presence of impurities in the cavity may increase the apparent loss and second, there is a possibility that a new type of absorption effect enters at these high frequencies, in which the electromagnetic quanta are large enough to induce some electronic transitions from the superconducting to the

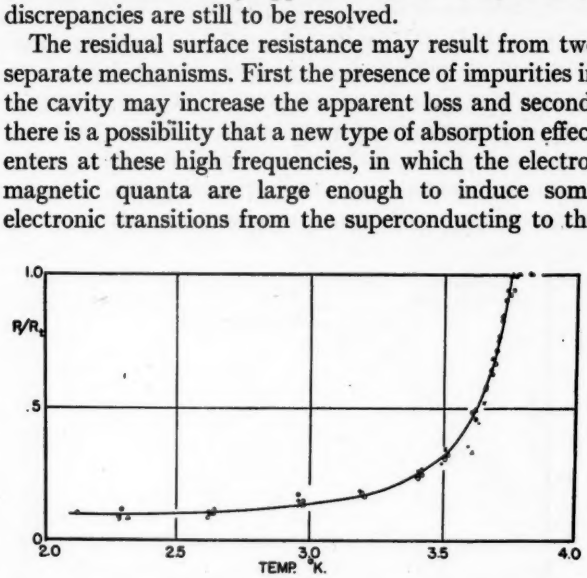

FIG. 7. Surface resistance of Sn in the superconducting state. Data for Johnson-Matthey 2135 Sn.

⊙	Cavity L	1-12-48
△	Cavity L	1- 5-48
×	Cavity L	1- 6-48
○	Cavity M	1- 6-48
●	Cavity H	12-11-47

[ΔΔΔ] This appears to be in accord with some recent results of W. B. Nowak at M.I.T. See W. B. Nowak, M.I.T. Ph.D. thesis, 1949.

[10] A. B. Pippard, Nature 162, 68 (1948).

normal state. These transitions would substitute normal for superconducting electrons and thus introduce losses by absorbing energy for the transition and by the creation of additional normal electrons which could lose energy to the lattice by collisions. This "photoelectric" absorption would of course be more effective at higher frequencies.

Either or both of these mechanisms may be operative in these experiments. In Pippard's 1200 mc/sec. experiments he used dielectric spacers to support his resonator wires, and although he made corrections for the dielectric loss, it is conceivable that it was not entirely accounted for. The report of his work at 9200 mc/sec. contains no reference to such corrections; we do not know whether they played any part in those experiments. In our experiments no dielectrics were inserted in the cavity but it is possible that some contamination of the metal may have occurred in the process of fabrication.

Such absorption effects, whether by the pure metal itself, or by normal inclusions within the cavity, are not included in the theories presented earlier in this chapter, and for the purpose of reducing the data by the techniques described, these effects should be subtracted out. If the absorption effects are due to foreign bodies, the corrections are simple to make and can be done by merely subtracting out the value of R/R_t approached at 0°K, together with an appropriate change of scale. If the absorption is caused by electronic transitions, then it is not clear how to make this correction since the number of transitions per second may depend on the temperature. Since no other way of making the correction appears to be clearly indicated, we have subtracted out the constant amount of 0.09 from R/R_t for the purpose of making our calculations.

Further experiments are evidently necessary to decide whether or not the finite residual resistance is really due to the edge of an absorption band. These experiments should be extended to include measurements at higher frequencies, lower temperatures, and other materials, and should include control of the specimen purity. It is of some interest to compare the behavior of these tin

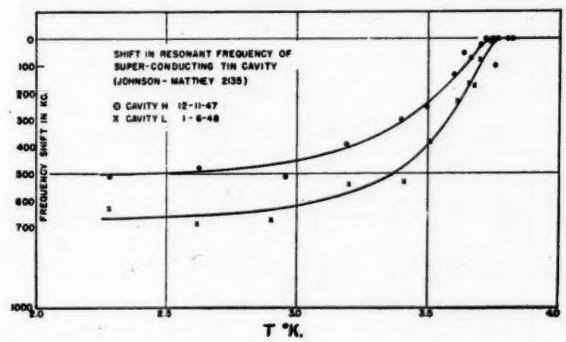

FIG. 8. Shift in resonant frequency of Sn cavity as a function of temperature.

⊙ Cavity H
× Cavity L

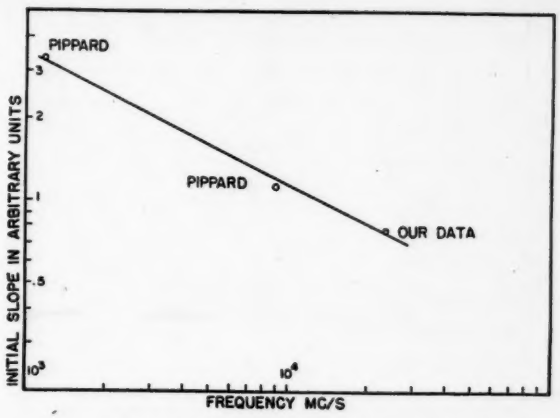

FIG. 9. Data on initial slopes of transition curves as a function of frequency.

cavities with some earlier results† obtained with Hilger lead cavities in this laboratory, also at a frequency of 24,000 mc/sec. In those experiments it was not possible to observe the transition region with an accuracy due to the fact that the transition occurs at 7.2°K, just above the liquid helium range. Between 4.2° and 2.0°K, however, measurements were possible, and of course the surface resistance could be determined fairly well just above the transition temperature. These measurements indicate a total change in surface resistance for lead of about 70 to 1 between 7.2°K and 2°K, about seven times as great as was observed with tin. This conforms to the expectation that the metal with the lower transition temperature should have an absorption band extending to lower frequencies.

II. Shift in Resonant Frequency of Cavity

The shift of resonant frequency of the cavity as a function of temperature is plotted in Fig. 8 for two different cavities. The reason for the differences in the two curves is not known. For purposes of calculation the two curves were averaged.

III. Interpretation

The usual way of treating a superconductor in which normal as well as superconducting electrons are present is to consider the total current as consisting of two components which are separately identified with the two kinds of electrons. The superconducting electron current density is related to the electric field strength by the London theory and the normal electron density by either Ohm's law or whatever modification is deemed appropriate. Thus H. London[4] assumed the validity of Ohm's law in his treatment but used an effective value for the a.c. conductivity much lower than the d.c. conductivity; Pippard[5] used the "ineffectiveness concept." In our treatment, however, we use the theory of Reuter and Sondheimer[6] to give the relation between the normal current density and the electric field. The Reuter and

† Obtained by J. B. Garrison.

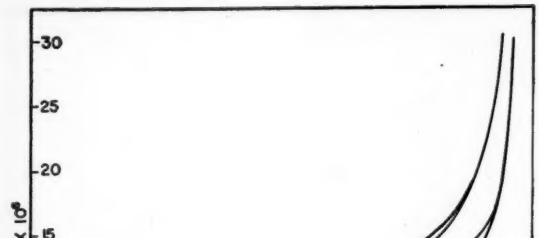

FIG. 10. Static penetration depth λ calculated from data by various methods.

A Reuter and Sondheimer theory, $p=0$, $\lambda_0=10^{-5}$ cm.
B Reuter and Sondheimer theory, $p=1$, $\lambda_0=10^{-5}$ cm.
C Reuter and Sondheimer theory, $p=1$, $\lambda_0=7.5\times10^{-6}$ cm.
D Pippard theory
E London theory

Sondheimer treatment is then modified by the addition of a term for the supercurrent and the integral equations may be solved by the same general techniques. The surface resistance and reactance of the superconductor may then be expressed in terms of three parameters, δ_{et}, the resistive skin depth just above the transition, $\lambda(T)$, the static field penetration depth, and the fraction of normal electrons at any temperature, $f_n(T)$. If we assume a relation between $f_n(T)$ and $\lambda(T)$, such for example that the sum of normal and superconducting electrons is constant, then we can determine both. They may both be related to $\lambda_0=\lambda(0)$. By combining the information given by both the surface resistance measurements and the shift in resonant frequency of the cavity (which is related to the surface reactance) λ_0 is evaluated.

The details of this treatment are given in Appendix A. We have also derived the formulas given by London and Pippard in terms of the same three parameters in order to exhibit the differences among these three modes of handling the problem.

IV. Initial Slopes

According to the theory given in Appendix A the initial slope of the R/R_t curve should go as $\omega^{-\frac{1}{3}}$. Figure 9 is a logarithmic plot of the initial slope $(d/dT)(R/R_t)$ *vs.* the frequency, on which we have plotted Pippard's results at 1200 and 9200 mc/sec. and ours at 23,910 mc/sec. and fitted the best straight line. It is seen that the observed frequency variation is more nearly $\omega^{-0.48}$ or $\omega^{-\frac{1}{2}}$ rather than $\omega^{-\frac{1}{3}}$.

Equation (A77) of Appendix A, for the initial slope of the inductive skin depth, indicates an initial negative slope. Further, since the inductive skin depth approaches λ_0 as the temperature goes toward zero, the curve must have a maximum in the neighborhood of $T=T_t$. However, the data are not good enough to detect any detailed structure in this region.

Penetration Depths

In Fig. 10 we have plotted curves of λ *vs.* T for our data on tin, calculated according to the data reduction techniques described in Appendix A. Taking $\lambda_0=10^{-5}$ cm, two curves are shown for the cases $p=0$ and $p=1$, using the extended R. S. method as herein expounded. For $\lambda_0=7.5\times10^{-6}$ cm, we show three curves, one for the extended B. S. method using $p=1$, one for Pippard's method, and one for London's method. It is seen that the three methods are in fair agreement at lower temperatures, and that London's and Pippard's methods are in good agreement near the transition temperature. However, these two methods yield a greater slope near the transition temperature than does the extended Reuter and Sondheimer theory.

The best choice of λ_0 is determined by comparing the curves $\Delta\lambda'$, the change in inductive skin depth,†† as determined from the shift in cavity resonant frequency, with these calculated from the R/R_t curve for different λ_0's. The calculated curves for $\lambda_0=7.5\times10^{-6}$ and $\lambda_0=10^{-5}$ are given in Fig. 11 together with that obtained from the frequency shift data. It is seen that $\lambda_0=10^{-5}$ cm, provides a fairly good fit. Pippard's best determination of λ_0, on the other hand, was 7.5×10^{-6} cm.

In Fig. 12 we compare our results for λ with those found by other experimenters.[5,11,12] The comparison is made on the basis of $\Delta\lambda$, the change in penetration depth referred to 2.1°K. Pippard's data[5] are derived from his 1200 mc/sec. frequency shift data while the other two sets of data were obtained from magnetic susceptibility

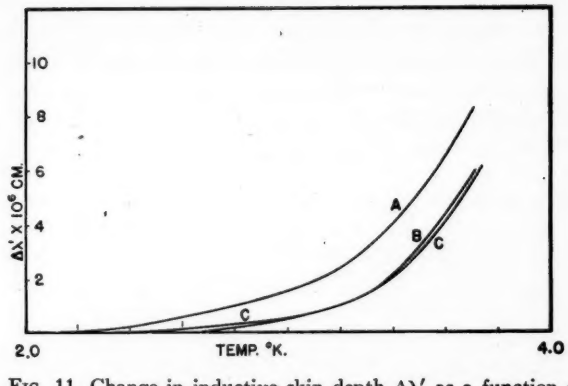

FIG. 11. Change in inductive skin depth $\Delta\lambda'$ as a function of temperature as derived from R/R_t data and from frequency shift data.

A—from R/R_t, $\lambda_0=7.5\times10^{-6}$ cm.
B—from R/R_t, $\lambda_0=10^{-5}$ cm.
C—Experimental

†† The quantity λ' is the same as δ' defined phenomenologically in Eq. (14).

[11] M. Desirant and D. Shoenberg, Proc. Phys. Soc. **60**, 413 (1948).

[12] E. Laurmann and D. Shoenberg, Nature **160**, 747 (1947).

measurements. Our results appear to agree fairly well with Desirant and Shoenberg[11] and Laurmann and Shoenberg[12] at "high" temperatures and are somewhat closer to Pippard's at low temperatures. Within the specified limits of error of the data they are consistent with Desirant and Shoenberg's results over the entire range. No precision indices are available for Pippard's and Laurmann and Shoenberg's measurements.

Our data for $\Delta\lambda$ as determined from R/R_t are consistent with the calculations of ΔX_s determined from the cavity resonant frequency shift and therefore may be regarded as calculated directly from the frequency shift. From Eqs. (A37) and (A43) of Appendix A it is seen that this involves principally assuming the London Theory with the theory for the normal electrons entering as a second order correction. Thus, as has been pointed out,[13] high frequency measurements do not furnish information about λ independently of some assumption concerning the London equations.

We are greatly indebted to many of our colleagues for assistance and helpful suggestions in the course of this work. We particularly wish to acknowledge the work of Dr. John B. Garrison (now at the University of Chicago) who is jointly responsible with one of us for the development of many of the experimental techniques described and who obtained the data given for lead, and to Mr. Ralph J. Harrison of the Research Laboratory of Electronics (M.I.T.) for many valuable and illuminating discussions. We are grateful for the use of the facilities of the Research Laboratory of Electronics and the enthusiastic support of Professor J. A. Stratton and the members of the staff, particularly Messrs. R. P. Cavileer, P. Nicholas, W. B. Nowak, and E. C. Ingraham.

APPENDIX A. THE SURFACE IMPEDANCE OF METALS IN THE SUPERCONDUCTING STATE

I. Introduction

The measurements of surface resistance and change of surface reactance are related to the physical characteristics of the superconducting state by introducing the current of superconducting electrons (London current) into the electrodynamic equations governing the normal state. A certain number of normal electrons are assumed to be present at each temperature. The normal electrons in the superconductor contribute to the current according to Eq. (14) of reference 6, the supercurrent adds a term to this. Maxwell's equations yield a new integral equation for the field. The surface resistance and reactance then depend on three parameters—the resistive skin depth just above the transition δ_{et} and two quantities characteristic of the superconducting state, the static field penetration depth $\lambda(T)$ and the fraction of normal electrons which remain at any temperature, $f_n(T)$. Assumptions about the relation between the latter two parameters lead to their evaluation from the data. In particular they may both be related to single constant $\lambda_0=\lambda(0)$. The best value of λ_0 is found by computing the expected change in surface reactance from the surface resistance curve as a function of T, and choosing λ_0 to give best agreement with observed values of the reactance change. Tables of the numerical values of the integrals which are needed to carry out these calculations have been given elsewhere.[3]

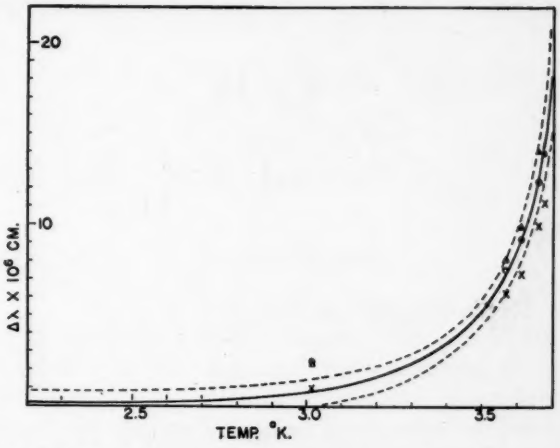

FIG. 12. Comparison of our data for $\Delta\lambda$, the change in penetration depth referred to 2.1°K, with other determinations.

△ Desirant and Shoenberg
× Pippard
⊙ Laurmann and Shoenberg

Solid curve from our data for R/R_t *vs.* temperature; dotted curves correspond to estimated uncertainties in our measurements.

It is also of interest to reduce the formulas used by London and those used by Pippard to depend on the same three parameters and thus exhibit their differences. The normal electrons were treated by different physical assumptions in their work, hence comparison of the calculated values of $\lambda(T)$ on each theory reveals the validity of their assumptions insofar as they approximate to the more accurate and more elaborate treatment given here.

II. Electrodynamic Equations for Superconductors

The field equations lead (in this one-dimensional case) to the electric field-current equation

$$\frac{\partial^2 E_x}{\partial z^2}=\frac{4\pi\dot{J}}{c^2}. \tag{A1}$$

$J=J_N+J_s$ (neglecting displacement current),
$J=$ total current at depth z in the metal,
$J_N=$ current of normal electrons,
$J_s=$ current of superconducting electrons. (A2)

Put

$$\dot{J}_s=\frac{c^2E_x}{4\pi\lambda^2} \tag{A3}$$

[13] Daunt, Miller, Pippard, and Shoenberg, Phys. Rev. 74, 842 (1948).

and

$$J_N=\tfrac{3}{4}\sigma_N l e^{i\omega t}\left[p\int_{-\infty}^{\infty}E(t)k\left(\frac{z-t}{l}\right)dt+(1-p)\int_{0}^{\infty}E(t)k\left(\frac{z-t}{l}\right)dt\right] \quad \text{(A4)}$$

where

$$E_x(z,t)=E(z)e^{i\omega t} \quad \text{(A5)}$$

and $k(u)$ is defined††† in reference 6, Eq. (15).

$\lambda(T)$ = the static magnetic field penetration depth into the superconductor. Equation (A3) may be interpreted as an acceleration equation for the superconducting electrons which do not collide with the lattice but accelerate under the action of the electric field in the metal at a rate determined by their inertia. When a static magnetic field is introduced, the induced electric field does the accelerating leaving behind a permanent eddy current when the steady static value is reached. This picture leads to $\lambda^2=m_s c^2/4\pi n_s\epsilon^2$, but (A3) is assumed to be more general than this specific model in which the mass and number of electrons m_s and n_s are uncertain.

Equation (A4) treats the normal electrons in the same way as the normal metal treatment of reference 6, but σ_N, the equivalent d.c. conductivity associated with the normal electrons will take account of the temperature dependence of the number of normal electrons.

From Eq. (29) of Appendix I, R.L.E. 109, or Eqs. (19) and (20) of reference 6,

$$\sigma_N=\frac{n_N\epsilon^2 l}{mv_m}=\frac{\epsilon^2}{h}\cdot\frac{2\pi^{\frac{1}{3}}}{3^{\frac{1}{3}}}h_N^{\frac{1}{3}}l. \quad \text{(A6)}$$

Putting (A2), (A3), and (A4) into (A1) and replacing $E(z)$ by $f(x)$ where $x=z/l$ gives the integro-differential equation for the field involving three parameters

$$''(fx)=\alpha_N i\left[p\int_{-\infty}^{\infty}f(y)k(x-y)dy+(1-p)\int_{0}^{\infty}f(y)k(x-y)dy+\alpha' f(x)\right], \quad \text{(A7)}$$

$$\alpha_N=\frac{3}{2}\frac{l^2}{\delta^2};\quad \delta_N=\left(\frac{c^2}{2\pi\omega\sigma_N}\right)^{\frac{1}{2}}, \quad \text{(A8)}$$

$$\alpha'=\frac{l}{\lambda^2}. \quad \text{(A9)}$$

Equation (A7) can be solved in the two limiting cases $p=1$ and $p=0$ by a slight variation of the procedure in Reuter's and Sondheimer's paper.[6]

III. Case $p=1$

$$f''(x)=i\alpha_N\int_{-\infty}^{\infty}f(y)k(x-y)dy+\alpha' f(y). \quad \text{(A10)}$$

Take the Fourier transform of (A10) with respect to x, employing the Faltung theorem on the product of Fourier transforms and introduce a discontinuity in $f'(x)$ at $x=0$; $f(x)$ has been taken even in x.

$$-2\mu-t^2\phi(t)=i\alpha_N\phi(t)\kappa(t)+\alpha'\phi(t) \quad \text{(A11)}$$

where††††

$$\mu=f'(+0)=-f'(-0), \quad \text{(A12)}$$

$$\phi(t)=\int_{-\infty}^{\infty}f(x)e^{-ixt}dx, \quad \text{(A13a)}$$

$$\kappa(t)=\int_{-\infty}^{\infty}k(x)e^{-ixt}dx=\frac{2}{t^2}\{(1+t^2)\tan^{-1}t-t\}. \quad \text{(A14)}$$

(A11) gives

$$\phi(t)=\frac{-2\mu}{t^2+\alpha'+i\alpha_N\kappa(t)}. \quad \text{(A13b)}$$

Inverting the Fourier transform; using (A14)

$$f(x)=\frac{1}{2\pi}\int_{-\infty}^{\infty}\phi(t)e^{ixt}dt=-\frac{2\mu}{\pi}\int_{0}^{\infty}\frac{\cos xt\,dt}{t^2+\alpha'+i\alpha_N\kappa(t)}. \quad \text{(A15)}$$

The surface impedance of the superconductor is given by

$$Z_s=-i\left(\frac{8}{3}\right)^{\frac{1}{3}}A_N\alpha^{\frac{1}{3}}\frac{f(0)}{f'(0)}=-i\frac{4\pi\omega}{c^2}l\frac{f(0)}{f'(0)} \quad \text{(A16)}$$

where (A15) gives

$$\frac{f(0)}{f'(0)}=-\frac{2}{\pi}\int_{0}^{\infty}\frac{dt}{t^2+\alpha'+i\alpha_N\kappa(t)}. \quad \text{(A17)}$$

Since α_N is very large at superconducting temperatures (10^6 to 10^8), it is useful to develop (A17) in inverse powers of α_N, (actually $\alpha_N^{\frac{1}{3}}$). The first two terms are:

$$\frac{f(0)}{f'(0)}=\frac{-2}{\pi}\left[\frac{1}{(\pi\alpha_N)^{\frac{1}{3}}}\int_{0}^{\infty}\frac{ydy}{y^3+\beta y+i}+\frac{4i}{\pi(\pi\alpha_N)^{\frac{2}{3}}}\int_{0}^{\infty}\frac{dy}{(y^3+\beta y+i)}+O\left(\frac{1}{\pi\alpha_N}\right)\right] \quad \text{(A18)}$$

where

$$\beta=\frac{\alpha'}{(\pi\alpha_N)^{\frac{2}{3}}}. \quad \text{(A19)}$$

††† This is not the wave number k used in the section on Surface Impedance of a Metal.

†††† κ is not the wave number used in the formulas of the section on Surface Impedance but is defined here in Eq. (A14).

The integrals in (A18) are evaluated by partial fraction expansions to give

$$I_1(\beta)=\int_0^\infty \frac{ydy}{y^3+\beta y+i}=\begin{cases}\dfrac{a}{1+2a^3}\left\{\pi+i\left[\tfrac{3}{2}\ln a-\dfrac{1+\dfrac{2}{a^3}}{\left(\dfrac{4}{a^3}-1\right)^{\frac{1}{2}}}\tan^{-1}\left(\dfrac{4}{a^3}-1\right)^{\frac{1}{2}}\right]\right\}; & a\leq 4^{\frac{1}{3}}\\ \dfrac{a}{1+2a^3}\left\{\pi+i\left[\tfrac{3}{2}\ln a-\dfrac{\tfrac{1}{2}+\dfrac{1}{a^3}}{\left(1-\dfrac{4}{a^3}\right)^{\frac{1}{2}}}\ln\dfrac{1+\left(1-\dfrac{4}{a^3}\right)^{\frac{1}{2}}}{1-\left(1-\dfrac{4}{a^3}\right)^{\frac{1}{2}}}\right]\right\}; & a\geq 4^{\frac{1}{3}}\end{cases} \tag{A20}$$

where a is the largest root of the cubic $x^3-\beta x-1=0$, and is given explicitly in terms of β by:

$$\begin{aligned} a&=\left(\frac{4\beta}{3}\right)^{\frac{1}{2}}\cosh\left[\tfrac{1}{3}\cosh^{-1}\tfrac{1}{2}\left(\frac{3}{\beta}\right)^{\frac{3}{2}}\right]; \quad \beta\leq\frac{3}{4^{\frac{1}{3}}}=1.89,\\ a&=\left(\frac{4\beta}{3}\right)^{\frac{1}{2}}\cos\left[\tfrac{1}{3}\cos^{-1}\tfrac{1}{2}\left(\frac{3}{\beta}\right)^{\frac{3}{2}}\right]; \quad \beta\geq\frac{3}{4^{\frac{1}{3}}}=1.89.\end{aligned} \tag{A21}$$

The next order term in (A18) is given by

$$I_2(\beta)=\int_0^\infty \frac{dy}{(y^3+\beta y+i)^2}=\frac{2}{3i}\left(1+\beta\frac{d}{d\beta}\right)\int_0^\infty \frac{dy}{y^3+\beta y+i} \tag{A22}$$

where

$$I_0(\beta)=\int_0^\infty \frac{dy}{y^3+\beta y+i}=\begin{cases}\dfrac{a}{1+2a^3}\left[\tfrac{3}{2}\ln a+\dfrac{3}{2(1-4/a^3)^{\frac{1}{2}}}\ln\left(\dfrac{1+(1-4/a^3)^{\frac{1}{2}}}{1-(1-4/a^3)^{\frac{1}{2}}}\right)-\pi i\right]; & a^3\geq 4\\ \dfrac{a}{1+2a^3}\left[\tfrac{3}{2}\ln a+\dfrac{3}{(4/a^3-1)}\tan^{-1}\left(\dfrac{4}{a^3}-1\right)^{\frac{1}{2}}-\pi i\right]; & a^3\leq 4\end{cases} \tag{A23}$$

$$I_2(\beta)=\begin{cases}\dfrac{-6a^3iI_0(\beta)}{(1+2a^3)^2}-\dfrac{4ai(a^3-1)}{(1+2a^3)^2}\left[\dfrac{a^3-1}{a^3-4}-\dfrac{3}{2a^3(1-4/a^3)^{\frac{1}{2}}}\ln\dfrac{1+(1-4/a^3)^{\frac{1}{2}}}{1-(1-4/a^3)^{\frac{1}{2}}}\right]; & a^3\geq 4\\ \dfrac{-ba^3iI_0(\beta)}{(1+2a^3)^2}-\dfrac{4ai(a^3-1)}{(1+2a^3)^2}\left[\dfrac{1-a^3}{4-a^3}+\dfrac{3}{a^3(4/a^3-1)^{\frac{1}{2}}}\tan^{-1}\left(\dfrac{4}{a^3}-1\right)^{\frac{1}{2}}\right]; & a^3\leq 4\end{cases} \tag{A24}$$

and (A16), (A18) give

$$Z_s=\frac{2\pi\omega}{c^2}\left(\frac{l}{\alpha_N}\right)^{\frac{1}{3}}\left(\frac{4}{\pi^{4/3}}I_1(\beta)i-\frac{16}{\pi^{8/3}}\frac{I_2(\beta)}{\alpha_N^{\frac{1}{3}}}\cdots\right). \tag{A25}$$

At the transition temperature, $\lambda=\infty$, $\beta=0$, $a=1$, and from (A20, A24)

$$I_1(0)=\frac{\pi}{3}(1-i/3^{\frac{1}{2}}), \tag{A26}$$

$$I_2(0)=-\frac{2\pi}{9}(1+i/3^{\frac{1}{2}})=-\tfrac{2}{3}iI_0(0), \tag{A27}$$

$$Z_t=\frac{2\pi\omega}{c^2}\frac{l}{\alpha_t^{\frac{1}{3}}}\frac{4}{3^{\frac{1}{2}}\pi^{\frac{1}{3}}}\left[\left(1+\frac{8\cdot 3^{\frac{1}{2}}}{3\pi(\pi\alpha_t)^{\frac{1}{2}}}\right)+i\left(3^{\frac{1}{2}}+\frac{8}{3\pi(\pi\alpha_t)^{\frac{1}{2}}}\right)\right], \tag{A28}$$

which agrees with results of reference 6 and Eq. (24), Appendix I of R.L.E. 109.

As $T\to 0$, if all electrons become superconducting, i.e., $n_N\to 0$, then $\delta_N\to 0$, $\beta\to\infty$, $a\to\infty$, $\alpha_N\to 0$. Approximations to the limiting forms of R_s and X_s may be obtained from the first term of (A25). This gives

$$R_s=\frac{4\pi\omega\lambda^4}{c^2}\frac{\alpha_N}{l^3}(3\ln\beta-1), \tag{A29}$$

$$X_s=\frac{4\pi\omega\lambda}{c^2}\left(1-\frac{1}{\beta^{\frac{1}{2}}}+\frac{5}{8\beta^3}\cdots\right). \tag{A30}$$

Equation (A30) gives the correct limiting form of X_s as $T\to 0$ if all electrons become superconducting.

Putting

$$R_t=\frac{2\pi\omega\delta_{et}}{c^2} \tag{A31}$$

where (A28) gives[a]

$$\delta_{et}=\frac{l}{\alpha_t^{\frac{1}{2}}}\cdot\frac{4}{3^{4/3}\pi^{\frac{1}{2}}} \tag{A32}$$

(which is the effective resistive skin depth at the transition temperature) and using

$$\frac{\alpha_N}{\alpha_t}=\frac{n_N^{\frac{1}{2}}}{n_t^{\frac{1}{2}}}=f_N^{\frac{1}{2}} \tag{A33}$$

so that (A31), (A32) give

$$\frac{\alpha_N}{l^3}=\frac{64}{8\cdot 3^{\frac{1}{2}}\pi}\cdot\frac{f_N^{\frac{1}{2}}}{\delta_{et}^3} \tag{A34}$$

and

$$\beta=\frac{1}{\lambda^2\pi^{\frac{1}{2}}}\left(\frac{l}{\alpha_N^{\frac{1}{2}}}\right)^2=\frac{27}{16}\frac{\delta_{et}^2}{\lambda^2 f_N^{4/9}} \tag{A35}$$

then (A29), (A30) become, using (A32) and (A34), as $T\to 0$,

$$\frac{R_s}{R_t}=0.2904\frac{\lambda^4 f_N^{\frac{1}{2}}}{\delta_{et}^4}\left(3\ln\frac{27}{16}-1-\ln\frac{\lambda^2 f_N^{4/9}}{\delta_{et}^2}\right), \tag{A36}$$

$$X_s=\frac{4\pi\omega\lambda}{c^2}\left(1-\frac{64}{81\cdot 3^{\frac{1}{2}}}\cdot\frac{\lambda^3 f_N^{\frac{1}{2}}}{\delta_{et}^3}+\frac{5}{8}\left(\frac{4}{3\cdot 3^{\frac{1}{2}}}\right)\frac{\lambda^6 f_N^{4/3}}{\delta_{et}^6}\cdots\right). \tag{A37}$$

More generally note that (A25) gives:

$$\frac{R_s}{R_t}=\frac{1}{f_N^{2/9}}\cdot\frac{ImI_1(\beta)}{ImI_1(0)};\quad \frac{X_s}{X_t}=\frac{1}{3^{\frac{1}{2}}}\frac{X_s}{R_t}=\frac{1}{f_N^{2/9}}\frac{ReI_1(\beta)}{ReI_1(0)}. \tag{A38}$$

[a] It is assumed that $\alpha_t^{\frac{1}{2}}\gg 1$ and hence the second-order terms in (A28) may be dropped.

Similar expressions will now be derived for the case $p=0$ and for London's and Pippard's treatments.

IV. Case $p=0$

$$f''(x)=\alpha_N i\int_0^\infty f(y)k(x-y)dy+\alpha' f(x). \tag{A39}$$

The more complicated manipulation which leads to a solution of this Wiener-Hopf type integral equation is given by Reuter and Sondheimer and is too long to outline here. The procedure, which follows that of Wiener and Hopf, introduces a function equal to the difference of the two sides of (A39) for $x<0$, but zero for $x\sim 0$, takes the Laplace Transform of this function again using the Faltung theorem, discusses the regions of existence of the various transforms and separates the transform equation into a side which is regular in the left-half plane and a side regular in the right-half plane with an overlapping region of regularity. The two sides therefore determine an integral function; determining the asymptotic behavior of this integral function identifies the integral function and thence the transform of $f(x)$. The ratio $f(0)/f'(0)$ is then expressed in terms of the transform and found explicitly. The modification introduced by the term $\alpha' f(x)$ in (A39) is to alter the characteristic equation whose roots must be located to separate the transform equation properly. We now find for $\alpha'>1$, the characteristic equation has no roots in the strip $1\le Re\, s\le 1$ for all x.

$\left(s \text{ is the transform variable and } F(s)=\int_{-\infty}^{\infty} e^{-xs}f(x)dx\right)$.

We finally find the quantity of interest in the form

$$\frac{f(0)}{f'(0)}=-\frac{1}{\nu+1};\qquad \nu=\frac{1}{\pi}\int_0^\infty \ln\left(\frac{t^2+\alpha'+i\alpha_N\kappa(t)}{t^2+1}\right)dt \tag{A40}$$

where

$$\kappa(t)=\frac{2}{t^3}\{(1+t^2)\tan^{-1}t-t\}. \tag{A41}$$

Integrate (A40) by parts, put $\kappa(t)\sim\pi/t$ and get,

$$\nu+1=\frac{2i\alpha_N}{\pi}\int_0^\infty\frac{\frac{3}{2}\frac{\pi}{t}+\frac{\alpha'}{i\alpha_N}}{t^2+\alpha'+i\frac{\alpha_N\pi}{t}}dt=\frac{3i(\alpha_N\pi)^{\frac{1}{2}}}{\pi}$$

$$\times\int_0^\infty\frac{dy}{y^3+\beta y+i}+\frac{2\alpha'}{\pi(\pi\alpha_N)^{\frac{1}{2}}}\int_0^\infty\frac{ydy}{y^3+\beta y+i}$$

$$=\tfrac{3}{4}i(\pi\alpha_N)^{\frac{1}{2}}[I_0(\beta)-\tfrac{2}{3}i\beta I_1(\beta)]. \tag{A42}$$

From (A16), (A40), (A42) we get

$$Z_s=\frac{4\pi\omega l}{c^2}\frac{\pi}{3(\pi\alpha_N)^{\frac{1}{2}}}\frac{1}{[I_0(\beta)-\frac{2}{3}i\beta I_1(\beta)]}. \quad \text{(A43)}$$

(Equation (A43) corresponds to the first term of (25).)

At $T=T_t$, $\beta=0$, using (A26), (A43) becomes

$$Z_t=\frac{2\pi\omega}{c^2}\frac{l}{\alpha_t^{\frac{1}{2}}}\frac{3^{\frac{1}{2}}}{2\pi^{\frac{1}{2}}}(1+3^{\frac{1}{2}}i);\quad p=0. \quad \text{(A44)}$$

Again as in the case of (A29) and (A30), as $T\to 0$, $\beta\to\infty$

$$I_0(\beta)\to\frac{3}{2}\frac{\ln\beta}{\beta}-\frac{\pi i}{2\beta}. \quad \text{(A45)}$$

Then (A45) in (A43) with (A19) and (A9) give, as $T\to 0$

$$Z_t\to\frac{4\pi\omega}{c^2}\frac{\pi}{3}\frac{l}{(\pi\alpha_N)^{\frac{1}{2}}}\left[\frac{1}{\frac{2}{3}-i\beta\frac{\pi}{2\beta^{\frac{1}{2}}}}\right]$$

$$=\frac{4\pi i\omega}{c^2}\frac{l}{(\pi\alpha_N)^{\frac{1}{2}}}\frac{1}{\beta^{\frac{1}{2}}}=\frac{4\pi i\omega\lambda}{c^2} \quad \text{(A46)}$$

which agrees with (A30).

Note that (A44), and (A32) lead to

$$\delta_{et}=\frac{l}{\pi_t^{\frac{1}{2}}}\cdot\frac{3^{\frac{1}{2}}}{2\pi^{\frac{1}{2}}} \quad \text{(A47)}$$

hence as in (A35), using (A33)

$$\beta=\frac{1}{\lambda^2\pi^{\frac{1}{2}}f_N^{4/9}}\cdot\left(\frac{l}{\alpha_t^{\frac{1}{2}}}\right)^2=\frac{4}{3}\frac{\delta_{et}^2}{\lambda^2 f_N^{4/9}}\quad (p=0) \quad \text{(A48)}$$

and, as in (A34),

$$\frac{l}{\alpha_N^{\frac{1}{2}}}=\frac{2\pi^{\frac{1}{2}}}{3^{\frac{1}{2}}}\frac{\delta_{et}}{f_N^{2/9}}. \quad \text{(A49)}$$

V. Pippard's Treatment

This differs from the above in treating the current due to the normal electrons by means of an effective conductivity derived from the "ineffectiveness concept."

$$Z=-\frac{4\pi i\omega}{c^2}\frac{E(0)}{\dfrac{\partial E(0)}{\partial z}}\ \text{(equivalent to (A16))}. \quad \text{(A50)}$$

From (A1), (A2)

$$\frac{\partial^2 E}{\partial z^2}=\frac{4\pi\dot{J}}{c^2};\quad =\dot{J}_s+\dot{J}_N=\frac{c^2E}{4\pi\lambda^2}+\sigma_e E. \quad \text{(A51)}$$

The effective conductivity

$$\sigma_e=\frac{\delta_s}{l}\sigma_N \quad \text{(A52)}$$

is assumed to be a fraction δ_s/l smaller than the d.c. conductivity of the normal electrons (using the "ineffectiveness concept"). Here δ_s is the penetration depth of the field into the superconductor.

Since $J(z)$ is now proportional to $E(z)$ (for harmonic time dependence $e^{i\omega t}$) (A51) leads to a wave equation for E. We have

$$E(z)=E_0e^{-i\kappa z} \quad \text{(A53)}$$

$$\kappa^2=-\left(\frac{1}{\lambda^2}+\frac{4\pi i\omega\sigma_e}{c^2}\right)=-\left(\frac{1}{\lambda^2}+\frac{2i}{\delta_e^2}\right). \quad \text{(A54)}$$

Therefore

$$\left.\begin{aligned}&\kappa=\kappa_r+i\kappa_i\\&\kappa_r=\frac{1}{\lambda}\left(\frac{q-1}{2}\right)^{\frac{1}{2}}\\&\kappa_i=-\frac{1}{\lambda}\left(\frac{q-1}{2}\right)^{\frac{1}{2}}\\&q=(1+4\lambda^4/\delta_e^4)^{\frac{1}{2}}\end{aligned}\right\}. \quad \text{(A55)}$$

From (A50), (A53), (A55)

$$Z_s=\frac{4\pi\omega}{c^2}\frac{1}{\kappa}=\frac{4\pi\omega}{c^2}\lambda\left[\frac{1}{q}\left(\frac{q-1}{2}\right)^{\frac{1}{2}}+\frac{i}{q}\left(\frac{q+1}{2}\right)^{\frac{1}{2}}\right]. \quad \text{(A56)}$$

Now

$$\frac{\delta_e^2}{\delta_{et}^2}=\frac{\sigma_{et}}{\sigma_e}=\frac{\dfrac{\delta_{et}}{l}\sigma_{Nt}}{\dfrac{\delta_s}{l}\sigma_N}=\frac{\delta_{et}}{\delta_s}\frac{1}{f_N^{\frac{1}{2}}}. \quad \text{(A57)}$$

This assumes l is constant, i.e., the d.c. conductivity in presence of a magnetic field greater than critical is constant. Hence using (A55)

$$\frac{f_N^{\frac{1}{2}}}{\delta_{et}^3}=\frac{1}{\delta_s}\cdot\frac{1}{\delta_e^2}=-\frac{\kappa_i}{\delta_e^2}=\frac{1}{\lambda}\left(\frac{q+1}{2}\right)^{\frac{1}{2}}\left(\frac{q^2-1}{2\lambda^2}\right)^{\frac{1}{2}} \quad \text{(A58a)}$$

or

$$(q+1)(q^2-1)=\frac{8\lambda^6 f_N^{4/3}}{\delta_{et}^6}. \quad \text{(A58b)}$$

As $T\to 0$, $q\to 1$ and (A58) may be solved for q as an expansion in powers of $2\lambda^6 f_N/\delta_{et}^6$. Then any function of

q may be expanded similarly. Thus

$$R_s=\frac{4\pi\omega\lambda}{c^2}\left(\frac{q-1}{2q^2}\right)^{\frac{1}{2}}=\frac{4\pi\omega\lambda}{c^2}\cdot\frac{\lambda^3 f_N^{\frac{1}{2}}}{\delta_{et}^3}\times\left[1-3\left(\frac{\lambda}{\delta_{et}}\right)^6 f_N^{4/3}+13\left(\frac{\lambda}{\delta_{et}}\right)^{12} f_N^{8/3}-64\left(\frac{\lambda}{\delta_{et}}\right)^{18} f_N^4\cdots\right]. \quad \text{(A59)}$$

Noting

$$R_t=\frac{2\pi\omega\delta_{et}}{c^2}, \quad \text{(A60)}$$

$$\frac{R_s}{R_t}=\frac{2\lambda^4 f_N^{\frac{1}{2}}}{\delta_{et}^4}\left[1-3\left(\frac{\lambda}{\delta_{et}}f_N^{2/9}\right)^6+13\left(\frac{\lambda}{\delta_{et}}f_N^{2/9}\right)^{12}-64\left(\frac{\lambda}{\delta_{et}}f_N^{2/9}\right)^{18}+\cdots\right], \quad \text{(A61)}$$

$$X_s=\frac{4\pi\omega\lambda}{c^2}\left(\frac{q+1}{2q^2}\right)^{\frac{1}{2}}=\frac{4\pi\omega\lambda}{c^2}\left[1-\frac{3}{2}\left(\frac{\lambda}{\delta_{et}}f_N^{2/9}\right)^6+\frac{47}{8}\left(\frac{\lambda}{\delta_{et}}f_N^{2/9}\right)^{12}-\frac{443}{16}\left(\frac{\lambda}{\delta_{et}}f_N^{2/9}\right)^{18}\cdots\right]. \quad \text{(A62)}$$

It is of interest to compare (A61) with the approximate expression obtained by Pippard

$$\frac{R_s}{R_t}=\frac{2\left(\frac{\lambda}{\delta_{et}}\right)^4 f_N^{\frac{1}{2}}}{\left[1+6f_N^{4/3}\left(\frac{\lambda}{\delta_{et}}\right)^6\right]^{\frac{1}{2}}}=2\left(\frac{\lambda}{\delta_{et}}\right)^4 f_N^{\frac{1}{2}}\times\left[1-3\left(\frac{\lambda}{\delta_{et}}f_N^{2/9}\right)^6+\frac{27}{2}\left(\frac{\lambda}{\delta_{et}}f_N^{2/9}\right)^{12}-\frac{135}{2}\left(\frac{\lambda}{\delta_{et}}f_N^{2/9}\right)^{18}\cdots\right]. \quad \text{(A63)}$$

Also the correction factor for normal electrons in (A62), which Pippard evaluates in terms of the ratio $r=R_s/R_t$, may be rigorously expanded in terms of r and f_N.

$$\left(\frac{q+1}{2q^2}\right)^{\frac{1}{2}}=1-0.5304f_N^{\frac{1}{2}}r^{\frac{1}{2}}-0.1094f_N^{\frac{1}{2}}r^3\cdots. \quad \text{(A64)}$$

Pippard takes $f_N=1$, since the terms in r are small when $f_N\neq 1$, but near the transition where the correction factor differs from 1, $f_N=1$. (Note that f_N here differs from Pippard because he takes the conductivity proportional to n_N whereas we use $n_N^{\frac{1}{2}}$ corresponding to a degenerate Fermi gas of electrons.)

VI. London's Treatment

The normal electrons are now treated as having an effective a.c. conductivity (smaller than the d.c. conductivity) which is assumed to vary as $n_N^{\frac{1}{2}}$ but not with the penetration depth of the field i.e. no "ineffectiveness concept" is used. As in Pippard' streatment Eqs. (A50), (A51), (A53), (A54), (A55), (A56) hold but not (A52) or (A57). Instead we have

$$\frac{\delta_e^2}{\delta_{et}^2}=\frac{\sigma_{et}}{\sigma_e}=\frac{1}{f_N^{\frac{1}{2}}}. \quad \text{(A65)}$$

Hence

$$q=\left(1+\frac{4\lambda^4}{\delta_e^4}\right)^{\frac{1}{2}}=\left(1+\frac{4\lambda^4}{\delta_e^4}f_N^{4/3}\right)^{\frac{1}{2}}, \quad \text{(A66)}$$

$$\frac{R_s}{R_t}=\frac{2\lambda}{\delta_{et}}\left(\frac{q-1}{2q^2}\right)^{\frac{1}{2}}=\frac{2\lambda^3 f_N^{\frac{1}{2}}}{\delta_{et}^3}\times\left[1-\frac{5}{2}\left(\frac{\lambda f_N^{\frac{1}{2}}}{\delta_{et}}\right)^4-\frac{71}{8}\left(\frac{\lambda f_N^{\frac{1}{2}}}{\delta_{et}}\right)^8\cdots\right], \quad \text{(A67)}$$

$$X_s=\frac{4\pi\omega\lambda}{c^2}\left(\frac{q+1}{2q^2}\right)^{\frac{1}{2}}=\frac{4\pi\omega\lambda}{c^2}\times\left[1-\frac{3}{2}\left(\frac{\lambda f_N^{\frac{1}{2}}}{\delta_{et}}\right)^4+\frac{35}{8}\left(\frac{\lambda f_N^{\frac{1}{2}}}{\delta_{et}}\right)^8\cdots\right]. \quad \text{(A68)}$$

VII. Calculation procedures

The experimental data consist of R_s/R_t as a function of T, the absolute value of R_t, and the change in X_s from the transition temperature down. The theory can be applied to the data in several ways. λ can be found as a function of T if $f_N(T)$ is known, or if a relation is assumed between f_N and λ. The most reasonable relation in the light of present theories relates f_N and λ but introduces the constant λ_0, the value of λ when all electrons are superconducting. By using the $\Delta X_s(T)$ data also, λ_0 can then be fixed. In addition the theory gives some simple quantitative relations which can be checked on the data; namely the frequency dependence of the initial slope of the resistance curve and of the resistance at temperatures well below the transition, and the slope of the reactance curve (or inductive skin depth curve) at T_t.

To relate f_N and λ, put

$$n_N+n_s=n_0 \quad \text{(A69)}$$

(where n_0 is number of normal electrons at the transition temperature).

$$\frac{\lambda^2}{\lambda_0^2}=\frac{n_0}{n_s}. \quad \text{(A70)}$$

Equations (A69) and (A70) give

$$f_N=\frac{n_N}{n_0}=1-\frac{n_s}{n_0}=1-\frac{\lambda_0^2}{\lambda^2}. \quad \text{(A71)}$$

Equation (A69) is part of the "two fluid" assumption about electrons in superconductors, the constant total is divided between superconducting and normal electrons which behave independently. Equation (A70) is based on the acceleration picture of superconducting electrons with inertia but no resistance; then $\lambda^2=m_s c^2/4\pi n_s e^2$. The mass m_s is unknown; even though superconducting electrons do not interact with lattice vibrations, there is no reason to think the potential field of the crystal does not affect the mass.

Calculation of $\lambda(T)$ using the extended theory of Reuter and Sondheimer to treat the normal electrons for the case $p=0$ is based on the following equations.

$$\left.\begin{aligned}
&\frac{R_s}{R_t}=\frac{1}{f_N^{2/9}}\frac{ImI_1(\beta)}{ImI_1(0)}; \qquad f_N=1-\frac{\lambda_0^2}{\lambda^2}\\
&\beta=\frac{27}{16}\frac{\delta_{et}^2}{\lambda^2 f_N^{4/9}}; \qquad \delta_{et}^2=\frac{c^2R_t}{2\pi\omega}\\
&\frac{c^2X_s}{4\pi\omega}=\delta_{et}\frac{3^{\frac{1}{2}}}{2}\frac{ReI_1(\beta)}{f_N^{2/9}ReI_1(0)}\\
&\frac{c^2X_t}{4\pi\omega}=\delta_{et}\frac{3^{\frac{1}{2}}}{2}
\end{aligned}\right\}. \tag{A72}$$

The procedure is to choose λ_0, calculate $f_N(\lambda)$, $\beta(\lambda)$, using the known value of R_t to find δ_{et}, $(R_s/R_t)(\lambda)$ using tables[b] of $ImI_1(\beta)$, hence from $(R_s/R_t)(T)$ find $\lambda(T)$. From tables of $ReI_1(\beta)$, the inductive skin depth $c^2X_s(\lambda)/4\pi\omega$ is found, hence $c^2X_s(T)/4\pi\omega$ from $\lambda(T)$. The values of $(c^2/4\pi\omega)[X_s(T)-X_s(T_t)]$ are compared with experimental values found from the frequency shift of the cavity. λ_0 is adjusted for best fit of the reactance data.

For the case $p=0$, we use the following relations.

$$\left.\begin{aligned}
&\frac{R_s}{R_t}=\frac{1}{f_N^{2/9}}\frac{ReI_3(\beta)}{ReI_3(0)}\left|\frac{I_3(0)}{I_3(\beta)}\right|^2;\\
&I_3(\beta)=I_0(\beta)-\tfrac{2}{3}i\beta I_1(\beta),\\
&\beta=\frac{4}{3}\frac{\delta_{et}^2}{\lambda^2 f_N^{4/9}}; \qquad \delta_{et}=\frac{c^2R_t}{2\pi\omega},\\
&\frac{c^2X_s}{4\pi\omega}=\delta_{et}\frac{3^{\frac{1}{2}}}{2}\frac{ImI_3(\beta)}{ImI_3(0)}\cdot\left|\frac{I_3(0)}{I_3(\beta)}\right|^2.
\end{aligned}\right. \tag{A73}$$

Calculations based on Pippard's equations use

$$\left.\begin{aligned}
&\frac{R_s}{R_t}=\frac{\lambda}{\delta_{et}}\left(\frac{2(q-1)}{q^2}\right)^{\frac{1}{2}}; \qquad f_N=1-\frac{\lambda_0^2}{\lambda^2}\\
&q^2=1+\frac{8\lambda^6 f_N^{4/3}}{\delta_{et}^6}\cdot\frac{1}{q+1}
\end{aligned}\right\}. \tag{A74}$$

[b] Tables of these integrals as well as those appearing in Eq. (A73) have been given in R.L.E. 109.

As above λ_0 is chosen, $f_N(\lambda)$ found, $q(\lambda)$ found by solving the cubic for q using the known value of δ_{et}. Hence we find $(R_s/R_t)(\lambda)$ and then from $(R_s/R_t)(T)$, $\lambda(T)$ is found. The $\lambda(T)$ and $q(\lambda)$ then lead to $c^2X_s/4\pi\omega$. The cubic in q is quickly solved by tabulating or plotting the root as a function of the single parameter, Newton's rule can be used to improve a first guess. (The desired root is unity when $f_N=0$). Various λ_0's may then be tried to fit the reactance data best.

Calculations on London's equations use the same equations as above except for the one giving q. This becomes

$$q=\left(1+\frac{4\lambda^4}{\delta_{et}^4}f_N^{4/3}\right)^{\frac{1}{2}}. \tag{A75}$$

Initial Slopes

The frequency dependence of the initial slope is found from (A38), (A20), (A35). (For the case $p=1$)

$$\begin{aligned}
\frac{d}{dT}\frac{R_s}{R_t}(T)\Big]_{T=T_t}&=-\frac{2}{9}\frac{\frac{R_s}{R_t}(T)}{T_t}\left(\frac{df_N}{dT}\right)_{T=T_t}\\
&\quad+\frac{1}{f_N^{2/9}}\frac{d}{d\beta}\left(\frac{ImI_1(\beta)}{ImI_1(0)}\right)\frac{d\beta}{dT}\Big]_{T=T_t}\\
&=\left(\frac{2}{9}-\frac{27}{16}\frac{3^{\frac{1}{2}}}{\pi}\frac{\delta_{et}^2}{\lambda_0^2}\right)\frac{1}{n_0}\left(\frac{dn_s}{dT}\right)_{T=T_t}
\end{aligned} \tag{A76}$$

using

$$\frac{d}{dT}\left(\frac{\lambda_0^2}{\lambda^2}\right)=\frac{1}{n_0}\frac{dn_s}{dT} \tag{A77}$$

and

$$\frac{df_N}{dT}=-\frac{d}{dT}\left(\frac{\lambda_0^2}{\lambda^2}\right); \qquad \frac{d\beta}{dT}=\frac{27}{16}\delta_{et}^2\frac{d}{dT}\left(\frac{1}{\lambda^2}\right). \tag{A78}$$

The 2/9 term in (A76) is only a few percent of the other term in the case of interest and since $dn_s/dT<0$, $(d/dT)(R_s/R_t)(T)>0$. Since $\delta_{et}=(4/3^{\frac{1}{2}}\pi^{\frac{1}{2}})(l/\alpha_t^{\frac{1}{2}})$ and $\alpha=(2\pi^{4/3}3^{\frac{1}{2}}/hc^2)e^2\omega n^{\frac{1}{3}}l^{\frac{2}{3}}$, the frequency dependence of the initial slope is closely $\omega^{-\frac{1}{2}}$.

The initial slope of the inductive skin depth $c^2X_s/4\pi\omega$ is similarly found to be

$$\frac{d}{dT}\frac{c^2X_s}{4\pi\omega}=\frac{3^{\frac{1}{2}}}{9}\delta_{et}\frac{1}{n_0}\left(\frac{dn_s}{dT}\right)_{T=T_t} \tag{A79}$$

which is negative. Since $c^2X_s/4\pi\omega$ at lower temperatures decreases to λ_0, the curve goes through a maximum near T_t. At higher frequencies, however; we may have $\delta_{et}\leq\lambda_0$ and the character of the curve will change.

Well below the transition, the limiting value of R_s/R_t has the form given by Eq. (A36).

Absorption of Gamma-Rays in Aluminum

W. C. PARKINSON
H. M. Randall Laboratory of Physics, University of Michigan, Ann Arbor, Michigan
(Received July 21, 1949)

The scattering cross section for gamma-rays in aluminum was measured by two independent methods at the three energies 1.11, 1.71, and 2.76 Mev. The results 0.156, 0.125, and 0.0996 cm^{-1}, respectively, for the three energies are in agreement with the predictions of theory within the experimental error of ± 1 percent. The essential features of the measurements are: (1) Choice of gamma-ray energies and absorbing material such that Compton scattering is the only important process. (2) Use of a geometry which effectively eliminates single and multiple scattering and permits an accurate determination of the background. (3) Elimination of errors due to the other gamma-ray energies emitted by the source. (4) Determination of corrections for absorber impurities, counter deadtime, and random fluctuations in the counters and counter circuits. The two methods of measurement differ primarily in the way in which the errors due to the other gamma-rays emitted by the source are removed.

INTRODUCTION

DURING the course of the last twenty years, many attempts have been made to verify experimentally the Klein-Nishina formula[1] which predicts the angular distribution and total cross section for scattering of gamma-rays. Meitner and Hupfeld,[2] Chao,[3] and Tarrant[4] measured the cross section for carbon using the 2.6-Mev gamma-rays of ThC'' by the straight absorption method. Their results were in agreement with the theory within their experimental accuracy of approximately 5 percent. The cross section in carbon and aluminum in the region from 0.04 to 0.6 Mev was investigated by Hewlett,[5] Allen,[6] and Read and Lauritsen[7] using Coolidge x-ray tubes and crystal spectrometers as a source of monochromatic radiation. Their results were in reasonable agreement with theory although it was necessary to make large corrections for the photoelectric cross section. Numerous measurements[8] were made in the region from 0.6 to 2.6 Mev with results deviating as much as 20 percent from the theory. The large variation in results in the intermediate region led the author to review the methods of measurement with a view toward making a more accurate determination of the validity of the formula.

A check of the Klein-Nishina formula is provided by a measurement either of the angular distribution of the scattered gamma-rays or of the total scattering cross section. In order to determine the total cross section with reasonable accuracy, several sources of error must be considered. First, it is necessary to eliminate or at least take accurate account of the other two of the three principal processes by which gamma-rays are absorbed; namely, the photoelectric effect and pair formation. Since it is extremely difficult experimentally to distinguish reliably between the three, it is essential that the measurements be made in the energy region from one to three Mev, where, for elements of low atomic number, the photoelectric and pair formation cross sections are very small compared to that of the Compton process. An additional factor which undoubtedly contributed to the variations in the results of the earlier investigators is single and multiple scattering. Fortunately, the strong sources now available through the facilities of the Atomic Energy Commission make possible the use of a geometry which effectively eliminates this difficulty, as may be verified both by calculation and by measurement. However, the use of such sources introduces a third source of error which is demonstrated very strikingly in the case of Sb^{124}, for which until the recent work of Kern[9] and co-workers, only two gamma-rays were reported. It is now apparent that gamma-rays of five different energies are emitted. Therefore, it is necessary that the methods employed for the measurement be capable of selecting one energy of the several emitted by the source so that the final measurements can be made with essentially monoenergetic radiation. Other factors which may introduce errors are the impurity of the absorber, bremsstrahlung of the beta-rays and secondary electrons, and instability in the measuring equipment.

METHODS OF MEASUREMENT

Four methods of measurement were investigated but, of these, two were ultimately rejected as being unsuitable for producing accurate results. The first, which utilized the proportional properties of the crystal counter as a means of separating in energy the various gamma-rays emitted by the source, was discarded

[1] O. Klein and Y. Nishina, Zeits. f. Physik **52**, 853 (1929).
[2] L. Meitner and H. Hupfeld, Zeits. f. Physik **67**, 147 (1930).
[3] C. Y. Chao, Phys. Rev. **36**, 1519 (1930).
[4] G. T. B. Tarrant, Proc. Roy. Soc. **128**, 345 (1930).
[5] C. W. Hewlett, Phys. Rev. **17**, 284 (1921).
[6] S. J. M. Allen, Phys. Rev. **27**, 266 (1926).
[7] J. Read and C. C. Lauritsen, Phys. Rev. **45**, 433 (1934).
[8] W. Genter lists the references for many of the earlier papers in J. de phys. et rad. **6**, 274 (1935). Some of the later papers are: C. C. Lauritsen and J. R. Oppenheimer, Phys. Rev. **46**, 80 (1934); G. Groetzinger and L. Smith, Phys. Rev. **67**, 53 (1945); J. M. Cork and R. W. Pidd, Phys. Rev. **66**, 227 (1944); J. M. Cork, Phys. Rev. **67**, 53 (1945); C. L. Cowan, Phys. Rev. **74**, 1841 (1948); and, C. L. Davisson and R. D. Evans, Phys. Rev. **73**, 1239 (1948). The results of the last two papers are in reasonably good agreement with the predictions of theory.
[9] Kern, Zaffarano, and Mitchell, Phys. Rev. **73**, 1142 (1948).

because of polarization effects in the crystal. The second, in which a beta-ray spectrometer was used to distinguish between the gamma-rays by selecting the secondary electrons ejected from a thin lead target, was rejected primarily because of the low counting rate obtained with a geometry suitable for eliminating errors due to scattering. The two methods actually used are termed the "filter" and the "coincidence" methods.

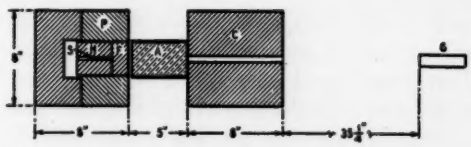

FIG. 1. Geometrical arrangement of the source S, absorber A, collimator C, and Geiger gamma-ray counter G, for the filter method. F=filter, H=source holder, P=lead shield.

The Filter Method

This method, which for the ideal case of a monoenergetic source would be the most straightforward, is the one employed by the majority of the earlier investigators. The geometrical arrangement is shown in Fig. 1. The measured absorption coefficient is defined through the relation $\tau_m=(1/x)\log N_0/N$ where x is the thickness of the absorbing material and N and N_0 are the true counting rates, proportional to the number of quanta transmitted unscattered, with and without the absorber in the beam, respectively. For a monoenergetic source τ_m is the true value of the absorption coefficient for the material of the absorber. In the actual case in which more than one energy of gamma-rays is emitted, it may be shown that by filtering the radiation, say through lead, the measured coefficient approaches the true value for that energy which has the least absorption in the filter. A check on the theory is obtained by plotting τ_m as a function of the filter thickness and comparing these data with the curve calculated using the theoretical values of the coefficients.

The principal features of the geometry are, first, the small solid angle subtended by the counter and, second, the method of determining the background counting rate. The background was measured for each filter thickness both with and without the absorber in the path by filling the axial hole in the collimator with lead. It was shown that this eliminated all the radiation reaching the counter through the collimator. Hence, the background includes all scattered radiation reaching the counter by paths other than through the collimator, and this is independent of whether a measurement is being made of the actual counting rate or of the background associated with it. Therefore, the only error in the measurement due to background is that due to single and multiple scattering occurring within the slit of the collimator. This was shown to be less than one percent by measuring the absorption coefficient as a function of the distance of the counter from the collimator. The results are in good agreement with calculations which show that the total error due to scattering[10] should be less than 0.2 percent.

The Coincidence Method

The coincidence method was essentially that used by Groetzinger and Smith.[11] The geometrical arrangement was the same as that in Fig. 1, with the exception that the filter was omitted and the single counter was replaced by two beta-counters with their thin mica windows facing each other. An aluminum filter placed between the counters was just thick enough to stop completely the beta-rays ejected from the first counter by the lower energy gamma-rays. The coincidence counting rate was then determined with and without the absorber in the collimated beam. The background, due mainly to accidental coincidences, was determined with an aluminum absorber between the counters just thick enough to stop completely the electrons ejected from the first counter by the highest energy gamma-rays. These data then permitted a determination of the absorption coefficient for the highest energy line emitted by the source.

INSTRUMENTATION

Although the only instrumentation involved in the final measurements was usual counting equipment, a detailed knowledge of the operating characteristics was necessary for accurate measurements. The regulated high voltage supply for the Geiger counters was stable to better than 1 percent for large fluctuations in the line voltage. A scale of 64 counting circuit was constructed having a resolving time of about 20 microseconds, sufficiently fast considering the deadtime of the counters. The coincidence circuit was a modified Rossi type, with a resolving time of 1.6 microseconds, again sufficient for the relatively low counting rates used. The counting time was determined by two synchronous electric clocks connected in parallel, a precaution found to be necessary for the particular type of clock used.

The Geiger counters were constructed especially for the measurements. The gamma-ray counters were made from brass tubing four inches long and one inch in diameter fitted with an eight-mil central wire. The beta-counters were the end-fire type, one inch in diameter with mica windows approximately one mil thick. One counter was two inches long but the other, placed nearest the collimator was only $1\frac{1}{8}$ inches long. The reason for such small length to width ratio is clear on consideration of the angle of scattering *versus* energy of the secondary Compton electrons.

All the counters were subjected to periodic tests. Whenever the slope of the plateau curve became greater than 3 percent per 100 volts for the gamma-counters and 5 percent per 100 volts for the beta-counters, or whenever the length of the plateau became

[10] I am indebted to Dr. E. S. Lennox for making this calculation.
[11] G. Groetzinger and L. Smith, Phys. Rev. 67, 53 (1945).

less than 150 volts, the counters were refilled. An alcohol-argon mixture at 11 cm pressure was used. Because of their short length and large mica window, the beta-counters showed considerable hysteresis, thus care was taken not to reduce the applied voltage during the period of measurement. Statistical checks were made occasionally to be sure that multiple counts were not occurring. Because of the difference in counting rates with and without the absorber in the beam, it was necessary to correct for the counting losses due to the counter deadtime. For low counting rates it is difficult to measure the counting losses with accuracy. Therefore, the corrections were based on the measured value of the deadtime. Because the deadtime is a sensitive function of the voltage above the threshold, the counters were always operated 100 volts above the threshold.

EXPERIMENTAL PROCEDURE AND RESULTS

In order to reduce the errors due to random variations, a definite procedure was followed in taking the data. The equipment was allowed to warm up for approximately twenty minutes. The four counting rates necessary to calculate τ_m were determined in the following time sequence: (1) without absorber in the beam, 100 seconds, (2) with the absorber, 300 seconds, (3) background with absorber, 100 seconds, and (4) background without absorber, 100 seconds. This sequence was repeated many times so that in one set of data variations of the counters, circuits, natural background, or decay of the source would average out. The thickness of the aluminum absorber was adjusted so that the counting rate with the absorber in the beam was approximately one-third that without the absorber. The optimum thickness (to obtain the greatest statistical accuracy in a given time) is a function of the ratio of the counting rate to the background.[12] With the low counting rates sometimes prevailing in these measurements, the ratio was relatively small; hence, the absorber thickness was optimized for this condition. For the filter method, each point plotted on the filter curve is an average of two or three such sets, while at least ten sets were obtained at each energy by the coincidence method.

The three sources employed in these measurements were Zn^{65}, Sb^{124}, and Na^{24}. The energies of the gamma-rays emitted were taken from the latest published data.[13] The first two sources were obtained from Oak Ridge, while the Na^{24} was made in the Michigan cyclotron by bombarding sodium meta-borate with deuterons. The source was allowed to stand 24 hours before being used for the filter method to allow decay of the short half-life impurities which could exist. Tests were made which indicated there were no impurities present of energies comparable with those of Na^{24} at the time of measurement.

A filter curve was obtained for two of the three sources. It was not feasible in the case of Zn^{65} because of the low intensity of the annihilation radiation compared to the intensity of 1.11-Mev line. To obtain a curve required such thickness of filter that the counting rates were reduced below practical values. Plots of the experimental data for Sb^{124} and Na^{24} are given in Figs. 2 and 3, respectively, along with the calculated filter curves. The short vertical lines represent the standard deviation for each point based on the total number of counts.

The results of the coincidence measurements for the three sources are given in Table I. The data include certain corrections which are discussed below. The theoretical values of the absorption coefficients were calculated from the formulas given in Heitler,[14] using the latest values of the fundamental constants.

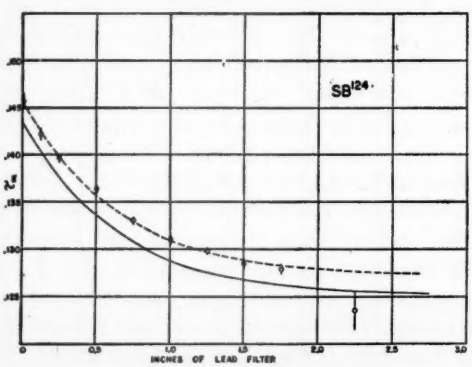

FIG. 2. The measured absorption coefficient *versus* thickness of lead filter for Sb^{124}. The vertical lines through each point represent the standard deviation based on the total number of counts. The solid curve was calculated using the theoretical values of the absorption coefficients. The dotted curve was obtained by adjusting slightly the values of k and τ in lead, holding fixed the value of τ in aluminum.

DISCUSSION OF RESULTS

The filter curves (solid curves in Figs. 2 and 3) were calculated using the theoretical values of the absorption coefficients by the relation

$$\tau_m = \tau_2^a + \frac{1}{x_2}\log\frac{[1+\sum k_i e^{(\tau_1^a-\tau_1^i)x_1}]}{[1+\sum k_i e^{(\tau_1^a-\tau_1^i)x_1 e^{(\tau_2^a-\tau_2^i)x_2}}]},$$

where the subscripts 1 and 2 refer to lead and aluminum, respectively, and the letter superscripts refer to a particular gamma-ray energy. Thus, τ_2^a indicates the total absorption coefficient in aluminum for the gamma-ray of energy a. $k^i=\epsilon_i N_0^i/\epsilon_a N_0^a$, where ϵ is the counter efficiency for energy i, and N_0^i is the number of gamma-rays emitted by the source per

[12] This calculation was an extension of one of the cases treated by R. Peierls, Proc. Roy. Soc. A149, 467 (1935). More recently M. E. Rose and M. M. Shapiro, Phys. Rev. 74, 1853 (1948), have treated this and additional cases in some detail.

[13] Kern, Zaffarano, and Mitchell, reference 9; C. Sharp Cook and L. M. Langer, Phys. Rev. 73, 1149 (1948); Jensen, Laslett, and Pratt, Phys. Rev. 73, 529 (1948); K. Siegbahn, Phys. Rev. 70, 127 (1946).

[14] W. Heitler, *The Quantum Theory of Radiation* (Clarendon Press, Oxford, 1944).

second of energy i. Thus, to obtain the curve, it is necessary to know the energies and the intensities of all the gamma-rays emitted by the source, as well as the efficiency of the counter for the various rays. For the sources used in these measurements, the energies are believed known to about 1 percent and the intensities to perhaps 5 percent. The efficiency of a Geiger counter for the various cathode materials as a function of energy was determined by Bradt and co-workers.[15] A check on the consistency of these data was made for Na^{24}, which emits two lines of equal intensity, by plotting the usual absorption curve. From this curve the ratio k may be determined and compared with the calculated value.

A comparison of the data with the calculated filter curve for Sb^{124} might be considered as indicating a discrepancy of approximately 2 percent in view of the fact that the shapes of the curves agree very well. By increasing the value of $\tau_2{}^a$ by 2 percent, the curves may be brought into very good agreement. However, this indicates clearly the difficulty of the method, particularly when so many energies are emitted by the source that it is not feasible to check the consistency of the data as indicated above. The value of k depends on the efficiency of the counter and the intensities of the lines. The efficiency depends somewhat on the geometry of the counter and thus the values taken from Bradt should not be considered accurate unless his geometry is reproduced.[16] Likewise, the intensities are not known with certainty. In addition, although the energies of the gamma-rays are known to 1 percent, the values of the total absorption coefficients in lead for the various energies are not known with that accuracy. The dotted curve which fits the data very well was obtained by adjusting slightly the values of k and τ in lead, holding fixed the value of τ in aluminum, which depends only on the Compton cross section. It might be pointed out that for the data available[17] prior to Kern's, no reasonable fit was possible.

The case for Na^{24} is less open to question as only two lines are believed to exist. The calculated curve is about 0.5 percent low. A slight change in the coefficients for lead and in k, well within their uncertainty, gives very good agreement as is indicated by the dotted curve. There is apparently some very low energy radiation present which is rapidly filtered out.

Although a filter curve was not obtained for Zn^{65}, a measurement was made of the apparent coefficient without any filter. When corrected for the three to five percent annihilation radiation emitted,[18] the measured value becomes 0.1567 cm^{-1}, which is in good agreement with the theoretical value of 0.1572 cm^{-1}.

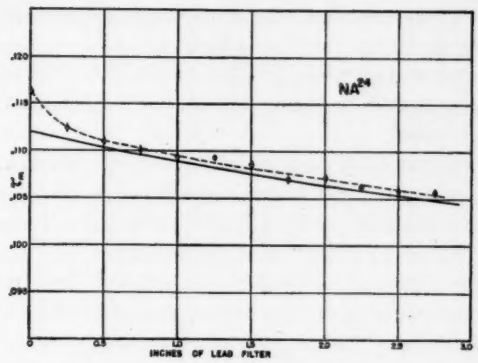

FIG. 3. The filter curve for Na^{24}.

The results of the coincidence method are less susceptible to these uncertain errors, and the measured values show agreement with the theoretical values within the standard deviation of the data. Of the three energy values for which the coefficient was measured in aluminum, perhaps the most reliable is that at 1.11 Mev. The photoelectric and pair cross sections are completely negligible at this energy, and the source is the most ideal of the three, the only other energy emitted being the annihilation radiation which is sufficiently far removed to allow good filtering of the secondary electrons. Perhaps the least reliable is antimony. At the time of measurement, it was believed that the highest energy emitted was 1.71 Mev. The subsequent values listed by Kern indicated a weak gamma-ray at 2.04 Mev, with an intensity of 3 percent. It would, therefore, be expected that the data would be slightly lower than the theoretical value for 1.71 Mev.

As was indicated previously, certain corrections were applied to the original data. The solid angle subtended by the counter was such that radiation scattered through slightly less than 1° would reach the counter. On the basis of the differential cross section, this amounts to an error of about 0.2 percent in the counting rate with the absorber in the beam. A second correction is the loss of true counts due to the deadtime of the counter. For the counting rates used, the correction to τ amounted to less than 0.5 percent for the filter method and approximately 0.9 percent for the coincidence method. An additional correction of 0.3 percent was made for the impurity of the absorber. The aluminum was analyzed by quantitative spectroscopic means and was found to contain iron as the major impurity. The error due to bremsstrahlung of the beta-rays emitted by the source was completely negligible.

A check on the stability of the circuits was furnished by comparing the standard deviation calculated from the number of counts with the standard deviation calculated from the deviation of the individual sets from the mean. These were in close agreement for zinc and sodium indicating no large random fluctuations. However, for antimony, the first energy measured, there was an appreciable difference. This was later found to

[15] H. Bradt *et al.*, Helv. Phys. Acta **19**, 77 (1946).
[16] K. Siegbahn also indicates a discrepancy, Phys. Rev. **70**, 127 (1946).
[17] W. E. Meyerhof and G. Scharff-Goldhaber, Phys. Rev. **72**, 273 (1947).
[18] W. M. Good and W. C. Peacock, Phys. Rev. **69**, 680 (1946); E. N. Jensen (private communication).

be due to fluctuations in the counter supply and the coincidence circuit, and were subsequently eliminated. The standard deviation given in Table I for antimony was calculated from the deviation of the individual sets from the mean.

The measured values for the total cross section are in very good agreement (approximately 1 percent) with the predictions of theory (Table I and Figs. 2 and 3). Any attempt to obtain a closer check at the present time would have little meaning inasmuch as the energies of the gamma-rays are known only to about 1 percent. The results of this investigation indicate, therefore, that the Klein-Nishina formula is in agreement with experiment in the energy range one to three Mev for aluminum.

TABLE I. Absorption coefficients for aluminum (cm^{-1}).

Energy Mev	Theoretical Compton	Photo-electric	Pair	Total	Measured value
1.11	0.1572	0.0001	——	0.157	0.156±0.001
1.708	0.1253	——	0.0009	0.126	0.125±0.002
2.76	0.0949	——	0.0042	0.0991	0.0996±0.0008

ACKNOWLEDGMENTS

The work described in this paper has proceeded at intervals over a period of the last two years. During the course of this time, many people have contributed to the end result. The author would like to express his appreciation to Professors H. R. Crane and J. M. Cork, who originally suggested the investigation, and to Professor D. M. Dennison, all of whom offered valuable advice during the early part of the work. I am indebted to Messrs. Roger Grismore, J. S. King, and J. W. Teener for the many hours they have spent in taking and analyzing data, and to Messrs. H. Westrick and O. Haas for their invaluable aid in building and altering equipment as needed. This work was supported in part by the Bureau of Ordnance, U. S. Navy, under Contract NOrd-7924.

PHYSICAL REVIEW VOLUME 76, NUMBER 9 NOVEMBER 1, 1949

Theory of Complex Spectra. IV

GIULIO RACAH
The Hebrew University, Jerusalem, Israel
(Received February 7, 1949)

The calculation of the coefficients of fractional parentage and of the energy matrices for the configurations f^n is simplified very much by the use of the theory of groups. Tables of results are given.

1. INTRODUCTION

IT was shown in two previous papers[1] that the calculations on complex spectra may be simplified by the introduction of tensor operators and coefficients of fractional parentage. These coefficients may be calculated by Eqs. (9) of III and (11) of III, but it appears that for the configurations f^n Eqs. (11) of III are too cumbersome for practical use.

By considering the meaning and the properties of the coefficients of fractional parentage from the standpoint of the theory of groups, we shall see that these calculations may be somewhat simplified and that a very fortunate and important simplification takes place exactly for the configurations f^n.

In Section 4 we shall classify the states of f^n as the basis of some group representations and in Section 5 we shall find some properties of the coefficients of fractional parentage which will avoid the use of Eqs. (11) of III; the results of the calculations will be given in Tables III and IV. The energy matrices will be calculated in Section 6, and also these calculations will be simplified by group-theoretical considerations.

Before treating the very argument of this paper, we shall give in Section 2 a formula which should have its natural place in Section 5 of III, but was unfortunately obtained only after the publication of that paper, and we shall prove in Section 3 a corollary of Schur's lemma, which will be very useful in the following calculations.

2. THE MATRIX OF SYMMETRIC SCALAR OPERATORS

The matrix components between two states of l^n of the scalar operator (30) of III were calculated in (33a) of III by taking only the last term of the summation and then multiplying the result by $\frac{1}{2}n(n-1)$. It appears, on the contrary, more convenient to limit the sum of (30) of III to the first $n-1$ electrons and then to multiply by $n/(n-2)$. Thus, we obtain easily

$$(l^n\alpha SL|G|l^n\alpha' SL)$$
$$=[n/(n-2)]\sum_{\alpha_1\alpha_1' S_1L_1}(l^n\alpha SL\{|l^{n-1}(\alpha_1S_1L_1)lSL)$$
$$\times(l^{n-1}\alpha_1S_1L_1|G|l^{n-1}\alpha_1'S_1L_1)$$
$$\times(l^{n-1}(\alpha_1'S_1L_1)lSL|\}l^n\alpha' SL). \quad (1)$$

[1] G. Racah, Phys. Rev. **62**, 438 (1942) and **63**, 367 (1943) (which will be referred to as II and III. We refer to these papers for definitions and notations.

This formula advantageously replaces (33a) of III, since it does not need the use of (32) of III. Moreover, if it is used for operators the eigenvalues of which are already known, it gives a great number of equations between the coefficients of fractional parentage. Operators of this type are not only the operator Q defined by (34) of III and the operator R which will be defined by (23), but, first of all, the operators

$$\sum_{i<j}(\mathbf{l}_i\cdot\mathbf{l}_j)=[L(L+1)-nl(l+1)]/2 \tag{2}$$

and

$$\sum_{i<j}(\mathbf{s}_i\cdot\mathbf{s}_j)=\tfrac{1}{2}S(S+1)-3n/8. \tag{3}$$

3. A LEMMA

The irreducible representations $(a|U_A(s)|a')$ of a group $\mathfrak{g}$ are generally reducible as representations of a subgroup $\mathfrak{h}$ of $\mathfrak{g}$; i.e., a constant matrix R_A exists, so that for every element t of $\mathfrak{h}$,

$$\sum_{aa'}(\beta Bb|R_A^{-1}|a)(a|U_A(t)|a')(a'|R_A|\beta'B'b')=(b|V_B(t)|b')\delta(BB')\delta(\beta\beta'), \tag{4}$$

where the $(b|V_B(t)|b')$ are the irreducible representations of $\mathfrak{h}$. Instead of the representations $U_A(s)$, we shall always consider the equivalent representations ("reduced with respect to $\mathfrak{h}$"),

$$(\beta Bb|W_A(s)|\beta'B'b')=(\beta Bb|R_A^{-1}U_A(s)R_A|\beta'B'b'); \tag{5}$$

it follows from (4) and (5) that for every element t of $\mathfrak{h}$,

$$(\beta Bb|W_A(t)|\beta'B'b')=(b|V_B(t)|b')\delta(BB')\delta(\beta\beta'). \tag{6}$$

The external (Kronecker's) product of two irreducible representations of $\mathfrak{g}$ is generally reducible, i.e., a constant matrix S exists, so that

$$\sum_{\beta_1B_1b_1\beta_2B_2b_2\beta_1'B_1'b_1'\beta_2'B_2'b_2'}(A_1A_2\alpha A\beta Bb|S^{-1}|A_1\beta_1B_1b_1;A_2\beta_2B_2b_2)(\beta_1B_1b_1|W_{A_1}(s)|\beta_1'B_1'b_1')$$

$$\times(\beta_2B_2b_2|W_{A_2}(s)|\beta_2'B_2'b_2')(A_1\beta_1'B_1'b_1';A_2\beta_2'B_2'b_2'|S|A_1A_2\alpha'A'\beta'B'b')=(\beta Bb|W_A(s)|\beta'B'b')\delta(AA')\delta(\alpha\alpha'). \tag{7}$$

Also the external product of two irreducible representations of $\mathfrak{h}$ is generally reducible and a constant matrix T exists, so that

$$\sum_{b_1b_2b_1'b_2'}(B_1B_2\gamma Bb|T^{-1}|B_1b_1B_2b_2)(b_1|V_{B_1}(t)|b_1')\times(b_2|V_{B_2}(t)|b_2')(B_1b_1'B_2b_2'|T|B_1B_2\gamma'B'b')=(b|V_B(t)|b')\delta(BB')\delta(\gamma\gamma'). \tag{8}$$

From (8), (6), and (7) we obtain

$$\sum_{b_1b_2b''}(b|V_B(t)|b'')(B_1B_2\gamma Bb''|T^{-1}|B_1b_1B_2b_2)\times(A_1\beta_1B_1b_1;A_2\beta_2B_2b_2|S|A_1A_2\alpha A\beta B'b')$$

$$=\sum_{b_1bb''}(B_1B_2\gamma Bb|T^{-1}|B_1b_1B_2b_2)\times(A_1\beta_1B_1b_1;A_2\beta_2B_2b_2|S|A_1A_2\alpha A\beta B'b'')\times(b''|V_{B'}(t)|b'), \tag{9}$$

and it follows from the lemma of Schur that the constant matrix $T^{-1}S$ is diagonal with respect to B and b and is independent of b:

$$\sum_{b_1b_2}(B_1B_2\gamma Bb|T^{-1}|B_1b_1B_2b_2)\times(A_1\beta_1B_1b_1;A_2\beta_2B_2b_2|S|A_1A_2\alpha A\beta B'b')=(A_1\beta_1B_1+A_2\beta_2B_2|X_\gamma|\alpha A\beta B)\delta(BB')\delta(bb'). \tag{10}$$

Multiplying from the left by T we have, finally,

$$(A_1\beta_1B_1b_1;A_2\beta_2B_2b_2|S|A_1A_2\alpha A\beta Bb)=\sum_\gamma(B_1b_1B_2b_2|T|B_1B_2\gamma Bb)\times(A_1\beta_1B_1+A_2\beta_2B_2|X_\gamma|\alpha A\beta B); \tag{11}$$

this formula will be very useful for practical calculations, since it expresses the dependence of the matrix S on b_1, b_2, and b by means of the simpler matrices T.

4. THE GROUP-THEORETICAL CLASSIFICATION OF THE TERMS OF l^n

1. The Spin and the Orbital Momentum

The configuration l^n has $\binom{4l+2}{n}$ independent states which may be characterized by a set of quantum numbers Γ; if the $4l+2$ eigenfunctions $\phi(m_s m_l)$ of the individual electrons undergo a linear unimodular transformation,

$$\phi'(m_s'm_l')=\sum_{m_sm_l}\phi(m_sm_l)c(m_sm_l;m_s'm_l'), \tag{12}$$

the eigenfunctions $\psi(l^n,\Gamma)$ undergo the linear transformation which is induced by (12) on the ansitymmetrical tensors of degree n in the $(4l+2)$-dimensional space; i.e., the $\Psi(l^n,\Gamma)$ are the basis of the antisymmetrical representation $\{\mathfrak{c}_{4l+2}\}^n$ of the linear unimodular group $\mathfrak{c}_{4l+2}$. The rows and columns of this representation are characterized by the quantum numbers Γ.

If we limit $\mathfrak{c}_{4l+2}$ to the subgroup $\mathfrak{c}_2\times\mathfrak{c}_{2l+1}$ defined by

$$c(m_sm_l;m_s'm_l')=\gamma(m_sm_s')c(m_lm_l'), \tag{13}$$

where γ and c are two independent linear unimodular transformations, the representation $\{\mathfrak{c}_{4l+2}\}^n$ breaks up into irreducible representations of $\mathfrak{c}_2\times\mathfrak{c}_{2l+1}$, each of which is the external product of a representation $\mathfrak{D}_S$ of $\mathfrak{c}_2$ and a representation $\mathfrak{H}_{n,S}$ of $\mathfrak{c}_{2l+1}$. It is well known that the symmetry schemes of $\mathfrak{D}_S$ and $\mathfrak{H}_{n,S}$ must be

TABLE I. Reduction of $\mathfrak{B}_W$ as representation of G_2.

Values of S and v I		II								
S	v	S	v	W	U					
0	0	7/2	7	(000)	(00)					
1/2	1	3	6	(100)	(10)					
1	2	5/2	5	(110)	(10)	(11)				
0	2	5/2	7	(200)	(20)					
3/2	3	2	4	(111)	(00)	(10)	(20)			
1/2	3	2	6	(210)	(11)	(20)	(21)			
1	4	3/2	5	(211)	(10)	(11)	(20)	(21)	(30)	
0	4	3/2	7	(220)	(20)	(21)	(22)			
1/2	5	1	6	(221)	(10)	(11)	(20)	(21)	(30)	(31)
0	6	1/2	7	(222)	(00)	(10)	(20)	(30)	(40)	

dual; since the scheme of $\mathfrak{D}_S$ has two lines, the lengths of which are, respectively, $(n/2)+S$ and $(n/2)-S$, the scheme of $\mathfrak{H}_{n,S}$ will have two columns of these lengths. The basis of these representations of $\mathfrak{c}_2 \times \mathfrak{c}_{2l+1}$ are the functions $\Psi(l^n S M_S \Delta)$; the quantum number M_S characterizes the rows and columns of $\mathfrak{D}_S$, the quantum numbers Δ those of $\mathfrak{H}_{n,S}$.

If we limit $\mathfrak{c}_{2l+1}$ to its subgroup composed by the elements of the representation $\mathfrak{D}_l$ of order $2l+1$ of the three-dimensional rotation group $\mathfrak{d}_3$, the representation $\mathfrak{H}_{n,S}$ breaks up into representations $\mathfrak{D}_L$ of $\mathfrak{d}_3$, the basis of which are the functions $\Psi(l^n \alpha S L M_S M_L)$. The quantum number (or set of quantum numbers) α must be introduced in order to distinguish the different equivalent representations of $\mathfrak{d}_3$ which may appear in the reduction of $\mathfrak{H}_{n,S}$, i.e., the different terms of the same kind which are allowed in l^n.

In order to classify in a suitable way these different terms, it is convenient to perform the passage from $\mathfrak{c}_{2l+1}$ to $\mathfrak{d}_3$ by successive steps.

2. The Seniority Number

As a first step, we limit $\mathfrak{c}_{2l+1}$ to the orthogonal subgroup $\mathfrak{d}_{2l+1}$ which leaves invariant the quadratic form

$$\sum_{-l}^{l}{}_m (-1)^m \phi(m)\phi(-m), \tag{14}$$

and the representations $\mathfrak{H}_{n,S}$ then break up into irreducible representations $\mathfrak{B}_W$ of $\mathfrak{d}_{2l+1}$; since the group $\mathfrak{d}_{2l+1}$ is of rank l, each $\mathfrak{B}_W$ is characterized by a set W of l integral numbers

$$w_1 \geqslant w_2 \geqslant \cdots \geqslant w_l \geqslant 0, \tag{15}$$

and since in the symmetry scheme of $\mathfrak{H}_{n,S}$ no row has a length greater than 2, also the w_i will not be greater than 2 and it will be

$$w_1 = \cdots = w_a = 2, \quad w_{a+1} = \cdots = w_{a+b} = 1, \quad w_{a+b+1} = \cdots = w_l = 0. \tag{16}$$

It is known from the theory of tensors that the passage from the linear to the metric space (or from $\mathfrak{c}_r$ to $\mathfrak{d}_r$) allows the decomposition of tensors by trace operation or contraction, i.e., some linear combinations

Table II. Reduction of $\mathfrak{C}_U$ as representation of $\mathfrak{d}_3$.

U	$12g(U)$	L
(00)	0	S
(10)	6	F
(11)	12	PH
(20)	14	DGI
(21)	21	$DFGHKL$
(30)	24	$PFGHIKM$
(22)	30	$SDGHILN$
(31)	32	$PDFFGHHIIKKLMNO$
(40)	36	$SDFGGHIIKLLMNQ$

of the components of tensors of degree n transform themselves as components of tensors of degree $n-2$; the classification of the terms of l^n according to the representations of $\mathfrak{d}_{2l+1}$ will therefore introduce a correspondence between some of them and the terms of l^{n-2}. It is easy to see that this correspondence is the same which was introduced in Section 6, Subsection 2 of III i.e., that the separation of the terms with $Q \neq 0$ from those with $Q=0$ is equivalent to the decomposition of a tensor by trace operation.

If we subtract (54), III, from (37), III, and add (52), III, we get

$$q_{ij} = -\tfrac{1}{2} - 2(\mathbf{s}_i \cdot \mathbf{s}_j) - 2\sum_{1}^{l}{}_t (4t-1)(\mathbf{u}_i^{(2t-1)} \cdot \mathbf{u}_j^{(2t-1)}); \tag{17}$$

owing to (38) of III and to (3) we have, for Q, the expression

$$Q = \tfrac{1}{4}n(4l+4-n) - S(S+1) - \sum_{1}^{l}{}_t (4t-1)\mathbf{U}^{(2t-1)^2}, \tag{18}$$

and it may be shown that

$$\sum_{1}^{l}{}_t (4t-1)\mathbf{U}^{(2t-1)^2} = (2l-1)G(\mathfrak{d}_{2l+1}), \tag{19}$$

where $G(\mathfrak{d}_{2l+1})$ is Casimir's[2] operator G for the group $\mathfrak{d}_{2l+1}$.

It may also be shown that the numbers a and b, which characterize the representations $\mathfrak{B}_W$ according to (16), are connected to the spin and the seniority number by the relations

$$a = (v/2) - S, \quad b = \min(2S, 2l+1-v). \tag{20}$$

The basis of the representations $\mathfrak{B}_W$ are the functions $\Psi(l^n \alpha v S L M_S M_L)$.

The seniority number could also be introduced before the spin number, by limiting $\mathfrak{c}_{4l+2}$ to its symplectic subgroup which leaves invariant the bilinear antisymmetric form

$$\sum_{-\frac{1}{2}}^{\frac{1}{2}}{}_{m_s} \sum_{-l}^{l}{}_{m_l} (-1)^{m_s+m_l-\frac{1}{2}} \phi_1(m_s m_l)\phi_2(-m_s, -m_l). \tag{21}$$

[2] H. Casimir, Proc. Roy. Acad. Amsterdam 34, 844 (1931).

TABLE IIIa. $(WU|W'U'+f)$ for $W'=(000), (100), (110), (200), (111), (210)$.

		$W'U'$										
		(000)	(100)	(110)		(200)		(111)			(210)	
W	U	(00)	(10)	(10)	(11)	(20)	(00)	(10)	(20)	(11)	(20)	(21)
(000)	(00)	0	1	0	0	0						
(100)	(10)	1	0	$(1/3)^{\frac{1}{2}}$	$(2/3)^{\frac{1}{2}}$	1						
(110)	(10)	0	1	0	0	0	$(3/35)^{\frac{1}{2}}$	$(2/5)^{\frac{1}{2}}$	$(18/35)^{\frac{1}{2}}$	$(2/5)^{\frac{1}{2}}$	$(3/5)^{\frac{1}{2}}$	0
	(11)	0	1	0	0	0	0	$-(1/10)^{\frac{1}{2}}$	$-(9/10)^{\frac{1}{2}}$	0	$(3/35)^{\frac{1}{2}}$	$(32/35)^{\frac{1}{2}}$
(200)	(20)	0	1	0	0	0	0	0	0	$(2/15)^{\frac{1}{2}}$	$(9/35)^{\frac{1}{2}}$	$(64/105)^{\frac{1}{2}}$
(111)	(00)			1	0	0	0	-1	0	0	0	0
	(10)			$(2/3)^{\frac{1}{2}}$	$-(1/3)^{\frac{1}{2}}$	0	$-(1/7)^{\frac{1}{2}}$	$-(3/8)^{\frac{1}{2}}$	$(27/56)^{\frac{1}{2}}$	0	0	0
	(20)			$(2/9)^{\frac{1}{2}}$	$-(7/9)^{\frac{1}{2}}$	0	0	$(1/8)^{\frac{1}{2}}$	$-(7/8)^{\frac{1}{2}}$	0	0	0
(210)	(11)			1	0	1	0	0	0	0	0	0
	(20)			$(7/9)^{\frac{1}{2}}$	$(2/9)^{\frac{1}{2}}$	1	0	0	0	0	0	0
	(21)			0	1	1	0	0	0	0	0	0
(211)	(10)						$(27/35)^{\frac{1}{2}}$	$-(9/40)^{\frac{1}{2}}$	$(1/280)^{\frac{1}{2}}$	$-(3/5)^{\frac{1}{2}}$	$(2/5)^{\frac{1}{2}}$	0
	(11)						0	$(9/10)^{\frac{1}{2}}$	$-(1/10)^{\frac{1}{2}}$	0	$(32/35)^{\frac{1}{2}}$	$-(3/35)^{\frac{1}{2}}$
	(20)						0	$(7/8)^{\frac{1}{2}}$	$(1/8)^{\frac{1}{2}}$	$(1/3)^{\frac{1}{2}}$	$(2/7)^{\frac{1}{2}}$	$-(8/21)^{\frac{1}{2}}$
	(21)						0	0	1	$(3/16)^{\frac{1}{2}}$	$-(25/112)^{\frac{1}{2}}$	$(33/56)^{\frac{1}{2}}$
	(30)						0	0	1	0	$(1/7)^{\frac{1}{2}}$	$(6/7)^{\frac{1}{2}}$
(220)	(20)									$(8/15)^{\frac{1}{2}}$	$-(16/35)^{\frac{1}{2}}$	$(1/105)^{\frac{1}{2}}$
	(21)									$-(1/8)^{\frac{1}{2}}$	$(27/56)^{\frac{1}{2}}$	$(11/28)^{\frac{1}{2}}$
	(22)									0	0	1

3. The Special Case of f^n

It was remarked in Section 6 of III that the seniority number suffices to distinguish the different terms of the same kind in d^n, but not for greater l; for $l \geqslant 3$ we must therefore seek for a subgroup of $\mathfrak{d}_{2l+1}$ which contains $\mathfrak{D}_l$, and it is a very fortunate chance that such a subgroup exists exactly for $l=3$: it is the subgroup of $\mathfrak{d}_7$ which leaves invariant the trilinear antisymmetric form

$$\sum_{mm'm''} V(333; mm'm'')\phi_1(m)\phi_2(m')\phi_3(m''), \quad (22)$$

where $V(abc; \alpha\beta\gamma)$ is defined by (17′) of II. This group is the first of the five simple groups which exist besides the four great classes of simple groups, and is usually denoted as G_2.

If we limit $\mathfrak{d}_7$ to its subgroup G_2, the representations $\mathfrak{B}_W$ break up into irreducible representations $\mathfrak{C}_U$ of G_2; since G_2 is of rank 2, the $\mathfrak{C}_U$ are characterized by a set $U\equiv(u_1u_2)$ of two integral numbers. If we limit G_2 to its subgroup composed by the elements of the representation $\mathfrak{D}_3$ of $\mathfrak{d}_3$, the $\mathfrak{C}_U$ also break up into representations $\mathfrak{D}_L$ of $\mathfrak{d}_3$, the basis of which are the functions $\Psi(f^n\alpha U v S L M_S M_L)$, and these functions will form our definitive system of eigenfunctions of f^n.

The law of reduction of $\mathfrak{B}_W$ as representation of G_2 is given in Table I, that of $\mathfrak{C}_U$ as representation of $\mathfrak{d}_3$ is given in Table II; we see from this last table that the quantum number α must be maintained only for $U\equiv(31)$ and $U\equiv(40)$.

Also the quantum numbers U could be introduced in a similar way as the seniority number in Section 6 of III, by classifying the terms of f^n according to the eigenvalues of

$$R=\sum_{i<j} r_{ij}, \quad (23)$$

where the scalar operator r_{ij} is defined by the relation

$$(f^2LM|r_{ij}|f^2LM)=6\delta(L,3); \quad (24)$$

the equations which correspond to (17), (18), and (19) are

$$r_{ij}=\tfrac{1}{2}-2(\mathbf{s}_i\cdot\mathbf{s}_j)-2q_{ij}-18(\mathbf{u}_i^{(1)}\cdot\mathbf{u}_j^{(1)})-66(\mathbf{u}_i^{(5)}\cdot\mathbf{u}_j^{(5)}), \quad (25)$$

$$R=\tfrac{1}{4}n(n+26)-S(S+1)-2Q-9\mathbf{U}^{(1)2}-33\mathbf{U}^{(5)2}, \quad (26)$$

and

$$9\mathbf{U}^{(1)2}+33\mathbf{U}^{(5)2}=12G(G_2); \quad (27)$$

TABLE IIIb. $(WU|(211)U'+f)$.

			U'				
W	U	N	(10)	(11)	(20)	(21)	(30)
(111)	(00)	1	1	0	0	0	0
	(10)	$24^{-\frac{1}{2}}$	-1	$8^{\frac{1}{2}}$	$15^{\frac{1}{2}}$	0	0
	(20)	$5832^{-\frac{1}{2}}$	1	$-56^{\frac{1}{2}}$	$135^{\frac{1}{2}}$	$2560^{\frac{1}{2}}$	$3080^{\frac{1}{2}}$
(210)	(11)	$42^{-\frac{1}{2}}$	$-7^{\frac{1}{2}}$	0	$15^{\frac{1}{2}}$	$20^{\frac{1}{2}}$	0
	(20)	$1701^{-\frac{1}{2}}$	$98^{\frac{1}{2}}$	$448^{\frac{1}{2}}$	$270^{\frac{1}{2}}$	$-500^{\frac{1}{2}}$	$385^{\frac{1}{2}}$
	(21)	$672^{-\frac{1}{2}}$	0	$-7^{\frac{1}{2}}$	$-60^{\frac{1}{2}}$	$220^{\frac{1}{2}}$	$385^{\frac{1}{2}}$
(211)	(10)	$72^{-\frac{1}{2}}$	$-5^{\frac{1}{2}}$	$40^{\frac{1}{2}}$	$-27^{\frac{1}{2}}$	0	0
	(11)	$126^{-\frac{1}{2}}$	$35^{\frac{1}{2}}$	0	$-27^{\frac{1}{2}}$	$64^{\frac{1}{2}}$	0
	(20)	$2520^{-\frac{1}{2}}$	$-245^{\frac{1}{2}}$	$-280^{\frac{1}{2}}$	$-867^{\frac{1}{2}}$	$-512^{\frac{1}{2}}$	$616^{\frac{1}{2}}$
	(21)	$315^{-\frac{1}{2}}$	0	$35^{\frac{1}{2}}$	$-27^{\frac{1}{2}}$	$-176^{\frac{1}{2}}$	$77^{\frac{1}{2}}$
	(30)	$315^{-\frac{1}{2}}$	0	0	$27^{\frac{1}{2}}$	$64^{\frac{1}{2}}$	$-224^{\frac{1}{2}}$

TABLE IVa. $(UL|U'L'+f)$ for $U'=(00), (10), (11), (20)$.

		$U'L'$						
		(00)	(10)	(11)			(20)	
U	L	S	F	P	H	D	G	I
(00)	S	0	−1	0	0	0	0	0
(10)	F	1	1	$(3/14)^{\frac{1}{2}}$	$(11/14)^{\frac{1}{2}}$	$-(5/27)^{\frac{1}{2}}$	$-(1/3)^{\frac{1}{2}}$	$-(13/27)^{\frac{1}{2}}$
(11)	P	0	1	0	0	$(10/21)^{\frac{1}{2}}$	$-(11/21)^{\frac{1}{2}}$	0
	H	0	1	0	0	$(20/189)^{\frac{1}{2}}$	$(65/231)^{\frac{1}{2}}$	$-(182/297)^{\frac{1}{2}}$
(20)	D	0	1	$-(27/49)^{\frac{1}{2}}$	$-(22/49)^{\frac{1}{2}}$	−4/7	$(33/49)^{\frac{1}{2}}$	0
	G	0	1	$(33/98)^{\frac{1}{2}}$	$-(65/98)^{\frac{1}{2}}$	$(55/147)^{\frac{1}{2}}$	$-(125/539)^{\frac{1}{2}}$	$(13/33)^{\frac{1}{2}}$
	I	0	1	0	1	0	$(3/11)^{\frac{1}{2}}$	$(8/11)^{\frac{1}{2}}$
(21)	D			$-(22/49)^{\frac{1}{2}}$	$(27/49)^{\frac{1}{2}}$	$(33/49)^{\frac{1}{2}}$	4/7	0
	F			$-(11/14)^{\frac{1}{2}}$	$(3/14)^{\frac{1}{2}}$	$-(55/126)^{\frac{1}{2}}$	$-(8/77)^{\frac{1}{2}}$	$(91/198)^{\frac{1}{2}}$
	G			$(65/98)^{\frac{1}{2}}$	$(33/98)^{\frac{1}{2}}$	$(13/882)^{\frac{1}{2}}$	$(104/147)^{\frac{1}{2}}$	$(5/18)^{\frac{1}{2}}$
	H			0	1	$(13/27)^{\frac{1}{2}}$	$-(16/33)^{\frac{1}{2}}$	$-(10/297)^{\frac{1}{2}}$
	K			0	1	0	$(16/33)^{\frac{1}{2}}$	$-(17/33)^{\frac{1}{2}}$
	L			0	1	0	0	1
(30)	P					$(11/21)^{\frac{1}{2}}$	$(10/21)^{\frac{1}{2}}$	0
	F					$(143/378)^{\frac{1}{2}}$	$-(130/231)^{\frac{1}{2}}$	$(35/594)^{\frac{1}{2}}$
	G					$(11/18)^{\frac{1}{2}}$	$(2/33)^{\frac{1}{2}}$	$-(65/198)^{\frac{1}{2}}$
	H					$(26/63)^{\frac{1}{2}}$	$(18/77)^{\frac{1}{2}}$	$(35/99)^{\frac{1}{2}}$
	I					0	$(8/11)^{\frac{1}{2}}$	$-(3/11)^{\frac{1}{2}}$
	K					0	$(17/33)^{\frac{1}{2}}$	$(16/33)^{\frac{1}{2}}$
	M					0	0	1

TABLE IVb. $(UL|(21)L'+f)$.

			L'					
U	L	N	D	F	G	H	K	L
(11)	P	$1344^{-\frac{1}{2}}$	$220^{\frac{1}{2}}$	$-539^{\frac{1}{2}}$	$-585^{\frac{1}{2}}$	0	0	0
	H	$4928^{-\frac{1}{2}}$	$-270^{\frac{1}{2}}$	$147^{\frac{1}{2}}$	$-297^{\frac{1}{2}}$	$1078^{\frac{1}{2}}$	$1470^{\frac{1}{2}}$	$-1666^{\frac{1}{2}}$
(20)	D	$31360^{-\frac{1}{2}}$	$8910^{\frac{1}{2}}$	$8085^{\frac{1}{2}}$	$351^{\frac{1}{2}}$	$-14014^{\frac{1}{2}}$	0	0
	G	$4312^{-\frac{1}{2}}$	$330^{\frac{1}{2}}$	$147^{\frac{1}{2}}$	$1287^{\frac{1}{2}}$	$1078^{\frac{1}{2}}$	$-1470^{\frac{1}{2}}$	0
	I	$18304^{-\frac{1}{2}}$	0	$-1911^{\frac{1}{2}}$	$1485^{\frac{1}{2}}$	$220^{\frac{1}{2}}$	$4590^{\frac{1}{2}}$	$10098^{\frac{1}{2}}$
(21)	D	$5390^{-\frac{1}{2}}$	$375^{\frac{1}{2}}$	$1960^{\frac{1}{2}}$	$-1144^{\frac{1}{2}}$	$1911^{\frac{1}{2}}$	0	0
	F	$154^{-\frac{1}{2}}$	$-40^{\frac{1}{2}}$	7	$-65^{\frac{1}{2}}$	0	0	0
	G	$630630^{-\frac{1}{2}}$	−74360	455	$226941^{\frac{1}{2}}$	−51744	70560	0
	H	$15730^{-\frac{1}{2}}$	$-2535^{\frac{1}{2}}$	0	$1056^{\frac{1}{2}}$	$-3179^{\frac{1}{2}}$	$7260^{\frac{1}{2}}$	$1700^{\frac{1}{2}}$
	K	$2860^{-\frac{1}{2}}$	0	0	$-192^{\frac{1}{2}}$	$968^{\frac{1}{2}}$	$-85^{\frac{1}{2}}$	$1615^{\frac{1}{2}}$
	L	$572^{-\frac{1}{2}}$	0	0	0	$-40^{\frac{1}{2}}$	$-285^{\frac{1}{2}}$	$247^{\frac{1}{2}}$
(30)	P	$2688^{-\frac{1}{2}}$	34	$-245^{\frac{1}{2}}$	$1287^{\frac{1}{2}}$	0	0	0
	F	$112^{-\frac{1}{2}}$	$-39^{\frac{1}{2}}$	0	$24^{\frac{1}{2}}$	7	0	0
	G	$7920^{-\frac{1}{2}}$	$1375^{\frac{1}{2}}$	$2450^{\frac{1}{2}}$	$-858^{\frac{1}{2}}$	$1617^{\frac{1}{2}}$	$1620^{\frac{1}{2}}$	0
	H	$640640^{-\frac{1}{2}}$	−42250	−455	$3971^{\frac{1}{2}}$	$261954^{\frac{1}{2}}$	$490^{\frac{1}{2}}$	$124950^{\frac{1}{2}}$
	I	$9152^{-\frac{1}{2}}$	0	$1274^{\frac{1}{2}}$	$2750^{\frac{1}{2}}$	$1320^{\frac{1}{2}}$	$2125^{\frac{1}{2}}$	$-1683^{\frac{1}{2}}$
	K	$1040^{-\frac{1}{2}}$	0	0	$-204^{\frac{1}{2}}$	$-136^{\frac{1}{2}}$	$605^{\frac{1}{2}}$	$95^{\frac{1}{2}}$
	M	$64^{-\frac{1}{2}}$	0	0	0	0	$-15^{\frac{1}{2}}$	−7
(22)	S	1	0	1	0	0	0	0
	D	$640^{-\frac{1}{2}}$	$-130^{\frac{1}{2}}$	$195^{\frac{1}{2}}$	$297^{\frac{1}{2}}$	$18^{\frac{1}{2}}$	0	0
	G	$51480^{-\frac{1}{2}}$	$18590^{\frac{1}{2}}$	65	$-429^{\frac{1}{2}}$	−23826	−4410	0
	H	$6160^{-\frac{1}{2}}$	$980^{\frac{1}{2}}$	−2450	$1078^{\frac{1}{2}}$	$-132^{\frac{1}{2}}$	$245^{\frac{1}{2}}$	−1275
	I	$18304^{-\frac{1}{2}}$	0	$1105^{\frac{1}{2}}$	$9163^{\frac{1}{2}}$	$-2244^{\frac{1}{2}}$	−4802	$990^{\frac{1}{2}}$
	L	$364^{-\frac{1}{2}}$	0	0	0	$152^{\frac{1}{2}}$	$-147^{\frac{1}{2}}$	$-65^{\frac{1}{2}}$
	N	$16^{-\frac{1}{2}}$	0	0	0	0	$-5^{\frac{1}{2}}$	$11^{\frac{1}{2}}$

it may also be shown[3] that the eigenvalues of $G(G_2)$ are

$$g(U)=g(u_1u_2)=(u_1^2+u_1u_2+u_2^2+5u_1+4u_2)/12. \quad (28)$$

Although this method of introducing the quantum numbers U avoids the explicit use of the theory of groups, the group-theoretical definition appeared this time more convenient, since the properties of the coefficients of fractional parentage and of the energy matrices, which are connected with this classification and will be obtained in the next sections, could be demonstrated only with the use of the theory of groups.

[3] The general expression of the eigenvalues of Casimir's operator G for every semisimple group will be published elsewhere.

TABLE IVc. $(UL|(30)L'+f)$.

U	L	N	P	F	G	H	I	K	M
						L'			
	D	$490^{-\frac{1}{2}}$	$-54^{\frac{1}{2}}$	$-91^{\frac{1}{2}}$	$189^{\frac{1}{2}}$	$-156^{\frac{1}{2}}$	0	0	0
(20)	G	$5929^{-\frac{1}{2}}$	$-330^{\frac{1}{2}}$	$910^{\frac{1}{2}}$	$126^{\frac{1}{2}}$	$-594^{\frac{1}{2}}$	$2184^{\frac{1}{2}}$	$-1785^{\frac{1}{2}}$	0
	I	$22022^{-\frac{1}{2}}$	0	$-245^{\frac{1}{2}}$	$-1755^{\frac{1}{2}}$	$-2310^{\frac{1}{2}}$	$-2106^{\frac{1}{2}}$	$-4320^{\frac{1}{2}}$	$-11286^{\frac{1}{2}}$
	D	$2695^{-\frac{1}{2}}$	$-578^{\frac{1}{2}}$	$1092^{\frac{1}{2}}$	$700^{\frac{1}{2}}$	$325^{\frac{1}{2}}$	0	0	0
	F	$1694^{-\frac{1}{2}}$	$-55^{\frac{1}{2}}$	0	$-560^{\frac{1}{2}}$	$-715^{\frac{1}{2}}$	$-364^{\frac{1}{2}}$	0	0
	G	$630630^{-\frac{1}{2}}$	$-83655^{\frac{1}{2}}$	$-87360^{\frac{1}{2}}$	$-56784^{\frac{1}{2}}$	$-3971^{\frac{1}{2}}$	$227500^{\frac{1}{2}}$	$171360^{\frac{1}{2}}$	0
(21)	H	$55055^{-\frac{1}{2}}$	0	$12740^{\frac{1}{2}}$	$-7644^{\frac{1}{2}}$	$18711^{\frac{1}{2}}$	$-7800^{\frac{1}{2}}$	$-8160^{\frac{1}{2}}$	0
	K	$165165^{-\frac{1}{2}}$	0	0	$-16848^{\frac{1}{2}}$	$77^{\frac{1}{2}}$	$-27625^{\frac{1}{2}}$	$79860^{\frac{1}{2}}$	$-40755^{\frac{1}{2}}$
	L	$17017^{-\frac{1}{2}}$	0	0	0	$-1785^{\frac{1}{2}}$	$-1989^{\frac{1}{2}}$	$-1140^{\frac{1}{2}}$	$12103^{\frac{1}{2}}$
	P	$16^{-\frac{1}{2}}$	0	$13^{\frac{1}{2}}$	$3^{\frac{1}{2}}$	0	0	0	0
	F	$1232^{-\frac{1}{2}}$	$429^{\frac{1}{2}}$	$-77^{\frac{1}{2}}$	$273^{\frac{1}{2}}$	$-33^{\frac{1}{2}}$	$-420^{\frac{1}{2}}$	0	0
	G	$55440^{-\frac{1}{2}}$	$-3465^{\frac{1}{2}}$	$-9555^{\frac{1}{2}}$	$7203^{\frac{1}{2}}$	$27797^{\frac{1}{2}}$	$1300^{\frac{1}{2}}$	$-6120^{\frac{1}{2}}$	0
(30)	H	$11440^{-\frac{1}{2}}$	0	$-195^{\frac{1}{2}}$	$-4693^{\frac{1}{2}}$	$1232^{\frac{1}{2}}$	$2600^{\frac{1}{2}}$	$2720^{\frac{1}{2}}$	0
	I	$32032^{-\frac{1}{2}}$	0	$5880^{\frac{1}{2}}$	$520^{\frac{1}{2}}$	$-6160^{\frac{1}{2}}$	$-1911^{\frac{1}{2}}$	$15680^{\frac{1}{2}}$	$-1881^{\frac{1}{2}}$
	K	$510510^{-\frac{1}{2}}$	0	0	$33813^{\frac{1}{2}}$	$89012^{\frac{1}{2}}$	$-216580^{\frac{1}{2}}$	$8085^{\frac{1}{2}}$	$163020^{\frac{1}{2}}$
	M	$3808^{-\frac{1}{2}}$	0	0	0	0	$153^{\frac{1}{2}}$	$960^{\frac{1}{2}}$	$2695^{\frac{1}{2}}$

5. THE CALCULATION OF THE FRACTIONAL PARENTAGES OF f^n

1. General Properties

The eigenfunctions of l^n, which are the basis of $\{\mathfrak{c}_{4l+2}\}^n$, may be obtained by reduction of the representation $\{\mathfrak{c}_{4l+2}\}^{n-1}\times(\mathfrak{c}_{4l+2})$:

$$\Psi(l^n\alpha vSLM_SM_L)=\sum\Psi(l^{n-1}\alpha'v'S'L'M_S'M_L')\phi(m_sm_l)\times(l^{n-1}\alpha'v'S'L'M_S'M_L',\,lm_sm_l|\,l^n\alpha vSLM_SM_L);\quad(29)$$

owing to the particular choice of the scheme which was made in the preceding section, it follows from the lemma (11) that the coefficients of this transformation break up in a product of different factors, each of which depends only from a smaller number of variables:

$$(l^{n-1}\alpha'v'S'L'M_S'M_L',\,lm_sm_l|\,l^n\alpha vSLM_SM_L)=(S'\tfrac{1}{2}M_S'm_s|\,S'\tfrac{1}{2}SM_S)(L'lM_L'm_l|\,L'lLM_L)\times(W'\alpha'L'+l|\,W\alpha L)(l^{n-1}v'S'+l|\,\}l^nvS).\quad(30)$$

Confronting this expression with (10) of III, we see that the coefficients of fractional parentage are the product of two factors:

$$(l^{n-1}(\alpha'v'S'L')lSL|\,\}l^n\alpha vSL)=(W'\alpha'L'+l|\,W\alpha L)(l^{n-1}v'S'+l|\,\}l^nvS);\quad(31)$$

the relations (58) of III are particular cases of this result. Owing to the unitary of all our transformations, the factors of (31) satisfy the orthogonality relations

$$\sum_{v'S'}(l^nvS\{|\,l^{n-1}v'S'+l)(l^{n-1}v'S'+l|\,\}l^nvS)=1\quad(32)$$

and

$$\sum_{\alpha'L'}(W\alpha L|\,W'\alpha'L'+l)(W'\alpha'L'+l|\,W''\alpha''L)=\delta(WW'')\delta(\alpha\alpha'').\quad(33)$$

For the particular case $l=3$, owing to the existence of the intermediate group G_2, the coefficients of fractional parentage are the product of three factors:

$$(f^{n-1}(\alpha'U'v'S'L')fSL|\,\}f^n\alpha UvSL)=(U'\alpha'L'+f|\,U\alpha L)(W'U'+f|\,WU)\times(f^{n-1}v'S'+f|\,\}f^nvS),\quad(34)$$

and the orthogonality relations (33) break up into

$$\sum_{U'}(WU|\,W'U'+f)(W'U'+f|\,W''U)=\delta(WW'')\quad(35)$$

and

$$\Big|\sum_{\alpha'L'}^{\prime}(U\alpha L|\,U'\alpha'L'+f)(U'\alpha'L'+f|\,U''\alpha''L)=\delta(UU'')\delta(\alpha\alpha'').\quad(36)$$

In order to find also relations of the type (61) of III, we consider now the identical representations of $\mathfrak{d}_{2l+1}$ which appears in the reduction of $\mathfrak{B}_{W_1}\times\mathfrak{B}_{W_2}$. Such representations may only appear if $W_1=W_2$, and since the tensors of odd degree are diagonal with respect to W (see (70) of III), we obtain in the same way as in Section 6 of II that

$$(W_1\alpha_1L_1+W_2\alpha_2L_2|\,(00\cdots0)0)=[(2L_1+1)/g_{W_1}]^{\frac{1}{2}}\delta(W_1W_2)\delta(\alpha_1\alpha_2)\delta(L_1L_2),\quad(37)$$

where g_{W_1} is the order of the representation $\mathfrak{B}_{W_1}$. Owing to the value (16′) of II of $(LLMM'|\,LL00)$, we get also

$$(W_1\alpha_1L_1M_1,\,W_2\alpha_2L_2M_2|\,W_1W_2,\,(00\cdots0)00)=g_{W_1}^{-\frac{1}{2}}(-1)^{L_1-M_1}\delta(W_1W_2)\delta(\alpha_1\alpha_2)\times\delta(L_1L_2)\delta(M_1,-M_2).\quad(38)$$

TABLE V. $c(UU'(40))$.

	(00)	(10)	(11)	(20)	(21)	(30)	(22)	(31)	(40)
(00)	0	0	0	0	0	0	0	0	1
(10)	0	0	0	0	0	1	0	1	1
(11)	0	0	0	0	1	1	0	1	1
(20)	0	0	0	1	1	1	1	2	2
(21)	0	0	1	1	2	2	2	3	2
(30)	0	1	1	1	2	2	1	3	2
(22)	0	0	0	1	2	1	1	2	2
(31)	0	1	1	2	3	3	2	5	3
(40)	1	1	1	2	2	2	2	3	3

If, in the general formula,[4]

$$\int (W_1\alpha_1L_1M_1|R|W_1\alpha_1'L_1'M_1') \times (W_2\alpha_2L_2M_2|R|W_2\alpha_2'L_2'M_2') \times (W\alpha LM|R|W\alpha'L'M')^* dR = g_W^{-1}(W_1\alpha_1L_1M_1, W_2\alpha_2L_2M_2|W_1W_2, W\alpha LM) \times (W_1W_2, W\alpha'L'M'|W_1\alpha_1'L_1'M_1', W_2\alpha_2'L_2'M_2') \times \int dR, \quad (39)$$

we consider the special case $W\equiv(00\cdots0)$ and introduce (38), we get

$$\int (W_1\alpha_1L_1M_1|R|W_1\alpha_1'L_1'M_1') \times (W_2\alpha_2L_2M_2|R|W_2\alpha_2'L_2'M_2')dR = g_W^{-1}(-1)^{L_1+L_1'-M_1-M_1'}\delta(W_1W_2) \times \delta(\alpha_1\alpha_2)\delta(L_1L_2)\delta(M_1,-M_2) \times \delta(\alpha_1'\alpha_2')\delta(L_1'L_2')\delta(M_1',-M_2')\int dR, \quad (40)$$

and confronting this result with the orthogonality relation[5]

$$\int (W_1\alpha_1L_1M_1|R|W_1\alpha_1'L_1'M_1')^* \times (W_2\alpha_2L_2M_2|R|W_2\alpha_2'L_2'M_2')dR = g_{W_1}^{-1}\delta(W_1W_2)\delta(\alpha_1\alpha_2)\delta(L_1L_2)\delta(M_1M_2) \times \delta(\alpha_1'\alpha_2')\delta(L_1'L_2')\delta(M_1'M_2')\int dR, \quad (41)$$

we obtain from the well-known corollary of Schwarz's inequality that

$$(W\alpha LM|R|W\alpha'L'M')^* = (-1)^{L+L'-M-M'}(W\alpha L-M|R|W\alpha'L'-M'). \quad (42)$$

Applying this result to the first and third factor in the left side of (39), we have

$$(W_1\alpha_1L_1M_1, W_2\alpha_2L_2M_2|W_1W_2, W\alpha LM(W_1W_2, W\alpha'L'M'|W_1\alpha_1'L_1'M_1', W_2\alpha_2'L_2'M_2') = (-1)^{L+L'-M-M'-L_1-L_1'+M_1+M_1'}(g_W/g_{W_1})(W\alpha L-M, W_2\alpha_2L_2M_2|WW_2, W_1\alpha_1L_1-M_1) \times (WW_2, W_1\alpha_1'L_1'-M_1'|W\alpha'L'-M', W_2\alpha_2'L_2'M_2'), \quad (43)$$

and since, owing to (16′) of II and (19a) of II,

$$(L_1L_2M_1M_2|L_1L_2LM) = (-1)^{L_2+M-M_1}[(2L+1)/(2L_1+1)]^{\frac{1}{2}} \times (LL_2-MM_2|LL_2L_1-M_1), \quad (44)$$

we have also

$$(W_1\alpha_1L_1+W_2\alpha_2L_2|W\alpha L)(W\alpha'L'|W_1\alpha_1'L_1'+W_2\alpha_2'L_2') = (-1)^{L+L_2-L_1+L'+L_2'-L_1'} [(2L_1+1)(2L_1'+1)/(2L+1)(2L'+1)]^{\frac{1}{2}}(g_W/g_{W_1}) \times (W\alpha L+W_2\alpha_2L_2|W_1\alpha_1L_1) \times (W_1\alpha_1'L_1'|W\alpha'L'+W_2\alpha_2'L_2'). \quad (45)$$

This equation may be satisfied only if

$$(W\alpha L+W_2\alpha_2L_2|W_1\alpha_1L_1) = (-1)^{L_1-L_2-L+x}[(2L+1)g_{W_1}/(2L_1+1)g_W]^{\frac{1}{2}} \times (W_1\alpha_1L_1+W_2\alpha_2L_2|W\alpha L), \quad (46)$$

where x is independent of the L and depends only on the W. The value of x is to a some extent arbitrary, since it depends from our choice of phases. For the particular case $W_2\equiv(10\cdots0)\equiv l$, which is important for us, we put $x=l=L_2$, and therefore,

$$(W\alpha L+l|W'\alpha'L') = (-1)^{L-L'} \times [(2L+1)g_{W'}/(2L'+1)g_W]^{\frac{1}{2}}(W'\alpha'L'+l|W\alpha L); \quad (47)$$

the relation (61) of III is a particular case of this result.

It is easy to see that for $l=3$ the relation (47) breaks up into

$$(WU+f|W'U') = (g_Ug_{W'}/g_{U'}g_W)^{\frac{1}{2}}(W'U'+f|WU) \quad (48)$$

and

$$(U\alpha L+f|U'\alpha'L') = (-1)^{L-L'} \times [(2L+1)g_{U'}/(2L'+1)g_U]^{\frac{1}{2}}(U'\alpha'L'+f|U\alpha L). \quad (49)$$

2. The Calculation of $(l^{n-1}v'S'+l|\,\}\,l^nvS)$

Applying (1) to (3) and owing to (31) and (33), we have

[4] See E. Wigner, *Gruppentheorie* (Friedrich Vieweg and Sohn, Braunschweig, 1931), p. 204, Eq. (22).

[5] Reference 4, p. 110, Eq. (11).

TABLE VIa. $(U|\chi(L)|U')$ for $U, U' \neq (31), (40)$.

$(U\|\chi\|U')$	S	P	D	F	G	H	I	K	L	M	N
$(20\|\chi\|20)$	0	0	143	0	−130	0	35	0	0	0	0
$(11\|\chi\|21)$	0	0	0	0	0	1	0	0	0	0	0
$(20\|\chi\|21)$	0	0	$-39\sqrt{2}$	0	$4(65)^{\frac{1}{2}}$	0	0	0	0	0	0
$(21\ \chi_1\|21)$	0	0	377	455	−561	49	0	−315	245	0	0
$(21\ \chi_2\|21)$	0	0	13	−65	55	−75	0	133	−75	0	0
$(10\|\chi\|30)$	0	0	0	1	0	0	0	0	0	0	0
$(11\|\chi\|30)$	0	$-13(11)^{\frac{1}{2}}$	0	0	0	$(39)^{\frac{1}{2}}$	0	0	0	0	0
$(20\|\chi\|30)$	0	0	0	0	$-13(5)^{\frac{1}{2}}$	0	30	0	0	0	0
$(21\|\chi\|30)$	0	0	0	$12(195)^{\frac{1}{2}}$	$8(143)^{\frac{1}{2}}$	$11(42)^{\frac{1}{2}}$	0	$-4(17)^{\frac{1}{2}}$	0	0	0
$(30\|\chi\|30)$	0	−52	0	38	−52	88	25	−94	0	25	0
$(20\|\chi\|22)$	0	0	$3(429)^{\frac{1}{2}}$	0	$-38(65)^{\frac{1}{2}}$	0	$21(85)^{\frac{1}{2}}$	0	0	0	0
$(21\|\chi\|22)$	0	0	$45(78)^{\frac{1}{2}}$	0	$12(11)^{\frac{1}{2}}$	$-12(546)^{\frac{1}{2}}$	0	0	$-8(665)^{\frac{1}{2}}$	0	0
$(22\|\chi\|22)$	260	0	−25	0	94	104	−181	0	−36	0	40

TABLE VIb. $(U|\chi(L)|31)$.

L	$(10\|\chi\|31)$	$(11\|\chi\|31)$	$(20\|\chi\|31)$	$(21\|\chi\|31)$	$(30\|\chi\|31)$	$(31\|\chi\|31)$
P	0	$11(330)^{\frac{1}{2}}$	0	0	$76(143)^{\frac{1}{2}}$	−6644
D	0	0	$-8(78)^{\frac{1}{2}}$	$-60(39/7)^{\frac{1}{2}}$	0	4792
F	0	0	0	$-312(5)^{\frac{1}{2}}$	$-48(39)^{\frac{1}{2}}$	$\begin{Vmatrix} 4420 & 336(143)^{\frac{1}{2}} \\ 336(143)^{\frac{1}{2}} & -902 \end{Vmatrix}$
F'	1	0	0	$12(715)^{\frac{1}{2}}$	$-98(33)^{\frac{1}{2}}$	
G	0	0	$5(65)^{\frac{1}{2}}$	$2024/(7)^{\frac{1}{2}}$	$20(1001)^{\frac{1}{2}}$	−2684
H	0	$11(85)^{\frac{1}{2}}$	0	$31(1309/3)^{\frac{1}{2}}$	$-20(374)^{\frac{1}{2}}$	$\begin{Vmatrix} -2024 & -48(6545)^{\frac{1}{2}} \\ -48(6545)^{\frac{1}{2}} & 2680 \end{Vmatrix}$
H'	0	$-25(77)^{\frac{1}{2}}$	0	$103(5/3)^{\frac{1}{2}}$	$-44(70)^{\frac{1}{2}}$	
I	0	0	$10(21)^{\frac{1}{2}}$	0	$-57(33)^{\frac{1}{2}}$	$\begin{Vmatrix} -12661/5 & -3366(34)^{\frac{1}{2}}/5 \\ -3366(34)^{\frac{1}{2}}/5 & 17336/5 \end{Vmatrix}$
I'	0	0	0	0	$18(1122)^{\frac{1}{2}}$	
K	0	0	0	$-52(323/23)^{\frac{1}{2}}$	$-494(19/23)^{\frac{1}{2}}$	$\begin{Vmatrix} 123506/23 & 144(21318)^{\frac{1}{2}}/23 \\ 144(21318)^{\frac{1}{2}}/23 & -85096/23 \end{Vmatrix}$
K'	0	0	0	$-336(66/23)^{\frac{1}{2}}$	$73(1122/23)^{\frac{1}{2}}$	
L	0	0	0	$-24(190)^{\frac{1}{2}}$	0	−4712
M	0	0	0	0	$-21(385)^{\frac{1}{2}}$	−473
N	0	0	0	0	0	1672
O	0	0	0	0	0	220

TABLE VIc. $(U|\chi(L)|40)$.

L	$(00\|\chi\|40)$	$(10\|\chi\|40)$	$(20\|\chi\|40)$	$(30\|\chi\|40)$	$(40\|\chi\|40)$
S	1	0	0	0	−1408
D	0	0	$-88(13)^{\frac{1}{2}}$	0	−44
F	0	1	0	$90(11)^{\frac{1}{2}}$	1078
G	0	0	$53(715/27)^{\frac{1}{2}}$	$-16(1001)^{\frac{1}{2}}$	$\begin{Vmatrix} -16720/9 & -34(2618)^{\frac{1}{2}}/9 \\ -34(2618)^{\frac{1}{2}}/9 & 10942/9 \end{Vmatrix}$
G'	0	0	$7(15470/27)^{\frac{1}{2}}$	$64(442)^{\frac{1}{2}}$	
H	0	0	0	$-72(462)^{\frac{1}{2}}$	−704
I	0	0	$34(1045/31)^{\frac{1}{2}}$	$-9(21945/31)^{\frac{1}{2}}$	$\begin{Vmatrix} -2453/31 & 60(74613)^{\frac{1}{2}}/31 \\ 60(74613)^{\frac{1}{2}}/31 & 36088/31 \end{Vmatrix}$
I'	0	0	$-12(1785/31)^{\frac{1}{2}}$	$756(85/31)^{\frac{1}{2}}$	
K	0	0	0	$-84(33)^{\frac{1}{2}}$	−132
L	0	0	0	0	$\begin{Vmatrix} -4268/31 & 924(1995)^{\frac{1}{2}}/31 \\ 924(1995)^{\frac{1}{2}}/31 & 11770/31 \end{Vmatrix}$
L'	0	0	0	0	
M	0	0	0	$-99(15)^{\frac{1}{2}}$	−1067
N	0	0	0	0	528
Q	0	0	0	0	22

$$S(S+1)-3n/4 = [n/(n-2)]\sum_{v'S'}[S'(S'+1)-3(n-1)/4] \times (l^{n-1}v'S'+l|\}l^nvS)^2; \quad (50)$$

since S' may have only the two values $S-\frac{1}{2}$ and $S+\frac{1}{2}$, we obtain from (32) and (50) that

$$\begin{aligned} \textstyle\sum_{v'}(l^{n-1}v'S-\tfrac{1}{2}+l|\}l^nvS)^2 &= (n+2S+2)S/n(2S+1), \\ \textstyle\sum_{v'}(l^{n-1}v'S+\tfrac{1}{2}+l|\}l^nvS)^2 &= (n-2S)(S+1)/n(2S+1). \end{aligned} \quad (51)$$

Since, for $n=v$, v' may have only the value $v-1$, we get

$$(l^{v-1}v-1\ S-\tfrac{1}{2}+l|\}l^vvS)^2=(v+2S+2)S/v(2S+1),$$
$$(l^{v-1}v-1\ S+\tfrac{1}{2}+l|\}l^vvS)^2=(v-2S)(S+1)/v(2S+1),$$

and owing to (58) of III,

$$\begin{aligned} &(l^{n-1}v-1\ S-\tfrac{1}{2}+l|\}l^nvS)^2 \\ &\quad=(4l+4-n-v)(v+2S+2)S/2n(2l+2-v)(2S+1), \\ &(l^{n-1}v-1\ S+\tfrac{1}{2}+l|\}l^nvS)^2 \\ &\quad=(4l+4-n-v)(v-2S)(S+1)/2n(2l+2-v)(2S+1); \end{aligned} \quad (52a)$$

TABLE VII. $x((210), UU')$.

	(11)	(20)	(21)
(11)	0	0	$12(455)^{\frac{1}{2}}$
(20)	0	$-6/7$	$6(66)^{\frac{1}{2}}/7$
(21)	$12(455)^{\frac{1}{2}}$	$6(66)^{\frac{1}{2}}/7$	$3/7, 0$

TABLE VIII. $x((211), UU')$.

	(10)	(11)	(20)	(21)	(30)
(10)	0	0	0	0	$-20(143)^{\frac{1}{2}}$
(11)	0	0	0	$10(182)^{\frac{1}{2}}$	10
(20)	0	0	$-8/7$	$4(33)^{\frac{1}{2}}/7$	$4\sqrt{3}$
(21)	0	$10(182)^{\frac{1}{2}}$	$4(33)^{\frac{1}{2}}/7$	$4/7, 3$	2
(30)	$-20(143)^{\frac{1}{2}}$	10	$4\sqrt{3}$	2	2

subtracting (52a) from (51) we also get

$$\begin{aligned}&(l^{n-1}v+1\ S-\tfrac{1}{2}+l|\,\}l^nvS)^2\\&=(n-v)(4l+6-v+2S)S/2n(2l+2-v)(2S+1),\\&(l^{n-1}v+1\ S+\tfrac{1}{2}+l|\,\}l^nvS)^2\\&=(n-v)(4l+4-v-2S)(S+1)/\\&\qquad 2n(2l+2-v)(2S+1).\end{aligned}\tag{52b}$$

The phases of $(l^{n-1}v'S'+l|\,\}l^nvS)$ are independent of n and will be denoted by $\epsilon(v'S'|\,\}vS)$; they are arbitrary as long as the phases of $(W'\alpha'L'+l|W\alpha L)$ are not fixed. The latter are partially fixed by (47), and, comparing it with (61) of III, we have

$$\epsilon(v+1S'|\,\}vS)=(-1)^{l+S-S'+\frac{1}{2}}\epsilon(vS|\,\}v+1S'),$$

or, in a more general form,

$$\epsilon(v'S'|\,\}vS)=(-1)^{l+S-S'+(v'-v)/2}\epsilon(vS|\,\}v'S').\tag{53}$$

Another partial limitation in the choice of $\epsilon(v'S'|\,\}vS)$ is given by the fact that, according to (20), every value of W corresponds to two couples of v and S, which are related by the equations,

$$v_1+2S_2=v_2+2S_1=2l+1;\tag{54}$$

it may be shown that from this fact follows the relation

$$\begin{aligned}&\frac{\epsilon(v_1-2\ S_1|\,\}v_1-1\ S_1-\frac{1}{2})\epsilon(v_1-1\ S_1-\frac{1}{2}|\,\}v_1S_1)}{\epsilon(v_1-2\ S_1|\,\}v_1-1\ S_1+\frac{1}{2})\epsilon(v_1-1\ S_1+\frac{1}{2}|\,\}v_1S_1)}\\&=\frac{\epsilon(v_2S_2+1|\,\}v_2+1\ S_2+\frac{1}{2})\epsilon(v_2+1\ S_2+\frac{1}{2}|\,\}v_2S_2)}{\epsilon(v_2S_2+1|\,\}v_2-1\ S_2+\frac{1}{2})\epsilon(v_2-1\ S_2+\frac{1}{2}|\,\}v_2S_2)},\end{aligned}\tag{55}$$

when v_1, S_1, v_2, and S_2 satify (54).

In order to satisfy (53) and (55), the following choice of phases was made for $l=3$:

$$\begin{aligned}&\epsilon(v'S'|\,\}vS)=(-1)^{S'} && \text{for } v \text{ odd},\\&\epsilon(v'S'|\,\}vS)=(-1)^{S'+(v'-v)/2} && \text{for } v \text{ even}.\end{aligned}\tag{56}$$

3. The Calculation of $(W'U'+f|WU)$ and $(U'L'+f|UL)$

The coefficients of fractional parentage of f and f^2 are equal to unity; those of f^3 were calculated from (9) of III, and, in the cases where two doublets with the same L were allowed, $(f^2(^3F)f\,L|\,\}f^3\alpha\,L)$ was put equal to 0 in one of them, since for doublets of f^3 with $U\equiv(21)$ the eigenvalue of R vanishes according to (26), (27), and (28).

From the coefficients of fractional parentage of f, f^2, and f^3, several elements of $(W'U'+f|WU)$ and $(U'L'+f|UL)$ were obtained and are given in Tables III and IV. These tables were then extended by using (48), (49), (35), (36), and also (1) as it was pointed out in Section 2. In the very few cases where these equations were not sufficient for the determination of some elements, additional equations were obtained from (23) of III by requiring that $(f^nUvSL\|U^{(5)}\|f^nU'v'SL')$ should vanish unless $v=v'$ and $U=U'$, since the tensor $\mathbf{U}^{(5)}$ commutes with Q and R.

Owing to the present status of the experimental classification of the spectra of the rare earths, the terms of lower multiplicity are not yet interesting; we limited therefore Tables III and IV to those elements which are of use in the calculation of the coefficients of fractional parentage for f^4 and for the two highest multiplicities of f^5, f^6, and f^7.

6. THE SPECTRA OF f^n

1. The Choice of the Parameters

In Section 4 of II we considered the coefficients of Slater's integrals F^k as scalar products of tensors in the three-dimensional space; we shall now show that they may also be considered as particular components of tensors in the $(2l+1)$-dimensional space.

In full analogy to Section 3 of II it is possible to define as an irreducible tensor of the "type" W in the $(2l+1)$-dimensional space each operator whose components transform by a $(2l+1)$-dimensional rotation as the elements of the basis of the representation $\mathfrak{B}_W$ of $\mathfrak{d}_{2l+1}$.

In the three-dimensional space $\mathbf{u}^{(k)}$ was a tensor, and its components $u_q^{(k)}$ transformed as the spherical harmonics $Y(kq)$; in the $(2l+1)$-dimensional space $\mathbf{u}^{(k)}$ alone is no longer a tensor, but it may be shown that the quantities $(2k+1)^{\frac{1}{2}}u_q^{(k)}$ transform as the functions $\psi((20\cdots0)kq)$ if k is even, and as the functions $\psi((110\cdots0)kq)$ if k is odd, i.e., all the quantities $(4t+1)^{\frac{1}{2}}u_q^{(2t)}$ or $(4t-1)^{\frac{1}{2}}u_q^{(2t-1)}$ for $1\leqslant t\leqslant l$ are *together* the components of a sole tensor.

TABLE IX. $x((220), UU')$.

	(20)	(21)	(22)
(20)	3/14	$3(55)^{\frac{1}{2}}/7$	$-3(5/28)^{\frac{1}{2}}$
(21)	$3(55)^{\frac{1}{2}}/7$	$-6/7, -3$	$3/(7)^{\frac{1}{2}}$
(22)	$-3(5/28)^{\frac{1}{2}}$	$3/(7)^{\frac{1}{2}}$	3/2

TABLE X. $x((221), UU')$.

	(10)	(11)	(20)	(21)	(30)	(31)
(10)	0	0	0	0	$5(143)^{\frac{1}{2}}$	$-15(429)^{\frac{1}{2}}$
(11)	0	0	0	$14(910/11)^{\frac{1}{2}}$	$2(10)^{\frac{1}{2}}$	$2(39)^{\frac{1}{2}}/11$
(20)	0	0	2/7	$-10(6)^{\frac{1}{2}}/7$	$\sqrt{3}$	$9(3/7)^{\frac{1}{2}}$
(21)	0	$14(910/11)^{\frac{1}{2}}$	$-10(6)^{\frac{1}{2}}/7$	$-1/7, 12/11$	$5(2/11)^{\frac{1}{2}}$	$3\sqrt{2}/11$
(30)	$5(143)^{\frac{1}{2}}$	$2(10)^{\frac{1}{2}}$	$\sqrt{3}$	$5(2/11)^{\frac{1}{2}}$	$-1/2$	$3/2(11)^{\frac{1}{2}}$
(31)	$-15(429)^{\frac{1}{2}}$	$2(39)^{\frac{1}{2}}/11$	$9(3/7)^{\frac{1}{2}}$	$3\sqrt{2}/11$	$3/2(11)^{\frac{1}{2}}$	$1/22$

TABLE XI. $x((222), UU')$.

	(00)	(10)	(20)	(30)	(40)
(00)	0	0	0	0	$-30(143)^{\frac{1}{2}}$
(10)	0	0	0	$-3(1430)^{\frac{1}{2}}$	$9(1430)^{\frac{1}{2}}$
(20)	0	0	6/11	$-3(42/11)^{\frac{1}{2}}$	$9\sqrt{2}/11$
(30)	0	$-3(1430)^{\frac{1}{2}}$	$-3(42/11)^{\frac{1}{2}}$	-3	$1/(11)^{\frac{1}{2}}$
(40)	$-30(143)^{\frac{1}{2}}$	$9(1430)^{\frac{1}{2}}$	$9\sqrt{2}/11$	$1/(11)^{\frac{1}{2}}$	3/11

In the seven-dimensional space the quantities

$$\sum_{kqk'q'} [(2k+1)(2k'+1)]^{\frac{1}{2}} u_1^{(k)}{}_q u_2^{(k')}{}_{q'} \times ((200)(20)kq, (200)(20)k'q' | WUKQ) \quad (57)$$

will transform as $\psi(WUKQ)$, and, in particular, the quantities

$$\sum_{kq}(2k+1) u_1^{(k)}{}_q u_2^{(k)}{}_{-q}(kkq-q | kk00) \times ((200)(20)k+(200)(20)k | WU0)$$
$$= \sum_k (2k+1)^{\frac{1}{2}} (\mathbf{u}_1^{(k)} \cdot \mathbf{u}_2^{(k)}) \times ((200)(20)k+(200)(20)k | WU0) \quad (58)$$

will have the tensorial properties of $\psi(WUS)$.

Since, according to (45) of II,

$$f_k(f^2L) = (f^2LM | (\mathbf{C}_1^{(k)} \cdot \mathbf{C}_2^{(k)}) | f^2LM),$$

or also

$$f_k(f^2L) = (3\|C^{(k)}\|3)^2 (f^2LM | (\mathbf{u}_1^{(k)} \cdot \mathbf{u}_2^{(k)}) | f^2LM), \quad (59)$$

we shall substitute to the f_k the linear combinations

$$N_i \sum_k (2k+1)^{\frac{1}{2}} (3\|C^{(k)}\|3)^{-2} f_k \times ((200)(20)k+(200)(20)k | W_i U_i S), \quad (60)$$

where the N_i are convenient normalization factors and

$$W_1U_1 \equiv (000)(00), \quad W_2U_2 \equiv (400)(40), \quad W_3U_3 \equiv (220)(22). \quad (61)$$

Since the only parents of the functions $\psi((000)(00)S)$, $\psi((400)(40)S)$, and $\psi((220)(22)S)$ are, respectively, the functions

$\psi((100)(10)F)$, $\psi((300)(30)F)$, and $\psi((210)(21)F)$,

the coefficients

$$((200)(20)k+(200)(20)k | W_i U_i S)$$

will be proportional to $((20)k+f|(10)F)$, $((20)k+f|(30)F)$ and $((20)k+f|(21)F)$, which are given in Table IV. Taking the values of $(3\|C^{(k)}\|3)$ from (51) of II and remembering that

$$f^k = D_k f_k, \quad (62)$$

where the D_k are the denominators of Table II[6] of TAS,* we define for the configurations f^n,

$$\begin{aligned} e_0 &= f^0 = n(n-1)/2, \\ e_1 &= 9f^0/7 + f^2/42 + f^4/77 + f^6/462, \\ e_2 &= 143f^2/42 - 130f^4/77 + 35f^6/462, \\ e_3 &= 11f^2/42 + 4f^4/77 - 7f^2/462; \end{aligned} \quad (63)$$

the term $9f^0/7$ was added for convenience in e_1 without changing its tensorial properties, since both f^0 and e_1 are scalars in the seven-dimensional space.

The general expression of the energy matrices of f^n will be

$$e_0E^0 + e_1E^1 + e_2E^2 + e_3E^3 \quad (64)$$

instead of

$$f^0F_0 + f^2F_2 + f^4F_4 + f^6F_6; \quad (65)$$

the E^i are linear combinations of Slater's parameters, which are, however, different from those adopted empirically in (96) of II:

$$\begin{aligned} E^0 &= F_0 - 10F_2 - 33F_4 - 286F_6, \\ E^1 &= (70F_2 + 231F_4 + 2002F_6)/9, \\ E^2 &= (F_2 - 3F_4 + 7F_6)/9, \\ E^3 &= (5F_2 + 6F_4 - 91F_6)/3; \end{aligned} \quad (66)$$

TABLE XII. $c(WW'(220))$.

	(000)	(100)	(110)	(200)	(111)	(210)	(211)	(220)	(221)	(222)
(000)	0	0	0	0	0	0	0	1	0	0
(100)	0	0	0	0	0	1	0	0	1	0
(110)	0	0	1	0	0	0	1	1	1	0
(200)	0	0	0	1	0	0	1	1	0	1
(111)	0	0	0	0	1	1	1	1	1	0
(210)	0	1	0	0	1	2	1	0	2	1
(211)	0	0	1	1	1	1	3	1	2	1
(220)	1	0	1	1	1	0	1	2	1	1
(221)	0	1	1	0	1	2	2	1	3	1
(222)	0	0	0	1	0	1	1	1	1	1

* E. U. Condon and G. H. Shortley, *Theory of Atomic Spectra* (Cambridge University Press, London, 1935).

TABLE XIII. $c(UU'(22))$.

	(00)	(10)	(11)	(20)	(21)	(30)	(22)	(31)	(40)
(00)	0	0	0	0	0	0	1	0	0
(10)	0	0	0	0	1	0	0	1	0
(11)	0	0	1	0	0	1	1	1	0
(20)	0	0	0	1	1	1	1	1	1
(21)	0	1	0	1	2	1	0	2	2
(30)	0	0	1	1	1	2	1	2	1
(22)	1	0	1	1	0	1	2	1	1
(31)	0	1	1	1	2	2	1	3	2
(40)	0	0	0	1	2	1	1	2	2

the formulas for f^2 assume now the form

$$
\begin{aligned}
&{}_0{}^1S = E^0 + 9E^1 && {}_2{}^3P = E^0 + 33E^3 \\
&{}_2{}^1D = E^0 + 2E^1 + 286E^2 - 11E^3 && {}_2{}^3F = E^0 \\
&{}_2{}^1G = E^0 + 2E^1 - 260E^2 - 4E^3 && {}_2{}^3H = E^0 - 9E^3 \\
&{}_2{}^1I = E^0 + 2E^1 + 70E^2 + 7E^3
\end{aligned}
\qquad (67)
$$

For $n>2$, the e_i are matrices whose order equals the number of allowed states for a given SL; the elements of these matrices may be calculated by means of (1), but most of the calculations may be avoided by considering the tensorial properties of the e_i.

e_1 is a scalar also in the seven-dimensional space; it is therefore diagonal in the $vUSL$ scheme, and its eigenvalues are independent of L and U. We have from (67) that

$$e_1(f^2SL) = q_{12} + \tfrac{1}{2} - 2(\mathbf{s}_1 \cdot \mathbf{s}_2), \qquad (68)$$

and owing to (50) of III and (3) we obtain that, in general, the eigenvalues of e_1 are

$$e_1(f^n vUSL) = 9(n-v)/2 + v(v+2)/4 - S(S+1). \qquad (69)$$

The matrices e_2 and e_3 are particular components of tensors in the seven-dimensional space. The dependence of their elements on U and L will be analogous to (28) of II, but the result is somewhat more complicated, since, in the decomposition of the external product of two irreducible representations of $\mathfrak{d}_7$, some representation may appear more than once. We now have

$$(f^n vWUSL | e_i | f^n v'W'U'SL) = \sum_\alpha A_\alpha (W'U'L + W_i U_i S | \alpha WUL); \qquad (70)$$

or, owing to an obvious extension of (46),

$$(f^n vWUSL | e_i | f^n v'W'U'SL) = \sum_\beta B_\beta (WUL + W'U'L | \beta W_i U_i S)/(2L+1)^{\frac{1}{2}}. \qquad (71)$$

The number of values which may be assumed by α and β equals the number of times that the representation $\mathfrak{B}_{W_i}$ appears in the decomposition of $\mathfrak{B}_W \times \mathfrak{B}_{W'}$ and will be denoted by $c(WW'W_i)$. A method for calculating these numbers is given by Weyl.[6]

TABLE XIVa. $(U|\varphi(L)|U')$ for $U, U' \neq (31), (40)$.

$(U \; U')$			S	P	D	F	G	H	I	K	L	M	N
(11	φ	11)	0	−11	0	0	0	3	0	0	0	0	0
(20	φ	20)	0	0	−11	0	−4	0	7	0	0	0	0
(10	φ	21)	0	0	0	1	0	0	0	0	0	0	0
(20	φ	21)	0	0	$6\sqrt{2}$	0	$(65)^{\frac{1}{2}}$	0	0	0	0	0	0
(21	φ	21)	0	0	−57	63	55	−105	0	−14	42	0	0
(11	φ	30)	0	$(11)^{\frac{1}{2}}$	0	0	0	$(39)^{\frac{1}{2}}$	0	0	0	0	0
(20	φ	30)	0	0	0	0	$2(5)^{\frac{1}{2}}$	0	3	0	0	0	0
(21	φ	30)	0	0	0	$(195)^{\frac{1}{2}}$	$-(143)^{\frac{1}{2}}$	$-2(42)^{\frac{1}{2}}$	0	$-4(17)^{\frac{1}{2}}$	0	0	0
(30	φ	30)	0	83	0	−72	20	−15	42	−28	0	6	0
(00	φ	22)	1	0	0	0	0	0	0	0	0	0	0
(20	φ	22)	0	0	$3(429)^{\frac{1}{2}}$	0	$4(65)^{\frac{1}{2}}$	0	$3(85)^{\frac{1}{2}}$	0	0	0	0
(22	φ	22)	144	0	69	0	−148	72	39	0	−96	0	56

TABLE XIVb. $(U|\varphi(L)|31)$.

L	(10|φ|31)	(11|φ|31)	(21|φ|31)	(30|φ|31)	(31|φ|31)
P	0	$(330)^{\frac{1}{2}}$	0	$17(143)^{\frac{1}{2}}$	209
D	0	0	$12(273)^{\frac{1}{2}}$	0	−200
F	1	0	$-36(5)^{\frac{1}{2}}$	$-16(39)^{\frac{1}{2}}$	$\begin{Vmatrix} 624 & -80(143)^{\frac{1}{2}} \\ -80(143)^{\frac{1}{2}} & -616 \end{Vmatrix}$
F'	0	0	$-3(715)^{\frac{1}{2}}$	$24(33)^{\frac{1}{2}}$	
G	0	0	$11(7)^{\frac{1}{2}}$	$4(1001)^{\frac{1}{2}}$	836
H	0	$(85)^{\frac{1}{2}}$	$-2(1309/3)^{\frac{1}{2}}$	$(187/2)^{\frac{1}{2}}$	$\begin{Vmatrix} -1353/2 & -5(6545)^{\frac{1}{2}}/2 \\ -5(6545)^{\frac{1}{2}}/2 & 703/2 \end{Vmatrix}$
H'	0	$(77)^{\frac{1}{2}}$	$-74(5/3)^{\frac{1}{2}}$	$31(35/2)^{\frac{1}{2}}$	
I	0	0	0	$30(33)^{\frac{1}{2}}$	$\begin{Vmatrix} -2662/5 & 528(34)^{\frac{1}{2}}/5 \\ 528(34)^{\frac{1}{2}}/5 & -88/5 \end{Vmatrix}$
I'	0	0	0	0	
K	0	0	$-28(323/23)^{\frac{1}{2}}$	$4(437)^{\frac{1}{2}}$	$\begin{Vmatrix} 6652/23 & 96(21318)^{\frac{1}{2}}/23 \\ 96(21318)^{\frac{1}{2}}/23 & -5456/23 \end{Vmatrix}$
K'	0	0	$42(66/23)^{\frac{1}{2}}$	0	
L	0	0	$-6(190)^{\frac{1}{2}}$	0	−464
M	0	0	0	$-6(385)^{\frac{1}{2}}$	814
N	0	0	0	0	−616
O	0	0	0	0	352

[6] H. Weyl, *The Classical Groups* (Princeton University Press, Princeton, New Jersey, 1939), p. 229.

TABLE XIVc. $(U|\varphi(L)|40)$.

L	$(20\|\varphi\|40)$	$(21\|\varphi\|40)$	$(22\|\varphi\|40)$
S	0	0	$2(2145)^{\frac{1}{2}}$
D	$11(13)^{\frac{1}{2}}$	$-6(26)^{\frac{1}{2}}$	$9(33)^{\frac{1}{2}}$
F	0	$3(455)^{\frac{1}{2}}$	0
G	$-4(715/27)^{\frac{1}{2}}$	$-131(11/27)^{\frac{1}{2}}$	$-4(11/27)^{\frac{1}{2}}$
G'	$(15470/27)^{\frac{1}{2}}$	$17(238/27)^{\frac{1}{2}}$	$-17(238/27)^{\frac{1}{2}}$
H	0	$-12(21)^{\frac{1}{2}}$	$3(286)^{\frac{1}{2}}$
I	$7(1045/31)^{\frac{1}{2}}$	0	$3(3553/31)^{\frac{1}{2}}$
I'	$3(1785/31)^{\frac{1}{2}}$	0	$75(21/31)^{\frac{1}{2}}$
K	0	$-2(119)^{\frac{1}{2}}$	0
L	0	$22(105/31)^{\frac{1}{2}}$	$4(627/31)^{\frac{1}{2}}$
L'	0	$-84(19/31)^{\frac{1}{2}}$	$12(385/31)^{\frac{1}{2}}$
N	0	0	$-(2530)^{\frac{1}{2}}$

TABLE XV. $y(f^3, {}_v{}^2U, {}_{v'}{}^2U')$.

	${}_2{}^2(11)$	${}_2{}^2(20)$	${}_2{}^2(21)$
${}_1{}^2(10)$	0	0	$-6(22)^{\frac{1}{2}}$
${}_2{}^2(11)$	2	0	0
${}_2{}^2(20)$	0	10/7	$2(66)^{\frac{1}{2}}/7$
${}_2{}^2(21)$	0	$2(66)^{\frac{1}{2}}/7$	2/7

2. The Calculation of e_2

For the values of W and W' which satisfy (16), $c(WW'(400))$ equals unity if $W=W'$ and $w_1=2$, and vanishes in any other case; it follows that e_2 is diagonal with respect to v and vanishes for $v=2S$, and also that for $v>2S$.

$$(f^n vWUSL|e_2|f^n vWU'SL) = b(nvS)(WUL+WU'L|(400)(40)S)/(2L+1)^{\frac{1}{2}}. \quad (72)$$

By considerations which are very similar to the method used in Section 7 of II for calculating the energy matrices of d^n (and in particular for the proof that the relative positions of the quartets and sextets of d^5 are exactly opposed to those of the terms of d^2 with the same L), it may be shown that $b(nvS)$ is independent of n and that for two values of v and S which correspond to the same value of W the $b(nvS)$ differ only in the sign. We can therefore write

$$(f^n vUSL|e_2|f^n vU'SL)=\pm(WUL|e_2|WU'L), \quad (73)$$

where the upper sign holds for the values of v and S which appear in the first column of Table I, and the lower sign for the second column.

The actual calculation of $(WUL|e_2|WU'L)$ is simplified by the lemma (11): introducing it in (72) we have that

$$(WUL|e_2|WU'L)=\sum_\gamma x_\gamma(W,UU')(U|\chi_\gamma(L)|U'), \quad (74)$$

where x_γ is independent of L and $\chi_\gamma(L)$ is independent of W; the maximal number of independent $(U|\chi_\gamma(L)|U')$ is $c(UU'(40))$ and is given in Table V.

Not only $(WUL|e_2|WU'L)$, but also

$$\sum_{L_2}(UL|U_2L_2+f)(U_2|\chi_{\gamma_2}(L_2)|U_2') \times(U_2'L_2+f|U'L) \quad (75)$$

TABLE XVI. $y(f^4, {}_v{}^3U, {}_{v'}{}^3U')$.

	${}_4{}^3(10)$	${}_4{}^3(11)$	${}_4{}^3(20)$	${}_4{}^3(21)$	${}_4{}^3(30)$
${}_2{}^3(10)$	0	0	0	$-12(33/5)^{\frac{1}{2}}$	0
${}_2{}^3(11)$	0	6/5	0	0	6
${}_4{}^3(10)$	0	0	0	$8(11/15)^{\frac{1}{2}}$	0
${}_4{}^3(11)$	0	29/15	0	0	$-1/3$
${}_4{}^3(20)$	0	0	6/7	$-8(11/147)^{\frac{1}{2}}$	$4/\sqrt{3}$
${}_4{}^3(21)$	$8(11/15)^{\frac{1}{2}}$	0	$-8(11/147)^{\frac{1}{2}}$	$-2/21$	$-4/3$
${}_4{}^3(30)$	0	$-1/3$	$4/\sqrt{3}$	$-4/3$	1/3

TABLE XVII. $y(f^4, {}_v{}^1U, {}_{v'}{}^1U')$.

	${}_4{}^1(20)$	${}_4{}^1(21)$	${}_4{}^1(22)$
${}_0{}^1(00)$	0	0	$-12(22)^{\frac{1}{2}}$
${}_2{}^1(20)$	$3(3/175)^{\frac{1}{2}}$	$-4(33/35)^{\frac{1}{2}}$	$-(3/5)^{\frac{1}{2}}$
${}_4{}^1(20)$	221/140	$8(11/245)^{\frac{1}{2}}$	$-(7/80)^{\frac{1}{2}}$
${}_4{}^1(21)$	$8(11/245)^{\frac{1}{2}}$	2/7	0
${}_4{}^1(22)$	$-(7/80)^{\frac{1}{2}}$	0	1/4

TABLE XVIII. $y(f^5, {}_v{}^4U, {}_{v'}{}^4U')$.

	${}_5{}^4(10)$	${}_5{}^4(11)$	${}_5{}^4(20)$	${}_5{}^4(21)$	${}_5{}^4(30)$
${}_3{}^4(00)$	0	0	0	0	0
${}_3{}^4(10)$	0	0	0	$9(11)^{\frac{1}{2}}$	.0
${}_3{}^4(20)$	0	0	$3/(7)^{\frac{1}{2}}$	$(33/7)^{\frac{1}{2}}$	$-2(21)^{\frac{1}{2}}$
${}_5{}^4(10)$	0	0	0	$-(55/3)^{\frac{1}{2}}$	0
${}_5{}^4(11)$	0	$-1/3$	0	0	$-5/3$
${}_5{}^4(20)$	0	0	5/7	$5(11/147)^{\frac{1}{2}}$	$2/\sqrt{3}$
${}_5{}^4(21)$	$-(55/3)^{\frac{1}{2}}$	0	$5(11/147)^{\frac{1}{2}}$	$-4/21$	$-2/3$
${}_5{}^4(30)$	0	$-5/3$	$2/\sqrt{3}$	$-2/3$	$-1/3$

is expressible as linear combination of the $(U|\chi_\gamma(L)|U')$; it is therefore convenient to calculate at first the expressions (75), and then to assemble the results in the summation (1), where the coefficients of fractional parentage have the form (34). It is also possible to avoid at all the summations (75) for most of the values of L, after the different $(U|\chi_\gamma(L)|U')$ allowed by Table V are obtained from few simple $\chi_{\gamma_2}(L_2)$.

Although almost all the allowed χ_γ appear in the expressions (75), the linear combinations (74) are generally proportional to each other, and it is therefore possible to express the results by means of one $\chi(L)$ for every couple UU', with the sole exception of $U=U' \equiv(21)$, where both $\chi_\gamma(L)$ allowed by Table V are necessary for expressing the different $e_2(W)$. The functions $(U|\chi(L)|U')$ are tabulated in Tables VI, the values of $x(W, UU')$ in Tables VII–XI.

3. The Calculation of e_3

Together with e_3 it is useful to consider the operator

$$\Omega=-462^{\frac{1}{2}}\sum_k(2k+1)^{\frac{1}{2}}\mathbf{U}^{(k)^2} \times((110)(11)k+(110)(11)k|(220)(22)S) =33(\mathbf{U}^{(1)^2}-\mathbf{U}^{(5)^2}), \quad (76)$$

TABLE XIX. $y(f^5, {}_v{}^2U, {}_5{}^3U')$.

	${}_5{}^3(10)$	${}_5{}^3(11)$	${}_5{}^3(20)$	${}_5{}^3(21)$	${}_5{}^3(30)$	${}_5{}^3(31)$
${}_1{}^2(10)$	0	0	0	$36/(5)^{\frac{1}{2}}$	0	$-36\sqrt{2}$
${}_3{}^2(11)$	0	$3/\sqrt{2}$	0	0	$3(5)^{\frac{1}{2}}/2$	$-(39/8)^{\frac{1}{2}}$
${}_3{}^2(20)$	0	0	$3/7$	$-11(6)^{\frac{1}{2}}/7$	$-4\sqrt{3}$	0
${}_3{}^2(21)$	$3(33/10)^{\frac{1}{2}}$	0	$-3(33/98)^{\frac{1}{2}}$	$3/7(11)^{\frac{1}{2}}$	$-3/2\sqrt{2}$	$3/2(22)^{\frac{1}{2}}$
${}_5{}^2(10)$	0	0	0	$43/(30)^{\frac{1}{2}}$	0	$4\sqrt{3}$
${}_5{}^2(11)$	0	$-5/6$	0	0	$-5(5/72)^{\frac{1}{2}}$	$-(13/48)^{\frac{1}{2}}$
${}_5{}^2(20)$	0	0	$11/7$	$-11/7(6)^{\frac{1}{2}}$	$4/\sqrt{3}$	0
${}_5{}^2(21)$	$43/(30)^{\frac{1}{2}}$	0	$-11/7(6)^{\frac{1}{2}}$	$25/231$	$29/6(22)^{\frac{1}{2}}$	$1/22\sqrt{2}$
${}_5{}^2(30)$	0	$-5(5/72)^{\frac{1}{2}}$	$4/\sqrt{3}$	$29/6(22)^{\frac{1}{2}}$	$-1/12$	$1/4(11)^{\frac{1}{2}}$
${}_5{}^2(31)$	$4\sqrt{3}$	$-(13/48)^{\frac{1}{2}}$	0	$1/22\sqrt{2}$	$1/4(11)^{\frac{1}{2}}$	$1/44$

TABLE XX. $y(f^6, {}_4{}^5U, {}_6{}^5U')$.

	${}_6{}^5(11)$	${}_6{}^5(20)$	${}_6{}^5(21)$
${}_4{}^5(00)$	0	0	0
${}_4{}^5(10)$	0	0	$-6(11)^{\frac{1}{2}}$
${}_4{}^5(20)$	0	$-2(2/7)^{\frac{1}{2}}$	$2(33/7)^{\frac{1}{2}}$

which has the same tensorial properties as e_3; from (24) of III and (27) we have

$$\Omega=\tfrac{1}{2}L(L+1)-12G(G_2), \tag{77}$$

and therefore its matrix is diagonal in the UL scheme and has the eigenvalues

$$\omega(U, L)=\tfrac{1}{2}L(L+1)-12g(U). \tag{78}$$

We have from (67) that

$$e_3(f^2\,{}^3L)=-3\omega, \tag{79}$$

and since for every n

$$\Omega=66\sum_{i<j}((\mathbf{u}_i^{(1)}\cdot\mathbf{u}_j^{(1)})-(\mathbf{u}_i^{(5)}\cdot\mathbf{u}_j^{(5)})), \tag{80}$$

we obtain that for every term of f^n with maximal spin

$$e_3(f^{n\ n+1}L)=-3\omega(U, L). \tag{81}$$

The values of $c(WW'(220))$ are given in Table XII' but the results are much simpler than could be expected from that table. The calculations show that

$$(f^nvUSL|e_3+\Omega|f^nvU'SL)=a(n, v)(f^vvUSL|e_3+\Omega|f^vvU'SL), \tag{82}$$

$$(f^6\,{}_6L|e_3+\Omega|f^6\,{}_6L)=(f^7\,{}_7L|e_3+\Omega|f^7\,{}_7L)=0; \tag{83}$$

for $n\leqslant 7$ it is

$$\begin{aligned} a(v+2, v)&=(1-v)/(7-v),\\ a(v+4, v)&=-4/(7-v), \end{aligned} \tag{84}$$

and it may be noted that these equations satisfy the relation

$$\sum_v^{14-v}{}_n(f^nvUSL|e_3+\Omega|f^nvU'SL)=0. \tag{85}$$

The fact that $a(n, v)$ depends on v but not on S suggests that Eqs. (82) to (85) are connected with the properties of the symplectic group which leaves invariant the form (21), but the investigation of these properties is beyond the scope of this paper.

For $v\neq v'$ we found also

$$\begin{aligned} (f^5\,{}_1{}^2L|e_3|f^5\,{}_3{}^2L)&=(2/5)^{\frac{1}{2}}(f^3\,{}_1{}^2L|e_3|f^3\,{}_3{}^2L),\\ (f^6\,{}_0{}^1L|e_3|f^6\,{}_4{}^1L)&=(9/5)^{\frac{1}{2}}(f^4\,{}_0{}^1L|e_3|f^4\,{}_4{}^1L),\\ (f^6\,{}_2L|e_3|f^6\,{}_4L)&=(1/6)^{\frac{1}{2}}(f^4\,{}_2L|e_3|f^4\,{}_4L),\\ (f^7\,{}_1{}^2L|e_3|f^7\,{}_5{}^2L)&=(3/2)^{\frac{1}{2}}(f^5\,{}_1{}^2L|e_3|f^5\,{}_5{}^2L). \end{aligned} \tag{86}$$

The values of $c(UU'(22))$ are given in Table XIII, but the calculations show that also when $c(UU'(22))>1$ we can write without any exception

$$(f^nvUSL|e_3+\Omega|f^nv'U'SL)=y(f^n, vSU, v'SU')(U|\varphi(L)|U'). \tag{87}$$

The functions $(U|\varphi(L)|U')$ are tabulated in Tables XIV, the values of $y(f^n, vSU, v'SU')$ which do not follow from (81), (82), (83), or (86) are given in Tables XV–XXIV.

TABLE XXI. $y(f^6, {}_v{}^3U, {}_6{}^3U')$.

	${}_6{}^3(10)$	${}_6{}^3(11)$	${}_6{}^3(20)$	${}_6{}^3(21)$	${}_6{}^3(30)$	${}_6{}^3(31)$
${}_2{}^3(10)$	0	0	0	$-48(2/5)^{\frac{1}{2}}$	0	-36
${}_2{}^3(11)$	0	$(6/5)^{\frac{1}{2}}$	0	0	$\sqrt{3}$	$3(13/10)^{\frac{1}{2}}$
${}_4{}^3(10)$	0	0	0	$46/(15)^{\frac{1}{2}}$	0	$-8(6)^{\frac{1}{2}}$
${}_4{}^3(11)$	0	$11/3(5)^{\frac{1}{2}}$	0	0	$-19/3\sqrt{2}$	$(13/60)^{\frac{1}{2}}$
${}_4{}^3(20)$	0	0	$-6\sqrt{2}/7$	$-22/7\sqrt{3}$	$8(2/3)^{\frac{1}{2}}$	0
${}_4{}^3(21)$	$-(110/3)^{\frac{1}{2}}$	0	$(22/147)^{\frac{1}{2}}$	$-16/21(11)^{\frac{1}{2}}$	$5/3\sqrt{2}$	$1/(22)^{\frac{1}{2}}$
${}_6{}^3(30)$	0	$-(5)^{\frac{1}{2}}/3$	$4(2/3)^{\frac{1}{2}}$	$4/3(11)^{\frac{1}{2}}$	$1/3\sqrt{2}$	$-1/(22)^{\frac{1}{2}}$

TABLE XXII. $y(f^0, {}_2{}^1U, {}_6{}^1U')$.

	${}_6{}^1(00)$	${}_6{}^1(10)$	${}_6{}^1(20)$	${}_6{}^1(30)$	${}_6{}^1(40)$
${}_2{}^1(20)$	0	0	$6/(55)^{\frac{1}{2}}$	$2(42/5)^{\frac{1}{2}}$	$6(2/55)^{\frac{1}{2}}$
${}_4{}^1(20)$	0	0	$-61/(770)^{\frac{1}{2}}$	$8(3/5)^{\frac{1}{2}}$	$-6/(385)^{\frac{1}{2}}$
${}_4{}^1(21)$	0	$3(22)^{\frac{1}{2}}$	$(2/7)^{\frac{1}{2}}$	$-\sqrt{3}$	$1/(7)^{\frac{1}{2}}$
${}_4{}^1(22)$	$-4(33/5)^{\frac{1}{2}}$	0	$-1/(22)^{\frac{1}{2}}$	0	$2/(11)^{\frac{1}{2}}$

TABLE XXIII. $y(f^1, {}_3{}^4U, {}_7{}^4U')$.

	${}_7{}^4(20)$	${}_7{}^4(21)$	${}_7{}^4(22)$
${}_3{}^4(00)$	0	0	$-12(11)^{\frac{1}{2}}$
${}_3{}^4(10)$	0	$6(33)^{\frac{1}{2}}$	0
${}_3{}^4(20)$	$-(5/7)^{\frac{1}{2}}$	$2(11/7)^{\frac{1}{2}}$	-1

TABLE XXIV. $y(f^1, {}_3{}^2U, {}_7{}^2U')$.

	${}_7{}^2(00)$	${}_7{}^2(10)$	${}_7{}^2(20)$	${}_7{}^2(30)$	${}_7{}^2(40)$
${}_3{}^2(11)$	0	0	0	$2(10)^{\frac{1}{2}}$	0
${}_3{}^2(20)$	0	0	$-16/(77)^{\frac{1}{2}}$	$-2(6)^{\frac{1}{2}}$	$6(2/77)^{\frac{1}{2}}$
${}_3{}^2(21)$	0	$-(66)^{\frac{1}{2}}$	$(6/7)^{\frac{1}{2}}$	1	$(3/7)^{\frac{1}{2}}$

From (71) and from the orthogonality between the functions $\psi((00)S)$, $\psi((40)S)$, and $\psi((22)S)$ follow the relations

$$\sum_L(2L+1)(U|\chi(L)|U) = \sum_L(2L+1)(U|\varphi(L)|U)=0 \quad (88)$$

and

$$\sum_L(2L+1)(U|\chi(L)|U')(U'|\varphi(L)|U)=0, \quad (89)$$

which were useful for checking Tables VI and XIV.

PHYSICAL REVIEW VOLUME 76, NUMBER 9 NOVEMBER 1, 1949

The Moment of Inertia and Electric Dipole Moment of CsF from Radiofrequency Spectra*

J. W. TRISCHKA**
Columbia University, New York, New York

(Received July 1, 1949)

The electric resonance method of molecular beam spectroscopy was used to obtain spectra resulting from induced changes in the space-quantization of the rotational state $J=1$ of CsF in a homogeneous electric field. An analysis of the spectra for several values of the field intensity and for two different vibrational states gave the following molecular constants, $I_e=(151\pm6)10^{-40}$ g cm², $\mu_e=(7.88\pm0.17)10^{-18}$ e.s.u., $B_e=(185\pm7)10^{-3}$ cm^{-1}, $\alpha_e=(1.85\pm0.19)10^{-3}$ cm^{-1}, $r_e=(2.34\pm0.05)10^{-8}$ cm, $\omega_e=270\pm30$ cm^{-1}. I_e is the moment of inertia, μ_e is the electric dipole moment, B_e and α_e are rotational constants, r_e is the internuclear distance and ω_e is the vibrational constant.

THE molecular beam electric resonance method[1] yields spectra in the radiofrequency region resulting from changes in the space-quantization of a single rotational state of the molecule when the molecule passes through a homogeneous electric field, upon which is superposed a weak, transverse, oscillating field. In previous experiments with CsF determinations were made of the moment of inertia and electric dipole moment,[1] and of several nuclear-molecular interaction constants.[2] In this paper the results of further experiments with CsF under the high resolution conditions described in reference 2 are presented. The moment of inertia and electric dipole moment are redetermined with considerably greater accuracy and additional constants are obtained from a study of the vibrational effects.

The apparatus has been described in detail elsewhere.[1,2] The spectra were observed by fixing the frequency of the oscillating electric field and varying the magnitude of the steady, homogeneous field, a valid method of observation if the electric field intensity is sufficiently strong,[2] as was the case in the present experiments. Frequency was measured to 1 part in 10,000 with a General Radio Type 624A heterodyne frequency meter, which had been checked against standard frequencies broadcast by WWV. The electric field intensity in the homogeneous field was calculated from the potential drop across the field and the distance between the parallel plates forming the field boundaries.[3] "B" batteries were used as a voltage supply. A Type K potentiometer, connected to a calibrated volt box, was used to measure voltage to 1 part in 5000. The standard cell of the potentiometer was checked with another cell recently calibrated at the Bureau of Standards. No effects due to thermal e.m.f.'s were observed.

All voltage readings were corrected for the contact potential difference between the plates of the homogeneous field. This quantity was measured by making a run with the applied field intensity in one direction,

* Publication assisted by the Ernest Kempton Adams Fund for Physical Research of Columbia University.

** Now at Syracuse University, Syracuse, New York.

[1] H. K. Hughes, Phys. Rev. 72, 614 (1947).

[2] J. W. Trischka, Phys. Rev. 74, 718 (1948).

[3] There is a typographical error in the value of the field gap reported in reference 2. The distance between the plates was 0.4931 ± 0.0004 cm.

TABLE I. Quantities required for the calculation of μ and I for the first two vibrational states.

ν (mc/sec.)	E (volts/cm)	$E^2\times10^{-4}$	ν/E^2
	$v=0$		
18.180	206.15	4.2498	427.78±0.39
44.460	322.67	10.412	427.01±0.35
94.520	471.57	22.238	425.04±0.41
189.53	670.49	44.956	421.59±0.32
297.37	843.80	71.200	417.65±0.31
	$v=1$		
18.021	202.78	4.1121	438.24±0.34
94.520	465.81	21.698	435.62±0.38
297.37	833.68	69.502	427.86±0.30

then a second run with the field in the opposite direction. The contact potential difference found as a result of several such runs at several different applied field intensities was 0.07±0.01 volt.

LINE POSITIONS

The transitions observed for CsF with the electric resonance apparatus at strong field intensities were between the states $m_J=0$ and $m_J=\pm1$ for the rotational state $J=1$. The nature and theory of the spectra have been discussed in detail in references 1 and 2. For the purposes of the present paper the positions of the spectral lines may be represented by

$$\nu'=\nu+\nu_n,$$

where ν is the frequency corresponding to the transitions between states given by the $\mu\cdot E$ term in the Hamiltonian, and ν_n is the shift from ν produced by the nuclear-molecular interactions. μ is the electric dipole moment and E is the electric field intensity. If the electric field intensity is such that

$$e^2q'Q\ll\lambda^2\hbar^2/2I\ll J(J+1)(\hbar^2/2I), \qquad (1)$$

ν_n is, within present experimental error, independent of the field intensity. $e^2q'Q$ is a measure of the nuclear quadrupole interaction, I is the moment of inertia, and $\lambda=\mu E/(\hbar^2/2I)$.

In order to calculate μ and I it is necessary first to determine ν. Since ν_n is known for the CsF spectra,[2] this calculation is hindered only by the fact that the fine-structure produced by ν_n is unresolved at the values of E required for an accurate determination. Thus, for the transition $(1, 0)\rightarrow(1, \pm1)$, a single line is observed for molecules in a given vibrational state. In the absence of an exact knowledge of the shape of the spectral window the shape of this line could not be accurately predicted from the known fine-structure. Fortunately, an accurate prediction was not necessary because of the relatively small extent, 500 kc/sec., of the fine-structure. Therefore, two extreme estimates of the line shape were made, one estimate based on a rectangular spectral window, the other on a triangular window. With these estimates as a guide the following scheme was decided on as the best one for finding the position of ν: the outermost lines of the fine structure were assumed to be equidistant from the sides of the experimental line at one-third its maximum intensity.

Since the experimental lines were actually a result of the variation of beam intensity with changes in E', while the frequency was held constant, the quantity actually found by the above procedure was E. This required no essential change in the scheme described above because the extent of the fine-structure was always small compared with the frequencies at which observations were made.

Table I shows the calculated values of E and the corresponding frequencies. The determination of the value of E at 18 mc/sec. was made by a method different from that described above. At this frequency there was sufficient resolution to use one of the fine-structure lines as a basis for finding ν. Calculations were made to insure that the observations met the conditions specified by Eq. (1).[4]

CALCULATION OF μ AND I

The best representation of the data in Table I is in a plot of ν/E^2 *versus* E^2. Such a plot of the data results in the straight line

$$\nu/E^2=a-bE^2. \qquad (2)$$

This corresponds in form to Brouwer's theoretical formula,[1,5] but closer study reveals that for the values of λ covered in these experiments Lamb's exact formula[1] must be employed. Since the experimental results are best summarized by Eq. (2), the following, linear, least-squares approximation to Lamb's curve was made for the range $\lambda=0.1$ to $\lambda=0.6$.

$$\Delta\epsilon/\lambda^2=0.14998-0.01031\lambda^2, \qquad (3)$$

where $\epsilon=h\nu/(\hbar^2/2I)$ and $\Delta\epsilon=\epsilon_{1,0}-\epsilon_{1,\pm1}$.[6]

The values of the constants in Eq. (2) and of the molecular constants obtained by use of Eqs. (2) and (3) are given in Table II.[7] The values of a and b were determined from the least-squares line fitting the data in Table I.

TABLE II. Molecular constants for the first two vibrational states.

v	0	1
I, 10^{-40} g cm^2	152±6	152±7
μ, 10^{-18} e.s.u.	7.89±0.17	7.98±0.18
μ^2I, 10^{-76}	9443±28	9674±30
a	428.48±0.26	438.98±0.30
b, 10^{-5}	1.52±0.06	1.60±0.07

[4] The author wishes to thank Dr. M. Slotnick for making these calculations.

[5] F. Brouwer, dissertation (Amsterdam, 1930).

[6] Hughes has recently made a detailed comparison of the Lamb and Brouwer formulas for the transition $(1, 0)\rightarrow(1, \pm1)$. See H. K. Hughes, to be submitted for publication in Phys. Rev.

[7] The field intensity in Table I is in international volts/cm. It was necessary, therefore, to convert to absolute volts, using the relation: 1 international volt=1.00034 absolute volts (Circular C459 of the National Bureau of Standards, 1947). The conversion formula 1 statvolt=299.796 absolute volts was also used.

EFFECT OF VIBRATION

The values of I, μ and $\mu^2 I$ in Table II must be interpreted as the result of averaging over the vibration.[2] This means that for a given vibrational state I and μ should be denoted by I_v and μ_v, where[8]

$$I_v = m/\langle 1/r^2 \rangle_{Av}, \tag{4}$$

and, to a first approximation

$$\mu_v = e_{\text{eff}} \langle r \rangle_{Av}. \tag{5}$$

r is the internuclear distance at any instant during the vibration, and e_{eff} is, by definition, the effective charge.

Knowing I_v and μ_v for two vibrational states it should be possible to calculate I_e and μ_e, the values of I and μ for the hypothetical state of no vibration. In addition, the small constant, α_e, could then be computed from the equation[9]

$$B_v = B_e - \alpha_e(v+\tfrac{1}{2}), \tag{6}$$

where B is the rotational constant. Finally, it should then be possible to calculate the coefficient, g, of the cubic term in the potential function from[10]

$$\alpha_e = 24 B_e^3 r_e^3 g/\omega_e^3 - 6B_e^2/\omega_e. \tag{7}$$

At present g can be found with an accuracy of about ± 40 percent because of the poor accuracy of ω_e, the vibrational constant.[2]

An examination of Table II shows that the errors in μ_v and I_v are too large to allow their use in a direct calculation of I_e, μ_e, α_e or g. Therefore, the calculation of these quantities must proceed in a more roundabout way from the values of I_v and μ_v, and from the difference between $\mu_0^2 I_0$ and $\mu_1^2 I_1$.

Because $\mu_v^2 I_v$ involves the averaging over a vibration of both μ and I it is not at once clear what will be the individual contributions of μ and I in the process. To clarify this question we can state to a first approximation that

$$\Delta\mu_v^2 I_v/\mu_0^2 I_0 = 2\Delta\mu_v/\mu_e + \Delta I_v/I_e, \tag{8}$$

where the Δ symbolizes the difference between the values of a quantity for $v=1$ and $v=0$. From Eqs. (4) and (5) we deduce

$$\Delta\mu_v/\mu_e = \Delta\langle r - r_e\rangle_{Av}/r_e, \tag{9}$$

and, approximately,

$$\Delta I_v/I_e = \Delta\langle 1/r^2\rangle_{Av}/(1/r_e^2). \tag{10}$$

From Eqs. (6) and (10) we can then conclude that, approximately,

$$\Delta I_v/I_e = \alpha_e/B_e = 2\Delta\langle r - r_e\rangle_{Av}/r_e - 3\Delta\langle (r-r_e)^2\rangle_{Av}/r_e^2. \tag{11}$$

But this is the basis for the calculations leading to Eq. 7. Hence, from Eqs. (7), (8), (9) and (11), we obtain

$$\alpha_e/B_e = \Delta\mu_v^2 I_v/2\mu_0^2 I_0 - 3B_e/\omega_e. \tag{12}$$

Substituting B_0 for B_e in Eq. (12), a first approximation to α_e results. Using this value the errors introduced by the various approximations can be corrected and a final value of α_e achieved. From this point on the calculation of the other constants for the "state" of no vibration is simple.

Table III shows the constants deduced from the CsF spectra. The value of ω_e, already reported in reference 2, is included for completeness. Results computed from the two vibrational states were averaged to give the values in the table.

TABLE III. Moecular constants of CsF.

Quantity	Value
I_e, 10^{-40} g cm^2	151±6
μ_e, 10^{-18} e.s.u.	7.88±0.17
B_e, 10^{-3} cm^{-1}	185±7
α_e, 10^{-3} cm^{-1}	1.85±0.19
r_e, 10^{-8} cm	2.34±0.05
ω_e, cm^{-1}	270±30

EXPERIMENTAL ERRORS

The experimental errors in the quantities reported in Tables I, II, and III arise from two kinds of errors, systematic errors and random errors. The separation of errors into these two categories was made on the following basis. Errors which were common to all the values of ν/E^2 in Table I were called systematic errors, since they could be taken into account after a and b were determined. Errors which did not have this property were called random errors.

The most important systematic error was that in the magnitude of the field gap. This error was conservatively considered as the sum of the error in the length of the spacers separating the plates of the field, ±0.04 percent, and the deviation from planeness of the plates, ±0.05 percent. The error in the contact potential difference between the plates of the homogeneous field was considered to be a systematic error for the vibrational state $v=1$ and a random error for $v=0$. This situation occurred because the applied field intensities were in the same direction for all of the measurements for $v=1$, whereas, this was not the case for $v=0$.

The random errors were the error in the voltage measurement, ±0.02 percent, the error in frequency measurement, ±0.01 percent, and the error in the estimation of line position, ±0.01 percent on the average.

The errors given for ν/E^2 in Table I are the sum of the propagated random errors. No errors in E^2 are shown since the errors in this quantity have a negligible effect on the values of a and b. The errors in a and b in Table II were computed by applying the least-squares law of propagation of errors to the least-squares

[8] Gerhard Herzberg, *Molecular Spectra and Molecular Structure* (Prentice-Hall, Inc., New York, 1939), p. 113.
[9] G. Herzberg, reference 8, p. 114.
[10] E. Teller, Hand-u Jahrb. d. chem. Phys. 9, II, 43 (1934). The formula is reprinted in Herzberg, reference 8, p. 116.

formulas for the slope and intercept of a straight line. The error in I in Table II came entirely from the errors in a and b, since the absolute value of the field intensity is not required to find I. The error in μ in this table includes errors in a and b and the error in the field gap. The error in $\mu^2 I$ is a result of the propagation of the errors in a, in the field gap, and in Planck's constant, h.[11]

In Table III, r_e and B_e are derived from I_e and their errors result only from the error in this quantity. The errors in I_e and μ_e are the same as the errors in I_v and μ_v, since negligible error is introduced by the error in α_e. The errror in α_e is a result of the propagation of the errors in B_e, ω_e, and $\Delta\mu^2 I/\mu_0^2 I_0$. In computing the error in the last mentioned quantity only random errors need be taken into account. Furthermore, the error in the volt box, which produces part of the random error in $\mu^2 I$, will not appear here since the data for both vibrational states was taken with the same setting of the volt-box. Hence, $\Delta\mu^2 I/\mu_0^2 I_0 = 231 \pm 6$. An error comparable to this is introduced in α_e/B_e by the term $3B_e/\omega_e$, so that $\alpha_e/B_e = (10.0 \pm 0.6)10^{-3}$. Multiplication of this quantity by B_e gives α_e.

DISCUSSION

The constant r_e in Table III is of considerable interest because it is at such wide variance with the value 2.67A computed from the empirical formula of Schomaker and Stevenson.[1,12] Since their formula gives agreement within a few percent with the experimental values for other alkali halides, including some Caesium halides,[13] CsF appears to be a striking exception. The peculiar nature of CsF is made more emphatic by the fact that its interatomic distance is less than that for CsH,[14] for which $r_e = 2.49$A.

A rough check on the present experiments can be obtained by a comparison with the results of Hughes,[1,6] who found $r = 2.55 \pm 0.16$A. Because of his low resolution his value corresponds to a distance somewhere between the interatomic distances for the first and second vibrational states, for which $r_0 = 2.35$A and $r_1 = 2.36$A, according to the present experiments. There is, then, agreement within experimental error.

In view of the seemingly anomalous value of r_e and the small overlapping with Hughes' value the work reported here was very carefully reviewed for errors, and several additional runs were made to check the data. The evidence for the correct identification of the rotational state has already been presented.[2] The value of I_e, from which r_e is computed, depends only on relative values of the electric field intensity. Hence, any systematic errors in E drop out.

As a check on the assumptions made in the theory of the experiment, order of magnitude calculations were made for the effect of distortion of the molecular electrons by the electric field and for the effect of the field on the vibrational states. Both effects were found to be entirely negligible.

The amount of ionic character, defined by μ/r_e, e being the electronic charge, is 70 percent.

The author is indebted to Professor I. I. Rabi for his helpful interest in these experiments. The help of Messrs. L. Grabner and S. Jacobson in the laboratory is gratefully acknowledged.

[11] The value of h used in all calculations was $(6.6234 \pm 0.0011) \times 10^{-27}$ erg sec. [see J. W. M. DuMond and E. R. Cohen, Rev. Mod. Phys. **20**, 82 (1948)].

[12] Schomaker and Stevenson, J. Am. Chem. Soc. **63**, 37 (1941).

[13] Maxwell, Hendricks, and Mosley, Phys. Rev. **52**, 968 (1937).

[14] G. M. Almy and M. P. Rassweiler, Phys. Rev. **53**, 890 (1938).

PHYSICAL REVIEW VOLUME 76, NUMBER 9 NOVEMBER 1, 1949

On Realistic Field Theories and the Polarization of the Vacuum

DAVID FELDMAN*
The Institute for Advanced Study, Princeton, New Jersey
(Received July 27, 1949)

The formal prescription for the regularization of divergent expressions in quantum electrodynamics which has been recently suggested by Pauli implies very strongly that these same divergences may be similarly canceled in a realistic theory wherein one has a mixture of fields in the manner of Pais and Sakata. Indeed, it may be readily seen that the Pauli regulator scheme corresponds field-theoretically to a family of spinor fields interacting with a family of neutral vector meson fields; the formalism is mathematically consistent (at least to the second order in the coupling constants) but physically unsound owing to the appearance of imaginary coupling constants. An attempt to remedy this defect by considering the most general mixture which is possible within the framework of ordinary field theory also leads to failure. Specifically, the current density which is induced in the vacuum by an external electromagnetic field is calculated to order e^2 for a variety of situations but it turns out that no combination of charged scalar, spinor and vector fields—with or without anomalous magnetic moments—leads to a full compensation of the divergences although the photon self-energy by itself may be made to vanish. It is concluded that, although the notion of a realistic approach to the theory of elementary particles remains an attractive one, the usual linear field theories do not in themselves seem to be adequate for this purpose; there is also always the possibility that it is the perturbation theory which is at fault.

1. FORMALISTIC *VS.* REALISTIC THEORIES

IN a recent critique of some of the current procedures in quantum electrodynamics, Pauli[1] has emphasized that the present theory involves the handling of divergent and conditionally convergent integrals the evaluations of which cannot be inferred in an unambiguous way from the theory but must be defined in each instance. Pending the development of new concepts, he has suggested that one handle the divergences of the theory in a purely formal way by first regularizing all singular expressions and then performing a limiting process. Specifically, if $f(x, m)$ is a singular function depending on the space-time coordinate x_μ and the mass m, the regularized function $f_R(x)$ may be defined by the formula

$$f_R(x)=\Sigma c_i f(x, M_i) \tag{1}$$

with $c_0=1$, $M_0=m$. The coefficients c_i are subjected to the restrictions

$$\Sigma c_i=0, \tag{2}$$

$$\Sigma c_i M_i^2=0, \tag{2'}$$

and the limiting process consists in letting the auxiliary masses M_i $(i=1, 2, \cdots)$ tend to infinity. The conditions (2) and (2') are sufficient to insure that the functions $\bar{\Delta}_R$ and $\Delta_R^{(1)}$ are free of singularities on the light cone unlike their unregularized counterparts.[2] These conditions are also enough to lead to convergent expressions for the electron self-energy and the polarization of the vacuum by an external electromagnetic field (with a correspondingly vanishing photon self-energy) provided one additional rule is added, *viz.*, these expressions must be regularized as a whole and not in parts. Upon performing the final limiting process, logarithmic divergences reappear in the unobservable charge and mass renormalization factors for the electron (unless new conditions are imposed on the c_i's).

The above procedure constitutes, in the terminology of Pauli and Villars, a "formalistic theory" wherein a purely formal recipe for the performance of calculations is given, in contrast to a "realistic theory" in which the mathematical device which effects convergence—in the case at hand, it is the introduction of the auxiliary masses—is not an *ad hoc* affair but rather a consequence of physical concepts. By a "realistic theory" we shall mean, in particular, one which attempts to take into account **all** of the interactions of the elementary particles with one another. It is the aim of this paper to determine whether or not a realistic (though semi-phenomenological) description of elementary particles can be obtained within the domain of ordinary field theory. It is perhaps not surprising that the result will turn out to be negative.

The term "ordinary field theory" as we use it in this work is meant to denote the canonical formalism of Heisenberg and Pauli as applied to the quantization of the scalar Klein-Gordon equation, the Dirac equation and the Maxwell-Proca equations leading to a description of particles with spin zero, one-half and one respectively and with assorted masses and charges. In treating the interaction of these fields with one another, one must add to the vacuum Lagrangians additional terms which are required to be in accord with the general principles of relativistic and gauge invariance. For simplicity, however, one also imposes on the interaction terms the more special restrictions that they involve no derivatives of spinor field variables, no derivatives higher than the first of Bose field variables and, in either case, that they contain the field variables which characterize any one field no more than bilinearly. It need hardly be stressed that, in view of the divergent nature of these theories, all computations must be carried through in a manifestly covariant way; this is feasible at the present time only if the coupling between fields is assumed to be weak.

2. A FIELD-THEORETICAL INTERPRETATION OF THE REGULARIZATION PROCEDURE

In actual fact, the need for a realistic approach to quantum electrodynamics *per se* is much less acute than it seemed two years ago since the present theory works

* AEC Postdoctoral Research Fellow.

[1] W. Pauli, unpublished letter to J. Schwinger; W. Pauli and F. Villars, Rev. Mod. Phys. 21, 434 (1949).

[2] The Δ, $\bar{\Delta}$ and $\Delta^{(1)}$ functions which we use in this paper are as tabulated in the Appendix of reference 5.

well and the modifications to be expected of a future correct theory will surely be of an ultra-relativistic nature. On the other hand, it appears very unlikely that the corresponding problem of the interaction of nucleons and mesons can be solved except within a realistic framework and we assume, with Pais[3] and Sakata,[4] that only in a theory which takes into account the mutual interactions of all the elementary particles can one hope to eliminate the divergences; the essential limitation of the present investigation is contained in the fact that we have restricted ourselves to mixtures of ordinary type fields.

It is perhaps interesting to consider first a field-theoretical model which seems to be the most literal transcription of the Pauli regulator scheme but which contains important difficulties in its physical interpretation and hence cannot be taken too seriously from a realistic point of view. It has, on the other hand, the virtue of being mathematically consistent and completely convergent (at least to the second order in the coupling constants) and does seem to explain the apparent arbitrariness of the regularization procedure.

It is most natural to regard the auxiliary masses which are involved in the regulator functions and which accordingly play a mathematical role only as being associated with real additional fields; we consider, therefore, the case of a family of spinor fields (including the electron field) interacting with a family of neutral vector Bose fields (including the photon field) with vector coupling linking each spinor and Bose field. One then finds, to the second order in the coupling constants, that all the particle self-energies converge as well as the current densities induced in the vacuum by external electromagnetic and mesonic fields provided certain simple relations exist among the masses and coupling constants which bear a close resemblance to conditions (2) and (2′). The photon self-energy is zero.

For simplicity, let us assume that we have, besides the electron field, two additional spinor fields and, besides the photon field, one additional Bose field. Let e_i, g_i and m_i denote the electric charge, mesonic charge and mass of the ith spinor field and let μ be the mass of the Bose particles. It then follows in a trivial way from the results of Schwinger[5] that one has for the current density induced in the vacuum by an external electromagnetic field described by the potential $A_\mu(x)$,[6]

$$\delta j_\mu(x)=i/2\cdot\int d\omega'\cdot\epsilon(x-x') \times\sum_{i=0}^{2}\langle[j_\mu(x,m_i),j_\nu(x',m_i)]\rangle_0 A_\nu(x') \quad (3)$$

with

$$j_\mu(x,m_i)=ie_i/2\cdot[\bar\psi(x,m_i)\gamma_\mu\psi(x,m_i) -\bar\psi'(x,m_i)\gamma_\mu\psi'(x,m_i)];$$

here, $\psi(x,m_i)$, $\bar\psi(x,m_i)$ and $\psi'(x,m_i)$, $\bar\psi'(x,m_i)$ are the field variables which describe the ith spinor and charge conjugate spinor fields respectively, $d\omega'$ is the four-dimensional element of volume and $\epsilon(x-x')$ is, as usual, $+1$ or -1 according as the space-like surface associated with x lies in the future or the past with respect to the corresponding surface associated with x'. It is then a consequence of the sufficiency of the regulator conditions (2) and (2′) that $\delta j_\mu(x)$ will converge and the photon self-energy will vanish provided

$$e_0^2+e_1^2+e_2^2=0, \quad e_0^2m_0^2+e_1^2m_1^2+e_2^2m_2^2=0. \quad (4)$$

In a similar way, for the mesonic current density induced in the vacuum by an external mesonic potential $U_\mu(x)$ one finds

$$\delta J_\mu(x)=i/2\cdot\int d\omega'\cdot\epsilon(x-x') \times\sum_{i=0}^{2}\langle[J_\mu(x,m_i),J_\nu(x',m_i)]\rangle_0 U_\nu(x') \quad (3')$$

with

$$J_\mu(x,m_i)=ig_i/2\cdot[\bar\psi(x,m_i)\gamma_\mu\psi(x,m_i) -\bar\psi'(x,m_i)\gamma_\mu\psi'(x,m_i)].$$

Both $\delta J_\mu(x)$ and correspondingly the self-energy of the neutral vector meson will converge if

$$g_0^2+g_1^2+g_2^2=0, \quad g_0^2m_0^2+g_1^2m_1^2+g_2^2m_2^2=0. \quad (4')$$

Finally, for the self-energy density operator of the ith spinor particle $\mathfrak{K}^{(i)}$, one has

$$\mathfrak{K}^{(i)}=1/2\cdot[\bar\psi^{(i)}(x)\chi^{(i)}(x)+\text{charge conjugate}], \quad (5)$$

where $(\partial_\lambda\equiv\partial/\partial x_\lambda)$

$$\begin{aligned}\chi^{(i)}(x)&=e_i^2\int d\omega'\{\bar D(x-x')(\gamma_\lambda\partial_\lambda+2m_i)\Delta^{(1)}(x-x',m_i^2)\\&+D^{(1)}(x-x')(\gamma_\lambda\partial_\lambda+2m_i)\bar\Delta(x-x',m_i^2)\}\psi^{(i)}(x')\\&+g_i^2\int d\omega'\{\bar\Delta(x-x',\mu^2)(\gamma_\lambda\partial_\lambda+2m_i)\Delta^{(1)}(x-x',m_i^2)\\&+\Delta^{(1)}(x-x',\mu^2)(\gamma_\lambda\partial_\lambda+2m_i)\\&\times\bar\Delta(x-x',m_i^2)\}\psi^{(i)}(x'). \quad (5')\end{aligned}$$

This converges if

$$e_i^2+g_i^2=0, \quad (6)$$

whence it is clear that one may set

$$g_i=ie_i \quad (6')$$

[3] A. Pais, "On the theory of elementary particles," Verh. Kon. Ac. Amsterdam, Vol. 19 (1947).
[4] S. Sakata, Prog. Theor. Phys. 2, 145 (1947).
[5] J. Schwinger, Phys. Rev. 75, 651 (1949).
[6] We employ natural units throughout with $\hbar=c=1$. The symbol $\langle F\rangle_0$ denotes the vacuum expectation value of F.

which is fully compatible with the earlier restrictions (4) and (4′). We wish also to remark that the self-stress of the ith spinor particle vanishes in this formalism; one gets for $S=\int T_{11}d^3x$ evaluated for a particle at rest the value $m_i/2\pi\cdot(e_i^2+g_i^2)/4\pi$ which eqaals zero by (6).[1,7]

We observe that in order to obtain convergence in this scheme it has been found necessary to employ imaginary coupling constants. This has the consequence that the Hamiltonian is not Hermitian and probability is not conserved. The physical meaning of the present formalism is hence obscure unless a limiting process is performed, in which case the whole affair reduces to a purely formal prescription for performing calculations.

It is interesting to see what this formalism (which is suggested by the use of regulators in quantum electrodynamics in problems of order e^2) implies for the kind of regularization to be used for transitions of higher order. One infers that all internal photon lines are to be regulated separately; also, that each closed electron loop is to be regulated as a single unit (the terminology "internal photon line" and "closed electron loop" is that associated with the Feynman diagram).[8] It is clear that one will lose the gauge invariance of the theory by regulating independently the individual segments which constitute a closed electron loop for charge would be no longer conserved in detail. The simplest case of a closed electron loop occurs in the calculation of the polarization of the vacuum where one must regularize the expression as a whole.[1,9]

3. THE POLARIZATION OF THE VACUUM

We ask finally the question: Can one obtain a mathematically and indeed physically consistent picture of elementary particles by the expedient of mixing ordinary fields? To answer this question, it turns out to be sufficient to consider the polarization of the vacuum by an external electromagnetic field. The requirements of gauge invariance somewhat restrict the number of possible situations which need to be investigated and we have accordingly considered the cases of an electromagnetic field interacting with a scalar field, with a spinor field (with vector and tensor coupling) and with a vector field (with vector and tensor coupling). (The first two of these five possibilities have already been extensively treated in the literature,[1,5,10] but we include them here for the sake of comparison. We must also remark that we have not considered the cases of particles with spin higher than one or the case of charged massless vector mesons—these remain as real though perhaps academic possibilities.)

The basic theory which has been used is that of Schwinger[5] except as modifications have become necessary whenever one has had to transcribe an expression containing time derivatives from the Schrödinger to the interaction representation.[11] The equation of motion in the interaction representation assumes the form

$$i\delta\Psi[\sigma]/\delta\sigma=\mathfrak{H}(x,\sigma)\Psi[\sigma], \tag{7}$$

where $\Psi[\sigma]$ is the state vector of the system and $\mathfrak{H}(x,\sigma)$ is the Hamiltonian density for the interaction between one of the fields in question and the external electromagnetic field. To the first order in the coupling constant, one may then write for the solution of (7)

$$\Psi[\sigma]=\left(1-i\int_{-\infty}^{\sigma}\mathfrak{H}(x',\sigma')d\omega'\right)\Psi[-\infty],$$

where $\Psi[-\infty]$ is the state vector which characterizes the initially undisturbed vacuum state of the system. For the induced current density $\delta j_\mu(x)$ one then finds

$$\begin{aligned}\delta j_\mu(x)&=(\Psi[\sigma],\, j_\mu(x,\sigma)\Psi[\sigma])-\langle(j_\mu(x,\sigma))_{A=0}\rangle_0\\&=\langle j_\mu(x,\sigma)-(j_\mu(x,\sigma))_{A=0}\rangle_0\\&\qquad -i\int_{-\infty}^{\sigma}\langle[j_\mu(x,\sigma),\mathfrak{H}(x',\sigma')]\rangle_0 d\omega'.\end{aligned} \tag{8}$$

We have used the notation $j_\mu(x,\sigma)$ in the right-hand side to emphasize that the operator which enters into (8) must be appropriate to the interaction representation. We remark, however, that, since we are interested in corrections to the current density of order e^2, it is only the linear part of the Hamiltonian $\mathfrak{H}_1(x')$, say, which is relevant, and indeed it is only the linear part of the current density operator, say, $j_\mu(x)$ which enters into the commutator. Furthermore, we discard that part of $\langle j_\mu(x,\sigma)\rangle_0$ which does not involve the external field. Assuming, finally, that the external electromagnetic field cannot create pairs, we may rewrite (8) somewhat more conveniently, *viz.*,

$$\begin{aligned}\delta j_\mu(x)&=\langle j_\mu(x,\sigma)-(j_\mu(x,\sigma))_{A=0}\rangle_0\\&\qquad -i/2\cdot\int\langle[j_\mu(x),\mathfrak{H}_1(x')]\rangle_0\epsilon(x-x')d\omega'.\end{aligned} \tag{8′}$$

We consider the application of (8′) to the several individual cases.

(*a*) *Charged scalar field.* Let $U(x)$ and $U^*(x)$ be the field variables which characterize the charged scalar field and let $A_\mu(x)$ denote the unquantized potential in

[7] A. Pais and S. T. Epstein, Rev. Mod. Phys. **21**, 445 (1949).
[8] F. J. Dyson, Phys. Rev. **75**, 486 (1949).
[9] J. Rayski, Phys. Rev. **75**, 1961 (1949).
[10] A. Pais and G. E. Uhlenbeck, Phys. Rev. **75**, 1321 (1949); Umezawa, Yukawa, and Yamada, Prog. Theor. Phys. **3**, 317 (1948), **4**, 25 (1949); R. Jost and J. Rayski, Helv. Phys. Acta, in press. We have recently learned from Professor H. Yukawa that H. Umezawa and R. Kawabe (Prog. Theor. Phys., in press) have also examined the case of vector mesons with vector coupling using basically non-covariant methods with results that are essentially in agreement with ours; in particular, they are led to impose the same conditions that we do (Eqs. (29) and (29′)) to insure the vanishing of the photon self-energy.

[11] S. Kanesawa and S. Tomonaga, Prog. Theor. Phys. **3**, 1, 101 (1948).

terms of which the external electromagnetic field is described. The external current $J_\mu(x)$ is then given by $J_\mu(x)=-(\delta_{\mu\nu}\Box-\partial_\mu\partial_\nu)A_\nu(x)$. The Lagrangian density for a charged scalar field interacting with an external electromagnetic field is[12]

$$\mathfrak{L}=-D_\mu^*U^*\cdot D_\mu U-m^2U^*U,$$

where $D_\mu=\partial_\mu-ieA_\mu$, $D_\mu^*=\partial_\mu+ieA_\mu$; one then finds for the charge-current four vector s_μ which is associated with the above Lagrangian

$$s_\mu=\delta\int\mathfrak{L}d\omega/\delta A_\mu=ie(D_\mu^*U^*\cdot U-U^*D_\mu U).$$

On going over to the interaction representation one has

$$\left.\begin{aligned}\mathfrak{IC}_1&=-ie(\partial_\mu U^*\cdot U-U^*\partial_\mu U)A_\mu,\\ j_\mu&=ie(\partial_\mu U^*\cdot U-U^*\partial_\mu U)-2e^2U^*U(A_\mu+n_\mu n_\nu A_\nu),\end{aligned}\right\}(9)$$

where $n_\mu(x)$ is the unit normal to the spacelike surface σ at the point x ($n_\mu^2=-1$). After a brief calculation wherein one employs the relations

$$\left.\begin{aligned}[U(x),\,U^*(x')]&=[U^*(x),\,U(x')]=i\Delta(x-x'),\\ \langle U^*(x)U(x')+U^*(x')U(x)\rangle_0&=\Delta^{(1)}(x-x'),\end{aligned}\right\}(10)$$

one finds from (8′) and (9) that

$$\delta j_\mu(x)=-e^2\int K_{\mu\nu}(x-x')A_\nu(x')d\omega',\qquad(11)$$

where

$$\begin{aligned}K_{\mu\nu}=&-\partial_\mu\Delta^{(1)}\cdot\partial_\nu\bar\Delta-\partial_\nu\Delta^{(1)}\cdot\partial_\mu\bar\Delta\\&+\partial_\mu\partial_\nu\Delta^{(1)}\cdot\bar\Delta+\Delta^{(1)}\cdot\partial_\mu\partial_\nu\bar\Delta\\&+\delta_{\mu\nu}(-\Delta^{(1)}\cdot\Box\bar\Delta-\Box\Delta^{(1)}\cdot\bar\Delta+2m^2\Delta^{(1)}\bar\Delta).\end{aligned}\qquad(11')$$

The induced current density no longer involves the timelike normals $n_\mu(x)$ which is as it should be, cancellation of the surface-dependent terms having been effected by use of the identity

$$\begin{aligned}-1/2\cdot\int d\omega'F(x,x')\partial_\mu\epsilon(x-x')\cdot\partial_\nu\Delta(x-x')\\=n_\mu(x)n_\nu(x)F(x,x).\end{aligned}\qquad(12)$$

As has been emphasized by Jost and Rayski,[10] the induced current $\delta j_\mu(x)$ as given by (11) is by no means clearly gauge invariant; indeed, for gauge invariance one should have $\partial K_{\mu\nu}/\partial x_\nu=0$ but instead one finds $\partial K_{\mu\nu}/\partial x_\nu=2\delta(x)\partial_\mu\Delta^{(1)}$ which is undetermined.

A detailed evaluation of (11) wherein the method of integration is along the lines described in references 1* and 5 leads ultimately to the following expression ($\alpha=1/137$):

$$\begin{aligned}\delta j_\mu(x)=&-i\alpha/4\pi\\&\cdot\int_{-1}^{1}dy[\exp\{im^2z-iz/4\cdot(1-y^2)\Box\}/z]_{z=0}A_\mu(x)\\&-\alpha/24\pi\cdot g_2J_\mu(x)-\alpha/120\pi\cdot(\Box/m^2)J_\mu(x)\\&-\alpha/1680\pi\cdot(\Box/m^2)^2J_\mu(x)+\cdots.\end{aligned}\qquad(13)$$

In tabulating these and succeeding results, it has been convenient to employ the notations

$$\left.\begin{aligned}g_1&=1/im^2\cdot\int_{-\infty}^{\infty}\exp(im^2z)/z^2\cdot\epsilon(z)dz;\\ g_2&=\int_{-\infty}^{\infty}\exp(im^2z)/z\cdot\epsilon(z)dz,\end{aligned}\right\}\qquad(14)$$

where $\epsilon(z)=z/|z|$ and z is a scalar invariant with the dimensionality of a coordinate squared; it is then clear that I_1 diverges as $(1/z)_{z=0}$ or as the square of a momentum while I_2 goes as $(\log z)_{z=0}$. We shall reserve a discussion of (13) until later.

(*b*) *Charged spinor field with magnetic moment* $e/2m-e\delta$. Let $\psi(x)$, $\bar\psi(x)$ and $\psi'(x)$, $\bar\psi'(x)$ designate the spinor field and its charge conjugate field, respectively. It is then well known that the addition to the Lagrangian density

$$\begin{aligned}\mathfrak{L}=&-1/2\cdot\bar\psi(\gamma_\mu\partial_\mu+m)\psi-1/2\cdot\bar\psi'(\gamma_\mu\partial_\mu+m)\psi'\\&+ie/2\cdot(\bar\psi\gamma_\mu\psi-\bar\psi'\gamma_\mu\psi')A_\mu\end{aligned}$$

of a term of the form

$$\mathfrak{L}'=ie\delta/4\cdot(\bar\psi\sigma_{\mu\nu}\psi-\bar\psi'\sigma_{\mu\nu}\psi')F_{\mu\nu},$$

where $\sigma_{\mu\nu}=(\gamma_\mu\gamma_\nu-\gamma_\nu\gamma_\mu)/2$ and $F_{\mu\nu}=\partial_\mu A_\nu-\partial_\nu A_\mu$ is the external electromagnetic field, leads to an anomalous magnetic moment for the spinor particle amounting to $-e\delta$.[13] Indeed, the current density is now properly given by

$$\begin{aligned}s_\mu=\delta\int(\mathfrak{L}+\mathfrak{L}')d\omega/\delta A_\mu=&ie/2\cdot(\bar\psi\gamma_\mu\psi-\bar\psi'\gamma_\mu\psi')\\&-ie\delta/2\cdot\partial_\nu(\bar\psi\sigma_{\nu\mu}\psi-\bar\psi'\sigma_{\nu\mu}\psi').\end{aligned}$$

It seems to be of some importance to consider this possibility as a real one for there is no *a priori* reason why spin one-half particles (apart from the electron and positron) should be described without an anomalous magnetic moment term. It is a simple matter to determine the Hamiltonian density and the current density

[12] G. Wentzel, *Quantentheorie der Wellenfelder* (Deuticke, Wien, 1943).

* In performing the integrations, we have followed the convention of Pauli and Villars in assigning to $\int d^4k\cdot k_\mu k_\nu\exp(izk_\lambda^2)$ the value $-\delta_{\mu\nu}(\pi^2/2z^3)\epsilon(z)$ although it might seem just as appropriate to have written $-\delta_{\mu\nu}(\pi^2/2z^3)(\epsilon(z)-z\delta(z))$. In any case, it may be readily seen that the only essential effect of the inclusion of the $\delta(z)$ term is to modify all quadratic divergences in the same way so that none of our conclusions with respect to the compensation of the divergences are in any way affected.

[13] W. Pauli, Rev. Mod. Phys. **13**, 203 (1941).

in the interaction representation, *viz.*,

$$\mathcal{H}=\mathcal{H}_1=-ie/2\cdot(\bar{\psi}\gamma_\mu\psi-\bar{\psi}'\gamma_\mu\psi')A_\mu - ie\delta/4\cdot(\bar{\psi}\sigma_{\mu\nu}\psi-\bar{\psi}'\sigma_{\mu\nu}\psi')F_{\mu\nu}, \quad (15)$$

$$j_\mu=ie/2\cdot(\bar{\psi}\gamma_\mu\psi-\bar{\psi}'\gamma_\mu\psi')-ie\delta/2\cdot\partial_\nu(\bar{\psi}\sigma_{\nu\mu}\psi-\bar{\psi}'\sigma_{\nu\mu}\psi') -e^2\delta(\bar{\psi}\psi+\bar{\psi}'\psi')(A_\mu+n_\mu n_\nu A_\nu) -e^2\delta^2/4\cdot\{\bar{\psi}[\sigma_{\rho\lambda}(\gamma_\mu+n_\mu n_\nu\gamma_\nu)+(\gamma_\mu+n_\mu n_\nu\gamma_\nu)\sigma_{\rho\lambda}]\psi +\bar{\psi}'[\sigma_{\rho\lambda}(\gamma_\mu+n_\mu n_\nu\gamma_\nu) +(\gamma_\mu+n_\mu n_\nu\gamma_\nu)\sigma_{\rho\lambda}]\psi'\}F_{\rho\lambda}. \quad (15')$$

Equations (8'), (15), and (15') together with the relations

$$\left.\begin{aligned}[\psi_\alpha(x),\bar{\psi}_\beta(x')]_+&=-iS_{\alpha\beta}(x-x'),\\ \langle\bar{\psi}_\alpha(x)\psi_\beta(x')\rangle_0&=(S^{(1)}(x'-x)-iS(x'-x))_{\beta\alpha}/2\end{aligned}\right\} \quad (16)$$

lead ultimately to the following expressions for the induced current density. It is convenient to write $\delta j_\mu(x)$ as the sum of three parts, *viz.*,

$$\delta j_\mu(x)=\delta j_\mu{}^{(v)}(x)+\delta j_\mu{}^{(vt)}(x)+\delta j_\mu{}^{(t)}(x); \quad (17)$$

$\delta j_\mu{}^{(v)}(x)$ is the current density one would get if one had the vector interaction only between the spinor particle and the electromagnetic field (corresponding to an electric charge but no anomalous magnetic moment), $\delta j_\mu{}^{(t)}(x)$ is the current density one would get if one had the tensor interaction only (corresponding to an anomalous magnetic moment but no electric charge) and $\delta j_\mu{}^{(vt)}(x)$ is the cross term. Then

$$\delta j_\mu{}^{(v)}(x)=-e^2\int K_{\mu\nu}(x-x')A_\nu(x')d\omega', \quad (18)$$

where

$$K_{\mu\nu}=4[\partial_\mu\Delta^{(1)}\cdot\partial_\nu\bar{\Delta}+\partial_\nu\Delta^{(1)}\cdot\partial_\mu\bar{\Delta} -\delta_{\mu\nu}(\partial_\lambda\Delta^{(1)}\cdot\partial_\lambda\bar{\Delta}+m^2\Delta^{(1)}\bar{\Delta})]; \quad (18')$$

$$\delta j_\mu{}^{(vt)}(x)=8e^2\delta m\int\Delta^{(1)}(x-x')\bar{\Delta}(x-x')J_\mu(x')d\omega'; \quad (19)$$

$$\delta j_\mu{}^{(t)}(x)=4e^2\delta^2\int M_{\mu\rho\sigma}(x-x')F_{\rho\sigma}(x')d\omega', \quad (20)$$

where

$$M_{\mu\rho\sigma}=\partial_\nu[\delta_{\sigma\mu}(\partial_\nu\Delta^{(1)}\cdot\partial_\rho\bar{\Delta}+\partial_\rho\Delta^{(1)}\cdot\partial_\nu\bar{\Delta}) +\delta_{\nu\rho}(\partial_\sigma\Delta^{(1)}\cdot\partial_\mu\bar{\Delta}+\partial_\mu\Delta^{(1)}\cdot\partial_\sigma\bar{\Delta}) -\delta_{\nu\rho}\delta_{\mu\sigma}(\partial_\lambda\Delta^{(1)}\cdot\partial_\lambda\bar{\Delta}-m^2\Delta^{(1)}\bar{\Delta})]. \quad (20')$$

We observe once more that $\delta j_\mu(x)$ no longer involves surface-dependent terms, these having canceled in view of (12). We also note that, while $\delta j_\mu{}^{(v)}(x)$ is in fact not gauge invariant—indeed, as Pauli has pointed out,[1] $\partial K_{\mu\nu}/\partial x_\nu=-4\delta(x)\partial_\mu\Delta^{(1)}$—the introduction of tensor coupling does not lead to any new non-gauge invariant terms. This means that, insofar as the question of the photon self-energy is concerned, it is irrelevant whether or not we have tensor coupling.

Upon carrying through a more explicit evaluation, one finds eventually that

$$\delta j_\mu{}^{(v)}(x)=i\alpha/2\pi\cdot\int_{-1}^{1}dy[\exp\{im^2z-iz/4\cdot(1-y^2)\Box\}/z]_{z=0}A_\mu(x) -\alpha/6\pi\cdot g_2J_\mu(x)-\alpha/15\pi\cdot(\Box/m^2)J_\mu(x) -\alpha/140\pi\cdot(\Box/m^2)^2J_\mu(x)+\cdots, \quad (21)$$

$$\delta j_\mu{}^{(vt)}(x)=\alpha\delta m/\pi\cdot g_2J_\mu(x)+\alpha\delta m/3\pi\cdot(\Box/m^2)J_\mu(x) +\alpha\delta m/30\pi\cdot(\Box/m^2)^2J_\mu(x)+\cdots, \quad (21')$$

$$\delta j_\mu{}^{(t)}(x)=-\alpha\delta^2m^2/2\pi\cdot{}_2J_\mu(x) -\alpha\delta^2m^2/12\pi\cdot(g_2+2)(\Box/m^2)J_\mu(x) -\alpha\delta^2m^2/20\pi\cdot(\Box/m^2)^2J_\mu(x)+\cdots. \quad (21'')$$

(*c*) *Charged vector field with magnetic moment* $(1-\gamma)e/2m$. Let $U_\mu(x)$ and $U_\mu{}^*(x)$ be the field variables which characterize the charged vector field. Here, too, it is possible to add to the Lagrangian density[12]

$$\mathfrak{L}=-1/2\cdot(D_\mu{}^*U_\nu{}^*-D_\nu{}^*U_\mu{}^*)(D_\mu U_\nu-D_\nu U_\mu)-m^2U_\nu{}^*U_\nu$$

a term of the form

$$\mathfrak{L}'=ie\gamma/2\cdot(U_\mu{}^*U_\nu-U_\nu{}^*U_\mu)F_{\mu\nu};$$

this extra term leads to an alteration of the magnetic moment of the vector meson from $e/2m$ to $(1-\gamma)e/2m$.[13] There is again no obvious reason why the vector form of interaction should be favored over the tensor and we consider both possibilities. The current density which is associated with the total Lagrangian is given by

$$s_\mu=\delta\int(\mathfrak{L}+\mathfrak{L}')d\omega/\delta A_\mu =ie[U_\nu{}^*(D_\nu U_\mu-D_\mu U_\nu)-(D_\nu{}^*U_\mu{}^*-D_\mu{}^*U_\nu{}^*)U_\nu] -ie\gamma\partial_\nu(U_\nu{}^*U_\mu-U_\mu{}^*U_\nu).$$

On carrying through the transition to the interaction representation, one finds for the linear terms in the Hamiltonian density

$$\mathcal{H}_1=-ie(U_\nu{}^*f_{\nu\mu}-f_{\nu\mu}{}^*U_\nu)A_\mu -ie\gamma/2\cdot(U_\mu{}^*U_\nu-U_\nu{}^*U_\mu)F_{\mu\nu}, \quad (22)$$

where $f_{\nu\mu}=\partial_\nu U_\mu-\partial_\mu U_\nu$. The current density operator assumes much more formidable proportions (we keep

terms to e^2):

$$
\begin{aligned}
&j_\mu \\
&=\{ie(U_\nu^* f_{\nu\mu}-f_{\nu\mu}^* U_\nu) \\
&-e^2[(A_\mu U_\sigma^*-A_\sigma U_\mu^*)U_\sigma+U_\sigma^*(A_\mu U_\sigma-A_\sigma U_\mu)] \\
&-e^2 n_\mu n_\nu[(A_\nu U_\sigma^*-A_\sigma U_\nu^*)U_\sigma+U_\sigma^*(A_\nu U_\sigma-A_\sigma U_\nu)] \\
&-e^2 n_\sigma n_\nu[(A_\mu U_\nu^*-A_\nu U_\mu^*)U_\sigma+U_\sigma^*(A_\mu U_\nu-A_\nu U_\mu)] \\
&-e^2/m^2\cdot n_\lambda n_\nu(f_{\lambda\mu}^* f_{\nu\sigma}+f_{\nu\sigma}^* f_{\lambda\mu})A_\sigma \\
&-e^2\gamma/m^2\cdot n_\lambda n_\nu(f_{\nu\mu}^* U_\sigma+U_\sigma^* f_{\nu\mu})F_{\lambda\sigma}\} \\
&+\{-ie\gamma\partial_\nu(U_\nu^* U_\mu-U_\mu^* U_\nu) \\
&-e^2\gamma/m^2\cdot\partial_\lambda'[\{f_{\lambda\nu}^*(x')U_\mu(x)+U_\mu^*(x)f_{\lambda\nu}(x')\}A_\nu(x')]_{x=x'} \\
&-e^2\gamma n_\nu n_\lambda[U_\nu^*(A_\lambda U_\mu-A_\mu U_\lambda)+(A_\lambda U_\mu^*-A_\mu U_\lambda^*)U_\nu] \\
&-e^2\gamma/m^2\cdot n_\nu n_\lambda(f_{\sigma\lambda}^*\partial_\nu U_\mu+\partial_\nu U_\mu^*\cdot f_{\sigma\lambda})A_\sigma \\
&+e^2\gamma/m^2\cdot[(n_\mu n_\nu\partial_\rho'+n_\nu n_\rho\partial_\mu'+n_\rho n_\mu\partial_\nu'+2n_\mu n_\nu n_\rho n_\lambda\partial_\lambda') \\
&\cdot(\{U_\nu^*(x)f_{\sigma\rho}(x')+f_{\sigma\rho}^*(x')U_\nu(x)\}A_\sigma(x'))]_{x=x'} \\
&-e^2\gamma^2/m^2\cdot\partial_\lambda'[\{U_\nu^*(x')U(_\mu x)+U_\mu^*(x)U_\nu(x')\}F_{\lambda\nu}(x')]_{x=x'} \\
&-e^2\gamma^2/m^2\cdot n_\nu n_\rho(U_\sigma^*\partial_\nu U_\mu+\partial_\nu U_\mu^*\cdot U_\sigma)F_{\sigma\rho} \\
&-e^2\gamma^2/m^2\cdot[(n_\mu n_\nu\partial_\sigma'+n_\nu n_\sigma\partial_\mu'+n_\sigma n_\mu\partial_\nu'+2n_\mu n_\nu n_\sigma n_\lambda\partial_\lambda') \\
&\cdot(\{U_\nu^*(x)U_\rho(x')+U_\rho^*(x')U_\nu(x)\}F_{\sigma\rho}(x'))]_{x=x'}\}; \qquad (22')
\end{aligned}
$$

the first grouping of terms on the right-hand side of (22′) is the interaction representation transcription of the "vectorial" part of the current density with the second grouping corresponding to the "tensorial" part.

One may next calculate the induced current density $\delta j_\mu(x)$ using (8′), (22) and (22′) together with the relations

$$
\left.
\begin{aligned}
&[U_\mu(x), U_\nu^*(x')]=[U_\mu^*(x), U_\nu(x')] \\
&\qquad =i(\delta_{\mu\nu}-1/m^2\cdot\partial_\mu\partial_\nu)\Delta(x-x'), \\
&\langle U_\mu^*(x)U_\nu(x')+U_\nu^*(x')U_\mu(x)\rangle_0 \\
&\qquad =(\delta_{\mu\nu}-1/m^2\cdot\partial_\mu\partial_\nu)\Delta^{(1)}(x-x').
\end{aligned}
\right\} \qquad (23)
$$

It is again convenient to express $\delta j_\mu(x)$ as the sum of a pure vector part $\delta j_\mu{}^{(v)}(x)$, a pure tensor part $\delta j_\mu{}^{(t)}(x)$ and a cross term $\delta j_\mu{}^{(vt)}(x)$, i. e.,

$$
\delta j_\mu(x)=\delta j_\mu{}^{(v)}(x)+\delta j_\mu{}^{(vt)}(x)+\delta j_\mu{}^{(t)}(x), \qquad (24)
$$

where

$$
\delta j_\mu{}^{(v)}(x)=-e^2\int K_{\mu\nu}(x-x')A_\nu(x')d\omega' \qquad (25)
$$

with

$$
\begin{aligned}
K_{\mu\nu}=3[&-\partial_\mu\Delta^{(1)}\cdot\partial_\nu\bar{\Delta}-\partial_\nu\Delta^{(1)}\cdot\partial_\mu\bar{\Delta} \\
&+\partial_\mu\partial_\nu\Delta^{(1)}\cdot\bar{\Delta}+\Delta^{(1)}\cdot\partial_\mu\partial_\nu\bar{\Delta} \\
&+\delta_{\mu\nu}(-\Delta^{(1)}\cdot\Box\bar{\Delta}-\Box\Delta^{(1)}\cdot\bar{\Delta}+2m^2\Delta^{(1)}\bar{\Delta})] \\
&-2/m^2\cdot[\partial_\mu\partial_\nu\Delta^{(1)}\cdot\Box\bar{\Delta}+\Box\Delta^{(1)}\cdot\partial_\mu\partial_\nu\bar{\Delta} \\
&-\partial_\mu\partial_\rho\Delta^{(1)}\cdot\partial_\nu\partial_\rho\bar{\Delta}-\partial_\nu\partial_\rho\Delta^{(1)}\cdot\partial_\mu\partial_\rho\bar{\Delta} \\
&+\delta_{\mu\nu}(\partial_\rho\partial_\sigma\Delta^{(1)}\cdot\partial_\rho\partial_\sigma\bar{\Delta}-\Box\Delta^{(1)}\cdot\Box\bar{\Delta})]; \qquad (25')
\end{aligned}
$$

$$
\begin{aligned}
\delta j_\mu{}^{(vt)}(x)=-2e^2\gamma\int d\omega'[&\Delta^{(1)}(x-x')\bar{\Delta}(x-x') \\
&-1/m^2\cdot\partial_\sigma\Delta^{(1)}(x-x')\cdot\partial_\sigma\bar{\Delta}(x-x')]J_\mu(x'); \qquad (26)
\end{aligned}
$$

$$
\delta j_\mu{}^{(t)}(x)=-e^2\gamma^2\int M_{\mu\rho\sigma}(x-x')F_{\rho\sigma}(x')d\omega' \qquad (27)
$$

with

$$
\begin{aligned}
M_{\mu\rho\sigma}=\partial_\nu[&2\delta_{\mu\sigma}\delta_{\nu\rho}\Delta^{(1)}\bar{\Delta} \\
&+1/m^2\cdot\delta_{\nu\rho}(\partial_\mu\Delta^{(1)}\cdot\partial_\sigma\bar{\Delta}+\partial_\sigma\Delta^{(1)}\cdot\partial_\mu\bar{\Delta}) \\
&-1/m^2\cdot\delta_{\mu\sigma}(\Delta^{(1)}\cdot\partial_\rho\partial_\nu\bar{\Delta}+\partial_\rho\partial_\nu\Delta^{(1)}\cdot\bar{\Delta}) \\
&-1/m^4\cdot\delta_{\nu\rho}(\partial_\sigma\partial_\lambda\Delta^{(1)}\cdot\partial_\mu\partial_\lambda\bar{\Delta}+\partial_\mu\partial_\lambda\Delta^{(1)}\cdot\partial_\sigma\partial_\lambda\bar{\Delta} \\
&-\partial_\mu\partial_\sigma\Delta^{(1)}\cdot\Box\bar{\Delta}-\Box\Delta^{(1)}\cdot\partial_\mu\partial_\sigma\bar{\Delta})]. \qquad (27')
\end{aligned}
$$

To bring about the cancellation of the surface-dependent terms in $\delta j_\mu(x)$, use was made of (12) plus the additional identity

$$
\begin{aligned}
-1/2\cdot\int d\omega' F(x,x')\{&\partial_\nu\partial_\mu\partial_\rho[\epsilon(x-x')\Delta(x-x')] \\
&-\epsilon(x-x')\partial_\nu\partial_\mu\partial_\rho\Delta(x-x')\} \\
=[(n_\mu n_\nu\partial_\rho'+n_\nu n_\rho\partial_\mu'+n_\rho n_\mu\partial_\nu' &\\
+2n_\mu n_\nu n_\rho n_\sigma\partial_\sigma')F(x,x')]_{x=x'}. \qquad (12')
\end{aligned}
$$

We note that, as in the spinor case, it is $\delta j_\mu{}^{(v)}(x)$ which is not gauge invariant and the introduction of the tensor coupling does not lead to any new non-gauge invariant terms which means, as before, that the amount of tensor coupling will not play a role in the discussion of the photon self-energy. Indeed, we observe that the first part of $K_{\mu\nu}$ (25′) is exactly three times the corresponding quantity for the case of a charged scalar field (11′) whereas the second part leads to a gauge invariant current; one may readily verify that for the charged vector meson field $\partial K_{\mu\nu}/\partial x_\nu=6\delta(x)\partial_\mu\Delta^{(1)}$.

The ultimate evaluation of $\delta j_\mu(x)$ leads to the following results:

$$
\begin{aligned}
\delta j_\mu{}^{(v)}(x)=&-3i\alpha/4\pi \\
&\cdot\int_{-1}^{1}dy[\exp\{im^2z-iz/4\cdot(1-y^2)\Box\}/z]_{z=0}A_\mu(x) \\
&+\alpha/4\pi\cdot(g_1-g_2/2)J_\mu(x) \\
&-\alpha/24\pi\cdot(g_2+3/5)(\Box/m^2)J_\mu(x) \\
&-17\alpha/1680\pi\cdot(\Box/m^2)^2J_\mu(x)+\cdots, \qquad (28)
\end{aligned}
$$

$$
\begin{aligned}
\delta j_\mu{}^{(vt)}(x)=&-\alpha\gamma/2\pi\cdot(g_1+g_2/2)J_\mu(x) \\
&+\alpha\gamma/8\pi\cdot(g_2-2/3)(\Box/m^2)J_\mu(x) \\
&+\alpha\gamma/40\pi\cdot(\Box/m^2)^2J_\mu(x)+\cdots, \qquad (28')
\end{aligned}
$$

$$
\begin{aligned}
\delta j_\mu{}^{(t)}(x)=&-\alpha\gamma^2/4\pi\cdot(g_1-g_2)J_\mu(x) \\
&+\alpha\gamma^2/16\pi\cdot(g_1-2g_2/3+4/3)(\Box/m^2)J_\mu(x) \\
&-\alpha\gamma^2/96\pi\cdot(g_2+4/5) \\
&\times(\Box/m^2)^2J_\mu(x)+\cdots. \qquad (28'')
\end{aligned}
$$

4. DISCUSSION

The essential content of the preceding section is contained in Eqs. (13), (21–21″) and (28–28″). We have already remarked that the amount of tensor coupling has no bearing on the photon self-energy whether we are considering spinor or vector mesons. If we let N_{sc}, N_{sp} and N_v denote the number of charged scalar, spinor and vector fields which interact simultaneously with the external electromagnetic field and $m_{sc}^{(i)}$, $m_{sp}^{(i)}$ and $m_v^{(i)}$ the corresponding masses, then it is evident that the photon self-energy will vanish provided

$$2N_{sp}=N_{sc}+3N_v, \tag{29}$$

$$2\Sigma(m_{sp}^{(i)})^2=\Sigma(m_{sc}^{(i)})^2+3\Sigma(m_v^{(i)})^2; \tag{29'}$$

these equations are the analogs of the regulator conditions (2) and (2′) and clearly allow many possibilities.

A corresponding cancellation of the divergences which arise in the gauge invariant terms in the current density is not possible however. As has been observed by many authors,[10] the charge renormalization factors in the scalar and spinor cases (the latter with vector coupling only) diverge logarithmically and have the same sign. The introduction of an anomalous magnetic moment for the spinor field intensifies the difficulty in that it leads to a logarithmically divergent $\Box J_\mu$ term. Unfortunately, this last infinity cannot be canceled by the corresponding one which occurs in the case where we have a charged vector meson field (with vector coupling only) for here, again, the signs in the two situations are the same. Indeed, in the vector meson case we obtain also a quadratic divergence in the charge renormalization term. Finally, the introduction of tensor coupling for the vector meson field leads to a $(\Box)^2 J_\mu$ divergence.

The inference to be drawn from all this is certainly not that the realistic approach is an incorrect one. Indeed, the very closedness of quantum electrodynamics on the one hand together with the complete failure of all meson theories on the other are fully compatible with and emphasize the necessity for a realistic description of elementary particles. We can only conclude that the usual linear field theories do not seem to be adequate for the job although the possibility that it is actually the perturbation theory which is at fault cannot be completely ignored.

It gives me pleasure to express my thanks to Professors R. Oppenheimer, H. Yukawa and Dr. A. Pais for their interest in this work. I want also to thank Dr. Pais for having made available to me the manuscript of Pauli and Villars and that of Jost and Rayski.

On the Theory of Electron Multiplication in Crystals

FREDERICK SEITZ*
Carnegie Institute of Technology, Pittsburgh, Pennsylvania
(Received July 8, 1949)

The theory of the multiplication of electrons in strong electrostatic fields is investigated. It is found that the non-polar coupling between electrons and lattice has an important effect on the retardation of electrons in polar materials as well as in non-polar ones if the electron is to be accelerated to an energy at which it may ionize the bulk material. The retardation arising from this coupling is a maximum when the energy of the electron corresponds to a value near the boundary of the Brillouin zone, in contrast with the retardation arising from purely polar interaction in polar crystals which has its maximum when the energy is near the energy of the polar modes. The existence of the non-polar interaction seems to make the difference between the breakdown criteria of von Hippel and Fröhlich of less practical importance than was supposed hitherto. It is found that statistical fluctuations in the velocity of the electrons plays a very important role in determining electron multiplication and that the field required to produce breakdown in a standard specimen actually is no more than twenty percent of the value obtained from the criteria of von Hippel and Fröhlich.

1. INTRODUCTION

THE theory of the production of free electrons in crystals in the presence of high electrostatic fields and relatively low temperatures, where thermal currents do not play a role, has been the subject of relatively intense but somewhat diversified activity during the past fifteen years. In this development principal interest has focused on dielectric breakdown because of its great practical importance.[1] On the other hand there are secondary phenomena which are of equal interest from the standpoint of fundamental development. For example it has been observed by von Hippel[2] and his co-workers that a measurable current exists within the alkali halides for fields somewhat lower than that required to induce breakdown. These pre-breakdown currents grow in magnitude as the field is raised. Although the breakdown current usually appears as a discontinuity on the rising pre-breakdown current, it seems reasonable to suppose that the pre-breakdown current is related to breakdown. Haworth and Bozorth,[3] who studied pre-breakdown phenomena in glass, observed that the current is exceedingly noisy; that is, the current occurs in pulses (Fig. 1) which grow in magnitude as the field increases. Pulses of this type have been observed[4] in a qualitative manner in many cases. Their presence suggests that electron avalanches occur at fields lower than that required to produce breakdown and grow rapidly in magnitude as the breakdown field is approached.

Theoretical developments concerning breakdown phenomena have flowed in three somewhat separate channels, each of which has had its own exponents:

(1) One of the first systematic development along modern lines is that of Zener,[5] who proposed that breakdown occurs when the electrostatic field becomes sufficiently strong to ionize the atoms of the insulator by a process akin to field emission. In effect, the electrons of the bulk solid are able to tunnel from the filled band of levels to the conduction band. This effect was investigated subsequently by Houston[6] and by Franz.[7] The latter focused attention particularly on the problem of breakdown, however, Houston's calculations are somewhat more accurate. These investigators find that the probability per unity time that an electron is ejected from the filled to the empty band when the field intensity is E is

$$P=(2\pi deE/\hbar)(e^{-\alpha}/(1-e^{-\alpha})^2), \tag{1}$$

where

$$\alpha=(\Delta\epsilon)^2md/eE\hbar^2. \tag{2}$$

Here $\Delta\epsilon$ is the gap in energy between filled and empty band, d is the lattice spacing (for the one-dimensional model employed) and e and m are the electron charge and mass. Franz has shown that this leads to a current of the order of 1 amp per cm^2 when E takes the value

$$E=0.33\cdot10^6(\Delta\epsilon)^2(\text{volts per cm}). \tag{3}$$

Here E is given in volts per cm when $\Delta\epsilon$ is expressed in electron volts. The lattice spacing d is assumed to have the value $3\cdot10^{-8}$ cm corresponding to the nearest-neighbor spacing in sodium chloride. Now the spacing between filled and empty conduction bands is about 10 ev in the case of sodium chloride, if present interpretation[8] of the ultraviolet absorption spectra of the alkali halides is correct. Thus (3) leads to a breakdown potential of about $3\cdot10^7$ volts per cm, which is at least

* Now at the University of Illinois, Urbana, Illinois.

[1] The principal survey articles on the field of dielectric breakdown in solids are as follows: A von Hippel, J. App. Phys. **8**, 815 (1937); Trans. Faraday Soc. (Conference on Dielectrics) **40**, 78 (1946); W. Franz, Zeits. f. Physik **113**, 607 (1939); H. Fröhlich, Reports on Progress in Physics **6**, 411 (1939); N. F. Mott and R. W. Gurney, *Electronic Processes in Ionic Crystals* (Oxford University Press, New York, 1940); A. E. W. Austen and S. Whitehead, Proc. Roy. Soc. **176**, 33 (1940). More recent papers are as follows: H. Fröhlich, Proc. Roy. Soc. **188**, 521, 532 (1947); J. W. Davisson, Phys. Rev. **70**, 685 (1946).

[2] A. von Hippel, Phys. Rev. **54**, 1096 (1938).

[3] F. E. Haworth and R. M. Bozorth, Physics **5**, 15 (1934).

[4] The writer is indebted to Professor R. J. Maurer for a discussion of observations on pre-breakdown noise.

[5] C. M. Zener, Proc. Roy. Soc. **145**, 523 (1934).

[6] W. V. Houston, Phys. Rev. **57**, 184 (1940).

[7] W. Franz, see reference 1.

[8] N. F. Mott and R. W. Gurney, see reference 1, p. 95.

a factor 10 larger than the observed[9] value at room temperature of $1.5 \cdot 10^6$ volts per cm. Even without this evidence, which is subject to criticism on the ground that the absolute theoretical values may contain large calculational inaccuracies, the measurements of Buehl and von Hippel[9] on the temperature dependence of the breakdown field in the alkali halides seem to rule out the field emission theory. This work shows that the breakdown field decreases with decreasing temperature in the range below room temperature. This effect is very difficult to explain on the field emission theory, whereas it is explained very naturally on an avalanche theory.

The value of $\Delta\epsilon$ is not accurately known in diamond; however it is probably less than 10 ev and probably nearer to 7 ev. Moreover the lattice spacing in diamond is about half the value for sodium chloride. As a result, the field corresponding to that given by Eq. (3) is somewhat less than 10^7 volts per cm. We shall have cause to refer to this value in later sections.

(2) In 1932 von Hippel[10] proposed that breakdown in solids is a by-product of the production of electron avalanches through electron impact. He pointed out that any electron which finds itself free in a solid in the presence of an electrostatic field will be subject to two opposing influences: It will tend to be accelerated by the field and retarded by the "friction" resulting from interaction with the vibrational waves of the lattice. He postulated that breakdown occurs when the average electron gains energy more rapidly from the field than it loses it to the lattice for all velocities of motion less than the value needed to produce ionization by impact. von Hippel also proposed that the electron would encounter the greatest friction in ionic crystals when its energy is of the order of $h\nu_0$ where ν_0 is the frequency of the optically active mode of lattice vibration. In other words the barrier is greatest when the electron has energy in the thermal range.

Seeger and Teller[11] supplemented von Hippel's theory by deriving an expression for the rate at which a conduction electron would lose energy to the lattice. Unfortunately this calculation alone does not provide a very satisfactory test of the theory because the collision frequency is so large in the velocity range where the friction is greatest that there is no reliable method of determining the rate of loss. For example, quantum mechanical perturbation techniques are not accurately applicable. In spite of the fact that von Hippel's theory is not subject to precise treatment, it evidently has many attractive features. For example it does give the correct order of magnitude of breakdown field and it does explain the occurrence of avalanches at least qualitatively. In addition it predicts temperature dependence of the general type that is observed.

(3) In 1937 Fröhlich[12] proposed an independent impact ionization theory which differs from von Hippel's primarily in regard to the condition employed for breakdown. Fröhlich also postulated that breakdown occurs as a result of acceleration of electrons through a friction barrier arising from interaction between electrons and lattice waves. However, he has been guided by the intuitive notion that the critical conditions are determined by the behavior of electrons which have an energy sufficient to ionize the atoms of the solid. As a result he has proposed an equation for the breakdown field which differs from von Hippel's and which states that the field should be sufficiently strong that electrons having energy sufficient to ionize gain more energy from the field than they lose to the lattice waves. As far as the writer can judge, Fröhlich believes that von Hippel's condition is too stringent because it requires that every electron be accelerated on the average. Apparently Fröhlich believes that breakdown will occur when any electron which has by whatever means possible reached the ionization energy will gain more

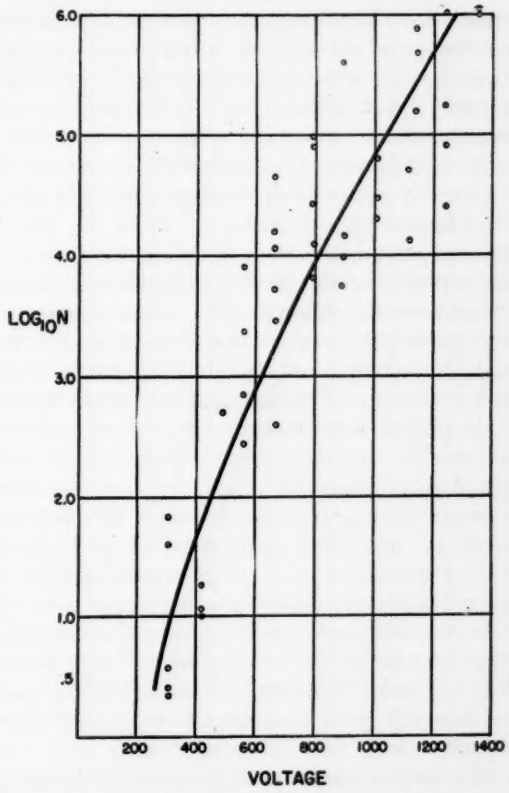

FIG. 1. Variation of the size of electron avalanches in Pyrex with applied voltage (after Haworth and Bozorth). The ordinate is expressed in units of the electron charge.

[9] A. von Hippel, Zeits. f. Physik **75**, 145 (1932); Ergebn. d. exakt. Naturwiss. **14**, 79 (1935); R. C. Buehl and A. von Hippel, Phys. Rev. **56**, 941 (1939); A. E. W. Austen and S. Whitehead, see reference 1.

[10] A. von Hippel, Ergeb. d. exakt. Naturwiss. **14**, 79 (1935); J. App. Phys. **8**, 815 (1937); A. E. W. Austen and S. Whitehead, see reference 1.

[11] R. J. Seeger and E. Teller, Phys. Rev. **54**, 515 (1938); **56**, 352 (1939).

[12] H. Fröhlich, Proc. Roy. Soc. **160**, 230 (1937); **172**, 94 (1939); **178**, 493 (1941); **188**, 521, 532 (1947); Phys. Rev. **61**, 200 (1942).

energy from the field than it loses to the lattice vibrations. In essense, his theory appears to rest on the assumption that when the breakdown field is reached the distribution function describing the spread of electron energies will have a maximum well below the ionization energy, but will possess some type of tail in the region of the ionization energy. The behavior of the electrons in this tail determines breakdown. In partial support of this viewpoint, Fröhlich has shown recently in a somewhat idealized calculation[12] that the distribution function actually possesses a portion which rises with increasing energy above the ionization energy. This calculation is deficient in the sense that it does not include the influence of the ionization process itself on the distribution function. Inasmuch as this influence is probably great, it must be admitted that Fröhlich's case still rests primarily on intuitive grounds.

Since Fröhlich, like von Hippel and Seeger and Teller, assumed that the maximum friction occurs when the electron has energies near $h\nu_0$ and that the curve describing dissipation of energy to the lattice falls at higher energies, his condition for breakdown would lead to a lower value of the breakdown if both groups of investigators employed in same function. Actually both arrive at about the same values of the breakdown field because they employ functions which differ essentially by a multiplicative constant. The difference arises from the manner in which the screening of electrons by the polarization of the lattice is included. Seeger and Teller assume that the electron is shielded by a polarization charge determined by the dielectric constant of the medium, whereas Fröhlich assumes that this screening is not of great importance for energies near the ionization potential.

As we shall see in Section 4 both groups of investigators neglect the interaction of electrons with non-polar modes of vibration. The calculations of the present paper seem to show that this interaction, which is peaked at energies of the order of several electron volts and which is of primary importance in non-polar crystals, plays a very important role in ionic solids and should modify the application of either of the criteria for breakdown described above. In fact, the present work seems to show that the criteria of von Hippel and Fröhlich do not differ appreciably from a practical viewpoint since the electron friction arising from interaction with lattice vibrations is almost as large when the electron can ionize as it is when the electron has energies near $k_0\theta$ in the case of polar crystals. Moreover the present work indicates that statistical fluctuations are sufficiently important that both criteria are too stringent.

It should be emphasized in connection with this summary that experimental aspects of the topic of breakdown still merit a great deal of further investigation. The best available data on the subject is derived from direct voltage measurements which are carried out to the point at which rupture occurs. It is conventional to assume that the applied electrostatic field is relatively uniform and that the electrodes play a minor role in the breakdown process when relatively reproducible results are achieved. Early work of Gudden and Pohl and more recent work of McKay[13] indicates that the introduction of as few as 10^{10} electrons into a crystal can have an appreciable influence upon the potential distribution through the formation of space charge within the specimen as a result of the trapping of electrons. It is possible that the large electrostatic fields which are achieved near breakdown in the best insulators sweep away this space charge. However this point, as well as the influence of ionic polarization, merits much more study than the topic has received to date. Similarly it is possible that the character of the pre-breakdown currents is determined primarily by the electrode-crystal junction.

These uncertainties will have relatively little influence on the following discussion since we shall be primarily interested in the manner in which electrons may be multiplied as a result of acceleration within the crystal. It seems reasonable to assume at present that this process is intimately related to the breakdown problem in many crystals even though we may not have complete understanding of the relationship between the applied voltage and the distribution of field in a specimen for which the applied voltage is near the breakdown value.

2. VIEWPOINT OF PRESENT ANALYSIS

The present paper is devoted to a re-examination of the impact ionization theory in order to attempt to obtain a somewhat clearer view of the multiplicative process. In the opinion of the writer, von Hippel's approach to the problem of dielectric breakdown provides a more fruitful starting point than Fröhlich's since it attempts to follow the dynamical behavior of a free electron throughout its life cycle as it passes from cathode to anode. It is difficult to believe that it will lead to essentially incorrect results if due attention is paid to all of the effects which influence the electron. It cannot of course be denied that Fröhlich's more formal approach could lead to identical results; however it appears to be very difficult to subject his method to the type of detailed approximation which is so valuable in obtaining a feeling for the inner working of a problem.

In the last analysis the central problem of dielectric breakdown in solids is this: At what field strength are free electrons produced in sufficient numbers to produce disruption? We shall suppose that the free electrons are produced by an avalanche effect in which one initial free electron produces a secondary by impact ionization; the pair then produce a second pair and the process continues through n generations at the end of which

[13] B. Gudden and R. W. Pohl, Zeits. f. Phys. **7**, 69 (1921); K. G. McKay, Phys. Rev. **74**, 1606 (1948).

time there are 2^n free electrons. For a given material and field strength n will be proportional to the time the electrons spend within the crystal and hence upon the dimensions of the specimen and the point at which the first electron is initiated, as well as on the bulk properties of the material.

The following arguments may be employed to obtain an estimate of the value n should attain for breakdown to be induced. We shall see in the following sections that a typical free electron will migrate through a crystal with a mobility in the vicinity of 1 cm² per volt-sec. when the field is near the breakdown value of say 10^6 volts per cm. Thus the electron will traverse a distance of 1 cm in about 10^{-6} sec. In addition to drifting in the direction of the field, the electron will undergo Brownian motion or diffusion in the plane normal to the field. The diffusion coefficient, which is $\lambda v/3$, where λ is the mean free path and v is the velocity of motion, has a value in the neighborhood of 1 cm² per sec. Thus in travelling 1 cm in the direction of the field, the electron will on the average wander through a circle of radius 10^{-3} cm in the plane normal to the field. We shall assume that its progeny, produced by impact ionization, also lie within a circle of this radius. Since the diffusion coefficient of heat in most solids is less than 1 cm² per sec., the energy which the electrons transfer to the atoms of the lattice in the collisions between electrons and lattice vibrations will not diffuse out of this tube in the time in which the electrons migrate 1 cm. Now if the field is 10^6 volts per cm, each electron will transfer 10^6 ev to the group of atoms in the tube. The material in the tube would be seriously disrupted if each atom received as much as 10 ev (230,000 cal. per mole). Thus it seems safe to assume that breakdown will occur if the primary electron produces one electron for each 10^5 atoms in the tube. Since there are about 10^{17} atoms in the tube, we conclude that the primary electron will produce breakdown if it generates 10^{12} progeny. The foregoing calculation has been made as if the 10^{12} electrons were present during the entire traversal of the tube. Actually the atoms in the tube will begin to receive energy from the electrons at the estimated rate of 10 ev per atom only after the 10^{12} electrons have been produced. Thus only the material near the end of the tube would be disrupted.

It is clear that if 10^{12} electrons were produced in a distance shorter than 1 cm, and hence in a time less than 10^{-6} sec., the energy transferred per atom to the atoms in the tube having a radius equal to the distance the electron diffuses normal to the field would be greater than 10 ev because this radius varies as the square root of the time. Conversely less than 10^{12} electrons would be needed to produce the desired disruption. We shall neglect this variation of the number of electrons needed with the distance in which they are produced since it is relatively small for the variations in electrode spacing normally employed in experiments.

The value of n for which $2^n = 10^{12}$ is 40. Thus we conclude that about 40 generations of secondary electrons should be produced between electrodes from a single primary if breakdown is to occur as a result of impact ionization. It is evident that this is a fairly approximate value; however it is sufficiently accurate for the purposes for which we shall use it.

The preceding conditions for breakdown may also be expressed in the following way: An average free electron must produce a secondary electron in travelling a distance $L = D/40$ in the direction of the field if D is the spacing between electrodes. Since the electrode spacing enters into this formulation of the condition for breakdown, it follows that the breakdown field should depend upon the electrode spacing, being larger the smaller the spacing. It has been well established for mica[14] that the breakdown field varies inversely as the electrode spacing. However the measurements of Austen and Whitehead do not permit a precise determination of the relation.

If the distance Λ which the electron travels in producing a secondary is greater than L but less than D it will start an avalanche; however this avalanche will not reach sufficient proportions to cause breakdown, even though it may be great enough to be detected relatively easily as a current pulse.

We may expect the distance Λ to decrease continuously with increasing field strength. Thus as the field intensity is increased we may generally expect to find a region in which pre-breakdown avalanches are observed whenever breakdown is caused by impact ionization. The size of the avalanches will increase continuously with increasing field until they become sufficiently large to produce breakdown.

Should the current produced by field emission of the type described by Zener and Franz cause breakdown before Λ is smaller than D, the free electrons will not be able to produce progeny and the pre-breakdown current will not be very noisy, that is, will not contain avalanches larger than those produced by the random arrival of electrons at the anode.

In the following sections an attempt will be made to analyze the factors which determine the ability of electrons to multiply in strong fields in somewhat more detail than has been done hitherto. Since quantum mechanical perturbation methods form the basis for most of this discussion, it is necessary to emphasize, along with other investigators,[15] that these methods cease to be accurate as soon as the collision frequency exceeds a value of about $3 \cdot 10^{13}$ sec.$^{-1}$. Since the collision frequency actually does exceed this value in the most interesting range of electron velocity, the results obtained with perturbation theory have only semi-quantitative value and must be employed with full recognition of this limitation. They can be employed only to infer the type of behavior that may be expected

[14] A. E. W. Austen and S. Whitehead, see reference 1.

[15] The applicability of perturbation theory is discussed in a previous paper by the writer, Phys. Rev. 73, 550 (1948).

TABLE I. Characteristic energies associated with free electrons at boundary of Brillouin zone (expressed in electron volts).

	ϵ min.	ϵ max.	ϵ_s
Diamond	8.9 ev	11.9	11.5
NaCl	3.6	4.8	4.6

to occur in practice; precise values of the various parameters should be determined either with the use of experiment or by application of methods other than those based on perturbation theory. In spite of these drawbacks the theoretical values to be derived and discussed lead to interesting conclusions.

3. FACTORS EFFECTING FREE ELECTRON

Consider the behavior of an electron which finds itself free in an insulating crystal. We shall assume that the electron possesses thermal energy initially and that there is a uniform electrostatic field of intensity E within the crystal. If the electron did not interact with the crystal, it would be uniformly accelerated at a rate eE/m and would with certainty obtain sufficient energy to excite or ionize the electrons of the insulator provided there is sufficient potential drop between the point of origin of the free electron and the anode toward which the electron is accelerated. As von Hippel has pointed out, the lattice provides in effect a source of "friction" for the motion of the electron which prevents the electron from being accelerated at the rate eE/m. The various sources of friction may be catalogued in the following way.

(1) Excitation of Polar (Optical) Modes of Vibration

In polar crystals the electron will interact strongly with the polar or optical modes of vibration of the lattice. This interaction has been examined in various approximations by von Hippel, Fröhlich and Mott, Seeger and Teller, and Callen who obtain results that are similar semi-quantitatively. The maximum interaction occurs when the electron has an energy of the order of $h\nu_0$, where ν_0 is the frequency of the polar mode of longest wave-length in the reduced zone scheme. The electron may lose energy to the lattice, provided it has sufficient energy to excite the polar modes, or it may gain energy if the lattice is thermally excited. Both types of encounter cause the electron to be scattered so that it undergoes Brownian motion. Fröhlich and Mott have distinguished carefully between the transverse and longitudinal polar modes of vibration, which generally have different frequencies even in a cubic crystal, and have shown that the longitudinal modes are principally responsible for the interaction. As far as the writer is aware all of the investigators who have considered the friction encountered by an electron in being accelerated have placed principal emphasis upon the interaction with polar modes and have neglected a second effect which seems to him to be as important for the problem.

(2) Interaction with Non-Polar Modes

The electron will interact with non-polar modes of vibration even in a polar crystal. This type of interaction is usually considered only in non-polar crystals since the polar modes are absent in these materials and the non-polar modes provide the principal source of scattering. However, the non-polar modes are of considerable interest even for polar crystals, for, as we shall see below, their influence is greatest when the energy of the electron is a hundred or so times larger than $h\nu_0$ and the influence of the polar modes has diminished. The neglect of the non-polar modes of polar crystals is undoubtedly justifiable in a discussion of the ordinary problem of electronic conduction for which the kinetic energy of the electrons does not differ greatly from $h\nu_0 \cong k\theta$ (θ = characteristic temperature). However these modes should be included when the electron has either a high energy or a very low energy. The interaction with these modes evidently is a principal subject of discussion for the problem of electron multiplication in non-polar crystals.

In addition to the foregoing impediments to the acceleration of an electron there are two more obstacles which merit attention.

(3) Laue Scattering

If in the course of being accelerated, an electron passes near to the boundary of a Brillouin zone, it has a finite chance of undergoing Laue scattering. Although such scattering will not alter the energy of the electron, it will alter its direction of motion and hence alter the rate at which the electron gains energy. This process is particularly important if the free electron does not possess sufficient energy to excite the bound electrons when it is in the first Brillouin zone associated with free electrons. If the bands associated with free electrons overlap and if the frequency with which the electron makes collisions with the lattice vibrations is sufficiently great, the electron will jump from one zone to the next without spending an appreciable time near the boundary of zones. However if the frequency of collisions with the lattice vibrations is small once the electron has gained energy, or if the neighboring energy bands associated with free electrons are separated by a gap in energy that is large compared with the energy of the lattice vibrational quanta, as is the case between filled and empty bands for the normal valence electrons of an insulator, the accelerated electron will eventually reach the boundary of the zone and undergo Laue reflection. We shall assume in the following that the conduction bands overlap, as is probably the case for most insulators. We shall see later that the frequency of collisions with lattice vibrations is sufficiently large in this case that the electron probably does not spend appreciable time near the boundary of the Brillouin zone.

The first two columns of Table I show the maximum and minimum energies that would be associated with the boundaries of the first conduction zone in diamond and sodium chloride if the electron were perfectly free. The third column gives an average ϵ_s that will be defined later.

(4) Production of Excitons

As J. B. Sampson and the writer emphasized a number of years ago,[16] the first electronic excitation process of which the accelerated electron may be capable is the production of excitation waves. In fact this should be the case with certainty if our present picture of the electronic states in good insulators is correct. Unless the excitation waves are decomposed into free electrons and holes by the field or by other means, the accelerated electron will lose the energy expended in excitation waves without producing secondary charged particles which can be accelerated in turn.

4. ENERGY LOSS BY LATTICE COLLISIONS IN POLAR AND NON-POLAR CRYSTALS

A. Non-Polar Crystals[17]

The interaction between free electrons and the lattice vibrations of non-polar crystals may be treated in a straightforward way if it is assumed that the lattice vibrations alter the potential field of the crystal in the manner first proposed by Bloch which is sometimes called the deformable atom hypothesis. It is assumed in essence that the perturbing potential V_p satisfies the equation

$$V_p(r) = -R \cdot \text{grad} V_n(r). \tag{4}$$

Here $V_n(r)$ is the unperturbed potential and R is a continuous function whose values at the positions of the atoms describe the motion of the atoms as a result of the vibrational waves. The use of the Bloch perturbing potential is supported by the fact that it leads to a $T^{\frac{1}{2}}$ dependence of mobility upon temperature at temperatures below the characteristic temperature, in agreement with experimental observations in pure diamond, silicon, and germanium. As a result, we may feel justified in employing the results of a previous paper to discuss the interaction between the electrons and lattice vibrations in non-polar materials.

It has been shown that the probability per unit time p that the electron will interact with the acoustical modes is

$$p = \frac{2\pi}{\hbar}\frac{2\hbar C^2}{9NM}\int \sigma^4(2n(\sigma)+1)\frac{\delta(E_1-E_2)}{\omega(\sigma)}\rho 2\pi \sin\theta d\theta d\sigma. \tag{5}$$

Here C is an energy parameter describing the coupling between electron and lattice, N is the number of unit cells in the crystal under consideration, M is the mass of the atoms of which the lattice is composed, σ is the wave number vector of the vibrational quanta, $n(\sigma)$ is the number of quanta of each type of vibration that is stimulated as a result of thermal excitation, $\omega(\sigma)$ is the circular frequency associated with the vibrational wave having wave number σ, ρ is the density of values of σ in wave number space, E_1 and E_2 are the energies of the system consisting of electron plus lattice before and after a collision of the electron with the wave having wave number σ. In the collision, the wave number k of the electron is transformed to k' where

$$k' = k + \sigma \tag{6}$$

so that $E_1 - E_2 = \epsilon(k) - \epsilon(k') \pm \hbar\omega$ if $\epsilon(k)$ is the energy of an electron having wave number k. If we assume that the electrons are completely free so that $\epsilon(k) = \hbar^2k^2/2m$, we find

$$E_1 - E_2 = -(\hbar^2/2m)(\sigma^2 + 2k\sigma\cos\theta) \pm \hbar\omega, \tag{7}$$

in which θ is the angle between k and the vector σ which satisfies (6) and the equation

$$E_1 - E_2 = 0. \tag{8}$$

The integration in (5) extends over all permitted values of σ and θ; however the presence of the delta-function reduces the integration to one dimension. In general when one desires to obtain the total probability per unit time as given by the integral (5) instead of the differential probability as a function of angle, it is convenient to replace the integration over θ by one over the variable $E_1 - E_2$, using (7) to connect the two variables. Equation (5) is then reduced to a single integration over the scalar wave number σ. Provided k lies well within the first Brillouin zone, the integration over σ extends from zero to $2k$ and leads to the results described in I. On the other hand, if k lies so close to the zone boundary that the upper limit of σ required by Eqs. (6) and (7) would lie outside the first zone in σ space, the integration becomes much more involved. The simplest procedure to follow is to set the upper limit of integration of σ equal to a constant σ_m that is of order of magnitude of the average radius of the first zone boundary. This procedure can also be adopted when k lies well outside the first zone.

As long as k lies well inside the first Brillouin zone, so that there is no limitation on the integration over σ imposed by the zone boundaries, the calculations of I show that the electron is scattered isotropically. However once the range of σ is no longer $2k$, forward scattering predominates. The transition between the two cases occurs when k approaches the zone boundary.

When the electron has thermal energy, as was assumed to be the case in I, $n(\sigma)$ may be set equal to $k_0T/\hbar\omega$, where k_0 is Boltzmann's constant and T is the absolute temperature. In this case the 1 appearing with

[16] F. Seitz, *Modern Theory of Solids* (McGraw-Hill Book Company, New York, 1940), p. 563. The basic theory of excitons may be found in the following: J. Frenkel, Phys. Rev. **37**, 17, 1276 (1931); Physik. Zeits. Sowjetunion **9**, 158 (1936); R. Peierls, Ann. Physik **13**, 905 (1932); J. C. Slater and W. Shockley, Phys. Rev. **50**, 705 (1936); G. Wannier, Phys. Rev. **52**, 191 (1937).

[17] This paper by the writer, Phys. Rev. **73**, 550 (1948), will be referred to as I in the text.

$2n(\sigma)$ in the integral can be neglected and we find, as in I,

$$p=\frac{4}{9\pi}\frac{C^2k_0T}{\hbar^3c^2n_0}\frac{m_k}{M} \tag{9}$$

in which n_0 is the density of unit cells. If the entire factor $(2n+1)$ in the integrand is included, the result is readily found to be

$$p=\frac{4}{9\pi}\frac{C^2k^2}{\hbar^2n_0c}\frac{m}{M}\left(\frac{k_0T}{\hbar ck}+\frac{2}{3}\right) \tag{10}$$

where c is the velocity of the longitudinal modes of vibration.

Equation (9) and its extended form (10) are valid only when the wave number vector of the electron lies well within the first Brillouin zone associated with the free electrons. When k does approach the edge of the zone or extend beyond it, the range of integration of σ becomes limited as we saw above. This limitation is particularly important when k lies outside the first zone, since it alters entirely the dependence of p upon k. A simple investigation shows that the quantity in parenthesis in (10) becomes independent of k, whereas the coefficient varies as $1/k$. In other words, the collision frequency attains its maximum value when k is near the boundary of the first Brillouin zone.

The rate of energy loss exhibits a similar behavior. This quantity, which we shall designate as $d\epsilon/dt$, may be computed by replacing the factor $2n+1$ in the integral (5) by $\hbar\omega$ and carrying out the corresponding integrals. As long as k lies well within the first zone, the result is

$$(-d\epsilon/dt)=(4/9\pi)(C^2/\hbar)(k^3/n_0)(m/M), \tag{11}$$

whereas this quantity falls off as $1/k$ when k lies outside the first zone. Temperature no longer plays a role because the electron loses and gains energy at the same rate from the temperature-stimulated component of the modes of vibration. If we evaluate the temperature-independent part of (10) for diamond under the assumption that m is the mass of a perfectly free electron, that C^2 has the value 936 ev^2 and that k has the value k_z satisfying the equation

$$(4\pi/3)k_z^3\rho=N, \tag{12}$$

where $\rho=V/8\pi^3$ is the density of points in wave number space and N is the number of cells in the specimen, we obtain

$$\frac{1}{\tau}=\frac{16\pi}{9}\frac{1}{\hbar}\frac{C^2}{(2mc^2\epsilon_z)^{\frac{1}{2}}}\frac{m}{M}=1.9\cdot10^{15}\ \text{sec.}^{-1}. \tag{13}$$

It is interesting to observe that $\epsilon_z=\hbar^2k_z^2/2m$ has a value of 11.5 ev (see Table I). The collision frequency (13) would give rise to a mobility of the order of magnitude of 0.94 cm^2/volt-sec. which is about 100 times smaller than the value for conduction electrons in thermal equilibrium at room temperature. In fact this value of the mobility is so low that the perturbation methods used to obtain it are no longer accurately valid, for the reasons discussed in I. The mobility and collision frequency may be employed only as rough approximations.

Recently Klick and Maurer[18] have carried out Hall effect measurements in diamond which permit an experimental determination of the mobility. They find a value of 900 cm^2/volt-sec. for thermal electrons instead of the value of 156 cm^2/volt-sec. calculated in I. If we arbitrarily assume that this difference of a factor 6 arises from an overestimate of the coupling constant C^2 in I for diamond by that amount, the collision frequency (13) is lowered to $3.1\cdot10^{14}$ sec.$^{-1}$ and the mobility for $\epsilon=\epsilon_z$ is 5.6 cm^2/volt-sec.

The interaction of a free electron with the optical modes of vibration in a non-polar crystal possessing two atoms per unit cell was discussed in I. Two cases were treated. If in a reduced zone scheme, we let $\sigma=0$ designate the optical mode of highest energy, that is the mode which would have highest wave number in the extended zone scheme, the conservation of wave number is expressed by the equation

$$k'=k+\sigma. \tag{14}$$

One of the cases considered was that in which the matrix component of interaction does not vanish when $\sigma=0$, whereas the second case was that in which it does. The first case will be the normal one and we shall assume that it is valid. The equation analogous to (5) may readily be integrated as is shown in I and the resulting collision frequency is

$$p=\frac{1}{\pi}\frac{D^2\hbar^2K^2 2m}{\hbar\omega_0}\frac{m^2}{M}\frac{k}{\hbar^2n_0}\left\{\begin{matrix}n\\ n+1\end{matrix}\right\}\left(1\pm\frac{\hbar\omega_0}{\epsilon}\right)^{\frac{1}{2}}. \tag{15}$$

D is an energy parameter, analogous to C in (5) and K is the first non-vanishing reciprocal vector of the lattice. This result (see Eq. (59) of I) is derived under the assumption that the frequency of the optical modes is essentially constant. The upper value of the quantity in braces is valid in collisions in which the electron gains energy and the lower is valid in collisions in which the electron loses energy. The corresponding signs before $\hbar\omega/\epsilon$ apply in the two cases. n will be very small and may be neglected in comparison with unity, if the temperature of the crystal is small compared with the characteristic temperature. We shall focus attention on this case in discussing the collision frequency since n will be of the order of unity at most and the principal effect of the optical modes can be obtained without considering the thermal quanta.

The rate at which the moving electron loses energy is obtained by multiplying (15) by $\hbar\omega$ and setting $n=0$.

[18] C. C. Klick and R. J. Maurer, Bull. Am. Phys. Soc. **24**, No. 4, 26 (1949).

This result is valid even when n is not zero because of the cancelation of collisions in which the electron loses and gains energy. The ratio of the rate of energy loss in collisions with acoustic modes of vibration to the loss in collisions with optical modes is

$$R=(16/9)(C^2/D^2)(k^2/K^2). \tag{16}$$

When k approaches the boundary of a zone the ratio k^2/K^2 approaches unity. Thus R becomes essentially equal to C^2/D^2. The simplest supposition is that D is nearly equal to C so that R is near unity when k approaches the zone boundary. Unfortunately there seems to be little experimental evidence bearing on the point. If C and D are comparable in materials such as silicon and germanium one would expect the mobility in pure crystals to exhibit deviations from the $T^{\frac{3}{2}}$ law in the vicinity of the characteristic temperatures, which are 600°K and 290°K respectively, as the optical modes of vibration become sufficiently stimulated to scatter the electrons. The fact that such deviations are not observed may mean that D actually is smaller than C and that the influence of the optical modes is almost negligible in these materials. In either case the influence of the optical modes will not effect markedly the qualitative behavior of the function representing the collision frequency of the electrons as a function of energy or wave number: In both cases the collision frequency varies from about 10^{13} sec.$^{-1}$ when the energy of the electron is of the order of $kT=0.025$ ev to about 10^{15} sec.$^{-1}$ when the wave number vector approaches the zone boundary, where the curve has its maximum (Fig. 2).

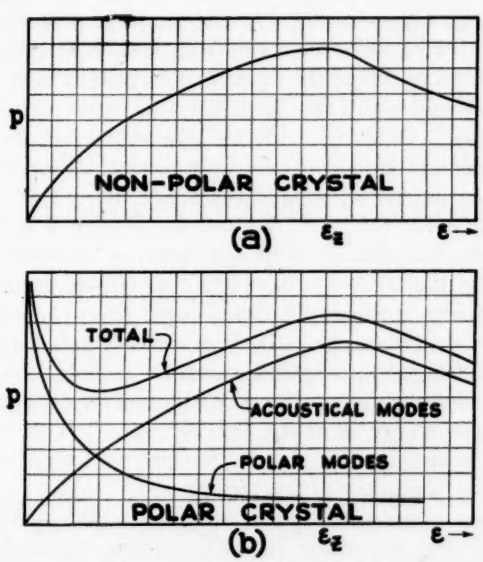

FIG. 2. Schematic representation of the collision frequency p as a function of energy ϵ in polar and non-polar crystals. Figure 2 (a) represents the collision probability in the case of a non-polar crystal such as diamond. The frequency has a maximum for an energy near ϵ_z. Both the optical and acoustical branches contribute to the peak. The collision frequency increases monotonically toward the peak and then falls. In Fig. 2 (b), for a polar crystal, the contributions from the polar and acoustical modes are shown separately, as well as their sums. The collision frequency for polar modes attains its maximum when ϵ is near $k\theta$, that is, of the order of 0.1 ev, whereas the collision frequency for non-polar modes attains its maximum near ϵ_z as in (a). The collision frequency possesses two maxima.

B. Polar Crystals

The most important interaction between electron and lattice in polar crystals is that with the polar modes of vibration when the energy of the electron is not too different from $k\theta$, as has been emphasized by Fröhlich. Mott and Fröhlich[19] have shown that the collision frequency of interest for transport theory is

$$p=\frac{1}{\tau_0}(\exp(h\nu_l/kT)-1), \tag{17}$$

when the energy of the electron is less than $k\theta$ so that it may only gain energy from the polar modes. Here[20]

$$\tau_0=\frac{3}{4\pi}\frac{\hbar v}{e^2(\kappa-\kappa_0)}\frac{\nu_l}{\nu_t^2}\frac{k_\nu}{k}, \tag{18}$$

where ν_l and ν_t are, respectively, the frequencies of the longitudinal and transverse polar modes of longest wave-length. These frequencies are related by the equation

$$\nu_t^2=(\kappa-\kappa_0+1)\nu_t^2, \tag{19}$$

in which κ is the static dielectric constant of the crystal and κ_0 is that arising from electron polarization alone. The v in (18) is the electron velocity, which is also equal to $\hbar k/m$. k_ν is defined by the equation

$$\hbar^2k_\nu^2/2m=h\nu_l. \tag{20}$$

Since τ_0 defined by (18) is independent of k, because of the presence of the ratio v/k, the collision frequency (17) is determined primarily by the temperature of the crystal, and becomes very small at low temperatures. When T approaches θ, (17) leads to values of the collision frequency of the order of $1/\tau_0$, which is of the order of $0.43\cdot10^{15}$ sec.$^{-1}$, and hence is sufficiently great that perturbation theory is not accurately applicable, as Fröhlich and Mott have emphasized.

It is to be stressed that the collision frequencies calculated by Fröhlich and Mott are those of interest for determining the mobility of the electrons and represent the frequency with which the electron is deflected through an angle that is 90° on the average. We shall discuss the true collision frequency later. This point is

[19] H. Fröhlich and N. F. Mott, Proc. Roy. Soc. **171**, 496 (1939).

[20] H. Callen has re-examined the interaction of polar origin in polar crystals more carefully than previous investigators in order to determine the extent to which von Hippel's criterion for breakdown will provide numerical agreement with the observed breakdown measurements. This work employs standard perturbation theory and hence is subject to the uncertainties arising from this source if it is to be employed for quantitative purposes. The writer is indebted to Dr. Callen for an opportunity of seeing a copy of his manuscript prior to publication.

not of major concern in the preceding discussion of non-polar crystals since the scattering is practically isotropic as long as the electron resides in the first zone.

When the energy of the electron exceeds $k\theta$, it may both give to as well as receive energy from the polar modes and the expression, for the transport collision frequency is

$$p=\frac{1}{\tau_0}\left(1+\frac{2}{e^{\theta/T}-1}\right). \tag{21}$$

Fröhlich has found that as long as the wave number vector of the electron lies inside the first zone, but still lies in the range for which the energy of the electron is greater than $k\theta$,

$$\frac{1}{\tau_0}=\frac{e^4 n_0}{\hbar^2 v_0 k}\frac{m}{M}, \tag{22}$$

in which n_0 is the density of ions, which is $1/a^3$ in the sodium-chloride lattice if a is the nearest-neighbor distance, and ν_0 is taken as the frequency of the transverse polar modes. Since k appears in the denominator, it follows that the collision frequency decreases as the wave number vector approaches the zone boundary, in contrast with the situation described previously for the interaction in non-polar crystals. We readily find that $1/\tau_0$ is of the order of $1.5\cdot 10^{13}$ for a typical crystal such as NaCl when $k=k_z$. Thus the collision frequency falls from a very high value when the energy of the electron is of the order of $k\theta$ to a relatively low value when the energy is of the order of several electron volts, corresponding to an energy near the zone boundary. In fact the mobility of the fast electron would be comparable to that of a thermal electron in a non-polar crystal if no other influence arose to affect the collision frequency.

Fröhlich has shown that the transport collision frequency falls as $1/k^3$ once the electron has an energy well outside the first zone.

The true collision frequency p', which does not contain an angular weighting factor of the type introduced by Fröhlich, is readily obtained from the material presented in Fröhlich's paper. In fact the derivation follows closely the procedure outlined in Section 5 of his paper in which the rate of energy transfer is calculated. This transfer is the sum

$$h\nu_0(p_+-p_-), \tag{23}$$

in which p_+ is the frequency of collisions in which the electrons transfer energy to the lattice and p_- is the frequency of collisions in which the electron receives energy. It is easily found from Fröhlich's work that

$$p'=2\pi\frac{e^4}{a^3}\frac{m}{M}(2n+1)\frac{1}{h\nu_0}\frac{1}{\hbar k}\int_{\sigma_1}^{\sigma_2}\frac{d\sigma}{\sigma}, \tag{24}$$

in which σ, as previously, is the wave number of the lattice wave (in the reduced scheme) and σ_1 and σ_2 are respectively the minimum and maximum values associated with a given value of k. The value of σ_1 (which Fröhlich calls w') is

$$\sigma_1=\frac{2\pi m\nu_0}{\hbar k}. \tag{25}$$

The maximum is $2k$ when k lies well inside the zone, whereas it may be chosen to be a constant, as an approximation, when k is well outside the first zone. In either case the integral in (24), which has the value $\log(\sigma_2/\sigma_1)$, may be treated as if nearly constant. It is to be noted that the ratio of (24) to (21) is $\log(\sigma_2/\sigma_1)$ which shows that the collisions are nearly isotropic when k is inside the zone. The ratio is much larger when k extends well outside the first zone and increases as $k^2\log(\sigma_2/\sigma_1)$ since the collisions cease to be nearly isotropic.

The preceding scattering is the result of interaction between the electron and the polarization field arising from displacement of the ions. This field is identical with that which would be obtained from a lattice of point ions if they underwent oscillatory motion. Let us now consider the extent to which this scattering is augmented by scattering arising from variations in the local potential field analogous to that considered for non-polar crystals. There is no doubt that any such supplementary scattering is negligible when the energy of the electron is near $k\theta$, however it could be important for other ranges of energy. The simplest procedure to follow is to assume that this additional scattering can be treated by use of the equations derived for non-polar crystals and based on the deformable atom picture. In this case a material such as germanium becomes an approximate stand-in for a crystal such as NaCl since the characteristic temperatures are about the same (Ge: 290°K, NaCl: 281°K) and the density of atoms in the first material is about the same as the density of ions in the second. However, the atomic weight of germanium is about 2.5 times larger than the average atomic weight in the salt. If a correction is made for this, it is found, using the equations derived in I, that the collision frequency for a conduction electron having thermal energy is about $0.7\cdot 10^{13}$ sec.$^{-1}$. This would yield a mobility of about 250 cm^2 volt-sec. in the absence of additional scattering.

If we employ the equations in I which relate the parameters occurring in (10) to the characteristic temperature and employ Eq. (12) for the determination of k_z we find that the collision frequency arising from the acoustical modes is $1.8\cdot 10^{14}$ sec.$^{-1}$ when $k=k_z$. This value is not negligible in comparison with the contribution from the polar modes derived with the use of Fröhlich's equations, namely $1.5\cdot 10^{13}$ sec.$^{-1}$. In other words the non-polar contribution to scattering in polar crystals would be appreciable at energies above the thermal range if it were comparable to that expected in non-polar crystals. This conclusion is valid, even if the

contribution from acoustical modes of vibration alone is considered.

It seems entirely reasonable to assume that non-polar scattering is as important in polar crystals as in non-polar materials. The basis for the use of the deformable atom model, which leads to the relation (4) in determining the scattering from non-polar fields, rests on the assumption that the relative distribution of the valence electrons in any unit cell is altered when a vibrational wave passes through the lattice. Since the valence electrons on the negative ions play as important a role in determining the interatomic forces in ionic crystals, principally through the Born repulsive term in the expression for the total energy, as do the valence electrons in non-polar crystals, we may expect non-polar scattering to be of comparable magnitudes in the two materials.

We should also expect the optical branches as well as the acoustical to contribute to the non-polar component of scattering in polar crystals by an amount comparable with that found in non-polar crystals if the surmise of the preceding paragraph is correct. Since the non-polar component becomes most important in polar crystals when the electron has a wave number near the zone boundary and since the magnitudes of the scattering associated with the two branches of the vibrational spectrum are then comparable (Eq. 16), the inclusion of the higher branch will at most multiply the collision frequency computed from the acoustical branch by a factor two.

To summarize, the collision frequency when plotted as a function of energy should have the form shown in Fig. 2 for polar and non-polar crystals. In the first case the curve has two maxima of comparable height, whereas only one maximum occurs in the second case.

5. BEHAVIOR OF AN AVERAGE ELECTRON

Let us now consider the field E_H at which a free electron would receive on the average more energy from the applied field than it expends in exchange with lattice vibrations for all values of its kinetic energy. This is the field at which breakdown would occur, according to von Hippel's theory. The condition satisfied by E_H is

$$d\epsilon/dt)_E + d\epsilon/dt)_L = 0 \tag{26}$$

for the energy ϵ at which $d\epsilon/dt)_L$ is a maximum. Here $d\epsilon/dt)_E$ is the rate of gain of energy from the field and $d\epsilon/dt)_L$ is the rate of transfer of energy to the lattice vibrations. We shall assume that the average electron undergoes Brownian motion and possesses a mobility

$$\mu = (e/m)\tau_m \tag{27}$$

in which τ_m^{-1} is the transport collision frequency. The rate of gain of energy from the field is thus

$$d\epsilon/dt)_E = (e^2/m)E^2\tau_m. \tag{28}$$

Since the largest values of $d\epsilon/dt)_L$ occur in the range of energy in which the collisions are essentially isotropic, the transport collision frequency and the true value do not differ greatly. The source of error that would result from the assumption that they are equal would probably not be larger than that made in employing perturbation theory in calculating the collision frequency. As a result, we shall occasionally replace τ_m by the true value τ_t.

The rate of transfer of energy to the lattice was discussed in the previous section and is given in various cases by Eqs. (11), (16), and (23) which may be placed in the form

$$-d\epsilon/dt)_L = \hbar ck(1/\tau_1), \tag{29}$$

$$1/\tau_1 = (4/9\pi)(C^2k^2/\hbar^2 n_0 c)(m/M) \times[1+(9/16)(D^2K^2/C^2k^2)], \tag{29a}$$

$$-d\epsilon/dt)_L = h\nu_0(1/\tau_2), \tag{30}$$

$$1/\tau_2 = (1/\tau_0)\log(\sigma_2/\sigma_1), \tag{30a}$$

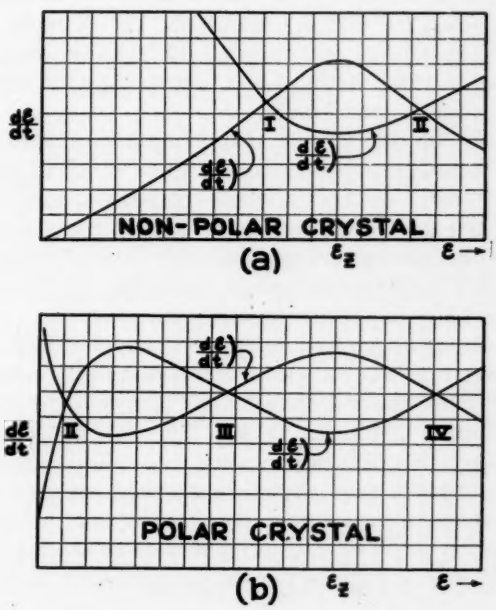

FIG. 3. Schematic picturization of the curves representing energy gain and loss as a function of time in polar and non-polar crystals. Figure 3 (a) shows the gain and loss curves corresponding to the two terms in Eq. (26). The case illustrated represents one in which the electrostatic field is less than but nearly equal to E_H, so that $d\epsilon/dt)_E$ crosses $d\epsilon/dt)_L$ twice. An electron having energy less than that associated with the first crossing, namely I, will be accelerated on the average. The second crossing, designated as II, represents a point of instability. If the electron has greater energy it will be accelerated on the average. Electrons having energy between the cross-points will move toward I on the average. Figure 3 (b) shows the corresponding case for a polar crystal. In this case there are four cross-points, of which only three are shown (designated as II, III, and IV). The cross-point of lowest energy which could be designated as I, is not shown since it occurs too close to the origin. The cross-points I and III represent energies of relative stability for the electron distribution whereas II and IV are unstable points. III and IV evidently are the analogues of I and II in Fig. 3 (a). (*Note:* Through an error the subscripts are omitted in the quantities $d\epsilon/dt$ which designate the gain and loss curves. The lower symbol designates the loss curve in both figures.)

in which τ_0 is given by (18) or (22). Equation (29) is to be employed for the non-polar interaction in polar and non-polar crystals when k is near the zone boundary, whereas (30) is to be employed for the polar interaction in polar crystals when the electron energy is near $k_0\theta$.

In terms of the quantities defined above E_H[2] is given by the maximum value of the quantity

$$m/e^2(\hbar ck/\tau_m\tau_1) \tag{31}$$

in non-polar crystals, and by the maximum value of either (31) or

$$m/e^2(hv_0/\tau_m\tau_2) \tag{32}$$

in polar crystals.

In diamond, the maximum value of (29a) is about $3.8\cdot10^{15}$ sec.$^{-1}$ and E_H is about $4.0\cdot10^7$ volts per cm if we take $C^2=936$ ev^2. It should be emphasized again that the absolute value of this may be considerably in error because of the inaccuracy accompanying the use of perturbation theory and inaccuracies in the numerical values used for various parameters. For example, the values are $0.6\cdot10^{15}$ sec.$^{-1}$ and $6.7\cdot10^6$ volts per cm if we decrease C^2 by a factor of 6 as suggested by the experiments of Klick and Maurer.

In sodium chloride, the peak in scattering frequency near thermal energies leads to a value of E_H of about $1.6\cdot10^6$ volts per cm, whereas the peak arising from non-polar scattering produces a value of about $1.2\cdot10^6$ if we assume the collision frequency is $3.6\cdot10^{14}$ sec.$^{-1}$. In other words the values are essentially equal within the accuracy of the present analysis.

In the absence of an external electrostatic field, the free electrons which occur in an insulator will possess a velocity distribution given by the Maxwell-Boltzmann distribution function. As the field intensity grows, however, the distribution may be radically altered because an electron possessing thermal energies may gain energy from the field more rapidly than it loses it to the lattice. This rate of gain is given by Eq. (28) which may be expressed in the approximate form

$$d\epsilon/dt)_E=(e^2/m)(E^2/p), \tag{33}$$

since $1/\tau_m$ is closely equal to the true collision frequency. Thus, as E increases toward E_H, the distribution function will be affected first in ranges of energy most distant from the peaks in p. This means that the Maxwell-Boltzmann distribution will be altered most easily in non-polar materials, which have high mobilities in the thermal range of energies. The mobility of diamond is about 900 cm^2 volt-sec. at room temperature according to Klick and Maurer. In this case the thermal electrons begin to gain energy from the field more rapidly than they lose it when the electrostatic field is about 5 kv per cm. Hence, the distribution is pushed to higher energies when the field exceeds this value and the electrons are no longer in thermal equilibrium with the lattice. The distribution which does obtain may be expected to be stable as long as E is small compared to E_H, which has been estimated above to lie between $6\cdot10^6$ and $4\cdot10^7$ volts/cm, because p increases and hence $d\epsilon/dt)_E$ decreases with increasing energy. The average energy of the electrons in this type of stable distribution is determined by the value of ϵ at which Eq. (26) is satisfied for the value of E applied to the crystal. This energy is 1 ev for diamond when E is about $3\cdot10^5$ volts per cm, if we assume the room temperature mobility is 900 cm^2/volt-sec.

The Maxwell-Boltzmann distribution should be much more stable in ionic crystals than in non-polar substances because the collision frequency possesses a maximum for energies near $k\theta$. The mobility of electrons in sodium chloride is about 100 times less than in diamond at room temperature. It follows that the Maxwell distribution will be radically distorted only when E becomes comparable to E_H.

We saw in the previous section that the collision frequency of electrons in ionic crystals possesses two maxima (see Fig. 2) when regarded as a function of energy. Equation (26) may possess four roots, two lying on each side of the maxima of $p(\epsilon)$ (Fig. 3) when E is sufficiently large, but still smaller than E_H. An electron which finds itself on the high energy side of the second root, which lies on the high energy side of the maximum in $p(\epsilon)$ occurring near $k\theta$, will gain energy from the field on the average and eventually reach the energy corresponding to the third root which lies on the low energy side of the peak that occurs near ϵ_2. Thus just as in non-polar crystals, there may be a group of electrons which possess energies that are large compared with kT and yet preserve an energy balance. The difference between the behavior in the two crystals lies in the fact that the high energy group is the only one in non-polar crystals whereas it contains only those electrons which escape the thermal distribution in polar crystals.

6. EXTENT OF DEVIATIONS FROM AVERAGE BEHAVIOR

In the preceding section we discussed the average behavior of a free electron. We shall now examine the extent to which an appreciable deviation from the average behavior can occur. This problem is of interest in trying to decide whether or not breakdown and related properties are determined by the average electron or by improbable fluctuations.

As a typical problem let us consider an electron which moves in the direction of the force exerted by the field and which starts with energy ϵ_1. Consider the probability that it will be accelerated to energy ϵ_2 without making any collisions. An electron of this type would be accelerated at the rate eE/m, where E is the field intensity. Hence it would gain energy from the field at the rate

$$d\epsilon/dt=eEv=eE(2\epsilon/m)^{\frac{1}{2}}. \tag{34}$$

The probability $P(t)$ that it will move for a time t without making a collision satisfies the differential equation

$$dP/dt=-pP \tag{35}$$

in which p is the average frequency of collision, which we have discussed in previous sections. Since p is known as a function of energy and since the energy is known as a function of time in the problem of interest to us in this paragraph, p may be regarded as a function of time. Hence,

$$P(t)=\exp\left(-\int_0^t p\,dt\right)=\exp\left(-\int_{\epsilon_1}^{\epsilon_2}\frac{p\,d\epsilon}{d\epsilon/dt}\right). \tag{36}$$

In the following, we shall assume that fluctuations in which the electrons make no collisions, or at most a very small number of collisions, are the most important group and shall employ (36) to estimate the probability for the group. It is apparently very difficult to treat quantitatively the frequency of collisions intermediate between the average and the extreme case represented by (36) because of the absence of a simple relation of the type (34). We shall see below that fluctuations of the type (36) play an important role in lowering the breakdown field below the value E_H determined by assuming that only the average behavior of electrons is important. If intermediate distributions of collisions are more important than those in which essentially no collisions occur, the breakdown field will be lowered even further, so that the following discussion can be viewed as giving a lower limit to the importance of fluctuations.

The following semi-quantitative argument seems to indicate that the fluctuations which are most important in determining breakdown in practice probably are those in which the electron is accelerated essentially from rest to the energy required for breakdown without making any collisions. Let us consider a somewhat idealized situation in which the collision frequency p is independent of energy. This assumption actually represents, to a fair approximation, the situation which occurs in ionic crystals if the curves of Fig. 2 are similar to the actual case. We shall also assume that the electron loses all of its forward momentum on the average each time it makes a collision with the lattice so that the kinetic energy it gains from the field between two collisions a time t apart is $(eEt)^2/2m$, irrespective of its kinetic energy at the time of the first collision. Thus if the electron starts from rest and makes n collisions spaced a distance t apart, the kinetic energy gained from the field is $(eEt)^2/2m$. In the following we shall consider time intervals between collisions which are sufficiently long and applied fields that are sufficiently strong that the collisions can be regarded as elastic. This means, of course, that we will be treating cases well removed from the average behavior in which gain and loss balance one another.

If I is the energy required to produce ionization and if this energy is obtained after n collisions, which we shall regard for simplicity as equally spaced, the time t between collisions must satisfy the equation

$$I=n(eEt)^2/2m.$$

Thus the time required to gain the energy I after a sequence of n collisions is $(n)^{\frac{1}{2}}t_1$, where t_1 is the time that would be required if the electron were accelerated with no collisions.

The probability that the electron shall undergo n collisions in the time $(n)^{\frac{1}{2}}t_1$ is given by the expression

$$P_n=\frac{(pt_1)^n n^{n/2}}{n!}\exp(-(n)^{\frac{1}{2}}pt_1) \tag{A}$$

in which p is the average number of collisions per unit time. Moreover the probability that the electron shall spend a time t_1 without making a collision in the time interval $(n)^{\frac{1}{2}}t_1$ is

$$G=p((n)^{\frac{1}{2}}-1)t_1\exp(-pt_1). \tag{B}$$

The ratio of (A) to (B) may be placed in the form

$$P_n/G=((n)^{\frac{1}{2}}-1)^{-1}\exp(-((n)^{\frac{1}{2}}-1)pt_1-(n/2)\log n+n+(n-1)\log pt_1) \tag{C}$$

if Stirling's approximation is employed. We shall set

$$n=\lambda^2 \quad \text{and} \quad pt_1=\alpha$$

so that the exponent in (C) becomes

$$-\alpha\lambda+\lambda^2-\lambda^2\log\lambda+\lambda^2\log\alpha+\alpha-\log\alpha. \tag{D}$$

For given α this function has roots at the points

$$\lambda=\alpha(1-x) \quad \text{and} \quad \lambda=1+y,$$

where

$$x=\left(\frac{2\alpha-\log}{3\alpha^2}\right)^{\frac{1}{2}}, \quad y=\frac{1}{\alpha-1-2\log\alpha}.$$

There is a minimum between these roots at $\lambda=0.3\alpha$ in which we are principally interested. Equation (C) has the value

$$-0.11\alpha^2+\alpha-\log\alpha$$

at this minimum. At fields near observed breakdown values α varies between about 10 and 30 if p is assumed to have a constant value near 10^{15} sec.$^{-1}$. For $\alpha=10$, (D) has the value -3.3, so that G is only slightly larger than P_n and we may expect a mixture of fluctuations to be important, those in which the electron is accelerated to the ionization energy with very few collisions being only moderately preferred if at all. On the other hand, (D) is -13 and -74 when α is 15 and 30, respectively, so that G is then far larger than P_n for values of n near the minimum.

The quantity (D) possesses a positive maximum when $\lambda=\alpha$ or when $n=p^2t_1^2$. In this case the time interval $(n)^{\frac{1}{2}}t_1$ is pt_1^2 for which the mean number of collisions is $p^2t_1^2$. Thus this maximum corresponds to the average situation and not one in which fluctuations are occurring.

The previous calculation for the case in which p is constant shows that the group of statistical fluctuations in which the electron is accelerated to the energy I with very few collisions is favored strongly over types intermediate between this and average behavior whenever α is 15 or greater. We may assume that the same conclusion is valid when the integral in the exponent of (36) is 15 or larger.

Let us consider the special case of interaction with the acoustical modes of vibration when the crystal is at the absolute zero of temperature. In this event we see from Eq. (10) that

$$p=A\epsilon, \quad A=\frac{16}{27\pi}\frac{C^2}{\hbar^4 n_0 c}\frac{m^2}{M}. \tag{37}$$

Combining this with (34), we readily find that the integral in (36) is

$$(2/3)(1/Ee)(m/2)^{\frac{1}{2}}(\epsilon_2)^{\frac{1}{2}}p_2-(\epsilon_1)^{\frac{1}{2}}p_1), \tag{38}$$

in which p_1 and p_2 are the values of p when the electron energy has the values ϵ_1 and ϵ_2, respectively. If we take ϵ_1 to be of the order of thermal energy and ϵ_2 to be of

the order ϵ_s, the second term in parenthesis is completely negligible in comparison with the first. Moreover, if we assume $p_2=3.8\cdot10^{15}$ sec.$^{-1}$ and $\epsilon_s=11.5$ which are essentially the values for diamond used in the previous section, (38) is

$$4.8\cdot10^5/E, \tag{39}$$

or $1.5\cdot10^8/E$, if E is expressed in units of volts per cm. If E is taken to have the value of $4\cdot10^7$ ev found in the last section for E_H, the integral becomes about 3.8. Hence

$$P=\exp(-3.8)=0.023. \tag{40}$$

This result is valid not only for the hypothetical example chosen. We note from Eqs. (31) and (32) that E_H^2 is proportional to $1/\tau_m\tau_t$ where τ_m is the collision time of interest for determining the mobility and other transport coefficients and τ_t is the true collision time. Since τ_t and τ_m are nearly equal for the electron energies of interest to us, it follows that E_H is proportional to the quantity p_2 appearing in (38). As a consequence P may generally be expressed in the approximate form

$$P=\exp(-3.8E_H/E) \tag{41}$$

for fields near E_H in any material for which (38) is valid.

The integral appearing in (36) may be evaluated by methods similar to those used above in the case in which the collision frequency p is determined by polar modes of vibration. In this case p varies as $1/(\epsilon)^{\frac{1}{2}}$ when ϵ exceeds the peak value which occurs near $\epsilon=k\theta$. The expression analogous to (38) is

$$(1/Ee)(m/2)^{\frac{1}{2}}(\epsilon_1)^{\frac{1}{2}}p_1\log(\epsilon_2/\epsilon_1). \tag{42}$$

Here ϵ_1 may be taken to be $k\theta$, $\epsilon_2=\epsilon_s$ and p_1 is the peak value of the collision frequency. The value of P derived from this expression when $E=E_H$ does not differ substantially from that derived with the use of (38) if values of the constants are chosen to correspond to the case of NaCl described in the previous sections.

We may note in passing that the time required to accelerate an electron from rest to an energy of 10 ev when the field is E, is mv/eE, where v is the terminal velocity namely $2\cdot10^8$ cm sec. The time has the value $3\cdot10^{-15}$ sec. for the example employed in the previous paragraph when $E=E_H=4\cdot10^7$ volts per cm.

The time required for an electron to drift 1 cm in a field of strength E is approximately $m/eE\tau_m$, where, as previously, τ_m is the collision frequency of interest for transport. During this time the electron will make $m/eE\tau_m\tau_t$ collisions. This is also the number of "trys" the electron will have to be accelerated to an energy of the order of 10 ev without making a collision during the period in which it migrates 1 cm. The product of the number of trys and the probability P of success per try is the number of times the electron would actually be accelerated to 10 ev without a collision in travelling unit distance. The reciprocal of this quantity is simply Λ, the average distance the electron travels before receiving sufficient energy to produce a secondary (see Section 2):

$$\Lambda=E(e/m)\tau_m\tau_t\exp(3.8E_H/E). \tag{43}$$

This equation may also be placed in the form

$$\Lambda=\frac{E\epsilon'}{eE_H^2}\exp(3.8E_H/E), \tag{44}$$

with the use of (31) and (32). ϵ' designates the quantity $h\nu_0$ appearing in (32) in the case in which E_H is evaluated from the polar modes and designates an appropriate mean value of $\hbar ck$ in the case when E_H is evaluated from the non-polar ones.

In the example cited early in this section, for which E_H is taken to be $4\cdot10^7$ ev and p_2 is $3.8\cdot10^{15}$ sec.$^{-1}$, corresponding to diamond, the time required for an electron to drift 1 cm on the average in a field of magnitude E_H is about $5.3\cdot10^{-8}$ sec. The electron would make about $2\cdot10^8$ collisions during this period of time. Correspondingly the coefficient of the exponential in (44) is of the order of $8\cdot10^{-9}$ cm if ϵ' is taken to be of the order of 0.1 ev. Thus, Λ is about $4\cdot10^{-7}$ cm when $E=E_H$.

The dependence of Λ upon E evidently arises principally through the exponential term in (44). For practical purposes the coefficient may be taken to be equal to ϵ'/eE_H when E is near E_H. Λ is of the order of 1 cm when $E=0.2E_H$.

Thus the present calculations show that in general the distance which the electron travels before producing a secondary electron varies from about 1 cm to about 10^{-6} cm as E varies from $0.2E_H$ to E_H. Evidently the field for which $\Lambda=D/40=0.025D$ lies within this range when D has the value associated with a normal test specimen. In other words the value of the field for which breakdown occurs is usually less than E_H, although it is close to this value, when the impact ionization theory is valid. Statistical fluctuations play an important role in the sense that they permit breakdown to occur before the field reaches E_H provided the specimen is larger than about 10^{-6} cm. As described in Section 2, we may expect to observe avalanches in the range of field strength between that for which $\Lambda=D$ and that for which it is $0.025D$.

The value of E at which Λ is $0.025D$, which we may call E_B, is determined by the equation

$$E_B=3.8E_H/\log\frac{0.025eE_H^2D}{E_B\epsilon'}. \tag{45}$$

It follows readily from (43) that Λ will decrease by a factor 40 if E is increased by about 20 percent when E is in the vicinity of $0.2E_H$. Hence the value of the field strength at which avalanches begin should be only about 20 percent smaller than the breakdown field if the coefficient 3.8 appears in the exponent of (44). Now this coefficient was derived from (38) by setting $E=E_H$ and is essentially the ratio $(\epsilon_s/mc^2)^{\frac{1}{2}}$ where c is

the velocity of the longitudinal sound waves. As a result, it should be relatively insensitive to the errors in the various quantities computed in the previous sections.

Figure 1, which shows the avalanches observed by Haworth and Bozorth in Pyrex, indicates that the field must change by a factor of about 5 in order to have the avalanches change in size from one electron to a value of the order of 10^6 electrons. This dependence on field strength corresponds to a coefficient in the exponent of (44) that is of the order of 50 times smaller than that we have derived. In other words, the avalanches observed by these investigators seem to be much less sensitive to field strength than those predicted from Eq. (44). The electronic pre-breakdown currents observed by von Hippel and others also appear to be much less sensitive to field than currents based on Eq. (44) would be.

The behavior of the avalanches observed by Haworth and Bozorth would be readily understood if it could be postulated that the electrons involved need tunnel through a much smaller portion of the friction barrier than that considered in the evaluation of (38). This would be the case, for example, if these avalanches were produced as the result of the freeing by impact of relatively loosely bound electrons which are attached to foreign atoms. In this case the electron being accelerated would require a lower energy than is needed to ionize the atoms of the bulk material. Hence the electron would be required to make a much less improbable transition through the friction barrier. This point would be worth detailed experimental investigation, for it may prove possible to obtain pre-breakdown avalanches of controlled size by selected contamination of suitably chosen solids.

The value of the breakdown field for diamond determined from the foregoing avalanche theory is about $8 \cdot 10^6$ volts per cm. This is very close to the value to be expected from the field ionization theory of Zener and Franz. The absolute values of the breakdown fields obtained from the approximate equations which have been derived for the two types of theories cannot be given great credance. However the results suggest that breakdown may actually occur by field ionization in diamond.

7. THE EXCITATION PROCESS

Consider now the behavior of an electron which has an energy near to or greater than ϵ_s and which is in a field sufficiently strong that it will gain more energy from the field than it loses to the lattice. An electron of this type will be accelerated until it is sufficiently energetic to excite or ionize the electrons of the lattice, the process on which attention will be focused in this section.

For simplicity, we shall assume that the cross section for excitation when regarded as a function of energy can be expressed in the form

$$\sigma(\epsilon)=\sigma_m(\epsilon_m/\epsilon)\log(\epsilon/\epsilon_e) \quad (\epsilon \geqslant \epsilon_e). \tag{46}$$

Here σ_m is the maximum value of the cross section, ϵ_e is the threshold energy at which excitation is possible and $\epsilon_m=2.71\epsilon_e$ is the energy at which the maximum in σ occurs. This expression is to be employed only when $\epsilon \geqslant \epsilon_e$.

The probability dq that the electron will make a collision resulting in excitation of the bulk atoms of the solid in time dt is

$$dq=\sigma n_0 v dt \tag{47}$$

where n_0 is the density of atoms and v is the velocity of the electron. We shall assume that the electron gains energy from the field at the rate veE, so that (47) may be written

$$dq=(\sigma n_0 d\epsilon/Ee). \tag{48}$$

An electron which starts with an energy less than ϵ_e will have unit probability of producing excitation when its energy has attained the value satisfying the equation

$$\log^2(\epsilon/\epsilon_e)=(2Ee/\sigma_m n_0 \epsilon_m). \tag{49}$$

The quantity on the right has a value between 0.1 and 0.01 for diamond when E has the range of values of $0.2E_H$ estimated previously provided σ_m is given the value 10^{-16} cm^2 corresponding to a typical atomic cross section. The values for sodium chloride lie in the same vicinity. In both of these cases, Eq. (49) is satisfied when ϵ/ϵ_e lies between 1.3 and 1.1. The principal conclusion to be drawn is that the electron does not produce excitation or ionization as soon as its energy reaches the threshold value ϵ_e when σ_m has a more or less normal value. Instead the electron continues to be accelerated and produces excitation or ionization only when the energy is somewhat larger than ϵ_e. It follows that the primary electron will be left with an energy larger than $k\theta$ on the average after the excitation process although it may not have an energy as large as ϵ_s. Thus even in an ionic crystal the primary electron will usually end with an energy in the range where it can be accelerated further until it is blocked by the peak associated with lattice collisions occurring near ϵ_s. This conclusion evidently is valid only if E is near to E_H.

If the excitation collision produces a second free electron, the primary and secondary electrons should divide the energy in excess of that needed to produce ionization so that both will end up with an energy larger than $k\theta$.

One of the most important conclusions to be drawn from the preceding discussion is the following: Once an electron which is free in an ionic crystal has escaped from the portion of the velocity distribution which occurs on the low energy side of the peak in collision frequencies near $\epsilon=k\theta$, it will continue to remain out of this portion of the distribution during its subsequent history. This conclusion is valid provided E is suffici-

ently close to E_H that the electron gains more energy from the field than it loses to the lattice in the range of energy between the two peaks occurring near $k\theta$ and ϵ_s. Moreover, any secondary electrons it produces will not join the distribution on the low energy side of $k\theta$. This means that a free electron and its progeny will behave in essentially the same way in polar and non-polar crystals when the field is strong once the electron has been accelerated beyond the low energy range.

Consider next the excitation of impurity atoms which are present in concentration n_i, which we shall suppose to be appreciably smaller than n_0. Let us suppose that the primary electron has been accelerated to an energy sufficient to ionize the impurity atom as a result of an unusual fluctuation, the energy of this electron being of the order of 2 ev above that of the average electron which is at energy equilibrium. If σ_i is the cross section for ionization of the impurity atom, the probability that the unusually energetic primary will produce ionization of one of the impurity atoms in time t is

$$\pi(t)=n_i\sigma_i vt, \tag{50}$$

in which v is the average speed of the electron.

The unusually energetic electron will eventually lose its excess energy since on the average it suffers an unfavorable balance of exchange of energy with the lattice. For example, if its energy is 2 ev higher than average and if it loses about 0.1 ev on the average in each collision with the lattice, it will fall back among the average electrons in the time required for about 20 collisions. If T is the time the electron has the excess energy, the probability that it will ionize an impurity atom during this period is

$$\pi_i=n_i\sigma_i vT. \tag{51}$$

This is of the order of 10^{-6} if we assume that $n_i=10^{16}$ per cc, $\sigma_i=10^{-16}$ cm^2, $v=10^8$ cm per sec. and $T=10^{-14}$ sec.

Consider now the distance Λ_i that the electron must travel in order to ionize an impurity atom. Equation (44) was derived under the assumption that the primary electron will ionize an atom of the bulk material the first time it has been accelerated to the region where it has sufficient energy to do so. The discussion which centers about Eq. (49) of the present section shows that this assumption is reasonable as long as σ_m has a typical atomic value. The equation for Λ_i which replaces (44) will have the approximate form

$$\Lambda_i=\frac{1}{\pi_i}\frac{E\epsilon'}{eE_H^2}\exp(\alpha E_H/E). \tag{52}$$

Here α is a constant considerably smaller than the corresponding constant 3.8 which appears in (44) since it assumed that the primary electron need not experience as radical a fluctuation in gaining energy sufficient to ionize an impurity atom as is necessary to ionize an atom of the bulk solid. The coefficient $1/\pi_i$ takes account of the fact that the primary electron which gains sufficient energy to ionize the impurity atom as the result of a fluctuation need not actually produce ionization. The remaining coefficient in (52) is assumed to be the same as in (44) since the frequency of collisions with the lattice will be nearly the same when the electron has energy sufficient to ionize impurities and to ionize the atoms of the bulk material.

Λ_i has the value D when E satisfies the relation

$$E=\alpha E_H/\log(eE_H^2\pi_i D/E\epsilon'). \tag{53}$$

This in turn is about $\alpha E_H/10$ if π_i is assumed to be 10^{-6} and the other quantities are given typical values. In other words, avalanches which result from the ionization of impurity atoms by electron impact will begin to be observed at fields that are much smaller than E_H. Moreover, the size of these avalanches should grow much less rapidly with field strength than those which originate in the ionization of the bulk material. It seems possible that avalanches of this type were observed by Bozorth and Haworth, and that the noisy pre-breakdown currents observed in other materials originate in the same way. It has also been suggested that these avalanches are associated with sudden changes in the electrode-crystal contact as a result of the strong field there.

8. THE FIELD-DECOMPOSITION OF EXCITONS

It is generally supposed at the present time that the first excited states in an insulating solid correspond to excitation waves which are the analogue of the discrete excited electronic levels of an atomic or molecular system in which the electrons remain bound to the nuclei. Unless the excitation waves become decomposed into free electrons and holes by some agency, the accelerated electron which has produced the wave will have expended its energy without having produced a secondary charged particle. In this case the first excitation process would present a barrier analogous to the processes in which the electron transfers its energy to the lattice vibrations described previously. The electron would need to pass the excitation barrier in order to obtain sufficient energy to produce secondary free electrons.

Let us consider the possibility that the excitation waves are decomposed by the applied field in the manner first proposed by Oppenheimer[21] for the hydrogen atom. The theory of this effect has been highly developed for atomic hydrogen by Lanczos[22] who obtained excellent agreement with observations of von Traubenberg[23] on the disappearance of the spectral lines of atomic hydrogen in the presence of an electrostatic field. These investigators find that the $H\gamma$ line of the Balmer

[21] J. R. Oppenheimer, Phys. Rev. **31**, 66 (1928).
[22] C. Lanczos, Zeits. f. Physik **62**, 518 (1930); **68**, 204 (1931).
[23] H. Rausch v. Traubenberg, Zeits. f. Physik **54**, 307 (1929); **56**, 254 (1929); **62**, 289 (1930); **71**, 291 (1931).

spectrum, which originates in a transition from the level having total quantum number $n=5$ to the level for which $n=2$, vanishes when the field intensity is about 700 kv per cm. The lifetime of the level for which $n=5$ then becomes less than the time required for emission of radiation (about 10^{-8} sec.). The level for which $n=5$ has a binding energy of 0.54 ev in the field-free atom. An analysis of Lanczos' results for levels in the neighborhood of $n=5$ shows that the critical field varies about as $1/n^4$. In other words, it varies essentially as the square of the ionization energy of the level.

The binding energy of the excitation states of the crystals are not accurately known. To obtain approximate values, we may assume that the electron and hole attract one another with a Coulomb force that is screened as a result of the high frequency dielectric polarization of the lattice. The energy states of the excitation wave associated with zero translational momentum are then given by an equation of the hydrogenic form:

$$E_n=\frac{e^4m}{2\mu^4\hbar^2n^2}. \tag{54}$$

Here μ is the refractive index of the crystal and n is a quantum number which may take the values $n=1, 2, 3, \cdots$. The factor two in the denominator enters because the reduced mass of the system is half the electronic mass. This expression should be more nearly valid for large quantum numbers than for small. Relative to the dissociated state the first excited state possesses the energy

$$E_2=-(1.7/\mu^4)(\text{ev}). \tag{55}$$

Since the indices of refraction of diamond and sodium chloride are 2.42 and 1.54, respectively, E_2 is 0.049 ev and 0.30 ev in the two cases.

In the case of diamond, the excitation states would be dissociated by a field well under 100 kv per cm, that is by a field that is very small compared with E_H. In fact the excitation waves should be dissociated as a result of thermal fluctuations in the vicinity of room temperature if this estimate of the binding energy of electron and hole is at all reliable.

The case of sodium chloride is more questionable since E_2 does not differ greatly from the value for the level $n=5$ in hydrogen. In fact, Mott[8] has proposed on the basis of an analysis of the ultraviolet absorption bands of the alkali halides that the energy of the first excitation state is about -1.7 ev relative to the dissociated state. Presumably the field required to dissociate this excitation state would be near to if not actually greater than E_H.

The calculations of the preceding section show that if σ_m is in the neighborhood of 10^{-16} cm^2, which is a typical value, the average accelerated electron makes its first exciting collision with the electrons of the bulk material when its energy is about 1.2 times larger than the threshold value. The threshold is about 7.5 ev in sodium chloride, according to measurements of optical absorption. It follows that the electron may well have sufficient energy, namely 9 ev, to produce ionization when it first transfers energy to the electrons of the bulk solid. In other words the probability that the electron which has been accelerated will produce a free electron and hole instead of an excitation wave is not negligible compared with unity. This process will be of major importance for breakdown in the alkali halides and other ionic crystals. It will also occur in non-polar materials, but need not occupy the same critical position if excitation waves are decomposed as easily as the results derived from (51) suggest.

To summarize, it appears reasonable to suppose the excitation waves which are stimulated by an accelerated electron will decompose in fields that are much smaller than E_H in a non-polar insulator such as diamond. On the other hand, the situation seems to be much more nearly on the border line in the case of an ionic crystal such as sodium chloride. In this case it is possible that the primary electron is able to produce secondaries when the field is below or near E_H only as a result of fluctuations in which the electron succeeds in obtaining sufficient kinetic energy to produce pairs directly, or at least to produce excitation waves which are sufficiently high in the spectrum that they can be dissociated by the field.

9. INFLUENCE OF BRILLOUIN ZONE

The calculations of Section 3 (Table I) show that a perfectly free electron would meet the first Brillouin zone when its energy lies between 3.6 ev and 4.8 ev in sodium chloride, depending upon its direction of travel. In diamond the corresponding energies are 8.9 ev and 11.9 ev. The crystalline potential will modify these values to some extent. In any event, it seems probable that the accelerated electron must cross a zone boundary before it can produce electronic excitation or ionization in sodium chloride, whereas this is probably not the case in diamond.

The semi-quantitative features of this problem have been investigated by Houston[6] in the case in which lattice collisions can be neglected. He has shown that the wave number vector of the electron approaches the zone boundary and undergoes a Bragg reflection as it reaches the plane boundary when the field is not too strong. Thus, in the absence of other disturbances, the electron alternately would be accelerated and decelerated by the field and the action of Bragg reflections. Two disturbances are provided by the fact that the electron may either undergo field "emission" from one zone to the next or be transferred by a collision with lattice waves. The second process will occur only if the bands overlap or at least are not separated by more than the energy of the highest lattice vibrational quantum. It seems safe to assume that the conduction bands overlap in the insulators of interest to us.

The probability of the electron tunneling across the zone boundary is determined by the quantity α appearing in Eq. (1) in the theory of Zener, Houston, and Franz. If we select $\Delta\epsilon$ to be 0.5 ev, α is close to unity in both diamond and sodium chloride when $E=E_H$. Thus, the electron has an appreciable probability of jumping the gap through field perturbation in one cycle of motion, provided the gap is 1 ev or less and the field is near E_H.

Now we know from the discussion of Section 6 that on the average an electron will make several inelastic collisions with the lattice waves during the time in which it is being accelerated to an energy near ϵ_s. Thus if the bands overlap, as we assume to be the case, the collisions with lattice waves should bring about a transfer from one zone to another.

In other words the barrier presented by the zone boundaries does not appear to offer a serious impediment to the acceleration of electrons. Apparently it may be surmounted either by field perturbation when E is near E_H or as a result of collisions with lattice waves.

10. ANISOTROPY OF BREAKDOWN FIELD

The disruption that accompanies breakdown in almost all crystalline substances exhibits crystalline symmetry.[24] In brief, the breakdown paths usually are oriented along very definite crystallographic directions. On the other hand, the measurements of von Hippel and Davisson[25] on the influence of the breakdown field on crystallographic orientation seem to show that the field is isotropic. In any event this appears to be the case in sodium chloride at room temperature. It seems very difficult to reconcile these two facts on the basis of any of the theories of breakdown proposed to date. As von Hippel and Davisson have emphasized, one would expect both the tunnelling theories of Zener and Franz and the impact-ionization theories to lead to anisotropy in the general case. It is possible that sodium chloride is a special exception. It is also possible that the actual breakdown field in the alkali halides is determined by the condition that the field be sufficiently strong to decompose the excitons produced as a result of impact excitation. In the latter case it is possible that the field required is independent of crystal orientation.

11. SUPPLEMENTARY COMMENTS

Professor R. de L. Kronig[26] has pointed out to the writer that liquid argon exhibits breakdown at fields of about $1\cdot10^6$ volts per cm. Kronig has interpreted this breakdown in terms of Zener's theory, although it is by no means certain that the avalanche theory is not valid. To obtain agreement with Zener's theory it is necessary to assume that $\Delta\epsilon$ in Eq. (2) is about 3 ev. It is possible that the nature of the breakdown could be determined by studying the dependence of the breakdown field upon temperature since this field would fall with decreasing temperature if the avalanche theory is correct. Since liquid argon is definitely a non-polar substance, one would expect only a single peak in the electron friction curve; moreover this should occur at energies of several electron volts. We may infer from the experimental results on argon that the collision frequency at this maximum would be of the order of $5\cdot10^{14}$ sec.$^{-1}$ if the preceding theory is correct. The corresponding mobility is about 3 cm^2 volt-sec.

Hutchinson[27] has measured the mobility of conduction electrons in liquid argon in fields of the order of 10 kv per cm by measuring transit times and finds values of 40 cm^2/volt-sec., which are reasonable for a non-polar material for electrons having energies in the thermal range. Hutchinson also reports electron multiplication in solid argon; however it is difficult to say whether or not this multiplication is the result of volume avalanches.

12. CONCLUSION

The principal conclusions to be drawn from the preceding investigation are as follows:

(1) The interaction between a free electron and the lattice vibrations is qualitatively different in polar and non-polar crystals. In non-polar crystals, such as diamond, silicon, and germanium, there is a single peak in "electron friction" which occurs when the free electron is near the boundary of the first Brillouin zone and its energy is of the order of several electron volts, depending upon the crystal. The previous treatments of the interaction between an electron and the lattice in an ionic crystal have neglected the influence of non-polar modes of vibration and have taken into account only the interaction with polar modes, which is a maximum when the electron energy is near $k_0\theta$ (k_0=Boltzmann's constant, θ=characteristic temperature). It is proposed that the influence of non-polar modes is as large as that of the polar modes. The function describing electron friction in polar crystals has two peaks. One peak, arising from polar interaction, occurs for energies near $k_0\theta$ and the second, arising from non-polar interaction, occurs for energies near the zone boundary. The existence of the second peak reduces considerably the practical difference between the criteria for breakdown proposed by von Hippel and by Fröhlich since the high energy peak occurs near the energy at which ionization begins.

(2) The lowest value of an applied electrostatic field

[24] L. Inge and A. Walther, Zeits. f. Physik **64**, 830 (1930); **71**, 627 (1931); A. von Hippel, Zeits. f. Physik **67**, 707 (1931); **68**, 309 (1931); J. Lass, Zeits. f. Physik **69**, 313 (1931). The most extensive work in the field has been carried out by J. W. Davisson, Phys. Rev. **70**, 685 (1946).

[25] A. von Hippel and J. W. Davisson, Phys. Rev. **57**, 156 (1940).

[26] R. de L. Kronig and A. E. van der Vooren, Physics **9**, 139 (1942); R. de L. Kronig, Zeits. f. Physik **118**, 452 (1942).

[27] G. W. Hutchinson, Nature **162**, 610 (1948).

for which a free electron of arbitrary energy will gain energy more rapidly from the field than it loses energy to the lattice vibrations is determined. This field strength, which is designated E_H, is the value at which breakdown would occur according to von Hippel's theory of the breakdown process. It is found that statistical fluctuations in the energies which free electrons possess in the presence of a field are so great that breakdown actually can occur when the field is as small as $0.2E_H$ for specimens of normal size. Calculations have been made on the assumption that fluctuations in which the electron makes very few collisions are the most important. This breakdown occurs as the result of the production of electron avalanches in which 10^{12} electrons are freed by impact collisions. E_H is estimated to lie between $4.0 \cdot 10^7$ and $6 \cdot 10^6$ volts per cm in diamond depending upon the coupling constant employed between lattice and electron. The corresponding value is about $1.5 \cdot 10^6$ volts per cm in sodium chloride. Since the derivation of these values involves improper use of perturbation theory they can be regarded only as rough approximations, as is true of the theoretical results of previous investigators. The breakdown field for diamond, estimated with the use of avalanche theory thus lies between $8 \cdot 10^6$ and $1.2 \cdot 10^6$ volts per cm, whereas the theoretical value for NaCl is about $0.3 \cdot 10^6$ volts per cm. The difference between the calculated value for NaCl and the observed value of $1.5 \cdot 10^6$ volts per cm near room temperature indicates the approximate character of the calculations. The value of the breakdown potential calculated for diamond with the use of the impact theory is not very different from the value estimated with the use of the field emission theory of Zener and Franz. The calculations are not sufficiently accurate to be decisive.

(3) An investigation of the dependence of the size of energy fluctuations on field strength shows that the size of avalanches caused by impact ionization of the bulk material should increase by a factor of 10^{12} when the electrostatic field changes by about 20 percent if the field is near the breakdown value. The avalanches observed by Haworth and Bozorth in Pyrex correspond to an exponent about 50 times smaller. It is concluded that these avalanches may arise from the ionization by impact of impurity atoms which have relatively loosely bound electrons. The pre-breakdown currents observed by von Hippel and his co-workers may have the same origin.

(4) Since the electron friction is relatively small for electrons having thermal energies in non-polar crystals, the free electrons cease to be at thermal equilibrium with the lattice at relatively weak fields. It is estimated that the average energy of free electrons in diamond is 1 ev when the applied field is about $3 \cdot 10^5$ ev. It is evident that electrons in this distribution should be able to excite impurity atoms in such a way as to produce effects such as ionization and luminescence. Two groups of free electrons will be a quasi-equilibrium in polar crystals in strong fields somewhat below the value for breakdown. One of these groups is essentially in thermal equilibrium with the lattice, whereas the second group resembles the average group present in non-polar crystals in having a much higher average energy.

(5) It is concluded that excitation waves are decomposed by the applied field in diamond when the field is near the breakdown value. The theoretical evidence is less conclusive in the case of the alkali halides. It is possible that breakdown occurs in these materials only when the field is sufficiently strong that the electron has an appreciable probability of running through the excitation range associated with the production of excitation waves without actually producing such waves and produces ionization instead.

(6) The barrier presented by the gaps at the boundaries of the Brillouin zones does not offer an appreciable impediment to the acceleration of electrons. The electron can jump between zones as a result of scattering collisions with the lattice if the zones overlap. In any case the perturbation produced by the field probably will permit the electron to leak through the barrier as long as the field is near the breakdown value.

(7) Experiments of Kronig and van der Vooren and of Hutchinson on the breakdown field of rare-gas liquids and solids support the viewpoint that non-polar coupling between electron and lattice is large when the energy of the electron is near a value associated with the Brillouin zone if it is assumed that breakdown in these materials is the result of electron avalanches. Unfortunately the experiments do not make it possible to determine whether this mechanism or that of Zener and Franz prevails.

Electric Breakdown in Ionic Crystals*

HERBERT B. CALLEN
Randal Morgan Laboratory of Physics, University of Pennsylvania, Philadelphia, Pennsylvania
and
Laboratory for Insulation Research, Massachusetts Institute of Technology, Cambridge, Massachusetts
(Received June 16, 1949)

The electric breakdown strength of ionic crystals at low and moderate temperatures is calculated on the basis of von Hippel's low energy criterion. Fröhlich's method of calculation, modified to take account of the electronic polarizability of the ions, is employed. The breakdown strength at $T=0°$ is F_0(volts/cm) $=134\times10^6(\hbar\omega_l)_{ev}[(\epsilon_s-\epsilon_0)/(\epsilon_s\epsilon_0^2)^{\frac{1}{2}}](m^*/m)$ where $(\hbar\omega_l)_{ev}$ is the reststrahl energy in electron volts, ϵ_s and ϵ_0 are the static and optical values of the dielectric constant, and (m^*/m) is the ratio of the effective mass to the free electron mass. The breakdown strength increases slowly with increasing temperature. The lack of dependence of the breakdown strength on crystallographic orientation and the strong directional dependence of the breakdown paths are qualitatively accounted for.

I. INTRODUCTION

TWO distinct mechanisms have been proposed for the breakdown process in ionic crystals under high field-strengths, at low and moderate temperatures. It has been proposed by von Hippel[1] that breakdown occurs when the applied field is high enough to accelerate electrons of *any* given energy in the conduction band to sufficient energy to further ionize the ions of the crystal by collision, thus leading to an exponential increase in the number of electrons in the conduction band. It may be easily seen that the applied field necessary to accelerate (on the average) an electron of given energy has a maximum when considered as a function of electron energy, as indicated schematically in Fig. 1. For, in order to accelerate an electron, the applied field must compensate the energy lost by this electron to the lattice; but slow electrons have insufficient energy to excite the vibrational modes of the lattice, whereas very fast electrons interact for too short a time with the ions which they pass to transfer energy to them with appreciable probability. The breakdown strength, according to von Hippel's "low energy" criterion, therefore corresponds to the maximum in Fig. 1, and an electron brought into the conduction band with low energy is immediately accelerated to the ionization energy and produces an additional conduction electron, the process thus building up in the form of an avalanche. Alternatively, Fröhlich[2] has suggested that an applied field sufficient only to accelerate electrons already having the ionization energy may lead to an instability and to electric breakdown.

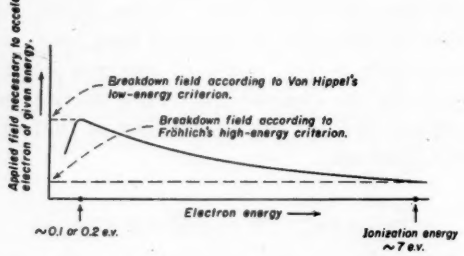
Applied field necessary to accelerate electron of given energy.
Breakdown field according to Von Hippel's low-energy criterion.
Breakdown field according to Fröhlich's high-energy criterion.
Electron energy
~0.1 or 0.2 e.v.
Ionization energy ~7 e.v.

FIG. 1. The field necessary to accelerate an electron of given energy (schematic).

Unfortunately it does not seem possible as yet to give a definitive *a priori* proof of the necessity of von Hippel's low energy criterion or of the sufficiency of Fröhlich's high energy criterion. It therefore seems desirable to compute the breakdown strength of crystals on the basis of each criterion, and to make an *a posteriori* choice of the criterion which most closely predicts the experimental facts.

Fröhlich[2] has developed a method of treatment of the interaction between a conduction electron and the vibrational modes of an ionic lattice, the method being a modification of the methods developed in the electron theory of metals. Utilizing this method he has given a breakdown theory based on the high energy criterion. Seeger and Teller[3] have a given a low energy breakdown theory based on Bohr's classical calculation of the energy loss of alpha-particles in a gas. The calculations of Fröhlich and of Seeger and Teller differ in two fundamental respects. Firstly, as discussed above, Fröhlich adopts what we have called the high energy criterion, whereas Seeger and Teller adopt the low energy criterion. Secondly, Fröhlich has explicitly considered the effect of the tortuosity of the path of the electron, and has given a treatment of this effect in terms of an electronic relaxation time. In the present paper Fröhlich's method,[4] modified to take account of the

* This work was supported under Contract NObs-42487 at the University of Pennsylvania, and was sponsored by the ONR, the Army Signal Corps and the Air Force under ONR contract N5 ori-78, T. 0.1 at M.I.T.

[1] See A. von Hippel, Trans. Faraday Soc. **42A**, 78 (1946), and A. von Hippel and R. S. Alger, Phys. Rev. **76**, 127 (1949) for recent accounts of this point of view and for a more complete bibliography.

[2] H. Fröhlich, Proc. Roy. Soc., London, **A160**, 230 (1937).

[3] R. J. Seeger and E. Teller, Phys. Rev. **54**, 515 (1938).

[4] Fröhlich has pointed out (Phys. Rev. **61**, 200 (1942), and private communication with the author) that certain qualitative consequences of his breakdown theory follow from the treatment

electronic polarizability, is applied to the low energy criterion, leading to results in fair agreement with experiment. The structure of the calculation follows closely that of Fröhlich's paper, and many of the equations are modifications of equations obtained by him. We have, however, thought it preferable to present a complete and self-contained account of the theory, rather than to attempt to refer to and modify Fröhlich's equations in those cases where such a procedure would be possible.

The electric field required to accelerate an electron of given energy is determined by the condition that the rate of energy loss from the electron to the lattice is just compensated by the rate of energy input from the field to the electron. This latter energy input is, however, simply Fev_d, where F is the field and v_d is the drift velocity. It is thus necessary to calculate the rate of energy loss from electron to lattice, and the drift velocity, as functions of electronic energy. These calculations are accomplished by treating the effect of the lattice vibrations on the electron as a time-dependent perturbation. The breakdown field is identified with the maximum value of the field so obtained.

II. THE VIBRATIONAL MODES OF THE LATTICE

According to the lattice dynamics of Born and von Karman[5] the normal vibrational modes of a diatomic crystal may be represented in the form of plane waves. The wave-vectors σ ($|\sigma|=1/\lambda$) take N discrete values lying within the first Brillouin zone, where N is the number of unit cells in the crystal. To each value of σ there correspond six modes, which can be grouped into three "optical" modes of relatively high frequency and three "acoustical" modes of relatively low frequency. Of the three modes of each type, one is longitudinal and two are transverse.

For a mode of wave vector σ let $\mathbf{u}_{1\sigma}(\mathbf{r})$ or $\mathbf{u}_{2\sigma}(\mathbf{r})$ be the deviation from its equilibrium position of the ion at the point $\mathbf{r}$, if the ion is of type 1 or type 2, respectively. Then a standing wave description of the longitudinal mode of wave-vector σ may be written as[5]

$$\begin{cases} \mathbf{u}_{1\sigma}(\mathbf{r})=-\dfrac{\sigma}{\sigma}\left(\dfrac{2}{M_1N}\right)^{\frac{1}{2}} b_\sigma(t)\,\xi_{1\sigma}\begin{Bmatrix}\sin\\ \cos\end{Bmatrix}(2\pi\sigma\cdot\mathbf{r}), \\ \mathbf{u}_{2\sigma}(\mathbf{r})=-\dfrac{\sigma}{\sigma}\left(\dfrac{2}{M_2N}\right)^{\frac{1}{2}} b_\sigma(t)\,\xi_{2\sigma}\begin{Bmatrix}\sin\\ \cos\end{Bmatrix}(2\pi\sigma\cdot\mathbf{r}), \end{cases} \tag{1}$$

where $\xi_{1\sigma}$ and $\xi_{2\sigma}$ determine the relative amplitudes of $\mathbf{u}_{1\sigma}$ and $\mathbf{u}_{2\sigma}$ and are so defined that

$$\xi_{1\sigma}^2+\xi_{2\sigma}^2=1. \tag{2}$$

According to our convention, if the cosine function in Eq. (1) is adopted for the mode σ, the sine function must be adopted for the mode $-\sigma$ to insure orthogonality of the modes. Both the natural frequency of the mode (ν_σ) and $\xi_{1\sigma}$ depend on σ in a fairly complicated manner. The total deviation of the ion at $\mathbf{r}$ is, of course,

$$\mathbf{u}_1(\mathbf{r})=\sum_\sigma \mathbf{u}_{1\sigma}(\mathbf{r}),\quad \mathbf{u}_2(\mathbf{r})=\sum_\sigma \mathbf{u}_{2\sigma}(\mathbf{r}), \tag{3}$$

where the summations are over all 6N modes.

If the kinetic and potential energies of the lattice are expressed in terms of the variables b_σ and $\dot{b}_\sigma$, a Lagrangian and a Hamiltonian function can be obtained, and $\dot{b}_\sigma$ is found to be the momentum conjugate to b_σ. The Hamiltonian is

$$H=\tfrac{1}{2}\sum_\sigma[\dot{b}_\sigma^2+\omega_\sigma^2 b_\sigma^2], \tag{4}$$

which is formally identical to the Hamiltonian of a collection of 6N one-dimensional, independent, harmonic oscillators. The wave function describing the vibrational state of the lattice is the product of 6N harmonic oscillator wave functions of individual quantum numbers $n_1, n_2\cdots n_\sigma\cdots$. The corresponding energy eigenvalue is

$$E_{n_1,\,n_2\cdots n_\sigma\cdots}=\sum_\sigma(n_\sigma+\tfrac{1}{2})\hbar\omega_\sigma. \tag{5}$$

Neglecting the fine structure of the dielectric, the mode σ can be considered as producing a polarization $\mathbf{P}_\sigma$;

$$\mathbf{P}_\sigma=\frac{e^*}{2a^3}(\mathbf{u}_{+,\sigma}-\mathbf{u}_{-,\sigma}) \tag{6}$$

and consequently a charge density ρ_σ;

$$\rho_\sigma=-\nabla\cdot\mathbf{P}_\sigma, \tag{7}$$

where e^* is an effective charge per ion (see Section II) and where a is the interionic distance ($2a^3$ is the volume of a unit cell). This charge density ρ_σ represents the accumulation of positive and of negative ions at the alternate nodes of a longitudinal wave and it is easily seen from the form of Eqs. (1) that ρ_σ differs from zero only for a longitudinal mode. The Coulomb interaction between a conduction electron and the charge density ρ_σ supplies a means of interaction whereby the electron can be scattered by the vibrational modes. Of course this is not the only interaction energy between a conduction electron and a phonon, and any vibrational mode alters the periodicity of the potential in which the electron moves and therefore scatters the electron, even though the mode may not give rise to a charge density ρ_σ. However, the Coulomb interaction with ρ_σ is the dominant term[6] in the complete interaction, as indicated by the empirical fact that the mean free path of elec-

of the relaxation time rather than from what we have termed the high-energy criterion. Thus the temperature dependence and the dependence of breakdown strength on impurity content are similar in the present theory to that in Fröhlich's high energy theory.

[5] See, for instance, F. Seitz, *The Modern Theory of Solids* (McGraw-Hill Book Company, Inc., New York, 1940).

[6] F. Seitz, in a paper presented to the New York meeting of the American Physical Society, January 28, 1949, has pointed out that for very fast electrons the Coulomb interaction with ρ_σ ceases to be the dominant term.

trons in polar crystals is very much shorter than that in non-polar crystals. We therefore neglect other interaction terms, and we consider the conduction electrons to be scattered only by the longitudinal modes. For the longitudinal modes

$$\mathbf{P}_\sigma=\frac{e^*}{2a^3}\frac{\sigma}{\sigma}\left(\frac{2}{N}\right)^{\frac{1}{2}}b_\sigma\left(\frac{\xi_{+,\sigma}}{M_+^{\frac{1}{2}}}-\frac{\xi_{-,\sigma}}{M_-^{\frac{1}{2}}}\right)\left\{\begin{matrix}\sin\\ \cos\end{matrix}\right\}(2\pi\boldsymbol{\sigma}\cdot\mathbf{r}). \quad (8)$$

For every value of σ there are two longitudinal modes, one in the acoustical branch and one in the optical branch. The acoustical modes are characterized by the fact that $\xi_{+,\sigma}/\xi_{-,\sigma}$ is positive, whence neighboring positive and negative ions vibrate in phase. For the optical modes $\xi_{+,\sigma}/\xi_{-,\sigma}$ is negative, and neighboring positive and negative ions vibrate 180° out of phase. The optical longitude modes therefore produce a much larger polarization $\mathbf{P}_\sigma$ and a much larger charge density ρ_σ than do the acoustical longitudinal modes. In fact, for the acoustical longitudinal modes of long wave-length, which are of principal importance in our theory, the ratio of the amplitudes of positive and negative ions is unity so that $\xi_{+,\sigma}/M_+^{\frac{1}{2}}=\xi_{-,\sigma}/M_-^{\frac{1}{2}}$, and $\mathbf{P}_\sigma=\rho_\sigma=0$. For the optical longitudinal modes of long wave-length the ratio of amplitudes is

$$u_{+,\sigma}/u_{-,\sigma}=-M_-/M_+ \quad (9)$$

whence

$$\xi_{+,\sigma}/M_+^{\frac{1}{2}}-\xi_{-,\sigma}/M_-^{\frac{1}{2}}=(1/M_++1/M_-)^{\frac{1}{2}}=1/M^{\frac{1}{2}}, \quad (10)$$

where M is the reduced mass of the ions. As a simplifying assumption we take $\mathbf{P}_\sigma=\rho_\sigma=0$ as true for all the acoustical longitudinal modes, and Eqs. (9) and (10) as true for all the optical longitudinal modes. In this way the longitudinal modes of long wave-length, which are of principal importance in the theory, are treated correctly, and the over-estimation of the polarization produced by the short optical modes is compensated by the underestimation of the polarization due to the short acoustical modes. Only the optical longitudinal modes are effective in scattering a conduction electron.

In the optical branch the frequency is a fairly insensitive function of wave-length and may, to a good approximation, be taken as constant, independent of wave-length. We therefore attribute to every optical longitudinal mode the frequency of the optical longitudinal modes of long wave-length, which we denote by ν (or by $\omega\equiv 2\pi\nu$). The relation of ν to the reststrahl frequency ν_t, or to the frequency of the long wave-length optical transverse modes, will be considered in the next section.

III. THE FREQUENCY OF THE LONG WAVE-LENGTH LONGITUDINAL OPTICAL MODES

It has been shown by Lyddane and Herzfeld[7] and by Fröhlich and Mott[8] that the frequency of the long** wave-length optical longitudinal modes exceeds the frequency of the long wave-length optical transverse modes in ionic diatomic crystals. In a longitudinal mode there are regions of charge accumulation which set up electric fields within the crystal, and these fields contribute to the restoring force-constant. In a transverse mode of long wave-length, however, the electric fields are "short-circuited" at the crystal boundaries and do not contribute to the restoring force-constant. Lyddane, Sachs, and Teller[9] have computed the relation between these frequencies taking proper account of the electronic polarizability of the ions.† We now reformulate this analysis in a form appropriate for the calculation, in the next section, of the phonon-electron interaction energy.

Following Lyddane, Sachs, and Teller, consider the ions of the crystal to be given the displacements corresponding to a long wave-length longitudinal optical mode, so that the relative displacement of the positive and negative ions is

$$\mathbf{X}_\sigma=\mathbf{u}_{+,\sigma}-\mathbf{u}_{-,\sigma}. \quad (11)$$

This displacement produces a polarization which, to the first order, is linear in $\mathbf{X}_\sigma$. Accordingly we write

$$\mathbf{P}_\sigma=(e^*/2a^3)\mathbf{X}_\sigma, \quad (12)$$

where e^* is an effective charge, which differs from the true ionic charge because of the distortion of the electronic shells and the electronic polarization caused by the internal fields which are set up by the displacement. This polarization is associated with an internal field

$$\mathbf{E}_\sigma=-4\pi\mathbf{P}_\sigma=-(2\pi e^*/a^3)\mathbf{X}_\sigma, \quad (13)$$

and this field is associated with an electrostatic energy density

$$U_\sigma'=\epsilon_0/8\pi[(2\pi e^*/a^3)\mathbf{X}_\sigma]^2. \quad (14)$$

In a transverse mode the electrostatic field of Eq. (13) is absent, so that U_σ' represents the difference in energy density of longitudinal and transverse modes with the same values of X_σ. Writing the total energy density associated with a mode in the form

$$U=(\tfrac{1}{2}M\omega^2/2a^3)X_\sigma^2, \quad (15)$$

where M is the reduced mass of the ions and ω is the natural angular frequency we thus find

$$(\tfrac{1}{2}M\omega^2/2a^3)X_\sigma^2=\tfrac{1}{2}M\omega_t^2/2a^3X_\sigma^2+\epsilon_0/8\pi[(2\pi e^*/a^3)\mathbf{X}_\sigma]^2$$

or

$$\omega^2=\omega_t^2+2\pi\epsilon_0e^{*2}/Ma^3, \quad (16)$$

where ω is the natural angular frequency of the longi-

[7] R. H. Lyddane and K. F. Herzfeld, Phys. Rev. 54, 846 (1938).
[8] H. Fröhlich and N. F. Mott, Proc. Roy. Soc. A171, 496 (1939).
** A mode of long wave-length is to be considered as one for which $\lambda\gg a$ (a is the inter-ionic distance), but it is assumed that λ is small compared with the dimensions of the crystal in order that the boundary conditions shall not be significant.
[9] Lyddane, Sachs, and Teller, Phys. Rev. 59, 673 (1941). The author is indebted to Dr. Sachs for calling his attention to this paper.
† Fröhlich and Mott (see reference 8) have also obtained an equation relating the two frequencies, neglecting the effect of electronic polarizability.

tudinal mode and ω_t is the natural angular frequency of the transverse mode.

An equation analogous to the familiar Born[10] formula, relating ω_t to ϵ_0, ϵ_s and e^*, may be obtained by similar reasoning. Consider a crystal in which the ions are given the relative displacement $\mathbf{X}$. The energy density is then

$$U=(\tfrac{1}{2}M\omega^2/2a^3)X^2 =(M/4a^3)[\omega_t^2+(2\pi\epsilon_0 e^{*2}/Ma^3)]X^2. \quad (17)$$

As in Eq. (13) the internal field is

$$\mathbf{E}=-(2\pi e^*/a^3)\mathbf{X}, \quad (18)$$

and the electrostatic energy density is

$$U'=(\epsilon_0/8\pi)[-(2\pi e^*/a^3)\mathbf{X}]^2. \quad (19)$$

If an external field $\mathbf{D}$, parallel to $\mathbf{X}$, is now imposed on the crystal it will induce an additional electronic polarization, the total polarization now being

$$\mathbf{P}=(e^*/2a^3)\mathbf{X}+(1/4\pi)[(\epsilon_0-1)/\epsilon_0]\mathbf{D}, \quad (20)$$

and the internal field becoming

$$\mathbf{E}=-(2\pi e^*/a^3)\mathbf{X}+(1/\epsilon_0)\mathbf{D}. \quad (21)$$

The electrostatic energy density is thus increased to

$$U'=(\epsilon_0/8\pi)[(1/\epsilon_0)\mathbf{D}-(2\pi e^*/a^3)\mathbf{X}]^2, \quad (22)$$

and consequently the total energy density becomes

$$U=(M/4a^3)\omega_t^2X^2+\epsilon_0/8\pi[(1/\epsilon_0)\mathbf{D}-(2\pi e^*/a^3)\mathbf{X}]^2. \quad (23)$$

If the displacement $\mathbf{X}$ is allowed to adjust itself the equilibrium value will be that which minimizes the energy, or

$$\mathbf{X}=[a^3e^*/(Ma^3\omega_t^2+2\pi\epsilon_0e^{*2})]\mathbf{D}. \quad (24)$$

With this value of $\mathbf{X}$ the equilibrium polarization becomes, from Eq. (20),

$$\mathbf{P}=\tfrac{1}{2}[e^{*2}/(Ma^3\omega_t^2+2\pi\epsilon_0e^{*2})]\mathbf{D}+(1/4\pi)(\epsilon_0-1/\epsilon_0)\mathbf{D}. \quad (25)$$

But, by definition of ϵ_s (the static dielectric constant),

$$\mathbf{P}\equiv(1/4\pi)[(\epsilon_s-1)/\epsilon_s]\mathbf{D}, \quad (26)$$

whence

$$\omega_t^2=(2\pi e^{*2}/Ma^3)[\epsilon_0^2/(\epsilon_s-\epsilon_0)], \quad (27)$$

which reduces to the Born equation if $(e^*\epsilon_0)^2$ is put equal to e^2. Combining Eq. (26) with Eq. (16) we find

$$\omega^2=(2\pi e^{*2}/Ma^3)[\epsilon_0\epsilon_s/(\epsilon_s-\epsilon_0)] \quad (28)$$

and

$$\omega^2/\omega_t^2=\epsilon_s/\epsilon_0. \quad (29)$$

Equations (29) and (27) allow us to compute both ω and e^* in terms of the experimentally observed reststrahl frequency, which is practically identical to ω_t.

[10] See M. Born and M. Goeppert-Mayer, *Handbuch der Physik*, Vol. 24/2, p. 646.

IV. THE PHONON-ELECTRON INTERACTION ENERGY

We have seen that, within our approximations, the interaction energy between an electron and any vibrational mode other than those of the longitudinal optical branch, is zero. Using the method of the previous section we can now evaluate the interaction energy of an electron and a longitudinal optical mode. Consider a crystal in which we establish the ionic displacements $\mathbf{X}_\sigma$ and into which we insert an excess conduction electron. If the conduction electron produces an electric displacement $\mathbf{D}$ the energy density is, by Eq. (23),

$$U=(M/4a^3)\omega_t^2\mathbf{X}_\sigma^2 +(\epsilon_0/8\pi)[(1/\epsilon_0)\mathbf{D}-(2\pi e^*/a^3)\mathbf{X}_\sigma]^2 \quad (30)$$

so that the increment in energy density due to the interaction is

$$\Delta U=\frac{e^*}{2a^3}\mathbf{X}_\sigma\cdot\mathbf{D}. \quad (31)$$

By Eqs. (1) and (16) the relative displacement has the form

$$\mathbf{X}_\sigma=\frac{\sigma}{\sigma}\left(\frac{2}{MN}\right)^{\frac{1}{2}}b_\sigma\begin{Bmatrix}\sin\\ \cos\end{Bmatrix}(2\pi\sigma\cdot\mathbf{r}). \quad (32)$$

If the electron is at the point $\mathbf{r}_e$ we have

$$\mathbf{D}=-\frac{e}{|\mathbf{r}-\mathbf{r}_e|^3}(\mathbf{r}-\mathbf{r}_e). \quad (33)$$

Introducing the new variables

$$\boldsymbol{\rho}\equiv\mathbf{r}-\mathbf{r}_e \quad (34)$$

and

$$\cos\theta\equiv\frac{\sigma}{\sigma}\cdot\frac{\mathbf{r}-\mathbf{r}_e}{|\mathbf{r}-\mathbf{r}_e|} \quad (35)$$

we have

$$\Delta U=\frac{ee^*}{2a^3}\left(\frac{2}{MN}\right)^{\frac{1}{2}}b_\sigma\begin{Bmatrix}\sin\\ \cos\end{Bmatrix}2\pi(\sigma\cdot\boldsymbol{\rho}+\sigma\cdot\mathbf{r}_e)(\cos\theta/\rho^2), \quad (36)$$

and the total interaction energy $W_{\sigma,\mathbf{r}_e}$ becomes

$$W_{\sigma,\mathbf{r}_e}=\frac{ee^*}{2a^3}\left(\frac{2}{MN}\right)^{\frac{1}{2}}b_\sigma\int_0^\infty\int_0^\pi\begin{Bmatrix}\sin\\ \cos\end{Bmatrix}2\pi(\sigma\cdot\boldsymbol{\rho}+\sigma\cdot\mathbf{r}_e) \times(\cos\theta/\rho^2)2\pi\rho^2\sin\theta d\theta d\rho. \quad (37)$$

The integral may be evaluated easily and gives

$$W_{\sigma,\mathbf{r}_e}=\frac{ee^*}{a^3\sigma}\left(\frac{2}{MN}\right)^{\frac{1}{2}}b_\sigma\begin{Bmatrix}-\cos\\ \sin\end{Bmatrix}(2\pi\sigma\cdot\mathbf{r}_e), \quad (38)$$

which reduces to Fröhlich's result[2] if one puts $e^*=e$.

V. TRANSITION PROBABILITIES

If the interaction energy between the vibrational modes and a conduction electron in the lattice is treated

as a perturbation (assuming so few conduction electrons that each can be treated independently), the unperturbed wave function is the product of a free electron wave function and 6N harmonic oscillator wave functions of quantum numbers $n_{\boldsymbol{\sigma}}$:

$$\psi_{\mathbf{K},\, n_1\cdots n_{\boldsymbol{\sigma}}\cdots}=V^{-\frac{1}{2}}e^{2\pi i\mathbf{K}\cdot\mathbf{r}}\prod_{\boldsymbol{\sigma}}\psi_{n\boldsymbol{\sigma}}, \tag{39}$$

where V is the volume of the crystal and $\mathbf{K}$ is the wave vector of the electron. The unperturbed energy is

$$E_{\mathbf{K},\, n_1\cdots n_{\boldsymbol{\sigma}}\cdots}=\frac{h^2K^2}{2m^*}+\sum_{\boldsymbol{\sigma}}(n_{\boldsymbol{\sigma}}+\tfrac{1}{2})\hbar\omega, \tag{40}$$

where m^* is the effective mass of the electron.

The probability per unit time of a transition in which the electron goes from state $\mathbf{K}$ to state $\mathbf{K}'$ and the longitudinal optical mode of wave-vector $\boldsymbol{\sigma}$ goes from state $n_{\boldsymbol{\sigma}}$ to state $n_{\boldsymbol{\sigma}}'$ is given by the time-dependent perturbation theory as

$$\Phi_{\boldsymbol{\sigma}}=1/\hbar^2|M_{KK'\sigma}|^2(\partial/\partial t)(\sin^2\xi t/\xi^2), \tag{41}$$

where

$$\hbar\xi=\tfrac{1}{2}[(h^2/2m^*)(K'^2-K^2)+(n_{\boldsymbol{\sigma}}'-n_{\boldsymbol{\sigma}})\hbar\omega], \tag{42}$$

and the matrix element $M_{KK'\sigma}$ is

$$M_{KK'\sigma}=\int\int\int\int V^{-\frac{1}{2}}e^{-2\pi i\mathbf{K}'\cdot\mathbf{r}}\psi_{n'\boldsymbol{\sigma}}^*W_{\boldsymbol{\sigma},\mathbf{r}}V^{-\frac{1}{2}}\times e^{2\pi i\mathbf{K}\cdot\mathbf{r}}\psi_{n\boldsymbol{\sigma}}d\mathbf{r}db_{\boldsymbol{\sigma}}. \tag{43}$$

Inserting the values of $\psi_{n\boldsymbol{\sigma}}$ and $W_{\boldsymbol{\sigma},\mathbf{r}}$ and using the orthogonality and recursion properties of the Hermite polynomials, one obtains

$$\Phi_{\boldsymbol{\sigma}}=\left(\frac{ee^*}{2a^3\sigma}\right)^2\frac{1}{NM\hbar\omega}\delta(\mathbf{K}-\mathbf{K}'\pm\boldsymbol{\sigma},0)\times[n_{\boldsymbol{\sigma}}\delta(n_{\boldsymbol{\sigma}}',n_{\boldsymbol{\sigma}}-1)+(n_{\boldsymbol{\sigma}}+1)\delta(n_{\boldsymbol{\sigma}}',n_{\boldsymbol{\sigma}}+1)]\times(\partial/\partial t)(\sin^2\xi t/\xi^2). \tag{44}$$

The delta-function $\delta(\mathbf{K}-\mathbf{K}'\pm\boldsymbol{\sigma},0)$ may be taken as the requirement of conservation of momentum in the transition. The factor $(\partial/\partial t)(\sin^2\xi t/\xi^2)$ has an appreciable value only in the vicinity of $\xi=0$, or if energy is approximately conserved.

The delta-functions $\delta(n_{\boldsymbol{\sigma}}',n_{\boldsymbol{\sigma}}-1)$ and $\delta(n_{\boldsymbol{\sigma}}',n_{\boldsymbol{\sigma}}+1)$ require that the quantum number of the vibrational mode change only by unity in the transition. The ratio of the probabilities of the transitions $n_{\boldsymbol{\sigma}}\rightarrow n_{\boldsymbol{\sigma}}+1$ and $n_{\boldsymbol{\sigma}}\rightarrow n_{\boldsymbol{\sigma}}-1$ is seen to be $(n_{\boldsymbol{\sigma}}+1)/n_{\boldsymbol{\sigma}}$, so that the electrons tend to lose energy to the vibrational modes.*

The simultaneous conservation of energy and momentum determines the angle between the wave vectors of an electron and a mode with which it can interact. The conservation of momentum gives

$$\mathbf{K}'=\mathbf{K}\pm\boldsymbol{\sigma} \tag{45}$$

and the approximate conservation of energy gives

$$(h^2K'^2/2m^*)=(h^2K^2/2m^*)\pm\hbar\omega+2\hbar\xi \quad \begin{cases}+ \text{ for absorption by electron}\\ - \text{ for emission by electron,}\end{cases} \tag{46}$$

where $\xi\simeq 0$.

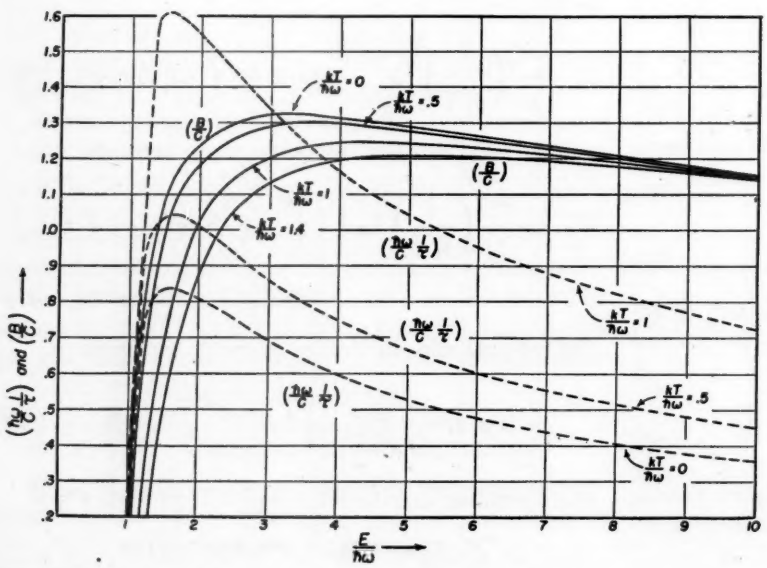

FIG. 2. Dependence of rate of energy loss and of relaxation time on energy and temperature.

* If the electron originally has an energy less than $\hbar\omega$, however, the emission process is impossible and it will gain energy from the lattice.

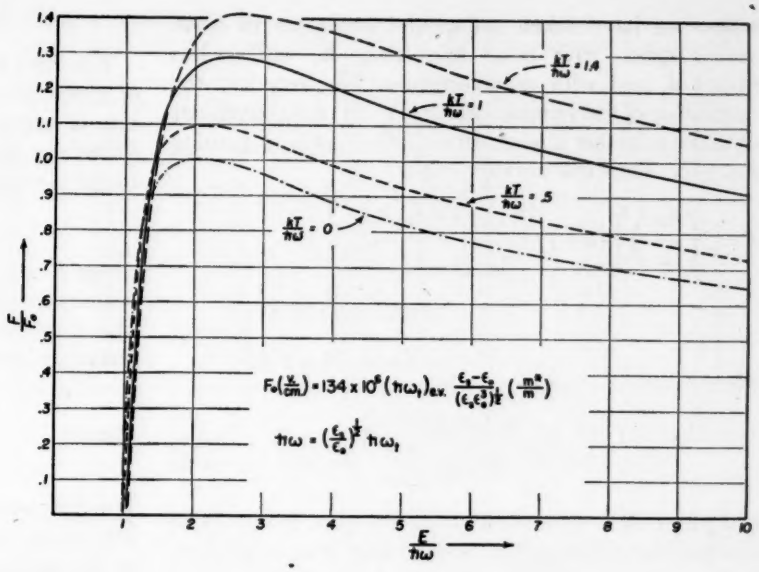

FIG. 3. Dependence of accelerating field on energy and temperature.

If α is the angle between $\mathbf{K}$ and $\boldsymbol{\sigma}$ one easily finds

$$\cos\alpha=-(\sigma/2K)+(2m^*/\hbar^2)[(2\hbar\xi\pm\hbar\omega)/2K\sigma] \quad \begin{cases}+ \text{ for absorption.}\\ - \text{ for emission.}\end{cases} \tag{47}$$

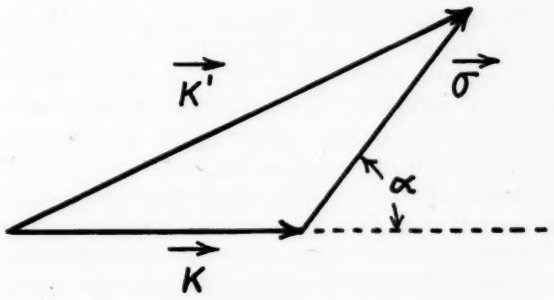

For a given K the electron can only interact with modes having wave vectors such that the right-hand member of Eq. (47) is less than unity in absolute value. Putting $\xi\simeq 0$, and introducing the notation

$$K_\nu^2\equiv 2m^*\nu/\hbar \tag{48}$$

so that K_ν is the wave vector of an electron with energy $h\nu$, we thus find as the limiting values* of σ which can interact with a given K:

$$\sigma_{\max}=K[1+(1\pm K_\nu^2/K^2)^{\frac{1}{2}}] \quad \begin{cases}+ \text{ for absorption}\\ - \text{ for emission,}\end{cases} \tag{49}$$

$$\sigma_{\min}=\pm K[-1+(1\pm K_\nu^2/K^2)^{\frac{1}{2}}] \quad \begin{cases}+ \text{ for absorption}\\ - \text{ for emission.}\end{cases} \tag{50}$$

In using Eq. (44) to calculate the probability of scattering of an electron we take for n_σ the average quantum number of a mode at the temperature T. This average value $\bar{n}$ is independent of σ and is given by

$$\bar{n}=\frac{\sum_n n\exp[-(n+\frac{1}{2})\hbar\omega/kT]}{\sum_n \exp[-(n+\frac{1}{2})\hbar\omega/kT]}=\frac{1}{\exp(\hbar\omega/kT)-1}. \tag{51}$$

VI. THE RATE OF LOSS OF ENERGY TO THE LATTICE

We have seen that, for an electron with energy greater than $\hbar\omega$, the probability of emission of a vibrational quantum exceeds the probability of absorption, and the electron tends to lose energy to the lattice. Following Fröhlich we now calculate the average rate of energy loss, which we denote by B. If $\Phi_\sigma{}^a$ is the probability of absorption and $\Phi_\sigma{}^e$ is the probability of emission we have, by Eqs. (44) and (51),

$$\Phi_\sigma{}^a=\left(\frac{ee^*}{2a^3\sigma}\right)^2\frac{\bar{n}}{NM\hbar\omega}\delta(\mathbf{K}-\mathbf{K}'\pm\boldsymbol{\sigma},0)\frac{\partial}{\partial t}\frac{\sin^2\xi t}{\xi^2}, \tag{52}$$

$$\Phi_\sigma{}^e=\left(\frac{ee^*}{2a^3\sigma}\right)^2\frac{\bar{n}+1}{NM\hbar\omega}\delta(\mathbf{K}-\mathbf{K}'\pm\boldsymbol{\sigma},0)\frac{\partial}{\partial t}\frac{\sin^2\xi t}{\xi^2}, \tag{53}$$

and

$$B=\hbar\omega\sum_\sigma\Phi_\sigma{}^e-\hbar\omega\sum_\sigma\Phi_\sigma{}^a, \tag{54}$$

where the limits on the first summation are appropriate to the emission process and those on the second summation are appropriate to the absorption process, as given by Eqs. (49) and (50). The summations over $\boldsymbol{\sigma}$ can be replaced by integrations in "wave vector space." Since there is one value of $\boldsymbol{\sigma}$ for each volume of $1/2Na^3$ in wave vector space we have

$$\sum_\sigma(\ )\rightarrow 2Na^3\int\int\int(\ )d\boldsymbol{\sigma}$$

$$=2Na^3\int\int\int(\ )2\pi\sigma^2\sin\alpha d\alpha d\sigma \tag{55}$$

* For sufficiently large K the value of $\sigma_{\max}$ given by Eq. (49) exceeds the maximum σ which can exist in the lattice—i.e., that at the furthest boundary of the Brillouin zone. Such fast electrons do not play a role in our low energy theory.

where we have taken spherical coordinates in wave vector space, with polar axis along $\mathbf{K}$, with radius vector σ, and with polar angle α. To carry out the evaluation of the summations in Eq. (54) it is convenient to make a further change of variable from α to ξ, using Eq. (47). Thus one obtains

$$B=C\left(\frac{\hbar\omega}{E}\right)^{\frac{1}{2}}\left[(\bar{n}+1)\ln\frac{1+(1-\hbar\omega/E)^{\frac{1}{2}}}{1-(1-\hbar\omega/E)^{\frac{1}{2}}}-\bar{n}\ln\frac{1+(1+\hbar\omega/E)^{\frac{1}{2}}}{-1+(1+\hbar\omega/E)^{\frac{1}{2}}}\right], \quad (56)$$

where

$$C=\frac{\pi(2m^*)^{\frac{1}{2}}(ee^*)^2}{Ma^3(\hbar\omega)^{\frac{1}{2}}}, \quad (57)$$

and where E is the energy of the electron. It should be recalled that this equation is valid only if $\sigma_{\max}$, as given by Eq. (49), lies indisde the first Brillouin zone. This requires that

$$E\lesssim\hbar^2/32m^*a^2, \quad (58)$$

or that the electron energy be less than about one to three electron volts for the various alkali halide crystals.

We have also assumed that the emission process is possible, so that we must have

$$E>\hbar\omega. \quad (59)$$

The quantity B/C is plotted against the "reduced energy" $E/\hbar\omega$ for various values of the "reduced temperature" $kT/\hbar\omega$ in Fig. 2.

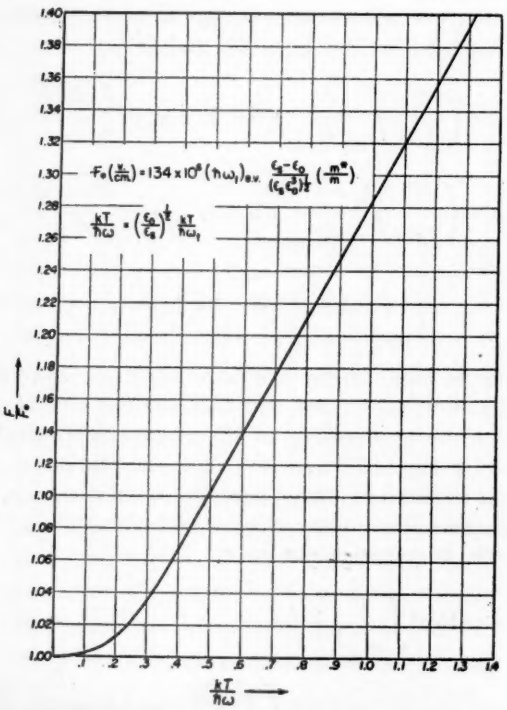

FIG. 4. Temperature dependence of breakdown field-strength.

VII. THE RELAXATION TIME

The field required to accelerate an average electron of given energy is obtained by equating the average rate of energy loss from the electron to the lattice, B, to the average rate of transfer of energy from the field to the electron, A. This latter rate of energy transfer is

$$A=eFv_d, \quad (60)$$

where F is the electric field strength and v_d is the drift velocity (which is a function of the energy and of F). The drift velocity may be expressed in terms of the relaxation time τ, defined by

$$v_d\equiv(e\tau/m^*)F, \quad (61)$$

whence

$$A=e^2F^2\tau/m^*. \quad (62)$$

The drift velocity, and thus also the relaxation time, is determined by the equilibrium between the tendency of the field to increase the z-directed velocity (assume the field along the z axis) and the tendency of the collisions to scatter the electrons away from the z axis and thus to decrease their z-directed velocity. Thus the drift velocity is determined by the equation

$$d\bar{v}_z/dt)_{\text{collisions}}=-d\bar{v}_z/dt)_{\text{field}}=-eF/m^*. \quad (63)$$

We consider the average effect of collisions on the electrons of energy E. Let an electron have its velocity $\mathbf{v}$ at an angle β with respect to the z-axis, so that its z-directed velocity v_z is $v\cos\beta$. Let a collision with a vibrational mode occur, after which the electron is deviated through the angle γ and has a velocity $\mathbf{v}'$. The probability of such a collision is clearly independent of the azimuthal angle of $\mathbf{v}'$ around $\mathbf{v}$. If we average over this azimuthal angle the final average z-directed velocity is $v'\cos\gamma\cos\beta$ and, on such a collision, the average change in v_z is

$$\Delta v_z=v'\cos\gamma\cos\beta-v\cos\beta=v_z[(v'/v)\cos\gamma-1]. \quad (64)$$

Maintaining v constant, and averaging both sides of the equation over the angle β, or over v_z;

$$\langle\Delta v_z\rangle=v_d[(v'/v)\cos\gamma-1], \quad (65)$$

where the drift velocity v_d is the average of v_z for all orientations of the electron. To find $d\bar{v}_z/dt)_{\text{collisions}}$ we must now average $\langle\Delta v_z\rangle$ over the angle γ, weighting each value of γ with the probability per unit time of a collision which scatters the electron through the angle γ. Indicating this averaging process by the notation $\langle\ \rangle_\gamma$, we have

$$d\bar{v}_z/dt)_{\text{collisions}}=v_d\langle(v'\cos\gamma-v)/v\rangle_\gamma \quad (66)$$

or, using Eqs. (62) and (60), and recalling that $\mathbf{v}$ is proportional to the wave vector $\mathbf{K}$;

$$1/\tau=\langle(K-K'\cos\gamma)/K\rangle_\gamma. \quad (67)$$

If α is the angle between the wave vector σ and the electronic wave vector $\mathbf{K}$ (see figure below Eq. (47)), we

TABLE I. Alkali halide data.

	ϵ_s	ϵ_0	$(\hbar\omega_t)_{e.v.}$	$a(10^{-8}$ cm)	$M(10^{-24}$ gms)	e^*/e	Theor. $F_0(10^6$ v/cm) $(m^*/m=1)$	Theor. $F_{15}^*(10^6$ v/cm) $(m^*/m=1)$	Exp't. $F_{15}^*(10^6$ v/cm)	$\frac{F_{15}^*(\text{Theor.})}{F_{15}^*(\text{Exp't.})}$
LiF	9.27	1.92	0.072	2.07	8.46	1.11	8.75	8.80	3.1	2.8
NaF	6.0	1.74	0.033	2.31	17.27	0.72	3.34	3.57	2.4	1.5
NaCl	5.62	2.25	0.024	2.81	23.2	0.56	1.35	1.57	1.5	1.1
NaBr	5.99	2.62	0.018	2.97	29.6	0.44	0.78	0.98	0.81	1.2
KF	6.05	1.85	0.03	2.66	21.2	0.84	2.72	2.96	1.9	1.6
KCl	4.68	2.13	0.019	3.14	30.8	0.55	0.965	1.20	1.0	1.2
KBr	4.78	2.33	0.015	3.29	43.6	0.50	0.63	0.85	0.70	1.2
KI	4.94	2.69	0.013	3.53	49.5	0.43	0.40	0.57	0.57	1.0
RbCl	5.0	2.19	0.017	3.27	41.6	0.63	0.88	1.12	0.83	1.3
RbBr	5.0	2.33	0.011	3.42	68.5	0.51	0.49	0.73	0.63	1.2
RbI	5.0	2.63	0.01	3.66	84.6	0.48	0.33	0.52	0.49	1.1

have

$$K'\cos\gamma = K+\sigma\cos\alpha \tag{68}$$

whence

$$1/\tau = \langle -\sigma\cos\alpha/K\rangle_{\sigma,\alpha}, \tag{69}$$

where we now average over σ and α, weighting each value with the probability per unit time of an appropriate collision. Thus

$$1/\tau = \sum_{\sigma}[-(\sigma/K)\cos\alpha\Phi_{\sigma^a}] + \sum_{\sigma}[-(\sigma/K)\cos\alpha\Phi_{\sigma^e}], \tag{70}$$

and transforming to integrals as in Eq. (55), we obtain

$$1/\tau = (B/2\hbar\omega)(\hbar\omega/E)+(C/\hbar\omega)(\hbar\omega/E)^{\frac{1}{2}} \times\{(\bar{n}+1)(1-\hbar\omega/E)^{\frac{1}{2}}+\bar{n}(1+\hbar\omega/E)^{\frac{1}{2}}\}. \tag{71}$$

The quantity $\hbar\omega/C\tau$ like B/C, depends only on the reduced energy $E/\hbar\omega$ and the reduced temperature $kT/\hbar\omega$, and is plotted against $E/\hbar\omega$ for various values of $kT/\hbar\omega$ in Fig. 2.

VIII. THE BREAKDOWN FIELD-STRENGTH

For a given electronic energy the average rate of energy loss B is independent of the applied field, but the average rate of energy gain from the field increases quadratically with the field intensity (Eq. (62)). There exists a certain field intensity for which the energy gain is just compensated by the energy loss, and any field strength greater than this value will, on the average, accelerate the electrons of the given energy. This "acceleration field strength" is determined by the equality

$$A=B \tag{72}$$

or, by Eq. (68),

$$F=((m^*)^{\frac{1}{2}}/e)(B/\tau)^{\frac{1}{2}} \tag{73}$$

which may be written

$$F=F_0[((\hbar\omega/C)(1/\tau))(B/C)]^{\frac{1}{2}}, \tag{74}$$

where

$$F_0=\frac{\sqrt{2}\pi m^* e e^{*2}}{Ma^3\hbar\omega}. \tag{75}$$

If e^* is expressed in terms of ω_t by Eq. (28) and ω is expressed in terms of ω_t by Eq. (29) we obtain

$$F_0=\frac{2^{\frac{1}{2}}\pi^2 m^* e}{h^2}\hbar\omega_t\frac{\epsilon_s-\epsilon_0}{(\epsilon_s\epsilon_0^3)^{\frac{1}{2}}} \tag{76}$$

or

$$F_0(\text{volts/cm})=134\times10^6(\hbar\omega_t)_{e.v.}\frac{\epsilon_s-\epsilon_0}{(\epsilon_s\epsilon_0^3)^{\frac{1}{2}}}\left(\frac{m^*}{m}\right) \tag{77}$$

where F_0 is in volts/cm and $(\hbar\omega_t)_{e.v.}$ is in electron-volts.

The quantity F/F_0, as given by Eq. (74), is easily obtained as a function of $E/\hbar\omega$ and $kT/\hbar\omega$ from Fig. 2. In Fig. 3 we plot F/F_0 against $E/\hbar\omega$ for various values of $kT/\hbar\omega$.

In accordance with the low energy criterion we adopt as the breakdown field at a given temperature the maximum of the corresponding curve in Fig. 3. We note that at $T=0$ the maximum occurs at $F/F_0=1$. *Thus F_0 is the breakdown field strength at $T=0$.* The maxima of the curves of Fig. 3 are plotted against the reduced temperature in Fig. 4, which therefore gives the temperature dependence of the breakdown strength.

The breakdown strength of a diatomic ionic crystal is obtained at $T=0$ from Eq. (77), and at other temperatures from Fig. 4. The breakdown strength depends only on the reststrahl frequency, the static and optical values of the dielectric constant, the effective mass, and the temperature.

In Table I we give the pertinent data for those alkali halides for which the reststrahl frequency is known, and the computed values of the breakdown strength assuming $m^*=m$.

IX. CONCLUSION—DIRECTIONAL EFFECTS

The theoretical values (assuming $m^*/m=1$) are compared with the experimental breakdown strengths in Table I. It is seen that the agreement is quite fair, the only notable exception being LiF.*

* Burstein, Oberly, and Plyler (Proc. Ind. Acad. Sci. 28, 388 (1948)) have presented evidence which indicates that there is an abnormally large amount of homopolar binding in LiF, and it should be noted that the presence of homopolar binding should tend to decrease the breakdown strength below the theoretical

It should be mentioned here that fluctuation effects, which have been neglected, may alter the breakdown criterion. Thus, although the field necessary to accelerate, on the *average*, an electron of given energy is as indicated in Fig. 3, there exists an appreciable probability than an electron will reach fairly high energies even without the benefit of the applied field, due to the statistical fluctuations in the interaction between the electron and the thermal vibrations of the lattice. Calculations of the effect of the fluctuations would involve a knowledge of the length of time an electron can afford to wait in the conduction band for a propitious fluctuation, before decaying into the lower almost-full band; that is, the treatment would require a knowledge of recombination probabilities, about which very little is known. Fortunately the curves of Fig. 3 are seen to be very flat in the neighborhood of their maxima, which tends to minimize the effect of fluctuations. Fluctuation effects may, however, be partially responsible for the fact that the theoretical breakdown strengths of Table I exceed the observed breakdown strengths and may perhaps be significant in the high-temperature region in which the temperature coefficient of the breakdown strength is observed to become negative.

The validity of the perturbation method also deserves some comment here. If the change in energy of an electron during a collision is $\hbar\omega$, and the mean time between collisions is Δt, a condition for the validity of the perturbation method is that $\Delta E \cdot \Delta t \gtrsim h$. If we compute the mean time between collisions for electrons in NaCl at $T=0°$ we find that for electrons of energy $\sim 3\hbar\omega$ (for which Δt is minimum) we obtain

$$\Delta E \cdot \Delta t \simeq 0.74h.$$

Thus the condition for validity of the perturbation method is not strictly satisfied, but the extrapolation is not so drastic that we may expect to obtain qualitatively incorrect results. The perturbation method is commonly found to be remarkably trustworthy, even when cruelly abused.

Finally, we wish to point out that the directional effects observed in breakdown experiments can be at least qualitatively undertood in terms of the present calculation. It is experimentally observed[11] that the breakdown strength of alkali halide crystals is independent of the orientation of the applied field relative to the crystallographic axes, but that the breakdown paths tend to lie in definite crystallographic axes. We have seen that the conservation rules for the collision between an electron and a vibrational mode restrict the range of wave vectors of the modes with which an electron of given energy can interact (see Eqs. (49) and (50)), and the maximum allowable σ increases with increasing electron energy. The slow electrons are thus insensitive to direction because the conservation rules permit them to interact only with modes near the origin of wave vector space, whereas the fast electrons are direction-sensitive because the conservation rules cause them to interact with modes at the zone boundaries. According to the low-energy criterion it is the slow electrons which determine the breakdown strength, but these electrons, once accelerated past a few tenths of an electron volt, travel relatively long distances through the crystal while being further accelerated to the ionization energy ($\sim$7 electron-volts). It is in this latter phase of their flight that they become direction sensitive* and form the direction-sensitive breakdown paths. It thus appears that the directional effects are associated with the symmetry of the Brillouin zones of the vibrational modes, and indeed Davisson[11] has shown that the directional properties of the breakdown paths are governed completely by the lattice symmetry, and not by the ionic characteristics or type of crystalline bonding. The directional effects seem to provide a potent argument in favor of the low energy criterion.

predictions. The goodness of the correlation between the deviation of theory and experiment, and the amount of homopolar binding found by Burstein *et al.*, seems to us to actually increase the confidence which one may place in the fundamental assumptions of the present theory.

[11] See A. von Hippel, Zeits. f. Physik **67**, 707 (1931); **68**, 309 (1931); A. von Hippel and J. Davisson, Phys. Rev. **57**, 156 (1940); J. W. Davisson, Phys. Rev. **70**, 685 (1946); **73**, 1194 (1948).

* Von Hippel (see reference 1) has suggested that the directional sensitivity of the fast electrons may arise from the symmetry properties of the forbidden and allowed energy bands, and this may also contribute to the effect.

PHYSICAL REVIEW VOLUME 76, NUMBER 9 NOVEMBER 1, 1949

Diffusion in Binary Alloys

J. BARDEEN
Bell Telephone Laboratories, Murray Hill, New Jersey
(Received July 5, 1949)

Darken has given a phenomenological theory of diffusion in binary alloys based on the assumption that each constituent diffuses independently relative to a fixed reference frame. It is shown that diffusion via vacant lattice sites leads to Darken's equations if it is assumed that the concentration of vacant sites is in thermal equilibrium. Grain boundaries and dislocations may act as sources and sinks for vacant sites and act to maintain equilibrium. The modifications required in the equations if the vacant sites are not in equilibrium are discussed.

I. INTRODUCTION

THERE has recently been much interest in diffusion in alloys from both an experimental and a theoretical standpoint. W. A. Johnson[1] has investigated the relation between diffusion of radioactive constituents of binary alloys of silver and gold and diffusion resulting from a gradient in the relative concentrations of the two metals. He finds that the chemical diffusion coefficient in an alloy in the 50–50 range of composition is larger than that of either of the constituents. Smigelskas and Kirkendall,[2] in a study of the migration of the boundary between 70–30 alpha-brass and copper as a result of diffusion, found that the diffusion is associated with a mass flow such as might be expected if zinc diffuses out of the brass more rapidly than copper diffuses in.

The theory of diffusion in alloys has been discussed recently by a number of authors from different points of view and apparently with differing results. Birchenall and Mehl[3] emphasize the role of the gradient of chemical potential as the motivating force in diffusion. Fisher, Hollomon, and Turnbull[4] treat the problem on the basis of the absolute theory of reaction rates, and consider diffusion via vacant lattice sites as well as by interstitial atoms. L. S. Darken[5] has developed the theory of diffusion in binary alloys from a phenomenological standpoint. He assumes that each constituent diffuses independently of the other. F. Seitz[6] treated the vacancy mechanism of diffusion from the standpoint of kinetic theory. The purpose of the present note is to point out the connection between these various treatments, and in particular to show that the vacancy mechanism leads to Darken's equations if it is assumed that the concentration of vacant sites is maintained in local thermal equilibrium.

The method of calculation which we use is similar to that of Seitz. From a consideration of the effect on rate of flow of terms in the free energy arising of nonideality of the solid solution, we are led to equations for diffusion rates which are essentially the same as those of Fisher, Hollomon, and Turnbull. These equations involve the concentration of vacant lattice sites. Darken's equations then follow if it is assumed that the vacant sites are maintained in thermal equilibrium.

In Part II we give a brief description of Darken's theory. This is followed in Part III by a discussion of the thermodynamics of a binary alloy with vacant lattice sites. Part IV gives the theory of diffusion based on a model similar to that of Seitz.

II. DARKEN'S THEORY

Darken assumes that each constituent diffuses independently of the other so that, in a binary alloy with constituents A and B in concentrations N_A and N_B, the currents of atoms of the two types relative to some fixed reference frame are:

$$i_A=-D_A(\partial N_A/\partial x);\quad i_B=-D_B(\partial N_B/\partial x). \tag{1}$$

Although Darken does not wish to be as specific, we will assume that the reference frame is the crystal lattice. Since

$$(\partial N_A/\partial x)=-(\partial N_B/\partial x), \tag{2}$$

the total flow of atoms across a plane fixed in the lattice is:

$$i_A+i_B=-(D_A-D_B)(\partial N_A/\partial x). \tag{3}$$

Relative to a moving reference frame for which this flow vanishes, the flow of A atoms is

$$i_A-f_A(i_A+i_B)=-(f_BD_A+f_AD_B)(\partial N_A/\partial x), \tag{4}$$

where f_A and f_B are the fractional concentrations:

$$f_A=N_A/(N_A+N_B),\quad f_B=N_B/(N_A+N_B). \tag{5}$$

The factor

$$D_c=f_BD_A+f_AD_B \tag{6}$$

is the chemical diffusion coefficient as measured by the usual methods.

If there is a gradient of the concentration, N_A^*, of a radioactive tracer, the flow of radioactive atoms in an alloy in which the total concentration of A atoms is

[1] W. A. Johnson, Trans. A.I.M.E. 147, 331 (1942).
[2] A. D. Smigelskas and E. O. Kirkendall, Trans. A.I.M.E. 171, 130 (1947).
[3] C. E. Birchenall and R. F. Mehl, Trans. A.I.M.E. 171, 143 (1947), and subsequent discussion.
[4] Fisher, Hollomon, and Turnbull, Metals Tech. Tech. Paper 2344 (February, 1948).
[5] L. S. Darken, Metals Tech. Tech. Paper 2311 (1948).
[6] Frederick Seitz, Phys. Rev. 74, 1513 (1948).

uniform is

$$i_A^* = -D_A^*(\partial N_A^*/\partial x). \quad (7)$$

Darken attributes differences between D_A and D_A^* to terms in the chemical potential other than those resulting from the entropy of mixing. It is the gradient of the chemical potential, μ_A, which is responsible for diffusion.

If in place of (2) or (7) we write

$$i_A = -C_A N_A \partial\mu_A/\partial x_A, \quad (8)$$

then C_A is the same for both chemical and radioactive diffusion. The chemical potential in the radioactive case involves only the entropy of mixing, so that, as for an ideal solution,

$$\mu_A^* = kT \log N_A^*. \quad (9)$$

Inserting (9) into (8) and comparing the result with (7), we find that

$$C_A = D_A^*/kT_A. \quad (10)$$

Comparing (8) and (2) for the case of chemical diffusion, we find the relation between D_A and D_A^* which was used by Darken:

$$D_A = D_A^*(d(\mu_A/kT)/d \log N_A). \quad (11)$$

For an ideal solution D_A and D_A^* are equal. In general, D_A may be either larger or smaller than D_A^*.

Similar equations apply to i_B. Darken points out that the thermodynamic equations of the alloy system,

$$d(\mu_A/kT)/d \log N_A = d(\mu_B/kT)/d \log N_B, \quad (12)$$

imply that

$$D_A/D_B = D_A^*/D_B^*. \quad (13)$$

Using values of μ_A from electrochemical data for the silver gold alloy Darken computed the value of the chemical diffusion coefficient, D_c, from the radioactive coefficients and found reasonable agreement with Johnson's measurements. Darken, of course, attributes a mass flow such as that found by Smigelskas and Kirkenall to a difference between D_A and D_B.

III. THERMODYNAMICS OF ALLOY WITH VACANT SITES

We suppose that of a total number of N sites, N_A are occupied by A atoms, N_B by B atoms, and N_v are vacant, so that

$$N = N_A + N_B + N_v. \quad (14)$$

We suppose that N_v is small compared with N_A and N_B. The Gibbs free energy may be expressed in the form:[7]

$$G = W(N_A, N_B, N_v) - kT(N \log N - N_A \log N_A - N_B \log N_B - N_v \log N_v), \quad (15)$$

where the second term comes from the entropy of mixing and the first from all other causes. The chemical potentials μ_A, μ_B, and μ_v are defined by equations of the form:

$$\mu_A = \partial G/\partial N_A = W/\partial N_A + kT \log f_A, \quad (16)$$

where f_A is the fractional concentration. In terms of the chemical potentials,

$$G = N_A\mu_A + N_B\mu_B + N_v\mu_v. \quad (17)$$

The potential μ_v is the free energy required to take an atom from the interior to the surface, forming an additional vacant site and increasing the total number of sites by one. If the vacant sites are in thermal equilibrium, $\mu_v = 0$. We do not assume this necessarily to be the case. In general,

$$\mu_v = kT \log(N_v/N_{ve}), \quad (18)$$

where N_v is the actual concentration of vacant sites and N_{ve} is the equilibrium concentration. In writing Eq. (18) we have assumed that $\partial W/\partial N_v$ is independent of N_v, as will be the case for small concentrations of vacancies. Equation (12) follows directly from Eq. (17) if it is assumed that $\mu_v = 0$, but is not strictly valid in the general case. Deviations from Eq. (12) will be small if the fractional concentration of vacant sites is small compared with unity or departs but little from equilibrium.

IV. DIFFUSION VIA VACANT SITES

We first discuss radioactive diffusion and then show how chemical diffusion is related to it. We assume, following Seitz,[6] that diffusion of both A and B atoms occurs by motion of atoms into neighboring vacant sites. For simplicity, we assume that the atomic volume is independent of concentration.

Consider two neighboring crystallographic planes, 1 and 2, which are normal to the x axis and which are separated by a distance λ. We suppose that there is a gradient in the concentration, N_A^*, of tracer atoms in an otherwise uniform alloy, so that the number per unit area on plane 1 is λN_A^* and on plane 2 is $\lambda(N_A^* + \lambda(\partial N_A^*/\partial x))$. The concentration of vacant sites is assumed to be uniform. The rate at which A^* atoms go from plane 1 to plane 2 is then:

$$k_A \lambda N_v N_A^*, \quad (19)$$

and from plane 2 to plane 1,

$$k_A \lambda N_v (N_A^* + \lambda(\partial N_A^*/\partial x)), \quad (20)$$

where k_A is proportional to the rate at which an A atom jumps into a neighboring vacant site. Expressions (19) and (20) are based on the assumption that the concentration of A atoms which have vacant sites as neighbors in the adjacent plane is proportional to the average concentration of A atoms in the given plane.[8] The net

[7] See, for example, M. W. Zemansky, *Heat and Thermodynamics* (McGraw-Hill Book Company, Inc., New York, 1943), p. 323.

[8] Dr. C. Herring has pointed out to the author that this assumption may not be valid. Consider the different ways in which a vacant site on the plane at $x+\lambda$ becomes adjacent to an A atom on the plane at x so that a forward jump of the A atom can take

flow of A^* atoms is the difference between (19) and (20)

$$i_A^* = -k_A\lambda^2 N_v(\partial N_A^*/\partial x), \tag{21}$$

giving for the radioactive diffusion coefficient:

$$D_A^* = k_A\lambda^2 N_v. \tag{22}$$

We next consider the case of chemical diffusion and assume a gradient in the concentration of vacant sites as well as of A and B atoms. The rate at which A atoms go from plane 1 to plane 2 is

$$k_f\lambda N_A(N_v+\lambda(\partial N_v/\partial x)) \tag{23}$$

and from plane 2 to plane 1

$$k_b\lambda N_v(N_A+\lambda(\partial N_A/\partial x)), \tag{24}$$

in which k_f and k_b are proportional to the frequency of jumps in the forward and backward directions, respectively. If, as a result of the concentration gradient in a non-ideal solution, the free energy of an A atom on plane 1 is slightly different from that of one on plane 2, the potential barrier over which diffusion takes place will not be symmetric, k_f will differ from k_b by terms of the order λ, and both will differ from k_A by terms of the same order.

The net rate of flow of A atoms is the difference between (23) and (24)

$$i_A = k_A\lambda^2\left(N_A\frac{\partial N_v}{\partial x} - N_v\frac{\partial N_A}{\partial x}\right) + (k_f - k_b)\lambda N_A N_v, \tag{25}$$

in which we have neglected higher order terms in λ. If ΔW is the change in free energy arising from non-ideality in the forward jump of an A atom,[9]

$$k_f/k_b = \exp(-\Delta W/kT) \simeq \left(1-\frac{\Delta W}{kT}\right). \tag{26}$$

The effective height of the barrier impeding diffusion is increased for a forward jump and decreased for a reverse jump, and the difference in effective heights in the two directions is ΔW. To a sufficient approximation,

$$k_f - k_b = k_A\Delta W/kT. \tag{27}$$

An expression for ΔW may be obtained as follows. In a forward jump, the number of A atoms on the plane at $x+\lambda$ is increased by one and the number of vacant sites is decreased by one. On the plane at x the opposite changes occur. Thus to terms of the order λ

$$\Delta W = \left(\frac{\partial W}{\partial N_A} - \frac{\partial W}{\partial N_v}\right)_{x+\lambda} - \left(\frac{\partial W}{\partial N_A} - \frac{\partial W}{\partial N_v}\right)_x = \lambda\frac{\partial}{\partial x}\left(\frac{\partial W}{\partial N_A} - \frac{\partial W}{\partial N_v}\right). \tag{28}$$

Using (27) and (28) in (25), we find

$$i_A = k_A\lambda^2 N_A N_v\frac{\partial}{\partial x}\left[\log N_v - \log N_A - \frac{1}{kT}\left(\frac{\partial W}{\partial N_A} - \frac{\partial W}{\partial N_v}\right)\right], \tag{29}$$

which may be written in the form:

$$i_A = -C_A N_A\partial(\mu_A - \mu_v)/\partial x, \tag{30}$$

where

$$C_A = k_A\lambda^2 N_v/kT = D_A^*/kT. \tag{31}$$

Equation (29) is essentially the same as Eq. (27) of Fisher, Hollomon, and Turnbull.

Equation (30) is the same as Eq. (8) if $\mu_v = 0$. Thus the mechanism of diffusion via vacant sites leads to Darken's phenomenological equations if the vacant sites are in local thermal equilibrium. No gradient of vacant sites is to be expected in the case of diffusion of a radioactive tracer. In chemical diffusion, where there is a vacancy current, grain boundaries and to a less extent dislocations will act as sources and sinks for vacant sites to help maintain local equilibrium. The associated plastic flow tends to keep the density of atoms constant.

If the concentration of vacant sites is not in thermal equilibrium, the more general Eq. (30), which is analogous to those of Seitz and of Fisher, Hollomon, and Turnbull, must be used. With use of Eq. (18) for μ_v, (30) includes a term in the concentration gradient of vacant sites. This could be transformed, following Seitz, to a term involving the current of vacant sites.

The author is indebted to Dr. C. Herring and to Dr. L. S. Darken for a number of valuable suggestions.

place. One of the ways is that in which a reverse jump has just taken place, an A atom on $x+\lambda$ going to the plane at x. The number of these which will occur will depend in part on the concentration of A atoms at $x+\lambda$ instead of x. In the extreme case in which motion can take place only along strings of atoms parallel to the concentration gradient, a flow of vacant sites could take place without any associated diffusion. According to Dr. Herring's calculations, the error made in calculating the radioactive diffusion coefficient in a cubic monatomic substance by the above method is about 10 percent.

[9] See S. Glasstone, H. J. Laidlen, and H. Eyring, *The Theory of Rate Processes* (McGraw-Hill Book Company, Inc., New York, 1941), p. 530.

Letters to the Editor

PUBLICATION of brief reports of important discoveries in physics may be secured by addressing them to this department. The closing date for this department is five weeks prior to the date of issue. No proof will be sent to the authors. The Board of Editors does not hold itself responsible for the opinions expressed by the correspondents. Communications should not exceed 600 words in length.

Alpha-Decay in Isotopes of Atomic Number Less Than 83

S. G. THOMPSON, A. GHIORSO, J. O. RASMUSSEN, AND G. T. SEABORG
Department of Chemistry and Radiation Laboratory, University of California, Berkeley, California
September 12, 1949

SOME time ago we started work in an attempt to observe alpha-particle decay in isotopes of atomic number less than 83. In the first experiments, thin targets of gold leaf were bombarded with 190-Mev deuterons in the 184-inch cyclotron. Two alpha-decay periods were observed in these targets; one of 0.7 minute half-life and another of 4.3 minutes half-life. The alpha-particle energies were 5.7 and 5.2 Mev, respectively. Chemical separations proved that the 4.3-minute period is due to a gold isotope and suggested that the 0.7-minute period is due to a mercury isotope. The mass numbers of these new isotopes have not been determined. However, the results of excitation functions in the production of the gold isotope by bombarding gold and platinum with protons suggest that its mass number lies in the range 185 to 188. The work on this isotope indicates that the alpha to electron capture branching ratio is of the order of magnitude of 10^{-4}, and that positron activity accompanies the 4.3-minute alpha-period.

Very recently Sm_2O_3, Gd_2O_3 and Dy_2O_3 tagets were bombarded similarly with 200-Mev protons. Several new alpha-decay periods were observed in the gadolinium and dysprosium targets, but significant alpha-activity was absent in the samarium target.

In the gadolinium bombardment there was present an alpha-decay period of approximately 7 minutes half-life and another of about 4 hours half-life, the alpha-particle energies being approximately 4.2 and 4.0 Mev, respectively, as determined with a pulse analyzer apparatus.

In the dysprosium bombardment, three alpha-decay periods were observed, namely ~7 minutes, ~20 minutes, and ~4 hours with alpha-particle energies of 4.2, 4.1, and 4.0 Mev, respectively. Present also was some electromagnetic radiation and a smaller amount of positron activity. With rough assumptions as to counting efficiency and geometry in the counting of the electromagnetic radiation with a Geiger counter, it appears that a minimum value for the ratio of alpha to electron capture is approximately 1 percent for the 4-hour activity.

The relationship between the alpha-particle energies and the half-lifes of these new isotopes places them in a new class. The energies are approximately the same as the alpha-particle energy of Th^{232} which has a half-life of 1.4×10^{10} years. These facts in themselves are proof that these new periods could not have been due to heavy isotope contamination.

Chemical identification of these rare earths has not been completed as yet. However, since the 4.0-hour and 7-minute activities were produced in gadolinium and dysprosium targets and not in samarium, they would appear to be associated with gadolinium or terbium isotopes. Since the 20-minute period was produced only in the dysprosium target it would appear to be an isotope of dysprosium or holmium.

Although it is probably premature to attempt now to interpret these rather limited data, it is tempting to suggest a difference between the alpha-emitting isotopes of the gold region and those of the rare earths. As has been pointed out on numerous occasions[1] it should be possible to observe artificial alpha-activity in sufficiently neutron deficient isotopes in the region between the rare earths and lead. The alpha-emitting isotopes of the gold region might be "normal" examples of this since they are observed to decay with short electron capture half-lives, and with small alpha to electron capture branching ratios. In this case alpha-particle decay would be largely the consequence of considerable neutron deficiency. The higher alpha to electron capture branching ratio of the new rare earth isotopes is probably due to (a) a more moderate degree of neutron deficiency giving rise to longer electron capture half-lives, and (b) exceptionally high alpha-particle energies giving rise to shorter alpha-half-lives. These new rare earth periods might, therefore, be correlated with the stable configuration of 82 neutrons[2] in such a way as to acquire the necessary extra alpha-disintegration energy. Just as the isotopes having neutron numbers in the range 127–130 of the region above lead (for example $_{84}Po^{211}$, $_{84}Po^{212}$, $_{84}Po^{213}$, or $_{85}At^{215}$) decay by unusually high energy alpha-particle emission as a consequence of their decay to or near the stable configuration of 126 neutrons,[3] so might isotopes such as $_{65}Tb^{149}$ or $_{66}Dy^{150}$ and those differing by a few neutrons (such as $_{65}Tb^{148}$, $_{65}Tb^{150}$, $_{66}Dy^{151}$, or $_{67}Ho^{153}$, etc.) decay by relatively high energy alpha-particle emission as a consequence of their decay to or near the stable configuration of 82 neutrons. Such isotopes would, therefore, be attractive possibilities for the assignment of these new rare earth periods. It would be more consistent with this view to assign the long-known natural radioactivity of samarium to $_{62}Sm^{147}$ (and/or $_{62}Sm^{148}$) rather than to $_{62}Sm^{152}$ (present best tentative assignment),[4] but, on the other hand, other stable configurations with a larger number of neutrons[5] may also be important.

In view of these new data it can be seen that alpha-decay in the lighter elements is more prevalent than hitherto recognized, and therefore these investigations are being continued. This letter is intended only as a very preliminary report and more complete results will be reported at some future date.

We wish to thank James Vale and the crew of the 184-inch cyclotron for their assistance in carrying out the work.

This work was performed under the auspices of the U. S. Atomic Energy Commission.

[1] See, e.g., T. P. Kohman, Phys. Rev. **76**, 448 (1949). This contains a rather complete list of references to other publications on this subject.
[2] See, e.g., Maria G. Mayer, Phys. Rev. **74**, 235 (1948).
[3] Perlman, Ghiorso, and Seaborg, Phys. Rev. **75**, 1730 (1948).
[4] A. J. Dempster, Phys. Rev. **73**, 1125 (1948).
[5] N. Feather, Nature **162**, 412 (1948).

Betatron-Produced Sources of High Specific Activity: Copper 62*

R. A. BECKER, F. S. KIRN, AND W. L. BUCK
Physics Research Laboratory, University of Illinois, Champaign, Illinois
August 15, 1949

THIN metallic foils have been activated, employing a probe technique, by bombardment with a 22-Mev. betatron. Specific activities in excess of 5 millicuries of Cu^{62} positron activity per gram have been obtained with 2-mm strips of half-mil copper foil (approximately 11 mg/cm²). These sources were employed to measure the positron spectrum by means of a 180-degree type magnetic spectrometer. The technique of activation is shown in Fig. 1. The electron beam, of small cross section, was caused to strike a lead converter, the resulting beam of x-rays in turn activating the folded foil. The presence of the converter greatly enhanced the strength of the activity since gamma-cross sections are of the order of 400 times larger than electron cross sections.[1] The specific activities thus obtained were more than a thousand times greater than those realized when the betatron is employed in the conventional manner with an x-ray donut. The procedure

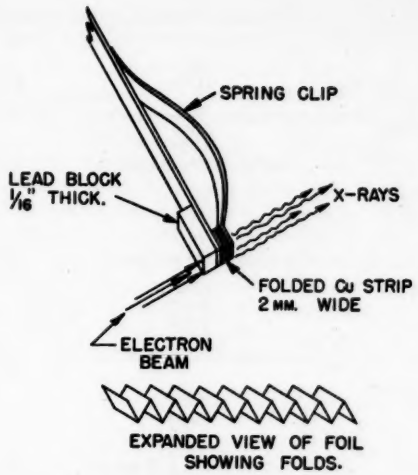

FIG. 1. Technique of activation of the foils.

took advantage of the tiny cross section of the beam at the probe, resulting in a high concentration of x-ray quanta in that region. After irradiation the foils, which had been cut to size prior to bombardment, were removed through an air lock, unfolded, and inserted in the spectrometer.

Figure 2 shows a Kurie plot of preliminary work with the 10-minute positron activity of Cu^{62}. Several sources were required because of the short decay time, and the major error arose from the normalization of the samples. The spectrometer had a resolution of about 1.25 percent. The field of the spectrometer was continuously monitored by comparing, with a null method, the e.m.f. generated by a rotating coil between the pole faces with that by a coil rotating in the gap of a standard permanent magnet. The latter was calibrated by means of the photoelectrons ejected from a 20 mg/cm² uranium foil by the gamma-rays of Co^{60}. The values of Lind *et al.*[2] for the Co^{60} lines were used. Two sets of measurements were obtained with a path radius of 10 cm, and one at 8 cm. The endpoints, respectively, were 2.88, 2.84, and 2.78 Mev. A mean was chosen to be 2.83±0.05 Mev. This figure is greater than that quoted by Crittenden.[3]

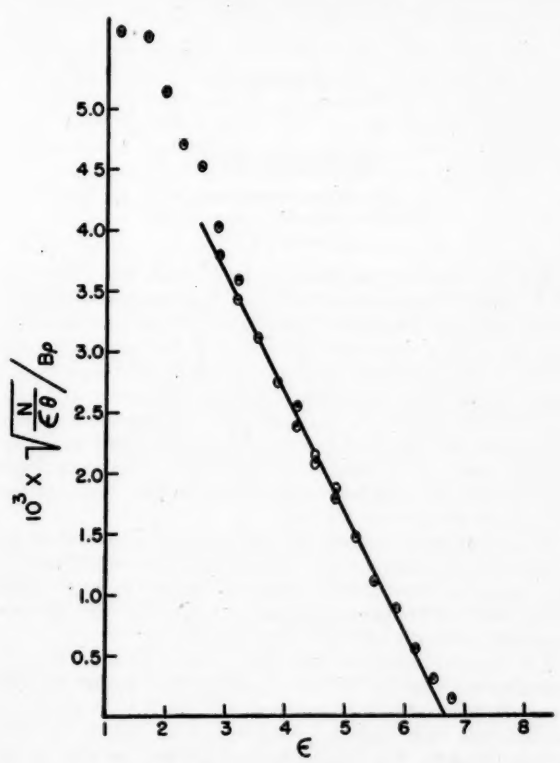

FIG. 2. Kurie plot of Cu^{62} positrons.

* Aided by the joint program of the ONR and AEC.
[1] Skaags, Laughlin, Hanson, and Orlin, Phys. Rev. 73, 420 (1948).
[2] Lind, Brown, and DuMond, Phys. Rev. 76, 591 (1949). The figure there quoted erroneously for the lower energy line was corrected by private communication from DuMond.
[3] E. C. Crittenden, Jr., Phys. Rev. 56, 709 (1939).

Energy of an Excited State of Li^7

MICHEL TER-POGOSSIAN, J. EUGENE ROBINSON, AND C. HAROLD GODDARD
Physics Department, Washington University, St. Louis, Missouri
September 15, 1949

IN a recent unpublished note, H. Primakoff and E. Feenberg suggested the possibility of the existence of two closely spaced excited states in Li^7. This hypothesis[1] appears necessary because of the selection rules in the Be^7 decay and the $B^{10}(n, \alpha)Li^{7*}$ reaction. The first step made to test this hypothesis was to compare the energies of the radiations emitted in the transitions $Li^{7*} \rightarrow Li^7$ for different methods of producing Li^{7*}. Many measurements of the energy of the radiation following the transition $Be^7 \rightarrow Li^{7*}$ have been reported,[2] but some of the energies reported for this radiation are sufficiently different from the energy of the gamma-radiation following the transition $B^{10}(n, \alpha)Li^{7*}$ reported by Elliott and Bell,[3] to allow the possibility of the existence in the Li^7 of two excited states, reached, one by the K-capture in Be^7 and the other by the emission of an alpha-particle by the compound nucleus B^{11}. The purpose of the present work is to restrict the possible existence of these excited states to a very narrow band by measuring the energy of the gamma-radiation following the transition $Be^7 \rightarrow Li^{7*}$ by comparing this energy with the energy of the gamma-radiation emitted by Au^{198}. This method was used by Elliott and Bell to determine the energy of the radiation following the transition $B^{10}(n, \alpha)Li^{7*}$. The source was prepared by bombarding an internal target of lithium metal in the Washington University cyclotron with 9-Mev deuterons for 17,000 microampere hours. The Be^7 was then chemically separated from the lithium following a procedure suggested by Dr. G. Friedlander[4] the final product about 5 mgs of beryllium acetate (about 5 mgs of beryllium carrier were added) was sealed in a glass tube. A source of Au^{198} obtained from the Oak Ridge pile was sealed in an identical tube. The energies of radiations emitted by the two sources were compared in a 180° beta-ray spectrometer[5] by comparing the energy of the photoelectrons produced in an uranium radiator of 50 mg/cm², and 1 mm wide. The measurements were made in the following order: measurement of the gold line, then the lithium line, gold again, then lithium again. These measurements were executed one immediately after the other. The bracketing of the lithium measurement between two measurements of the gold line, and the repetition of the lithium measurement showed that the field measuring device (flip coil connected to a galvanometer) did not vary during the experiment. The reference point for the measurement of momentum was taken at the peak of photoelectron lines. It should be noted that any point on the photoelectron lines could be taken as a reference since each of the four measured lines should be identical by virtue of the fact that the source was always located at the same position relative to the uranium radiator and that the same radiator was always used. Values obtained for the momentum in arbitrary units were (see also Fig. 1):

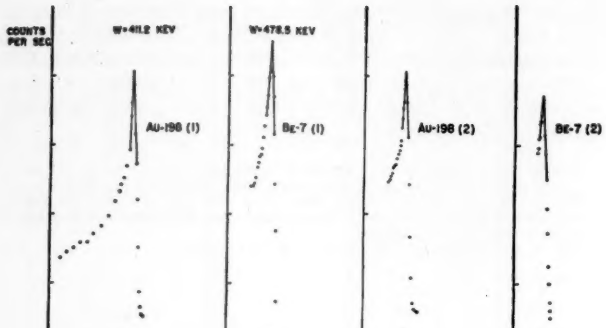

FIG. 1. Spectra of the photoelectrons ejected from a 50 mg/cm² uranium radiator by the gamma-rays of Au^{198} and Be^{7}. The ordinates representing the number of counts per second have been normalized to bring the lines to approximately the same height graphically; and are graduated in arbitrary units.

	Au(1)	Li(1)	Au(2)	Li(2)
Momentum	8.20	9.31	8.20	9.30

Taking for the gold line the value reported by DuMond:[6] 411.2 kev, we find for the energy of the excited state of Li^{7}: 478.5±0.5 kev. Elliott and Bell[3] reported the value of 478.5±1.5 kev for the energy of the excited state of Li^{7} reached $B^{10}(n, \alpha)Li^{7*}$. It appears from these results that if these two excited states are different they are not separated by more than 2 kev.

This work was assisted by the joint program of the ONR and AEC.

[1] B. T. Feld, Phys. Rev. 75, 1618 (1949) discusses the possible disintegration schemes proposed.
[2] R. M. Williamson and H. T. Richards, Phys. Rev. 76, 614 (1949). Reference to all previous measurements of the energy of this transition are given in this article.
[3] L. G. Elliott and R. E. Bell, Phys. Rev. 74, 1869 (1948).
[4] G. Friedlander (private communication).
[5] Ter-Pogossian, Robinson, and Cook, Phys. Rev. 75, 995 (1949).
[6] DuMond, Lind, and Watson, Phys. Rev. 73, 1392 (1948).

TABLE I. Values of I_0/I_{90} for targets of various diameters.

I Diameter of D_2O Holder	II I_0/I_{90}	III I_0/I_{90} Corrected for geometry
12 mm	0.393	
	0.354	
	average 0.374±7 percent	0.350
9 mm	0.318	
	0.361	
	0.347	
	0.357	
	average 0.346±6 percent	0.321
6 mm	0.245	
	0.304	
	0.364	
	0.279	
	average 0.298±16 percent	0.271
4.5 mm	0.299	
	0.282	
	0.264	
	0.257	
	0.354	
	average 0.276±19 percent	0.248

holders were made of steel tubing 0.0125 cm-thick and 5 cm-long. The outer diameters were 4.5, 6, 9, and 12 mm respectively. Column II of Table I shows the values of I_0/I_{90} for the different targets obtained on different runs lasting 12–24 hours. In column III are the average values for a given diameter of the results in column II corrected for geometry.

Assuming a linear dependence on radius of I_0/I_{90}, the extrapolated value for zero radius is 0.17. This yields a value of a/b of 0.205±.05.

The value previously reported by us[4] was not corrected properly. The present value is in agreement with Lassen's[5] corrected value and with Meiner's value.

[1] Hamermesh, Hamermesh, and Wattenberg, Phys. Rev. 76, 611 (1949).
[2] G. Graham and H. Halban, Rev. Mod. Phys. 17, 297 (1945).
[3] E. P. Meiners, Jr., Phys. Rev. 76, 259 (1949).
[4] Bernard Hamermesh and Albert Wattenberg, Phys. Rev. 75, 1290(A) (1949).
[5] N. O. Lassen, Phys. Rev. 75, 1099 (1949).

The Angular Distribution of the Photo-Neutrons from Deuterium at 2.76 Mev

BERNARD HAMERMESH AND ALBERT WATTENBERG
Argonne National Laboratory, Chicago, Illinois
September 22, 1949

THE apparatus and techniques used in the study of the photoneutrons from beryllium[1] have been used to study the photoneutrons produced in deuterium by 2.76-Mev γ-rays. The distribution is found to be of the form $I(\theta)=a+b\sin^2\theta$. The ratio a/b is best found by measurements made at 0° and 90°. The results are subject to two corrections, a geometrical one caused by the finite angles subtended by the source and counter at the target and a correction caused by neutrons being scattered inside the D_2O target. The former correction is readily estimated from the relative dimensions and spacings of the target, source and counter. The scattering correction may be estimated in a very rough manner.[1] However, because of the large effect of this correction on the a/b value for deuterium, an experimental study was made of the correction.

The method used is similar to the one of Graham and Halban[2] and Meiners.[3] Since the scattering effect should become smaller and smaller as the size of the D_2O target decreased a set of D_2O targets of varying diameters was used. The cylindrical D_2O

28.7-Hour Ba^{135}

B. E. ROBERTSON* and M. L. POOL
Ohio State University, Columbus, Ohio
September 23, 1949

WITH electromagnetically enriched Ba^{132}, Ba^{134}, Ba^{135}, and Ba^{136} ** now available, the previously reported 28.7-hour barium activity[1–3] has been investigated. It had been postulated that this activity was a metastable state of Ba^{135} although assignments to other mass numbers were not entirely ruled out.[3] It is the purpose of this letter to confirm the mass assignment of the 28.7-hour activity to Ba^{135}. As the degree of enrichment of the respective barium isotopes is not yet available, this mass assignment has been made on the basis of the specific activities per milligram of barium in the enriched barium samples after bombardments with deuterons and fast neutrons.

Bombardment of enriched $Ba^{134}(NO_3)_2$ with 10-Mev deuterons yielded the 28.7-hour activity in the barium fraction. Characteristic radiaions were 0.28-Mev negatively charged particles, barium x-rays, and a 0.30-Mev gamma-ray in agreement with the measurements previously reported.[1–3]

The bombardment of $Ba^{134}(NO_3)_2$ with 10-Mev deuterons produced more of the 28.7-hour activity than similar bombardments of the nitrates of the enriched Ba^{132}, Ba^{135}, Ba^{136}, and normal barium. The same chemical procedures were used in extracting barium fractions. The bombardment time was the same in each case. Decays were followed on a Wulf electrometer.

The resulting specific activities in terms of the time-off intensity of the 28.7-hour activity per milligram of bombarded barium were in the ratios 1.00:0.73:0.54:0.03:0.05 for the samples enriched in Ba^{134}, Ba^{132}, Ba^{135}, and Ba^{136}, and natural barium, respectively. Similar bombardments of the enriched barium isotopes in carbonate form with fast neutrons from Li+d produced the 28.7-hour activity with specific activities in the ratios 1.00:0.42:0.42:0.09:0.04 for the samples enriched in Ba^{135}, Ba^{132}, Ba^{134}, and Ba^{136}, and natural barium. Bombardments of Hilger CsCl with 10-Mev deuterons yielded the well-known 38.5-hour activity[4] of Ba^{133} in the barium fraction but no 28.7-hour activity, precluding assignment of the 28.7-hour activity to Ba^{133} or Ba^{134} as a result of the reaction $Cs^{133}(d, 2n)$ or $Cs^{133}(d, n)$. Bombardment of Hilger CsCl with 20-Mev alpha-particles did not produce the 28.7-hour activity in the barium fraction, ruling out assignment to Ba^{136} as a result of the reaction $Cs^{133}(\alpha, p)$.

On the basis of these data the 28.7-hour activity in barium is assigned to an isomeric state of Ba^{135} as a result of the reactions $Ba^{134}(d, p)$ and $Ba^{135}(n', n)$. Calculations of the cross sections for the reactions will be communicated when the isotopic analyses of the enriched barium isotopes are available.

* Captain, U. S. Air Forces, research done under auspices U.S.A.F. Institute of Technology, Wright Field, Dayton, Ohio.
** Supplied by the Y-12 plant, Carbide and Carbon Chemicals Corporation, through the Isotope Division, AEC, Oak Ridge, Tennessee.

[1] D. C. Kalbfell and R. A. Cooley, Phys. Rev. 58, 91 (1940).
[2] Weimer, Pool, and Kurbatov, Phys. Rev. 63, 59 (1943).
[3] Fu-Chun Yu and J. D. Kurbatov, Phys. Rev. 74, 34 (1948).
[4] G. T. Seaborg and I. Perlman, Rev. Mod. Phys. 20, 585 (1948).

Upper Limit for the Lifetime of the 411-Kev Excited State of Hg^{198}

R. E. Bell and H. E. Petch*
Chalk River Laboratory, National Research Council of Canada
Chalk River, Ontario, Canada
September 19, 1949

THE β-γ-coincidences arising from the Au^{198}—Hg^{198} β-disintegration have been examined with a coincidence circuit of short resolving time in an effort to measure the mean life of the 411-kev γ-emitting state of Hg^{198}. Using the method of delayed coincidences and resolving times $2\tau_0$ less than 10^{-8} sec., the mean life is found too short to detect, in contradiction to MacIntyre's recent result[1] for the same measurement.

The coincidence unit employs anthracene—1P21 scintillation counters operated with electrode voltages so high (~2000 v) that their output pulses do not require amplification. The pulses are equalized in Type 6AK5 pentodes and led along 95-ohm matched coaxial cable to a 50-ohm shorted coaxial cable clipper which determines their length, and thence to a 1N34 diode coincidence mixer. The pulses from either counter can be delayed by accurately known amounts by lengthening the appropriate signal cable. Checks have been made to see that the extra lengths of cable used to delay the pulses do not cause any loss of coincidences through attenuation. The selection of pulse heights and determination of counting rates in the individual counters is accomplished by feeding the individual counter pulses by separate cables into two ordinary linear amplifiers equipped with amplitude discriminators. The output pulses of these amplifiers are fed into a relatively slow (~2 μsec.) triple coincidence circuit with the unselected fast coincidence pulses, and the desired coincidence rate is counted at the triple coincidence output. In this way only those fast coincidences are recorded which correspond to pulses larger than a fixed size from the individual counters, and the difficulties of very fast pulse height discrimination are avoided.

The resolution curve of the coincidence unit was measured by observing the coincidence rate as a function of delay of the pulses from each counter in turn. Results have been recorded for Co^{60} γ-γ-coincidences, Cs^{134} γ-γ-coincidences, and Au^{198} β-γ-coincidences at two different resolving times, $2\tau_0=9\times10^{-9}$ sec. and $2\tau_0=5.5\times10^{-9}$ sec. To clarify the diagrams, only the Cs^{134} and Au^{198} results at the shorter resolving time are shown. (The Co^{60} results are indistinguishable from those for Cs^{134}.) Figure 1 shows the resolution curves observed for Cs^{134} γ-γ- and Au^{198} β-γ-coincidences. The two curves are identical within experimental error and both are highly symmetrical. If the Hg^{198} 411-kev excited state had a mean life τ long enough to be detectable in this experiment, the right-hand (β-pulse delay) portion of the Au^{198} resolution curve would have a tail falling off as $\exp(-T/\tau)$, where T is the delay time.[2] No such tendency is visible in Fig. 1. The slight shifts (~4×10^{-10} sec.) of the maxima of the curves of Fig. 1 with respect to each other and to the zero of time represent fixed delays due to differences in transit time of the electrons in the photomultiplier tubes at slightly different electrode voltages. As a check on this explanation, the voltage on one photo-multiplier was lowered by 30 percent: the resolution curve then moved, without change of shape, in the direction corresponding to a lag of 3.4×10^{-9} sec. in the pulses from that tube. A resolution curve was plotted for β-α-coincidences from ThC(β)ThC'(α)ThD to

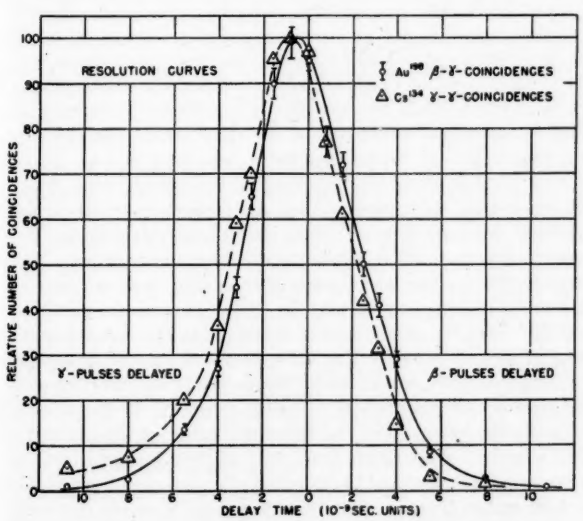

FIG. 1. Resolution curves of the coincidence unit for Au^{198} β-γ-coincidences and Cs^{134} γ-γ-coincidences.

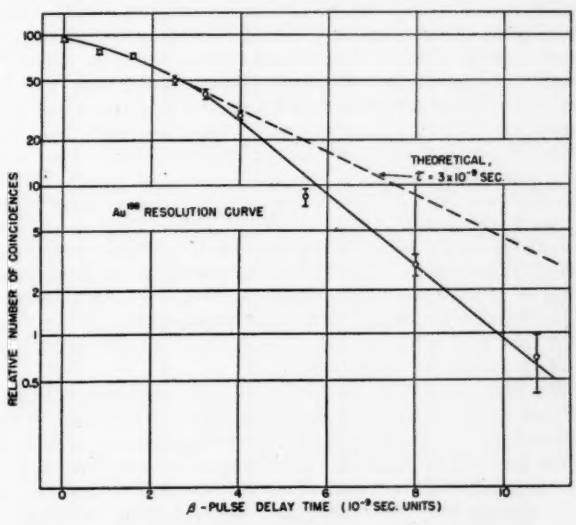

FIG. 2. β-pulse delay portion of Au^{198} resolution curve plotted on a logarithmic scale.

show that the apparatus is, in fact, capable of detecting delayed coincidences due to a finite lifetime. The shape of the resulting curve (not shown) was compatible with the 0.304-μsec. half-life[3] of ThC′.

In order to set an upper limit on the mean life τ of the 411-kev excited state of Hg^{198}, the β-pulse delay portion of the Au^{198} resolution curve has been plotted on a semilogarithmic scale in Fig. 2. The roughly exponential fall-off of the experimental curve is common to the results for Co^{60}, Cs^{134}, and Au^{198} and thus is instrumental. A dashed line in Fig. 2 indicates the shape the curve would have if the mean life of the Hg^{198} excited state were as long as 3×10^{-9} sec. Figure 2 demonstrates that the mean life τ of the 411-kev excited state of Hg^{198} is less than 3×10^{-9} sec.

An incidental result is that the excited states of Ni^{60} and Ba^{134} which are concerned in γ-γ-coincidences from Co^{60} and Cs^{134}, respectively, all have mean lives shorter than 3×10^{-9} sec.

MacIntyre's result for the mean life ($2.3\pm0.2\times10^{-8}$ sec.) can probably be explained by the fact that he compared β-γ-coincidences from Au^{198} with those from Na^{24}. The pulses from Na^{24} γ-rays (1.38 and 2.76 Mev) would be many times larger than those from Au^{198} γ-rays (0.411 Mev): in a coincidence system using amplifiers of finite rise time the result would be a greater lag in the detection of the Au^{198} γ-ray pulses and consequently an apparent finite lifetime of the Hg^{198} excited state.

* Visitor from McMaster University, Hamilton, Ontario.

[1] W. J. MacIntyre, Phys. Rev. **76**, 312 (1949).
[2] F. W. Van Name, Phys. Rev. **75**, 100 (1949).
[3] Bunyan, Lundby, and Walker, Proc. Phys. Soc. London **A62**, 253 (1949).

On the Spatial Alignment of Nuclei

R. V. POUND
Lyman Laboratory of Physics, Harvard University, Cambridge, Massachusetts
September 16, 1949

CONSIDERABLE interest centers on the problem of producing a system containing nuclei in a reasonably well-ordered state of alignment in space. Such a system makes possible studies of angular dependence of the scattering and absorption of polarized nucleons and of angular distributions in radioactive decay, relative to the spin axis of the nuclei.[1,2]

The most direct method of achieving a net alignment is to place the substance in a magnetic field H_0. If thermal equilibrium exists between the spin system and its surroundings, a Boltzmann distribution of the spins over the $2I+1$ equally spaced energy levels results, with the lowest level, corresponding to the spin nearly parallel or antiparallel to the field, becoming most heavily populated. Practical difficulties are presented by the fact that the nuclei must be put into an extremely strong field and at the same time must be in thermal contact with a paramagnetic substance in a weak field, because a reasonable degree of orientation is achieved only at the lowest temperatures so far attainable by adiabatic demagnetization, with the nuclei in the strongest field obtainable. A somewhat simpler method may be available for nuclei of paramagnetic ions, which may be oriented by the intense fields of the oriented ions themselves, at low enough temperatures.[3,4] In both cases the sample containing the nuclei must be kept in a field while the other experiments are performed lest random orientations be resumed.

The purpose of this note is to outline an experimentally less difficult method by which a partial alignment of nuclei might be achieved. It is known that the $2I+1$-fold degeneracy of a nucleus can be partially lifted through an interaction between the nuclear electric quadrupole moment and a crystalline electric field having axial symmetry.[5,6] The component m_I of angular momentum along the axis becomes a good quantum number, in the absence of a strong magnetic interaction, although levels differing only in sign of m_I are not separated. So far, because of difficulties attendant on finding suitable samples, only moderate quadrupole splittings have been found, such as the 720 kc/sec. in Al_2O_3.[6] On the other hand, it must be expected that very much larger splittings exist in, for instance, crystals composed of molecules having p-type covalent bonds.[7] One would expect, in fact, splittings of the order of hundreds or thousands of megacycles as in gaseous molecules[8] because the gradient of the electric field at the nucleus is determined by the other nuclei and the electrons of the molecule itself (in contrast to the situation in ionic crystals where the ion containing a nucleus is primarily in a singlet S state and probably contributes little to the gradient of the electric field at the nucleus).

A crystal having quadrupole splittings of this order of magnitude need only be brought into thermal equilibrium with a substance that has been adiabatically demagnetized to a temperature of a few hundredths of a degree and the nuclei will fall into the lowest energy levels. This would mean either the highest or lowest absolute values of the component of the nuclear spin along the major axis of the tensor grad $\mathbf{E}$ at the nucleus would predominate. Either case could be found depending upon the sign of the quadrupole coupling constant $eQ(\partial^2V/\partial z^2)$. Therefore, the nuclei would be aligned, respectively, either simultaneously almost parallel and antiparallel to this axis in the molecule, or precessing nearly in a plane perpendicular to this axis. If the molecules could be crystallized in such a way that this axis was alike for all, one achieves a certain kind of nuclear orientation. A fairly sizable single crystal or some technique of orienting small crystals would give the desired result if the crystal does not contain non-equivalent orientations of the molecules, with respect to the crystal axes.

Although the kind of alignment resulting is not as unambiguous as in the magnetic alignment, several advantages are apparent. In radioactive emission, anticipated angular distributions involve even powers of $\cos\theta$,[1] for which, if true, the ambiguity is not a disadvantage. The thermal contact with the paramagnetic substance may be easier to achieve because the nuclear sample can be put into the magnetic field while the paramagnetic magnetization and adiabatic demagnetization are performed. This is so because the magnetic splittings are only small perturbations on the electric ones. If the crystal containing the nuclear sample itself could be made also to contain the paramagnetic ions, the thermal contact could be very strong, and the paramagnetic ions, by their relaxation processes, could help to bring about thermal relaxation of the nuclear system. Once thermal equilibrium is established the sample may be completely removed from the magnetic field, simplifying some of the experiments on the aligned nuclei.

To find such a high frequency splitting and to demonstrate the temperature of the spin system, ordinary nuclear paramagnetic resonance experiments at moderate frequencies can be of assistance. With an odd half-integral spin, one could observe the resonance absorption in the transition between the still degenerate levels $m_I=\pm\frac{1}{2}$, when the degeneracy is removed by a magnetic field. If the axis of symmetry of the electric field lies along the magnetic field, one expects to find a resonance line at the frequency corresponding to the normal gyromagnetic ratio, but, if the quadrupole splitting is strong, the frequency would be very sensitive to a small angular displacement from this position. By a perturbation calculation, regarding the Zeeman energy as a small perturbation on the large quadrupole energy, one can find the amount of the quadrupole splitting.

If the intensity of the line is observed as the temperature is reduced to such a degree that $kT<h\nu$ where ν is the quadrupole splitting frequency, either of two things will occur, determined by the sign of the quadrupole coupling constant. If the $m_I=\pm\frac{1}{2}$ levels are the lowest, then the line would get more intense as $1/T$ until a critical temperature is reached where a fairly pronounced increase in intensity would accompany the preferential population of these states. If $m_I=\pm I$ are the lowest, the observed line would go through a maximum and then decrease as the $m_I=\pm\frac{1}{2}$ levels become depopulated.

Preliminary experimental work directed toward this end is underway. Details of the calculations of quadrupole interactions in fields of axial symmetry will be published elsewhere.

[1] J. A. Spiers, Nature **161**, 807 (1948).
[2] M. E. Rose, Phys. Rev. **75**, 213 (1948).
[3] C. J. Gorter, Physica **14**, 504 (1948).
[4] M. E. Rose, Phys. Rev. **75**, 213 (1948).
[5] R. V. Pound, Phys. Rev. **73**, 1247 (1948); **74**, 1203 (1948).
[6] R. V. Pound, Proc. Phys. Soc. **61**, 576 (1948).
[7] C. H. Townes, Phys. Rev. **71**, 909 (1947).
[8] Townes, Holden Bardeen, Merritt, Phys. Rev. **71**, 644 (1947); Townes, Merritt, and Wright, Phys. Rev. **73**, 1334 (1948); Gordy, Simmons, and Smith, Phys. Rev. **74**, 243 (1948).

Double-Probe Method for Determination of Electron Temperatures in Steady and Time-Varying Gas Discharges

E. O. JOHNSON AND L. MALTER
RCA Laboratories Division, Radio Corporation of America, Princeton, New Jersey

September 19, 1949

THE single-probe method of Langmuir and Mott-Smith[1] is not well suited for measurements in time-varying discharges and in particular not in decaying plasmas following the interruption of a discharge. In the latter case this follows from the fact that efforts to operate the probe above plasma potential are defeated by the fact that the plasma potential constantly recedes so as to maintain itself positive with respect to the probe. The use of two probes connected in a floating circuit overcomes the difficulties of the single-probe method and permits the determination of such quantities as electron temperature and density in both steady and time-varying discharges. Dow[2] has described a double-probe method for determining the electron temperature in the ionosphere. He appears to do this from values of i_e very close to the regions of VD_1 or VD_2 only (see Fig. 1). In these regions, the method appears to be less accurate and uses data which are generally discarded in the method here described.

Two probes are connected together through a resistor and a variable potential source V_B. The entire measuring system is permitted to float. By means of a scope across the resistor, the instantaneous current I_D can be determined. In practice one varies V_B and determines I_D and V_D, the potential difference between the probes.

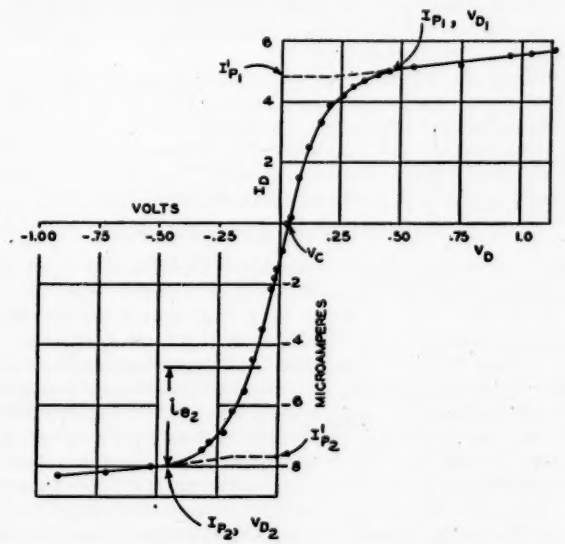

FIG. 1. Current *vs.* voltage characteristic of floating double-probe system immersed in plasma.

A typical plot is shown in Fig. 1. These data were obtained in an argon-filled hot-cathode diode, 100 μsec. following the interruption of a discharge.

From the equality of the total electron and ion currents to the probes, it follows that:

$$\left(\frac{I_{p1}+I_{p2}}{ie_2}-1\right)=k\exp[-11{,}600(V_d/T_e)]=\Gamma, \tag{1}$$

where

$$k=(A_1/A_2)(j_{01}/j_{02})\exp[+11{,}600(V_c/T_e)]. \tag{2}$$

A_1 and A_2 are the areas of probes 1 and 2. j_{01} and j_{02} are the random electron current densities at probes 1 and 2. ie_2, the electron current to probe No. 2, is equal to the difference between I_d and I_{p2}. The other symbols are defined in Fig. 1. The slope of log Γ *vs.* V_d yields T_e. Figure 2 is a plot of (1) for the data of Fig. 1. For this case, $T_e=1065°$K. The linear regions beyond I_{p1} and I_{p2} in Fig. 1 correspond to saturated ion current only, to one probe or the other. Since the current to one of the probes in these regions is purely ionic, the current flow is generally determined by space charge and not by orbital-limited-current relations.[1]

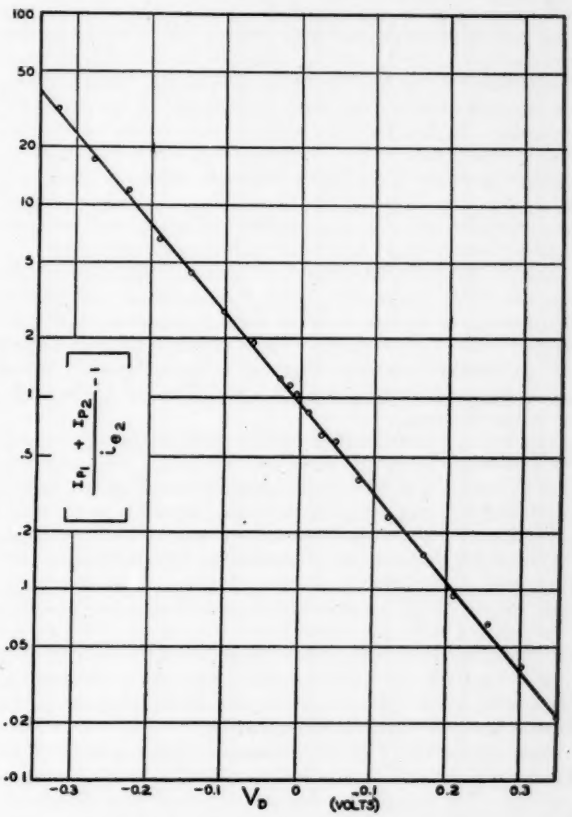

FIG. 2. Logarithmic plot for determination of electron temperature.

A more rapid determination of T_e can be obtained from Fig. 1, and the relation

$$T_e=11{,}600G(1-G)(dV_d/dI_d)_{V_d=0}(I_{p1}+I_{p2}), \tag{3}$$

where

$$G=\frac{[ie_2]_{V_D=0}}{I_{p1}+I_{p2}}. \tag{4}$$

If the slope of the regions of positive ion saturation is considerable, then in place of I_{p1} and I_{p2} one uses quantities obtained as follows: Extend the positive ion saturation curves linearly as shown in Fig. 2 and use for I_{p1} and I_{p2}, the ordinates at points $\frac{2}{3}$ of

the horizontal distance between the points of saturation (V_{D1} and V_{D2}) and the wall potential condition ($V_D = V_c$). These points are designated as I'_{p1} and I'_{p2} in Fig. 2. For the case of Fig. 2 this short method yields $T_e = 1025°K$.

[1] I. Langmuir and H. M. Mott-Smith, Gen. Elec. Rev. **27**, 449 (1924).
[2] W. G. Dow, Phys. Rev. **76**, 453 (1949).

Tests of Self-Regenerating Fillings for Geiger Counters

S. A. KORFF AND A. D. KRUMBEIN
New York University, New York, New York
September 12, 1949

ONE of the serious difficulties which faces the users of Geiger counters of the self-quenching types, is that the operating conditions change with time. This effect is due to the progressive decomposition of the quenching vapor. In the end enough vapor is decomposed so that the counter becomes useless. Unfortunately, this decomposition is a necessary concomitant of the quenching mechanism.[1] It has therefore seemed worth while to examine possible vapors with a view to seeking any which might show a synthesis as well as a decomposition in the discharge. Since it is well known that ammonia can be made by the Haber process, and since this gas will also produce self-quenching action in counters, some counters were filled with this gas and tested.

Some of these counters have now been in continuous use for over two years, operating, except for occasional unavoidable interruptions, at as high counting rates as possible. They have recorded some 3×10^{10} counts. These results appear consistent with the original hypothesis that the ammonia molecule is not only decomposed in quenching but is resynthesized in the active part of the discharge.

Counters were tested which were one cm in radius, 8 cm long, with 4 mil tungsten central wires, and filled to a total pressure of about 15 cm Hg with 80 percent ammonia and 20 percent argon. Another set with only ammonia (no argon) was also run. Cathodes of evaporated silver, evaporated copper, solid copper, aquadag, and nickel were tried. Counters containing 10 cm ammonia only operated at around 1200 volts with plateaus of some 100 to 125 volts, i.e., operating characteristics were comparable to those usually found with the conventional argon-alcohol fillings, although the latter sometimes have longer plateaus. At pressures of 5 cm of ammonia, the operating voltages are 850 to 900 and the plateaus 50 to 75 volts in length. Adding argon gives shorter plateaus but lower starting potentials.

These counters exhibited two interesting characteristics. First, the counters seem to show an increase in background during a long run. This background may be due to a large number of spurious counts. In some cases the background increases very much. However, if the counter is allowed to "rest" for a while, the background returns to normal. This effect has been noted also by Simpson.[2] Of the counters tested, those with aquadag cathodes recovered the fastest.

The second characteristic of these counters was an increase in photo-sensitivity. The counter with the aquadag cathode became photo-sensitive after some 3×10^8 counts, the one with solid copper cathode after 1.5×10^8 and that with nickel after 10^9 counts. The photo-sensitivity remained after "rest" periods. In one case, to see whether this sensitivity would decrease with time, a counter was taken out of the run; it is still photo-sensitive after ten months "rest." This photo-sensitivity extends to yellow and in two cases to red light.

The experiments are being continued and will be reported in detail at a later date.

[1] S. A. Korff and R. D. Present, Phys. Rev. **65**, 274 (1944); W. Spatz, Phys. Rev. **64**, 236 (1943).
[2] J. A. Simpson (private communication).

Reproducibility of Photo-Neutron Standards

L. F. CURTISS AND A. CARSON
National Bureau of Standards, Washington, D. C.
September 19, 1949

THE construction of two nearly identical radium beryllium photo-neutron standards has given us an opportunity to ascertain the degree of reproducibility which can be expected in making standards of this type. These standards were constructed following the suggestion of Gammertsfelder and Goldhaber[1] by enclosing a capsule of compressed radium containing approximately 1 gram of radium in the center of a beryllium sphere 4.00 cm in diameter. Each of the two spheres was turned and the two halves threaded to have the same dimensions to within ±0.0001 inch. The radium was enclosed in a sealed capsule of platinum-iridium having walls 0.2 mm thick. The external dimensions of the capsules, which were right cylinders, are 0.84 cm in diameter and 0.86 cm in height. The capsules were mounted in the geometrical center of the sphere in cavities machined just large enough to accept them, as shown in Fig. 1. These standards are prepared for

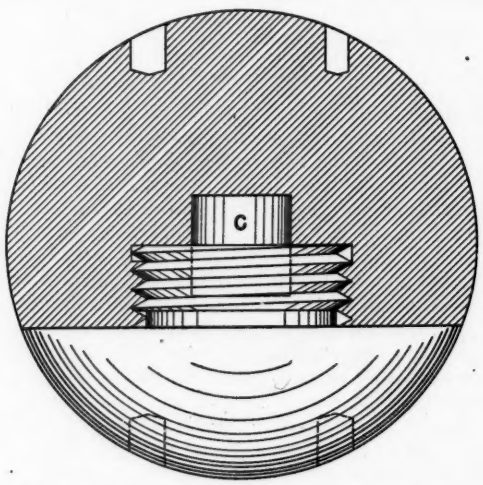

FIG. 1. Primary photo-neutron standard consisting of a 4-cm diameter beryllium sphere with 1-gram capsule of radium (*C*) at the center.

the purpose of serving as a national primary standard for measurement of sources of neutrons. They were made in duplicate so that one may be retained at the National Bureau of Standards as a reference source and the other loaned for comparison measurements when this seems desirable.

Although the radium capsules were made as nearly identical as possible it was found that from measurement of the external gamma-radiation the amount of radium contained in each after completion was not quite the same. In each case the radium salt had been compressed to maximum density. The ratio of the radium contents for standard I to standard II was found to be

$$I_\gamma/II_\gamma = 0.9897 \text{ with std. dev.} = 0.052 \text{ percent.}$$

After assembly in the beryllium spheres the ratio of the neutron intensity emitted by these sources was determined. These measurements were made by means of a long counter made in accordance with the procedure described by Hanson and McKibben.[2] The counter tube was filled with B^{10} enriched BF_3. For each measurement the standard was mounted on a base provided with pins which fitted into small holes in the beryllium sphere. This base was mounted at a fixed position on the axis of the neutron counter at a distance of approximately 21 cm. Therefore, it was comparatively easy to interchange the two standards for observations and have them at the same distance from the detector. The support was arranged so that the sources could be rotated about their vertical axes and measurements were repeated for each 90° of rotation to correct for any lack of symmetry. The

statistics of the counting yielded a standard deviation of 0.073 percent. The ratio of the neutron intensities determined in this way came out

$$I_N/II_N=0.9871.$$

The variation with rotation amounted to 0.17 percent.

The number of neutrons emitted from these spheres should also be proportional to the mass of beryllium present. Although these spheres were machined to be as nearly identical as possible a small difference in weight was found. The ratio of masses is given by

$$I_M/II_M=0.9968.$$

We may now correct the observed ratio of neutron intensities for the differences in the radium and beryllium in the two sources. We obtain

$$\left(\frac{I_N}{II_N}\right)_{corr}=0.9871\times\frac{1}{0.9897}\times\frac{1}{0.9968}=1.0006.$$

This indicates that this type of source is reproducible with an accuracy depending on the precision with which the radium and beryllium in it can be measured.

Recently, Bretscher, Cook, Morton, and Wilkinson[3] have prepared radium beryllium fluoride ($RaBeF_4$) as a reproducible source of neutrons suitable as standards. They show that the rate of neutron emission from this compound is proportional to the radium present within ± 0.5 percent. The chemical preparation of this compound must be carefully controlled to secure uniform results. Also, since this compound is an α, n source, there will be a growth of neutron activity corresponding to the growth of polonium in the source, which at equilibrium amounts to approximately 9 percent. These authors state that this compound yields 3.15×10^6 neutrons per sec. per gram of radium in the compound. Preliminary measurements show that our standards yield approximately 1.1×10^6 neutrons per second per gram of radium. Therefore, the photo-neutron standards described above have about 1/3 the efficiency and roughly 3 times the diameter of a comparable $RaBeF_4$ standard. These disadvantages are comsated for, to a large extent, by the simplicity of the preparation, the accuracy with which they can be reproduced, and the elimination of the effect of the growth of polonium. Furthermore, the radium can be removed from the photo-neutron sources in its original condition if at any time the source is to be discarded. A chemical separation is required to remove the radium from the $RaBeF_4$ sources.

[1] G. R. Gammertsfelder and M. Goldhaber, Phys. Rev. **69**, 369 (1946).
[2] A. O. Hanson and J. L. McKibben, Phys. Rev. **72**, 673 (1947).
[3] Bretscher, Cook, Morton, and Wilkinson, Proc. Roy. Soc. **196A**, 436 (1949).

Reflection and Polarization of Neutrons by Magnetized Mirrors

D. J. Hughes* and M. T. Burgy
Argonne National Laboratory, Chicago, Illinois
September 19, 1949

We have recently been studying the refraction of neutrons in magnetic materials by means of critical reflection from ferromagnetic mirrors. The original purpose of the experiments was to demonstrate the existence of two indices of refraction in iron[1-3] and to investigate the feasibility of production of polarized neutrons by reflection from magnetized iron. Since the work was begun, two valuable applications of the method have been suggested. Halpern[4] has pointed out that the critical angle observed with the mirror magnetized in the direction of neutron propagation is quite sensitive to the assumed form of the neutron-electron magnetic interaction and can be used to decide the correct form. Hamermesh[5] has suggested that completely polarized neutrons might be obtained by reflection from magnetized cobalt without the necessity of monochromatization because only one spin state will reflect regardless of neutron wave-length. Both suggestions have been followed successfully with results which are here reported briefly.

Neutrons from the thermal column of the Argonne heavy water pile were filtered through BeO and collimated by means of 0.1-in. slits 10 feet apart. The BeO filter transmits only those neutrons of the Maxwell distribution with $\lambda>4.4$A hence there is a sharp drop in the intensity reflected from a mirror when the critical angle θ_c for 4.4A is exceeded. As the mirror angle, θ, increases up to θ_c all incident wave-lengths are reflected and the intensity increases linearly with θ (because of the increasing number of neutrons intercepted by the mirror). Above θ_c the intensity drops off as $1/\theta^3$ because of the shape of the Maxwell distribution. Thus a single index is expected to give an intensity shown by the line marked "Bloch" in Fig. 1 while two indices (each operative for half the incident neutrons) would give the lower curve. As Halpern[4] has suggested, the dipole-dipole interaction used by Bloch[6] leads to the one index curve (with $\theta_c=23.8'$), while the Dirac interaction used by Schwinger[7] and by Halpern and Johnson[8] leads to the two index curve ($\theta_c=14.2'$ and $30.7'$). The curves of Fig. 1 are those calculated for the two interactions including slight corrections for the resolution of the apparatus and the finite reflectivity for angles just above critical. The experimental intensity points agree well with the two index curve and verify the correctness of the Dirac interaction. There is of course the possibility of short range forces which would give rise to angular distributions other than that of the Dirac interaction; it can only be said that their effect in the present experiment is much less than the normal magnetic scattering.[9]

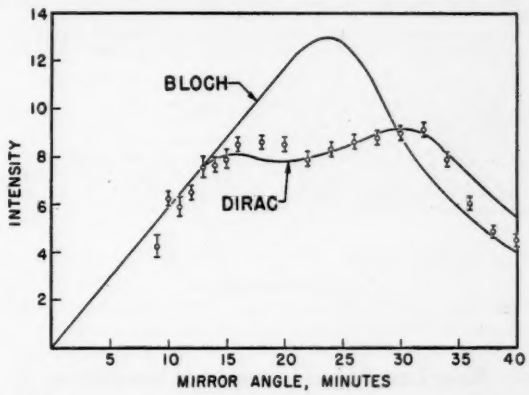

Fig. 1. Intensity of neutrons reflected from a ferromagnetic mirror.

The polarization of neutrons reflected from a mirror is measured by reflection from a second mirror. Ideally, a polarized beam will show complete reflection at a second mirror magnetized in the same direction as the first mirror, but zero reflection at a mirror magnetized in the reverse direction. This "double reflection" effect is completely analogous to the "double transmission" effect used to measure the polarization of neutrons produced by transmission. Actually, as for double transmission, it is extremely difficult to prevent depolarization and reorientation of the neutron spins in the stray fields between polarizer and analyzer. It is much simpler to keep both mirrors magnetized parallel and to measure the change in intensity resulting from depolarization of the beam between the mirrors. The depolarization is easily produced by insertion of a thin piece of unmagnetized iron in the beam, and the changes in intensity are just half those expected in the double reflection method, complete polarization being identified by a drop of one-half in intensity. This depolarization method of analysis was used in the production of polarized neutrons with cobalt mirrors. The cobalt mirrors (5 in.$\times$10 in.) were

produced by electroplating under the direction of H. Ross of the Argonne Shop. The first attempts resulted only in about 50 percent polarization but use of longer neutron wave-lengths (to reduce the possibility of non-adiabatic transitions) and of higher magnetizing currents, made complete polarization (within statistical accuracy of about 1 percent) attainable. Two distinct advantages of the reflection method of polarization are (1) no intensity loss occurs as in the transmission method, and (2) polarization of long wave-length neutrons is possible, unlike the transmission method which is applicable only for $\lambda<4.04$A (because iron becomes "transparent" to neutrons of longer wave-length).

The details of these and other mirror experiments will appear in a report now in preparation. Plans for the application of the mirror technique to other nuclear properties, such as the coherent hydrogen scattering amplitude are now being made. We wish to thank Dr. M. Hamermesh for his extremely helpful discussions during these experiments.

* Now at Brookhaven National Laboratory, Upton, Long Island, New York.

[1] Halpern, Hamermesh, and Johnson, Phys. Rev. **59**, 981 (1941).
[2] A. Achieser and J. Pomeranchuk, J. Exper. Theor. Phys. USSR **18**, 475 (1948).
[3] Hughes, Burgy, Heller, and Wallace, Phys. Rev. **75**, 565 (1949).
[4] O. Halpern, Phys. Rev. **75**, 343 (1949).
[5] M. Hamermesh, Phys. Rev. **75**, 1766 (1949).
[6] F. Bloch, Phys. Rev. **50**, 259 (1936).
[7] J. Schwinger, Phys. Rev. **51**, 544 (1937).
[8] O. Halpern and M. H. Johnson, Phys. Rev. **55**, 898 (1939).
[9] A recent paper by H. Ekstein (Phys. Rev. **76**, 1328 (1949)) summarizes the question of the neutron-electron magnetic interaction and its relation to experimental verification.

New Low Mass Isotopes of Emanation (Element 86)

A. Ghiorso, W. W. Meinke, and G. T. Seaborg
Department of Chemistry and Radiation Laboratory, University of California, Berkeley, California
September 12, 1949

AMONG the spallation products obtained from the 350-Mev proton bombardment of Th^{232} we have identified two gaseous alpha-emitters which apparently do not decay into any presently known alpha-decay chains. The half-lives observed for the decay of the alpha-activities are 23 minutes and 2.1 hours. These half-lives may be principally determined by an unknown amount of orbital electron capture. At least one alpha-emitting daughter (about 4 hours half-life) has been observed to grow from a gaseous parent, but it has not been determined whether it arises from alpha-decay or electron-capture.

Since these gaseous atoms emit alpha-particles it is assumed that they are isotopes of element 86 (emanation or radon) rather than a lighter rare gas. If they were heavy isotopes such as Em^{221} or Em^{223}, both unknown, they would decay into known alpha-decay series, the neptunium and actinium series, respectively, and so would grow known short-lived alpha-emitters which would have been detected. It thus appears reasonable that they must be lighter than the known emanation isotopes.

The lightest isotope of emanation observed prior to these experiments was Em^{216}, which arises from the U^{228} alpha-decay series[1] and which should have a half-life of approximately 10 microseconds as predicted by means of the new alpha-decay systematics.[2,3] The reappearance of longer half-lives, such as 23 minutes and 2.1 hours, with lower mass numbers is apparently due to the stable configuration of 126 neutrons. Thus these activities are to be assigned to the mass numbers 212 and lower (that is, Em^{212} and $Em^{<212}$). Therefore it appears that the plot of alpha-energy *versus* mass number for the isotopes of emanation goes through the same type of maximum and minimum as is observed for bismuth, polonium, and astatine.[2]

The method used to measure the emanation alpha-activities was very simple but designed to separate the emanation from tremendous amounts of other alpha-emitters, from bismuth to protactinium. The cyclotron target consisted of thin thorium metal strips sandwiched with thin aluminum foils to act as catchers for the transmuted atoms which were able to recoil out of the surface of the thorium. These aluminum foils were then heated at a very low temperature in a vacuum system. A slow stream of argon "carried" the emanation through two cold traps at -50°C and into a final trap at -90°C where the emanation should freeze out. From this storage trap it was possible to fill a cylindrical ion chamber in which alpha-pulses could be detected. In order to prove that a gas was involved it was shown that the activity could be quantitatively transferred back and forth many times by varying the temperature of the cold trap. After an emanation sample had been allowed to decay for some hours the gas was thoroughly pumped out of the chamber and the alpha-activity left behind (presumably due to the daughters) was followed for decay. It was not possible to measure alpha-energies in these first experiments and Geiger counter measurements were clouded by the probability of xenon and krypton fission product contaminants from which no careful separation had been made.

New equipment is now being built with which it should be possible to measure alpha-energies for these emanation isotopes and their daughters and to determine the proper mass assignments.

We wish to thank James Vale and the crew of the 184-inch cyclotron for their assistance in carrying out this work.

This work was performed under the auspices of the U. S. AEC.

[1] Meinke, Ghiorso, and Seaborg, Phys. Rev. **75**, 314 (1949).
[2] Perlman, Ghiorso, and Seaborg, Phys. Rev. **74**, 1730 (1948).
[3] Perlman, Ghiorso, and Seaborg, Phys. Rev. **75**, 1096 (1949).

Magnetic Moment of La^{139} *

W. C. Dickinson
Research Laboratory of Electronics, Massachusetts Institute of Technology, Cambridge, Massachusetts
September 12, 1949

THE ratio of the frequency of the nuclear magnetic resonance of La^{139} to that of the proton has been measured at 6700 gauss. Both resonances were observed in a single sample consisting of an aqueous solution of lanthanum chloride. A double-bridge magnetic resonance absorption method, similar to that used for the recent measurement of the Be^9-H^1 frequency ratio,[1] was employed so that further detail is not necessary here. However in this measurement, although the two frequencies correspond very closely to a 7:1 ratio as in the Be^9-H^1 measurement, advantage was not taken of the increased precision in frequency ratio measurement made possible by heterodyning the seventh harmonic of the one frequency with the fundamental of the other. For Be^9 the observed line width was $\sim\frac{1}{2}$ gauss and since it was possible to determine the center of this line to within 0.1 gauss in a field of 7000 gauss, a frequency ratio precision of at least 1 part in 70,000 could be utilized. However, the observed line width for La^{139} was $\sim$3 gauss and since the true line center could be determined only to within $\frac{1}{2}$ gauss at best, the precision given by a Zenith BC-221-T frequency meter was sufficient.

A total of six determinations was made. From these the following value for the ratio of the resonant frequencies in the same magnetic field was obtained:

$$\frac{\nu(La^{139})}{\nu(H^1)}=0.141251\pm0.000014.$$

The uncertainty given represents limit of error; all six values fall within the above limits. This result is in agreement with that of Chambers and Williams.[2]

The magnetic moment of La^{139} in units of the magnetic moment of the proton is hence:

$$\frac{\mu(La^{139})}{\mu(H^1)}=0.98876\pm0.00010.$$

This expression is uncorrected for the slight diamagnetic field at the nucleus of the La^{139} due to the Larmor precession of its atomic electrons in the applied field. The best value for this correction can be obtained by using a Hartree atom model calculation for Cs and making a short extrapolation. This gives $(\Delta H/H)La = 0.60$ percent.

The broadness of the La^{139} resonance line may be ascribed to a nuclear quadrupole moment Q which, however, has never been measured. Similar broad lines have been observed for I^{127} and Cs^{133},[3] and also the two Br isotopes,[4] all of which are known to have quadrupole moments.

* This work has been supported in part by the Signal Corps, the Air Materiel Command, and the ONR.

[1] W. C. Dickinson and T. F. Wimett, Phys. Rev. **75**, 1769 (1949).
[2] W. H. Chambers and D. Williams, Phys. Rev. **76**, 461 (1949).
[3] F. Bitter, private communication.
[4] R. V. Pound, Phys. Rev. **72**, 1273 (1947).

Nuclear Quadrupole Moments and Nuclear Shell Structure

C. H. Townes
Brookhaven National Laboratory, Upton, New York*
AND
H. M. Foley and W. Low**
Physics Department, Columbia University, New York, New York
September 23, 1949

CONSIDERABLY before the recent revival of interest in nuclear shell structure, Schmidt[1] had found a systematic variation with Z of the deviation of nuclear charge distributions from a sphere (which he derived from nuclear quadrupole moments) and pointed out minima of the magnitudes of nuclear quadrupole moments near the "magic numbers" $Z=50$ and 82. Schmidt's plot has been extended with more recent data[2,3] and quadrupole moments correlated to some extent with nuclear shell structure.[3,4]

The following simple model, based on nuclear shell considerations, leads to the proper behavior of known nuclear quadrupole moments, although predictions of the magnitudes of some quadrupole moments are seriously in error.

1. Neutrons and protons fit into single particle levels in a scheme similar to those proposed for correlating spins, thus producing what may be called proton and neutron shells.

2. Proton and neutron shells tend to be oriented or polarized to allow maximum overlap between proton and neutron distributions.

This model leads to the conclusions:

A. For an odd-proton nucleus, the quadrupole moment is primarily dependent on the number of protons P and can be written $Q_{p\text{odd}}=Q_p(P)$, where Q_p is always positive immediately before, and always negative immediately after a shell is filled.

B. For an odd-neutron nucleus, the magnitude of the quadrupole moment depends on the number of protons, but its sign is determined by the number of neutrons N, being given by $[Q_p(N)]/[|Q_n(N)|]$. $Q_n(N)$ is the electric quadrupole moment which would be produced by the neutrons if they were charged, and Q_n is very nearly the same function as Q_p.

C. For odd-odd nuclei, estimation of quadrupole moments is more complex and depends on the way in which the mechanical moments of the odd neutron and odd proton add. If these moments are essentially parallel, the quadrupole moment should be of the same sign and approximately the same magnitude as for a similar odd-proton nucleus, if the neutron and proton mechanical moments are not essentially parallel, the quadrupole moment magnitude should be considerably reduced.

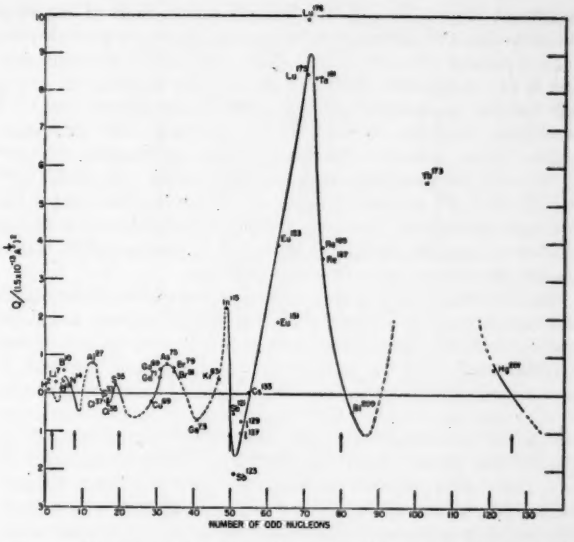

FIG. 1. Nuclear quadrupole moments divided by the square of the nuclear radius $(1.5\times10^{-13}A^{\frac{1}{3}})^2$. Known moments of odd-proton nuclei and odd-proton odd-neutron nuclei (excepting Li^6 and Cl^{36}) are plotted as circles against number of protons, moments of odd-neutron nuclei as crosses against number of neutrons. Arrows indicate closing of major nucleon shells. Solid curve represents regions where quadrupole moment behavior seems established, dashed curve more doubtful regions.

Known quadrupole moments appear to fit these expectations. Figure 1 shows nuclear quadrupole moments[5] as a function of number of nucleons.

The sign of Q near the closing of major shells is that expected in all cases except for Li^7. In view of uncertainties in the charge distributions in the molecules from which Q for Li^7 was derived, perhaps present indications that Q is positive should not be regarded as conclusive. The negative quadrupole moment of S^{33} and the reversal of sign to a positive moment for S^{35} is a striking illustration of the above rules since S^{35} has 19 neutrons, or one less than the filled shell of 20. This model would similarly predict that the quadrupole moments of K^{39} and K^{41} are positive, that of Sc^{45} and Zr^{91} negative.

Se^{77} seems from microwave measurements to have a quadrupole moment less than 0.001×10^{-24} cm^2, yet atomic spectra indicate a spin for this nucleus greater than 3/2. Both experiments may be correct, and the Se^{77} moment very small because of the spherical distribution of protons in this nucleus due to completion of the $4f$ sub-shell. Ca^{43} is a similar case which should have a complete proton shell and small quadrupole moment.

The negative quadrupole moment of Ge^{73} with 41 neutrons suggests that a completed sub-shell occurs at 40 neutrons (pointed out as a possibility by Nordheim) corresponding to filling the $3p$ levels in Nordheim's and Mayer's schemes.[6] If the neutron and proton shells fill in the same manner, the Cb^{93} quadrupole moment should also be negative and the Zr^{91} quadrupole moment small.

The odd-odd nuclei with known quadrupole moments consist of Li^6, B^{10}, N^{14}, Cl^{36}, and Lu^{176}. Their moments correspond to expectations from the model described above, and those cases for which the moments of neutron and proton shells are parallel (B^{10}, N^{14}, Lu^{176}) are plotted in Fig. 1.

Gordy's statement[3] that completion of a neutron shell tends to make quadrupole moments more negative does not follow from the above considerations. This is perhaps not serious because the evidence for this empirical observation is questionable. A number of quadrupole moments plotted by Gordy are values he predicts on the basis of an empirical relation between nuclear electric quadrupole moments and magnetic dipole moments. The most

significant applications of this relation are to cases of nuclei of the same spin and differing by two protons. In the only two known nuclear pairs of this type ($Cu^{65}-Ga^{69}$, $Ga^{71}-As^{75}$), Gordy's relation is in considerable error and in one case it gives the wrong sign for the quadrupole moment. Gordy has plotted the Cs^{133} quadrupole moment as $+0.3\times10^{-24}$ cm² and from this value derived other moments. However, known information on Cs^{133} allows only the conclusion that for this nucleus $|Q|\leq0.3\times10^{-24}$ cm². If the Cs^{133} moment is taken as zero or negative and if the predicted quadrupole moments are questioned, then no evidence appears to remain that completion of a neutron shell makes nuclear quadrupole moments more negative.

For the nuclei which contain closed proton shells plus or minus only one proton, the nuclear shell model gives not only a definite prediction of the sign of Q, but also, if the state of the odd proton is determined from the nuclear spin and magnetic moment, it gives a fairly definite value for the quadrupole moment magnitude. In the cases Li^7, N^{14}, and Bi^{209}, the calculated magnitudes are in substantial agreement with those observed. This model also gives roughly the proper ratios between the quadrupole moments of In^{113}, In^{115}, Sb^{121}, and Sb^{123} (protons differing by one from a closed shell of 50). However, in spite of the rather extensive success of this model, it appears difficult to reconcile the magnitudes of the In^{113}, In^{115}, and Sb^{123} quadrupole moments with a nuclear shell model including a closed shell at 50 nucleons. They are larger by a factor of four than can reasonably be produced by a single particle. In addition the very large quadrupole moments in the vicinity of $Z=71$ present difficulties to a nuclear shell model. To give Lu^{176} its quadrupole moment of 7×10^{-24} cm², approximately 35 protons in the most favorable orbits must contribute to Q. Since the first fifty protons are presumably in a closed shell and contribute nothing to Q, only 21 protons are available and even all of them could hardly be put in the few orbits which contribute most to a positive quadrupole moment.

Failure of the nuclear shell model to give correct quadrupole moments is in contrast to the situation with nuclear magnetic moments, which can all be accounted for by a suitable admixture of states of a single nucleon. In the shell model approximation, these large quadrupole moments must represent a considerable contribution from the protons in the closed shells. The polarization of this core would presumably require a sharing of angular momentum between the protons of the incomplete shell and those of the closed shells. The magnitude of the polarization, however, and the resulting large asymmetry of the nucleon distribution is hardly consistent with the single particle-central field quantization which is the basis of the shell structure model.

* Permanent Address: Columbia University, New York, New York.
** This author's work supported jointly by the Signal Corps and ONR.
[1] T. Schmidt, Naturwiss. 28, 565 (1940).
[2] J. Mattauch and S. Flügge, *Nuclear Physics Tables and An Introduction to Nuclear Physics* (Interscience Publishers, Inc., New York, 1946).
[3] W. Gordy, Phys. Rev. 76, 139 (1949).
[4] E. Feenberg and K. C. Hammack, Phys. Rev. 75, 1877 (1949); R. D. Hill, Phys. Rev. 76, 998 (1949).
[5] Data taken from table of nuclear moments by H. L. Poss (Brookhaven National Laboratory Report to be published).
[6] Feenberg, Hammack, and Nordheim, Phys. Rev. 75, 1968 (1949).

The Sm^{151} Beta-Ray Spectrum*

B. H. Ketelle and G. W. Parker
Oak Ridge National Laboratory, Oak Ridge, Tennessee
September 6, 1949

A LONG-LIVED samarium beta-emitter was first identified in mass spectrographic studies of R. J. Hayden and L. G. Lewis.[1] The half-life has been given recently by M. G. Inghram[2] to be about 200 years and independently by J. A. Marinsky[3] to be 1000±350 years. G. W. Parker and P. M. Lantz[4] have prepared sources of the activity and characterized its radiation by means of aluminum absorption curves. They report that maximum beta-energy to be approximately 65 kev.

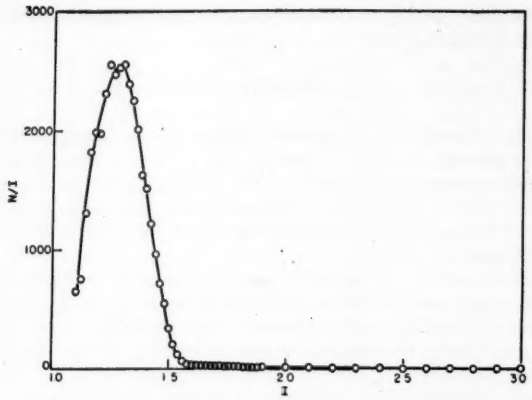

FIG. 1. Distribution of beta-rays of Sm^{151}. The counting rate per unit momentum is plotted against the coil current in amperes.

The source material used in this study was fission product samarium. Its chemical separation from the other fission products has been described elsehwere[4] in detail. The method consists of a gross separation of the fission products on an Amberlite IR-1 ion exchange column. This column effectively separates the trivalent cations from other cationic and anionic fission products and also separates the yttrium and cerium quite well from the other rare earths. After an intermediate separation of the cerium earths the fraction of eluate recognized by its gamma-activity to contain europium also contains the samarium and some element 61. Since the concentrations of other rare earth activities relative to the europium and samarium had been reduced, it was possible to achieve good separation of samarium from europium and element 61 by a final ion exchange column separation using optimum conditions for elution. The purified samarium was converted to the chloride and the aqueous solution was evaporated on a 50

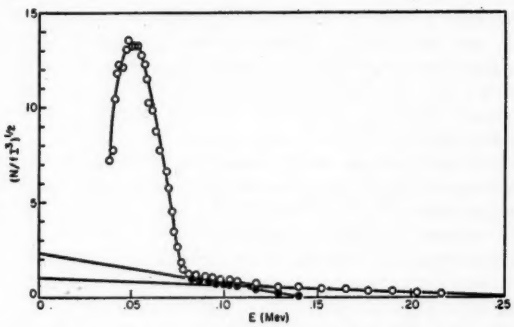

FIG. 2. Kurie plot of Sm^{151} source which contained Eu impurity.

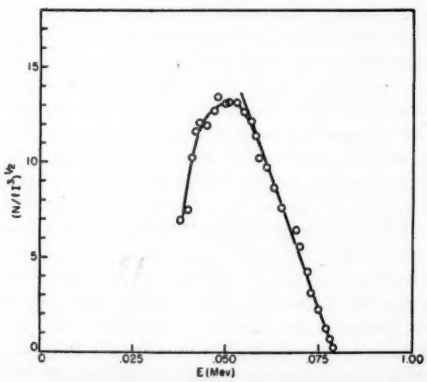

FIG. 3. Kurie plot of Sm^{151}.

$\mu g/cm^2$ laminated Formvar-polystyrene film. The source material itself was approximately 1 mg/cm^2 thick.

The beta-ray distribution curve shown in Fig. 1 was obtained on a thin lens beta-ray spectrometer similar to that described by Deutsch *et al.*[5] The counter tube window was 2 mg/cm^2-thick and no window corrections have been made. The Kurie plot of the data is shown in Fig. 2. There appear to be two higher energy components which are attributed to a small amount of Eu^{155} activity which was known to be present in the source. Figure 3 shows the Kurie plot of the samarium activity after the higher energy components have been subtracted. The beta-ray end point is 79 kev. Several determinations of the distribution give end-point energies which agree within three kilivolts of this value.

Because of the source thickness and the window cut-off an analysis of the shape of the spectrum would be meaningless and has not been attempted.

* This document is based on work performed under Contract Number W-7405 eng 26 for the AEP at Oak Ridge National Laboratory.

[1] R. J. Hayden and L. G. Lewis, Phys. Rev. **70**, 111 (1946).
[2] M. G. Inghram (private communication).
[3] J. A. Marinsky (private communication).
[4] G. W. Parker and P. M. Latz, AECD–2160.
[5] Deutsch, Elliott, and Evans, Rev. Sci. Inst. **15**, 178 (1944).

Hyperfine Structure and Nuclear Spin of Kr^{83} and Ne^{21} Investigated with Separated Isotopes

JØRGEN KOCH
Institute of Theoretical Physics, University of Copenhagen, Copenhagen, Denmark
AND
EBBE RASMUSSEN
Department of Physics, Royal Veterinary and Agricultural College, Copenhagen, Denmark
September 22, 1949

HIGHLY enriched samples of Kr^{83} and Ne^{21} have been prepared with a mass spectrograph[1] by collecting the ions of the separated isotopes in aluminum plates as previously described.[2] These plates were mounted as electrodes in Geissler tubes (volume ~30 cc) filled with helium at a pressure of 5–10 mm in order to obtain the most favorable conditions for exciting the small amounts of isotopes to be investigated.[3] The isotopes were released from the electrodes by h.f. induction heating. When cooled with liquid air the tubes yielded intense Kr- and Ne-spectra without any impurities.

In earlier investigations of the spectrum of normal krypton, the nuclear spin of the only odd isotope Kr^{83} (11.53 percent) has been determined to be 9/2 with high probability.[4,5] However, due to the predominance of the even isotopes, certain h.f.s. components were masked, and it therefore seemed desirable to check the spin value from the interval rule by means of enriched Kr^{83}.

By using a tube containing about 2 μ moles of Kr^{83} (separated in a four-hour run), interferograms were photographed with a Fabry-Perot etalon showing the structures of the $1s-2p$ combinations in the infra-red. Measurements of the components of 8059A ($1s_3-2p_4$), from which the spin can be most simply deduced because of the spherical symmetry of the only splitting upper term $2p_4$, at first turned out to be in disagreement with the spin value 9/2, which should give rise to a h.f.s. pattern as shown in Fig. 1. This disagreement was later found to be caused by the presence of about one percent Kr^{82}, probably brought into the beam of mass 83 by the formation of $(Kr^{82}H)^+$ ions,[6] which brings about a slight displacement of the component b toward a.

The intervals x and y can, however, be indirectly determined by measuring the total splitting $x+y$, and by using the fact that the center of gravity must be located at a point Z in a distance y from a. This fact follows simply from interval and intensity rules. The center of gravity Z again coincides with the position of the line from the even isotopes, if no isotope shift exists.

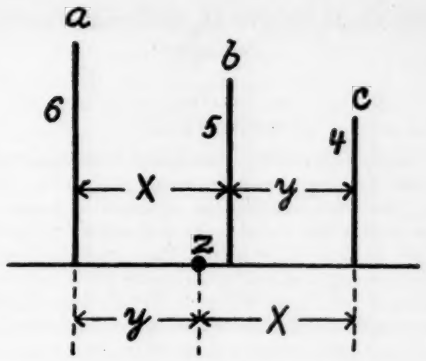

FIG. 1. Hyperfine structure of the Kr^{83} line 8059A.

In order to examine this last point, tubes containing very pure Kr^{82} and Kr^{84}, respectively, were prepared. By comparing interferograms taken alternately on the same plate with these tubes, an isotope shift of 0.002 cm^{-1} was detected for the line in question. This value is of the order of magnitude to be expected from Bohr's theory of the Rydberg constant, and consequently, the center of gravity Z for Kr^{83} must be situated symmetrically between the lines from Kr^{82} and Kr^{84}. By measuring interferograms taken in turn with Kr^{82}, Kr^{83}, and Kr^{84}, and by taking into account the isotope shift, the intervals x and y could be accurately determined. The final values were $x+y=0.192$ cm^{-1}, and $x/y=0.106/0.086$, which definitely give the spin value 9/2 (theor. val.: $x/y=0.1055/0.0865$).

An isotope shift of the same order of magnitude (0.002 to 0.004 cm^{-1}) was further found to exist for all measured $1s-2p$ combinations. In all cases the components of shorter wave-length belong to the heavier isotope. Finally, it should be mentioned that the intervals of the Kr line 7685A ($1s_2-2p_1$), for which only the lower term $1s_2$ splits up, were measured to be 0.138 and 0.108 cm^{-1}, which confirms the existence of a quadrupole moment of the Kr^{83} nucleus.[5]

The procedure here described was also used for investigating the h.f.s. of the rare isotope Ne^{21} (0.27 percent), since earlier experiments using neon, enriched by diffusion, showed no components from this isotope.[7] Interferograms photographed with a tube containing about 0.2 μ mole of Ne^{21}, collected in a ten-hour run, showed narrow h.f.s. structures of all $1s-2p$ combinations. Also in these experiments certain components were masked by a line originating from the lighter isotope (Ne^{20}), which in the final separation was present in nearly the same amount as Ne^{21}. This fact complicates accurate measurements of the structures, of which in most cases only one component could be observed, situated on the short wave-length side of the Ne^{20} line in distances of 0.05–0.07 cm^{-1}. However, by comparing intensities of the components of the lines 5852A ($1s_2-2p_1$), and 6266A ($1s_2-2p_3$), for which the structures are caused by the splitting of the lower and of the higher term, respectively, the magnetic moment was found to be negative and the spin to be 3/2 or possibly greater. The investigations with Ne^{21} will be continued, and further details for Kr^{83} will be published in the *Proceedings of the Royal Danish Academy of Science.*

We wish to thank Professor Niels Bohr for his continued interest in the present investigation. We should also like to thank Mr. F. Carlsen and Mr. S. Møller Holst for their help with the separation of the isotopes.

[1] J. Koch and B. Bendt-Nielsen, Kgl. Danske Vid. Sels. Math.-fys. Medd. 21, No. 8 (1944).
[2] J. Koch, Nature **161**, 566 (1948).
[3] E. Rasmussen, Zeits. f. Physik. **62**, 494 (1930); **80**, 726 (1933).
[4] H. Kopfermann and N. Wieth-Knudsen, Zeits. f. Physik **85**, 353 (3319.)
[5] H. Korsching, Zeits. f. Physik **109**, 349 (1938).
[6] Koch, Kofoed-Hansen, O. Kristensen, and Drost-Hansen, Phys. Rev. **76**, 279 (1949).
[7] R. Ritschl and H. Schober, Physik. Zeits. **38**, 6 (1937).

Wide Angle Sprays of Minimum Ionization Particles*

F. OPPENHEIMER AND E. P. NEY
University of Minnesota, Minneapolis, Minnesota
September 20, 1949

WE have observed wide angle sprays of soft minimum ionization particles emerging from lead plates of a cloud chamber. The cloud chamber was expanded at regular intervals of one per minute, and the pictures were taken during three hours at constant altitude of 14 g/cm². The cloud chamber was in a pressurized gondola attached to a General Mills balloon that had been launched from Camp Ripley at 55° geomagnetic latitude.

Figure 1 shows an example of one of the largest of such sprays in which it is possible to count about 30 tracks. Stereoscopic viewing shows that most of the tracks remain in the illuminated region as they traverse the section between the two ¼-in. lead plates; however, none of the spray particles appear to traverse the lower lead plate. Since the observed tracks show minimum ionization and have a range less than ¼ in. of Pb, they are probably electrons, and, in any event, have a mass not larger than about 20 electron masses. There is no indication of any further cascade process associated with the spray in Fig. 1.

In Table I we have tabulated the sprays observed during three hours during one of our flights. Although the events have been observed on several flights, we have used only this one in the tabulation because the condition of the chamber was particularly constant during this time.

The minimum ionization events reported in Table I certainly involve more than one type of phenomenon. Some of the events exhibit the narrow angle penetrating sprays that have been observed to emerge from "stars" seen in photographic emulsions. However, the fraction of soft wide angle sprays with and without associated heavy particles seems to be approximately independent of the size of the spray. The fact that the "star" particles are seen in only about one-third of the observed cases does not imply that the remaining two-thirds events were not accompanied by a star. From observations in photographic emulsions one would conclude that the range of most of the nucleons emerging from stars is not great enough to penetrate ⅛ in. of lead.

TABLE I. Minimum ionizotion sprays.*

Number of particles with between one and two times min. ionization	3 or more	3—5	6—9	10—15	>15
Number of events with min. ionization particles	100	56	31	10	3
Number of cases where spray is accompanied by heavily ionizing particles	34	20	10	3	1
Number of events in which one or more spray particles penetrate ¼ in. Pb	19	10	7	1	1
Number of events in which one or more spray particles multiply in ¼ in. Pb	10				
Number of stars of heavy particles and no min. ionization tracks in the same operating time	9				

* Not all sprays included are wide angle.

In the spray reproduced in Fig. 1, as well as in several other large angle sprays, it is impossible to project all the observed tracks back to a common center. Instead, several groups seem to emerge from a region in the lead plate about ½ cm in diameter. Since the observed sprays thus may be formed in some multiple type of event, we have looked for stars or sprays in the lead plates above and below the plates in which the sprays themselves were observed. The probability that a moderate energy gamma-ray will be degraded in only ¼ in. of Pb is not very large, and one might therefore expect to find small sprays in several plates. Some of the minimum ionization particles observed throughout the chamber may be associated with a star in the picture. However, there is only one case in the 100 events of Table I where the association appears at all plausible. Figure 2 shows an example from another flight in which a star may be time-coincident with a spray. Because of the difficulty of deciding the average direction of momentum transfer to the spray, and because of the large number of random tracks in the cloud chamber, it has not been possible to determine whether the sprays are initiated by ionizing or non-ionizing radiation.

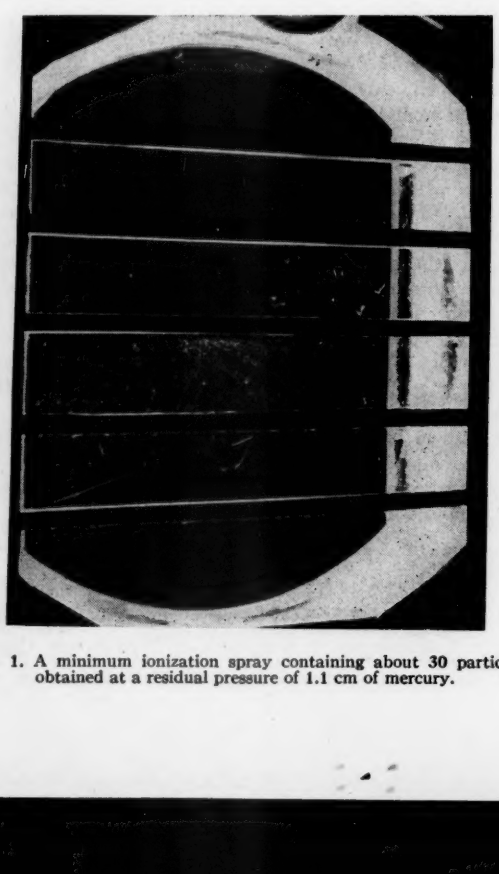

FIG. 1. A minimum ionization spray containing about 30 particles obtained at a residual pressure of 1.1 cm of mercury.

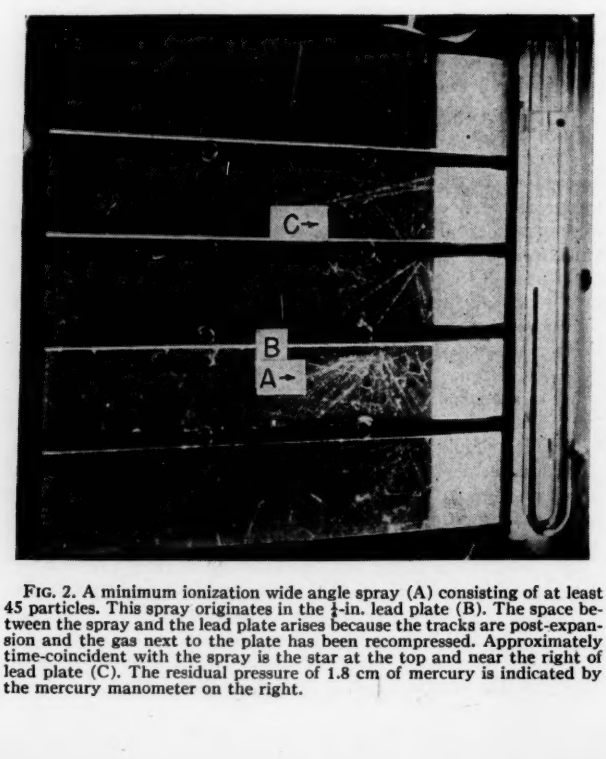

FIG. 2. A minimum ionization wide angle spray (A) consisting of at least 45 particles. This spray originates in the ¼-in. lead plate (B). The space between the spray and the lead plate arises because the tracks are post-expansion and the gas next to the plate has been recompressed. Approximately time-coincident with the spray is the star at the top and near the right of lead plate (C). The residual pressure of 1.8 cm of mercury is indicated by the mercury manometer on the right.

It is possible that the observed large angle sprays of electrons are due to the tail of large cascade showers whose core is traveling more or less parallel to the lead plates. There is little direct evidence against this explanation of the sprays. However, there are three factors which make it appear to be unlikely. (1) The frequent appearance of heavy particles associated with sprays. (2) The fact that only two large cascade showers, at any angle to the plates, have been observed in all the pictures we have obtained above 90,000 ft. (3) According to other workers, the appearance of such sprays of electrons is a very rare event to mountain and B-29 altitudes, even though the relative frequencies of showers as compared to stars is much greater at these lower altitudes than in out flights.[1] At 90,000 ft. the wide angle sprays are quite frequent. The cloud-chamber sensitive time represented in Table I is about 3.5 sec.

We plan to continue to gather statistics of the occurrence of the sprays reported here. Although we have now observed five carbon interactions, we have not observed any sprays initiated in carbon. We hope, in the future, to be able to measure the momentum of the spray particles.

The balloon flights and the development of the cloud-chamber equipment of this work has been made possible through the assistance of the ONR and the AEC.

* Reported at the Echo Lake Conference of Cosmic Rays, June 22–28, 1949.

[1] An event which appears to be of the type described here has been seen by R. P. Shutt, Phys. Rev. **69**, 271 (1946).

The Determination of the Molecular Structure of Bromosilane by Microwave Measurements

A. H. Sharbaugh, J. K. Bragg,* T. C. Madison, and V. G. Thomas
General Electric Research Laboratory, Schenectady, New York
September 12, 1949

THE second and third rotational transitions, $J=1\rightarrow 2$ and $J=2\rightarrow 3$ of $Si^{28}H_3Br^{79}$ and $Si^{28}H_3Br^{81}$, have been measured and analyzed. The $J=2\rightarrow 3$ transition of the rarer isotopic species of bromosilane, $Si^{29}H_3Br^{79}$, $Si^{29}H_3Br^{81}$, $Si^{30}H_3Br^{79}$, and $Si^{30}H_3Br^{81}$, were also observed. The nuclear and molecular constants are listed in Table I.

Table I. Nuclear and molecular constants of bromosilane.

		ν_0(mc/s)	$I_B\times10^{40}$ (g-cm^2)	$eQ(\partial^2V/\partial Z^2)$ (mc/s)	B_0(mc/s)
$J=2\rightarrow3$	$Si^{28}H_3Br^{79}$	25930.32	194.13	336	4321.72
	$Si^{28}H_3Br^{81}$	25755.89	195.44	278	4292.64
	$Si^{29}H_3Br^{79}$	25397.80	198.20		4232.96
	$Si^{29}H_3Br^{81}$	25222.21	199.58		4203.70
	$Si^{30}H_3Br^{79}$	24896.33	202.19		4149.39
	$Si^{30}H_3Br^{81}$	24720.57	203.63		4120.09
$J=1\rightarrow2$	$Si^{28}H_3Br^{79}$	17287.30	194.12		4321.82
	$Si^{28}H_3Br^{81}$	17170.45	195.44		4292.61

The theoretical hyperfine structure to be expected for a nuclear spin of 3/2 for beomine was in excellent agreement with the observed spectra for all the transitions involving Si^{28}. Since the second order quadrupole corrections were of the same order as the experimental error in frequency measurement (±0.08 mc/s), they were neglected. These measurements yield a ratio of 1.209 for the nuclear quadrupole moment of Br^{79} to that of Br^{81} which compares favorably with the figure of 1.197 for the corresponding methyl bromides.[1] Any possible quadrupole effect due to the Si^{29} or Si^{30} nuclei was sufficiently small as to be within the limits of resolution.

The experimental determination of six effective moments of inertia resulting from the different isotopic species permits the evaluation of the three structural parameters of the molecule. These were evaluated from the $J=2\rightarrow J=3$ transitions of $Si^{28}H_3Br^{79}$, $Si^{28}H_3Nr^{81}$, and $Si^{30}H_3Br^{79}$ and checked against the remaining three. The values are listed together with the estimated errors in Table II.

Table II. Structural parameters for bromosilane and chlorosilane.

	SiH_3Br	Covalent radii and tetrahedral angle	SiH_3Cl[2]	Covalent radii and tetrahedral angle
Si-Br Distance	2.209 ±0.001A	2.31	2.048A	2.16
Si-H Distance	1.57 ±0.03A	1.47	1.50A	1.47
H-Si-H Distance	111°20′ ±1°	109°28′	110°57′	109°28′

As observed with SiH_3Cl, there is considerable shortening of the Si—Br distance from the sum of the covalent radii, presumably due to appreciable double bond character of this bond. However, the difference of the Si—Cl and the Si—Br distances is the same as that of the corresponding covalent radii. Although not stated explicitly,[2] the number of significant figures available in the chlorosilane parameters may be expected to be the same as that in bromosilane; hence differences in these parameters listed in Table II are not necessarily real.

We wish to thank Dr. A. E. Newkirk of this laboratory for the preparation of the bromosilane used in these measurements.

* Present address: Chemistry Department, Cornell University, Ithaca, New York.

[1] Gordy, Simmons, and Smith, Phys. Rev. **74**, 243 (1948).

[2] Computed from microwave measurements. See Dailey, Mays, and Townes, Phys. Rev. **76**, 136 (1949), and A. H. Sharbaugh, Phys. Rev. **74**, 1870 (1948).

Erratum: The Application of Dyson's Methods to Meson Interactions

[Phys. Rev. **76**, 486 (1949)]

P. T. Matthews
Clare College, Cambridge, England

IN Eq. (6) the closures of the brackets in the factors of the form $P(\ldots)$ should follow the factor $j(x_n)$ in the first two terms and the factor $(j_\rho(x_{n-1})n_\rho(x_{n-1}))^2$ in the final term.

On the Photoelectron Spectrum of Ta^{182}

C. Harold Goddard and C. Sharp Cook
Department of Physics, Washington University, St. Louis, Missouri
September 16, 1949

A STUDY of the internal conversion electrons produced by the gamma-rays from the disintegration of Ta^{182} has led to a report[1] of some 28 gamma-rays in the energy range below 330 kev. The investigation herein reported is a study of the photoelectron spectrum of this isotope using a 14-cm radius of curvature uniform field spectrometer.[2] The only other reported investigation[3] of the photoelectron spectrum of this isotope gives only two gamma-rays in the above-mentioned region and two higher energy gammas at 1.13 and 1.22 Mev.

The region for gamma-ray energies below 330 kev was studied using both uranium and lead radiators, each of 50 mg/cm^2 thickness and the results are indicated in Parts (A) and (B) of Fig. 1, respectively. The higher energy region was studied only with the uranium radiator and the result is shown in Part (C) of Fig. 1.

The criterion for the assignment of gamma-ray energies in the low energy region was that the line must appear in both spectra if possible. Except for two low intensity lines in the uranium radiator spectrum such a matching process could be performed with the result that eight gamma-rays seem to be identified in the photoelectron spectrum. Further check indicates that each of these appear to correspond to a gamma-ray energy as determined by Cork *et al*[1] from the internal conversion spectrum. The results are indicated in Table I.

In addition, there appear to be three higher energy gamma-rays at 1.12, 1.19, and 1.23 Mev as indicated in Part (C) of Fig. 1. These are designated by the numbers 9, 10, and 11, respectively.

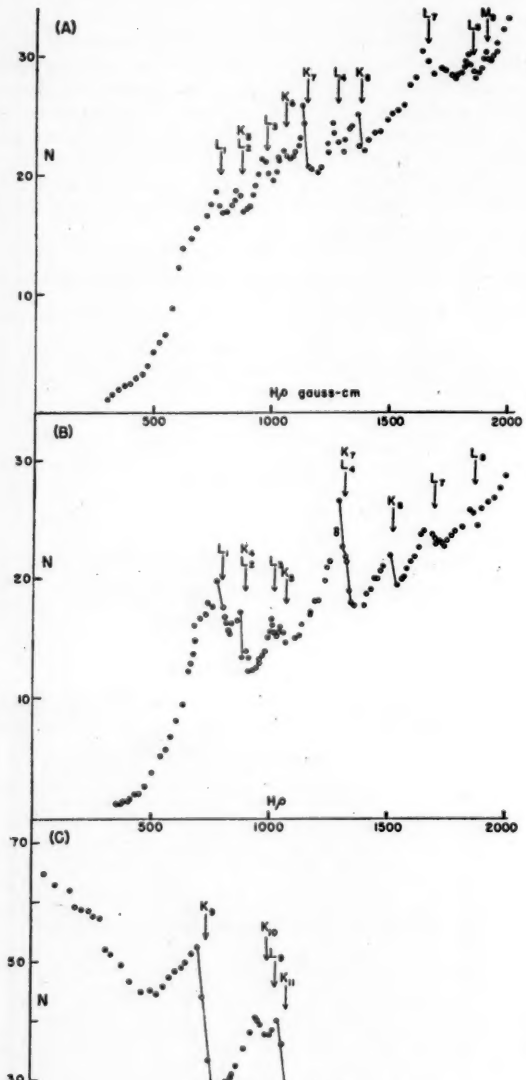

FIG. 1. The photoelectron spectrum of Ta^{182} (A) in the region below 2000 gauss-cm using an uranium radiator of 50 mg/cm²; (B) in the region below 2000 gauss-cm using a lead radiator of 50 mg/cm²; and (C) in the region 4000–6000 gauss-cm using an uranium radiator of 50 mg/cm².

TABLE I. List of gamma-rays found in photoelectron spectrum of Ta^{182}.

Our number	Gamma-energy	Cork's number
1[a]	71	5
2	84	7
3	103	9
4	151	16
5	180	20
6[b]	209	22
7	220	23
8	261	25

[a] These numbers have been arbitrarily assigned and are used as subscripts to indicate the K and L peaks for the individual gamma-rays in the spectra of Fig. 1.

[b] Only a low intensity K peak is found in the uranium radiator spectrum for this gamma-ray. Had it appeared in the lead radiator spectrum, it would have fallen on the leading edge of the line indicated as K_7, L_4, and because of its low intensity would probably be overshadowed by the two more intense lines.

Since completing this investigation, a report of further work on this subject by Wilkinson, Beach, and Peacock[4] has come to the attention of the authors. The gamma-ray energies as derived from the photoelectron spectrum reported therein are not always in agreement with the values reported here. However, the criterion stated above seems to lead to fairly definite indications that the gamma-rays listed in Table I do exist in the photoelectron spectrum of Ta^{182}.

The authors wish to thank Mr. Chang Chia-hua for his assistance in taking a portion of the data.

This work has been supported by the joint program of the ONR and the AEC.

[1] J. M. Cork, Phys. Rev. **72**, 581 (1947); Cork, Keller, Sazynski, Rutledge, and Stoddard, Phys. Rev. **75**, 1778 (1949).
[2] Ter-Pogossian, Cook, Goddard, and Robinson, Phys. Rev. **76**, 909 (1949).
[3] W. Rall and R. G. Wilkinson, Phys. Rev. **71**, 321 (1947).
[4] Indiana University Third Annual Report on Contract N6ori-48, Task Order I (August 1, 1949).

Photo-Neutrons from Neutron Capture Gamma-Rays

BERNARD HAMERMESH AND ALBERT WATTENBERG
Argonne National Laboratory, Chicago, Illinois
September 22, 1949

RECENT reports[1] on gamma-rays produced on neutron capture indicate that gamma-rays of energies as high as 9.5 Mev are produced. Since neutron-binding energies are usually between 6 and 8 Mev, the capture gamma-rays from some substances should be able to photo-disintegrate other substances.

A neutron beam from the thermal column of the Argonne heavy water pile was allowed to impinge upon various materials such as Cd, $Cl(C_2Cl_6)$, Au, and Fe. The gamma-rays emitted then struck various possible (γ, n) sources placed next to a detector. The detector was a BF_3 pulse ion chamber embedded in paraffin. The counter was well shielded from fast neutrons from the pile. Cadmium differences were measured with different combinations of source and target.

TABLE I. Cadmium differences in counts/minute.

Targets \ gamma-ray sources	Cl	Cd	Au	Fe
D_2O	470	1000	270	130
Pb	110	15	25	
Bi	25	15	15	
Hg	20	10	0	
Li(LiF)	20	10	35	
Fe	0	0		
Al	0	0		
Cd	0	0		

Table I shows the cadmium differences obtained in counts/minute after correcting for various backgrounds.

The statistical accuracy is ±10 counts per minute. Values other than zero are given only where a consistently positive effect was found. The efficiency of the detector was such that a one-millibarn (γ, n) cross section was the lowest that could give a positive effect, assuming that one percent of the capture gamma-rays are effective.

As more information is obtained about capture gamma-ray spectra, it may be possible to obtain values of photo-disintegration thresholds and cross sections for various elements in the region 6–10 Mev. With the present available thermal neutron beams, the above reactions do not seem to be useful sources of fast neutrons.

[1] H. Kubitschek and S. A. Dancoff, Phys. Rev. 76, 531 (1949).

The Nuclear Gyromagnetic Ratio of V^{51} *

W. D. KNIGHT** AND V. W. COHEN
Brookhaven National Laboratory Upton, Long Island, New York
September 15, 1949

RESONANCES due to V^{51} have been observed in $Pb(VO_3)_2$ and in V_2O_5, both in dry powder form and in acid solutions, using an automatic recording r-f spectrometer similar to that described by Pound.[1]

The resonance frequency for V^{51} was compared to that for Na^{23}, for fixed magnetic field, in a mixture containing V_2O_5, NaCl, and dilute HCl. This procedure eliminated the necessity of exchanging samples for comparison, and allowed one to be certain that the individual resonances occurred in the same region of the magnetic field. The magnetic field was stabilized by an electronic control which maintained the current constant to approximately one part in 10^5 over the time required for a series of measurements of comparison frequencies.

The ratio of the uncorrected g-values is given by the observed frequency ratio, which is:

$$g(V^{51})/g(Na^{23}) = 0.99394 \pm 0.00003.$$

Using Bitter's[2] value for the frequency ratio Na^{23}/H^1, and the value of Taub and Kusch[3] for $g(H^1) = 5.5870$ nuclear magnetons, the frequency ratio V^{51}/H^1 and $g(V^{51})$ are, respectively:

$$V^{51}/H^1 = 0.26290,$$
$$g(V^{51}) = 1.4713 \pm 0.0003 \text{ nuclear magnetons.}$$

For the latter value, a diamagnetic correction of 0.171 percent has been introduced (see discussion in reference 3).

Kopfermann and Rasmussen[4] have published a probable value of 7/2 for the nuclear spin of V^{51}, although this value is not certain. No previous value for $g(V^{51})$ has been published. Assuming the spin to be 7/2, one obtains the following value for the nuclear magnetic moment

$$\mu(V^{51}) = 5.150 \text{ nuclear magnetons.}$$

As is well known,[5] a plot of μ as a function of I for the odd proton nuclei shows two rather distinct groupings of the nuclei. The above value for V^{51} falls close to the region containing the upper group.

* Work performed at the Brookhaven National Laboratory under contract with the AEC.
** Permanent address, Department of Physics, Trinity College, Hartford, Connecticut.
[1] R. V. Pound, Phys. Rev. 72, 527 (1947).
[2] F. Bitter, Phys. Rev. 75, 1326 (1949).
[3] H. Taub and P. Kusch, Phys. Rev. 75, 1481 (1949).
[4] H. Kopfermann and E. Rasmussen, Zeits. f. Physik 98, 624 (1936).
[5] See the paper by L. W. Nordheim, Phys. Rev. 75, 1894 (1949) and the references cited there.

Angular Distribution of Neutrons from Targets Bombarded by 18-Mev Deuterons

P. AMMIRAJU
Department of Physics, University of California, Berkeley, California
August 30, 1949

RECENT measurements[1-3] on the angular distribution of fast neutrons from targets bombarded by deuterons of energy less than 20 Mev indicate that the neutrons are mostly emitted in the forward direction (i.e., the direction of the original deuteron beam). This letter reports a series of measurements on the spatial distribution of these neutrons with targets of different elements and copper as a threshold detector for all the elements investigated. In all cases there is a fairly sharp forward peak in the distribution of the emitted neutrons. Similar measurements[4] at 190-Mev deuteron energy have been carried out and the results are in good agreement with the stripping process worked out by Serber.[5] Although the present day theories are inadequate to explain fully the results obtained in this experiment, there is good agreement in the case of copper and beryllium targets with the stripping theory.

Deuterons of approximately 18-Mev energy were allowed to impinge on different targets and the resulting neutron intensity was detected by means of copper threshold detectors enclosed in cadmium boxes and placed in an arc of a circle of about 10½-inch radius with target as the center. The target materials used were Be, Na, Cu, Ta, Pb, and Th, and were thick enough for the deuterons to be stopped within the target thickness. Most of the activity in copper consisted of the ten-minute period showing thereby that the neutrons are emitted with sufficient energy to produce the reaction $Cu^{63}(n, 2n)Cu^{62}$ which has a threshold of 11 Mev.[6] The activity of the samples was measured by means of an ionization chamber with a F.P. 54 electrometer-tube.

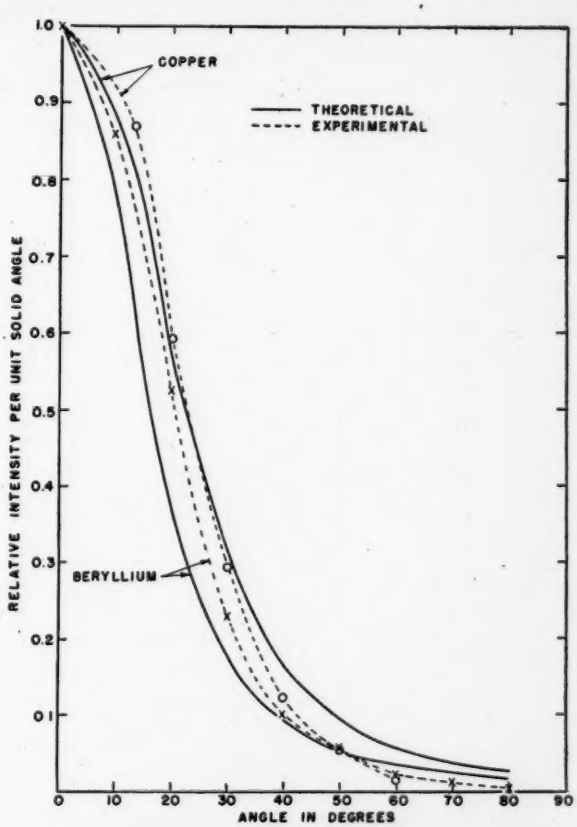

FIG. 1. Angular distribution of neutrons from Be and Cu. The theoretical curves are calculated from Serber's theory.

TABLE I. Summary of results obtained for the half-width.

Target	Half-width in degrees	
	Experimental	Stripping theory
Be	41°	31°
Cu	45°	46°
Pb	47°	70°

The distribution curves for Be and Cu, along with the curves calculated from Serber's theory, are reproduced in Fig. 1. In the case of Be and Cu there is a small amount of background (3 percent and 10 percent respectively of the maximum) for which correction is made in comparing the experimental curve with that obtained on the basis of stripping process. The agreement in the case of copper is good, but for beryllium the observed half-width (i.e., full width at half-maximum) is somewhat greater than that given by stripping theory. This indicates that in the case of Be, processes other than stripping might also be responsible for the observed distribution. In the case of Pb, there is a larger isotropic background (about 25 percent of the maximum) and after subtraction of the background there is a large discrepancy between the observed and calculated distributions in that the experimental half-width is considerably smaller than the theoretical half-width. Although there seems to be a perceptible increase in the half-width with increase in atomic number, the rate of increase is definitely not in agreement with stripping theory. Similar results on the variation of half-width with atomic number have been reported by Falk *et al.*[3] Professor V. F. Weisskopf has pointed out that for heavy elements the deuteron loses so much energy in climbing the potential barrier that the neutron can obtain sufficient momentum to cause the Cu(n, $2n$) reaction only by adding its internal momentum in the deuteron parallel to its external momentum. This will cause a sharp forward peak for essentially energetic reasons, the stripping neutrons at larger angles being of lower energy. Table I gives a summary of the results obtained for the half-width.

It is a great pleasure to thank Professor A. C. Helmholz for suggesting the problem and for guidance throughout the course of the investigation. I would like to take this opportunity to thank Professor R. Serber for valuable suggestions in the interpretation of data on the basis of stripping theory. My thanks are also due to the 60-inch cyclotron crew.

[1] R. B. Roberts and P. H. Abelson, Phys. Rev. **72**, 76 (1947).
[2] Falk, Creutz, and Seitz, Phys. Rev. **74**, 1226 (1948).
[3] Falk, Creutz, and Seitz, Phys. Rev. **76**, 322 (1949).
[4] Helmholz, MacMillan, and Sewell, Phys. Rev. **72**, 1003 (1947).
[5] R. Serber, Phys. Rev. **72**, 1008 (1947).
[6] McElhinney, Hanson, Becker, Duffield, and Diven, Phys. Rev. **75**, 542 (1949).